

# VIBRATIONS OF SOILS AND FOUNDATIONS

*F. E. Richart, Jr. (Professor)*  
*J. R. Hall, Jr. (Assoc. Professor)*  
*R. D. Woods (Asst. Professor)*

Department of Civil Engineering  
The University of Michigan  
Ann Arbor, Michigan

PRENTICE-HALL INTERNATIONAL, INC., *London*  
PRENTICE-HALL OF AUSTRALIA, PTY. LTD., *Sydney*  
PRENTICE-HALL OF CANADA LTD., *Toronto*  
PRENTICE-HALL OF INDIA PRIVATE LTD., *New Delhi*  
PRENTICE-HALL OF JAPAN, INC., *Tokyo*

*Prentice-Hall, Inc., Englewood Cliffs, New Jersey*

TA 710  
.R.46

© 1970 by  
PRENTICE-HALL, INC.  
Englewood Cliffs, N.J.

All rights reserved. No part of this  
book may be reproduced in any form  
or by any means without permission  
in writing from the publisher.

Current printing (last digit):

10 9 8 7 6 5 4 3 2 1

13-941716-8  
Library of Congress Catalog Card Number: 75-100361  
Printed in the United States of America

*Spencer  
Library  
1970*

## PREFACE

Problems related to vibrations of soils and foundations have required increased attention during the past two decades, and notable advances have been made during the past ten years. Recent contributions include new theoretical procedures for calculating dynamic responses of foundations, improved field and laboratory methods for determining dynamic behavior of soils, and field measurements to evaluate the performance of the prototype. It is the purpose of this text to describe the state-of-the-art as it relates to procedures for analysis, design, and measurements of the response of foundations to dynamic loadings, and the transmission of vibrations through soils. The primary emphasis is directed towards vibrations of the magnitudes generated by machinery, but the principles and many of the results can be adapted to the dynamic conditions resulting from earthquakes or blast loadings.

The book has developed from notes prepared for a graduate course in Soil Dynamics which has been taught by the authors, in succession, since 1961. It has been assumed that the reader has an adequate background in statics and elementary dynamics but probably has not completed a formal course in vibration theory. Chapter 2 reviews the elements of vibrations needed to understand the material presented in later chapters. The course notes, essentially in the present form, were prepared for a two-week short course during the summer of 1968 which was attended by practicing engineers and professors. It has been found that the contents of this book can be followed readily by practicing engineers and that this information may provide the basis for a first year graduate course.

Throughout the text notes are included to point out topics which need further investigation, both analytical and experimental. In particular, the

need for field evaluation of the behavior of prototype installations is emphasized. It is only through a feedback from prototype measurements to design procedures that we are able to gain confidence in and improve upon present design methods. Chapter 9 on Instrumentation is included to familiarize the reader with the principles and types of vibration measuring equipment which may be used for obtaining field and laboratory data on vibrations of soils and foundations.

The authors wish to acknowledge the stimulation and assistance offered by several senior advisors and by many colleagues. The number of times a name appears in the reference list indicates some measure of each individual's contribution to our background in the subject of vibrations of soils and foundations. The late Professor K. Terzaghi directed the attention of the senior author toward soil dynamics in 1951 and subsequently provided many forms of assistance and encouragement. Several of the recent improvements in the analyses of soil dynamics problems are based on methods developed by Professor N. M. Newmark, and his stimulation and interest have contributed to our continued efforts in this field. Discussions with Professor R. V. Whitman over the past decade have been especially significant in our selection and evaluation of topics for continued study. Many junior colleagues, particularly Dr. T. Y. Sung and Professors B. O. Hardin, J. Lysmer, and V. P. Drnevich have contributed directly to the ideas and methods presented in this text. Special thanks are extended to Mr. M. P. Blake for his careful reading of the notes and for his valuable comments.

Finally, the authors wish to acknowledge the generous assistance provided by the Department of Civil Engineering, The University of Michigan, to the development and preparation of this text. We have appreciated the careful typing of the manuscript which was done by Miss Pauline Bentley and Miss Reta Teachout.

F. E. RICHART, JR.  
J. R. HALL, JR.  
R. D. WOODS

*Ann Arbor Michigan*  
*January 1969*

## CONTENTS

<b>1</b>	<b>Introduction</b>	<b>1</b>
1.1	Design Criteria	2
1.2	Relations Between Applied Loads and Quantities which Govern Criteria	2
1.3	Evaluation of Soil Properties	3
1.4	Design Procedures	3
<b>2</b>	<b>Vibration of Elementary Systems</b>	<b>5</b>
2.1	Vibratory Motion	6
2.2	Vector Representation of Harmonic Motion	10
2.3	Single-Degree-of-Freedom Systems	11
2.4	Phase-Plane Analysis of Single-Degree-of-Freedom Systems	32
2.5	Systems with Two Degrees of Freedom	48
2.6	Natural Frequencies of Continuous Systems	57
<b>3</b>	<b>Wave Propagation in an Elastic, Homogeneous, Isotropic Medium</b>	<b>60</b>
3.1	Waves in a Bounded Elastic Medium	60
3.2	Waves in an Infinite, Homogeneous, Isotropic Elastic Medium	75
3.3	Waves in an Elastic Half-Space	80

<b>4</b>	<b><i>Elastic Waves In Layered Systems</i></b>	<b>93</b>
4.1	Distribution of Wave Energy at Boundaries	93
4.2	Elements of Seismic Methods	100
4.3	Steady-State Vibration Techniques	111
<b>5</b>	<b><i>Propagation of Waves in Saturated Media</i></b>	<b>121</b>
5.1	Introduction	121
5.2	Compression Waves in Ideal Fluids	123
5.3	Wave Propagation in Porous Saturated Solids	132
5.4	Effect of Water Table on Wave Propagation in Soils	136
5.5	Summary	139
<b>6</b>	<b><i>Behavior of Dynamically Loaded Soils</i></b>	<b>140</b>
6.1	Introduction	140
6.2	Behavior of Elastic Spheres in Contact	141
6.3	Behavior of Soils Under Small-Amplitude Vibratory Loading	151
6.4	Behavior of Soil Under Large-Amplitude Loading	170
<b>7</b>	<b><i>Theories for Vibrations of Foundations on Elastic Media</i></b>	<b>191</b>
7.1	Introduction	191
7.2	Lamb (1904) and the Dynamic Boussinesq Problem	192
7.3	Vertical Oscillation of Footings Resting on The Surface of The Elastic Half-Space	194
7.4	Torsional Oscillation of Circular Footings on the Elastic Half-Space	213
7.5	Rocking Oscillation of Footings Resting on the Elastic Half-Space	216
7.6	Sliding Oscillation of a Circular Disk Resting on the Elastic Half-Space	221
7.7	Geometrical Damping Associated with Vibrations of Rigid Circular Footings on the Elastic Half-Space	224
7.8	Coupled Rocking and Sliding of the Rigid Circular Footing on the Elastic Half-Space	227
7.9	Oscillation of the Rigid Circular Footing Supported by an Elastic Layer	230
7.10	Vibrations of Rigid Foundations Supported by Piles or Caissons	235

<b>8</b>	<b><i>Isolation Of Foundations</i></b>	<b>244</b>
8.1	Isolation by Location	244
8.2	Isolation by Barriers	247
<b>9</b>	<b><i>Instrumentation for Laboratory and Field Measurements</i></b>	<b>263</b>
9.1	Basic Electrical Elements	264
9.2	Instruments for Electrical Measurements	269
9.3	Vibration Transducers and Their Calibration	275
9.4	Cables and Connectors	289
9.5	Vibration Measurements for Field Tests	292
9.6	The Resonant-Column Test	300
<b>10</b>	<b><i>Design Procedures for Dynamically Loaded Foundations</i></b>	<b>308</b>
10.1	Introduction	308
10.2	Design Criteria	309
10.3	Dynamic Loads	322
10.4	Brief Review of Methods for Analyzing Dynamic Response of Machine Foundations	336
10.5	Lumped-Parameter Vibrating Systems	345
10.6	Analysis and Design for Vertical Vibrations of Foundations	353
10.7	Analysis and Design for Rocking Vibrations of Foundations	369
10.8	Conclusions	379
	<b>Appendix</b>	<b>381</b>
	<b>References</b>	<b>387</b>
	<b>Index</b>	<b>403</b>



## SYMBOLS

In selecting the symbols used in this text, an attempt was made to conform to the *List of Recommended Symbols for Soil Mechanics*, adopted in Paris (1961) by the International Society of Soil Mechanics and Foundation Engineering and "Nomenclature for Soil Mechanics," *Journal of the Soil Mechanics and Foundations Division, Proceedings, American Society of Civil Engineers*, Vol. 88, No. SM 3 (June 1962), Paper No. 3183. However, in a few cases symbols were adopted to conform to usage in other disciplines or to avoid confusion. Whenever the same symbol is used to represent two items—for example,  $e$  for void ratio and  $e$  as the base of natural logarithms—the distinction should be clear from the text.

Symbols are defined where they first appear in the text; those which occur several times are listed below. When a symbol represents a quantity having dimensions, the dimensions most commonly used are listed along with the symbol. If no dimension is indicated, the symbol represents a pure number.

$A$ (ft)	= displacement amplitude
$A$ (ft <sup>2</sup> )	= area
$A_x$ (ft)	= amplitude of horizontal oscillation
$A_z$ (ft)	= amplitude of vertical vibration
$A_{\Theta}$ (rad.)	= amplitude of angular rotation about vertical axis of symmetry
$A_{\psi}$ (rad.)	= amplitude of angular rotation about a horizontal axis

$a_o$	= dimensionless frequency, defined by Eq. (7-2)
$\bar{a}_o$	= dimensionless frequency factor for a single-degree-of-freedom system, defined by Eq. (2-72)
$a_{om}$	= dimensionless frequency at maximum amplitude of vibration
$B$ (lb/ft <sup>2</sup> )	= bulk modulus, or modulus of compressibility
$\bar{B}$	= dimensionless mass factor for a single-degree-of-freedom system, defined by Eq. (2-73)
$B_x$	= mass ratio for horizontal oscillation of rigid circular footing, defined by Eq. (7-56)
$B_z$	= mass ratio for vertical vibration of rigid circular footing on elastic half-space, defined by Eq. (7-23)
$B_\Theta$	= mass ratio for torsional oscillation of rigid circular footing about a vertical axis, defined by Eq. (7-38)
$B_\psi$	= mass ratio for rocking of rigid circular footing about a horizontal axis through base of footing, defined by Eq. (7-44)
$b$	= dimensionless mass ratio, defined by Eq. (7-3)
$C_i$	= arbitrary constant
$c$ (ft)	= half-length of the longer side of a rectangular foundation (see Fig. 7-12)
$c$ (lb-sec/in.)	= viscous-damping coefficient
$c_c$ (lb-sec/in.)	= critical damping, defined by Eq. (2-31)
$c_x$ (lb-sec/in.)	= damping constant for horizontal oscillation
$c_z$ (lb-sec/in.)	= damping constant for vertical vibration
$c_\psi$ (lb-sec/rad)	= damping constant for rocking of footing about horizontal axis
$c'$ (lb/ft <sup>2</sup> )	= effective cohesion intercept
$D$	= damping ratio, defined by Eq. (2-32)
$D_r$	= relative density of cohesionless soils, defined by Eq. (6-37)
$D_x$	= damping ratio for horizontal oscillation, defined by Eq. (7-63) for rigid circular footing
$D_z$	= damping ratio for vertical oscillation, defined by Eq. (7-62) for rigid circular footing
$D_\Theta$	= damping ratio for torsional oscillation, defined by Eq. (7-65) for rigid circular footing

$D_\psi$	= damping ratio for rocking of rigid circular footing about horizontal axis, defined by Eq. (7-53)
$d$ (ft)	= half-width of rectangular foundation (see Fig. 7-12)
$E$ (lb/in. <sup>2</sup> )	= modulus of linear deformation, Young's modulus
$e$	= void ratio (volume of voids per unit volume of solid constituents); also, base of natural logarithms
$e$ (in.)	= eccentricity, the radial distance from the center of gravity of a rotating mass to the center of rotation
$F$	= Lysmer's displacement function, defined by Eq. (7-21)
$F_1, F_2$	= components of Lysmer's displacement function $F$
$f$ (cycles/sec)	= frequency
$f_b$ (cycles/sec)	= beat frequency
$f_d$ (cycles/sec)	= damped natural frequency
$f_m$ (cycles/sec)	= resonant frequency for constant-force-amplitude excitation
$f_{mr}$ (cycles/sec)	= resonant frequency for rotating-mass-type excitation
$f_n$ (cycles/sec)	= undamped natural frequency
$f_1, f_2$	= components of Reissner's displacement function
$G$ (lb/in. <sup>2</sup> )	= modulus of shear deformation or shear modulus
$G_s$	= specific gravity, ratio of unit weight of a material to the unit weight of water
$g$ (ft/sec <sup>2</sup> )	= acceleration of gravity (32.17 ft/sec <sup>2</sup> )
$H$ (ft)	= thickness of layer of soil
$I$ (ft-lb-sec <sup>2</sup> )	= mass polar moment of inertia
$I_\Theta$ (ft-lb-sec <sup>2</sup> )	= mass moment of inertia of footing in rotation about a vertical axis
$I_\psi$ (ft-lb-sec <sup>2</sup> )	= mass moment of inertia of footing in rotation about horizontal axis
$i$	= $\sqrt{-1}$
$K_o$	= coefficient of earth pressure at rest (ratio between normal stress on a vertical section and normal stress on a horizontal section at a given point in a mass of soil)
$k$ (lb/in.)	= spring constant
$k_e$ (lb/in.)	= equivalent spring constant

$k_{zs}$ (lb/in.)	= spring constant relating horizontal displacement to applied horizontal force $Q_o$ , defined by Eq. (7-60) for rigid circular footing
$k_z$ (lb/in.)	= spring constant relating vertical displacement $z$ to applied force $Q_o$ ; spring constant for rigid circular footing on elastic half-space, defined by Eq. (7-26)
$k_{\Theta s}$ (in.-lb/rad)	= spring constant relating angular rotation about vertical axis to applied static torque, defined by Eq. (7-37)
$k_{\psi}$ (in.-lb/rad)	= spring constant for rotation
$k_{\psi s}$ (in.-lb/rad)	= spring constant relating angular rotation about horizontal axis to applied static moment, defined by Eq. (7-50)
$k'$ (lb/ft <sup>3</sup> )	= modulus of subgrade reaction
$L$ (ft)	= wave length
$L_R$ (ft)	= wave length of Rayleigh wave
$l$ (ft)	= length of beam or rod
$M$	= amplitude magnification factor
$M_r$	= amplitude magnification factor, defined by Eq. (7-25)
$M_x$	= amplitude magnification factor, defined by Eq. (7-58)
$M_{\Theta m}$	= amplitude magnification factor, defined by Eq. (7-39)
$M_{\Theta r m}$	= amplitude magnification factor, defined by Eq. (7-41)
$M_{\psi}$	= amplitude magnification factor, defined by Eq. (7-45)
$M_{\psi r}$	= amplitude magnification factor, defined by Eq. (7-47)
$m$ (lb-sec <sup>2</sup> /ft)	= mass ( $m = W/g$ )
$m_o$ (lb-sec <sup>2</sup> /ft)	= total eccentric mass in rotating-mass oscillator
$m_1$ (lb-sec <sup>2</sup> /ft)	= mass of each eccentric weight in multimass oscillator
$N$	= wave number ( $N = 2\pi/L$ )
$n$	= porosity, ratio between total volume of voids and total volume of soil
$P$ (lb)	= force
$P_o$ (lb)	= amplitude of periodic force acting on elastic body
$p$ (lb/ft <sup>2</sup> )	= fluid pressure
$Q$ (lb)	= time-dependent external force acting on elastic system
$Q_o$ (lb)	= amplitude of external force acting on elastic system

$R$ (ft)	= radius
$r$ (ft)	= radial distance from origin of coordinates
$r_o$ (ft)	= radius of circular footing
$\bar{r}$ (ft)	= radius of gyration
$S$	= degree of saturation
$T$ (sec)	= period
$T$ (ft-lb)	= torque
$T_b$ (sec)	= beat period
$T_n$ (sec)	= undamped natural period
$T_{\Theta}$ (ft-lb)	= torque about vertical axis
$T_{\psi}$ (ft-lb)	= torque about horizontal axis
$t$ (sec)	= time
$U(z)$	= spatial variation of displacement $u$
$u$ (ft)	= displacement in $x$ -direction
$\dot{u}$ (ft/sec)	= velocity in $x$ -direction
$u$ (lb/ft <sup>2</sup> )	= pore pressure in soils
$V$ (ft <sup>3</sup> )	= total volume
$V_s$ (ft <sup>3</sup> )	= total volume of solid particles
$V_v$ (ft <sup>3</sup> )	= total volume of voids
$v$ (ft/sec)	= velocity of wave propagation
$v_a$ (ft/sec)	= velocity of sound waves in air
$v_C$ (ft/sec)	= velocity of longitudinal or rod wave
$v_P$ (ft/sec)	= velocity of dilatation wave or primary wave ( $P$ -wave)
$v_R$ (ft/sec)	= velocity of Rayleigh wave ( $R$ -wave)
$v_S$ (ft/sec)	= velocity of shear wave ( $S$ -wave)
$v_w$ (ft/sec)	= velocity of sound wave in water
$\bar{v}$ (ft/sec)	= apparent velocity
$W$ (lb)	= weight
$W(z)$	= spatial variation of displacement $w$
$w$ (ft)	= displacement in $z$ -direction

$x$ (ft)	= horizontal distance
$x_c$ (ft)	= crossover distance, distance to point at which direct wave and refracted wave arrive at the same time in a refraction survey
$x_s$ (ft)	= horizontal displacement caused by static force $Q_o$ , defined by Eq. (7-59) for rigid circular footing
$x$ (ft)	= horizontal moment arm of unbalanced weights from center of rotation in rotating-mass oscillator
$z$ (ft)	= displacement in the vertical direction, positive downward
$z_o$ (ft)	= vertical displacement at center of circular area of loading on surface of elastic half-space
$z_s$ (ft)	= vertical displacement caused by static load $Q_o$
$\dot{z}$ (ft/sec)	= velocity in the vertical direction
$\ddot{z}$ (ft/sec <sup>2</sup> )	= acceleration in the vertical direction
$\alpha$ (1/ft)	= coefficient of attenuation, defined by Eq. (6-27)
$\alpha$	= parameter relating shear-wave velocity to compression-wave velocity:

$$\alpha = \sqrt{\frac{G}{\lambda + 2G}} = \sqrt{\frac{1 - 2\nu}{2 - 2\nu}}$$

$\gamma$ (lb/ft <sup>3</sup> )	= unit weight of soil
$\gamma_a$ (lb/ft <sup>3</sup> )	= unit dry weight of soil
$\gamma_s$ (lb/ft <sup>3</sup> )	= unit weight of solid particles
$\gamma_w$ (lb/ft <sup>3</sup> )	= unit weight of water (62.4 lb/ft <sup>3</sup> )
$\gamma'$ (lb/ft <sup>3</sup> )	= unit weight of submerged soil
$\gamma_{ij}$	= shear strain
$\gamma_{z\theta}$	= average maximum shear-strain amplitude developed in torsion of hollow cylindrical soil sample
$\delta$	= logarithmic decrement, defined by Eq. (2-39)
$\delta_L$ (rad)	= loss angle in a viscoelastic solid, defined by Eq. (6-30)
$\epsilon_i$	= linear strain in the $i$ -direction
$\bar{\epsilon}$	= cubic dilatation or volumetric strain of elastic body ( $\bar{\epsilon} = \epsilon_x + \epsilon_y + \epsilon_z$ )

$\bar{\epsilon}$	= cubic dilatation or volumetric strain in a fluid
$\theta$	= angle
$\Theta$	= angular rotation about axis of symmetry
$\Theta_s$	= angular rotation of rigid circular footing about a vertical axis caused by static torque
$\lambda$ (and $G$ ) (lb/in. <sup>2</sup> )	= Lamé's constants:
	$\left( \lambda = \frac{2\nu G}{1 - 2\nu} \right)$
$\mu$ lb-sec/in. <sup>2</sup>	= shear coefficient of viscosity
$\nu$	= Poisson's ratio
$\pi$	= 3.14159...
$\rho$ (lb-sec <sup>2</sup> /ft <sup>4</sup> )	= mass density ( $\rho = \gamma/g$ )
$\sigma_i$ (lb/ft <sup>2</sup> )	= total normal stress in the $i$ -direction
$\bar{\sigma}_o$ (lb/ft <sup>2</sup> )	= average effective normal stress or effective octahedral normal stress
$\tau_{ij}$ (lb/ft <sup>2</sup> )	= shear stress
$\tau_o$ (lb/ft <sup>2</sup> )	= octahedral shear stress, defined by Eq. (6-22)
$\Phi$	= potential function
$\phi'$ (deg)	= effective angle of internal friction in soils
$\varphi$	= phase angle
$\psi$	= angular rotation about a horizontal axis
$\psi_s$	= angular rotation of footing about horizontal axis caused by static moment
$\Psi$	= potential function
$\omega$ (rad/sec)	= circular frequency
$\omega_d$ (rad/sec)	= damped natural circular frequency
$\omega_n$ (rad/sec)	= undamped natural circular frequency
$\omega_z$ (rad/sec)	= natural frequency for uncoupled translation
$\omega_\psi$ (rad/sec)	= natural frequency for uncoupled rotation
$\nabla^2$	= Laplacian operator ( $\nabla^2 = \partial^2/\partial x^2 + \partial^2/\partial y^2 + \partial^2/\partial z^2$ for Cartesian coordinates)

**Notes about subscripts:**

- $x, y, z$  refer to Cartesian coordinates  
 $r, \theta, z$  refer to cylindrical coordinates  
 $1, 2, 3$  refer to directions of principal stresses or strains  
 $i, j, k$  represent general coordinate directions  
 $\exp$  used for base of natural logarithms

# INTRODUCTION

The problems associated with the design of foundations to resist dynamic loadings, either from supported machinery or from external sources, still require special solutions dictated by local soil conditions and environment. The foundation must first satisfy the criteria for static loadings, then it must be satisfactory for resisting the dynamic conditions.

Designing to resist dynamic loading conditions requires answering the following questions: (1) What should be considered "failure" of the chosen design function and what are the numerical limits on the failure criteria? (2) What are the relations between the applied loads and the quantities which are significant in the failure criteria? (3) How do we identify and evaluate these significant quantities? (4) Finally, after we have evaluated these significant quantities, what sort of a factor of safety (or statistical estimate of the reliability in evaluating these quantities) do we apply in the design process?

The basic reason for preparing this text is to provide recent information which assists in answering questions 1 through 4 in the design process. This information is intended to supplement the considerable amount of valuable information already available in such notable books on the subject as those by Rausch (1943), Lorenz (1960), Barkan (1962), Major (1962), and Harris and Crede (1961).\*

\* Complete references are listed alphabetically in the References sections at the end of the book.

### 1.1 Design Criteria

Establishing the design criteria is probably the most important step in the design process. This defines the problem to be solved and is the gage by which we judge our computed solution and, if possible, our measurements of the performance of the prototype. For dynamically loaded foundations the criteria are generally described in terms of limiting values of acceleration, velocity, or displacement under the operating conditions. Limiting values of these criteria are determined by what is considered to be a "failure" of the design function. Section 10.2 describes several limits of these design criteria for different requirements. It is significant to note, for example, that a vibration amplitude of 0.001 in. at a frequency of 1000 cycles/min would represent a satisfactory value for the displacement-frequency criterion if the design purpose was "to prevent serious damage to machinery," but would be entirely inadequate if the design purpose was "not to be noticeable to persons" (see Fig. 10-1). Consequently, it is essential that "ground rules" be established at the start of the design study.

### 1.2 Relations Between Applied Loads and Quantities which Govern Criteria

The first part of this topic is sometimes difficult to evaluate numerically. Dynamic loadings generated by the natural forces of earthquakes, wind, or water waves, or manmade forces from blasting, traffic, construction, or neighboring machinery may be transmitted to the foundation through a structural system or through the soil. In most of these cases, it is necessary to obtain field measurements under conditions similar to those for the proposed design, and to assume that these loadings will be encountered by the prototype. Consequently, it is necessary to have information on the transmission and interception of energy transmitted through the soil (Chaps. 3, 4, and 8) and some knowledge of methods for evaluating forces and motions in the field (Chap. 9). A discussion of the forces developed by certain simple machines is included in Chap. 10.

The link between the applied loads and the failure criteria is made analytically. Because the limiting value of the failure criteria for vibrating machine foundations usually involves motions of a few thousandths of an inch, the failure mechanism is in the range of elastic deformations of the supporting soil. Consequently, solutions based on a consideration of an elastic supporting system often provide satisfactory relations between the applied loads and dynamic response of foundations. Chapter 7 deals with a number of solutions for the response of foundations, primarily based on the theory of elasticity. These elasticity solutions require an evaluation of the

Poisson's ratio and shear modulus for the elastic material; in terms of our design process, this means that the significant quantities in questions 2 and 3 are the shear modulus and Poisson's ratio for the soil.

### 1.3 Evaluation of Soil Properties

The process of obtaining representative values for the critical soil properties is probably the most difficult part of the design study. Samples must be obtained from the proposed construction site and tested under conditions anticipated to represent the operating environment. Because the soil properties which influence the dynamic response of foundations are established for a different order of magnitude of deformations from those involved in static soil properties, a new set of laboratory- and field-testing procedures have been developed, primarily during the past decade. Chapter 6 includes a discussion of the dynamic soil properties needed for design purposes and some information on the influence of testing conditions on these properties. Further discussion of the test equipment is found in Chap. 9.

### 1.4 Design Procedures

There are several methods by which the design criteria may be satisfied for a particular installation. A few of these are discussed in Chap. 10, but particular emphasis is placed upon the lumped-parameter method. There is already a wealth of literature available concerning the solutions for lumped-parameter systems, but it has always been a problem to determine representative values for the lumped mass, spring, and dashpot. For dynamically loaded foundations supported directly on soils it has been found that the theory of foundations supported by the elastic half-space provides the key for determining satisfactory values for the damping and spring constant for a given foundation-soil system. The lumped mass represents the weight of the foundation and supported equipment. Examples are included in Chap. 10 to illustrate the application of the lumped-parameter method using damping and spring constants established from the elastic-half-space theory.

The consideration of soil as an elastic half-space has further advantages in application of solutions from geophysics to problems of wave propagation in soils and of isolation of foundations—namely, it permits extensions of the theoretical studies to problems of the refraction and diffraction of waves in soils by geometrical discontinuities.

The contents of this book are directed primarily toward the problems of analysis and design of machine foundations, including consideration of the wave energy transmitted through the supporting soil.

Information pertaining to these problems has been collected from the fields of seismology, theory of elasticity, soil dynamics, instrumentation, and machine design. Each of these fields has its special set of accepted terminology and symbols and these have been followed as closely as possible. It is recognized that the reader may have some difficulty while he becomes familiar with the terminology in a field outside his specialty. Instead of a cumbersome glossary of terms, a detailed index has been provided to direct the reader to the page where each term is defined. A list of symbols is included at the front of the book for convenient reference.

## 2

### VIBRATION OF ELEMENTARY SYSTEMS

To predict or analyze the response of a vibratory system, in many cases it is satisfactory to reduce it to an idealized system of lumped parameters. The simplest system is the classical single-degree-of-freedom system with viscous damping consisting of a mass, spring, and dashpot. Since this system is easily formulated mathematically, the solution is found in all textbooks on vibrations as well as in mathematical texts on differential equations. Yet, while such a system appears to be a gross simplification of any real system, there are many instances in which it provides a very satisfactory model with which to make a dynamic analysis, even though the real system may not physically resemble the mathematical model. For example, it will be shown in Chap. 7 that a footing resting on an elastic medium can be represented mathematically by elements associated with a single-degree-of-freedom system where the values of the physical constants are determined from the dimensions and properties of the foundation and elastic medium. Once a system has been reduced to a model, the next step is the analysis, which may be analytical or graphical depending upon the type of problem. In some cases nonlinearities must be included in the model in order to approximate the real system more closely. Although such conditions usually result in complicated mathematical expressions, graphical solutions may often be obtained readily.

For some systems a single-degree-of-freedom model will not represent accurately the dynamic response. In these cases a model having two or more degrees of freedom may be required. The analysis then becomes considerably more complicated and the use of a digital or analog computer becomes

necessary. For continuous systems which cannot be represented by lumped components of springs, masses, and dashpots, hand calculations are usually limited to the determination of the natural frequency of the system or of its response to steady vibration.

The following sections present the analytical, graphical, and numerical methods that form the basic tools required for vibration design and for analysis of foundations and basic mechanical and structural components.

## 2.1 Vibratory Motion

*Harmonic* or sinusoidal motion is the simplest form of vibratory motion and may be described mathematically by the equation

$$z = A \sin(\omega t - \varphi) \quad (2-1)$$

which is plotted as a function of time in Fig. 2-1. The quantity  $A$  represents the displacement amplitude from the mean position, sometimes referred to as *single amplitude*. The distance  $2A$  represents the *peak-to-peak-displacement amplitude*, sometimes referred to as *double amplitude*, and is the quantity most often measured from vibration records. The *circular frequency*  $\omega$  defines the rate of oscillation in terms of radians per unit time,  $2\pi$  rad being equal to one complete cycle of oscillation. The frequency of oscillation in terms of cycles per unit time is given by

$$f = \frac{\omega}{2\pi} \quad (2-2)$$

(In some literature the units of cycles per second are called *Hertz*, abbreviated Hz.) The time required for the motion to begin repeating itself is called the *period* of vibration and is given by

$$T = \frac{1}{f} = \frac{2\pi}{\omega} \quad (2-3)$$

It can be seen from Fig. 2-1 that to define physically harmonic motion two independent quantities are required. The most commonly used parameters are amplitude and frequency. In some instances a third quantity, the *phase angle*  $\varphi$ , is required to specify the time relationship between two quantities having the same frequency when their peak values having like sign do not occur simultaneously. In Eq. (2-1) the phase angle is a reference to the time origin. More commonly, however, the phase angle will be a reference to

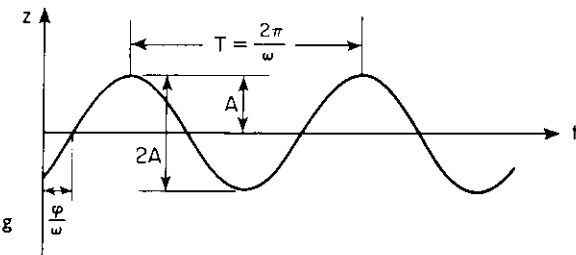


Figure 2-1. Quantities describing harmonic motion.

another quantity having the same frequency. For example, at some reference point in a harmonically vibrating system, the motion may be expressed by

$$z_1 = A_1 \sin \omega t \quad (2-4)$$

Motion at any other point in the system might be expressed by

$$z_i = A_i \sin(\omega t - \varphi_i) \quad (2-5)$$

with  $\pi \geq \varphi \geq -\pi$ .

For positive values of  $\varphi$  the motion at point  $i$  reaches its peak within one half-cycle after the peak motion occurs at point 1. The angle  $\varphi$  is then called a *phase lag*. For negative values of  $\varphi$  the peak motion at  $i$  occurs within one half-cycle ahead of the motion at 1 and  $\varphi$  is called a *phase lead*.

Obviously, all motion of vibrating bodies is not harmonic and, in fact, harmonic motion is generally obtained only under controlled laboratory conditions. In Fig. 2-2 three other types of motion are shown. *Periodic motion* (Fig. 2-2a) is of the type such that the displacement-time relationship repeats itself; whereas in *random motion*, as shown in Fig. 2-2b, the displacement-time pattern never repeats. Figure 2-2c shows a *transient*-type motion associated with damped systems where an impulsive-type disturbance has been applied over a short time interval. After the impulse the vibrations decay until the system returns to a rest condition. Problems involving transient motion will be considered in a later section.

When two harmonic motions of slightly different frequency are superimposed, a nonharmonic motion occurs, as shown in Fig. 2-3, which appears to be harmonic except for a gradual increase and decrease in amplitude. For such a condition the expression for motion may be written as the sum of two harmonic motions:

$$z = A_1 \sin(\omega_1 t - \varphi_1) + A_2 \sin(\omega_2 t - \varphi_2) \quad (2-6)$$

The dashed curve representing the envelope of the vibration amplitudes oscillates at a frequency, called the *beat frequency*, which corresponds to the



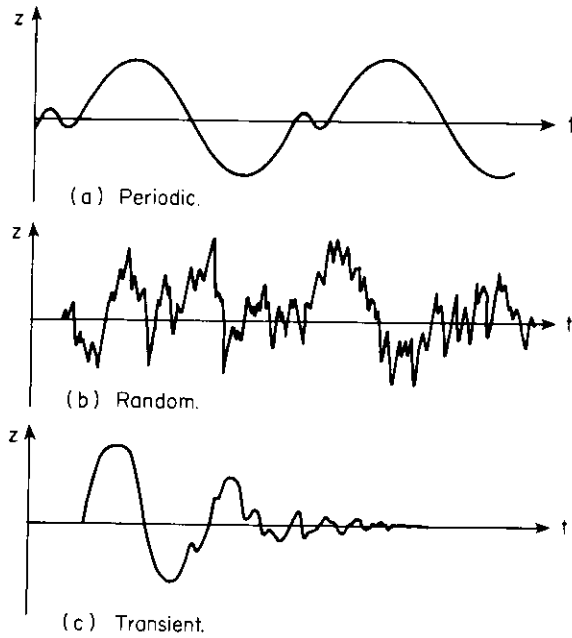


Figure 2-2. Periodic, random, and transient motion.

difference in the two source frequencies:

$$f_b = \frac{1}{T_b} = \frac{|\omega_1 - \omega_2|}{2\pi} \quad (2-7)$$

The frequency of the combined oscillations is the average of the frequencies of the two components and is given by

$$f = \frac{1}{T} = \frac{1}{2\pi} \frac{\omega_1 + \omega_2}{2} \quad (2-8)$$

The maximum and minimum amplitudes of motion are the sum and difference respectively of the amplitudes of the two sources:

$$\begin{aligned} z_{\max} &= A_1 + A_2 \\ z_{\min} &= |A_1 - A_2| \end{aligned} \quad (2-9)$$

Motion of the type described by Eq. (2-6) often occurs when vibrations are caused by two machines designed to operate at the same speed. Unless the drive systems of the two machines are synchronized, there will be a slight difference in their operating speed, resulting in vibrations having the beat frequency.

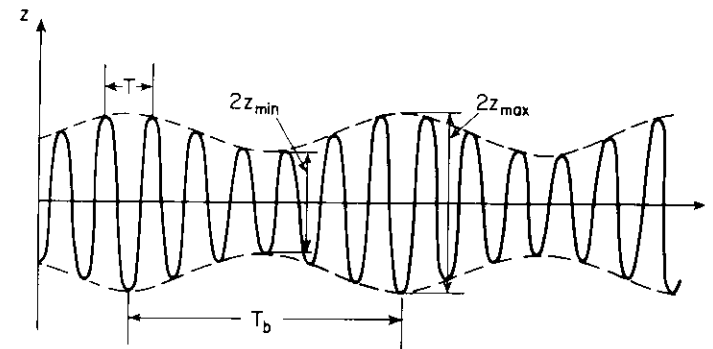


Figure 2-3. Motion containing a beat.

Up to now only displacement has been considered. In many problems one must also consider the first and second derivatives and in some cases the third derivative of displacement with respect to time. The quantities obtained from the derivatives of Eq. (2-1) are given below.

$$\text{Displacement} = z = A \sin(\omega t - \varphi) \quad (2-10a)$$

$$\text{Velocity} = \frac{dz}{dt} = \dot{z} = \omega A \cos(\omega t - \varphi) \quad (2-10b)$$

$$\text{Acceleration} = \frac{d^2z}{dt^2} = \ddot{z} = -\omega^2 A \sin(\omega t - \varphi) \quad (2-10c)$$

$$\text{Jerk} = \frac{d^3z}{dt^3} = -\omega^3 A \cos(\omega t - \varphi) \quad (2-10d)$$

The dot over the quantity indicates derivatives with respect to time. If a comparison of the quantities obtained is made, it is seen that with each succeeding derivative the amplitude of the quantity obtained is the amplitude of the previous quantity multiplied by  $\omega$ .

Thus, for harmonic motion the displacement amplitude along with the frequency is all that is needed to determine the amplitude of any of the other quantities. In fact, if any two amplitudes or any one amplitude along with the frequency are specified, then all other quantities are uniquely determined. In many instances a vibration nomograph, as shown in Fig. 2-4, provides a convenient conversion between the four quantities of frequency, displacement amplitude, velocity amplitude, and acceleration amplitude. It will be noted that in Fig. 2-4 the acceleration is expressed as a factor multiplied by  $g$ . The symbol  $g$  is used throughout this book to represent the acceleration of gravity, where

$$1g = 386 \text{ in./sec}^2 \quad (2-11)$$

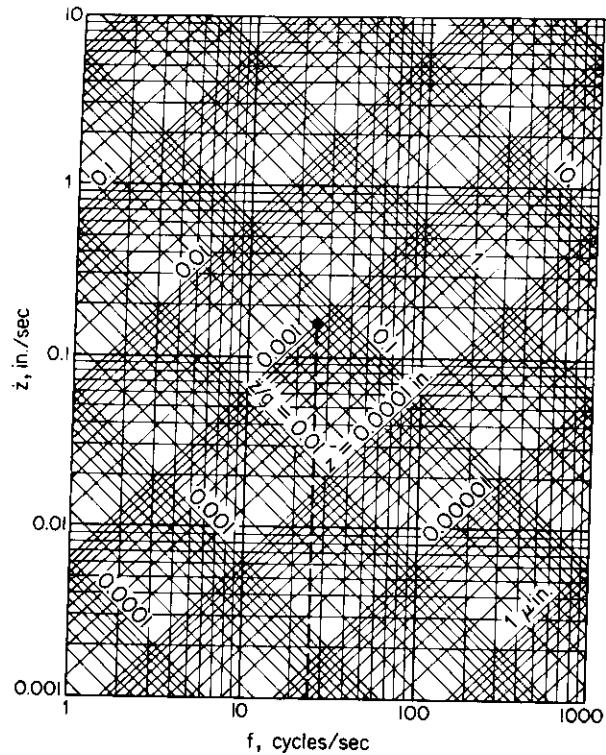


Figure 2-4. Vibration nomograph for harmonic motion.

When using Fig. 2-4 one must be consistent and use either single or double amplitude for all quantities. As an example, a peak displacement of 0.001 in. at 25 cycles/sec produces a peak velocity of 0.16 in./sec and a peak acceleration of 0.065 g. This point is shown in Fig. 2-4 by the circle and dashed line.

For motion other than harmonic motion, simple relationships do not exist between displacement, velocity, and acceleration, and the conversion from one quantity to the other must be accomplished by differentiation or integration.

### 2.2 Vector Representation of Harmonic Motion

In the solution of problems involving harmonic motion, a physical feeling can be obtained by use of the concept of rotating vectors. For problems of transient motion, however, the method fails, but graphical methods can be used in these cases.

Using displacement as the reference quantity and rewriting Eqs. (2-10) in terms of sine functions, we obtain

$$z = A \sin \omega t \tag{2-12a}$$

$$\dot{z} = \omega A \cos \omega t = \omega A \sin \left( \omega t + \frac{\pi}{2} \right) \tag{2-12b}$$

$$\ddot{z} = -\omega^2 A \sin \omega t = \omega^2 A \sin (\omega t + \pi) \tag{2-12c}$$

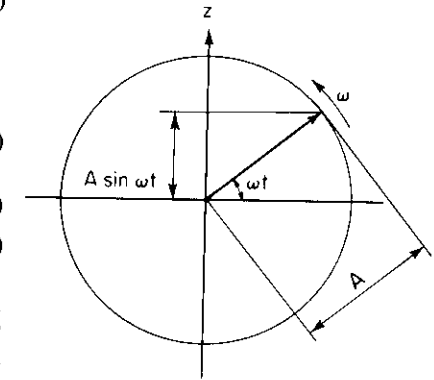


Figure 2-5. Vector representation of harmonic motion.

From Eqs. (2-12) it can be observed that velocity leads displacement by 90° and acceleration leads displacement by 180°. If a vector of length  $A$  is rotated counterclockwise about the origin, as shown in Fig. 2-5, its projection onto the vertical axis would be equal to  $A \sin \omega t$ , which is exactly the expression for displacement given in Eq. (2-12a). It follows that velocity can be represented by the vertical projection of a vector of length  $\omega A$  positioned 90° ahead of the displacement vector. Likewise, acceleration can be represented by a vector of length  $\omega^2 A$  located 180° ahead of the displacement vector. A plot of all three of the above quantities is shown in Fig. 2-6.

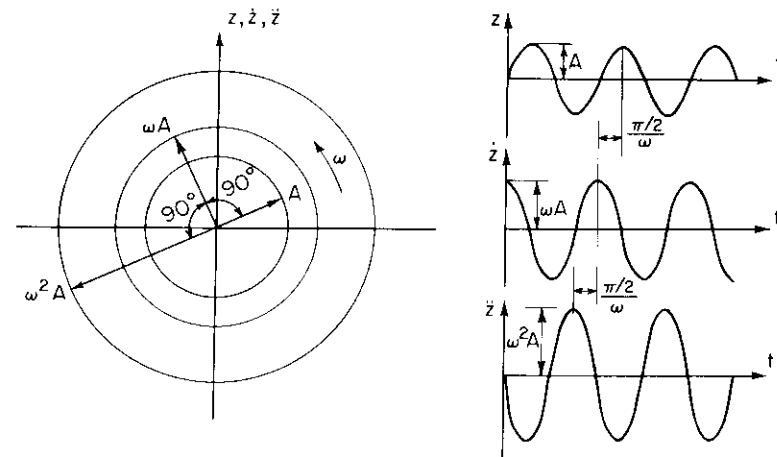


Figure 2-6. Vector representation of harmonic displacement, velocity and acceleration.

### 2.3 Single-Degree-of-Freedom Systems

We shall next consider the solutions to a vibratory system having only one degree of freedom. In such a system, the position of all parts of the system can be described by a single variable at any instant of time. If a system requires more than a single variable to define its configuration, then it has more than one degree of freedom. In general, the number of degrees of freedom of a system is equal to the number of independent variables required to define the position of all parts of the system at any instant of time.

#### Free Vibrations—Undamped

The system shown in Fig. 2-7a consists of a linear spring with a spring constant  $k$  and a weight  $W$  having a mass  $m = W/g$ . The spring constant  $k$  is defined as the change in force per unit change in length of the spring. The weight is restricted to move in the vertical direction without rotation. The solution to the problem is simplified by measuring the displacement  $z$  from a position  $z_s$  below the point at which the spring force is equal to zero. The distance represents the static deflection and is given by

$$z_s = \frac{W}{k} \quad (2-13)$$

The differential equation of motion is obtained from Newton's second law, which states that the net unbalanced force on a constant-mass system is equal to the mass of the system multiplied by its acceleration. If the system shown in Fig. 2-7a is displaced a distance  $z$  from the rest position, the force

(a)  $z = 0$  at Rest Position.

(b)

Figure 2-7. Spring-mass system without damping.

in the spring will be equal to  $(W + kz)$ , as shown in Fig. 2-7b. Thus, from Newton's second law,

$$W - (W + kz) = \frac{W}{g} \ddot{z} = m\ddot{z} \quad (2-14)$$

which reduces to

$$m\ddot{z} + kz = 0 \quad (2-15)$$

The solution of this equation, found in any text on differential equations, is

$$z = C_1 \sin \sqrt{\frac{k}{m}} t + C_2 \cos \sqrt{\frac{k}{m}} t \quad (2-16)$$

where the arbitrary constants  $C_1$  and  $C_2$  are evaluated from the initial conditions of the system. The quantity  $\sqrt{k/m}$  corresponds to the *undamped natural circular frequency* of the system, designated as

$$\omega_n = \sqrt{\frac{k}{m}} \text{ rad/sec} \quad (2-17a)$$

and the undamped natural frequency is

$$f_n = \frac{1}{2\pi} \sqrt{\frac{k}{m}} \text{ cycles/sec} \quad (2-17b)$$

The undamped natural frequency may be expressed in another form by substitution of  $W/g$  for  $m$  and  $z_s$  for  $W/k$ . Thus,

$$f_n = \frac{1}{2\pi} \sqrt{\frac{g}{z_s}} \quad (2-18)$$

Table 2-1 gives values of  $f_n$  for values of  $z_s$  within the practical range of most problems.

Table 2-1

$z_s$ (in.)	$f_n$ (cycles/sec)
0.001	99.0
0.01	31.3
0.1	9.90
1.0	3.13

From the above we can see that for free vibration of an undamped single-degree-of-freedom system, the motion is harmonic and occurs at a natural frequency  $f_n$ . The amplitude of motion is determined from the initial conditions, two of which must be specified. If displacement and velocity are specified at  $t = 0$  and denoted as  $z_0$  and  $\dot{z}_0$ , respectively, the following expressions are obtained for  $C_1$  and  $C_2$  in Eq. (2-16):

$$C_1 = \frac{\dot{z}_0}{\omega_n} \tag{2-19a}$$

$$C_2 = z_0 \tag{2-19b}$$

*Series and Parallel Springs*

Although it is convenient to symbolize a single-degree-of-freedom system as a single spring attached to a mass, in most real systems there are usually several springs required for stability. It is possible, however, to calculate an equivalent single spring to represent the assemblage of springs. In Fig. 2-8



(a) Series Springs.

(b) Parallel Springs.

Figure 2-8. Series and parallel spring systems.

two general types of spring arrangements are shown. For the *series* arrangement we have the condition of equal force in each spring. Two springs having spring constants of  $k_1$  and  $k_2$  as in Fig. 2-8a will deflect statically when loaded by a weight  $W$  by an amount

$$z_s = \frac{W}{k_1} + \frac{W}{k_2} = W \left( \frac{1}{k_1} + \frac{1}{k_2} \right) \tag{2-20}$$

Thus, the equivalent spring constant is

$$k_e = \frac{W}{z_s} = \frac{1}{\frac{1}{k_1} + \frac{1}{k_2}} \tag{2-21}$$

For a system with  $n$  springs in series, the expression for an equivalent spring is

$$k_e = \frac{1}{\frac{1}{k_1} + \frac{1}{k_2} + \dots + \frac{1}{k_n}} \tag{2-22}$$

The *parallel* spring arrangement in Fig. 2-8b must satisfy the condition of equal displacement in each spring and the sum of the forces in each spring must equal the weight  $W$ :

$$W = P_1 + P_2 = z_s k_1 + z_s k_2 \tag{2-23}$$

Thus, for parallel springs,

$$k_e = \frac{W}{z_s} = k_1 + k_2 \tag{2-24}$$

In general, a system with  $n$  parallel springs has an equivalent spring constant given by

$$k_e = k_1 + k_2 + \dots + k_n \tag{2-25}$$

*Free Vibrations—With Damping*

If an element is added to the spring-mass system in the above analysis in order to dissipate energy, a system is obtained which more closely behaves like a real system. The simplest mathematical element is the viscous damper or dashpot shown schematically in Fig. 2-9a. The force in the dashpot is directly proportional to velocity  $\dot{z}$  and has a value computed from the viscous damping coefficient  $c$  having units of lb/(in./sec). Thus, the dashpot exerts a force which acts to oppose the motion of the mass.

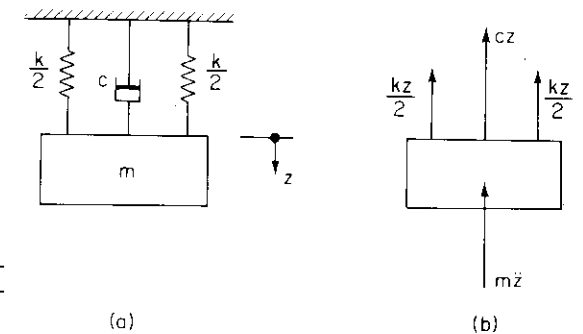


Figure 2-9. Single-degree-of-freedom system with viscous damping.

For free vibrations of the system in Fig. 2-9, the differential equation of motion may be obtained by making use of Newton's second law and measuring displacement from the rest position. A positive displacement will produce a spring force acting on the mass in the negative direction (restoring force) and a positive velocity will produce a damping force acting in the negative direction, all shown in Fig. 2-9b. Summation of vertical forces leads to

$$m\ddot{z} + c\dot{z} + kz = 0 \quad (2-26)$$

for free vibrations. If we let  $z = \exp(\beta t)$ ,

$$m\beta^2 + c\beta + k = 0 \quad (2-27)$$

which has the following solutions for  $\beta$ :

$$\beta_1 = \frac{1}{2m} [-c + \sqrt{c^2 - 4km}] \quad (2-28a)$$

$$\beta_2 = \frac{1}{2m} [-c - \sqrt{c^2 - 4km}] \quad (2-28b)$$

Three possible cases must be considered for the above equations, depending upon whether the roots are real, complex, or equal.

**CASE 1:**  $c^2 > 4km$ . For this case the two roots of Eq. (2-27) are real as well as negative and the solution to Eq. (2-26) is

$$z = C_1 \exp(\beta_1 t) + C_2 \exp(\beta_2 t) \quad (2-29)$$

Since  $\beta_1$  and  $\beta_2$  are both negative,  $z$  will decrease exponentially without change in sign, as shown on Fig. 2-10a. In this case no oscillations will occur and the system is said to be *overdamped*.

**CASE 2:**  $c^2 = 4km$ . This condition is only of mathematical significance, since the equality must be fulfilled in order for the roots of Eq. (2-27) to be equal. The solution is

$$z = (C_1 + C_2 t) \exp\left(-\frac{ct}{2m}\right) \quad (2-30)$$

This case is similar to the overdamped case except that it is possible for the sign of  $z$  to change once as in Fig. 2-10b. The value of  $c$  required to satisfy the above condition is called the critical damping coefficient,  $c_c$ , and Eq. (2-30) represents the *critically damped* case. Thus,

$$c_c = 2\sqrt{km} \quad (2-31)$$

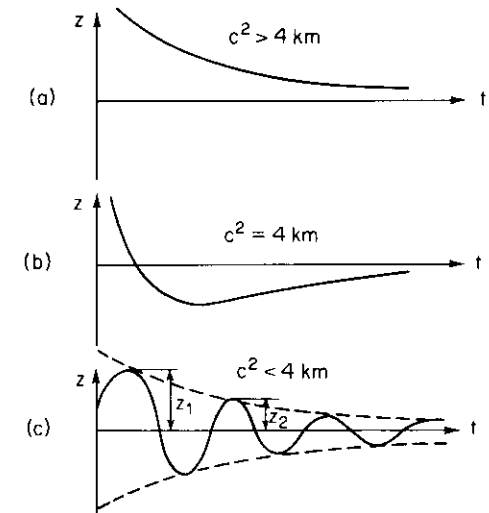


Figure 2-10. Free vibrations of a viscously damped system. (a) Overdamped. (b) Critically damped. (c) Underdamped.

The damping ratio,  $D$ , will be defined by

$$D = \frac{c}{c_c} \quad (2-32)$$

**CASE 3:**  $c^2 < 4km$ . For systems with damping less than critical damping, the roots of Eq. (2-27) will be complex conjugates. By introducing the relationship for  $c_c$ , the roots  $\beta_1$  and  $\beta_2$  become

$$\beta_1 = \omega_n(-D + i\sqrt{1 - D^2}) \quad (2-33a)$$

$$\beta_2 = \omega_n(-D - i\sqrt{1 - D^2}) \quad (2-33b)$$

Substitution of Eqs. (2-33) into Eq. (2-29) and conversion to trigonometric form with the aid of Euler's formula,  $\exp i\theta = \cos \theta + i \sin \theta$ , gives

$$z = \exp(-\omega_n D t) (C_3 \sin \omega_n t \sqrt{1 - D^2} + C_4 \cos \omega_n t \sqrt{1 - D^2}) \quad (2-34)$$

where  $C_3$  and  $C_4$  are arbitrary constants. Equation (2-34) indicates that the motion will be oscillatory and the decay in amplitude with time will be proportional to  $\exp(-\omega_n D t)$ , as shown by the dashed curves in Fig. 2-10c. Examination of Eq. (2-34) shows that the frequency of free vibrations is less than the *undamped natural circular frequency* and that as  $D \rightarrow 1$ , the frequency approaches zero. The natural circular frequency for damped oscillation in terms of the undamped natural circular frequency is given by

$$\omega_d = \omega_n \sqrt{1 - D^2} \quad (2-35)$$

and will be called the *damped natural circular frequency*. For systems with less than 40 per cent critical damping, the reduction in natural frequency is less than 10 per cent. For greater values of damping, the reduction in natural frequency is more pronounced.

Referring to Fig. 2-10, the amplitudes of two successive peaks of oscillation are indicated by  $z_1$  and  $z_2$ . These will occur at times  $t_1$  and  $t_2$ , respectively. Evaluating Eq. (2-34) at  $t_1$  and  $t_2$  we get

$$z_1 = \exp(-\omega_n D t_1)(C_3 \sin \omega_d t_1 + C_4 \cos \omega_d t_1) \quad (2-36a)$$

$$z_2 = \exp(-\omega_n D t_2)(C_3 \sin \omega_d t_2 + C_4 \cos \omega_d t_2) \quad (2-36b)$$

However,  $t_2 = t_1 + 2\pi/\omega_d$ . Thus,  $\omega_d t_2 = \omega_d t_1 + 2\pi$  and hence

$$\sin \omega_d t_2 = \sin(\omega_d t_1 + 2\pi) = \sin \omega_d t_1$$

Thus, the ratio of peak amplitudes is given by

$$\frac{z_1}{z_2} = \exp[-\omega_n D(t_2 - t_1)] = \exp\left(\omega_n D \frac{2\pi}{\omega_d}\right) \quad (2-37)$$

Substitution of Eq. (2-35) gives

$$\frac{z_1}{z_2} = \exp\left(\frac{2\pi D}{\sqrt{1 - D^2}}\right) \quad (2-38)$$

The *logarithmic decrement* is defined as the natural logarithm of two successive amplitudes of motion, or

$$\delta = \ln \frac{z_1}{z_2} = \frac{2\pi D}{\sqrt{1 - D^2}} \quad (2-39)$$

It can be seen that one of the properties of viscous damping is that the decay of vibrations is such that the amplitude of any two successive peaks is a constant ratio. Thus the logarithmic decrement can be obtained from any two peak amplitudes  $z_1$  and  $z_{1+n}$  from the relationship

$$\delta = \frac{1}{n} \ln \frac{z_1}{z_{1+n}} \quad (2-40)$$

It is also important to note that if the peak amplitude of vibration is plotted on a logarithmic scale against the cycle number on an arithmetic scale, the points will fall on a straight line if the damping is of the viscous type as assumed in Eq. (2-26).

### Forced Vibrations—Undamped

We shall next consider the response of the spring-mass system to the application of a harmonic force  $Q$  of amplitude  $Q_0$ , as shown in Fig. 2-11a. Using Newton's second law, we find the differential equation of motion to be

$$m\ddot{z} + kz = Q_0 \sin \omega t \quad (2-41)$$

The solution to this equation includes the solution for free vibrations, Eq. (2-16), along with the solution which satisfies the right-hand side of Eq. (2-41). In order to obtain a physical feeling for the problem, the particular

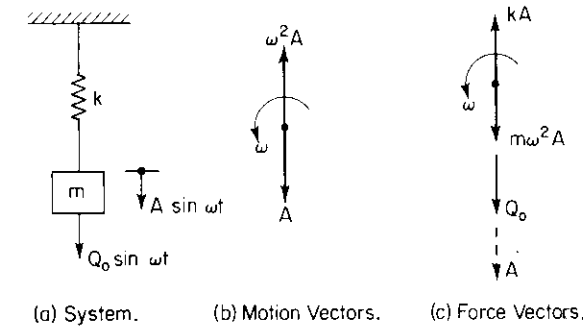


Figure 2-11. Forced vibrations of a single-degree-of-freedom system without damping.

solution will be obtained using the concept of rotating vectors. Since the applied force is harmonic, it is reasonable to assume that the internal spring force and inertia force will also be harmonic. Thus, the motion of the system will be of the form

$$z = A \sin \omega t \quad (2-42)$$

which is represented graphically in Fig. 2-11b. The forces acting on the mass are shown in Fig. 2-11c. The spring force acts opposite to the displacement and the inertia force acts opposite to the direction of acceleration. The exciting-force vector of amplitude  $Q_0$  is shown acting in phase with the displacement vector. Thus, from equilibrium requirements,

$$Q_0 + m\omega^2 A - kA = 0 \quad (2-43)$$

giving

$$A = \frac{Q_0}{k - m\omega^2} = \frac{Q_0}{k} \frac{1}{1 - \left(\frac{\omega}{\omega_n}\right)^2} \quad (2-44)$$

The complete solution obtained from Eqs. (2-44) and (2-16) is

$$z = \frac{\underline{Q}_0}{k} \frac{1}{1 - \left(\frac{\omega}{\omega_n}\right)^2} \sin \omega t + C_1 \sin \omega_n t + C_2 \cos \omega_n t \quad (2-45)$$

For a real system, the vibrations associated with the last two terms of Eq. (2-45) will eventually vanish because of damping, leaving the so-called *steady-state solution*:

$$z = \frac{\underline{Q}_0}{k} \frac{1}{1 - \left(\frac{\omega}{\omega_n}\right)^2} \sin \omega t \quad (2-46)$$

Investigation of Eq. (2-44) shows that for  $\omega < \omega_n$ ,  $A$  is positive, and that for  $\omega > \omega_n$ ,  $A$  is negative. However, by noting that  $-A \sin \omega t = A \sin (\omega t - \pi)$ , the amplitude of motion can always be taken as positive by introducing a phase angle between force and displacement equal to  $\pi$  for  $\omega > \omega_n$ . If the amplitude  $A$  is divided by the static displacement produced on the system by a force of amplitude  $\underline{Q}_0$ , the *dynamic magnification factor*  $M$  is obtained:

$$M = \frac{A}{\frac{\underline{Q}_0}{k}} = \frac{1}{1 - \left(\frac{\omega}{\omega_n}\right)^2} \quad (2-47)$$

This is plotted in Fig. 2-12 along with the relationship for the phase angle between force and displacement. The magnification factor becomes infinite when  $\omega = \omega_n$ , because no damping is included in the model. An important feature to point out in the solution is that for  $\omega < \omega_n$  the exciting force is in phase with the displacement and opposes the spring force. For  $\omega > \omega_n$  the exciting force is  $180^\circ$  out of phase with the displacement and opposes the inertia force. At  $\omega = \omega_n$  the inertia force and spring force balance, and the exciting force increases the amplitude of motion without bound.

*Forced Vibrations—Damped*

The introduction of viscous damping into the single-degree-of-freedom model provides a system which closely approximates the properties of many

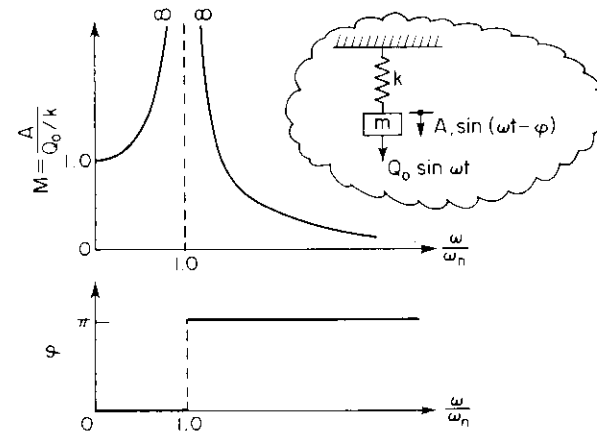


Figure 2-12. Dynamic magnification factor and phase angle between force and displacement of an undamped single-degree-of-freedom system.

real systems, since damping is always present in one form or another. Although the use of a viscous-type damping is for mathematical convenience, there are surprisingly few instances where it does not provide a satisfactory model. Figure 2-13a shows the system to be analyzed. Again, using the reasoning described for the undamped case, the particular solution to the differential equation

$$m\ddot{z} + c\dot{z} + kz = \underline{Q}_0 \sin \omega t \quad (2-48)$$

may be obtained using the concept of rotating vectors. The displacement, velocity, and acceleration vectors are shown in Fig. 2-13b. In this problem

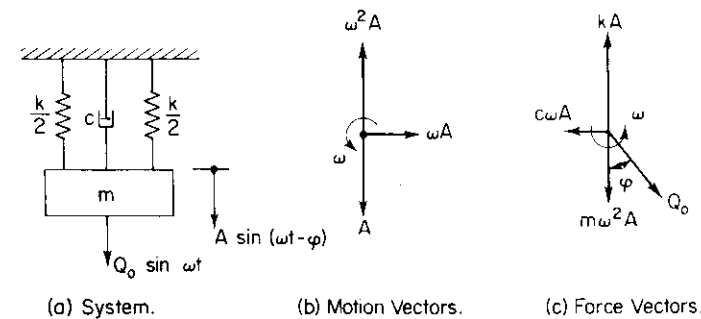


Figure 2-13. Forced vibrations of a single-degree-of-freedom system with viscous damping.

the displacement is assumed as

$$z = A \sin(\omega t - \varphi) \tag{2-49}$$

Hence, when the force vectors are drawn as in Fig. 2-13c, the exciting force will be  $\varphi$  degrees ahead of the displacement vector. In this case the existence of the phase angle is apparent since the damping force  $c\omega A$  is  $90^\circ$  out of phase with the spring and inertia forces. Summation of the vectors in the horizontal and vertical directions provides two equations with  $A$  and  $\varphi$  as unknowns:

$$kA - m\omega^2 A - Q_0 \cos \varphi = 0 \tag{2-50a}$$

$$c\omega A - Q_0 \sin \varphi = 0 \tag{2-50b}$$

Solving for  $A$  and  $\varphi$  gives

$$A = \frac{Q_0}{\sqrt{(k - m\omega^2)^2 + c^2\omega^2}} \tag{2-51}$$

$$\tan \varphi = \frac{c\omega}{k - m\omega^2} \tag{2-52}$$

Substitution of the expressions for  $D$  and  $\omega_n$  and rearrangement gives

$$M = \frac{A}{\frac{Q_0}{k}} = \frac{1}{\sqrt{\left[1 - \left(\frac{\omega}{\omega_n}\right)^2\right]^2 + \left[2D \frac{\omega}{\omega_n}\right]^2}} \tag{2-53}$$

$$\tan \varphi = \frac{2D \frac{\omega}{\omega_n}}{1 - \left(\frac{\omega}{\omega_n}\right)^2} \tag{2-54}$$

which are the dynamic magnification factor and phase angle between force and displacement for steady-state vibration. These equations are plotted in Fig. 2-14 for various values of  $D$  and will be referred to as the response curves for *constant-force-amplitude* excitation. Constant-force amplitude implies that  $Q_0$  is independent of  $\omega$ . It is noticed that the frequency at which the maximum amplitude occurs is not the undamped natural circular frequency  $\omega_n$ , but a frequency slightly less than  $\omega_n$ . The frequency at maximum amplitude,  $f_m$ , will be referred to as the *resonant frequency* for constant-force amplitude and is given by the expression

$$f_m = f_n \sqrt{1 - 2D^2} \tag{2-55}$$

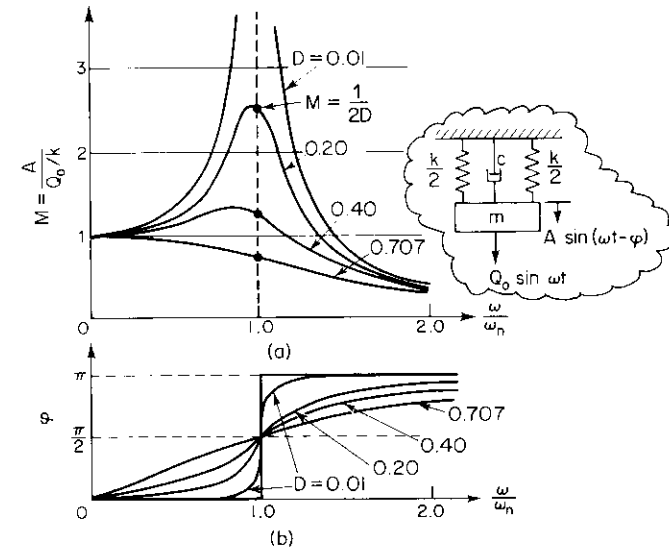


Figure 2-14. Response curves for a viscously damped single-degree-of-freedom system.

The value of  $M$  at this frequency is given by

$$M_{\max} = \frac{1}{2D\sqrt{1 - D^2}} \tag{2-56}$$

Inspection of the above equations reveals that for  $D = 1/\sqrt{2}$ ,  $f_m = 0$  and the maximum response is the static response. The curves showing the variation of  $\varphi$  with  $\omega/\omega_n$  have the properties that the point of maximum slope occurs at the resonant frequency and all curves have a value of  $\pi/2$  at  $\omega = \omega_n$ . Figure 2-14a is given in more detail in Appendix Fig. A-1.

*Rotating-Mass-Type Excitation*

For many systems the vibrations are produced by forces from unbalanced rotating masses. A common type vibration generator, shown in Fig.

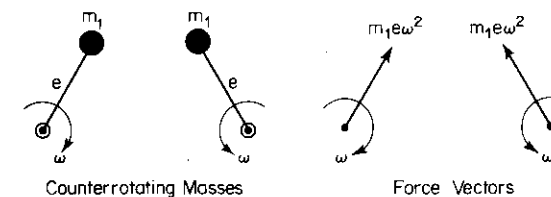


Figure 2-15. Forces produced by two counterrotating masses.



2-15, consists of two counterrotating eccentric masses  $m_1$  at an eccentricity  $e$ . The phase relationship between the masses is such that they both reach their top position simultaneously. Each mass produces a rotating-force vector equal to  $m_1 e \omega^2$ . Addition of these two vectors results in the cancellation of the horizontal components and the addition of the vertical components. The vibratory force is thus

$$Q = m_e e \omega^2 \sin \omega t \quad (2-57)$$

where  $m_e = 2m_1 =$  total eccentric mass. In contrast to the constant-force-amplitude case discussed previously, the rotating-mass-type force has an amplitude proportional to the square of the frequency of oscillation. The solution to the damped single-degree-of-freedom system acted upon by the force defined by Eq. (2-57) can be obtained by a substitution of  $m_e e \omega^2$  for  $Q_0$  in Eq. (2-51). Note that

$$\frac{m_e e \omega^2}{k} = \frac{m_e}{m} \frac{m}{k} e \omega^2 = \frac{m_e e}{m} \left( \frac{\omega}{\omega_n} \right)^2 \quad (2-58)$$

Thus, the quantity

$$A = \frac{C_r M}{K} \quad \frac{A}{m_e e} = \left( \frac{\omega}{\omega_n} \right)^2 M \quad (2-59)$$

where  $M$  is the dynamic magnification factor for the constant-force-amplitude case. The expression for  $\varphi$  obviously remains the same. Figure 2-16 is a

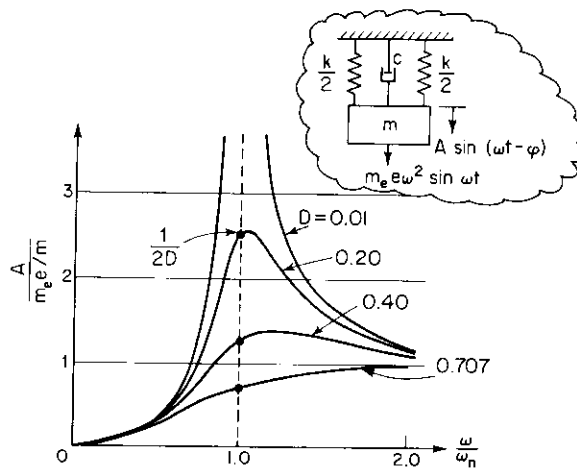


Figure 2-16. Response curves for rotating mass type excitation of a viscously damped single-degree-of-freedom system.

plot of Eq. (2-59) for various values of  $D$ . The curves are similar in appearance to those obtained for the constant-force-amplitude case. An important difference is that the resonant frequency occurs above the undamped natural frequency and is given by

$$f_{mr} = f_n \frac{1}{\sqrt{1 - 2D^2}} \quad (2-60)$$

The ordinate at  $f_{mr}$  is given by

$$\left[ \frac{A}{m_e e} \right]_{\max} = \frac{1}{2D\sqrt{1 - D^2}} \quad (2-61)$$

It should be pointed out that  $m$  is the total vibrating mass and includes the mass  $m_e$ . The physical significance of the quantity  $m_e e/m$  can be interpreted in two ways. When the eccentric mass is rotating at frequency  $\omega_n$ , it is producing a force having an amplitude of  $m_e e \omega_n^2$ . If this force amplitude is divided by the spring constant of the system, the quantity  $m_e e/m$  is obtained. From another, more practical viewpoint, it can be observed that in Fig. 2-16 the amplitude approaches the value  $m_e e/m$  as the frequency increases beyond the resonant condition. This is related to the physical phenomenon that a rotating mass, if unrestrained, will tend to rotate about its center of gravity. For this case the vibration amplitude is  $e$ , since  $m_e = m$ . However, for most systems  $m_e$  represents only part of the total mass resulting in a limiting vibration amplitude of  $(m_e/m)e$ . This phenomenon is the basis for adding more mass to a system vibrating above its resonant frequency in order to reduce its vibration amplitude.

Up to this point there have been two natural frequencies (undamped and damped) and two resonant frequencies (constant-force-amplitude and rotating-mass) associated with a single-degree-of-freedom system. As a comparison, all four of these have been plotted in terms of  $D$  in Fig. 2-17. For values of  $D$  less than 0.2, all frequencies are within 5 per cent of the undamped natural frequency. For higher values the differences between the frequencies become large. For  $D \geq 0.707$ , no peak exists in the curves for forced vibration; for  $D \geq 1.0$ , oscillatory motion does not exist for damped free vibrations.

### Geometrical Shape of Resonance Curves

If an experiment is run to determine the response curve of a single-degree-of-freedom system, it is possible to deduce properties of the system from the shape of the curve. Some of the significant points have already been noted in the previous discussion, but the ones given below are also useful. It is

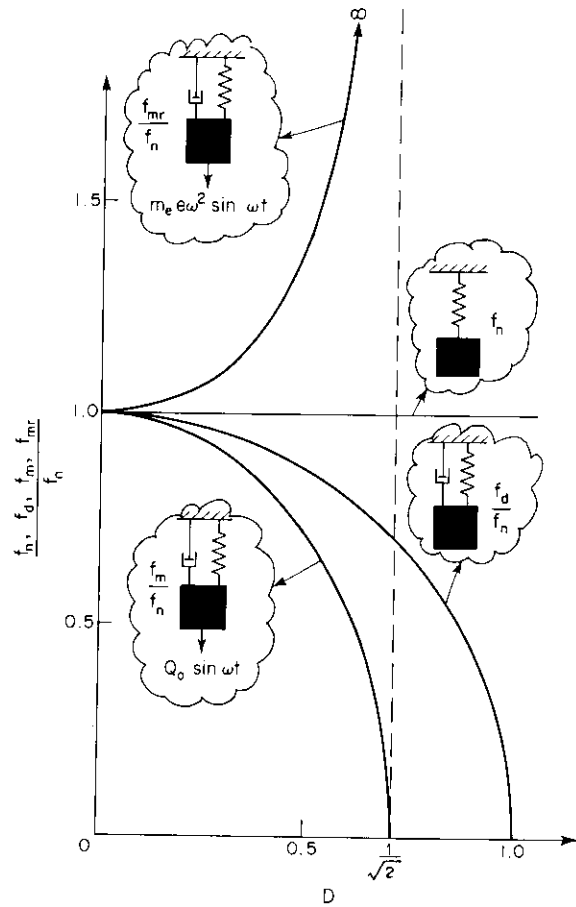


Figure 2-17. Frequencies of a single-degree-of-freedom system.

apparent from the fact that the curve starts at zero amplitude that Fig. 2-18a is the response curve for a rotating-mass-type excitation. If a line is drawn from the origin tangent to the response curve, its point of tangency coincides with the undamped natural frequency of the system. In addition, for any line drawn from the origin intersecting the curve at two points the following relationship exists:

$$f_1 \cdot f_2 = f_n^2 \tag{2-62}$$

where  $f_1$  and  $f_2$  are the frequencies at the points where the line intersects the curve. Thus, from a single experimental curve several independent calculations can be made and an average used to obtain the undamped natural frequency of the system. From this it is possible to calculate other properties such as  $m$ ,  $c$ , and  $k$  if the input force is known.

Figure 2-18b is a response curve for a single-degree-of-freedom system acted upon by a constant-force amplitude, as indicated from the finite value of  $A$  at  $f = 0$ . A classical method of measuring damping makes use of the relative width of the curve. Using the quantities indicated on the curve, the logarithmic decrement can be calculated from

$$\delta = \frac{\pi f_2^2 - f_1^2}{2 f_m^2} \sqrt{\frac{A^2}{A_{max}^2 - A^2} \frac{\sqrt{1 - 2D^2}}{1 - D^2}} \tag{2-63}$$

The equation must obviously be evaluated by trial and error, since the expression involves  $D$  on the right-hand side. When  $D$  is small, the last term

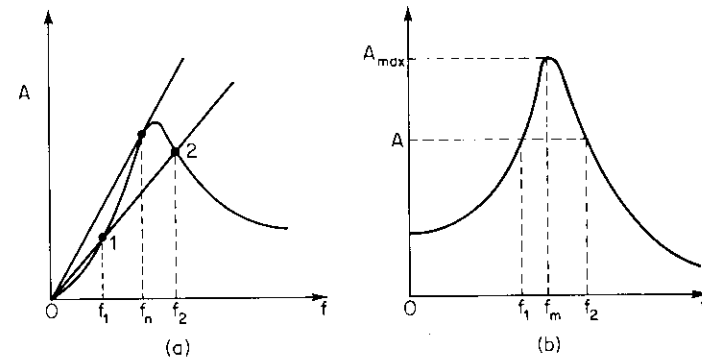


Figure 2-18. Geometric shapes of response curves for the determination of damping.

can be taken as equal to 1.0. An extremely simplified expression is obtained if  $D$  is small and  $A$  is chosen equal to  $0.707A_{max}$ . Then

$$\delta = \pi \frac{\Delta f}{f_m} \tag{2-64}$$

where  $\Delta f = f_2 - f_1$ .

*Response Due to Motion of the Support*

In many cases the vibration of a system is not due to forces acting directly on the mass but from motion of the base. The solution to this problem will also be obtained making use of vector representation of motion and forces. Figure 2-19a shows the problem to be analyzed. The motion of the base is taken as  $A_1 \sin \omega t$  and the response of the mass  $m$  is assumed to be  $A \sin(\omega t - \varphi_1)$ . The motion vectors along with the associated force vectors are shown in Figs. 2-19b and c, respectively. It is noted that a displacement of the

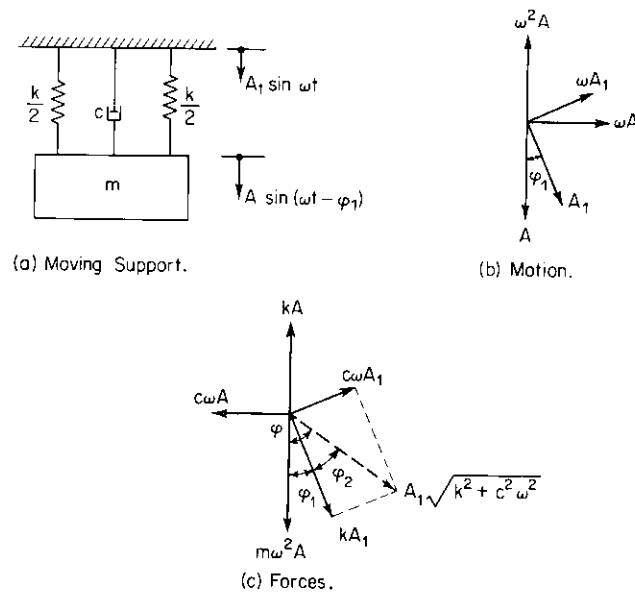


Figure 2-19. Motion and force vectors for the case of a moving support.

support causes a force to be applied to the mass in the same direction as the displacement, whereas the opposite is true for a displacement of the mass. The force vectors are obtained from the motion vectors, as shown in Fig. 2-19c. If the force components from the motion of the support are resolved into a resultant, the same vector diagram as in Fig. 2-13c is obtained. Hence, the solution for  $A$  may be obtained by substituting  $A_1\sqrt{k^2 + c^2\omega^2}$  for  $Q_0$  in Eq. (2-51), giving

$$A = \frac{A_1\sqrt{k^2 + c^2\omega^2}}{\sqrt{(k - m\omega^2)^2 + c^2\omega^2}} \quad (2-65)$$

which reduces to

$$\frac{A}{A_1} = \frac{\sqrt{1 + \left(2D \frac{\omega}{\omega_n}\right)^2}}{\sqrt{\left[1 - \left(\frac{\omega}{\omega_n}\right)^2\right]^2 + \left[2D \frac{\omega}{\omega_n}\right]^2}} \quad (2-66)$$

The expression for  $\varphi_1$  is found from the relationships shown in Fig. 2-19c. The angle  $\varphi$  is given by Eq. (2-52) and from the vector diagram

$$\varphi_2 = \tan^{-1} \frac{c\omega A_1}{kA_1} = \tan^{-1} \frac{c\omega}{k} \quad (2-67)$$

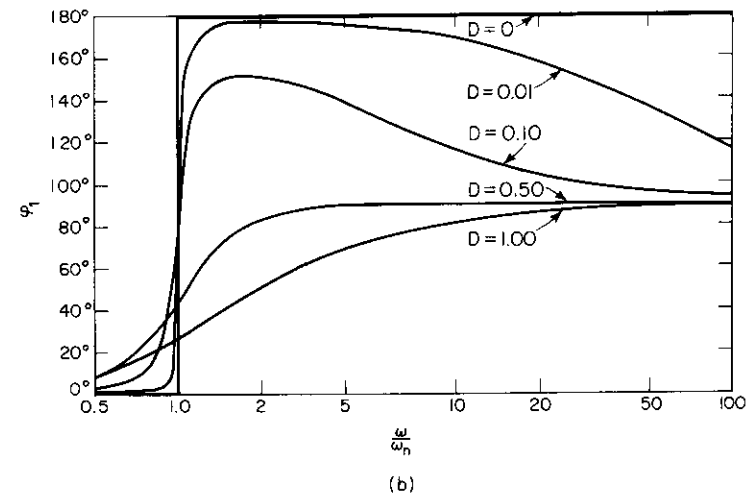
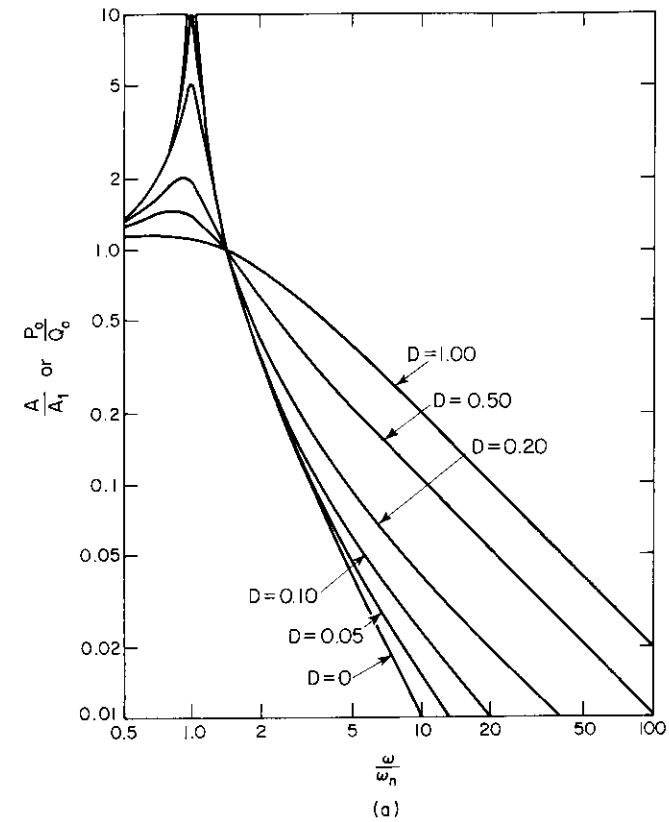


Figure 2-20. Solutions for motion of the support or force transmission.

Also  $\varphi_1 = \varphi - \varphi_2$  and, from the trigonometric expression for the tangent of the difference of two angles,

$$\tan \varphi_1 = \frac{2D \left(\frac{\omega}{\omega_n}\right)^3}{1 - \left(\frac{\omega}{\omega_n}\right)^2 (1 - 4D^2)} \quad (2-68)$$

Equations (2-66) and (2-68) have been plotted in Fig. 2-20 for various values of  $D$ . In problems of vibration isolation of sensitive equipment, the above solution affords a guide to the solution of designing the supporting system if the input from the base is known.

*Force Transmission*

When a force is applied to a mass, it is sometimes necessary to consider the force transmitted to the support. This essentially involves the computation of the resultant of the spring force and the damping force caused by the relative motion between the mass and its support. From Fig. 2-21 the transmitted force  $P_o$  is equal to

$$P_o = \sqrt{(kA)^2 + (c\omega A)^2} = A\sqrt{k^2 + c^2\omega^2} \quad (2-69)$$

Substitution of Eq. (2-51) into the above gives, upon simplification,

$$\frac{P_o}{Q_o} = \frac{\sqrt{1 + \left(2D \frac{\omega}{\omega_n}\right)^2}}{\sqrt{\left[1 - \left(\frac{\omega}{\omega_n}\right)^2\right]^2 + \left[2D \frac{\omega}{\omega_n}\right]^2}} \quad (2-70)$$

which is exactly the same as the relationship for  $A/A_1$  obtained for the case involving motion of the support.

The phase relationship between  $Q_o$  and the force transmitted to the support may be derived from Fig. 2-21, if we note that  $P_o$  is opposite in direction to the force applied to the mass. It can be seen that

$$\tan \varphi_2 = \frac{c\omega A}{kA} = \frac{c\omega}{k} \quad (2-71)$$

and  $\varphi_1 = \varphi - \varphi_2$ , giving exactly the same expression as Eq. (2-68).

In the presentation of the solutions to different cases involving the single-

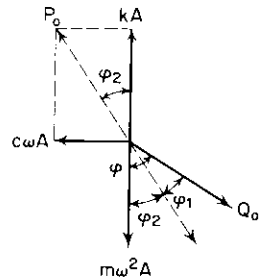


Figure 2-21. Phase relationship between applied force and transmitted force.

degree-of-freedom system, it is conventional to express the relationships in terms of the dimensionless parameters of  $c/(2\sqrt{km})$  and  $\omega\sqrt{m/k}$  which separate the effects of damping and frequency. However, in design or analysis problems the damping factor is probably the least used. In most cases it is the mass or spring constant of

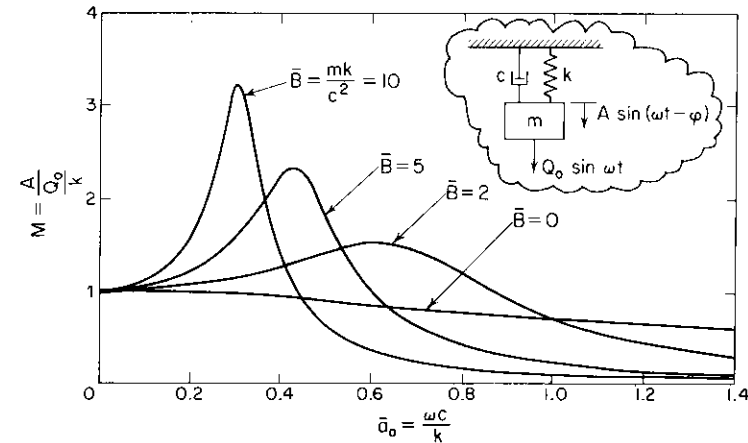


Figure 2-22. Response curves for a single-degree-of-freedom system with the effect of mass and frequency separated (after Lysmer, 1965).

the system which can most easily be changed or adjusted. Using curves such as those in Fig. 2-14, it is a very cumbersome task to determine the exact effect of changes in  $m$  and  $k$ , since they are interrelated between the abscissa and each of the family of curves. Lysmer (1965) separated the effects of mass and frequency and derived the set of relations given below (and shown in Fig. 2-22) in terms of a *dimensionless-frequency factor*

$$\bar{\omega}_o = \frac{\omega c}{k} \quad (2-72)$$

and *mass factor*

$$\bar{B} = \frac{mk}{c^2} \quad (2-73)$$

The dynamic magnification factor, phase angle, and other quantities for the *constant-force-amplitude case* are as follows:

$$M = \frac{1}{\sqrt{(1 - \bar{B}\bar{\omega}_o^2)^2 + \bar{\omega}_o^2}} \quad (2-74)$$

$$\tan \varphi = \frac{\bar{\omega}_o}{1 - \bar{B}\bar{\omega}_o^2} \quad (2-75)$$

$$M_{\max} = \frac{\bar{B}}{\sqrt{\bar{B} - \frac{1}{4}}} \quad (2-76)$$

$$\bar{\omega}_{om} = \frac{\sqrt{\bar{B} - \frac{1}{2}}}{\bar{B}} \quad (2-77)$$

## 2.4 Phase-Plane Analysis of Single-Degree-of-Freedom Systems

The previous section, covering the solutions to problems involving the single-degree-of-freedom system, made use of the method of rotating vectors in the formulation of the solutions. This concept is useful for visualization of the graphical procedures which will be described next. When the response of a vibrating system is plotted graphically in terms of  $z$  and  $\dot{z}/\omega_n$ , we obtain a curve referred to as the phase-plane trajectory. This curve is very useful for problems involving transient motion, since it allows the engineer to "see" how the properties of the system affect its response to impact or transient loads. The phase-plane method can also be applied to systems with nonlinear properties such as friction damping, nonlinear spring forces, and many others (see Jacobsen and Ayre, 1958).

### Free Vibrations of Spring-Mass Systems

From Eq. (2-16) we have the solution to free vibrations of a spring-mass system. By combining terms in the equation we can write the solution as

$$z = \sqrt{C_1^2 + C_2^2} \cos(\omega_n t - \varphi) \quad (2-78)$$

Differentiation with respect to time and division by  $\omega_n$  gives

$$\frac{\dot{z}}{\omega_n} = -\sqrt{C_1^2 + C_2^2} \sin(\omega_n t - \varphi) \quad (2-79)$$

Squaring Eqs. (2-78) and (2-79) and adding gives

$$z^2 + \left(\frac{\dot{z}}{\omega_n}\right)^2 = C_1^2 + C_2^2 \quad (2-80)$$

which is the equation of a circle with its center at the origin and having a radius of  $\sqrt{C_1^2 + C_2^2}$ . The constants  $C_1$  and  $C_2$  have been expressed in terms of initial conditions by Eqs. (2-19). Plotting Eqs. (2-78) and (2-79) on coordinates of  $z$  and  $\dot{z}/\omega_n$ , as shown in Fig. 2-23, gives a point starting at  $z_0$  and  $\dot{z}_0/\omega_n$  traveling clockwise on the circular arc, described by Eq. (2-80), and moving with an angular velocity of  $\omega_n$ . Thus, at any time  $t$ , the angular distance traveled around the circle is  $\omega_n t$ . The quantities  $z$  or  $\dot{z}/\omega_n$  can be obtained as a function of time  $t$  and plotted by extending lines from the phase-plane, as shown in Fig. 2-23. The fundamental relationships for free

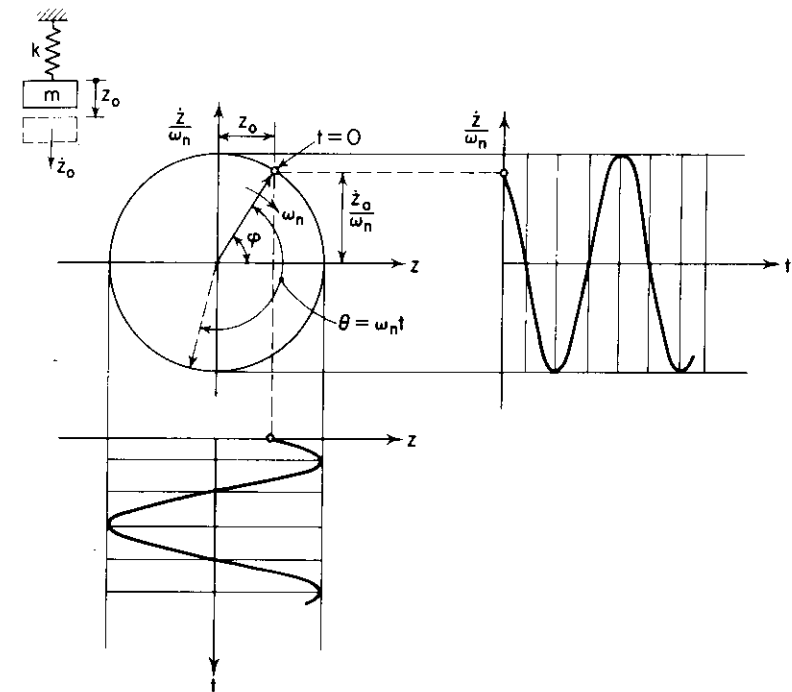


Fig. 2-23. Phase-plane solution for free-vibrations of an undamped single-degree-of-freedom system.

vibrations of a spring-mass system can be seen immediately from Fig. 2-23. For example, the maximum displacement and velocity in terms of the initial displacement and velocity are related to the radius of the circle. That is,

$$z_{\max} = \left(\frac{\dot{z}}{\omega_n}\right)_{\max} = \sqrt{z_0^2 + \left(\frac{\dot{z}_0}{\omega_n}\right)^2} \quad (2-81)$$

### Vibrations from a Step Function

If a constant force  $Q$  is instantaneously applied to a simple spring-mass system, the equation governing the motion is

$$z = C_3 \sin \omega_n t + C_4 \cos \omega_n t + \frac{Q}{k} \quad (2-82)$$

which can be rewritten as

$$z - \frac{Q}{k} = \sqrt{C_3^2 + C_4^2} \cos(\omega_n t - \varphi) \quad (2-83)$$

The expression for velocity is

$$\frac{\dot{z}}{\omega_n} = -\sqrt{C_3^2 + C_4^2} \sin(\omega_n t - \varphi) \quad (2-84)$$

Evaluation of the constants  $C_3$  and  $C_4$  from initial conditions gives

$$C_3 = \frac{\dot{z}_0}{\omega_n} \quad C_4 = z_0 - \frac{Q}{k} \quad (2-85)$$

Squaring and adding Eqs. (2-83) and (2-84) gives

$$\left(z - \frac{Q}{k}\right)^2 + \left(\frac{\dot{z}}{\omega_n}\right)^2 = C_3^2 + C_4^2 \quad (2-86)$$

which again is the equation of a circle, but this time with the center at  $z = Q/k$ . If the initial conditions are plotted on the phase-plane, a line drawn from  $(z = Q/k)$  to the point  $(z_0, \dot{z}_0/\omega_n)$  will be the radius of the circle, as shown in Fig. 2-24. It can be seen that the solution represents harmonic motion about a mean position ( $z = Q/k$ ) with an amplitude depending on the initial values of displacement and velocity. If the force  $Q$  changes at some time  $t_1$ , the values of  $z$  and  $\dot{z}/\omega_n$ , after rotation of  $\omega_n t_1$  rad, are used for the initial conditions starting at  $t = t_1$ , with the center of the circle shifting to the new value of  $Q/k$ . If the force  $Q$  varies with time, the construction of the phase-plane trajectory must be broken down into small time intervals in which the force  $Q$  is taken as the average value during each time interval. The degree of accuracy of the solution depends upon the number of time intervals chosen to represent the force  $Q$ .

**EXAMPLE.** In Fig. 2-25, a mass having a weight  $W = 100$  lb is shown attached to a spring having a spring constant  $k = 6000$  lb/in. The system is initially at rest. At time  $t = 0$  a force  $Q = 30$  lb is applied instantaneously and remains at this level until  $t = 0.015$  sec, after which it instantaneously changes to  $Q = -25$  lb and remains at that level until  $t = 0.020$  sec. After  $t = 0.020$  sec no force is applied to the system and it is allowed to oscillate in free vibration.

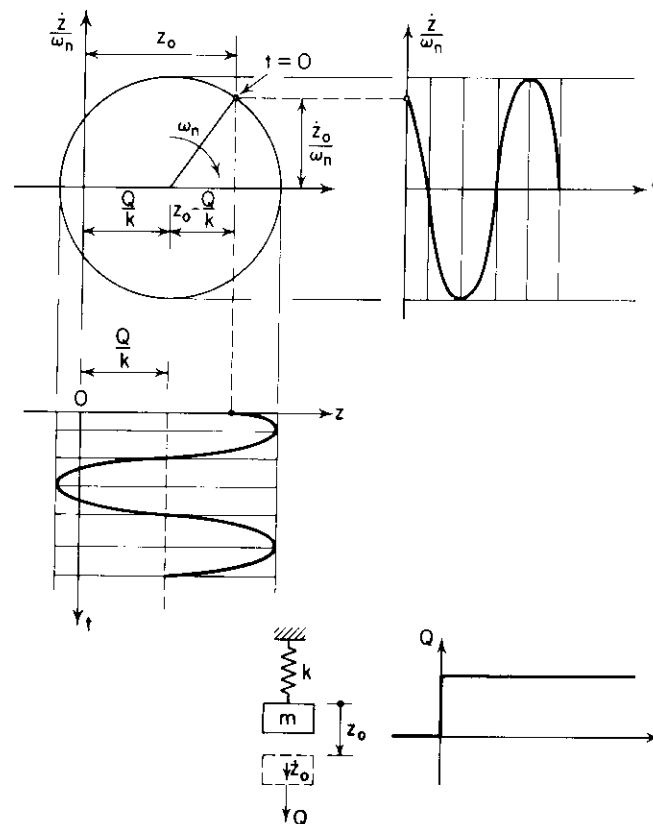


Figure 2-24. Phase-plane solution for an undamped single-degree-of-freedom system acted upon by a static force  $Q$ .

To solve for the response of the system, we first calculate its natural frequency and period.

$$f_n = \frac{1}{2\pi} \sqrt{\frac{kg}{W}} = \frac{1}{2\pi} \sqrt{\frac{(6000)(386)}{(100)}} = 24.3 \text{ cycles/sec}$$

$$T_n = \frac{1}{f_n} = 0.0412 \text{ sec}$$

The center of the phase-plane trajectory for  $0 \leq t \leq 0.015$  sec is given by

$$z_1 = \frac{Q}{k} = \frac{30}{6000} = 0.005 \text{ in.}$$

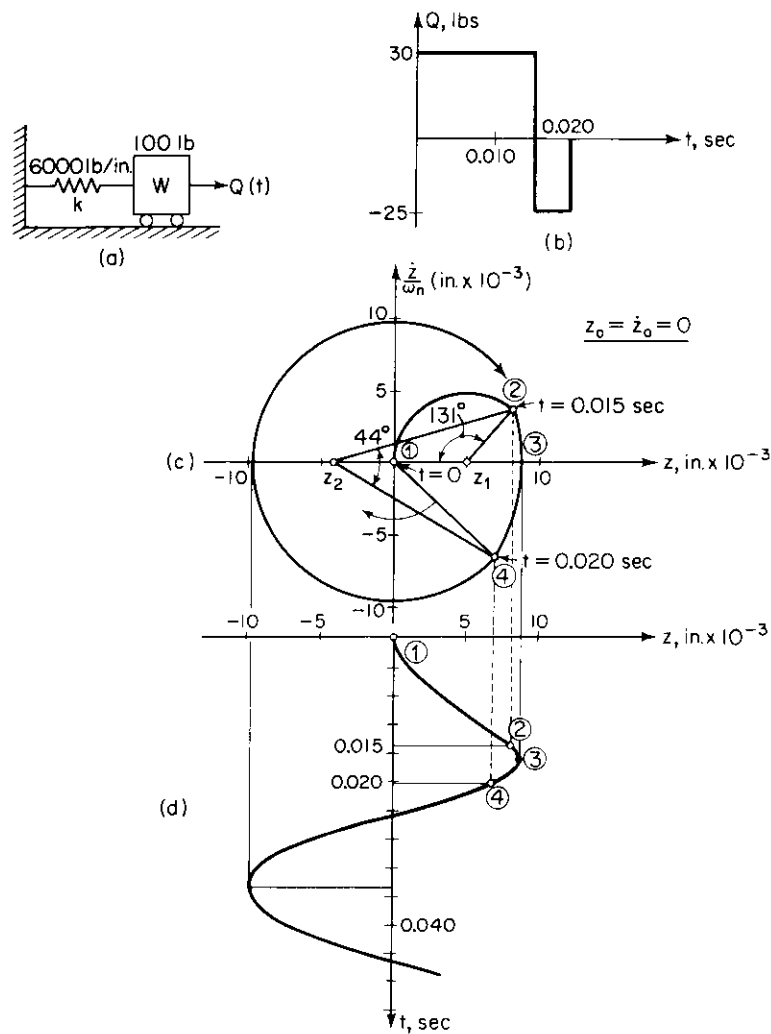


Figure 2-25. Phase-plane example.

and the arc constructed with this center will subtend an angle of

$$\theta = \frac{\Delta t}{T_n} (360) = \frac{0.015}{0.0412} (360) = 131^\circ$$

The construction from  $t = 0$  to  $t = 0.015$  sec is shown in Fig. 2-25 by the arc from point ① to point ②. For  $t = 0.015$  to  $t = 0.020$  sec the force acting on the system

is  $-25$  lb and the center of the phase-plane trajectory is shifted to

$$z_2 = \frac{-25}{6000} = -0.00417 \text{ in.}$$

Point ② now represents the initial conditions for the next segment of the phase plane and an arc is constructed through an angle of

$$\theta = \frac{0.005}{0.0412} (360) = 44^\circ$$

This is represented by the arc from point ② to point ④. For  $t > 0.020$  sec no external force acts on the system and the center of the phase-plane trajectory is shifted to the origin. Point ④ represents the initial conditions for the remaining part of the construction. Since no damping exists, the oscillations will continue at an amplitude equal to the radius from the origin to point ④. In Fig. 2-25d the displacement-time curve has been constructed by projecting points from the phase plane onto the  $z$ -axis. The time scale is calculated from the angular motion on the phase plane.

*Vibrations with Friction Damping*

This example will illustrate the application of the phase plane to friction damping, as shown by the system in Fig. 2-26. For this problem the initial displacement and velocity have been given and the solution for free vibration will be determined. The weight in Fig. 2-26a is resting on a surface having a coefficient of friction equal to 0.5. Thus, a friction force  $F = 40$  lb will act on the weight in a direction opposite to its instantaneous velocity. The solution to the problem is easily visualized if the friction force is treated like an exciting force. Hence, whenever the phase-plane trajectory is above the  $z$ -axis, the friction force acts in the negative  $z$ -direction, and when the trajectory is below the  $z$ -axis, the friction force acts in the positive  $z$ -direction. This defines the centers of the trajectory for free vibrations at  $z = \pm(40/400) = \pm 0.10$  in.

The undamped natural frequency and period of the system are

$$f_n = \frac{1}{2\pi} \sqrt{\frac{(400)(386)}{80}} = 6.98 \text{ cycles/sec}$$

$$\omega_n = 2\pi(6.98) = 43.8 \text{ rad/sec}$$

$$T_n = \frac{1}{f_n} = 0.1433 \text{ sec}$$

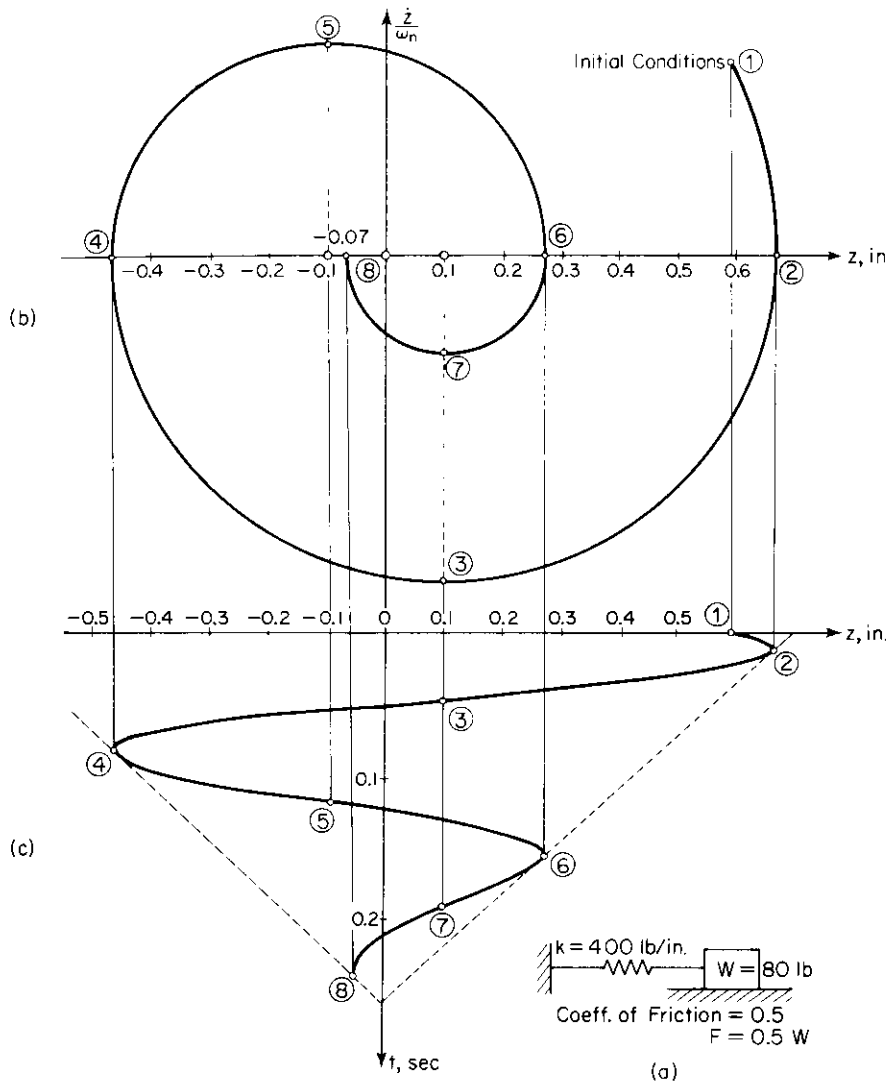


Figure 2-26. Phase-plane for friction damping.

The initial conditions are

$$z = 0.59 \text{ in.}$$

$$\dot{z} = 14.9 \text{ in./sec.}$$

For the phase-plane we need to divide the initial velocity by  $\omega_n$ . This gives  $\dot{z}/\omega_n = 0.34$  in. and is plotted along with the initial displacement to give point

① in Fig. 2-26b. Since the trajectory starts above the  $z$ -axis (positive velocity), the center will be located at  $z = -0.10$  in. and an arc is constructed to point ②. At point ② the trajectory crosses the  $z$ -axis, and the velocity changes sign, shifting the center to  $z = +0.10$  in. This center is used until the trajectory crosses the  $z$ -axis at point ④ and the center shifts to  $z = -0.10$  in. The construction is continued in this manner until finally a point is reached where the trajectory crosses the  $z$ -axis at a point between the location of the two centers. No further construction is possible and it is found that the system has come to a rest position which may or may not correspond to a position having zero force in the spring. This particular point illustrates a difference between viscous damping and friction damping. For friction damping the system comes to rest after some finite time interval, while a viscously damped system theoretically never stops moving. Another difference can be seen from the displacement-time diagram in Fig. 2-26c. The envelope of the peak points on the curve is a straight line as compared to the exponential envelope of a viscously damped system.

*Vibrations with Viscous Damping*

This example will illustrate the solution to free vibrations of a viscously damped system, as shown in Fig. 2-27a. Again it is useful to treat the viscous

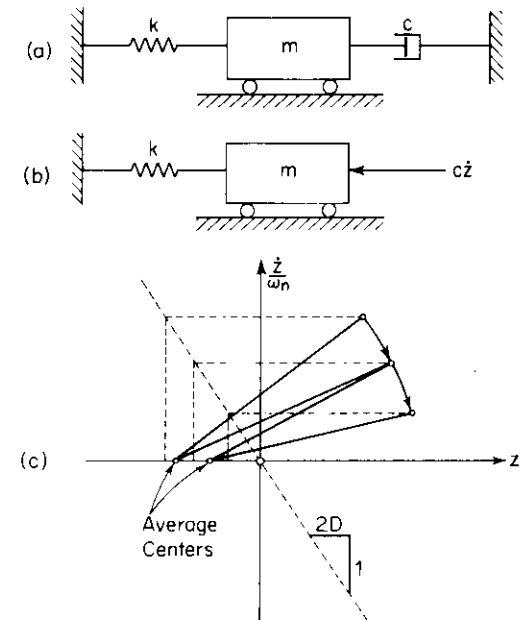


Figure 2-27. Phase-plane for viscous damping.



damper as an exciting force, which for this case is proportional to but opposite in direction to the velocity of the mass  $m$ , as shown in Fig. 2-27b. For free vibrations the instantaneous center of the phase-plane trajectory is given by

$$z = -\frac{c\dot{z}}{k} = -\frac{c\omega_n}{k} \frac{\dot{z}}{\omega_n}$$

or

$$z = -2D \frac{\dot{z}}{\omega_n} \quad (2-87)$$

To facilitate the phase-plane solution, the line representing Eq. (2-87) is plotted directly on the phase-plane. Since it is necessary to work with forces which are constant, an average center over a small velocity interval is used to construct a segment of the trajectory. This results in a trajectory having cusps at the beginning and end of each interval. The accuracy of the solution depends upon minimizing the sharpness of the cusps, because the exact solution in this case is a spiral. It should be noted that the correlation of displacement and time requires summation of the angles used for each increment of the phase plane construction.

#### Vibration from Motion of the Support

The above methods of treating the damping forces as exciting forces may be extended to many types of problems. However, there are some special cases which can be easily solved with slight modifications of the above procedures. Two such cases involve the response of systems when the excitation is due to motion of the support. In one case the absolute motion of the mass can be determined if the *displacement* of the support is known. In the other case the *relative motion* between the support and the mass can be obtained if the *acceleration* of the support is known.

**Displacement of the support.** If the displacement of the support of a spring-mass system is given, the differential equation of motion is

$$m\ddot{z} + k(z - z_b) = 0 \quad (2-88)$$

where  $z_b$  is the displacement of the support. Rearrangement gives

$$m\ddot{z} + kz = kz_b \quad (2-89)$$

Thus,  $kz_b$  can be considered to be the forcing function, and the center of the circular arc is  $z_b$ .

If viscous damping is included in the system, it is more convenient to specify the acceleration of the support and solve for the *relative motion* between the mass and the support.

**Acceleration of the support.** If  $z_r$  is the relative motion between the mass and the support, the differential equation of motion is

$$m(\ddot{z}_r + \ddot{z}_b) + c\dot{z}_r + kz_r = 0 \quad (2-90)$$

From this,

$$m\ddot{z}_r + kz_r = -m\ddot{z}_b - c\dot{z}_r \quad (2-91)$$

The right-hand side of this equation represents the equivalent force applied to the system; division by  $k$  gives the center as

$$\frac{-m\ddot{z}_b}{k} - \frac{c\dot{z}_r}{k} = -\frac{\ddot{z}_b}{\omega_n^2} - 2D \frac{\dot{z}_r}{\omega_n} \quad (2-92)$$

The left-hand side of Eq. (2-91) is written in terms of the *relative motion*, which will be the quantity obtained using the phase-plane solution. The first term on the right-hand side is obtained from the acceleration of the support and the second term is obtained during construction of the phase plane, using the procedure shown in Fig. 2-27.

#### Acceleration from the Phase Plane

Displacement, velocity, and time can all be readily determined from the phase plane. It is also possible to obtain acceleration from the phase plane. At any time  $t$  the radius will have a length  $r$  and will be positioned at an angle  $\theta$  with respect to the horizontal axis, as shown in Fig. 2-28. In a time interval of  $\Delta t$  the radius will move through an angle of  $\omega_n \Delta t$ , and the arc length at the end of the radius will be  $r\omega_n \Delta t$ . The change in velocity during this time interval is related to the vertical component of the distance  $r\omega_n \Delta t$  and is shown in Fig. 2-28 as  $\Delta\dot{z}/\omega_n$ . From geometry,

$$\cos \theta = \frac{\Delta\dot{z}}{\omega_n r\omega_n \Delta t} \quad (2-93)$$

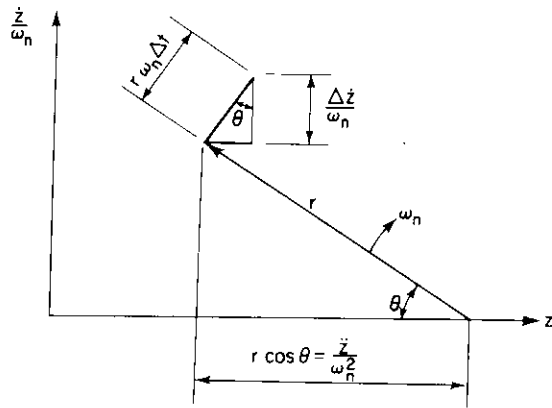


Figure 2-28. Calculation of acceleration from the phase plane.

From this,

$$\ddot{z} = \frac{\Delta \dot{z}}{\Delta t} = \omega_n^2 (r \cos \theta) \quad (2-94)$$

The quantity  $(r \cos \theta)$  is simply the projection of the radius onto the horizontal or  $z$ -axis. This projection is multiplied by  $\omega_n^2$  to give the acceleration. If the projection is to the *left* of the center of the arc, the acceleration is *positive*; while if it is to the *right*, the acceleration is *negative*.

### Multilinear Spring Systems

Many cases involve nonlinear restoring forces. These may usually be approximated by a series of linear relationships—as shown in Fig. 2-29, where the force-deformation relationship is defined by  $k_1$ ,  $k_2$ , and  $k_3$ . For displacements of the system within range I, the factor  $k_1$  governs its behavior.

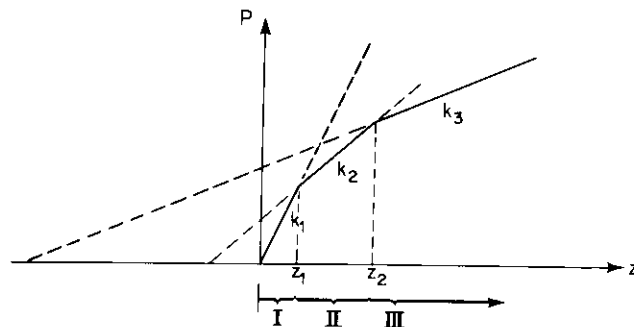


Figure 2-29. Force-deformation relationship for a multilinear system.

If the displacement of the system is in range II, then  $k_2$  governs its behavior. For each range of displacement, a particular linear relationship governs the behavior.

The solution to the above problem can be obtained by the addition of elements which produce forces proportional to and in the same direction as the displacement of the system. Detailed solutions using this method are given by Jacobsen and Ayre (1958). However, a slight modification in the phase-plane construction allows the exact solution to be obtained and in addition considerably reduces the time required to obtain a solution.

The concept used is that when the displacement of the system lies within a range where the restoring force has a linear relationship, the system behaves as if the same relationship was valid for all values of displacement. However, extrapolation of the force-deformation relationship to zero force does not give zero displacement. For the example shown in Fig. 2-29, zero restoring force for range II corresponds to a negative displacement and is the center for free vibrations when the displacement of the system is within range II. If the displacement of the system passes into range I, then the center of the circle shifts to the origin. For problems of this type it is convenient to construct the force-deformation relationship to scale and extend the straight line portions of each range. Having done this, the center of the circle can be obtained from the intersection of the value of the exciting force and the straight line compatible with the displacement of the system.

In addition to the change in the center of the circle when passing from one linear range to another, there are two changes resulting from the change in the undamped natural frequency. First of all, there is a change in relationship between rotation of the radius and time, since the radius will have a new angular velocity equal to the new value of  $\omega_n$ . Second, there is an instantaneous change in the quantity  $\dot{z}/\omega_n$ . Since the velocity of the system must necessarily be continuous (an instantaneous change in velocity requires an infinite force), the value of the ordinate is multiplied by  $\omega_{n1}/\omega_{n2}$ .

**Example.** The system shown in Fig. 2-30a consists of a mass placed between two equal springs designed so that they resist only compressive forces and so that each spring is precompressed by 1.5 in. For such a system the restoring-force-vs.-displacement curve has a discontinuity at a displacement of 1.5 in. For displacements less than 1.5 in., both springs act to produce a spring constant for the system equal to 400 lb/in. For displacements greater than 1.5 in., only one spring acts, providing a spring constant of 200 lb/in. Thus, the natural frequency for each range of displacement is

$$\omega_{n1} = \sqrt{\frac{400}{2}} = 14.1 \text{ rad/sec}$$

$$\omega_{n2} = \sqrt{\frac{200}{2}} = 10.0 \text{ rad/sec}$$

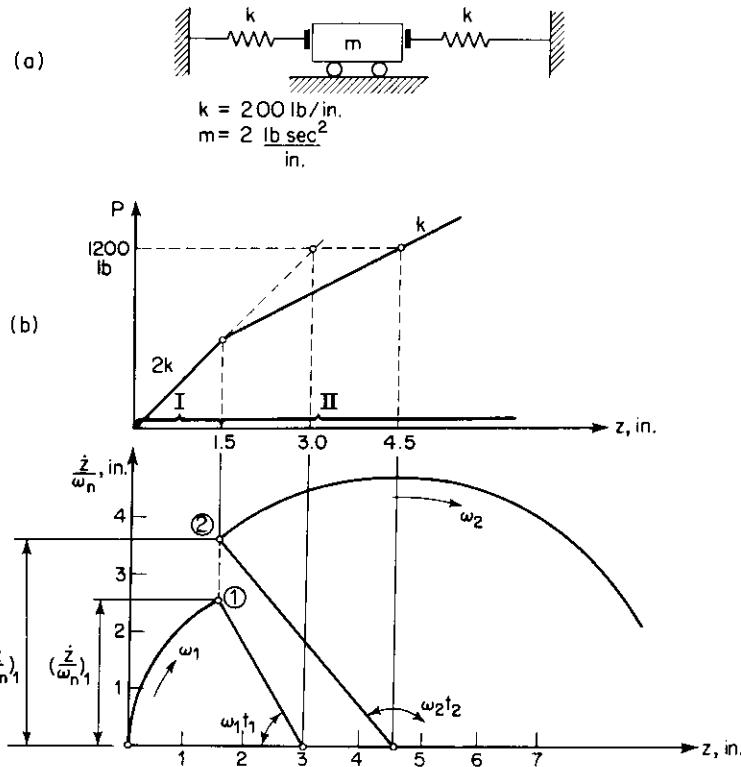


Figure 2-30. Phase-plane solution for a bilinear system.

In order to illustrate the method of solution, assume that a force of 1200 lb is applied instantaneously to the system and allowed to remain for a relatively long duration. For range I the center is located at  $z = 3.0$  in., which can be found either by dividing 1200 lb by 400 lb/in. or constructing a plot of restoring force vs. displacement with an extension of the initial straight-line portion as shown on the figure. Next, an arc is constructed from the origin to point ①. This is the point where the spring constant of the system changes and the center changes from 3.0 in. to 4.5 in. In addition, the ordinate on the phase plane must be multiplied by the factor  $(\omega_{n1}/\omega_{n2} = 1.41)$  to compensate for the change in natural frequency of the system. Using the new center and point ② on the phase plane, the second circular arc is continued until the displacement becomes less than 1.5 in. or the load is changed.

This method is not restricted in any way to a predetermined restoring-force-deformation relationship. In fact, one of the most useful applications involves the condition in which the system has a yielding modulus and an unloading modulus after yielding. This results in an energy-absorbing system which can be made to represent closely a real system.

Phase Plane with Oblique Coordinates

For problems involving viscously damped systems, a modification of the previous method is given by Jacobsen and Ayre (1958), from which the solution can be much more easily obtained.

The solution to free damped vibration can be expressed as

$$z = \exp(-D\omega_n t) [\sqrt{C_1^2 + C_2^2} \cos(\omega_d t - \varphi)] \quad (2-95)$$

$$\frac{\dot{z}}{\omega_n} = -\exp(-D\omega_n t) [\sqrt{C_1^2 + C_2^2} \sin(\omega_d t - \varphi - \varphi_1)] \quad (2-96)$$

where  $\sin \varphi_1 = D$ .

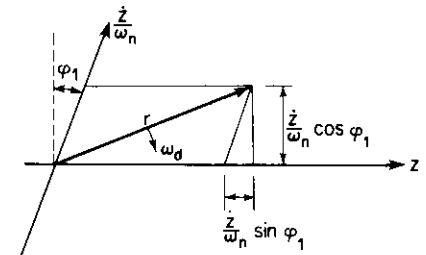


Figure 2-31. Oblique coordinate system.

By introducing the oblique set of coordinates shown in Fig. 2-31,

$$r^2 = \left(\frac{\dot{z}}{\omega_n} \cos \varphi_1\right)^2 + \left(z + \frac{\dot{z}}{\omega_n} \sin \varphi_1\right)^2 \quad (2-97)$$

$$r^2 = z^2 + \left(\frac{\dot{z}}{\omega_n}\right)^2 + 2z \frac{\dot{z}}{\omega_n} \sin \varphi_1 \quad (2-98)$$

and substitution of Eqs. (2-95) and (2-96) into Eq. (2-98) gives

$$r = (\sqrt{C_1^2 + C_2^2} \cos \varphi_1) \exp(-D\omega_n t) = r_o \exp(-D\omega_n t) \quad (2-99)$$

This is the equation of a logarithmic spiral. It is the trajectory traced by a radius having an angular velocity of  $\omega_d$  and a length that changes according to Eq. (2-99). For forced vibrations the center of the spiral is located at a displacement equal to  $Q/k$ . (An application of the above method is found in Chap. 10.)

In order to use the method of oblique coordinates, it is necessary to construct a template out of heavy paper to aid in the drawing of spiral curves. For values of  $D \leq 0.5$ , an approximate method using  $90^\circ$  circular arcs provides an accuracy of  $\pm 2$  per cent. The approximate spiral is exact at  $45^\circ$

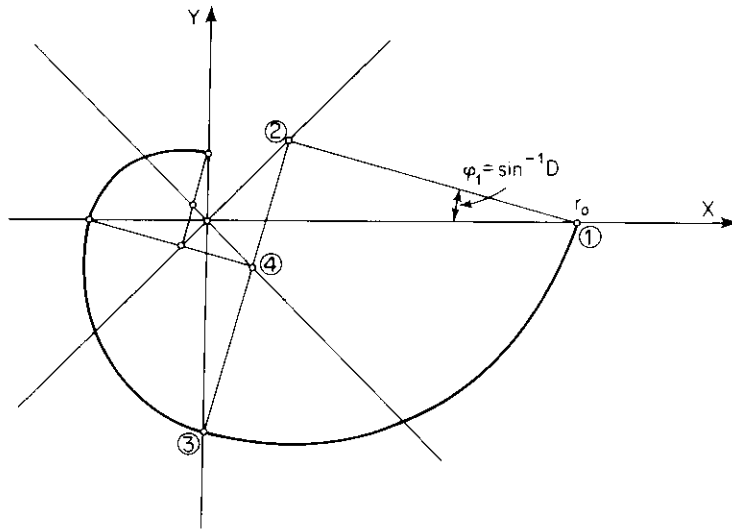


Figure 2-32. Approximate method for constructing a logarithmic spiral.

intervals. In Fig. 2-32 the geometry of the approximate spiral is shown. It is constructed by drawing lines at  $45^\circ$  to the  $x$ - $y$  coordinates through the origin. The size of the spiral is chosen to fit the personal preference of the user, and the maximum radius  $r_0$  is placed on the  $x$ -axis. Next, a line is drawn from point ① at an angle ( $\varphi_1 = \sin^{-1} D$ ) with the  $x$ -axis until it intersects the  $45^\circ$  line at point ②. Point ② is the center of the first  $90^\circ$  circular segment of the spiral from point ① to point ③. The center for the next  $90^\circ$  segment is at the intersection of the final radius and the next  $45^\circ$  line (point ④). The construction is repeated until the desired length of spiral is obtained.

*Acceleration on Oblique-Coordinate System*

The determination of acceleration from the phase plane with oblique coordinates is slightly different from that presented previously. In Fig. 2-33 the radius  $r$  at any time  $t$  makes an angle of  $\theta$  with respect to the  $z$ -axis. For an increment of time  $\Delta t$ , the radius  $r$  will travel through an angle of  $\omega_d \Delta t$ . If the length of  $r$  remained constant, the length of the phase plane trajectory would be  $r\omega_d \Delta t$ . However,  $r$  changes length such that the trajectory makes an angle  $\varphi_1$  with respect to a perpendicular at the end of the radius, making the length of the trajectory  $r\omega_d \Delta t / (\cos \varphi_1)$ . The resulting change in  $\dot{z}/\omega_n$  is

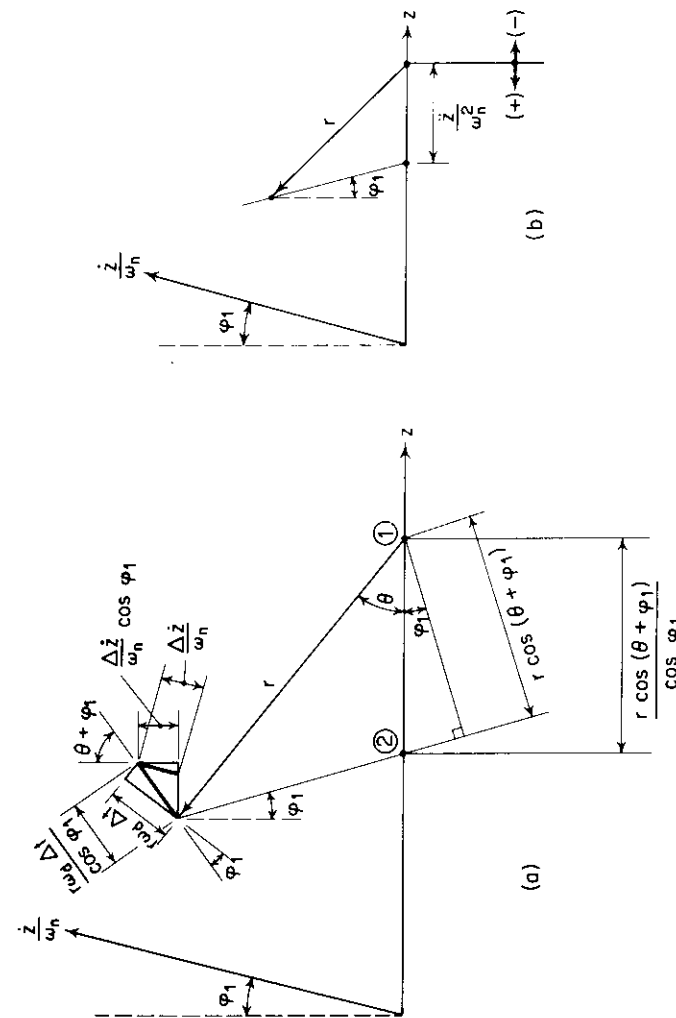


Figure 2-33. Acceleration from the phase-plane with oblique coordinates.

measured parallel to the oblique axis. From the geometry obtained,

$$\cos(\theta + \varphi_1) = \frac{\Delta \dot{z} \cos \varphi_1 \cos \varphi_1}{\omega_n r \omega_d \Delta t} \quad (2-100)$$

Solving Eq. (2-100) for  $\Delta \dot{z}/\Delta t$  gives

$$\ddot{z} = \frac{\Delta \dot{z}}{\Delta t} = \frac{r \omega_n \omega_d \cos(\theta + \varphi_1)}{\cos^2 \varphi_1} \quad (2-101)$$

However, since  $\sin \varphi_1 = D$ , then  $\cos^2 \varphi_1 = 1 - D^2$ . Also  $\omega_d = \omega_n \sqrt{1 - D^2}$ . Equation (2-101) can be rewritten as

$$\ddot{z} = \frac{\omega_n^2}{\sqrt{1 - D^2}} [r \cos(\theta + \varphi_1)] \quad (2-102)$$

From Fig. 2-33a  $[r \cos(\theta + \varphi_1)]$  is the side of a right triangle formed by the radius and a line inclined at an angle  $\varphi_1$ , with  $r$  as the hypotenuse. The distance from ① to ② on the  $z$ -axis is  $[r \cos(\theta + \varphi_1)]/(\cos \varphi_1)$ . Factoring this quantity out of Eq. (2-102) and substituting  $(\cos \varphi_1 = \sqrt{1 - D^2})$  gives

$$\ddot{z} = \frac{r \cos(\theta + \varphi_1)}{\cos \varphi_1} \omega_n^2 \quad (2-103)$$

Thus, if an inclined line is drawn from the tip of the radius to the  $z$ -axis, as shown in Fig. 2-33b, the distance from this point to the center is equal to  $\ddot{z}/\omega_n^2$ . This provides a relatively easy method of determining accelerations directly from the phase-plane solution.

## 2.5 Systems with Two Degrees of Freedom

Although many systems can be adequately modeled using a single-degree-of-freedom model, in some cases it is necessary to consider a model having two or more degrees of freedom. The simplest case is shown in Fig. 2-34, where two masses are connected in series. The more common case is

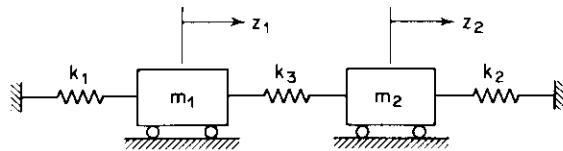


Figure 2-34. System with two degrees of freedom.

coupled rocking and sliding of a single mass, which occurs when the exciting and restoring forces do not all act through the center of gravity.

### Coupled Translation

Consider the two-mass system shown in Fig. 2-34, which is connected by three springs. Each mass is restricted to move horizontally and the displacement of each mass is designated by the two values  $z_1$  and  $z_2$ . The forces in springs  $k_1$  and  $k_2$  each depend upon the value of only one displacement, while the force in spring  $k_3$  depends upon the *relative* displacement between the two masses. The application of Newton's second law to each mass gives

$$m_1 \ddot{z}_1 = -k_1 z_1 - k_3 z_1 + k_3 z_2 \quad (2-104a)$$

$$m_2 \ddot{z}_2 = k_3 z_1 - k_3 z_2 - k_2 z_2 \quad (2-104b)$$

as the differential equations for free vibration. The motions for free vibrations are assumed harmonic and expressed by

$$z_1 = A_1 \sin \omega t \quad (2-105a)$$

$$z_2 = A_2 \sin \omega t \quad (2-105b)$$

Substitution of Eqs. (2-105) into Eqs. (2-104) gives

$$(k_1 + k_3 - m_1 \omega^2) A_1 - k_3 A_2 = 0 \quad (2-106a)$$

$$-k_3 A_1 + (k_2 + k_3 - m_2 \omega^2) A_2 = 0 \quad (2-106b)$$

The above homogeneous equations have a nontrivial solution only if the determinant of the coefficients is equal to zero. This provides a quadratic in  $\omega^2$  called the *frequency equation*, which is

$$(\omega^2)^2 - \left( \frac{k_1 + k_3}{m_1} + \frac{k_2 + k_3}{m_2} \right) \omega^2 + \frac{k_1 k_2 + k_1 k_3 + k_2 k_3}{m_1 m_2} = 0 \quad (2-107)$$

The two roots to Eq. (2-107) correspond to the natural frequencies of the system. The lowest value is the first-mode natural frequency,  $\omega_1$ , and the higher value is the second-mode natural frequency,  $\omega_{11}$ . From Eqs. (2-106),

$$\frac{A_2}{A_1} = \frac{k_1 + k_3 - m_1 \omega^2}{k_3} = \frac{k_3}{k_2 + k_3 - m_2 \omega^2} \quad (2-108)$$

Substitution of  $\omega_1$  into Eq. (2-108) always gives a positive value of  $A_2/A_1$ ,

while substitution of  $\omega_{II}$  gives a negative value. This means that for the first mode both masses move in phase, while for the second mode they move  $180^\circ$  out of phase.

Since both sine and cosine functions will yield the same frequency equation and since two frequencies are obtained as solutions, the general solution can be written as

$$z_1 = C_1 \sin \omega_I t + C_2 \cos \omega_I t + C_3 \sin \omega_{II} t + C_4 \cos \omega_{II} t \quad (2-109a)$$

$$z_2 = \alpha_I(C_1 \sin \omega_I t + C_2 \cos \omega_I t) + \alpha_{II}(C_3 \sin \omega_{II} t + C_4 \cos \omega_{II} t) \quad (2-109b)$$

representing a superposition of both modes. The quantities  $\alpha_I$  and  $\alpha_{II}$  are the values of  $A_2/A_1$  for the first and second modes, respectively. The four arbitrary constants  $C_1, C_2, C_3,$  and  $C_4$  are determined from the initial conditions, which include both the displacement and velocity for each mass.

It is sometimes convenient to calculate the natural frequencies making use of Mohr's circle, as described by Den Hartog (1956). The procedure is to first hold  $m_1$  fixed and calculate the natural frequency for  $m_2$ . This gives

$$\omega_A^2 = \frac{k_2 + k_3}{m_2} \quad (2-110)$$

Then, holding  $m_2$  fixed and calculating the frequency for  $m_1$  gives

$$\omega_B^2 = \frac{k_1 + k_3}{m_1} \quad (2-111)$$

A third quantity which is a measure of the coupling between  $m_1$  and  $m_2$  is

$$\omega_{AB}^2 = \frac{k_3}{\sqrt{m_1 m_2}} \quad (2-112)$$

Finally  $\omega_I^2$  and  $\omega_{II}^2$  are obtained from the Mohr diagram in Fig. 2-35.

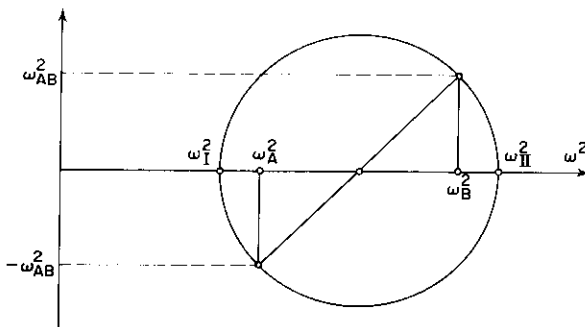


Figure 2-35. Mohr's circle construction for natural frequencies.

*Coupled Translation and Rotation*

Coupled translation and rotation of a single mass occurs when the forces and reactions do not coincide with the center of gravity of the mass. When subjected to a translatory acceleration, the inertia force acting through the center of gravity and the restoring forces acting on the mass produce a force couple. The net result is coupling between the translational and rotational modes of vibration.

The above problem is represented by the general system shown in Fig. 2-36. The system consists of a rigid mass  $m$  which is restrained so that the center of gravity can only translate in the  $z$ -direction, but which is free to rotate about the center of gravity.

Three springs are connected to the system at various locations. The center of pressure of the spring reactions for pure translation is at a distance  $R$  from the center of gravity. By definition of the center of pressure, the sum of the moments of the spring forces about the center of pressure is equal to zero. Taking clockwise as positive gives

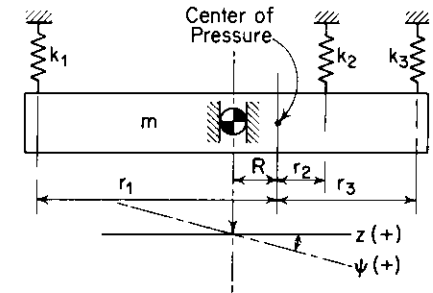


Figure 2-36. Coupled translation and rotation.

$$k_1 z r_1 - k_2 z r_2 - k_3 z r_3 = 0 \quad (2-113)$$

The effective spring constant for translation is given by

$$k_z = k_1 + k_2 + k_3 \quad (2-114)$$

and the spring constant for rotation about the center of pressure is defined as the moment per unit rotation

$$k_\psi = \frac{\text{Moment}}{\psi} = \frac{k_1 r_1 \psi r_1 + k_2 r_2 \psi r_2 + k_3 r_3 \psi r_3}{\psi} \quad (2-115a)$$

or

$$k_\psi = k_1 r_1^2 + k_2 r_2^2 + k_3 r_3^2 \quad (2-115b)$$

In order that we may obtain a better physical feeling for the parameters involved in the system, it will be converted to the equivalent system shown in Fig. 2-37, where the mass is concentrated in a ring having a radius of gyration  $\bar{r}$ ; and the springs have been replaced by two equal springs each at a distance  $r$  from the center of pressure. The springs each have a spring constant of  $k_z/2$ , making  $k_\psi = k_z \bar{r}^2$ . In order to set up the differential equations of

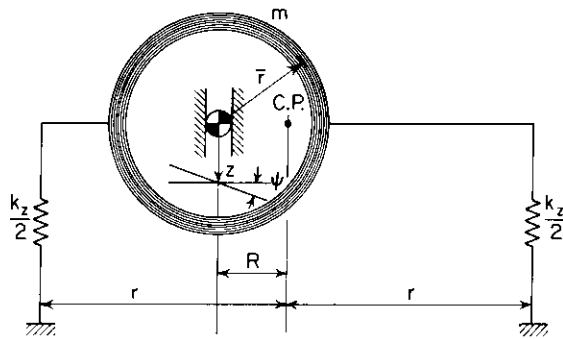


Figure 2-37. Simplified system equivalent to Fig. 2-36.

motion for free vibration, an arbitrary displacement and rotation are applied to the center of gravity. The restoring forces shown in Fig. 2-38 can be calculated from the resulting displacement and rotation of the center of pressure. Summing the forces and moments about the center of gravity and applying Newton's second law gives

$$m\ddot{z} = -k_z(z + R\psi) \tag{2-116a}$$

$$m\bar{r}^2\ddot{\psi} = -k_\psi\psi - k_z(z + R\psi)R \tag{2-116b}$$

Note, in the above equations, that the coupling is due to the fact that the center of gravity and the center of pressure do not coincide. If  $R = 0$ , the system is uncoupled and has two independent natural frequencies—one for translation and one for rotation.

These are defined as

$$\omega_z = \sqrt{\frac{k_z}{m}} \tag{2-117a}$$

$$\omega_\psi = \sqrt{\frac{k_\psi}{m\bar{r}^2}} \tag{2-117b}$$

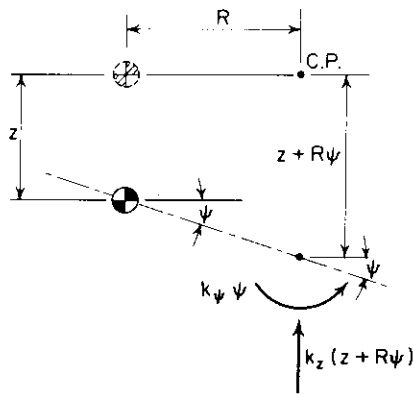
The equations for the coupled solution are obtained by substituting

$$z = A_z \sin \omega t \tag{2-118a}$$

$$\psi = A_\psi \sin \omega t \tag{2-118b}$$

and

Figure 2-38. Restoring forces for the system on Fig. 2-37.



into Eqs. (2-116), giving

$$(k_z - m\omega^2)A_z + k_zRA_\psi = 0 \tag{2-119a}$$

and

$$k_zRA_z + (k_\psi + k_zR^2 - m\bar{r}^2\omega^2)A_\psi = 0 \tag{2-119b}$$

The frequency equation is obtained by setting the determinant of the coefficients from Eqs. (2-119) equal to zero. This gives

$$(\omega^2)^2 - \left(\frac{k_z}{m} + \frac{k_\psi + k_zR^2}{m\bar{r}^2}\right)\omega^2 + \frac{k_\psi k_z}{m\bar{r}^2 m} = 0 \tag{2-120}$$

Equation (2-120) can be rearranged to give

$$\left(\frac{\omega^2}{\omega_z^2}\right)^2 - \left[1 + \left(\frac{r}{\bar{r}}\right)^2 + \left(\frac{R}{\bar{r}}\right)^2\right]\frac{\omega^2}{\omega_z^2} + \left(\frac{r}{\bar{r}}\right)^2 = 0 \tag{2-121}$$

which has been plotted for  $R/\bar{r} = 0$  and  $R/\bar{r} = 1$  in Fig. 2-39. When  $R/\bar{r} = 0$  the system is uncoupled, since the center of pressure and the center of gravity coincide. For this case the two frequencies correspond to a pure translation and a pure rotation. For  $R/\bar{r} = 1$  a coupled system is obtained, wherein the first-mode frequency is always less than  $\omega_z$  or  $\omega_\psi$ , whichever is smaller, and the second-mode frequency is always greater than  $\omega_z$  or  $\omega_\psi$ .

The mode shapes for such a system can be found from Eqs. (2-119), giving

$$\frac{A_z}{A_\psi} = \frac{k_zR}{m\omega^2 - k_z} = \frac{m\bar{r}^2\omega^2 - k_\psi - k_zR^2}{k_zR} \tag{2-122}$$

This quantity is actually the negative of the center of rotation—taking a positive center as meaning to the right—and is plotted as a function of  $\omega$  in

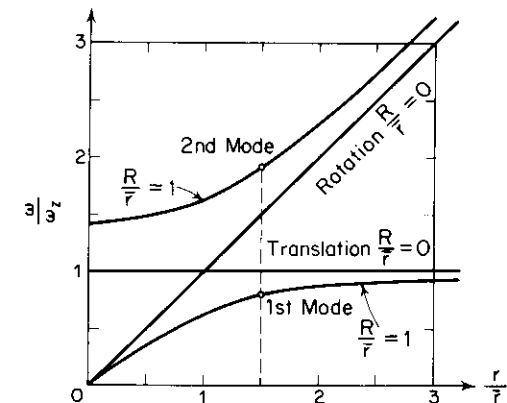


Figure 2-39. Solution to Eq. (2-121).

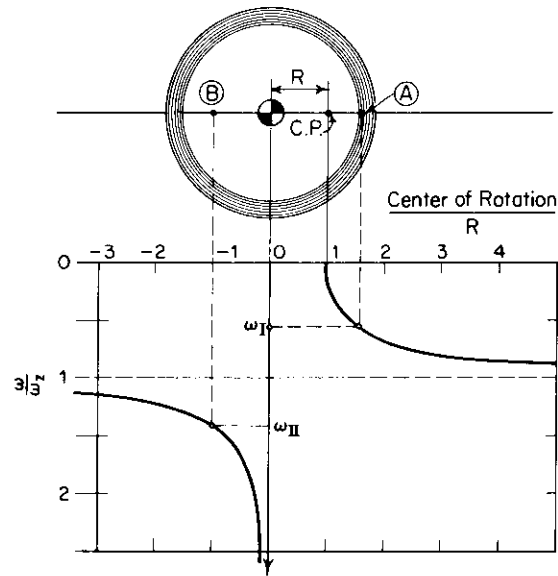


Figure 2-40. Center of rotation vs. natural frequency.

Fig. 2-40. The system shown in Fig. 2-40 will have two natural frequencies  $\omega_I$  and  $\omega_{II}$ . If the system is freely vibrating at  $\omega_I$ , its center of rotation will be point  $\textcircled{A}$ , which is to the right of the center of pressure. For  $\omega_{II}$  the center of rotation will be point  $\textcircled{B}$ , which is to the left of the center of gravity. For free oscillations involving a superposition of both modes, a center of rotation is meaningless.

*Forced Vibrations*

If an exciting force is applied to the system shown in Fig. 2-41, the Eqs. (2-119) become

$$(k_z - m\omega^2)A_z + k_zRA_\psi = Q_o \tag{2-123a}$$

$$k_zRA_z + (k_\psi + k_zR^2 - m\bar{r}^2\omega^2)A_\psi = Q_o s \tag{2-123b}$$

where  $s$  is the distance from the center of gravity to the point of force application. If the exciting force has been applied long enough for any transient motion to have decayed (in a real system some amount of damping is always present), the solution for  $A_z$  and  $A_\psi$  can be obtained using determinants. Thus,

$$A_z = \frac{\begin{vmatrix} Q_o & k_zR \\ Q_o s & k_\psi + k_zR^2 - m\bar{r}^2\omega^2 \end{vmatrix}}{\begin{vmatrix} (k_z - m\omega^2) & k_zR \\ k_zR & k_\psi + k_zR^2 - m\bar{r}^2\omega^2 \end{vmatrix}} \tag{2-124}$$

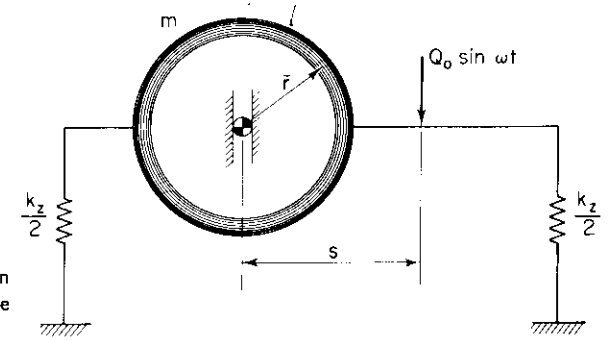


Figure 2-41. System shown on Fig. 2-37 with an exciting force applied.

Note that the denominator yields the frequency equation and thus has roots  $\omega = \omega_I$  and  $\omega_{II}$ . Equation (2-124) can be written as

$$A_z = \frac{Q_o}{m^2\bar{r}^2} \frac{(k_zR^2 + k_\psi - m\bar{r}^2\omega^2 - k_zRs)}{[\omega^2 - \omega_{II}^2][\omega^2 - \omega_I^2]} \tag{2-125}$$

Also, from Eqs. (2-123),

$$A_\psi = \frac{Q_o}{m^2\bar{r}^2} \frac{[-k_zR + (m\omega^2 - k_z)s]}{[\omega^2 - \omega_{II}^2][\omega^2 - \omega_I^2]} \tag{2-126}$$

The center of rotation is the negative of the ratio of the amplitudes:

$$\frac{A_z}{A_\psi} = \frac{k_zR^2 + k_\psi - m\bar{r}^2\omega^2 - k_zRs}{-k_zR + (m\omega^2 - k_z)s} \tag{2-127}$$

As previously mentioned, Eq. (2-127) is the same as the relationship for mode shapes when  $s = 0$ , as plotted in Fig. 2-40.

*Forced Translation and Rotation with Damping*

In order to illustrate the increase in complexity of the problem due to the addition of damping to the system, equations will be obtained for the solution of steady vibrations. The system to be analyzed will be reduced to the simplified system shown in Fig. 2-42. The viscous-damping coefficient for translation is  $c_z$ ; for rotation it is ( $c_\psi = c_z r_c^2$ ). The motion of the center of pressure and the resulting forces from the springs and dashpots are shown. Summation of forces about the center of gravity of the system gives

$$m\ddot{z} = -k_z(z + R\psi) - c_z(\dot{z} + R\dot{\psi}) + Q(t) \tag{2-128a}$$

$$m\bar{r}^2\ddot{\psi} = -k_\psi\psi - c_\psi\dot{\psi} - k_z(z + R\psi)R - c_z(\dot{z} + R\dot{\psi})R + Q(t)s \tag{2-128b}$$



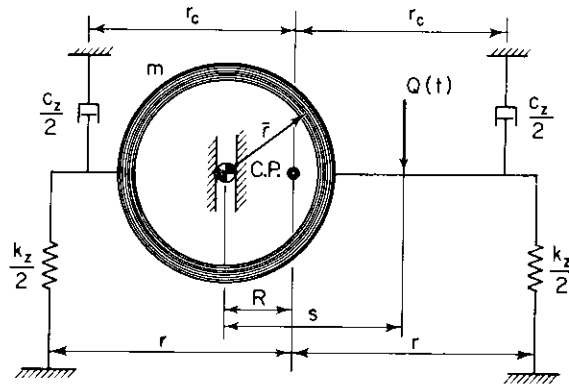


Figure 2-42. Coupled translation and rotation with damping.

The solutions to Eqs. (2-128) are most easily obtained using complex notation. Let

$$Q(t) = Q_o \exp(i\omega t) = Q_o(\cos \omega t + i \sin \omega t) \quad (2-129)$$

and

$$z = (A_{z1} + iA_{z2}) \exp(i\omega t) \quad (2-130a)$$

$$\psi = (A_{\psi1} + iA_{\psi2}) \exp(i\omega t) \quad (2-130b)$$

Then

$$\dot{z} = \omega(iA_{z1} - A_{z2}) \exp(i\omega t) \quad (2-131a)$$

and

$$\dot{\psi} = -\omega^2(A_{z1} + iA_{z2}) \exp(i\omega t) \quad (2-131b)$$

From Eqs. (2-130), the displacement amplitude and rotation amplitude are

$$A_z = \sqrt{A_{z1}^2 + A_{z2}^2} \quad (2-132a)$$

$$A_\psi = \sqrt{A_{\psi1}^2 + A_{\psi2}^2} \quad (2-132b)$$

which can be evaluated after obtaining values for  $A_{z1}$ ,  $A_{z2}$ ,  $A_{\psi1}$ , and  $A_{\psi2}$ .

The phase relationships between force, displacement, and rotation may also be obtained from the values of  $A_{z1}$ ,  $A_{z2}$ ,  $A_{\psi1}$ , and  $A_{\psi2}$ . Finally, to obtain  $A_{z1}$ ,  $A_{z2}$ ,  $A_{\psi1}$ , and  $A_{\psi2}$ , Eqs. (2-130) are substituted into Eqs. (2-128), separating the real and complex parts to obtain the following four equations:

$$(-m\omega^2 + k_z)A_{z1} - \omega c_z A_{z2} + Rk_z A_{\psi1} - R\omega c_z A_{\psi2} = Q_o \quad (2-133a)$$

$$\omega c_z A_{z1} + (-m\omega^2 + k_z)A_{z2} + \omega c_z R A_{\psi1} + Rk_z A_{\psi2} = 0 \quad (2-133b)$$

$$Rk_z A_{z1} - \omega c_z R A_{z2} + (-m\bar{r}^2 + k_\psi + k_z R^2)A_{\psi1} + (-\omega c_\psi - \omega c_z R^2)A_{\psi2} = Q_o s \quad (2-133c)$$

$$c_z \omega R A_{z1} + Rk_z A_{z2} + (\omega c_\psi + \omega c_z R^2)A_{\psi1} + (-m\bar{r}^2 + k_\psi + k_z R^2)A_{\psi2} = 0 \quad (2-133d)$$

Since all four equations must be solved for each value of frequency, it is necessary to make use of a digital or analog computer to obtain the solution.

### 2.6 Natural Frequencies of Continuous Systems

Although the main consideration of this text comprises foundations and soils, problems involving beams arise often enough to justify including a brief section on the subject. For beams, mass and elasticity are not physically isolated components and there are, theoretically, infinitely many natural frequencies; but for most practical problems the lowest natural frequencies are the most important. Figure 2-43 provides a means of calculating the first three natural frequencies of beams having uniform cross-section and uniformly distributed loads. If concentrated masses that are large with respect to the mass of the beam are placed on the beam, then the beam can be considered a weightless spring. If the above conditions are not met or if several masses are placed on the beam, then other methods must be used to find the lowest natural frequency.

#### Newmark's Method

The method devised by Newmark (1943) for calculating beam deflections can also be applied to the problem of finding natural frequencies of beams

Simple Support	$C_w = 9.87$ 	$C_w = 39.5$ 	$C_w = 89$ 
Cantilever	$C_w = 3.52$ 	$C_w = 22.4$ 	$C_w = 61.7$ 
Fixed Support	$C_w = 22.4$ 	$C_w = 61.7$ 	$C_w = 121$ 
Fixed Hinged	$C_w = 15.4$ 	$C_w = 50.0$ 	$C_w = 104$ 

$$\omega_n = C_w \sqrt{\frac{EI}{m \ell^3}} \text{ rad/sec}$$

$C_w$  = coefficient,  
 $E$  = Young's modulus (lb/in.<sup>2</sup>),  
 $I$  = moment of inertia (in.<sup>4</sup>),  
 $m$  = mass of entire beam (lb-sec<sup>2</sup>/in.),  
 $\ell$  = length of beam (in.).  
 (Nodes are shown as proportion of  $\ell$  from left end.)

Figure 2-43. Beam frequencies for various end supports.

having any variation of cross-section and mass loading. Space does not allow a detailed description of the method and the reader is referred to Godden (1965).

### Static-Deflection Methods

The relationship between potential and kinetic energy of a vibrating system provides the basis for approximate methods of calculating natural frequencies of more complex systems. Two methods are described below. For greater detail on the subject the reader is referred to Jacobsen and Ayre (1958). The Southwell-Dunkerley approximation provides a means of calculating a *lower bound* for the natural frequency, while the Rayleigh approximation provides an *upper bound* for the natural frequency. Both methods assume that the static deflection of the system is a reasonable approximation for the shape of the dynamic displacement. Hence they are referred to as static-deflection methods.

**Southwell-Dunkerley approximation.** This method provides a means of obtaining a lower bound for the lowest natural frequency of a multiple-degree-of-freedom system and is presented without proof. If a system is broken into parts, each part considered a single-degree-of-freedom system, then the lower bound for the coupled system is found by

$$\frac{1}{f_n^2} = \frac{1}{f_{n1}^2} + \frac{1}{f_{n2}^2} + \cdots + \frac{1}{f_{nj}^2}$$

where  $f_{nj}$  represents the natural frequency of the  $j$ th part. Using Eq. (2-18), it is possible to obtain the relationship

$$f_n = \frac{3.13}{\sqrt{z_{s1} + z_{s2} + \cdots + z_{sj}}} \text{ cycles/sec} \quad (2-134)$$

for the natural frequency of a beam broken down into  $j$  parts, where  $z_{sj}$  represents the deflection of the  $j$ th part in *inches*. As an illustration of the application of Eq. (2-134), consider Fig. 2-44, which shows a beam with four weights, each of which is large compared to the weight of the beam. The four systems to be analyzed which provide the static deflections in Eq. (2-134) are shown in Fig. 2-44b. The answer obtained is always less than the "exact" answer.

**Rayleigh approximation.** In the Rayleigh approximation an upper bound of the lowest natural frequency is obtained. As an illustration of this method

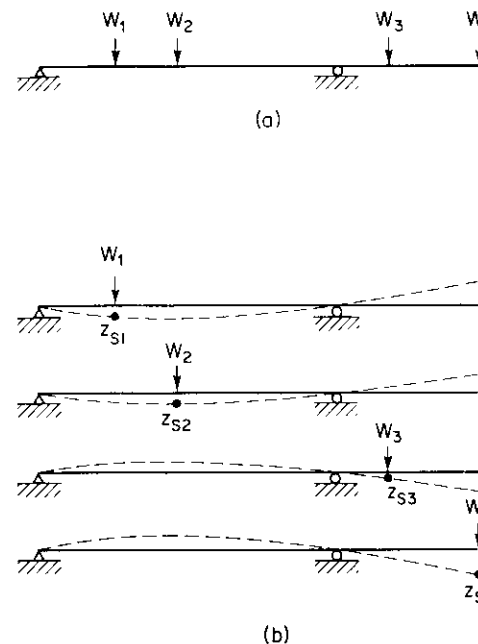


Figure 2-44. Static deflections used in the Southwell-Dunkerley approximation for the natural frequency of a beam supporting large weights compared to the weight of the beam.

consider again the same system. For the Rayleigh approximation *all* of the loads are applied simultaneously, with the condition that the forces of gravity act in opposite directions on opposite sides of supports, as shown in Fig. 2-45. The deflections in *inches* are calculated at each mass point and substituted into the equation

$$f_n = 3.13 \sqrt{\frac{W_1 z_{s1} + W_2 z_{s2} + W_3 z_{s3} + W_4 z_{s4}}{W_1 z_{s1}^2 + W_2 z_{s2}^2 + W_3 z_{s3}^2 + W_4 z_{s4}^2}} \text{ cycles/sec} \quad (2-135)$$

to provide an upper bound. All quantities in the equation are taken as positive regardless of the direction of the deflection

The advantages of the above two methods are that the calculations involve static deflections and both an upper and lower bound are obtained, providing a check as well as an indication of the accuracy of the solution.

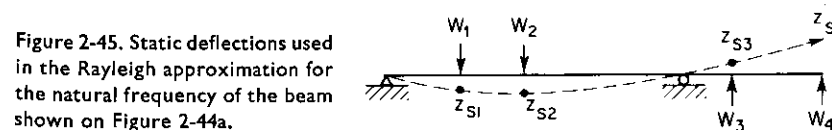


Figure 2-45. Static deflections used in the Rayleigh approximation for the natural frequency of the beam shown on Figure 2-44a.

# 3

## WAVE PROPAGATION IN AN ELASTIC, HOMOGENEOUS, ISOTROPIC MEDIUM

While it is considered more rigorous from the theoretical standpoint to develop a general solution and then impose boundary conditions to obtain specific solutions, it is more instructive in problems of wave propagation in elastic media to start with the specific problem of waves in a bounded medium.

### 3.1 Waves in a Bounded Elastic Medium

Various forms of physical systems subject to vibrations yield the identical equation of motion. The equation is called the *wave equation* and is expressed by the following partial-differential equation:

$$\frac{\partial^2 u}{\partial t^2} = v^2 \frac{\partial^2 u}{\partial x^2} \quad (3-1)$$

where  $v$  is the wave-propagation velocity. Some of the systems which can be described by the wave equation are rods in longitudinal vibration, rods in torsional vibration, pressure waves in an ideal fluid along the axis of the container, and the transverse vibrations of a taut string. Although the wave

equation is derived from any of these physical systems, the mathematical solution is identical in all cases. The wave equation, therefore, is one of the fundamental equations of mechanics.

#### Vibration in Rods

Three independent kinds of wave motion are possible in rods: longitudinal, torsional, and flexural. The first two kinds of motion result in the typical wave equation, while the third results in a dispersive equation of motion ("dispersive" here means that the velocity of the flexural waves depends on their frequency of excitation or wave length). Only longitudinal and torsional vibrations of rods will be considered here.

**Longitudinal waves.** Consider the free vibration of a rod with cross-sectional area  $A$ , Young's modulus  $E$ , and unit weight  $\gamma$ , as shown in Fig. 3-1. Assuming that each cross-section remains plane during motion and that the stress is uniform over the area,\* the equation of motion can be written directly. The stress on a transverse plane at  $x$  is  $\sigma_x$  and the stress on a transverse plane at  $(x + \Delta x)$  is  $[\sigma_x + (\partial\sigma_x/\partial x)\Delta x]$ . The sum of forces in the  $x$ -direction can be written as

$$-\sigma_x A + \left( \sigma_x + \frac{\partial\sigma_x}{\partial x} \Delta x \right) A = F$$

If the displacement of the element in the  $x$ -direction is designated as  $u$ ,

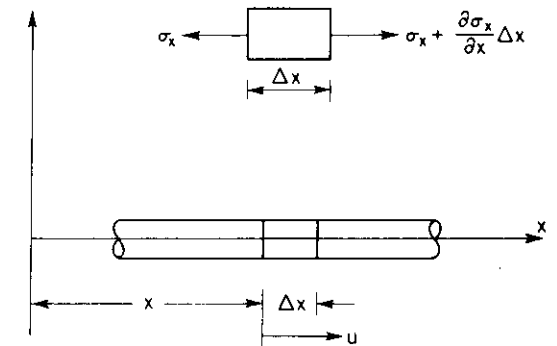


Figure 3-1. Longitudinal vibration of a rod.

\* In the above derivation inertia forces caused by the lateral motions of particles are neglected. The solution is, therefore, only approximate but is accurate as long as the wave length of the longitudinal waves is long in comparison with the cross-sectional dimensions of the rod.

Newton's second law can be written as

$$-\sigma_x A + \sigma_{x+\Delta x} A + \frac{\partial \sigma_x}{\partial x} \Delta x A = \Delta x A \frac{\gamma}{g} \frac{\partial^2 u}{\partial t^2}$$

or

$$\frac{\partial \sigma_x}{\partial x} = \frac{\gamma}{g} \frac{\partial^2 u}{\partial t^2} \quad (3-2)$$

The strain in the  $x$ -direction is  $\partial u / \partial x$  and the ratio of stress to strain is Young's modulus; therefore,

$$\sigma_x = E \frac{\partial u}{\partial x}$$

and

$$\frac{\partial \sigma_x}{\partial x} = E \frac{\partial^2 u}{\partial x^2}$$

Then using the mass density  $\rho = \gamma/g$ , Eq. (3-2) can be written

$$E \frac{\partial^2 u}{\partial x^2} = \rho \frac{\partial^2 u}{\partial t^2} \quad (3-3a)$$

or

$$\frac{\partial^2 u}{\partial t^2} = v_C^2 \frac{\partial^2 u}{\partial x^2} \quad (3-3b)$$

where

$$v_C^2 = \frac{E}{\rho} \quad (3-3c)$$

and  $v_C$  is defined as the phase velocity or longitudinal-wave-propagation velocity in a rod. Equation (3-3b) has the exact form of the wave equation.

The solution of Eq. (3-3b) may be written in the form

$$u = f(v_C t + x) + h(v_C t - x) \quad (3-4)$$

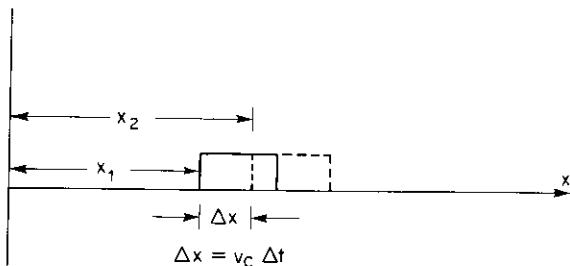


Figure 3-2. Motion of wave form in rod.

where  $f$  and  $h$  are arbitrary functions. The solution expressed in Eq. (3-4) has a simple physical interpretation. For a specific instant in time,  $t$ , both terms on the right-hand side of Eq. (3-4) are functions of  $x$  only. The second term can be represented by the solid block in Fig. 3-2, where the shape of the block is specified by the function  $h$ . After a time interval  $\Delta t$ , the argument of the function  $h$  becomes  $[v_C(t + \Delta t) - x]$ . If at the same time that  $t$  is increased by  $\Delta t$ ,  $x$  is increased by  $(\Delta x = v_C \Delta t)$ , the function  $h$  will remain unchanged, as follows:

$$u|_t = h(v_C t - x)$$

$$u|_{t+\Delta t} = h[v_C(t + \Delta t) - (x + \Delta x)]$$

$$u|_{t+\Delta t} = h[v_C t + v_C \Delta t - x - v_C \Delta t] = h(v_C t - x)$$

This demonstrates that the block in Fig. 3-2 at  $x_1$  and  $t$  moves unchanged in shape to  $x_2$  at  $(t + \Delta t)$ . It can now be stated that the right-hand term of Eq. (3-4) represents a wave traveling in the positive  $x$ -direction with velocity  $v_C$ . In a similar manner, it can be shown that the first term on the right in Eq. (3-4) represents a wave traveling in the negative  $x$ -direction with velocity  $v_C$ . This result could be anticipated from a consideration of the consequences of applying an instantaneous displacement  $u$  to a section of the rod in Fig. 3-1. It is obvious that the cross-section at  $(x + \Delta x)$  would experience a compressive stress and that the cross-section  $x$  would experience a tensile stress. Initially, only small zones close to these cross-sections would *feel* the stress, but as time passed larger zones would experience the stress caused by the displacement  $u$ . The results would be a tensile-stress wave traveling in the negative  $x$ -direction and a compressive wave traveling in the positive  $x$ -direction.

It is important to distinguish clearly between wave-propagation velocity  $v_C$  and the velocity of particles in the stressed zone,  $\dot{u}$ . To clarify this distinction, first consider the stressed zone at the end of the rod in Fig. 3-3a. When a uniformly distributed compressive-stress pulse of intensity  $\sigma_x$  and duration  $t_n$  (Fig. 3-3b) is applied to the end of the rod, initially only a small zone of the rod will experience the compression. This compression will be transmitted to successive zones of the rod as time increases. The transmission of the compressive stress from one zone to another represents a wave traveling along the rod at a velocity  $v_C$ .

During a time interval  $\Delta t$ , the compressive stress will travel along the rod a distance  $(\Delta x = v_C \Delta t)$ . At any time after  $t_n$ , a segment of the rod of length  $(x_n = v_C t_n)$  will constitute the compressed zone, and the amount of elastic shortening of this zone will be given by the displacement of the end

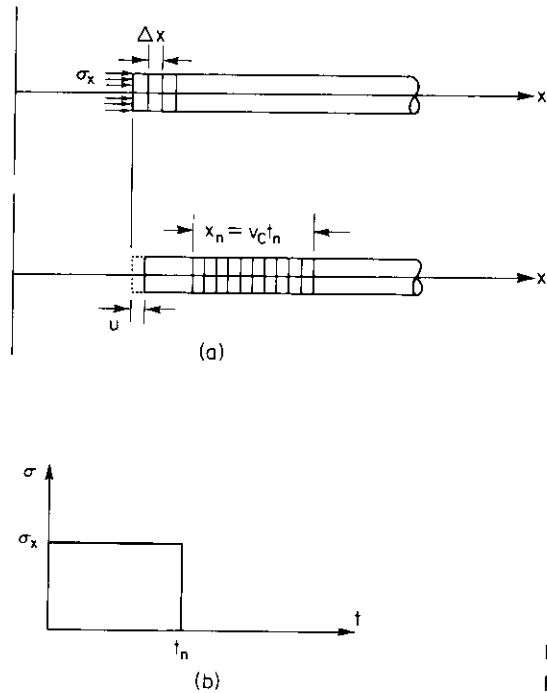


Figure 3-3. Phase velocity and particle velocity in prismatic rods.

of the rod

$$u = \frac{\sigma_x}{E} x_n = \frac{\sigma_x}{E} v_C t_n$$

or

$$\frac{u}{t_n} = \frac{\sigma_x v_C}{E}$$

Now, the displacement  $u$  divided by time  $t_n$  also represents the velocity of the end of the rod or particle velocity:

$$\dot{u} = \frac{\sigma_x v_C}{E} \tag{3-5}$$

It should be recognized that both wave-propagation velocity and particle velocity are in the same direction when a compressive stress is applied but that wave-propagation velocity is opposite to the particle velocity when a tensile stress is applied. Another important consideration is that the particle velocity  $\dot{u}$  depends on the intensity of the stress (see Eq. 3-5) but that the wave-propagation velocity  $v_C$  is only a function of the material properties (see Eq. 3-3c).

**Torsional waves.** The torque on a transverse section of a rod such as shown in Fig. 3-4a produces an angular rotation  $\theta$ . The torque can be written

$$T = G I_p \frac{\partial \theta}{\partial x} \tag{3-6}$$

where  $G$  = shear modulus (modulus of rigidity, lb/in.<sup>2</sup>),  
 $I_p$  = polar moment of inertia of the cross-section (in.<sup>4</sup>), and  
 $\frac{\partial \theta}{\partial x}$  = angle of twist per unit length of rod (rad/in.).

The torque due to the rotational inertia of an element of rod of length  $\Delta x$  can be written as

$$T = \rho I_p \Delta x \frac{\partial^2 \theta}{\partial t^2} \tag{3-7}$$

Applying Newton's second law to an element, as shown in Fig. 3-4b, yields

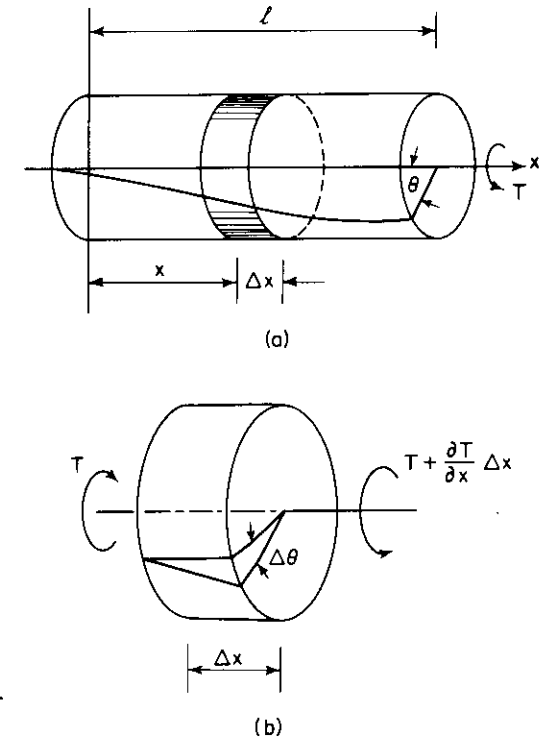


Figure 3-4. Torsion in circular rod.

the following:

$$-T + \left( T + \frac{\partial T}{\partial x} \Delta x \right) = \rho I_p \Delta x \frac{\partial^2 \Theta}{\partial t^2}$$

or

$$\frac{\partial T}{\partial x} = \rho I_p \frac{\partial^2 \Theta}{\partial t^2} \quad (3-8)$$

Now, substituting for  $T$  from Eq. (3-6), Eq. (3-8) becomes

$$\frac{\partial}{\partial x} \left( G I_p \frac{\partial \Theta}{\partial x} \right) = \rho I_p \frac{\partial^2 \Theta}{\partial t^2}$$

or

$$\frac{\partial^2 \Theta}{\partial x^2} = v_s^2 \frac{\partial^2 \Theta}{\partial t^2} \quad (3-9a)$$

where

$$v_s^2 = \frac{G}{\rho} \quad (3-9b)$$

Equation (3-9a) has the form of Eq. (3-3c), except that Young's modulus  $E$  has been replaced by the shear modulus  $G$ .

### End Conditions

There are several ways to examine the phenomena that occur at the ends of rods of finite length in which a stress wave is traveling. The approach presented here is that of a simple physical interpretation similar to the presentation by Timoshenko and Goodier (1951). Another approach is that of solving the wave equation for given boundary conditions as described by Kolsky (1963).

The wave equation is a linear differential equation with constant coefficients. If there are two solutions to this equation, the sum of these two solutions will also satisfy the wave equation, because superposition is valid. Now, consider an elastic rod in which a compression wave is traveling in the positive  $x$ -direction and an identical tension wave is traveling in the negative  $x$ -direction (Fig. 3-5a). During the time interval in which the two waves pass by each other in the crossover zone, the portion of the rod in which the two waves are superposed has zero stress (Fig. 3-5c) and a particle velocity equal to twice the particle velocity in either wave. The particle velocity doubles in the crossover zone because, as pointed out earlier, particle velocity in a compression wave is in the direction of wave travel, but particle velocity in a tension wave is opposite to the direction of wave travel. Since the compression and tension waves are traveling in opposite directions in

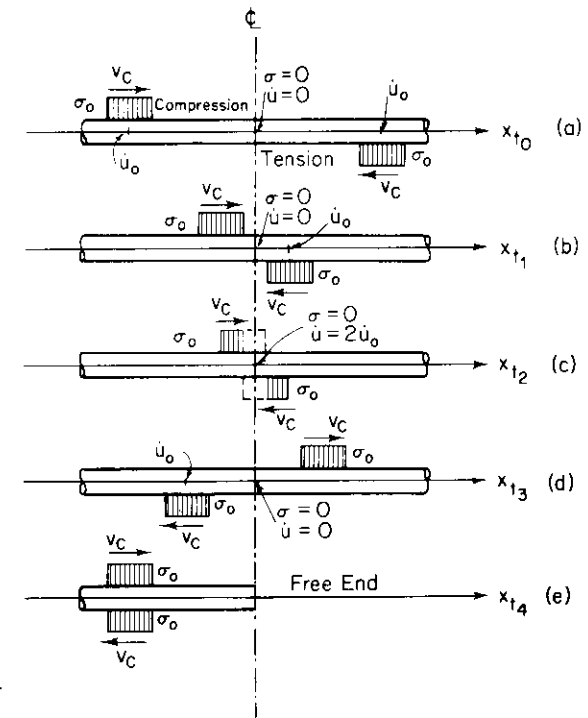


Figure 3-5. Wave in a rod—free-end condition.

Fig. 3-5, the particle velocities associated with both waves are additive. After the two waves have passed, the stress and velocity return to zero at the crossover point and the compressive and tensile waves return to their initial shape and magnitude. On the centerline cross-section, the stress is zero at all times. This stress condition is the same as that which exists at a free end of a rod. By removing one-half of the rod, the centerline cross-section can be considered a free end. Then, by examining the left side of Fig. 3-5e, we may see that a compression wave is reflected from a free end as a tension wave of the same magnitude and shape. Similarly, a tension wave is reflected as a compression wave of the same magnitude and shape.

Now, consider an elastic rod in which a compression wave is traveling in the positive  $x$ -direction and an identical compression wave is traveling in the negative  $x$ -direction (Fig. 3-6a). During the interval in which the two waves traverse the crossover zone, the cross-section through the centerline has a stress equal to twice the stress in each wave and a particle velocity equal to zero. After the waves pass by each other, they return to their original shape and magnitude.

The centerline cross-section remains stationary during the entire process and, hence, behaves like a fixed end of a rod. From an examination of the

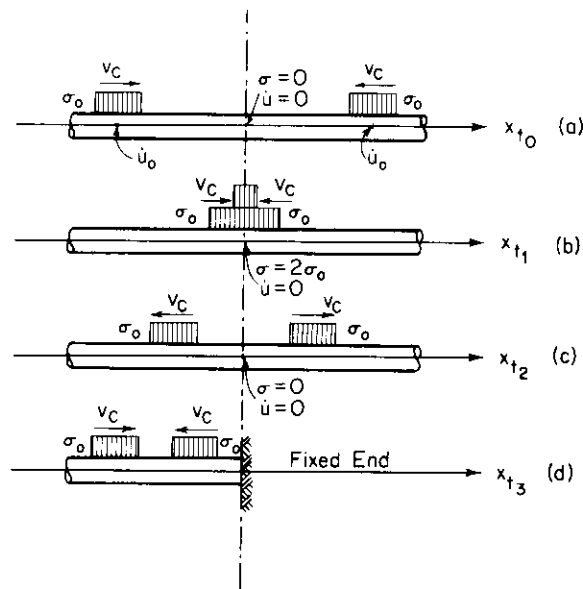


Figure 3-6. Wave in a rod—fixed-end condition.

left half of Fig. 3-6d, it can be seen that a *compression wave is reflected from a fixed end of a rod as a compression wave of the same magnitude and shape*; and that at the fixed end of a rod the stress is doubled.

The above conclusions were based on the waves of constant-stress amplitude. However, the same conclusions regarding wave propagation, superposition, and reflection of waves can be applied to stress waves of any shape.

*Rods of Finite Length*

So far, only infinite and semi-infinite rods have been considered. For finite rods with various boundary conditions, other solutions to the wave equations can be written as a trigonometric series

$$u = U(C_1 \cos \omega_n t + C_2 \sin \omega_n t) \tag{3-10}$$

where

- $U$  = the displacement amplitude along the length of the rod,
- $C_1, C_2$  = constants, and
- $\omega_n$  = the circular frequency of a natural mode of vibration.

This equation describes the displaced shape of a bar vibrating in a natural mode. Substitution of Eq. (3-10) into Eq. (3-3b) gives

$$\frac{d^2 U}{dx^2} + \frac{\omega_n^2}{v_c^2} U = 0$$

from which

$$U = C_3 \cos \frac{\omega_n x}{v_c} + C_4 \sin \frac{\omega_n x}{v_c} \tag{3-11}$$

For a rod of finite length, the displacement amplitude  $U$  must be determined separately for each of three possible end conditions. These end conditions are (1) both ends free (free-free), (2) one end fixed and one end free (fixed-free), and (3) both ends fixed (fixed-fixed).

**Free-Free.** For the rod of length  $l$  in Fig. 3-7a, the end conditions for the free-free case are that the stress and, consequently, the strain on the end planes must be zero. This means that  $dU/dx = 0$  at  $x = 0$  and at  $x = l$ . Now

$$\frac{dU}{dx} = \frac{\omega_n}{v_c} \left( -C_3 \sin \frac{\omega_n x}{v_c} + C_4 \cos \frac{\omega_n x}{v_c} \right) = 0 \tag{3-12}$$

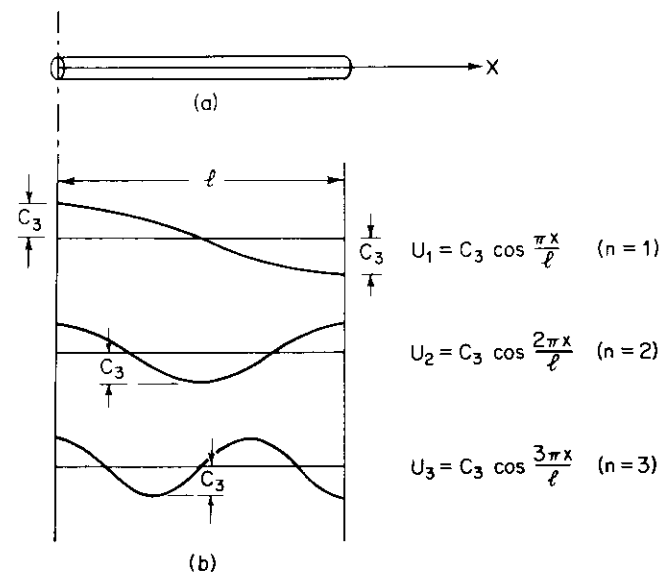


Figure 3-7. Normal modes for free-free rod.

By evaluating Eq. (3-12) at  $x = 0$ , we get  $C_4 = 0$ ; and by evaluating Eq. (3-12) at  $x = \ell$  and assuming a nontrivial solution ( $C_3 \neq 0$ ), we get

$$\sin \frac{\omega_n \ell}{v_C} = 0 \quad (3-13)$$

To satisfy Eq. (3-13),

$$\frac{\omega_n \ell}{v_C} = n\pi$$

or

$$\omega_n = \frac{n\pi v_C}{\ell}, \quad n = 1, 2, 3, \dots \quad (3-14)$$

Equation (3-13) is the *frequency equation* from which the frequencies of the natural modes of vibration of the free-free rod are found. Combining Eqs. (3-14) and (3-11), the distribution of displacement along the rod for any harmonic can be found. The first three harmonics are shown in Fig. 3-7b, and the displacement amplitude can be expressed as

$$U_n = C_3 \cos \frac{n\pi x}{\ell}, \quad n = 1, 2, 3, \dots \quad (3-15)$$

The general form of the displacement solution for the free-free rod is obtained by substituting Eq. (3-15) in Eq. (3-10) to get

$$u = \cos \frac{n\pi x}{\ell} \left[ (C_1)_n \cos \frac{n\pi v_C t}{\ell} + (C_2)_n \sin \frac{n\pi v_C t}{\ell} \right] \quad (3-16)$$

By superposing the solutions for many natural modes of vibration, any longitudinal vibration can be represented by

$$u = \sum_{n=1}^{\infty} \cos \frac{n\pi x}{\ell} \left[ (C_1)_n \cos \frac{n\pi v_C t}{\ell} + (C_2)_n \sin \frac{n\pi v_C t}{\ell} \right] \quad (3-17)$$

**Fixed-free.** The end conditions for the rod in Fig. 3-8a are as follows: at the fixed end ( $x = 0$ ) the displacement is zero ( $U = 0$ ); at the free end ( $x = \ell$ ) the strain is zero ( $\partial U / \partial x = 0$ ). Using the condition at  $x = 0$  in Eq. (3-11),  $C_3 = 0$ ; and using the condition at  $x = \ell$  in Eq. (3-12),

$$\cos \frac{\omega_n \ell}{v_C} = 0 \quad (3-18)$$

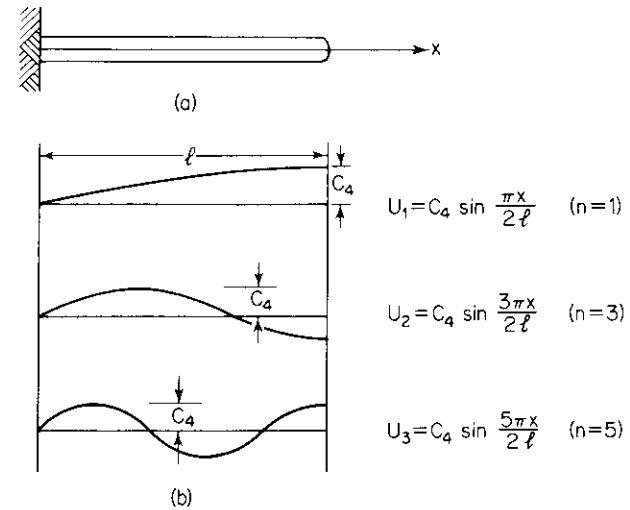


Figure 3-8. Normal modes for fixed-free rod.

For Eq. (3-18) to be satisfied,

$$\omega_n = \frac{n\pi v_C}{2\ell}, \quad n = 1, 3, 5, \dots \quad (3-19)$$

Now, the displacement amplitude can be written

$$U_n = C_4 \sin \frac{\omega_n x}{v_C} = C_4 \sin \frac{n\pi x}{2\ell} \quad (3-20)$$

The first three harmonics described by Eq. (3-20) are shown in Fig. 3-8b.

**Fixed-fixed.** The end conditions for the rod in Fig. 3-9a are as follows:  $U = 0$  at  $x = 0$  and at  $x = \ell$ . For this to be true,  $C_3 = 0$  and

$$\sin \frac{\omega_n \ell}{v_C} = 0 \quad (3-21)$$

From Eq. (3-21) we get

$$\omega_n = \frac{n\pi v_C}{\ell}, \quad n = 1, 2, 3, \dots \quad (3-22)$$

Then we can write

$$U_n = C_4 \sin \frac{n\pi x}{\ell}, \quad n = 1, 2, 3, \dots \quad (3-23)$$



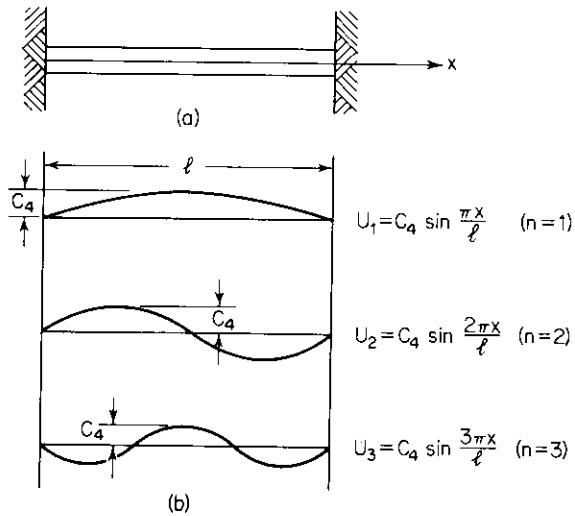


Figure 3-9. Normal modes for fixed-fixed rod.

The first three harmonics described by Eq. (3-23) are shown in Fig. 3-9b. All of the foregoing derivations for longitudinal waves can be applied directly to torsional waves.

#### Experimental Determination of Elastic Moduli

**Travel-time method.** The travel time of elastic waves can be used as the basis for the experimental determination of elastic moduli of the material of a rod. Using the appropriate electronic equipment, it is possible to determine the time for an elastic wave to travel a distance  $\ell_0$  along a rod. If  $t_c$  is the measured travel time for the longitudinal wave, then, from Eq. (3-3c), Young's modulus can be written

$$E = \frac{\gamma \ell_0^2}{g t_c^2} \quad (3-24)$$

If  $t_s$  is the measured travel time for a torsional wave, then, from Eq. (3-9b) the shear modulus can be written

$$G = \frac{\gamma \ell_0^2}{g t_s^2} \quad (3-25)$$

**Resonant-column method.** In this technique a column of material is excited either longitudinally or torsionally in one of its normal modes, and the wave velocity is determined from the frequency at resonance and from the dimensions of the specimen. For example, if a free-free rod could be excited longitudinally in the first normal mode of vibration and the frequency

$f_n$  measured, the velocity of the longitudinal wave could be calculated from Eq. (3-14), as follows:

$$\omega_n = 2\pi f_n = \frac{\pi v_C}{\ell}, \quad \text{for } n = 1$$

and then

$$v_C = 2f_n \ell \quad (3-26)$$

Similarly, for a torsionally excited free-free rod, the velocity of the torsional wave could be calculated as follows:

$$\omega_n = 2\pi f_n = \frac{\pi v_S}{\ell}, \quad \text{for } n = 1$$

and

$$v_S = 2f_n \ell \quad (3-27)$$

Because  $v_C$  is known from Eq. (3-26), Young's modulus can be computed from

$$E = \rho(2f_n \ell)^2 \quad (3-28)$$

and since  $v_S$  is known from Eq. (3-27), the shear modulus can be computed from

$$G = \rho(2f_n \ell)^2 \quad (3-29)$$

Various specimen configurations have been tried in the resonant-column approach. The most common arrangements are the free-free and the fixed-free configurations. The free-free arrangement is not entirely free at either end and the degree of freedom is not easily determined. Due to this difficulty, the free-free configuration is not as well-suited to the resonant-column technique as is the fixed-free configuration.

Another difficulty with the resonant-column technique is the necessity of exciting the specimen and measuring its motion. To accomplish this, driving and motion-monitoring instruments must be attached to the specimen, and these attachments alter the specimen boundary conditions. It is possible to compensate for the attachments at the free end of the fixed-free configuration by assuming that the attachments can be lumped into a mass, as shown in Fig. 3-10. The equations for the fixed-free rod do not apply, because the end conditions at the *free* end are changed. For longitudinal excitation, displacement is zero at the fixed end, but at the free end a force is exerted on the rod which is equal to the inertia force of the concentrated mass.

This force can be expressed as

$$F = \frac{\partial u}{\partial x} AE = -m \frac{\partial^2 u}{\partial t^2} \quad (3-30)$$

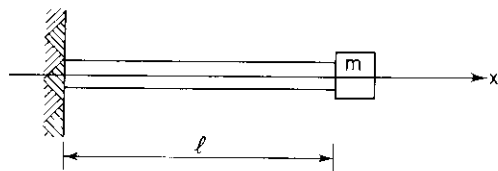


Figure 3-10. Fixed-free rod with mass attached to free end.

where  $A$  is the cross-sectional area of the rod and  $m$  is the mass of the equipment attached to the free end. Applying the end condition for  $x = 0$  to Eq. (3-11), we find that  $C_3 = 0$  and the displacement amplitude becomes

$$U = C_4 \sin \frac{\omega_n x}{v_C} \quad (3-31)$$

At  $x = \ell$ , we use Eq. (3-10) to get

$$\frac{\partial u}{\partial x} = \frac{\partial U}{\partial x} (C_1 \cos \omega_n t + C_2 \sin \omega_n t)$$

and

$$\frac{\partial^2 u}{\partial t^2} = -\omega_n^2 U (C_1 \cos \omega_n t + C_2 \sin \omega_n t)$$

Substituting these expressions in Eq. (3-30) gives

$$AE \frac{\partial U}{\partial x} = m \omega_n^2 U \quad (3-32)$$

Finally, we substitute  $U$  from Eq. (3-31) into Eq. (3-32) to obtain

$$AE \frac{\omega_n}{v_C} \cos \frac{\omega_n \ell}{v_C} = \omega_n^2 m \sin \frac{\omega_n \ell}{v_C}$$

which can be reduced to

$$\frac{A\ell\gamma}{W} = \frac{\omega_n \ell}{v_C} \tan \frac{\omega_n \ell}{v_C} \quad (3-33)$$

In Eq. (3-33) it should be recognized that  $A\ell\gamma$  is the weight of the rod and that  $W$  is the weight of the added mass. Equation (3-33) is the frequency equation for all normal modes of vibration for the system in Fig. 3-10. The right side of Eq. (3-33) can be written for convenience as  $(\beta \tan \beta)$ , where  $\beta = \omega_n \ell / v_C$ . Then, for any ratio of weight of rod to weight of added mass, the value of  $\beta$  can be found. Equation (3-33) is solved most easily by plotting

a curve of  $\beta$  vs.  $A\ell\gamma/W$  (see Fig. 7-24). The wave velocity can now be computed from the following equation, using the appropriate values of  $\beta$ :

$$v_C = \frac{2\pi f_n \ell}{\beta} \quad (3-34)$$

Young's modulus is then found from

$$E = \rho v_C^2 = \rho \left( \frac{2\pi f_n \ell}{\beta} \right)^2 \quad (3-35)$$

When the ratio  $A\ell\gamma/W \rightarrow \infty$ , the rod approaches the fixed-free condition. However, as the ratio  $A\ell\gamma/W \rightarrow 0$ , the system approaches a single-degree-of-freedom system with a spring constant  $k = AE/\ell$  and a suspended mass equal to  $W/g$ .

For torsional vibration, the equation comparable to Eq. (3-33) can be written as

$$\frac{I}{I_o} = \frac{\omega_n \ell}{v_S} \tan \frac{\omega_n \ell}{v_S} \quad (3-36)$$

where  $I$  is the mass polar moment of inertia of the specimen and  $I_o$  is the mass polar moment of inertia of the added mass.

### 3.2 Waves in an Infinite, Homogeneous, Isotropic, Elastic Medium

In Sec. 3.1 it was shown that wave motion in an elastic rod could be described by the wave equation and that a physical interpretation of wave motion was easily related to the mathematical expressions. In the case of an infinite elastic medium, however, physical interpretations are less obvious and it will be necessary to emphasize mathematical relationships. Nevertheless, it will still be possible to reduce the problem to the form of the wave equation.

#### Derivation of Equations of Motion

To derive the equations of motion for an elastic medium, it is necessary to examine the equilibrium of a small element, as shown in Fig. 3-11. Since this subject has been treated in detail by many other authors (Timoshenko and Goodier, 1951; Kolsky, 1963; Ewing, Jardetzky, and Press, 1957;

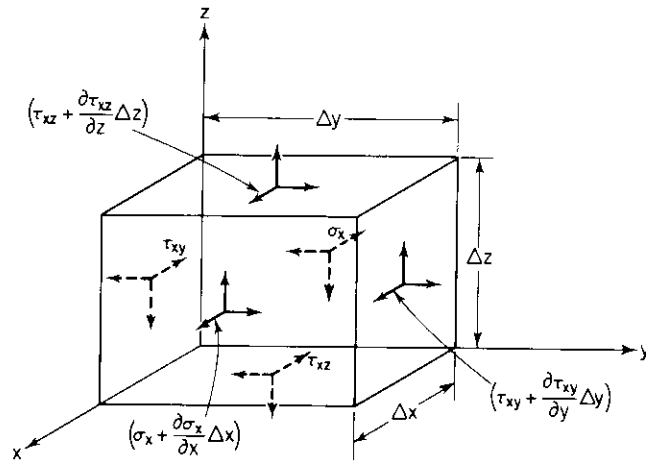


Figure 3-11. Stress on a small element of an infinite elastic medium.

Grant and West, 1965; and others), only the essential steps of the development of the equations of motion will be presented here.

First consider the variation in force on opposite faces of the small element in Fig. 3-11. The stresses on each face of this element are represented by sets of orthogonal vectors. The solid vectors are acting on the visible faces of the element and the dotted vectors are acting on the hidden faces. Translational equilibrium of this element can be expressed by writing the sum of forces acting parallel to each axis. In the  $x$ -direction the equilibrium equation is

$$\left(\sigma_x + \frac{\partial \sigma_x}{\partial x} \Delta x\right) \Delta y \Delta z - \sigma_x \Delta y \Delta z + \left(\tau_{xy} + \frac{\partial \tau_{xy}}{\partial y} \Delta y\right) \Delta x \Delta z - \tau_{xy} \Delta x \Delta z + \left(\tau_{xz} + \frac{\partial \tau_{xz}}{\partial z} \Delta z\right) \Delta x \Delta y - \tau_{xz} \Delta x \Delta y = 0 \quad (3-37)$$

Similar equations can be written for the summation of forces in the  $y$ - and  $z$ -directions. Neglecting body forces and applying Newton's second law in the  $x$ -direction gives

$$\left(\frac{\partial \sigma_x}{\partial x} + \frac{\partial \tau_{xy}}{\partial y} + \frac{\partial \tau_{xz}}{\partial z}\right) \Delta x \Delta y \Delta z = \rho(\Delta x \Delta y \Delta z) \frac{\partial^2 u}{\partial t^2} \quad (3-38)$$

Equations similar to Eq. (3-38) can be written for the  $y$ - and  $z$ -directions.

Then, the three equations of motion in terms of stresses can be written

$$\rho \frac{\partial^2 u}{\partial t^2} = \frac{\partial \sigma_x}{\partial x} + \frac{\partial \tau_{xy}}{\partial y} + \frac{\partial \tau_{xz}}{\partial z} \quad (3-39a)$$

$$\rho \frac{\partial^2 v}{\partial t^2} = \frac{\partial \tau_{yx}}{\partial x} + \frac{\partial \sigma_y}{\partial y} + \frac{\partial \tau_{yz}}{\partial z} \quad (3-39b)$$

$$\rho \frac{\partial^2 w}{\partial t^2} = \frac{\partial \tau_{zx}}{\partial x} + \frac{\partial \tau_{zy}}{\partial y} + \frac{\partial \sigma_z}{\partial z} \quad (3-39c)$$

where  $v$  and  $w$  are displacements in the  $y$ - and  $z$ -directions, respectively. To express the right-hand sides of Eqs. (3-39) in terms of displacements, the following relationships for an elastic medium will be used:

$$\begin{aligned} \sigma_x &= \lambda \bar{\epsilon} + 2G \epsilon_x & \tau_{xy} &= \tau_{yx} = G \gamma_{xy} \\ \sigma_y &= \lambda \bar{\epsilon} + 2G \epsilon_y & \tau_{yz} &= \tau_{zy} = G \gamma_{yz} \\ \sigma_z &= \lambda \bar{\epsilon} + 2G \epsilon_z & \tau_{zx} &= \tau_{xz} = G \gamma_{zx} \end{aligned} \quad (3-40)$$

$$G = \frac{E}{2(1+\nu)} \quad \lambda = \frac{\nu E}{(1+\nu)(1-2\nu)}$$

where  $\nu$  is Poisson's ratio,  $\lambda$  and  $G$  are Lamé's constants ( $G$  is also called the shear modulus or rigidity modulus), and  $\bar{\epsilon}$  is called the cubical dilatation (also called the dilation or volume expansion) and is defined by  $\bar{\epsilon} = \epsilon_x + \epsilon_y + \epsilon_z$ . We also need the following relationships for strain and rotation in terms of displacement:

$$\begin{aligned} \epsilon_x &= \frac{\partial u}{\partial x} & \gamma_{xy} &= \frac{\partial v}{\partial x} + \frac{\partial u}{\partial y} & 2\bar{\omega}_x &= \frac{\partial w}{\partial y} - \frac{\partial v}{\partial z} \\ \epsilon_y &= \frac{\partial v}{\partial y} & \gamma_{yz} &= \frac{\partial w}{\partial y} + \frac{\partial v}{\partial z} & 2\bar{\omega}_y &= \frac{\partial u}{\partial z} - \frac{\partial w}{\partial x} \\ \epsilon_z &= \frac{\partial w}{\partial z} & \gamma_{zx} &= \frac{\partial u}{\partial z} + \frac{\partial w}{\partial x} & 2\bar{\omega}_z &= \frac{\partial v}{\partial x} - \frac{\partial u}{\partial y} \end{aligned} \quad (3-41)$$

where  $\bar{\omega}$  is the rotation about each axis. Combining the appropriate expressions of Eq. (3-40) and (3-41) with Eq. (3-39a) gives

$$\rho \frac{\partial^2 u}{\partial t^2} = (\lambda + G) \frac{\partial \bar{\epsilon}}{\partial x} + G \nabla^2 u \quad (3-42)$$

Similarly, we can rewrite Eq. (3-39b) and (3-39c) as

$$\rho \frac{\partial^2 v}{\partial t^2} = (\lambda + G) \frac{\partial \bar{\epsilon}}{\partial y} + G \nabla^2 v \quad (3-43)$$

and

$$\rho \frac{\partial^2 w}{\partial t^2} = (\lambda + G) \frac{\partial \bar{\epsilon}}{\partial z} + G \nabla^2 w \quad (3-44)$$

where  $\nabla^2$  (the Laplacian operator in Cartesian coordinates) is defined as

$$\nabla^2 = \frac{\partial^2}{\partial x^2} + \frac{\partial^2}{\partial y^2} + \frac{\partial^2}{\partial z^2}$$

Equations (3-42), (3-43), and (3-44) are the equations of motion for an infinite homogeneous, isotropic, elastic medium.

#### Solutions for Equations of Motion

Two solutions can be found for the equations of motion: one solution describes the propagation of a wave of pure volume change (irrotational wave), while the other describes the propagation of a wave of pure rotation (equivoluminal wave). The first solution can be obtained by differentiating Eqs. (3-42), (3-43), and (3-44) with respect to  $x$ ,  $y$ , and  $z$ , respectively, and adding all three expressions together. This operation results in an equation of the form

$$\rho \frac{\partial^2 \bar{\epsilon}}{\partial t^2} = (\lambda + 2G) \nabla^2 \bar{\epsilon}$$

or

$$\frac{\partial^2 \bar{\epsilon}}{\partial t^2} = v_P^2 \nabla^2 \bar{\epsilon} \quad (3-45)$$

This is exactly the form of the *wave equation*, where

$$v_P = \sqrt{\frac{\lambda + 2G}{\rho}} \quad (3-46)$$

The dilatation  $\bar{\epsilon}$ , therefore, propagates at a velocity  $v_P$ . The other solution to the equations of motion can be obtained by differentiating Eq. (3-43) with

respect to  $z$  and Eq. (3-44) with respect to  $y$  and then eliminating  $\bar{\epsilon}$  by subtracting these two equations. This operation gives

$$\rho \frac{\partial^2}{\partial t^2} \left( \frac{\partial w}{\partial y} - \frac{\partial v}{\partial z} \right) = G \nabla^2 \left( \frac{\partial w}{\partial y} - \frac{\partial v}{\partial z} \right)$$

and by using the expression for rotation  $\bar{\omega}_x$  from Eq. (3-41), we get

$$\rho \frac{\partial^2 \bar{\omega}_x}{\partial t^2} = G \nabla^2 \bar{\omega}_x$$

or

$$\frac{\partial^2 \bar{\omega}_x}{\partial t^2} = v_S^2 \nabla^2 \bar{\omega}_x \quad (3-47)$$

Similar expressions can be obtained for  $\bar{\omega}_y$  and  $\bar{\omega}_z$ , which implies that rotation is propagated with velocity

$$v_S = \sqrt{\frac{G}{\rho}} \quad (3-48)$$

From the above analysis it can be seen that an *infinite elastic medium* can sustain two kinds of waves, that the two waves represent different types of body motions, and that the waves travel at different velocities. The two waves are usually referred to by the following terms:

- (1) *dilatational wave* (primary wave, *P-wave*, compression wave, irrotational wave), and
- (2) *distortional wave* (secondary wave, *S-wave*, shear wave, equivoluminal wave).

The dilatational wave propagates with a velocity  $v_P$  (Eq. 3-46), while the distortional wave propagates with a velocity  $v_S$  (Eq. 3-48). The terms “*P-wave*” and “*S-wave*” will generally be used in place of “dilatational wave” and “distortional wave” in this text.

It is informative to compare the wave velocities determined for an infinite elastic medium with those obtained in Sec. 3.1 for an elastic rod. The particle motion associated with the compression wave in the rod and the dilatational wave in the infinite medium is the same, but the wave-propagation velocities are different. In the rod  $v_C = \sqrt{E/\rho}$ , but in the infinite medium  $v_P = \sqrt{(\lambda + 2G)/\rho}$ . This means that the compression wave will travel faster in the infinite medium than in a rod. The compression wave travels faster in the infinite medium because there can be no lateral displacements, while in the rod lateral displacements are possible. The second type of wave motion

(distortional) propagates at the same velocity ( $v_S = \sqrt{G/\rho}$ ) in both the rod and the infinite medium.

### 3.3 Waves in an Elastic Half-Space

In Sec. 3.2 it was found that two types of waves were possible in an infinite elastic medium—waves of dilatation and waves of distortion. In an elastic half-space, however, it is possible to find a third solution for the equations of motion which corresponds to a wave whose motion is confined to a zone near the boundary of the half-space. This wave was first studied by Lord Rayleigh (1885) and later was described in detail by Lamb (1904). The elastic wave described by these investigators is known as the *Rayleigh wave* (*R-wave*) and is confined to the neighborhood of the surface of a half-space. The influence of the Rayleigh wave decreases rapidly with depth.

#### Rayleigh-Wave Velocity

A wave with the characteristics noted above can be obtained by starting with the equations of motion (Eqs. 3-42, 3-43, and 3-44) and imposing the appropriate boundary conditions for a free surface. We define the surface of the half-space as the  $x$ - $y$  plane with  $z$  assumed to be positive toward the interior of the half-space, as shown in Fig. 3-12. For a *plane wave* traveling in the  $x$ -direction, particle displacements will be independent of the  $y$ -direction. Displacements in the  $x$ - and  $z$ -directions, denoted by  $u$  and  $w$  respectively, can be written in terms of two potential functions  $\Phi$  and  $\Psi'$ :

$$u = \frac{\partial \Phi}{\partial x} + \frac{\partial \Psi'}{\partial z} \quad \text{and} \quad w = \frac{\partial \Phi}{\partial z} - \frac{\partial \Psi'}{\partial x}$$

The dilatation  $\bar{\epsilon}$  of the wave defined by  $u$  and  $w$  is

$$\bar{\epsilon} = \frac{\partial u}{\partial x} + \frac{\partial w}{\partial z} = \frac{\partial}{\partial x} \left( \frac{\partial \Phi}{\partial x} + \frac{\partial \Psi'}{\partial z} \right) + \frac{\partial}{\partial z} \left( \frac{\partial \Phi}{\partial z} - \frac{\partial \Psi'}{\partial x} \right) = \nabla^2 \Phi$$

and the rotation  $2\bar{\omega}_y$  in the  $x$ - $z$  plane is

$$2\bar{\omega}_y = \frac{\partial u}{\partial z} - \frac{\partial w}{\partial x} = \frac{\partial}{\partial z} \left( \frac{\partial \Phi}{\partial x} + \frac{\partial \Psi'}{\partial z} \right) - \frac{\partial}{\partial x} \left( \frac{\partial \Phi}{\partial z} - \frac{\partial \Psi'}{\partial x} \right) = \nabla^2 \Psi'$$

Now it can be seen that the potential functions  $\Phi$  and  $\Psi'$  have been chosen

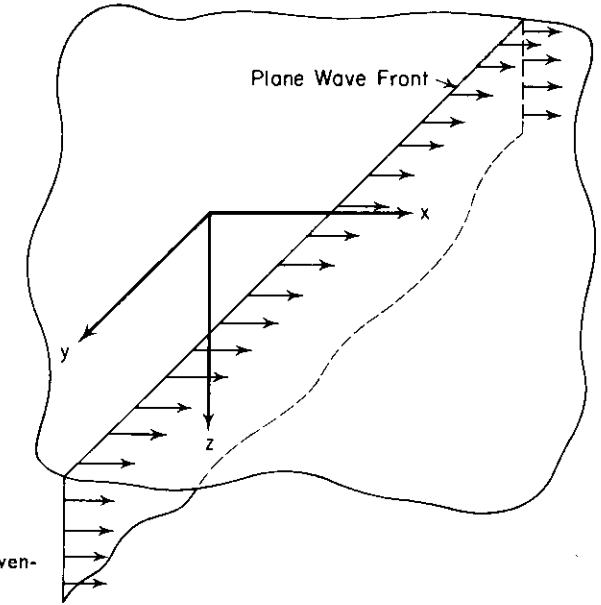


Figure 3-12. Coordinate convention for elastic half-space.

such that  $\Phi$  is associated with dilatation of the medium and  $\Psi'$  associated with rotation of the medium.

Substituting  $u$  and  $w$  into Eqs. (3-42) and (3-44) yields

$$\rho \frac{\partial}{\partial x} \left( \frac{\partial^2 \Phi}{\partial t^2} \right) + \rho \frac{\partial}{\partial z} \left( \frac{\partial^2 \Psi'}{\partial t^2} \right) = (\lambda + 2G) \frac{\partial}{\partial x} (\nabla^2 \Phi) + G \frac{\partial}{\partial z} (\nabla^2 \Psi') \quad (3-49)$$

and

$$\rho \frac{\partial}{\partial z} \left( \frac{\partial^2 \Phi}{\partial t^2} \right) - \rho \frac{\partial}{\partial x} \left( \frac{\partial^2 \Psi'}{\partial t^2} \right) = (\lambda + 2G) \frac{\partial}{\partial z} (\nabla^2 \Phi) - G \frac{\partial}{\partial x} (\nabla^2 \Psi') \quad (3-50)$$

Equations (3-49) and (3-50) are satisfied if

$$\frac{\partial^2 \Phi}{\partial t^2} = \frac{\lambda + 2G}{\rho} \nabla^2 \Phi = v_P^2 \nabla^2 \Phi \quad (3-51)$$

and

$$\frac{\partial^2 \Psi'}{\partial t^2} = \left( \frac{G}{\rho} \right) \nabla^2 \Psi' = v_S^2 \nabla^2 \Psi' \quad (3-52)$$

Now, by assuming a solution for a sinusoidal wave traveling in the positive  $x$ -direction, expressions for  $\Phi$  and  $\Psi'$  can be written

$$\Phi = F(z) \exp [i(\omega t - Nx)] \quad (3-53)$$

and

$$\Psi = \mathbf{G}(z) \exp [i(\omega t - Nx)] \quad (3-54)$$

The functions  $\mathbf{F}(z)$  and  $\mathbf{G}(z)$  describe the variation in amplitude of the wave as a function of depth, and  $N$  is the wave number defined by

$$N = \frac{2\pi}{L}$$

where  $L$  is the wave length.

Now, substituting the expressions for  $\Phi$  and  $\Psi$  from Eqs. (3-53) and (3-54) into Eqs. (3-51) and (3-52) yields

$$-\frac{\omega^2}{v_P^2} \mathbf{F}(z) = -N^2 \mathbf{F}(z) + \mathbf{F}''(z) \quad (3-55)$$

and

$$-\frac{\omega^2}{v_S^2} \mathbf{G}(z) = -N^2 \mathbf{G}(z) + \mathbf{G}''(z) \quad (3-56)$$

By rearranging Eqs. (3-55) and (3-56), we get

$$\mathbf{F}''(z) - \left(N^2 - \frac{\omega^2}{v_P^2}\right) \mathbf{F}(z) = 0 \quad (3-57)$$

and

$$\mathbf{G}''(z) - \left(N^2 - \frac{\omega^2}{v_S^2}\right) \mathbf{G}(z) = 0 \quad (3-58)$$

where  $\mathbf{F}''(z)$  and  $\mathbf{G}''(z)$  are derivatives with respect to  $z$ . Now, letting

$$q^2 = \left(N^2 - \frac{\omega^2}{v_P^2}\right) \quad (3-59)$$

and

$$s^2 = \left(N^2 - \frac{\omega^2}{v_S^2}\right) \quad (3-60)$$

Eqs. (3-57) and (3-58) can be rewritten as

$$\mathbf{F}''(z) - q^2 \mathbf{F}(z) = 0 \quad (3-61)$$

and

$$\mathbf{G}''(z) - s^2 \mathbf{G}(z) = 0 \quad (3-62)$$

The solutions of Eqs. (3-61) and (3-62) can be expressed in the form

$$\mathbf{F}(z) = A_1 \exp(-qz) + B_1 \exp(qz) \quad (3-63)$$

$$\mathbf{G}(z) = A_2 \exp(-sz) + B_2 \exp(sz) \quad (3-64)$$

A solution that allows the amplitude of the wave to become infinite with depth cannot be tolerated; therefore,

$$B_1 = B_2 = 0$$

and Eqs. (3-53) and (3-54) become

$$\Phi = A_1 \exp[-qz + i(\omega t - Nx)] \quad (3-65)$$

and

$$\Psi = A_2 \exp[-sz + i(\omega t - Nx)] \quad (3-66)$$

Now, the boundary conditions specifying no stress at the surface of a half-space imply that  $\sigma_z = 0$  and  $\tau_{zx} = 0$  at the surface  $z = 0$ . Therefore, at the surface,

$$\sigma_z = \lambda \bar{\epsilon} + 2G\epsilon_z = \lambda \bar{\epsilon} + 2G \frac{\partial w}{\partial z} = 0$$

and

$$\tau_{zx} = G\gamma_{zx} = G \left( \frac{\partial w}{\partial x} + \frac{\partial u}{\partial z} \right) = 0$$

Using the definitions of  $u$  and  $w$  and the solutions for  $\Phi$  and  $\Psi$  from Eqs. (3-65) and (3-66), the above equations for boundary conditions can be written

$$\sigma_z|_{z=0} = A_1[(\lambda + 2G)q^2 - \lambda N^2] - 2iA_2GNs = 0 \quad (3-67)$$

and

$$\tau_{zx}|_{z=0} = 2iA_1Nq + A_2(s^2 + N^2) = 0 \quad (3-68)$$

Upon rearranging, Eqs. (3-67) and (3-68) become

$$\frac{A_1(\lambda + 2G)q^2 - \lambda N^2}{A_2} - 1 = 0 \quad (3-69)$$

and

$$\frac{A_1}{A_2} \frac{2qiN}{(s^2 + N^2)} + 1 = 0 \quad (3-70)$$

Now we add these two equations to get

$$\frac{(\lambda + 2G)q^2 - \lambda N^2}{2iGNs} = -\frac{2qiN}{s^2 + N^2} \quad (3-71)$$

and cross-multiply in Eq. (3-71) to obtain

$$4qGsN^2 = (s^2 + N^2)[(\lambda + 2G)q^2 - \lambda N^2] \quad (3-72)$$

Squaring both sides of Eq. (3-72) and introducing  $q$  from Eq. (3-59) and  $s$  from Eq. (3-60), we get

$$16G^2N^4 \left( N^2 - \frac{\omega^2}{v_P^2} \right) \left( N^2 - \frac{\omega^2}{v_S^2} \right) = \left[ (\lambda + 2G) \left( N^2 - \frac{\omega^2}{v_P^2} \right) - \lambda N^2 \right]^2 \left[ N^2 + \left( N^2 - \frac{\omega^2}{v_S^2} \right) \right]^2 \quad (3-73)$$

Now, dividing through by  $G^2N^8$ , we obtain

$$16 \left( 1 - \frac{\omega^2}{v_P^2 N^2} \right) \left( 1 - \frac{\omega^2}{v_S^2 N^2} \right) = \left[ 2 - \left( \frac{\lambda + 2G}{G} \right) \left( \frac{\omega^2}{v_P^2 N^2} \right) \right]^2 \left( 2 - \frac{\omega^2}{v_S^2 N^2} \right)^2 \quad (3-74)$$

Then, using the following relationships derived in the footnote\* gives

$$\frac{\omega^2}{v_P^2 N^2} = \frac{v_R^2}{v_P^2} = \alpha^2 K^2 \quad (3-75)$$

$$\frac{\omega^2}{v_S^2 N^2} = \frac{v_R^2}{v_S^2} = K^2 \quad (3-76)$$

$$\frac{\lambda + 2G}{G} = \frac{1}{\alpha^2} = \frac{2 - 2\nu}{1 - 2\nu} \quad (3-77)$$

\* By definition,

$$N = \frac{2\pi}{L}$$

or

$$L = \frac{2\pi}{N}$$

(Let  $L_R$  and  $v_R$  be the wave length and velocity, respectively, of the surface wave.)

Eq. (3-74) can be written

$$16(1 - \alpha^2 K^2)(1 - K^2) = \left( 2 - \frac{1}{\alpha^2} \alpha^2 K^2 \right)^2 (2 - K^2)^2 \quad (3-78)$$

After expansion and rearrangement, Eq. (3-78) becomes

$$K^6 - 8K^4 + (24 - 16\alpha^2)K^2 + 16(\alpha^2 - 1) = 0 \quad (3-79)$$

Equation (3-79) can be considered a cubic equation in  $K^2$  and real valued solutions can be found for given values of  $\nu$ . The quantity  $K$  represents a ratio between the velocity of the surface wave and the velocity of the shear wave.

Also,

$$L_R = \frac{v_R}{f} = \frac{2\pi v_R}{\omega}$$

and, from above,

$$L_R = \frac{2\pi}{N} = \frac{v_R 2\pi}{\omega}$$

therefore,

$$N = \frac{\omega}{v_R}$$

and

$$N^2 = \frac{\omega^2}{v_R^2}$$

Let  $K$  and  $\alpha$  be defined such that

$$\frac{v_R^2}{v_S^2} = K^2 \quad \text{and} \quad \frac{v_R^2}{v_P^2} = \alpha^2 K^2$$

Then

$$\frac{\omega^2}{v_P^2 N^2} = \frac{v_R^2}{v_P^2} = \alpha^2 K^2$$

and

$$\frac{\omega^2}{v_S^2 N^2} = \frac{v_R^2}{v_S^2} = K^2$$

Substitution of  $v_S$  and  $v_P$  from Eqs. (3-46) and (3-48) gives

$$\frac{1}{\alpha^2} = \frac{v_P^2}{v_S^2} = \frac{\frac{\lambda + 2G}{\rho}}{\frac{\rho}{\lambda}} = \frac{\lambda + 2G}{G}$$

and using

$$\nu = \frac{\lambda}{2(\lambda + G)}$$

we get

$$\frac{\lambda + 2G}{G} = \frac{2 - 2\nu}{1 - 2\nu} = \frac{1}{\alpha^2}$$

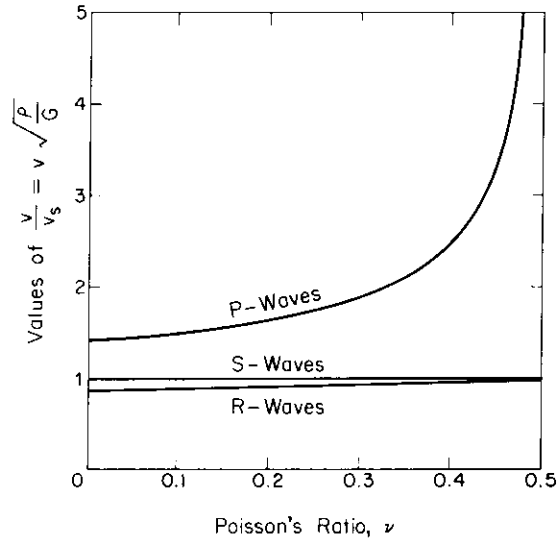


Figure 3-13. Relation between Poisson's ratio,  $\nu$ , and velocities of propagation of compression (P), shear (S), and Rayleigh (R) waves in a semi-infinite elastic medium (from Richart, 1962).

From this solution it is clear that  $K^2$  is independent of the frequency of the wave; consequently, the velocity of the surface wave is independent of frequency and is nondispersive.

Ratios of  $v_R/v_S$  and  $v_P/v_S$  can be obtained from Eq. (3-79) for values of Poisson's ratio  $\nu$  from 0 to 0.5. Curves of these ratios as a function of  $\nu$  are shown in Fig. 3-13.

*Rayleigh-Wave Displacement*

So far, a relationship for the ratio of the Rayleigh-wave velocity to the shear-wave velocity has been obtained, but additional information about the Rayleigh wave can be determined by obtaining the expressions for  $u$  and  $w$  in terms of known quantities. Upon substituting the expressions for  $\Phi$  and  $\Psi$  from Eqs. (3-65) and (3-66) into the expressions for  $u$  and  $w$ , we get

$$u = \frac{\partial\Phi}{\partial x} + \frac{\partial\Psi}{\partial z}$$

$$= -A_1 iN \exp[-qz + i(\omega t - Nx)] - A_2 s \exp[-sz + i(\omega t - Nx)]$$

(3-80)

and

$$w = \frac{\partial\Phi}{\partial z} - \frac{\partial\Psi}{\partial x}$$

$$= -A_1 iN \exp[-qz + i(\omega t - Nx)] + A_2 iN \exp[-sz + i(\omega t - Nx)]$$

(3-81)

From Eq. (3-70) we can get

$$A_2 = -\frac{2qiNA_1}{s^2 + N^2}$$

and substitution of  $A_2$  into Eqs. (3-80) and (3-81) gives

$$u = A_1 \left[ -iN \exp(-qz) + \frac{2iqsN}{s^2 + N^2} \exp(-sz) \right] \exp i(\omega t - Nx) \quad (3-82)$$

and

$$w = A_1 \left[ \frac{2qN^2}{s^2 + N^2} \exp(-sz) - q \exp(-qz) \right] \exp i(\omega t - Nx) \quad (3-83)$$

Equations (3-82) and (3-83) can be rewritten

$$u = A_1 Ni \left\{ -\exp \left[ -\frac{q}{N}(zN) \right] + \frac{2\frac{q}{N}\frac{s}{N}}{\frac{s^2}{N^2} + 1} \exp \left[ -\frac{s}{N}(zN) \right] \right\}$$

$$\times \exp i(\omega t - Nx) \quad (3-84)$$

and

$$w = A_1 N \left\{ \frac{2\frac{q}{N}}{\frac{s^2}{N^2} + 1} \exp \left[ -\frac{s}{N}(zN) \right] - \frac{q}{N} \exp \left[ -\frac{q}{N}(zN) \right] \right\}$$

$$\times \exp i(\omega t - Nx) \quad (3-85)^*$$

Now, from Eqs. (3-84) and (3-85), the variation of  $u$  and  $w$  with depth can be expressed as

$$U(z) = -\exp \left[ -\frac{q}{N}(zN) \right] + \frac{2\frac{q}{N}\frac{s}{N}}{\frac{s^2}{N^2} + 1} \exp \left[ -\frac{s}{N}(zN) \right] \quad (3-86)$$

and

$$W(z) = \frac{2\frac{q}{N}}{\frac{s^2}{N^2} + 1} \exp \left[ -\frac{s}{N}(zN) \right] - \frac{q}{N} \exp \left[ -\frac{q}{N}(zN) \right] \quad (3-87)$$

\* The significance of the presence of  $i$  in the expression for  $u$  (Eq. 3-84) and its absence in the expression for  $w$  (Eq. 3-85) is that the  $u$ -component of displacement is  $90^\circ$  out of phase with the  $w$ -component of displacement.



The functions  $U(z)$  and  $W(z)$  represent the spatial variations of the displacements  $u$  and  $w$ . Equations (3-59) and (3-60) can be rewritten

$$\frac{q^2}{N^2} = 1 - \frac{\omega^2}{N^2 v_p^2} \quad (3-88)$$

and

$$\frac{s^2}{N^2} = 1 - \frac{\omega^2}{N^2 v_s^2} \quad (3-89)$$

and then, using Eqs. (3-75) and (3-76), Eqs. (3-88) and (3-89) can be reduced to

$$\frac{q^2}{N^2} = 1 - \alpha^2 K^2 \quad (3-90)$$

and

$$\frac{s^2}{N^2} = 1 - K^2 \quad (3-91)$$

Now,  $U(z)$  and  $W(z)$  can be evaluated in terms of the wave number  $N$  for any given value of Poisson's ratio. For example, if  $\nu = \frac{1}{4}$ ,  $U(z)$  and  $W(z)$  are given by

$$U(z) = -\exp[-0.8475(zN)] + 0.5773 \exp[-0.3933(zN)] \quad (3-92)$$

and

$$W(z) = 0.8475 \exp[-0.8475(zN)] - 1.4679 \exp[-0.3933(zN)] \quad (3-93)$$

Figure 3-14 shows curves for  $U(z)$  and  $W(z)$  vs. distance from the surface in wave lengths of the Rayleigh wave ( $L_R$ ) for Poisson's ratios of 0.25, 0.33, 0.40, and 0.50.

#### Wave System at Surface of Half-Space

In preceding paragraphs expressions have been determined for the wave velocities of the three principal waves which occur in an elastic half-space. Knowing these velocities, we can easily predict the order in which waves will arrive at a given point due to a disturbance at another point. In addition to predicting the order of arrival of the waves along the surface, Lamb (1904) described in detail the surface motion that occurs at large distances from a point source at the surface of an ideal medium.

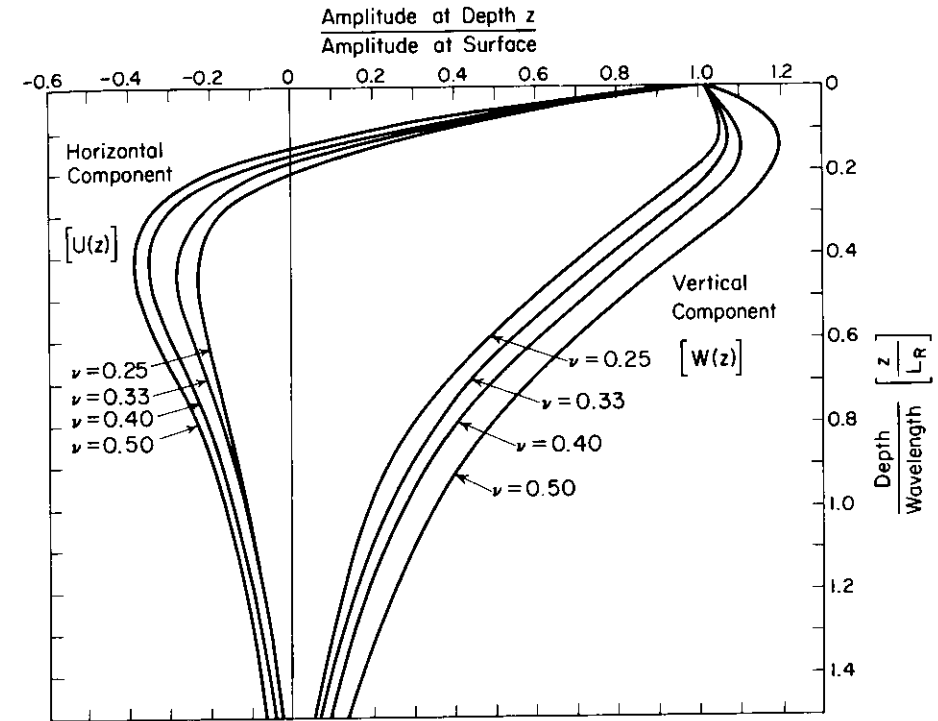


Figure 3-14. Amplitude ratio vs. dimensionless depth for Rayleigh wave.

Under the conditions considered by Lamb, a disturbance spreads out from the point source in the form of a symmetrical annular-wave system. The initial form of this wave system will depend on the input impulse; but if the input is of short duration, the characteristic wave system shown in Fig. 3-15 will develop. This wave system has three salient features corresponding to the arrivals of the  $P$ -wave,  $S$ -wave, and  $R$ -wave. The horizontal and vertical components of particle motion are shown separately in Fig. 3-15. A particle at the surface first experiences a displacement in the form of an oscillation at the arrival of the  $P$ -wave, followed by a relatively quiet period leading up to another oscillation at the arrival of the  $S$ -wave. These events are referred to by Lamb as the *minor tremor* and are followed by a much larger magnitude oscillation, the *major tremor*, at the time of arrival of the  $R$ -wave.

The time interval between wave arrivals becomes greater and the amplitude of the oscillations becomes smaller with increasing distance from the source. In addition, the minor tremor decays more rapidly than the major tremor. It is evident, therefore, that the  $R$ -wave is the most significant disturbance along the surface of a half-space and, at large distances from the source, may be the only clearly distinguishable wave.

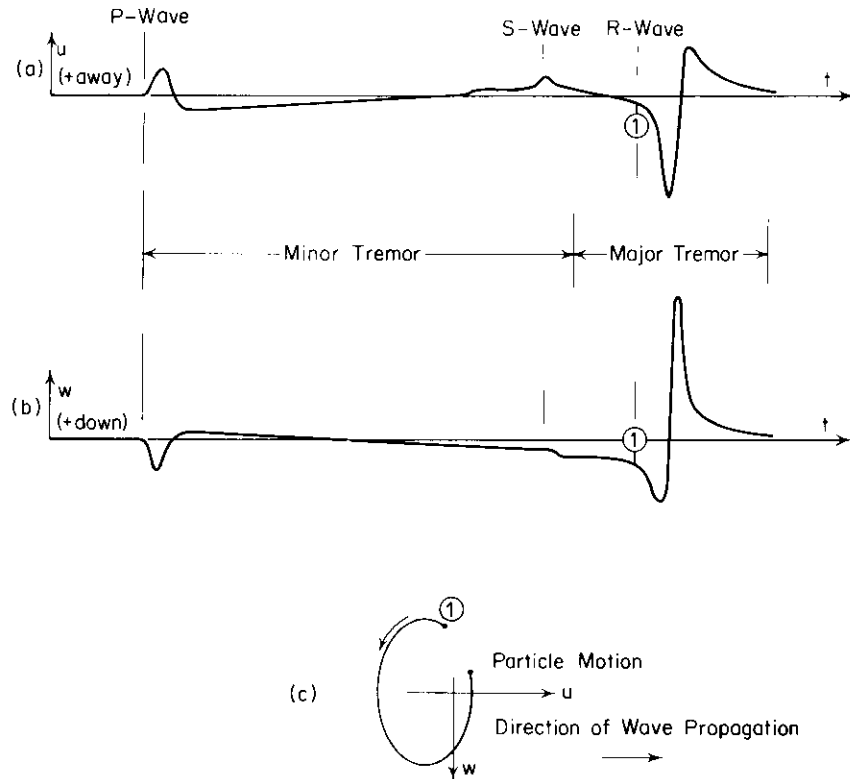


Figure 3-15. Wave system from surface point source in ideal medium (after Lamb, 1904).

By combining the horizontal and vertical components of particle motion starting at points ① in Figs. 3-15a and b, the locus of *surface-particle motion* for the *R-wave* can be drawn as shown in Fig. 3-15c. The path of the particle motion describes a retrograde ellipse, in contrast to the prograde-ellipse motion associated with water waves.

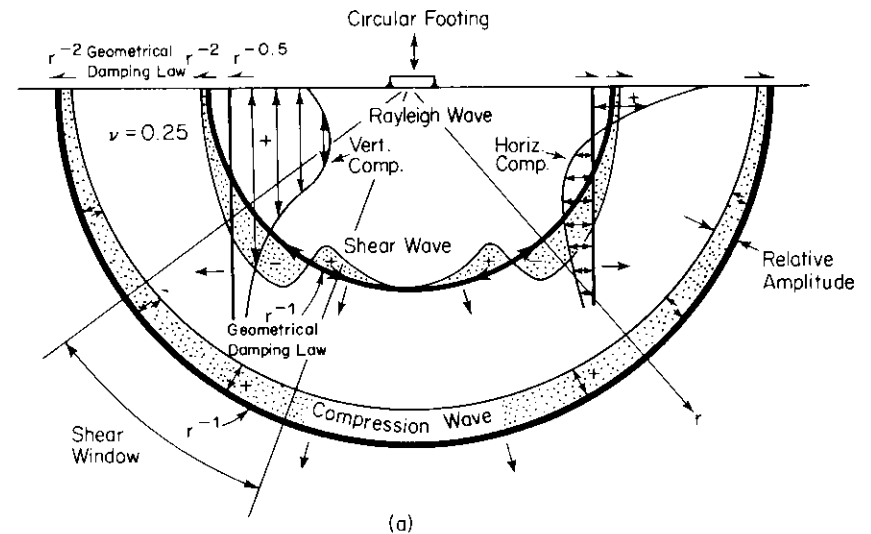
Most real earth-motion records are more complex than indicated in Fig. 3-15, due to the variation between ideal elastic-half-space theory and the real earth. Some of the deviations which account for the differences between the ideal and the real earth are (1) layering in the earth, (2) inhomogeneities in the earth, (3) the curvature of the earth's surface, and (4) multishock input sources instead of single impulse.

*Wave Field Generated by Circular Footing*

So far, the basic theory of waves in an ideal elastic half-space has been presented. Now we need to combine and expand on this information to

obtain a picture of the wave field generated by a circular footing undergoing vertical oscillations at the surface of a half-space. The energy coupled into the ground by a footing is transmitted away by a combination of *P*-, *S*-, and *R*-waves.

The basic features of this wave field at a relatively large distance\* from the source are shown in Fig. 3-16a. The distance from the source of waves to each wave front in Fig. 3-16a is drawn in proportion to the velocity of each wave for a medium with  $\nu = \frac{1}{4}$ . The *body waves* propagate radially outward from the source along a hemispherical wave front (heavy dark lines in Fig. 3-16a) and the *Rayleigh wave* propagates radially outward along a cylindrical wave front. All of the waves encounter an increasingly larger volume of



Wave Type	Per Cent of Total Energy
Rayleigh	67
Shear	26
Compression	7

(b)

Figure 3-16. Distribution of displacement waves from a circular footing on a homogeneous, isotropic, elastic half-space (from Woods, 1968).

\* According to Lysmer (1966), a distance of 2.5 wave lengths from the source is a large distance.

material as they travel outward; thus, the energy density in each wave decreases with distance from the source. This decrease in energy density or decrease in displacement amplitude is called *geometrical damping*. It can be shown (Ewing, Jardetzky, and Press, 1967, for example) that the amplitude of the body waves decreases in proportion to the ratio of  $1/r$  ( $r$  is the distance from the input source) except along the surface of the half-space, where the amplitude decreases as  $1/r^2$ . The amplitude of the Rayleigh wave decreases as  $1/\sqrt{r}$ .

The particle motion associated with the *compression wave* is a push-pull motion parallel to the direction of the wave front; the particle motion associated with the *shear wave* is a transverse displacement normal to the direction of the wave front; and the particle motion associated with the *Rayleigh wave* is made up of two components (horizontal and vertical) which vary with depth as shown in Fig. 3-16a. The shaded zones along the wave fronts for the body waves indicate the relative amplitude of particle displacement as a function of the dip angle (the angle measured downward from the surface at the center of the source) as calculated by Miller and Pursey (1954) and T. Hirona (1948). The region of the shear-wave front in which the larger amplitudes occur is referred to as the *shear window*.

For a vertically oscillating, uniformly distributed, circular energy source on the surface of a homogeneous, isotropic, elastic half-space, Miller and Pursey (1955) determined the distribution of total input energy among the three elastic waves to be (as shown on Fig. 3-16b) 67 per cent Rayleigh wave, 26 per cent shear wave, and 7 per cent compression wave. The facts that two-thirds of the total input energy is transmitted away from a vertically oscillating footing by the Rayleigh wave and that the Rayleigh wave decays much more slowly with distance than the body waves indicate that *the Rayleigh wave is of primary concern for foundations on or near the surface of the earth*.

## 4

### ELASTIC WAVES IN LAYERED SYSTEMS

An elastic half-space is appropriate as a model of the earth only as a first approximation. Wave-propagation phenomena resulting from elastic-half-space theory must be further refined to understand elastic-wave propagation in the earth. By considering a *layered half-space* as a model, it is possible to improve the correlation between wave-propagation theory and observed wave phenomena.

#### 4.1 Distribution of Wave Energy at Boundaries

##### *Two Half-Spaces in Contact*

\*In general, when a body wave traveling in an elastic medium encounters an interface with another elastic medium, some of the incident-wave energy will be reflected into the first medium and some energy will be transmitted into the second medium. Using the theory of elasticity, Zoeppritz (1919) determined the nature of the reflected and transmitted waves and the distribution of energy between these waves. There are, of course, two body waves to consider, but one of these—the shear wave—must be separated into two components before we may consider energy partition at an interface. The two components to be considered are the *SV-wave*, the component whose motion is in a plane perpendicular to the plane of the interface, and the *SH-wave*, the component whose motion is in a plane parallel to the interface.

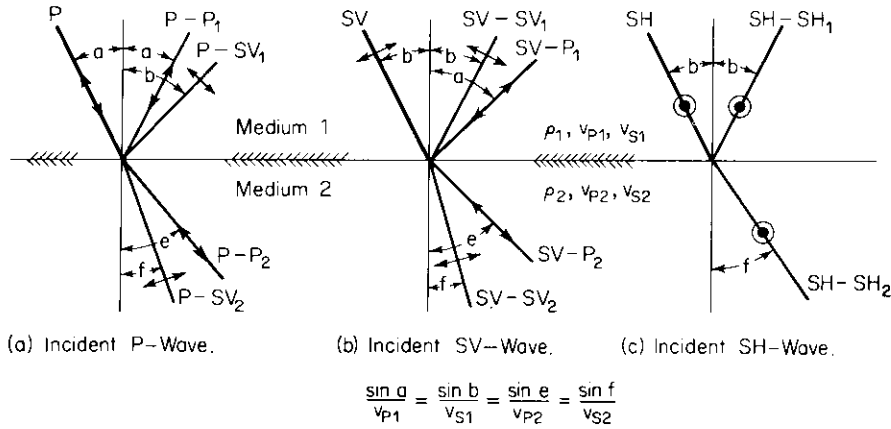


Figure 4-1. Partition of elastic wave at interface between two elastic media.

For an incident  $P$ -wave ( $P$ ), as shown in Fig. 4-1a, there will be four resultant waves: (1) a reflected  $P$ -wave ( $P-P_1$ ), (2) a reflected  $SV$ -wave ( $P-SV_1$ ), (3) a refracted  $P$ -wave ( $P-P_2$ ), and (4) a refracted  $SV$ -wave ( $P-SV_2$ ). The two components of the shear wave,  $SV$  and  $SH$ , must be considered separately in describing the resultant waves at an interface. The resultant waves from an incident  $SV$ -wave are: (1) a reflected  $SV$ -wave ( $SV-SV_1$ ), (2) a reflected  $P$ -wave ( $SV-P_1$ ), (3) a refracted  $SV$ -wave ( $SV-SV_2$ ), and (4) a refracted  $P$ -wave ( $SV-P_2$ ), shown in Fig. 4-1b. While incident  $P$  and  $SV$ -waves each produce resultant  $P$ - and  $SV$ -waves, an incident  $SH$ -wave produces only  $SH$ -waves. The  $SH$ -wave does not produce a  $P$ -wave because it has no component normal to the plane of the interface. The resultant waves from an incident  $SH$ -wave are reflected  $SH$ -wave ( $SH-SH_1$ ) and refracted  $SH$ -wave ( $SH-SH_2$ ), shown in Fig. 4-1c.

The angle at which a resultant wave leaves the interface depends on the angle at which the incident wave approaches the interface and the ratio of wave velocities of the two media. Exit angles for all waves can be found from Snell's law:

$$\frac{\sin a}{v_{P1}} = \frac{\sin b}{v_{S1}} = \frac{\sin e}{v_{P2}} = \frac{\sin f}{v_{S2}} \quad (4-1)$$

where the angles  $a$ ,  $b$ ,  $e$ , and  $f$  are measured from the normal to the interface and are defined in Fig. 4-1, and where

- $v_{P1}$  = velocity of the  $P$ -wave in medium 1,
- $v_{S1}$  = velocity of the  $S$ -wave in medium 1,
- $v_{P2}$  = velocity of the  $P$ -wave in medium 2, and
- $v_{S2}$  = velocity of the  $S$ -wave in medium 2.

Zoeppritz expressed the distribution of energy among the resultant waves in terms of incident- and resultant-wave amplitudes. (The energy transmitted by an elastic wave is proportional to the square of the displacement amplitude of the wave.) The equations are written as follows:

For incident  $P$ -wave—

$$(A - C) \sin a + D \cos b - E \sin e + F \cos f = 0 \quad (4-2)$$

$$(A + C) \cos a + D \sin b - E \cos e - F \sin f = 0 \quad (4-3)$$

$$-(A + C) \sin 2a + D \frac{v_{P1}}{v_{S1}} \cos 2b + E \frac{\rho_2}{\rho_1} \left( \frac{v_{S2}}{v_{S1}} \right)^2 \frac{v_{P1}}{v_{P2}} \sin 2e - F \frac{\rho_2}{\rho_1} \left( \frac{v_{S2}}{v_{S1}} \right)^2 \frac{v_{P1}}{v_{S2}} \cos 2f = 0 \quad (4-4)$$

$$-(A - C) \cos 2b + D \frac{v_{S1}}{v_{P1}} \sin 2b + E \frac{\rho_2}{\rho_1} \frac{v_{P2}}{v_{P1}} \cos 2f + F \frac{\rho_2}{\rho_1} \frac{v_{S2}}{v_{P1}} \sin 2f = 0 \quad (4-5)$$

For incident  $SV$ -wave—

$$(B + D) \sin b + C \cos a - E \cos e - F \sin f = 0 \quad (4-6)$$

$$(B - D) \cos b + C \sin a + E \sin e - F \cos f = 0 \quad (4-7)$$

$$(B + D) \cos 2b - C \frac{v_{S1}}{v_{P1}} \sin 2a + E \frac{\rho_2}{\rho_1} \frac{v_{S2}^2}{v_{S1} v_{P2}} \sin 2e - F \frac{\rho_2}{\rho_1} \frac{v_{S2}}{v_{S1}} \cos 2f = 0 \quad (4-8)$$

$$-(B - D) \sin 2b + C \frac{v_{P1}}{v_{S1}} \cos 2b + E \frac{\rho_2}{\rho_1} \frac{v_{P2}}{v_{S1}} \cos 2f + F \frac{\rho_2}{\rho_1} \frac{v_{S2}}{v_{S1}} \sin 2f = 0 \quad (4-9)$$

For incident  $SH$ -wave—

$$B + D - F = 0 \quad (4-10)$$

$$B - D - \frac{\rho_2}{\rho_1} \frac{v_{S2}}{v_{S1}} \frac{\cos f}{\cos b} F = 0 \quad (4-11)$$

where

- $A$  = amplitude of incident  $P$ -wave,
- $B$  = amplitude of incident  $S$ -wave,
- $C$  = amplitude of reflected  $P$ -wave,
- $D$  = amplitude of reflected  $S$ -wave,

$E$  = amplitude of refracted  $P$ -wave,  
 $F$  = amplitude of refracted  $S$ -wave,  
 $\rho_1$  = density of medium 1,  
 $\rho_2$  = density of medium 2,

and the angles  $a, b, e,$  and  $f$  are defined in Fig. 4-1.

After Eqs. (4-2) through (4-11) have been studied, it can be concluded that the amplitude of each resultant wave is a function of (1) the angle of incidence of the incident wave, (2) the ratio of the wave velocities in the two media, and (3) the ratio of densities of the two media. Therefore, for two specified media the amplitude of resultant waves is a function of the incident angle only. It is possible, therefore, to calculate the amplitude of each resultant wave for a given incident wave over a range of incident angles from

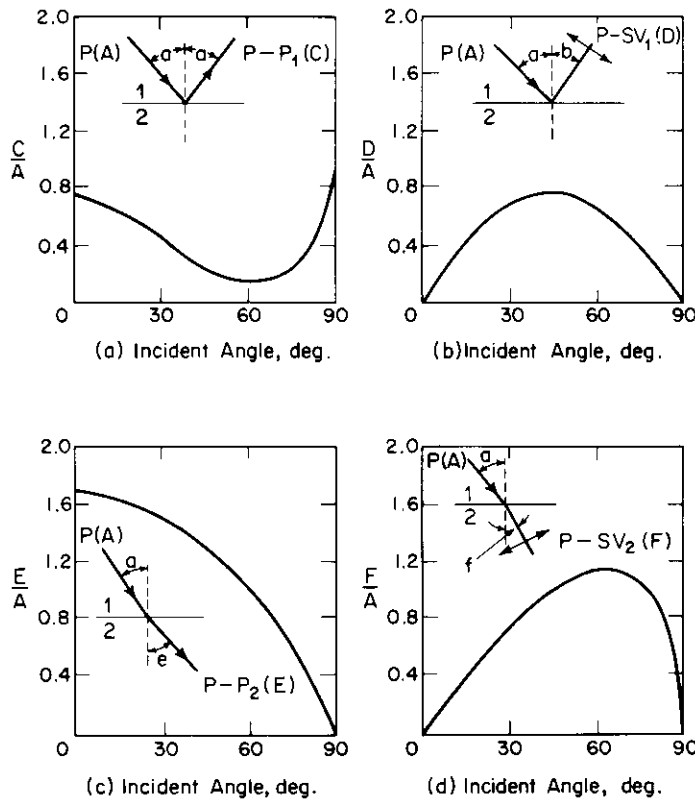


Figure 4-2. Amplitude ratio vs. incident angle for  $P$ -wave (after McCamy et al., 1962).

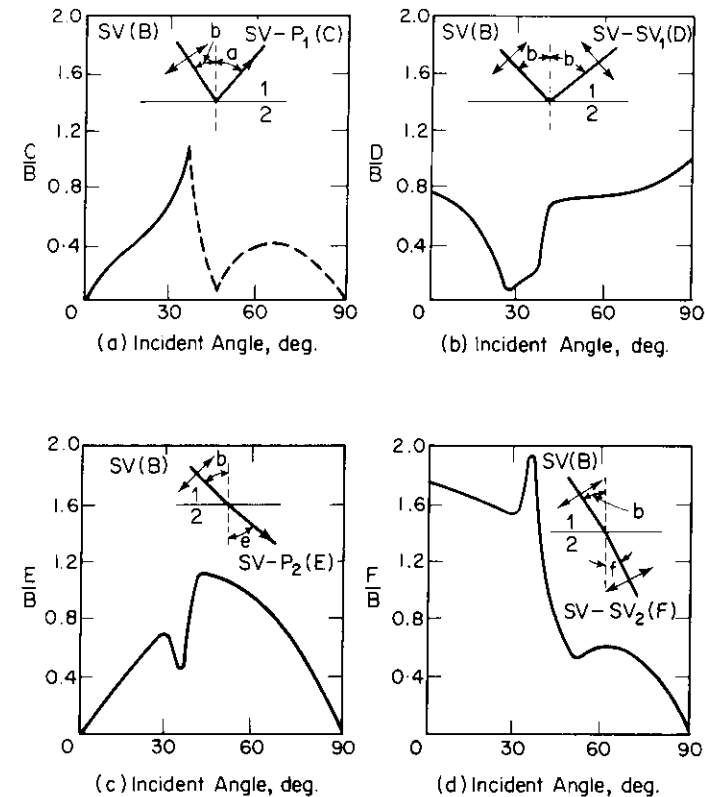


Figure 4-3. Amplitude ratio vs. incident angle for  $SV$ -wave (after McCamy et al., 1962).

$0^\circ$  to  $90^\circ$ . Equations (4-2) through (4-11) can be rearranged and solutions obtained for the ratio of resultant-wave amplitude to incident-wave amplitude. When the results of such calculations are plotted on a diagram of amplitude ratio vs. incident angle, an interesting and potentially useful phenomenon can be observed; namely, for a given incident wave, each resultant wave has relative maxima and minima amplitude ratios, depending on the incident angle. Figures 4-2 and 4-3 are examples of amplitude-ratio-vs.-incident-angle diagrams for a situation where wave velocities and density are greater in medium 1 than in medium 2. It can be seen, for example, in Fig. 4-2a that the amplitude ratio for the reflected  $P$ -wave ( $P-P_1$ ) is a minimum when the angle of incidence of the incoming wave is about  $60^\circ$ . In Fig. 4-3b it is seen that the minimum amplitude ratio for a reflected  $SV$ -wave ( $SV-SV_1$ ) from an incident  $SV$ -wave occurs at an angle of about  $27^\circ$ .

When the velocity of a reflected or refracted wave is greater than that of

the incident wave, there will be a critical angle of incidence for which the angle of reflection or refraction is  $90^\circ$ . For angles of incidence greater than the critical angle, a disturbance which decays rapidly with distance from the interface is created in place of the reflected or refracted wave. This disturbance does not transmit energy away from the interface; therefore, the incident-wave energy is partitioned among the remaining reflected and refracted waves. For incident angles greater than the critical angle, the sine of the exit angle is greater than unity, and complex functions must be introduced in Eqs. (4-2) through (4-11). This doubles the number of equations that must be solved; however, the imaginary amplitude ratios for resultant waves found from these equations have no physical significance, because these waves do not transmit energy away from the interface. The dashed portion of the curve in Fig. 4-3a represents this condition. It can be seen, for example, that for the  $SV-P_1$  wave to vanish, the incident angle must be greater than the critical angle  $i_c$ , which is given by

$$i_c = \arcsin \left( \frac{v_{S1}}{v_{P1}} \sin 90^\circ \right) \quad (4-12)$$

$$i_c = \arcsin \frac{v_{S1}}{v_{P1}} \quad (4-13)$$

It is clear that the critical angle is a function of the ratio  $v_{S1}/v_{P1}$  and this ratio in turn is a function of Poisson's ratio only.

#### Rayleigh Wave at Surface Discontinuity

We know from Chap. 3 that a large part of the total input energy from a surface source is carried away from the source in the form of Rayleigh waves; consequently, it is interesting to determine the mechanism that occurs when a Rayleigh wave encounters an interface of velocity and density contrast. This is essentially a problem of a surface wave at the interface of two quarter-spaces in contact. A complete theory for a surface wave at the interface between the two quarter-spaces is not currently available; however, some work has been reported on a related problem, a Rayleigh wave at a corner (Viktorov, 1958; deBremaecker, 1958; Knopoff and Gangi, 1960; Pilant et al., 1964; Kane and Spence, 1963). At a corner, an incident Rayleigh wave is partitioned among three types of waves: (1) a reflected Rayleigh wave, (2) a transmitted Rayleigh wave, and (3) reflected body waves, as shown in Fig. 4-4. The amount of energy carried away from the corner by each type wave is a function of Poisson's ratio and the corner angle. The ratio of reflected-Rayleigh-wave energy to incident-Rayleigh-wave energy

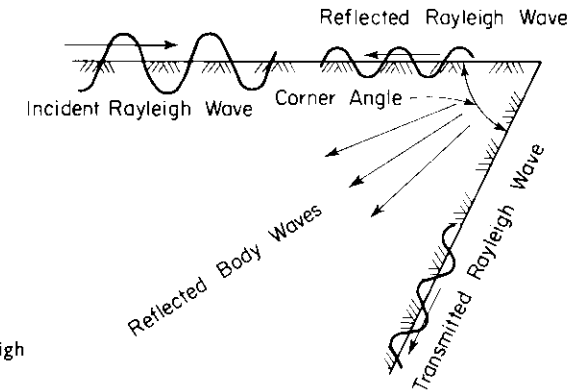


Figure 4-4. Partition of Rayleigh wave energy at a corner.

as a function of the corner angle was determined in model studies by three investigators (Viktorov, 1958; deBremaecker, 1958; Pilant et al., 1964) and is shown in Fig. 4-5. The interesting phenomenon to note is that minimum Rayleigh-wave energy is reflected at a corner angle of about  $80^\circ$ .

While the above information on  $R$ -waves at a corner does not apply directly to the problem of  $R$ -waves along the surface of two quarter-spaces in contact, it does present a basis upon which a qualitative estimate can be made. An incident  $R$ -wave may be partitioned into (1) a reflected  $R$ -wave, (2) reflected body waves, (3) a transmitted  $R$ -wave, (4) refracted body waves, and (5) an interface wave. The distribution of energy among these waves will depend on the angle of the interface and the properties of the two quarter-spaces.

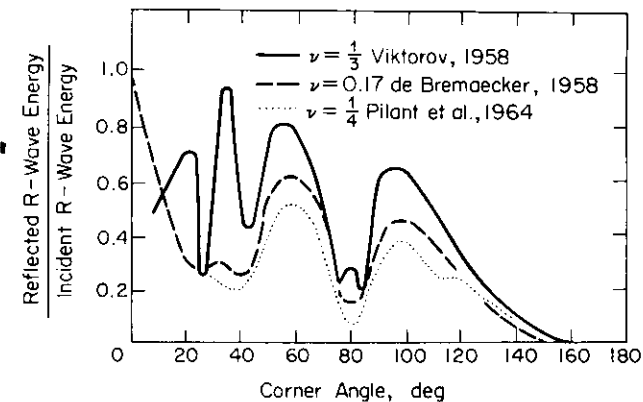


Figure 4-5. Ratio of reflected  $R$ -wave energy to incident  $R$ -wave energy vs. corner angle.

*Implications of Horizontal Layering*

It has been shown that elastic waves will be at least partially reflected at an interface between two media, and if horizontal layering occurs in a half-space—as shown in Fig. 4-6—some energy originating at the surface and traveling into the half-space will return to the surface. If more than one interface exists, waves may be reflected back to the surface from each layer. This reflected energy is partially responsible for the complications in seismic-wave arrival records obtained at recording stations at the surface of the earth.

When any reflected wave returns to the surface of the layered half-space, it encounters the interface between solid and void where it will be totally reflected. Multiple total reflections within the upper layer can generate a second type of surface wave called the *Love wave*. Love first described this wave in 1911; it consists of a horizontally polarized shear wave. Ewing, Jardetzky, and Press (1957) describe the Love wave as a “horizontally polarized shear wave trapped in a superficial layer and propagated by multiple total reflections.”

For Love waves to be confined to the superficial layer, it is necessary that the phase velocity of the Love wave be less than the shear-wave velocity in the next lower layer. A Love wave will not occur if the superficial layer is the higher-velocity layer. The Love wave travels with a velocity which is between the shear-wave velocity of the superficial layer  $v_{S1}$  and the shear-wave velocity of the next lower layer  $v_{S2}$ .

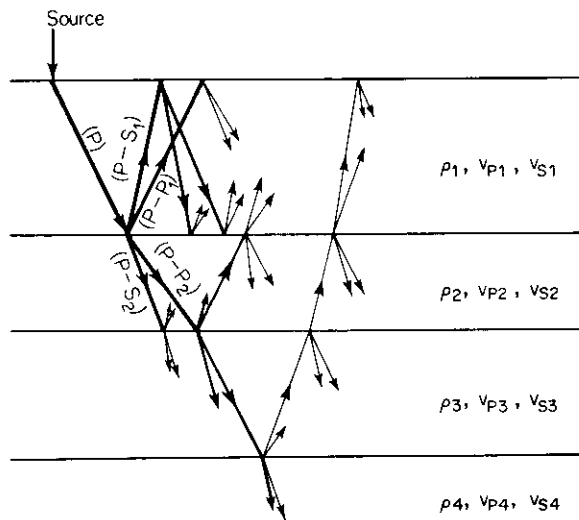


Figure 4-6. Multiple wave reflection and refraction in a layered half-space.

*4.2 Elements of Seismic Methods*

It is difficult to obtain information on *in-situ* soil properties below the uppermost layer of the earth by conventional sampling methods. There are important advantages, therefore, in using seismic methods which can be performed at the surface yet which yield wave propagation and profile information for materials situated at lower depths.

*Direct-Arrival Survey*

In problems concerning vibrations of soils and foundations, it is necessary to use soil moduli obtained from low amplitudes of vibration. Seismic methods are well suited for obtaining these moduli because they are based on elastic-wave theory. It was shown in Eq. (3-48), for example, that to compute the shear modulus it is necessary to determine the density of the material and the shear-wave velocity. At the surface of the earth, it is relatively easy to determine the density, and from seismic techniques it is easy to obtain the velocity of the shear wave, or of the Rayleigh wave, which is practically the same. With this information the shear modulus can be computed.

The wave system shown on Fig. 3-15 was generated by an impulsive source on the surface of an ideal half-space. Three distinct arrivals were indicated which represented waves traveling directly from the source to the receiver. By recording the wave system at several receivers located at increasing distances along a radius from the source, the velocity of all three waves can be determined. Figure 4-7a is a representation of an impulsive energy source and three receiver stations  $R_1$ ,  $R_2$ , and  $R_3$ . Figure 4-7b shows three travel-time curves constructed by plotting the wave system recorded at

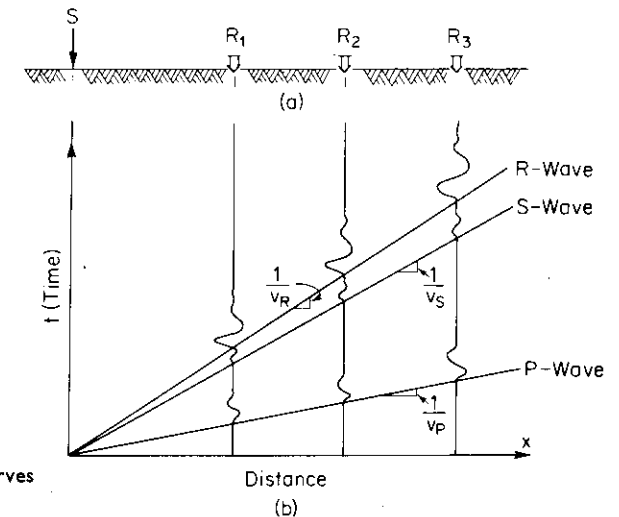


Figure 4-7. Travel-time curves from direct arrivals.

each receiver station. A line drawn through the first arrivals for each identifiable type of wave represents the travel-time curve for that particular wave. The slope of each travel-time curve is the reciprocal of the velocity of the wave it represents. While this technique for determining wave velocities is simple in concept, it is not often easy to accomplish. Wave-arrival records for receivers on real soils are usually complicated, and often the only clearly distinguishable arrival is that of the direct *P*-wave. Of course, if Poisson's ratio for the soil is known or can be estimated,  $v_S$  and  $v_R$  can be found from  $v_P$ , using the curves in Fig. 3-13. The wave-propagation velocities determined from the first *P*-wave arrival are representative only of the material along the surface, and other techniques must be employed to obtain wave-propagation data for lower layers.

*Reflection Survey*

The *P*-wave will be the first wave to arrive at a given point along any given path, and the first arrival is the easiest to identify; therefore, in the following discussions of seismic methods only the *P*-wave will be described. The wave front of the *P*-wave, as shown in Fig. 3-16a, is a hemisphere, but to simplify the diagrams in these discussions, ray theory will be used to represent traveling waves. In ray theory the wave path is represented by a ray which is perpendicular to the wave front and parallel to the direction of wave propagation.

In Fig. 4-8a a half-space with a horizontally oriented surface layer is shown. Assuming *S* to be an impulsive energy source and *R* a receiver, two paths can be traced along which wave energy can travel from *S* to *R*. One path is directly along the surface from *S* to *R*. This is the "direct-wave"

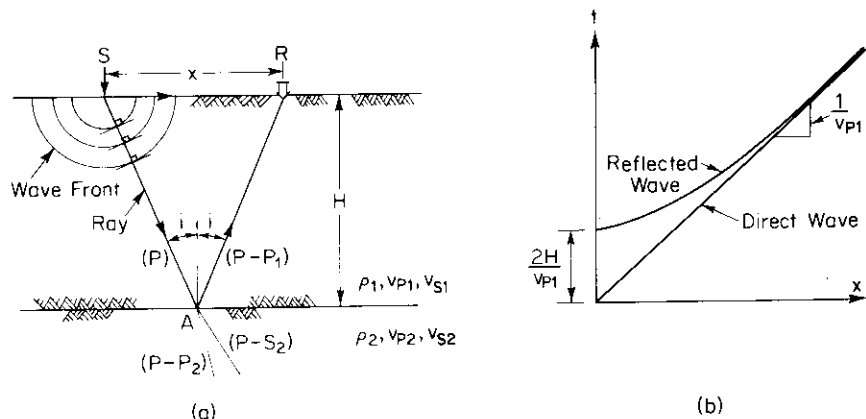


Figure 4-8. Ray paths and travel-time curves for direct and reflected waves.

path and the travel-time equation can be written as

$$t_d = \frac{x}{v_{P1}} \tag{4-14}$$

in which  $t_d$  is the travel time of the direct wave. The other path shown in Fig. 4-8a is composed of the ray from *S* to the interface *A* and back to the surface at *R*. This ray is called the "reflected wave" and its travel-time equation can be determined as follows:

$$\text{Total distance traveled} = 2\overline{SA}$$

$$2\overline{SA} = 2\sqrt{\left(\frac{x}{2}\right)^2 + H^2}$$

therefore,

$$t_r = \frac{\text{Distance traveled}}{\text{Wave velocity}} = \frac{2\overline{SA}}{v_{P1}} = \frac{\sqrt{x^2 + 4H^2}}{v_{P1}} \tag{4-15}$$

Equation (4-15) represents a hyperbolic relationship between  $x$  and  $t_r$ . Figure 4-8b shows the travel-time curves for both the direct wave and the reflected wave. For  $x$  very small,  $t_r$  is simply  $2H/v_{P1}$ ; for  $x$  very large,  $t_r$  approaches  $t_d$  asymptotically.

To perform a reflection survey, the arrival times for the direct and reflected waves are recorded for receivers at the source and at several distances from the source. Then the travel-time curves are plotted. For a layer in which the velocity is not a function of depth, both  $v_{P1}$  and  $H$  can be found. From the direct wave,  $v_{P1}$  is determined ( $v_{P1}$  = reciprocal of slope of travel-time curve); and then from the reflected wave the  $(x = 0)$ -intercept is scaled. The depth of the layer can be determined from the scaled  $(x = 0)$ -intercept value. If the wave velocity in the upper layer is a function of depth, the average wave velocity may be determined from the  $(x = 0)$ -intercept providing the thickness  $H$  can be determined independently. Reflections may also be recorded from additional deeper interfaces, if they exist. For an analysis of this more complex reflection problem, see Griffiths and King (1965) or Ewing, Jardetzky, and Press (1957).

There are limitations to the reflection method, however, the most important being that the reflected *P*-wave arrives at a recording station after the receiver has already been excited by direct waves. Under these circumstances, it is often difficult to distinguish clearly the exact time of the reflected-wave arrival. For this reason a seismic method which makes use of first arrivals only is a distinct advantage. The refraction survey described next is based on first arrivals only.



Refraction Survey

**Horizontal layering.** If the upper layer of a horizontally layered half-space has wave velocities lower than those of the second layer, a critical angle of incidence (see Sec. 4.1) can be found for a *P*-wave which originates at the surface and intersects the interface. The refracted *P*-wave (*P*-*P*<sub>2</sub>) generated by the critically incident *P*-wave will travel parallel to the interface in the lower medium, as shown in Fig. 4-9a. From ray theory, it would not be expected that this critically refracted wave could be detected at the surface. However, it can be shown by elasticity theory that the refracted wave causes a disturbance along the interface and that this disturbance generates a wave in the upper medium (Fig. 4-9b). This new wave is called the *head wave*, and travels at a velocity *v*<sub>*P*1</sub> in a direction inclined at (90° - *i*<sub>*c*</sub>) to the interface where *i*<sub>*c*</sub> is the critical angle of incidence.

All receivers along the surface at a distance from the source equal to or greater than (2*H* tan *i*<sub>*c*</sub>) will record a head-wave arrival. At receivers close to the source in Fig. 4-10 (*R*<sub>1</sub>, *R*<sub>2</sub>, . . .) the direct wave will arrive before either the reflected wave or the head wave, but there is some receiver *R*<sub>*n*</sub> at which the head wave will arrive before either of the other waves because it travels for a significant time in the higher-velocity lower medium. This wave—composed of the initial *P*-wave from *S* to *A*, the critically refracted wave from *A* to *B*, and the head wave from *B* to *R*<sub>*n*</sub>—will be referred to as the “refracted wave.”

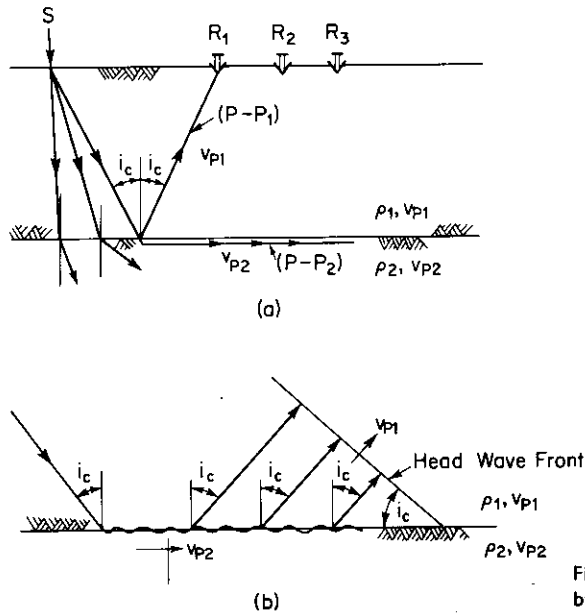


Figure 4-9. Head wave generated by critically refracted *P*-wave.

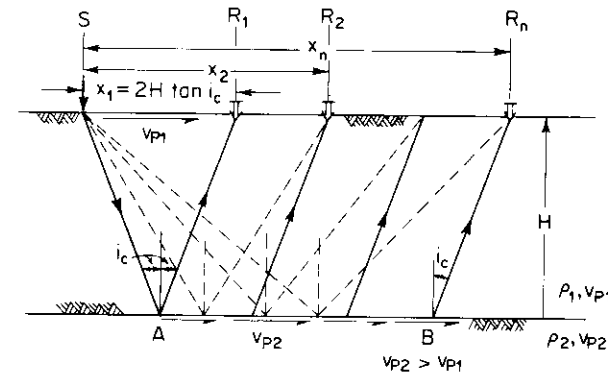


Figure 4-10. Ray paths for direct and head waves.

Travel-time equations can be written for the direct wave and the refracted wave. The travel time *t*<sub>*d*</sub> for the direct wave is given by Eq. (4-14) and is represented in Fig. 4-11b by the straight line through the origin with a slope of 1/*v*<sub>*P*1</sub>. Using the notation in Fig. 4-11a, the travel time *t*<sub>*h*</sub> for the refracted wave can be written as follows:

$$t_h = \frac{H}{v_{P1} \cos i_c} + \frac{1}{v_{P2}} (x - 2H \tan i_c) + \frac{H}{v_{P1} \cos i_c} \quad (4-16)$$

or

$$t_h = \frac{x}{v_{P2}} + 2H \left( \frac{1}{v_{P1} \cos i_c} - \frac{\tan i_c}{v_{P2}} \right) \quad (4-17)$$

Using the relationships

$$\sin i_c = \frac{v_{P1}}{v_{P2}} \quad \text{and} \quad \cos i_c = \sqrt{1 - \frac{v_{P1}^2}{v_{P2}^2}}$$

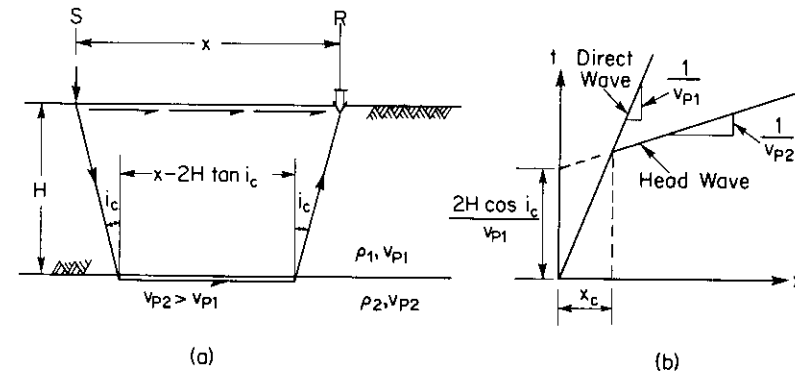


Figure 4-11. Ray paths and travel-time curves for direct and head waves.

Eq. 4-17 can be reduced to

$$t_h = \frac{x}{v_{P2}} + \frac{2H \cos i_c}{v_{P1}} = \frac{x}{v_{P2}} + 2H \sqrt{\frac{1}{v_{P1}^2} - \frac{1}{v_{P2}^2}} \quad (4-18)$$

Equation (4-18) represents a straight line in the  $x-t$  plane with a slope of  $1/v_{P2}$  and an intercept on the  $t$ -axis at  $(2H \cos i_c)/v_{P1}$ , as shown in Fig. 4-11b. The distance  $x_c$  from the source to the point at which the direct wave and the refracted wave arrive at the same time is called the *crossover distance* (at  $x_c, t_d = t_h$ ). By substituting  $x_c$  for  $x$  in Eqs. (4-14) and (4-18) and setting these equations equal, an expression for  $x_c$  can be found:

$$t_d = t_h$$

or

$$\frac{x_c}{v_{P1}} = \frac{x_c}{v_{P2}} + \frac{2H \cos i_c}{v_{P1}}$$

from which

$$x_c = 2H \sqrt{\frac{v_{P2} + v_{P1}}{v_{P2} - v_{P1}}} \quad (4-19)$$

Equation (4-19) can be rearranged and solved for the depth of the upper layer:

$$H = \frac{x_c}{2} \sqrt{\frac{v_{P2} - v_{P1}}{v_{P2} + v_{P1}}} \quad (4-20)$$

From a refraction survey three important unknowns can be obtained:  $v_{P1}$ ,  $v_{P2}$ , and  $H$ . Furthermore, this technique for obtaining seismic data is reliable because all data are based on first arrivals.

**Inclined layering.** Up to this point, the analysis of the refraction technique has been limited to soil profiles with horizontal layering. Before treating the more general problem of inclined layering, it is necessary to introduce the concept of apparent wave velocity. Apparent wave velocity is the velocity found by timing the passage of a wave between two closely spaced receivers. A portion of a wave front is drawn in Fig. 4-12, and this wave front is inclined to the surface as it arrives at receiver stations a distance  $x$  apart. The apparent velocity  $\bar{v}$  of this wave front along the surface is given by

$$\bar{v} = \frac{x}{t} \quad (4-21)$$

where  $t$  is the elapsed time between arrivals at  $R_m$  and  $R_n$ . The distance in the

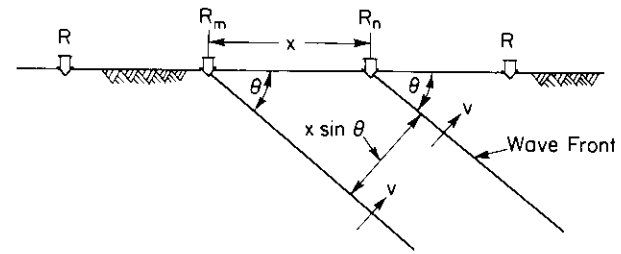


Figure 4-12. Apparent wave velocity.

direction of wave travel that the wave front moved is equal to  $(x \sin \theta)$ , where  $\theta$  is the angle of inclination. The elapsed time  $t$  can also be written

$$t = \frac{x \sin \theta}{v} \quad (4-22)$$

where  $v$  is the phase velocity of the wave. Now, substituting Eq. (4-22) into Eq. (4-21), the apparent velocity can be written

$$\bar{v} = \frac{v}{\sin \theta} \quad (4-23)$$

It can be seen from Eq. (4-23) that when the wave front is parallel to the surface ( $\theta = 0^\circ$ ) the apparent velocity is infinite and when the wave front is perpendicular to the surface ( $\theta = 90^\circ$ ) the apparent velocity is equal to the phase velocity.

It is of interest to digress and determine the apparent velocity of the head wave in the case of a horizontally layered system. This case is shown in Fig. 4-13. The angle  $\theta$  is  $i_c$ ; therefore the apparent velocity of the head wave

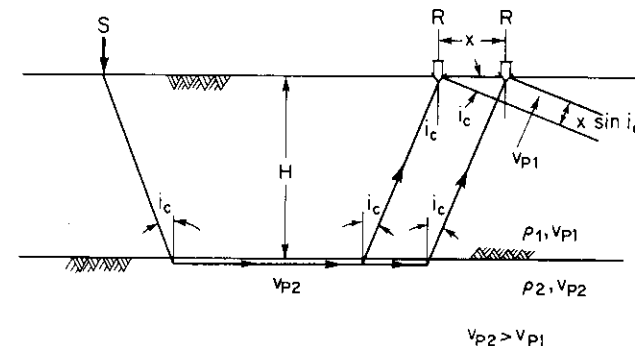


Figure 4-13. Apparent velocity of head wave for horizontal interface.

can be written

$$\bar{v}_h = \frac{v_{P1}}{\sin i_c}$$

but

$$\sin i_c = \frac{v_{P1}}{v_{P2}}$$

so

$$\bar{v}_h = v_{P2}$$

This confirms the fact that the apparent velocity in the case of a horizontal upper layer is equal to the  $P$ -wave velocity in the second medium,  $v_{P2}$ .

To analyze the problem of refractions from an inclined interface, the diagram shown in Fig. 4-14 will be used. Note that the angle  $\psi$  at which the interface is inclined is called the *apparent dip* and is equal to the *true dip*  $\delta$  only if the line from  $S$  to  $R$  is in the plane of the dip angle. This also implies that  $S$ ,  $A$ ,  $B$ , and  $R$  are not in a vertical plane unless  $\psi$  is the true dip angle.

Now, the travel-time equations for the direct wave and the refracted wave can be written. For the direct wave,  $t_d$  is given by Eq. (4-14). For the refracted wave,

$$t_h = \frac{\overline{SA}}{v_{P1}} + \frac{\overline{BR}}{v_{P2}} + \frac{\overline{AB}}{v_{P2}} \quad (4-24)$$

where

$$\overline{SA} = \frac{H_S}{\cos i_c} \quad (4-25)$$

$$\overline{BR} = \frac{H_R}{\cos i_c} \quad (4-26)$$

$$H_R = H_S + x \sin \psi \quad \text{and} \quad (4-27)$$

$$\overline{AB} = x \cos \psi - H_S \tan i_c - H_R \tan i_c \quad (4-28)$$

Substituting Eqs. (4-25) through (4-28) into Eq. (4-24) and using the relationship

$$\frac{1}{v_{P1} \cos i_c} - \frac{\tan i_c}{v_{P2}} = \frac{\cos i_c}{v_{P1}} \quad (4-29)$$

the travel time for the refracted wave can be written

$$t_h = x \left[ \frac{\sin(i_c + \psi)}{v_{P1}} \right] + \frac{2H_S \cos i_c}{v_{P1}} \quad (4-30)$$

Equation (4-30) is again the equation of a straight line with a slope given by

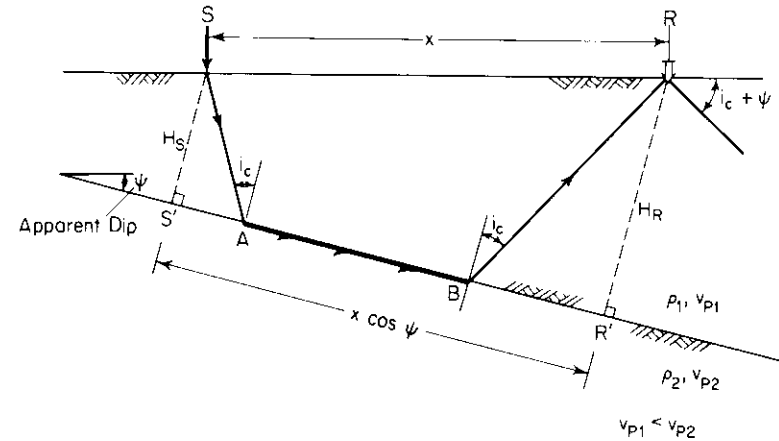


Figure 4-14. Head-wave path for inclined interface.

the first term on the right and a  $t$ -axis intercept given by the second term on the right. The travel-time curves for both direct and head waves are plotted in Fig. 4-15a. In Fig. 4-15a it can be seen that the apparent velocity of the second medium,  $\bar{v}_{P2}$ , is the reciprocal of the slope of the refracted-wave travel-time curve.

There are still, however, two unknowns in Eq. (4-30):  $i_c$  and  $\psi$ . To obtain the data required for a complete solution—including the depth to the interface, the apparent slope of the interface, and the  $P$ -wave velocities in both media—the analysis must be repeated reversing the positions of  $R$  and  $S$ , as shown in Fig. 4-16. Using this technique, called a *reversed profile*, it is possible to get a different refracted wave travel-time equation:

$$t'_h = x \left[ \frac{\sin(i_c - \psi)}{v_{P1}} \right] + \frac{2H_R \cos i_c}{v_{P1}} \quad (4-31)$$

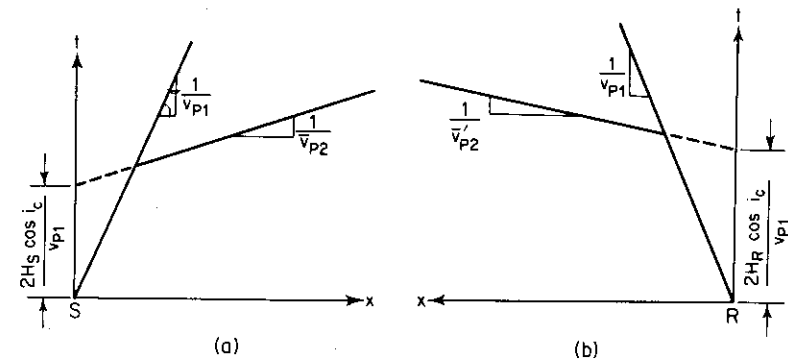


Figure 4-15. Travel-time curves for direct and head waves.

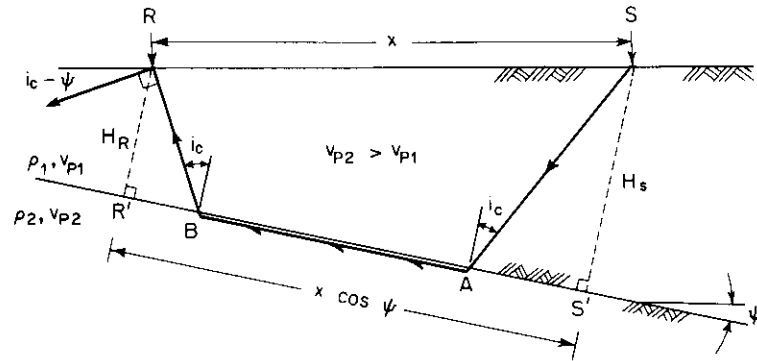


Figure 4-16. Reversed profile refraction survey.

Again,  $t_a$  is given by Eq. (4-14). Figure 4-15b shows these travel-time curves. The reciprocal of the slope of the refracted wave travel-time curve gives another value for the apparent velocity of the second medium,  $\bar{v}'_{P2}$ . By equating the apparent velocity  $\bar{v}_{P2}$  scaled from Fig. 4-15a to the bracketed term of Eq. (4-30) and equating the apparent velocity  $\bar{v}'_{P2}$  from Fig. 4-15b to the bracketed term of Eq. (4-31), it is possible to obtain two equations in two unknowns:

$$\frac{1}{\bar{v}_{P2}} = \left[ \frac{\sin(i_c + \psi)}{v_{P1}} \right] \quad (4-32)$$

and

$$\frac{1}{\bar{v}'_{P2}} = \left[ \frac{\sin(i_c - \psi)}{v_{P1}} \right] \quad (4-33)$$

Equations (4-32) and (4-33) can be rearranged as

$$i_c + \psi = \arcsin \frac{v_{P1}}{\bar{v}_{P2}} \quad (4-34)$$

and

$$i_c - \psi = \arcsin \frac{v_{P1}}{\bar{v}'_{P2}} \quad (4-35)$$

Equations (4-34) and (4-35) can be solved for  $\psi$  and  $i_c$ , and with known values of  $\psi$  and  $i_c$ ,  $v_{P2}$  can be computed from

$$\sin i_c = \frac{v_{P1}}{v_{P2}}$$

Then,  $H_S$  can be computed from Eq. (4-30) and  $H_R$  can be computed from Eq. (4-27).

It is possible to determine the true dip angle  $\delta$  of the interface by running two reversed profile refraction surveys along two lines intersecting at an angle  $\phi$ , as shown in Fig. 4-17a. For the line  $\overline{SR}$  the following relationship can be obtained from the geometry of Fig. 4-17b:

$$\sin \delta = \frac{\overline{RR'}}{\overline{ER}} \quad (4-36)$$

$$\sin \psi_1 = \frac{\overline{RR'}}{\overline{SR}} \quad (4-37)$$

$$\sin(90 - \theta) = \frac{\overline{ER}}{\overline{SR}} = \cos \theta \quad (4-38)$$

Combining Eqs. (4-36) through (4-38), the following expression can be obtained:

$$\sin \delta (\cos \theta) = \sin \psi_1 \quad (4-39)$$

Similarly, for the line  $\overline{SR''}$ ,

$$\sin \delta [\cos(\phi - \theta)] = \sin \psi_2 \quad (4-40)$$

Equations (4-39) and (4-40) can be solved simultaneously for the unknowns  $\delta$  and  $\theta$ , or they can be solved by sine vectors, as shown in Fig. 4-17c.

### 4.3 Steady-State-Vibration Technique

#### Rayleigh Waves in Elastic Half-Space

It was noted in Sec. 3.3 that the seismic waves generated by a vertically oscillating circular footing at the surface of a half-space were predominately Rayleigh waves. It would be expected, therefore, that a motion transducer with vertical motion sensitivity located at the surface of the half-space would sense the vertical component of the Rayleigh wave. The displaced shape of the half-space surface at any instant in time due to a sinusoidal-input source could be represented by a sine curve, as in Fig. 4-18. The distance between any two successive peaks (or troughs) is equivalent to one wave length of the Rayleigh wave (denoted as  $L_R$ ). The time variation of the vertical displacement at the vibration source can be expressed as

$$z(t) = \sin \omega t \quad (4-41)$$

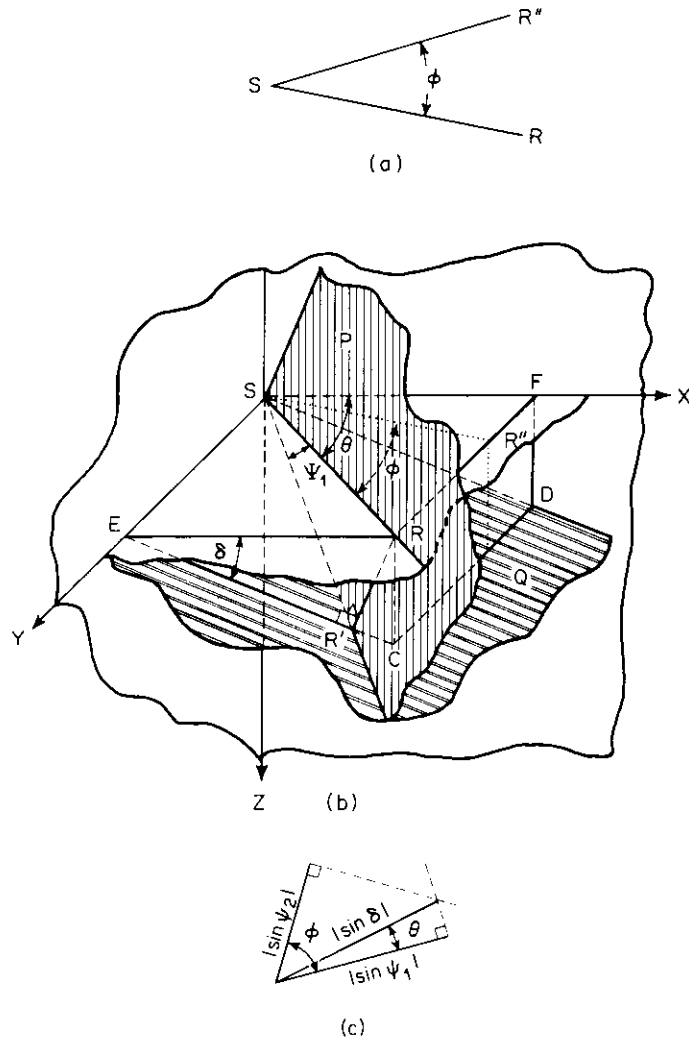


Figure 4-17. True dip angle determination.

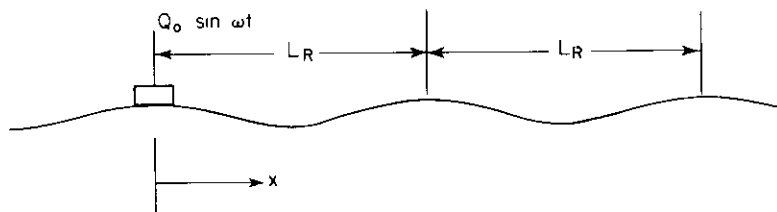


Figure 4-18. Deformed shape of a half-space surface.

At any other point on the surface of the half-space, the time variation of vertical displacement can be expressed as

$$z(t) = \sin(\omega t - \varphi) \tag{4-42}$$

where  $\varphi$  is a phase angle. Equation (4-42) can be rewritten as

$$z(t) = \sin(\omega t - \varphi) = \sin \omega \left( t - \frac{r}{v_R} \right) = \sin \left( \omega t - \frac{2\pi f r}{v_R} \right) \tag{4-43}$$

where  $r$  is the distance from the vibration input to the point. At the source of vibrations,  $r = 0$  and  $\varphi = 0$ , but at a distance  $r = L_R$  from the source,

$$\varphi = \frac{2\pi f L_R}{v_R} \tag{4-44}$$

At  $r = L_R$ , the phase angle is  $2\pi$ , and  $v_R$  can be written as

$$v_R = f L_R \tag{4-45}$$

It can be seen from Eq. (4-45) that  $v_R$  can be computed from the measured value of  $L_R$  at any input frequency  $f$ . Also, because  $v_R$  is approximately equal to  $v_S$ , the shear modulus can be computed by substituting  $v_R$  from Eq. (4-45) in Eq. (3-48).

In the United States, most of the development of steady-state-vibration techniques for subsurface soil exploration have been contributed by the U.S. Army Corps of Engineers, Waterways Experiment Station (WES), Vicksburg, Mississippi. Since about 1960, soils engineers at WES have conducted many steady-state-vibration surveys in conjunction with routine soil borings and seismic exploration to establish techniques by which reliable soil data can be obtained (see Fry, 1963 and 1965).

The theoretical attenuation with depth of both components of the  $R$ -wave were shown in Fig. 3-14. On the basis of those attenuation curves it is reasonable to assume that the bulk of the  $R$ -wave travels through a zone of the half-space about one-wave-length deep. It could further be postulated that the average properties within this zone approximate the properties at a depth of one-half wave length ( $L_R/2$ ).\*

By decreasing the frequency of the vibrations from an initial value, the wave length increases and the  $R$ -wave effectively samples a greater depth. Conversely, by increasing the frequency the wave length decreases and the

\* Field investigations reported by Heukelom and Foster (1960), Fry (1963), and Ballard (1964) indicate that this assumption is reasonable for uniform- and layered-soil media.

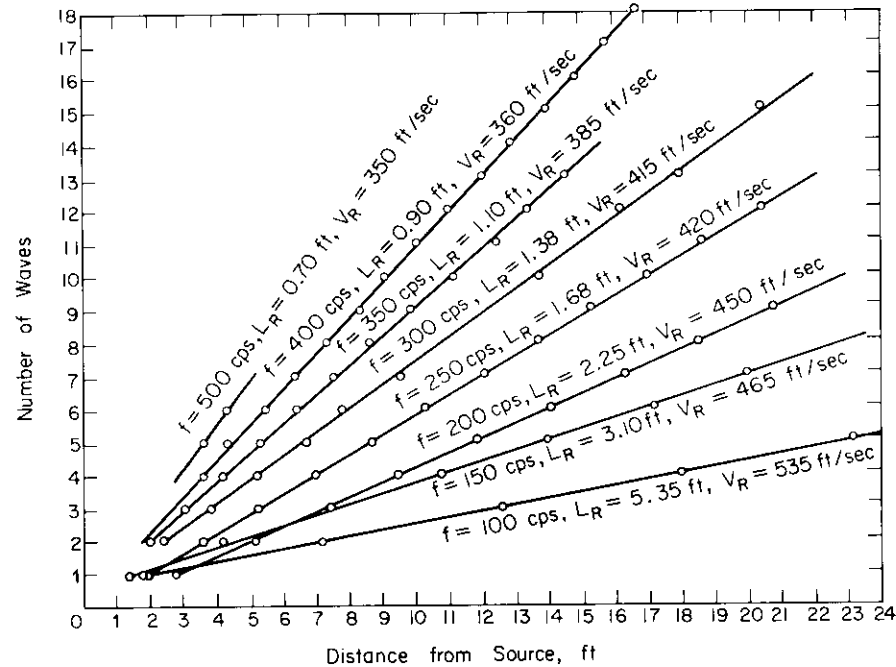


Figure 4-19. Determination of average wave length of Rayleigh wave.

sampled depth decreases. For a homogeneous, isotropic, elastic half-space the material properties are independent of depth; therefore, all frequencies will yield the same velocity. For an elastic half-space in which the elastic properties change gradually with depth,  $v_R$  varies with the frequency of the input excitation. In this case different wave lengths effectively sample material with different average elastic properties. It is possible, therefore, to obtain valuable information on the elastic properties of a half-space whose properties vary with depth from steady-state vibrations at the surface.

In a series of field tests, the authors investigated the variation with depth of elastic properties of a silty fine sand using the steady-state technique. For each of eight frequencies,  $L_R$  was determined. A straight line was fitted through points plotted on a graph of distance from the source vs. number of wave lengths from the source (Fig. 4-19). Each of the lines in Fig. 4-19 represents the data for one frequency. The reciprocal of the slope of each line is the average wave length associated with each frequency. The shear-wave velocity calculated for each frequency is plotted as a function of one-half the wave length in Fig. 4-20. This is equivalent to a shear-wave-velocity-vs.-depth profile. Borings at the site of these field tests showed that the soil was uniform within the upper four feet. The results shown in Fig.

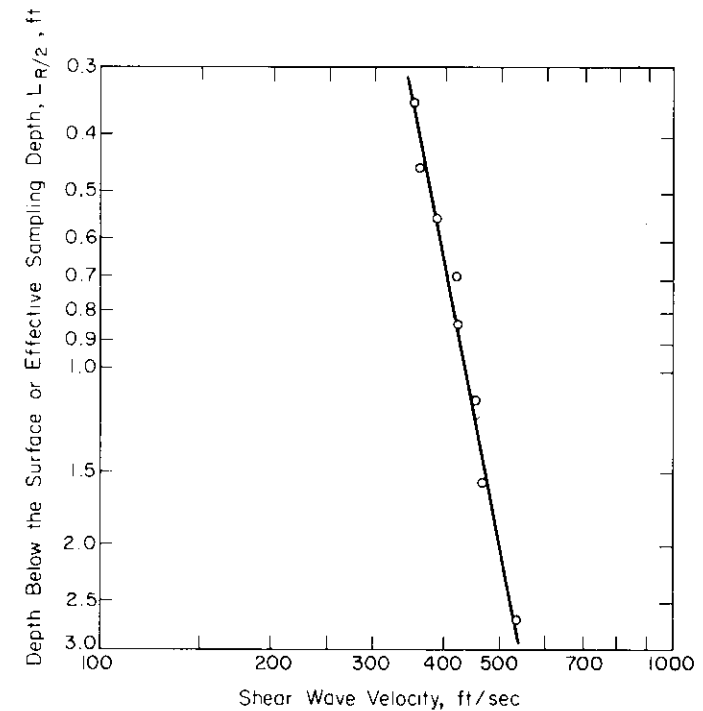


Figure 4-20. Shear-wave velocity vs. depth in fine, silty sand.

4-20, therefore, indicate a soil whose elastic properties are a function of overburden pressure. This is, of course, in agreement with known properties of granular materials like the silty fine sand at this site.

The results presented in Figs. 4-19 and 4-20 were for a relatively shallow depth. Investigators at the U.S. Army Corps of Engineers, Waterways Experiment Station have investigated deeper soil strata using steady-state vibrations. A plot of shear modulus-vs.-depth for a test in uniform sand was reported by Ballard and Casagrande (1967) and is reproduced in Fig. 4-21. In these tests the shear modulus was determined to a depth of 17 feet. At other sites Ballard (1964) reported that depths of up to 170 feet were sampled using the steady-state technique. In general, it has been found that greater depths may be sampled in materials with higher values of shear modulus.

#### *Rayleigh Wave in Layered Half-Space*

In a half-space consisting of a single layer over a semi-infinite medium, the analytical expressions for  $R$ -wave propagation are very complex. However, the elastic properties of the upper layer can be determined from

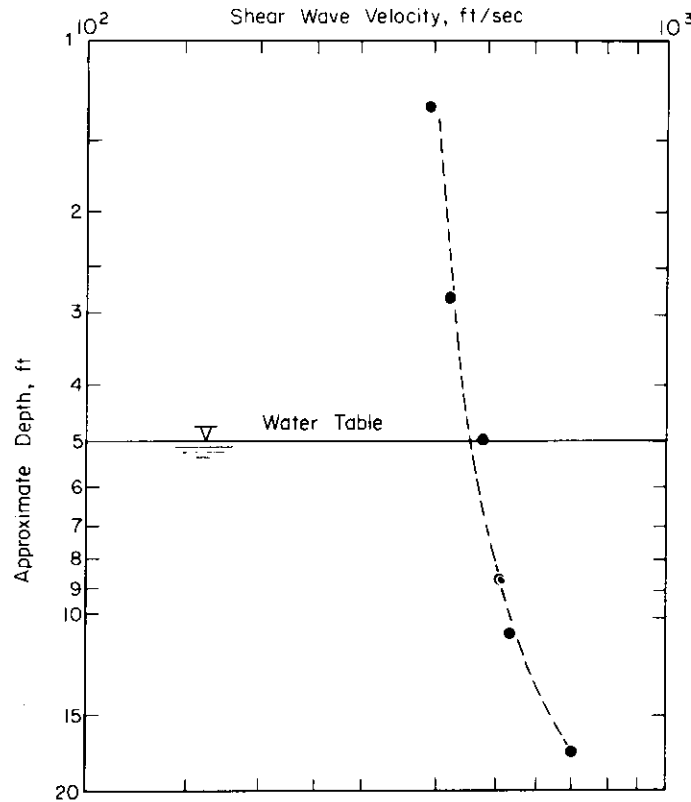


Fig. 4-21. Shear-wave velocity vs. depth in uniform, fine sand (after Ballard and Casagrande, 1967).

high-frequency (short wave-length) data, and the elastic properties of the lower medium can be obtained from low-frequency (long wave-length) data. For multilayered systems an analytical solution for  $v_R$  is almost prohibitive, but from field investigations it has been found that the  $R$ -wave propagates at a velocity commensurate with the material through which the greater part of the  $R$ -wave energy is transmitted. Heukelom and Foster (1960) reported an investigation in which they were able to identify three  $R$ -wave velocities in the four-layer highway profile, as shown in Fig. 4-22. In these tests the wave-velocity-vs.-half-wave-length data correlated well with the true profile. Fry (1965) reported on vibratory tests in which a layered rock was sampled to a depth of about 95 feet, and good correlation with borings was obtained, as shown in Fig. 4-23 on page 118.

A water table in a granular soil constitutes an interface to a compression wave, but Rayleigh waves are influenced only slightly by a water table,

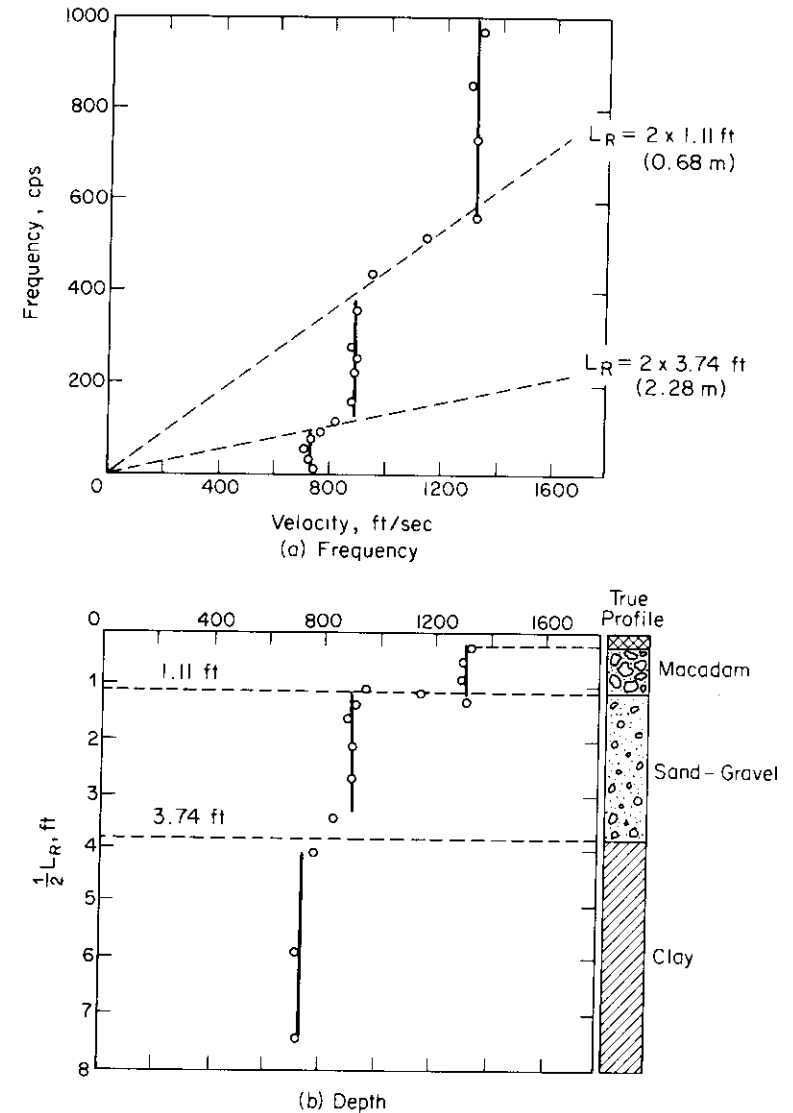


Figure 4-22. Wave velocities observed on stratified soil as a function of frequency and depth (after Heukelom and Foster, 1960).

because the pore water cannot transmit shear. The influence of pore water on shear-wave velocity is discussed in detail in Chap. 5. A general conclusion is that shear-wave velocity is insensitive to pore water. The insensitivity of the  $S$ -wave and  $R$ -wave to the water table represents a distinct advantage for steady-state techniques.

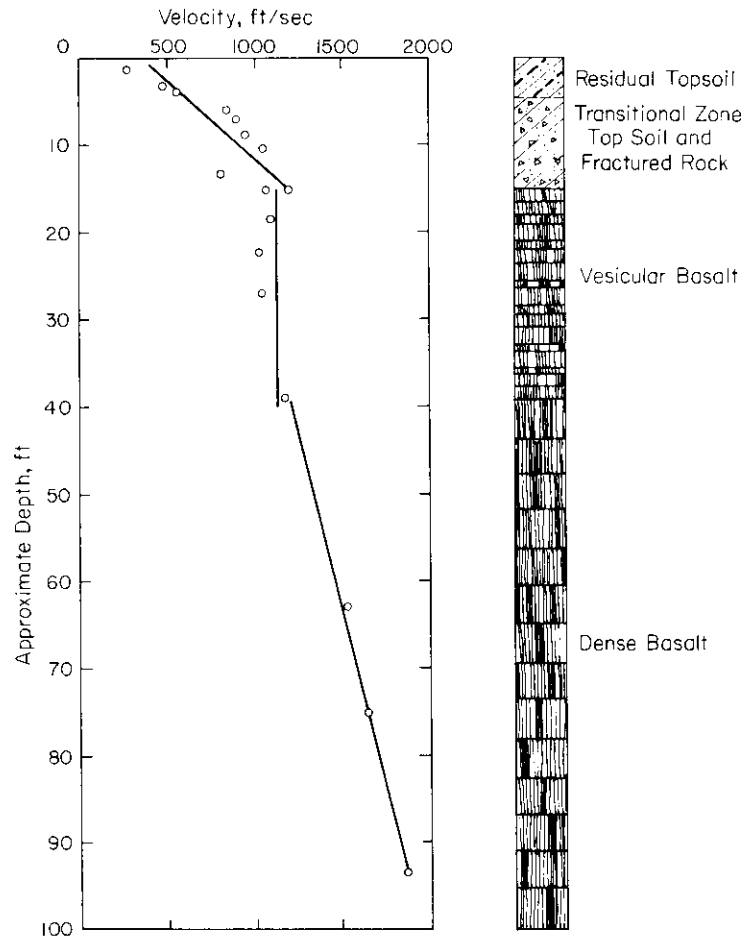


Figure 4-23. Shear-wave velocity vs. depth in rock profile (after Fry, 1965).

While the cited cases have in general shown a good profile correlation, the steady-state technique is not sufficiently sensitive to distinguish the exact location of an interface. A clearer determination of a horizontal interface can be obtained in some cases using Love waves as described in the next section.

*Love Wave in a Layered Half-Space*

For a medium with a low-velocity layer on top of a higher-velocity layer, Jones (1958) showed that steady-state Love waves could be used to determine the shear-wave velocity in the upper medium and the thickness of the

upper layer. For a single surface layer the frequency equation for the Love wave can be written as

$$\tan \frac{2\pi H}{L} \left( \frac{v^2}{v_{S1}^2} - 1 \right)^{1/2} = \frac{G_2}{G_1} \left( \frac{1 - \frac{v^2}{v_{S2}^2}}{\frac{v^2}{v_{S1}^2} - 1} \right)^{1/2} \tag{4-46}$$

where

- $L$  = wave length of vibrations,
- $v$  = phase velocity of the vibrations,
- $v_{S1}$  = phase velocity of shear waves in surface layer,
- $v_{S2}$  = phase velocity of shear waves in lower medium,
- $G_1$  = shear modulus in the surface layer,
- $G_2$  = shear modulus in the lower medium, and
- $H$  = thickness of the surface layer.

The principal mode of Love-wave propagation corresponds to the lowest branch of the tangent function for which

$$0 < \frac{2\pi H}{L} \left( \frac{v^2}{v_{S1}^2} - 1 \right)^{1/2} < \frac{\pi}{2} \tag{4-47}$$

For high frequencies (short wave lengths), an asymptotic solution for Eq. (4-46) indicates that the velocity of the Love wave approaches the shear-wave velocity for the upper layer. Similarly, at low frequencies (long wave lengths), the Love-wave velocity approaches the shear-wave velocity in the lower medium. A plot of distance-from-the-source-vs.-number-of-waves, similar to Fig. 4-19, can be used to determine the average wave length of the Love wave from which the shear-wave velocity may be calculated.

Jones also showed that for  $G_2/G_1$  ratios of 3 or greater in Eq. (4-46), the solutions were approximately the same as for a ratio of  $G_2/G_1$  equal to infinity. For the right-hand side of Eq. (4-46) equal to infinity, the principal mode yields the following expression:

$$\frac{2\pi H}{L} \left( \frac{v^2}{v_{S1}^2} - 1 \right)^{1/2} = \frac{\pi}{2} \tag{4-48}$$

from which

$$\frac{4H}{L} \left( \frac{v^2}{v_{S1}^2} - 1 \right)^{1/2} = 1$$

or, rearranging,

$$\frac{1}{v_{S1}^2} - \frac{1}{v^2} = \frac{1}{16f^2 H^2} \tag{4-49}$$



After further rearranging,

$$\frac{1}{v^2} = -\frac{1}{16H^2} \frac{1}{f^2} + \frac{1}{v_{S1}^2} \quad (4-59)$$

By plotting  $1/v^2$  vs.  $1/f^2$ , a straight line is obtained for which the slope is  $-(1/16H^2)$ , and the  $1/v^2$  axis intercept gives the value of  $1/v_{S1}^2$ . An example taken from Jones is given in Fig. 4-24. The data shown in Fig. 4-24 was obtained at a site which consisted of an upper layer of silty clay and a lower medium of gravel. The upper layer was about 5 feet thick and the ratio of  $G_2/G_1$  was about 10/1. The layer thickness calculated from the slope of the line in Fig. 4-24 is about 4.9 feet. Jones also presented a method for determining the depth of the upper layer in a system for which  $G_2/G_1$  was less than 3. This method made use of theoretical curves and a trial-and-error procedure, but the method will not be presented here.

A description of the field equipment and techniques required to perform the foregoing seismic tests can be found in Chap. 9.

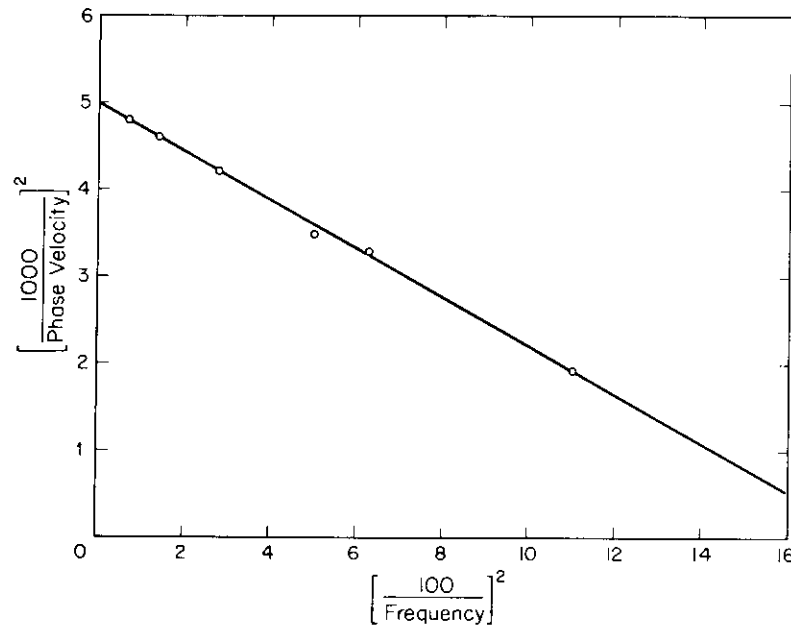


Figure 4-24. Evaluation of thickness of layer from Love wave data (after Jones, 1958).

## 5

### PROPAGATION OF WAVES IN SATURATED MEDIA

#### 5.1 Introduction

In Chaps. 3 and 4 the topics of wave propagation in ideal solids were treated. However, real soils have special characteristics which cause their responses to wave energy to differ from those developed by ideal solids. The voids in soil masses are filled with water, air, or mixtures of fluids, and these pore fluids may significantly influence the dynamic behavior of soils. This chapter includes a discussion of wave propagation in fluids and fluid-saturated solids to illustrate, qualitatively, the dynamic behavior which might be anticipated in fluid-saturated soils. Chapter 6 treats the dynamic behavior of soils, including the nonlinear and inelastic response of the soil structure.

Before considering wave propagations in fluid-saturated bodies, it is useful to review briefly the terminology employed in soil mechanics to describe the solid and fluid components of soils. An element of soil may be represented by a column of unit cross-sectional area and total height  $V$ . The volume of solid particles is then represented by a height  $V_s$  and the total volume of voids by a height  $V_v$ , as shown in Fig. 5-1. The porosity  $n$  describes the portion of the total volume represented by the void spaces—

$$n = \frac{V_v}{V} \quad (5-1)$$

—and the void ratio  $e$  describes the ratio of the volume of voids to the volume

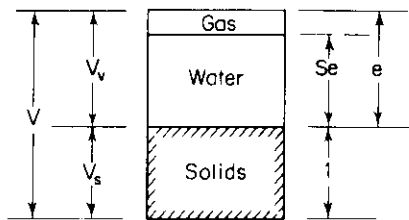


Figure 5-1. Phase diagram for elements of soil.

of solids—

$$e = \frac{V_v}{V_s} = \frac{n}{1 - n} \quad (5-2)$$

For a completely saturated soil the void space is completely filled with a liquid, usually water, and the *degree of saturation S* is 100 per cent. When gas is present in the void space, the degree of saturation is less than 100

per cent and the volume of fluid in the voids is described by  $Se$ , as noted in Fig. 5-1. The unit weight  $\gamma$  of soils at various conditions of water content is defined conveniently in terms of void ratio  $e$ . The *unit dry weight* of soil is defined as

$$\gamma_d = \frac{1}{1 + e} G_s \gamma_w \quad (5-3)$$

in which  $G_s$  represents the specific gravity of the solid particles in the soil and  $\gamma_w$  is the unit weight of water (62.4 lb/ft<sup>3</sup>). Addition of water in the void spaces increases the *total unit weight* of the soil to

$$\gamma = \frac{(G_s + Se)\gamma_w}{1 + e} \quad (5-4)$$

in which the degree of saturation  $S$  is expressed as a decimal ( $S = 1.0$  for complete saturation). When the element of soil is completely submerged in water, the *submerged unit weight* is

$$\gamma' = \frac{(G_s + e)\gamma_w}{1 + e} - \gamma_w = \frac{G_s - 1}{1 + e} \gamma_w \quad (5-5)$$

These fundamental relationships are required for the discussions of wave propagation in mixtures and in soils, which follow a brief treatment of wave propagation in ideal fluids.

In comparison with the theory for propagation of waves in elastic solids, the theory for propagation of compression waves in fluids is relatively simple. Since ideal fluids cannot develop shearing resistance, shear waves do not occur, and only the compression waves need be considered. There is an extensive body of literature in the field of hydrodynamics dealing with the propagation of compression waves in fluids (see, for example, Lord Rayleigh, 1877, 1945; Lamb, 1879, 1945; Morse, 1948; and Streeter, 1961). These

theoretical studies include the influences of many types of boundary conditions on wave propagation in fluids and help to bridge the gap between the theoretical behavior of ideal solids and the actual behavior of saturated or partially saturated soils.

The propagation of small-amplitude gravity waves in water is another phenomenon which is governed by the wave equation (Eq. 3-1) and which may be useful for estimating the propagation of waves in soils. Gravity waves are surface waves that have characteristics similar to Rayleigh waves in solids. Thus, from studies of the propagation characteristics and the refraction and diffraction of gravity waves in water (see for example, Wiegel 1964), we may obtain a qualitative picture of the behavior of Rayleigh waves in soils.

## 5.2 Compression Waves in Ideal Fluids

### Acoustic Waves in Air

Every elementary course in physics includes a discussion of the propagation of sound waves in air. The behavior of the waves of compression and rarefaction which propagate outward from a source in air is described by the *wave equation*:

$$\frac{\partial^2 p}{\partial t^2} = v_a^2 \nabla^2 p \quad (5-6)$$

in which

- $p$  = the pressure developed by the sound wave,
- $\nabla^2$  = the Laplacian operator ( $= \partial^2/\partial x^2 + \partial^2/\partial y^2 + \partial^2/\partial z^2$  for Cartesian coordinates), and
- $v_a$  = the velocity of sound in air.

Equation (5-6) applies for the particle displacement  $\xi$  and the density  $\rho$ , as well as for the pressure  $p$ , and it is identical in form to Eq. (3-1). The velocity of sound in air is

$$v_a = \sqrt{\frac{k_a p_a}{\rho_a}} \quad (5-7)$$

in which  $k_a$  is the ratio of specific heat at constant pressure to that at constant volume, and  $\rho_a$  is the mass density. For air,  $k_a = 1.403$ ,  $p_a = 2117$  lb/ft<sup>2</sup>, and  $\rho_a = 0.002337$  lb-sec<sup>2</sup>/ft<sup>4</sup> at the standard temperature of 20°C and standard pressure of 760 mm of Hg (2117 lb/ft<sup>2</sup> or 14.7 lb/in.<sup>2</sup>). This gives  $v_a = 1127$  ft/sec at the standard conditions. The wave velocity in air varies with the pressure and temperature. The wave velocity at any

temperature is related to the wave velocity at 0°C ( $v_{a0} = 1089$  ft/sec) by

$$v_a = 1089 \sqrt{1 + \frac{^\circ\text{C}}{273}} \quad (5-8)$$

in which °C is the temperature in degrees centigrade.

The acoustic pressure may be expressed on the *decibel scale* (db scale) as a value represented by 20 times the logarithm to the base 10 of the ratio of the actual pressure to a reference pressure. A standard reference pressure in audioacoustics corresponds to a sound pressure of  $p_0 = 0.000204$  dyne/cm<sup>2</sup> ( $2.96 \times 10^{-9}$  lb/in.<sup>2</sup> or  $4.26 \times 10^{-7}$  lb/ft<sup>2</sup>). Thus, the db value for a pressure of 1 lb/ft<sup>2</sup>, referred to the standard value, would be

$$\text{db}(p_0) = 20 \log_{10} \frac{1}{4.26 \times 10^{-7}} = 127.4$$

In some instances the db scale is simply used to represent ratios of the acoustic pressures; in these cases we may say that one quantity has a db value relative to the db value of the other. The db scale may also be applied to express the ratios of acoustic power by multiplying the logarithm to the base 10 of this ratio by a factor of 10. Further discussions of the application of the db scale are given by Morse (1948) and Albers (1960).

#### Pressure Waves in Water

Waves of compression and rarefaction, the dilatational or acoustic waves, are propagated in water according to the same laws that apply to acoustic waves in air. An empirical expression for the velocity of sound in fresh water at any temperature is

$$v_w = 141,000 + 421t - (3.7)t^2 \quad (5-9)$$

and for sea water at any temperature, salinity, and depth, it is (from Albers, 1960),

$$v_w = 141,000 + 421t - (3.7)t^2 + 110S + (0.018)d \quad (5-10)$$

In Eqs. (5-9) and (5-10),  $v_w$  is the velocity of wave propagation in centimeters per second,  $t$  is the water temperature in °C,  $S$  is the salinity in parts per thousand, and  $d$  is the depth below the surface in centimeters. Thus, for fresh water at 0°C,  $v_{w0} = 141,000$  cm/sec = 4630 ft/sec, and at 21.1°C (70°F),  $v_w = 4860$  ft/sec.

It is important to keep in mind that the wave velocity in water is on the order of 4800 ft/sec when measuring the propagation of the dilatational wave in saturated soils. By introducing this value of  $v_w = 4800$  ft/sec into the expression for wave propagation velocity in water,

$$v_w = \sqrt{\frac{B_w}{\rho_w}} \quad (5-11)$$

a typical value for the bulk modulus  $B_w$  (or modulus of volume compressibility) of fresh water may be obtained as

$$B_w = (4800)^2 \frac{62.4}{32.17} = 4.47 \times 10^7 \text{ lb/ft}^2 \quad \text{or} \quad 310,400 \text{ lb/in.}^2 \quad (5-12)$$

This calculation shows that the bulk modulus of fresh water is on the order of 300,000 lb/in.<sup>2</sup>. Therefore, water is essentially *incompressible* when compared with the compressibility of soils, and seismic methods for evaluating propagation of the compression wave in saturated soils may be measuring only the wave transmission in water.

#### Reflection, Refraction, and Diffraction of Waves

In this discussion, we shall consider a train of pressure waves propagating through an ideal fluid at a wave velocity  $v$ . The periodic variations in pressure may be represented by spherical surfaces, shown in Fig. 5-2a as a series of concentric circles. These circles represent the distance between the maximum peaks of the pressure oscillations. The progress of the waves may be identified by noting successive positions of these circles representing the peak positions, or the "wave front."

If we consider first the pressure wave propagating outward from a small spherical source (Fig. 5-2a), the wave-propagation velocity  $v$  remains constant but, because the wave energy is spread over a larger area as the spherical wave front expands, the *amplitude of vibration decreases according to*  $1/r$ .

The simple source represents a useful component of *Huygens' principle*, which states that every point on a wave surface becomes in turn a source for a new disturbance. Thus, every point on a spherical wave surface sets up new wavelets of spherical shape (see Fig. 5-2b). The enveloping surface for all these new wavelets forms the new wave surface. This principle is useful in explaining the propagation of a wave front at a reflecting surface, as shown in Fig. 5-2c. On this diagram a unit length of the incident-wave front propagating at a velocity  $v$  is represented by the line  $A-B$  just as  $A$  touches the

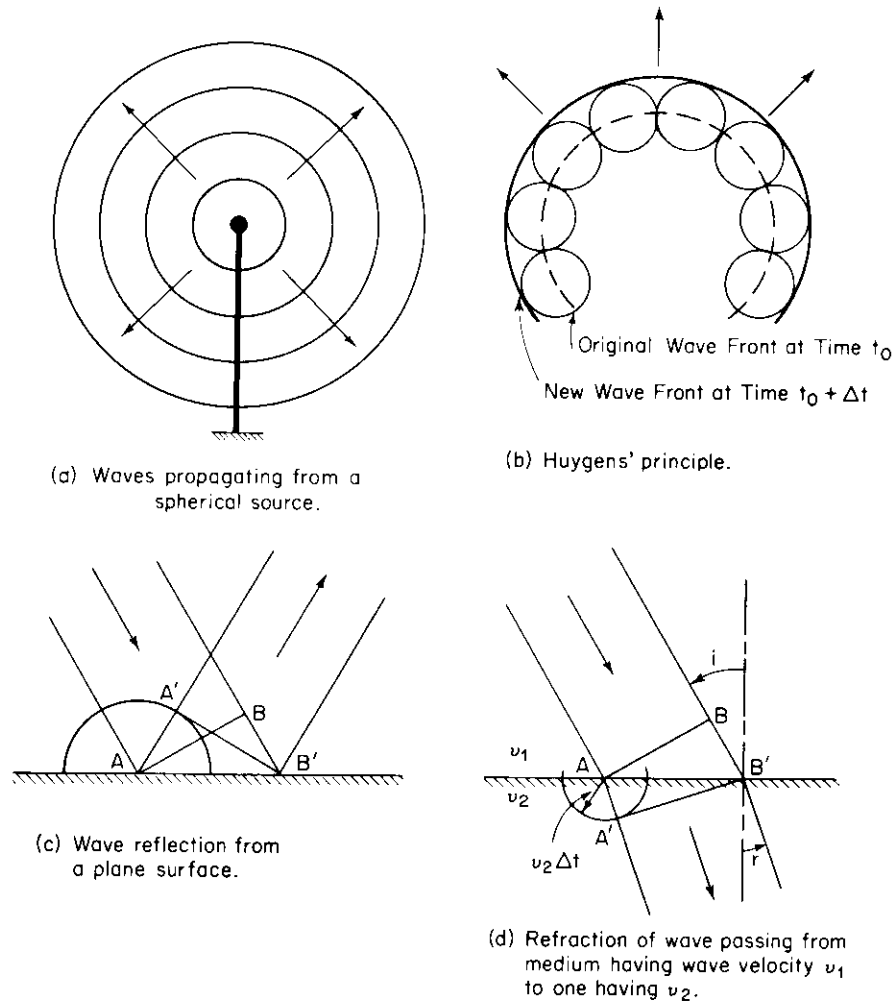


Figure 5-2. Wave phenomena in ideal fluids.

reflecting surface. After the interval of time  $\Delta t$  required for the wave to travel the distance  $B-B'$ , the point on the wave front originally at  $B$  has reached  $B'$  and the spherical front propagating from  $A$  at the same velocity  $v$  has also traveled a distance  $A-A'$  ( $A-A' = B-B'$ ) from  $A$ , as shown by the circle of radius  $A-A'$  in Fig. 5-2c. The new wave front is formed by the surface which passes through  $B'$  and is tangent to the wavelets formed at all points along the front, but represented by the wavelet from  $A$ . The new wave front is

represented by  $A'-B'$  in Fig. 5-2c. From the geometry of this figure, it is evident that the angle of incidence must equal the angle of reflection.

Huygens' principle may also be used to describe *refraction* or change in direction of the wave front as it passes from one medium with a wave velocity  $v_1$  to another medium with a wave velocity  $v_2$ . Again an element of the wave front  $A-B$  is shown in Fig. 5-2d just as  $A$  reaches the interface. After the interval of time required for  $B$  to travel to  $B'$  at the velocity  $v_1$  in medium 1, the wavelet from  $A$  has described a surface as shown by the circle in Fig. 5-2d having a radius  $v_2\Delta t$ . The new wave front  $A'-B'$  is now formed by the envelope to this circle and point  $B'$ , and the direction of propagation is perpendicular to  $A'-B'$ . Thus, the new wave front will have a different orientation to the interface than that for the incident wave. The relation between the angle of incidence  $i$  and the angle of refraction  $r$  is established by Snell's law:

$$\frac{\sin i}{\sin r} = \frac{B-B'}{A-A'} = \frac{v_1}{v_2} \quad (4-1)$$

Refraction occurs whenever a wave passes through an interface between materials which provide for different velocities of wave propagation. This phenomenon is most familiar when related to the propagation of light through different transparent materials, or sound through fluids having variations in wave velocity because of changes in temperature. The refraction of gravity waves in water, caused by changes in water depth, is similar to the refraction of waves in soils, caused by changes in wave-propagation velocity.

A reduction in the depth of water through which a gravity wave passes causes a reduction in wave velocity below that for deep water. Thus, gravity waves approaching the shoreline at an angle are bent or refracted because the inshore portion of the wave acts in shallower water and is slowed down; consequently, the waves tend to swing around and conform to the bottom contours. Considerations of refraction patterns of water waves are useful, primarily in a qualitative sense, for estimating the influences in the changes of the thicknesses and contours of soil layers on the patterns of propagation for Rayleigh waves. Both gravity waves in water and Rayleigh waves in soils are surface waves and are influenced by the ratio of thickness of the material to the length of the propagating waves if this ratio is less than about 1. Useful discussions of refraction of gravity waves in water are given by Johnson (1953) and Wiegel (1964).

Diffraction occurs for sound waves and for light waves, as well as for gravity waves in water of constant depth. The theoretical solutions have generally been developed for light or sound waves and then adapted to the problems of gravity waves. Wave diffraction is developed by the interception of incoming-wave energy by an irregular surface and the interaction of this

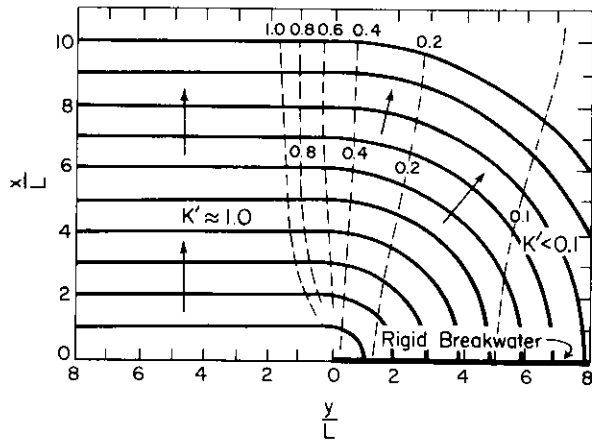


Figure 5-3. Wave fronts and lines of equal diffraction coefficients for a semi-infinite rigid impervious breakwater, with the incident waves normal to the breakwater (from Wiegel, 1964).

reflected and refracted wave energy with the original wave systems. The diffraction of gravity waves near the end of a semi-infinite breakwater illustrates this type of problem (Wiegel, 1964). Figure 5-3 shows a train of waves travelling perpendicular to a breakwater extending completely to the bottom of a body of water of constant depth. The breakwater is impermeable and rigid and extends an infinite distance to the right of point ( $y/L = 0$ ). At the time the incident-wave front reaches ( $x/L = 0$ ), it is still a straight line. However, at this point the wave to the right of point ( $y/L = 0$ ) is intercepted by the breakwater and reflected back to sea. The portion of the wave to the left of point ( $y/L = 0$ ) proceeds past the breakwater with the straight-line portions of the front propagating as straight lines and the wavelets originating from ( $y/L = 0$ ) producing a circular wave front which develops waves behind the breakwater.

It should be noted that dimensionless coordinates are used in Fig. 5-3 by relating the distances in the vicinity of the breakwater to the wave length  $L$  of the incoming wave. The solid lines in Fig. 5-3 represent the wave fronts, and the dotted lines represent values of the wave-diffraction coefficient  $K'$ . The wave-diffraction coefficient is the ratio of the wave amplitude in the zone affected by diffraction to the incoming-wave amplitude. Thus a value of  $K'$  less than 1.0 identifies a region for which the breakwater has some beneficial effect.

The pattern of wave reduction behind the breakwater indicates the type of shielding we might expect near the end of a semi-infinite trench excavated completely through a soil layer for the purpose of intercepting Rayleigh waves. A more realistic approximation to the case of a trench of finite depth in soil is produced by the wave-diffraction patterns around floating breakwaters where some portion of the incoming-wave energy passes beneath the structure and diffracts upward into the shielded zone.

### Propagation of Compression Waves in Mixtures

Solids suspended in liquids may produce an influence on the propagation of the compression wave because their presence influences both the mass density and the compressibility of the mixture. For the usual case of solid particles suspended in water, the mass density is

$$\rho_{\text{tot}} = \frac{\gamma_w G_s + e}{g(1 + e)} \quad (5-13)$$

in which  $G_s$  is the specific gravity of the solid particles and  $e$  is the void ratio. The compressibility of the mixture is made up of the compressibility of the fluid plus the compressibility of the solid particles in the form

$$\frac{1}{B} = \frac{e}{1 + e} \frac{1}{B_w} + \frac{1}{1 + e} \frac{1}{B_s} \quad (5-14)$$

in which

- $B$  = bulk modulus of elasticity of the mixture,
- $B_w$  = bulk modulus of elasticity of water, and
- $B_s$  = bulk modulus of elasticity of the solid particles.

Equation (5-14) is generally known as the *Wood equation* (Wood, 1930) for compressibility of mixtures.

If we consider a simple mixture of quartz particles (for which the specific gravity is 2.66 and the bulk modulus is  $4.45 \times 10^6$  lb/in.<sup>2</sup>) and water, we note from Eqs. (5-13) and (5-14) that the mass density and bulk modulus of the mixture are dependent on the void ratio  $e$ . Therefore, the wave-propagation velocity in the mixture, as defined by

$$v_{\text{mix}} = \sqrt{\frac{B}{\rho_{\text{tot}}}} \quad (5-15)$$

also varies with  $e$ . Figure 5-4 shows the influence of changes in void ratio on the ratio of compression-wave velocity in a mixture of quartz particles and water to the compression-wave velocity in water. Note that, for void ratios above about 1.2, the compression wave propagates more slowly in the mixture than it does in water alone.

This variation of wave velocity with void ratio is of interest to those involved with the reflection and absorption of sound waves at the sea bottom (see, for example, Shumway, 1960, and Hamilton, 1963). Both laboratory and *in-situ* sea-bottom tests have shown this decrease of sound-wave velocity

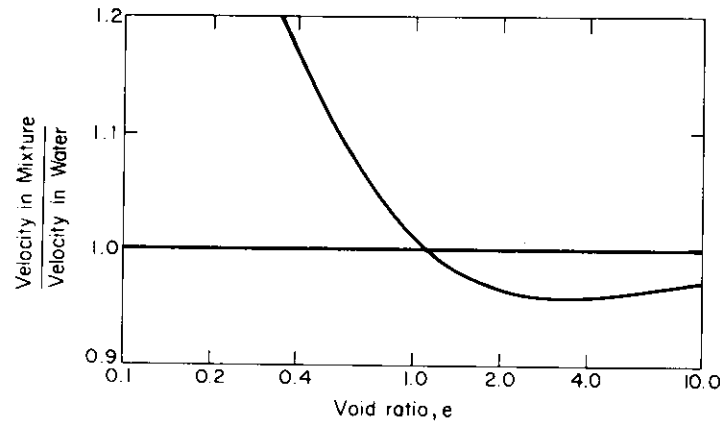


Figure 5-4. Relation between compression-wave velocity and void ratio for a mixture of quartz particles and water.

below that in water alone in bottom sediments for which the void ratio was greater than about 1.2.

The effect of *small amounts of air in the water* portion of the mixture is to reduce the wave-propagation velocity significantly. For less than 100 per cent saturation, the volumes of air and water per unit volume  $V$  of soil are (see Fig. 5-1)

$$V_a = \frac{(1-S)e}{1+e} V \quad (5-16)$$

$$V_w = \frac{Se}{1+e} V \quad (5-17)$$

in which  $S$  represents the degree of saturation expressed as a decimal. The volume of solid particles in this unit volume is

$$V_s = \frac{1}{1+e} V \quad (5-18)$$

The total mass density of the solid-air-water mixture is

$$\rho_{tot} = \frac{\gamma_w}{g} \left( \frac{Se}{1+e} + \frac{(1-S)e\gamma_a}{(1+e)\gamma_w} + \frac{G_s}{1+e} \right) \quad (5-19a)$$

or

$$\rho_{tot} \approx \frac{\gamma_w}{g} \left( \frac{Se}{1+e} + \frac{G_s}{1+e} \right) \quad (5-19b)$$

because the product  $(1-S)\gamma_a/\gamma_w$  is negligible:

The combined bulk modulus of a volume  $V$  of an *air-water mixture* is

$$B_{aw} = \frac{B_w}{1 + \frac{V_a}{V} \left( \frac{B_w}{B_a} - 1 \right)} \quad (5-20)$$

As an example, consider the influence of 0.10 per cent of air bubbles in the water on the bulk modulus of a unit volume of the air-water mixture. If we take the conditions for which  $v_w = 4800$  ft/sec in de-aired water, then  $B_w = 310,400$  lb/in.<sup>2</sup>. For air,  $B_a = 3000$  lb/ft<sup>2</sup> = 20.83 lb/in.<sup>2</sup> at atmospheric pressure. Then the bulk modulus for the air-water mixture is

$$B_{aw} = \frac{310,400}{1 + 0.001 \left( \frac{310,400}{20.83} - 1 \right)} = 19,500 \text{ lb/in.}^2 \quad (5-21)$$

showing that the bulk modulus is reduced by a factor of about 16. For the air-water mixture alone, the wave velocity is now

$$v_{aw} = \sqrt{\frac{B_{aw}}{\rho_{aw}}} = \sqrt{\frac{(19,500)(144)(32.17)}{(62.4)(0.999)}} = 1204 \text{ ft/sec} \quad (5-22)$$

Thus, by including this small volume of air bubbles (0.10 per cent) in the system, the wave-propagation velocity in the mixture is reduced by about a factor of 4. (Streeter and Wylie, 1967, have included a more comprehensive discussion of the effects of small amounts of air on the wave-propagation velocities in fluids.) For soil-water-air mixtures, the wave-propagation velocity can be evaluated from Eq. (5-15) after substituting  $B_{aw}$  for  $B_w$  in Eq. (5-14) and calculating  $\rho_{tot}$  from Eq. (5-19).

This discussion of the effects of small amounts of air (or gas) in the pore fluid of soils indicates that some control could be exerted on the wave-transmission characteristics of a saturated soil by introducing air bubbles. The comparable problem has been attempted in a full-scale situation in Dover, England, where a pneumatic breakwater was installed (see Evans, 1956; "A Wall of Bubbles . . .," 1959; Kurihara, 1958). A wall of bubbles was formed by compressed air escaping from a pipe laid on the sea bottom across the mouth of the harbor. It was expected that the presence of the bubbles would decrease the compressibility of the sea water in this location and thereby decrease the propagation of wave energy into the harbor. This pneumatic breakwater has been relatively successful, although there is some

difference of opinion as to whether it is because the bubbles affect the compressibility or because the bubbles cause a vertical current in the water.

Another application of bubbles in water to reduce dynamic forces has been described by Graves (1968), in which a curtain of air bubbles has effectively reduced hydraulic-blast forces on submerged structures.

### 5.3 Wave Propagation in Porous Saturated Solids

In Chap. 3 a discussion was presented of the propagation of waves in ideal elastic solids, and in Sec. 5.2 the propagation of compression waves in ideal fluids and mixtures was considered. A closer approximation to the solution for elastic waves in soils can be obtained by studying the behavior of porous elastic solids in which the pores are filled with a fluid, either air or water.

Morse (1952) considered a medium consisting of solid granular materials and fluid which filled the voids. Then he assumed the grains to be motionless and incompressible, thereby restricting his analysis to the wave propagated in the fluid, and evaluated the dissipation of the wave energy by viscous flow through the pores. Sato (1952) treated a sphere of material which contained a spherical hole full of fluid. Then he replaced this system by a sphere of different radius (but with the original compressibility) of homogeneous material and determined the elastic-wave velocities from this adjusted structure. Thus, he ignored the fluid motion. Zwikker and Kosten (1949), Paterson (1955), Brandt (1955), and Biot (1956) studied the elastic waves propagated in saturated porous materials. Zwikker and Kosten assumed one-dimensional strain in a porous elastic solid which contained air in the pores. They considered the coupled motion of the elastic structure and the air and obtained two different velocities which they termed the disturbed elastic-structure wave and the disturbed air wave. Brandt and Paterson studied the waves propagated in saturated granular materials, both theoretically and experimentally. The most complete treatment of the problem, presented by Biot (1956), will be discussed here in some detail.

#### *Biot Theory for Wave Propagation in Porous Saturated Solids*

Biot (1956) considered the general three-dimensional propagation of both shear and compressive waves in a fluid-saturated porous medium. The fluid was assumed to be a compressible liquid free to flow through the pores. Assuming a conservative physical system which was statistically isotropic,

Biot derived the following stress-strain relations containing four distinct elastic constants:

$$\sigma_x = 2G\epsilon_x + \lambda\bar{\epsilon} + C_Q\bar{\epsilon} \quad (5-23a)$$

$$\sigma_y = 2G\epsilon_y + \lambda\bar{\epsilon} + C_Q\bar{\epsilon} \quad (5-23b)$$

$$\sigma_z = 2G\epsilon_z + \lambda\bar{\epsilon} + C_Q\bar{\epsilon} \quad (5-23c)$$

$$\tau_{xy} = G\gamma_{xy}; \quad \tau_{yz} = G\gamma_{yz}; \quad \tau_{xz} = G\gamma_{xz} \quad (5-23d)$$

$$-p = C_Q\bar{\epsilon} + C_R\bar{\epsilon} \quad (5-23e)$$

in which  $\sigma_i$ ,  $\epsilon_i$ ,  $G$ , and  $\lambda$  are as defined in Sec. 3.2, and

$\bar{\epsilon}$  = dilatation in the elastic structure,

$\bar{\epsilon}$  = dilatation in the fluid,

$p$  = total pressure acting on the fluid per unit area of cross-section of porous material, and

$C_Q$ ,  $C_R$  = constants relating to the coupling between the fluid and solid constituents.

If the total volume of the aggregate is held constant, then  $\bar{\epsilon} = 0$  and  $C_R$  is seen to be a measure of the pressure required to push a certain additional volume of fluid into the aggregate. Thus,  $C_R = nB$ , where  $n$  is the porosity and  $B$  is given by Eq. (5-14). The constant  $C_R$  is a positive quantity. The constant  $C_Q$  is a coupling coefficient between the volume change of the solid and that of the fluid. If  $p$  is taken as zero, then

$$\bar{\epsilon} = -\frac{C_Q}{C_R}\bar{\epsilon} \quad (5-24)$$

If a pressure is applied to the elastic structure while  $p$  is zero, there will be a volume change of the solid material of the elastic structure and also a decrease in the porosity which causes a flow of fluid from the element. The volume change of the fluid thus produced should be a function of the Poisson's ratio of the solid, which indicates that  $C_Q$  probably has a value which may be estimated from

$$0 \leq \frac{C_Q}{C_R} \leq \nu \quad (5-25)$$

For a system in which the dissipative forces are disregarded, the dynamic equations of equilibrium in the  $x$ -direction are

$$\frac{\partial \sigma_x}{\partial x} + \frac{\partial \tau_{xy}}{\partial y} + \frac{\partial \tau_{xz}}{\partial z} = \frac{\partial^2}{\partial t^2} [\bar{\rho}u_x + \rho_A(u_x - U_x)] \quad (5-26a)$$

and

$$-\frac{\partial p}{\partial x} = \frac{\partial^2}{\partial t^2} [\bar{\rho}^* U_x + \rho_A (U_x - u_x)] \quad (5-26b)$$

in which

- $\bar{\rho}$  = mass density of the elastic structure (solid particles),
- $\rho^*$  = mass density of fluid, as given by the mass of fluid per unit volume of porous material,
- $\rho_A$  = mass density of an additional apparent mass which relates to the coupling between the fluid and the elastic structure,
- $u_x$  = displacement of particles of the elastic structure in the  $x$ -direction, and
- $U_x$  = displacement of the fluid particles in the  $x$ -direction.

Equations similar to Eqs. (5-26) may be written for equilibrium in the  $y$ - and  $z$ -directions.

By treating the equations of equilibrium (Eqs. 5-26) in a manner similar to that followed in Sec. 3.2, the velocities of the waves of rotation and dilatation may be obtained. Biot found that for the fluid-saturated solid there was only *one* rotational wave and that it involved coupled motion of the elastic structure and the fluid. The equation governing the rotational wave is

$$G \nabla^2 \bar{\omega} = \left( \bar{\rho} + \frac{\rho^* \rho_A}{\rho^* + \rho_A} \right) \frac{\partial^2 \bar{\omega}}{\partial t^2} \quad (5-27)$$

Equation (5-27) is the wave equation (see Eq. 5-6) expressed in terms of the rotation of particles of the elastic structure  $\bar{\omega}$ . The velocity of propagation of the wave described by Eq. (5-27) is

$$v_S = \left[ \frac{G}{\bar{\rho} + \frac{\rho^* \rho_A}{\rho^* + \rho_A}} \right]^{1/2} \quad (5-28)$$

which is the velocity of the shear wave in the elastic structure. Note that there is no structural coupling between the elastic structure and the fluid, because the fluid has no shearing stiffness. There is a rotation of the fluid,  $\bar{\omega}$ , which is related to the rotation of the elastic frame by

$$\bar{\omega} = \frac{\rho_A}{\rho^* + \rho_A} \bar{\omega} \quad (5-29)$$

The rotation of the fluid particles is in the same direction as that for the particles of the elastic structure. From Eqs. (5-27), (5-28), and (5-29), it is seen that the only coupling in the rotational or shearing mode of oscillation

is that developed by the relative motions of the solid and fluid as indicated by the term involving the apparent additional mass density  $\rho_A$ . In a real soil  $\rho_A$  will vary with the grain size and permeability but, as a first approximation, the total mass density of the saturated soil could be introduced into the denominator of Eq. (5-28) to evaluate the shear-wave velocity.

For the ideal fluid-saturated solid, Biot found that *two* dilatational waves are developed. One wave of dilatation (compression wave) is transmitted through the fluid and the other is transmitted through the elastic structure. These two waves are coupled through the stiffnesses of the solid and fluid components of the system as well as through the coupling effect produced by motions of the solid and fluid.

It is because Biot's theory clearly points out the strong influence of the structural coupling involved in the compression waves and the lack of structural coupling for the shear wave that we may feel confident that field measurements of shear waves in saturated soils determine the shear-wave velocity in the soil structure.

#### Example of Application of Biot's Theory

Hardin (1961) described an example of the application of Biot's theory to a water-saturated body of quartz sand. He included the effect of confining pressure on shear modulus of the elastic structure composed of granular particles by assuming that  $G$  varies with  $(\bar{\sigma}_0)^{1/3}$ . The other parameters of the system were chosen to be typical for a uniform quartz sand with a mean particle diameter of 0.35 mm. After substituting these typical values into the equations for wave-propagation velocity, Hardin obtained velocities of propagation for the three waves as shown in Fig. 5-5.

The wave having the highest velocity, shown in Fig. 5-5, represents the compression wave in the fluid. This was designated as the compression wave of the "first kind" by Biot. It has a velocity of propagation higher than that in water alone because of the "push" given by the vibrating elastic structure. The compression wave in the elastic structure (wave of the "second kind") is slightly lower than the compression wave for the dry condition because of the drag of the water in the pores. The shear wave in the elastic structure travels at the lowest velocity. Note that the velocity of the shear wave varies with  $(\bar{\sigma}_0)^{1/6}$  because of the assumption that  $G$  varies with  $(\bar{\sigma}_0)^{1/3}$ . The compression wave in the elastic structure varies approximately with  $(\bar{\sigma}_0)^{1/6}$ , but it is influenced by the coupling between the stiffnesses of the water and the elastic structure. Variations in confining pressure produce little effect on the wave-propagation velocity in the water.

The value of Biot's theory is primarily qualitative—to point out the existence of the three types of waves and the order of magnitude of the



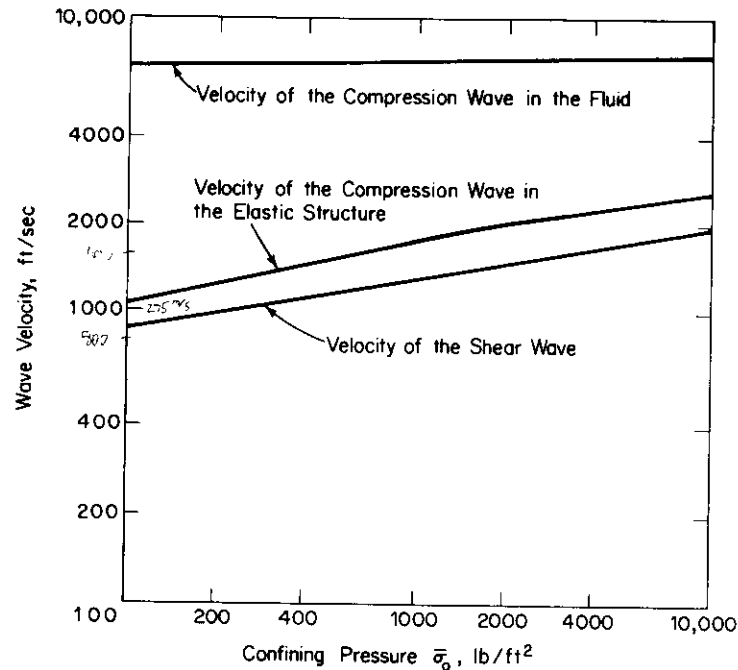


Figure 5-5. Theoretical variation of the two compression-wave velocities and the shear-wave velocity with confining pressure, as calculated from the Biot (1956) theory (from Hardin, 1961).

changes produced in these wave velocities by changes in the different parameters. This theory has also been used by Hardin (1961) to study the effects of changes in soil parameters on damping in the system.

#### 5.4 Effect of Water Table on Wave Propagation in Soils

In many important industrial installations, the water table is relatively close to the ground surface. Thus, the water-saturated soil may also be included in the zone of soil that transmits vibrations to or from a particular foundation. The preceding sections of this chapter have dealt with homogeneous masses of pure fluids, mixtures, or water-saturated solids. In this section we shall discuss, qualitatively, the influences of the boundary between the saturated soils and the dry or partially saturated soils. This boundary is generally designated as the "water table" for static conditions or as the "piezometric level" for seepage conditions. In either case, it describes the elevation of the water surface with respect to a plane of reference.

##### Horizontal Water Table

As the simplest example of the influence of the water table on wave propagation in soils, consider the static condition of a horizontal water table in clean cohesionless soils. We may also assume that the soil is relatively coarse-grained, so that any effects of a capillary zone can be ignored.

The first influence of the water table is on the static unit weight of the soil. For a soil which is homogeneous except for the water effects, the unit weight  $\gamma$  above the water table is given by Eq. (5-4), and the effective or submerged unit weight  $\gamma'$  below the water table is given by Eq. (5-5). Then the effective confining pressure  $\bar{\sigma}_o$  at any point ( $A$ ) within the soil mass is calculated from

$$(\bar{\sigma}_o)_A = \frac{1 + 2K_o}{3} \sum (h_1\gamma + h_2\gamma') \quad (5-30)$$

in which

$K_o$  = coefficient of horizontal earth pressure at rest at point  $A$ ,  
 $h_1$  = height of the column of unsaturated soil above point  $A$ , and  
 $h_2$  = height of the column of saturated soil above point  $A$ .

From Eq. (5-30) it is evident that the effective confining pressure acting at each point in a soil mass depends on the effective overburden pressure which is a function of the heights  $h_1$  and  $h_2$  of the unsaturated and saturated soils. It is shown in Chap. 6, particularly by Eqs. (6-18) and (6-20) and Fig. 6-8, that the shear-wave velocity in soils depends on  $(\bar{\sigma}_o)^{0.25}$ . The compression wave is affected similarly. Therefore, any effect which causes a change in  $\bar{\sigma}_o$  also causes a change in the wave-propagation velocity in the soil. Consequently, the wave-propagation velocity in soils may be changed if the water-table elevation is changed.

In the preceding paragraph it was noted that the presence of the water table in the soil mass changed the wave-propagation characteristics of the soil structure. Possibly even more important is the fact that the presence of the water table converts the soil mass into a *layered system*. The upper layer transmits wave energy through the soil structure, while the saturated layer transmits wave energy through both the soil structure and the fluid. Therefore, at the interface (water surface) the diagrams shown in Fig. 4-1 indicate the kinds of reflections and refractions which may occur. However, if layer 2 is a saturated soil, wave energy will be transmitted by shear and compression waves in the soil structure and by only compression waves in the water.

When the water table is relatively close to the surface of a deposit of cohesionless soil, seismic methods which measure the travel times of the compression waves in the soil will often identify the velocity of the compression wave in water rather than in the soil structure. For example, Ballard

and Casagrande (1966, 1967) have described seismic investigations at Roi-Namur, Kwajalein Atoll, Marshall Islands, and at Cape Kennedy, Florida, where the soils were uniform deposits of sands with the water table at about 6 ft below the surface. At the depth of 6 ft and below, the recorded values of the compression wave were 4800 ft/sec and 5000 ft/sec, as compared to the average values of 1050 ft/sec and 1100 ft/sec for the upper 6 feet at the respective sites. They also measured the shear-wave velocities, which did not show this discontinuity at the water surface.

In the description of the seismic-refraction surveys in Sec. 4.2, it was noted that the time of first arrival of the  $P$ -wave is governed by the layer closest to the surface, which transmits wave energy at the highest velocity. Thus, a "hard" layer (i.e., high modulus or high velocity of wave transmission) close to the surface will mask out a softer underlying layer in a seismic-refraction survey. Earlier in this chapter, it was noted that water has a bulk modulus of approximately 300,000 lb/in.<sup>2</sup>, which leads to a value of about 5000 ft/sec for the velocity of propagation of the compression wave. Thus, water behaves as a "hard" material with respect to wave propagation when compared to the behavior of soils under low confining pressures.

The discussion in the preceding paragraph indicates that recorded values of about 5000 ft/sec for  $P$ -wave propagation in soils may actually represent only the wave propagation in the fluid portion of saturated soils. Consequently, such measurements may not give any useful information about the modulus of the soil structure.

By contrast, the steady-state-vibration method, noted in Sec. 4.3, identifies the shear modulus of the soil structure at various depths within the soil mass. Because fluids cannot transmit shear waves, the only influences of the water table and pore fluids on the propagation of shear waves in the soil structure are through the buoyancy effects on unit weight of the soil and inertia forces (see Biot theory, Sec. 5.3). Thus, for *in-situ* evaluations of the wave-propagation characteristics of soils, it is recommended that both the seismic-refraction and the steady-state-vibration methods be used.

#### *Inclined Piezometric Surface*

An inclined piezometric surface is associated with water flow, or seepage, through soils. Thus, in addition to the usual buoyant effects produced by immersion of soil particles, the vertical component of the seepage forces must be considered in evaluating local variations of the unit weight of soil. At any point within the soil mass, the vertical component of the hydraulic gradient  $i_z$  may be evaluated. Then the effective submerged unit weight under seepage conditions is determined from

$$\gamma'_s = \frac{(G_s - 1)\gamma_w}{1 + e} \pm i_z \gamma_w \quad (5-31)$$

In Eq. (5-31) the + sign applies to the last term when the water flow is downward. Then  $\gamma'_s$  is substituted for  $\gamma'$  in Eq. (5-30) to evaluate the confining pressure in the soil at a particular point.

The effects of an inclined piezometric surface on the reflection and refraction of wave energy are similar to the effects of inclined layers, as discussed in Sec. 4.2.

#### *Fluctuating Water Table*

It is important to be able to estimate the probable ranges of fluctuation of the water table at any proposed site. This fluctuation may be seasonal and occur with some regularity, or may represent only a temporary condition. Variations of the water table during or because of construction, or because of floods or tides, may cause temporary changes in the dynamic characteristics of a foundation-soil system. These temporary conditions can usually be tolerated, but their influences should be examined during the design considerations. However, the seasonal changes may be significant, and this influence must be established, particularly if the design is based on dynamic soil characteristics obtained from field measurements obtained under only one set of field conditions.

### 5.5 Summary

This chapter emphasizes the important role water has in modifying the wave-propagation characteristics of soils. Because water is a "hard" material in comparison with many soils near the ground surface, it is capable of transmitting the compression wave at a higher velocity than does the soil structure. Seismic field tests may indicate compression-wave-propagation velocities of the order of 5000 ft/sec in saturated soils, which is about the wave-propagation velocity in water. Thus, this kind of field test may not describe the true behavior of the soil structure.

A brief discussion was included to illustrate the importance of small amounts of gas on the wave-propagation velocity in a fluid-gas mixture. Therefore, in unsaturated soils the highest velocity of propagation of the compression wave could range from that in the soil structure alone to that in the fluid.

As a result of the discussion in this chapter, it is recommended that field evaluations of the wave-propagation velocities in water-bearing soils be conducted by both the seismic-refraction and the steady-state-vibration methods.

# 6

## BEHAVIOR OF DYNAMICALLY LOADED SOILS

### 6.1 Introduction

Perhaps the most critical step in the design of a foundation-soil system to resist dynamic loads is the correct evaluation of the soil properties involved. These soil properties will be different for each construction site. Furthermore, the dynamic response of a given soil depends upon the loading conditions and strain distributions developed in the soil mass. Thus, it is impossible to present a concise discussion which describes all situations. Rather, the purpose of this chapter is to describe the general problems associated with the response of soils to dynamic loads and to discuss some typical test results for specific conditions. It will be left to the reader to estimate how well the examples presented herein approximate his design conditions and to add continually to his file of data in this rapidly developing field.

The primary emphasis in this chapter is directed toward the response of soils to vibratory stresses of relatively small magnitude. The small-amplitude stress-strain behavior of a soil mass governs the velocity of wave transmission through the soil (Chap. 3) and is the critical factor in determining the dynamic response of foundations supported directly on soils (Chap. 10). The characteristics of the stress-strain curve determine the ranges of strain associated with elastic or inelastic response and identify the energy losses which develop in soil masses following repeated loadings.

As a first step toward evaluating the dynamic responses of soils to small-amplitude loadings, it is useful to consider the soil particles to be represented by perfect elastic spheres. Mathematical solutions have been presented for the static and dynamic responses which describe the influence of the confining pressures and lateral deformations on the wave propagation, moduli, and damping in masses of these ideal spheres. These solutions serve as useful guides for estimating the dynamic response of real soils.

For dynamic strains of the same order of magnitude as those developed beneath machine foundations, it has been found that soils exhibit an approximately elastic behavior. Thus, it is necessary to evaluate these quasi-elastic soil characteristics for use in design. Methods are described in Sec. 6.3 for evaluating these quantities from both laboratory and field tests.

Finally, large-amplitude dynamic strains cause changes in the soil structure which result in settlements and often loss of strength in soil masses. Section 6.4 includes a brief description of the effects of large-amplitude strains similar to those produced by blasts, earthquakes, and compaction operations.

### 6.2 Behavior of Elastic Spheres in Contact

#### *Arrangements of Perfect Spheres*

For a first approximation to a mass of cohesionless soil, consider an array of perfect spheres. This model may be further restricted to spheres of identical size arranged in patterns in which the spheres are in contact and no large voids are present because of missing spheres. Thus, the mass of spheres is statistically homogeneous.

In Fig. 6-1a, a group of these identical spheres are shown in the *simple cubic* packing in which each sphere touches six neighbors. This is the loosest arrangement for equal spheres and produces a void ratio  $e = 0.91$ . This may be established by examining a cubic element (Fig. 6-1c) for which the volume of the cube is  $8R^3$  and the volume of the inscribed sphere is  $\frac{4}{3}\pi R^3$ . Thus, the void ratio is

$$e = \frac{V_v}{V_s} = \frac{V - V_s}{V_s} = \frac{8R^3 - \frac{4}{3}\pi R^3}{\frac{4}{3}\pi R^3} = 0.91$$

Figure 6-1a represents both the plan and elevation of the arrangement for the simple cubic packing.

A second arrangement of these identical spheres can be developed by a simple modification of Fig. 6-1a. If the arrangement in Fig. 6-1a is

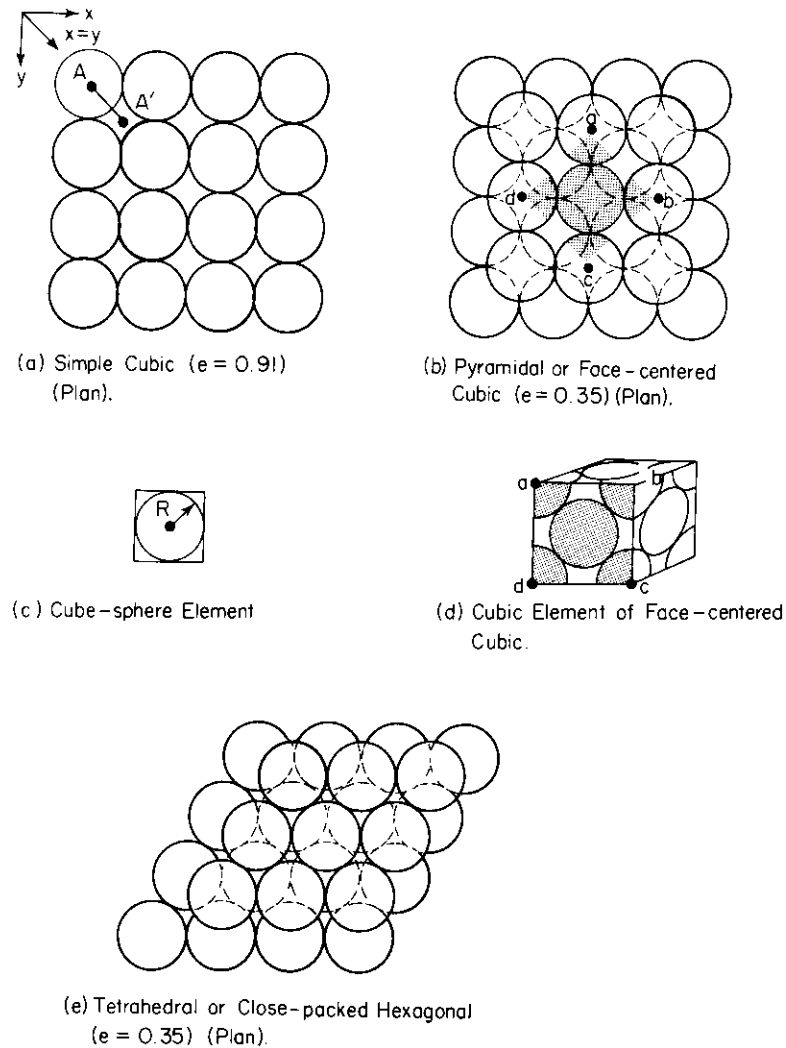


Figure 6-1. Modes of regular packing of equal spheres.

considered to represent the bottom layer of a pack of spheres and a second identical layer is added on top but translated along a path indicated by  $A-A'$  in Fig. 6-1a, then each sphere of the second layer will fit in the pocket formed by the depression between four spheres of the bottom layer. By adding successive layers, each with the plan arrangement of Fig. 6-1a but translated each time to allow the spheres to fit in the pocket between four spheres below, the *pyramidal* packing shown in Fig. 6-1b is formed. This packing is

sometimes called the *face-centered* cubic packing because a cubic element with a face  $abcd$  as shown in Fig. 6-1d also describes the packing. The corners  $a$ ,  $b$ ,  $c$ , and  $d$  of the face of the cubic element are indicated in Fig. 6-1b to show how it fits into the aggregate.

The void ratio of the pyramidal or face-centered cubic packing can be evaluated readily from Fig. 6-1d. The side of the cube has a length of  $4R/\sqrt{2}$  and a volume of  $(32/\sqrt{2})R^3$ . In this cubic element there are 6 hemispheres and 8 octants, or a total of 4 spheres each having a volume of  $\frac{4}{3}\pi R^3$ . Therefore, the void ratio is

$$e = \frac{V - V_s}{V_s} = \frac{\frac{32}{\sqrt{2}}R^3 - 4\left(\frac{4}{3}\pi R^3\right)}{4\left(\frac{4}{3}\pi R^3\right)} = 0.35$$

The *tetrahedral* or *close-packed hexagonal* arrangement of identical spheres shown in Fig. 6-1e also produces the minimum void ratio of  $e = 0.35$ . Lower values of void ratio are possible, of course, if smaller equal spheres are packed in the voids between the larger spheres.

The principal reason for the discussion of these arrangements of equal spheres is to demonstrate the large changes in void ratio possible just by rearrangement of particles. An aggregate of particles originally in the simple cubic packing can be transformed into the pyramidal packing quite readily if each layer moves along a path  $A-A'$  as illustrated in Fig. 6-1a. The settlement of a unit thickness for this rearrangement is

$$\Delta = \frac{\Delta e}{1 + e} = \frac{0.91 - 0.35}{1.91} = 0.293$$

or the layer is reduced by 29.3 per cent of its original thickness. Thus, changes in particle arrangements can lead to serious settlements in layers of cohesionless materials.

### Spheres Subjected to Normal Loads

In the process of evaluating the behavior of a mass of equal-sized spheres under normal loading, it is customary to begin with the Hertz theory (Hertz, 1881; see also Timoshenko and Goodier, 1951) for two spheres pressed together by a normal force  $P$ . Figure 6-2a shows two spheres of equal radius  $R$  just touching, and Fig. 6-2b illustrates the deformation which occurs when the normal force  $P$  presses the two spheres together. Upon application of the

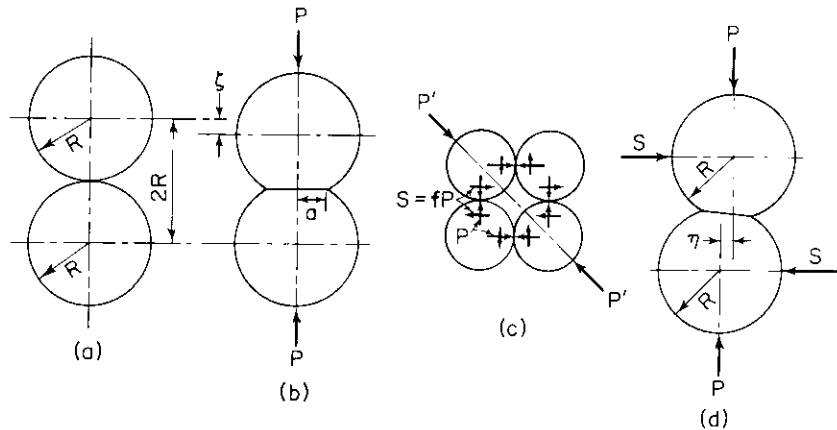


Figure 6-2. Behavior of equal spheres in contact. (a) Spheres just touching. (b) Deformation by normal force. (c) Shearing forces between particles in cubic packing. (d) Lateral deformation by shearing forces.

load, the point of contact develops into a flat circular area of contact of radius  $a$ . The size of this contact area depends on the shear modulus  $G$  and the Poisson's ratio  $\nu$  of the sphere material; on the radius  $R$  of the sphere; and on the normal force  $P$ . The radius of the contact area is

$$a = \sqrt[3]{\frac{3(1-\nu)}{8G} PR} \quad (6-1)$$

The displacement  $\zeta$  representing the reduction in the center-to-center distance between the two spheres is given by

$$\zeta = \frac{2a^2}{R} \quad (6-2)$$

On the plane of contact between the two spheres, the normal stress  $\sigma$  varies from a maximum at the center,  $r = 0$ , to a minimum at the radius,  $r = a$ , according to the expression

$$\sigma = \frac{3P}{2\pi a^2} \sqrt{1 - \left(\frac{r}{a}\right)^2} \quad (6-3)$$

Eq. (6-3) describes a parabolic distribution of contact pressure which has a maximum value of

$$\sigma_{\max} = \frac{3P}{2\pi a^2} = \frac{4Ga}{(1-\nu)\pi R} \quad (6-4)$$

that is  $1\frac{1}{2}$  times the average pressure.

Equations (6-1) through (6-4) demonstrate the nonlinear relations which exist between the applied normal force  $P$ , the area of contact, the displacement of the spheres, and the contact stresses. However, this is an *elastic* system for which the load-displacement curves follow the same path during loading or unloading (assuming that the spheres are made of an ideal elastic material), and no energy is lost during a loading-unloading cycle. This describes a nonlinear elastic behavior.

The normal compliance  $C$  of the two spheres in contact is the reciprocal of the tangent to the load-deformation curve, and its value depends upon the applied load  $P$ . It is expressed by

$$C = \frac{d\zeta}{dP} = \frac{4}{3} \left[ \frac{3(1-\nu)}{8G} \right]^{2/3} \left( \frac{1}{RP} \right)^{1/3} \quad (6-5)$$

Equation (6-5) represents the incremental motion of the centers of the two spheres as a consequence of an incremental normal force  $dP$ . From the compliance, we can develop a simple expression for the tangent modulus of elasticity for a simple cubic packing of equal spheres loaded along one coordinate axis of the cube (for example, the  $x$ -axis as shown in Fig. 6-1a). The average stress in the  $x$ -direction equals the force transmitted through a row of spheres divided by the effective square cross-section of the row (see Fig. 6-1c):

$$\sigma_x = \frac{P}{4R^2} \quad (6-6)$$

Equation (6-6) can be introduced into Eq. (6-5) to develop the tangent modulus  $E_T$  for uniaxial loading:

$$E_T = \frac{d\sigma_x}{d\epsilon_x} = \frac{1}{2CR} = \frac{3}{2} \left[ \frac{2G}{3(1-\nu)} \right]^{2/3} \sigma_x^{1/3} \quad (6-7)$$

The significant factor in Eq. (6-7) is that the tangent modulus depends upon the cube root of the axial stress. Equation (6-7) also leads to an expression for the modulus of volume compression  $B$ , which relates the hydrostatic stress  $\sigma_o$  to the volumetric strain. If we consider  $\sigma_o = \sigma_1 = \sigma_2 = \sigma_3$ , then the volumetric strain is three times the uniaxial strain given in Eq. (6-7), and the modulus of volume compression becomes

$$B = \frac{1}{2} \left[ \frac{2G}{3(1-\nu)} \right]^{2/3} \sigma_o^{1/3} \quad (6-8)$$

Because the deformation of spheres in contact is a local phenomenon, the

behavior described by Eqs. (6-7) and (6-8) could be superposed in any order as long as only normal forces are developed at the points of contact between the spheres. For example, the usual condition existing in soils corresponds to some allround confining pressure  $\sigma_0$  existing in the "at-rest" condition because of the weight of the soil. Then, if an additional stress is added in the  $x$ - or  $y$ -direction (see Fig. 6-1a), the tangent modulus for longitudinal deformation would correspond to that given by Eq. (6-7) if we substitute  $\sigma_0$  for  $\sigma_x$ .

It should be noted that the simple cubic packing of equal spheres is a structure primarily of academic interest. The load-deformation or stress-strain relations for this structure depend on normal forces at the points of contact only when the stresses are hydrostatic or act along the principal axes (i.e., axes  $x$  and  $y$  in Fig. 6-1a). When stresses are applied along a diagonal direction ( $x = y$  in Fig. 6-1a), both normal and shearing forces are developed at the points of contact, as shown in Fig. 6-2c. An additional theoretical treatment is required to cover the effects of shearing forces at the points of contact.

#### Effect of Tangential Forces at Contact Between Spheres

The case of two equal spheres pressed together by a normal force  $P$ , then subjected to a shearing force  $S$ , was studied theoretically by Cattaneo (1938), Mindlin (1949), and Mindlin and Deresiewicz (1953). The solutions treated the problem in which a constant normal force  $P$  was maintained as the shearing force  $S$  was varied and the horizontal displacement  $\eta$  of the vertical centerline through the spheres (see Fig. 6-2d) as well as the stresses on the contact surface were evaluated. They considered first the condition for *no slip* between the spheres at the contact surface, for which the theoretical distribution of shearing stresses was as indicated by the curve labeled, " $\tau$ —no slip," in Fig. 6-3. Note that the theoretical distribution indicates infinite shearing stresses at the periphery of the contact area. On a real material the limiting shearing stress which may be developed depends on the coefficient of friction between the two surfaces and the normal stress, or

$$\tau_f = f\sigma \quad (6-9)$$

In Eq. (6-9) the coefficient of friction  $f$  is assumed to be a constant. In order to make the theoretical solution conform to the realistic limits on the shearing stresses, an annular zone was determined in which the shearing stresses had the limiting value established by Eq. (6-9). This annular zone is shown in Fig. 6-3 as the region between ( $r = a$ ) and ( $r = c$ ). Within the central zone ( $r \leq c$ ) no slip occurred.

The theoretical prediction of slip on an annular ring of the contact surface was confirmed by experiments on glass spherical surfaces in contact

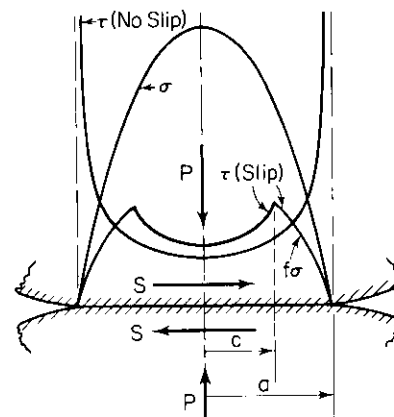


Figure 6-3. Distribution of normal ( $\sigma$ ) and shearing ( $\tau$ ) stresses on the contact surface between two spheres loaded by axial ( $P$ ) and shearing ( $S$ ) forces (from Mindlin, 1954).

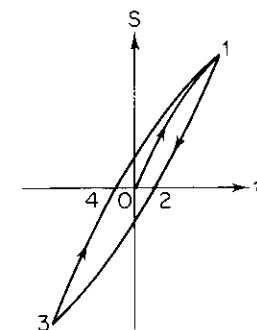


Figure 6-4. Hysteresis loop formed by shearing force-displacement relations for two equal spheres pressed together and subjected to shearing forces.

(Mindlin et al., 1951). Furthermore, the evidence of slip upon loading indicates a continual change in the shearing stress distribution during loading. Similarly, the distribution of shearing stresses will vary upon unloading, and residual stresses are developed in the slip zone when tangential force has been again reduced to zero. Mindlin and Deresiewicz (1953) studied these changes in slip, stress distribution, and displacement. They concluded that the changes in shearing forces and displacements depended not only on the initial state of loading, but also on the entire past history of loading and the instantaneous relative change of the normal and tangential forces. From theoretical studies they developed the shearing force-lateral displacement relations shown in Fig. 6-4 for a reversed loading. This diagram indicates a typical hysteresis loop from which the energy loss per loading cycle can be evaluated.

The behavior of an aggregate of equal spheres when both normal and shearing forces act at the contact points may be studied by considering the simple cubic packing (Fig. 6-1a) loaded along the ( $x = y$ )-direction. First a hydrostatic pressure  $\sigma_0$  is applied, then an additional uniaxial stress is applied in the ( $x = y$ )-direction. Because tangential forces are developed on loading, as indicated in Fig. 6-2c, there is a loss of energy upon loading. Upon unloading, the direction of the tangential forces is reversed and there is again a loss of energy at the contact. Deresiewicz (1958) has presented a theoretical solution for the stress-strain relationships during loading and unloading and for the criterion of failure. The stress-strain curve for loading is concave toward the strain axis and similar in shape to the curve 0-1 in Fig. 6-4. By

evaluating the strains parallel and perpendicular to the direction of loading, an effective value of Poisson's ratio for the array of spheres can be established. For example, if the Poisson's ratio for the sphere material is 0.25 and the coefficient of friction  $f$  between the spheres is chosen as 0.50, the effective Poisson's ratio varies from about 0.10 for small longitudinal stresses to 0.22 at the failure stress. The "failure" in this case is defined as the beginning of sliding between the spheres, which occurs when

$$\frac{\sigma_{(x=y)}}{\sigma_o} > \frac{2f}{1-f} \quad (6-10)$$

The longitudinal stress  $\sigma_{(x=y)}$  in Eq. (6-10) represents the axial stress ( $\sigma_1 - \sigma_o$ ) which is applied in the ( $x = y$ )-direction. Upon unloading from the maximum load applied, a stress-strain curve similar in shape to the curve 1-2 in Fig. 6-4 is developed. The significant fact derived from this study is that a stress-strain curve concave to the strain axis is developed when lateral expansion of the mass of spheres is permitted.

The arrangement of equal spheres in the face-centered cubic lattice was treated by Duffy and Mindlin (1957). They considered additional increments of the one-dimensional stress field acting on the array of spheres previously subjected to a hydrostatic stress  $\sigma_o$ . When the longitudinal stress acts parallel to the edge of the cube ( $x$ -direction, Fig. 6-1b), the stress-strain relation is

$$\frac{d\sigma_x}{d\epsilon_x} = \frac{2(8-7\nu)}{8-5\nu} \left[ \frac{3G^2\sigma_o}{2(1-\nu)^2} \right]^{1/3} \quad (6-11)$$

The modulus obtained from Eq. (6-11) is higher than that obtained from the Hertz theory (Eq. 6-7) because it includes the effects of the tangential stiffnesses at the contact points.

For the face-centered array of equal spheres under a hydrostatic stress  $\sigma_o$ , only normal forces exist at the points of contact between the spheres. Hendron, Fulton, and Mohraz (1963) have integrated the expression for incremental strain to determine the hydrostatic strain along any chosen axis as

$$\epsilon_o = \left( \frac{3(1-\nu)\sqrt{2}}{8G} \right)^{2/3} \sigma_o^{2/3} \quad (6-12)$$

Note that Eq. (6-12) represents a stiffer array than does Eq. (6-7) because 12 contacts per sphere are made in the face-centered array in contrast to 6 contacts per sphere in the simple cubic array. Hendron et al. (1963) also studied the case of one-dimensional compression of the face-centered array

of equal spheres. In this condition no lateral strain is permitted ( $\epsilon_x = \epsilon_y = 0$ ) and strain is developed only in the  $z$ -direction. During a monotonically increasing load, the strain is described by

$$\epsilon_z = \left[ \frac{3(1-\nu)\sqrt{2}}{8G(1+f)} \right]^{2/3} 2\sigma_z^{2/3} \quad (6-13)$$

By comparing Eqs. (6-12) and (6-13) it is seen that the ratio of axial strain at the same value of  $\sigma_z$  reduces to

$$\frac{\epsilon_z}{\epsilon_o} = \frac{2}{(1+f)^{2/3}} \quad (6-14)$$

Stress-strain curves representing Eqs. (6-12) and (6-13) are shown in Fig. 6-5 for the loading cycle. Because shearing forces are developed at the contact points for the one-dimensional strain condition, energy is lost during loading and unloading and the unloading curve is indicated by the dashed line in Fig. 6-5 for the condition of no lateral strain.

An examination of curves  $O-A$ ,  $O-B$ , and  $O-C$  in Fig. 6-5 reveals the significant factor governing the stress-strain behavior of arrays of equal spheres. The stiffest condition exists when the lateral strain is equal to the vertical strain under hydrostatic loading. When lateral strains are equal to zero, the behavior of the aggregate is still of the "strain-hardening" type (the stress-strain curve is concave toward the stress axis as it is for the hydrostatic stress condition), but greater axial strains are developed than for the hydrostatic loading. Finally, for the condition of constant lateral pressure (but no restriction on strains), the stress-strain curve is concave toward the strain axis. Therefore, we may conclude that the stress-strain behavior of an array of equal-sized spheres in initial contact depends on the amount of lateral strain developed during axial loading.

The particles of real soils are, of course, not perfect spheres arranged in a perfect packing. Furthermore, there are other variables which must

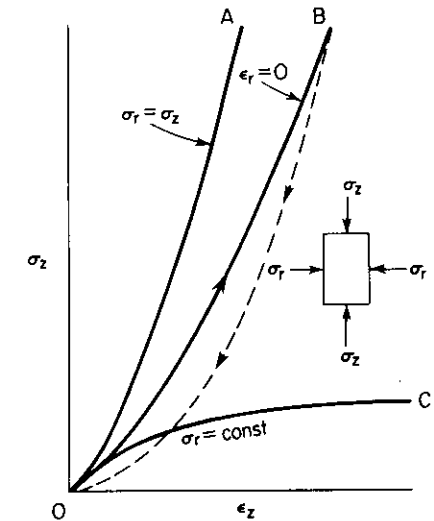


Figure 6-5. Theoretical stress-strain curves for triaxial tests of granular materials with various lateral restraints.

be considered when treating a material comparable to clean, dry, uniform sand: irregular *shape* of the grains; rotation and displacement of these grains during loading or unloading; nonuniform packing; and fracture of the grains during loading. In addition, the treatment so far has considered only single loading cycles involving *very small strains*. The effects of repeated applications of larger strains in real soils will be discussed in following sections.

### Resonant-Column Tests of "Perfect" Spheres

The previous discussion dealt with ideal spheres of exactly the same size. For aggregates composed of these spheres it was found (Eqs. 6-7 and 6-11) that the longitudinal modulus of elasticity varies with the  $\frac{1}{3}$  power of the normal stress. In such a medium it would be anticipated that a longitudinal wave would be propagated with a velocity

$$v_C = \sqrt{\frac{E}{\rho}} \quad (3-3)$$

or

$$v_C \propto \sigma_o^{1/6} \quad (6-15)$$

In order to evaluate this theoretical prediction, Duffy and Mindlin (1957) conducted an experimental study of the elastic-wave propagation in a rod composed of steel spheres. These spheres were high-tolerance ball bearings carefully sorted into two groups. The bearings in one group each had a tolerance on the diameter of  $\frac{1}{8}$  ( $\pm 0.000050$ ) in., and those in the other group each had a tolerance of  $\frac{1}{8}$  ( $\pm 0.000010$ ) in. These spheres were carefully arranged in a face-centered cubic array to form square bars. These bars were covered by a rubber membrane and a confining pressure was developed by vacuum within the porous bar. After applying the confining pressure, the bars were set into longitudinal vibration, and the wave velocity was established from the resonant frequency of forced vibration. Figure 6-6 shows the test results obtained for the two groups of spheres as well as the curve predicted by theory. It is significant to note that even for these spheres, which would be considered "perfect" by normal standards, there was a definite difference between the longitudinal velocities predicted by theory and those obtained by test.

In view of the discrepancies noted in Fig. 6-6, we cannot expect that the wave-propagation velocities developed in real granular soils will agree closely with the theoretical values predicted from theories for perfect spheres. The theoretical studies are useful as a guide, but we *must establish the wave-propagation velocities in real soils by experimental methods*.

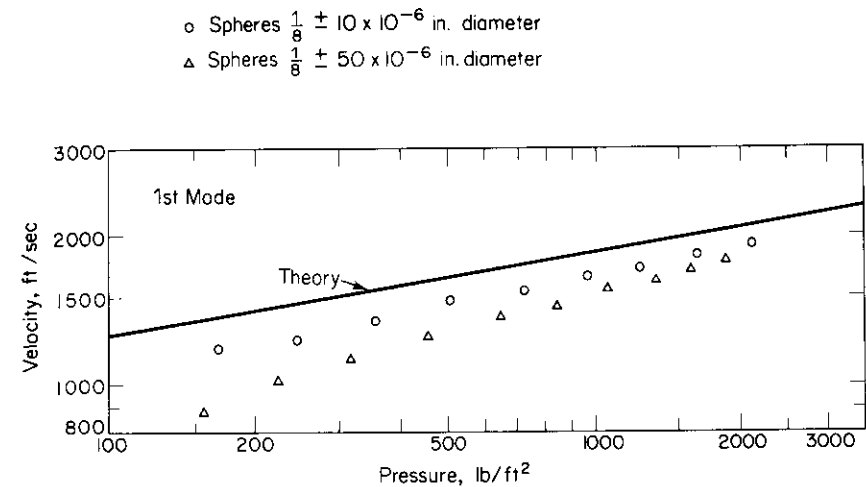


Figure 6-6. Variation of the velocity of the compression wave with confining pressure for bars composed of stainless steel spheres (from Duffy and Mindlin, 1957).

### 6.3 Behavior of Soils Under Small-Amplitude Vibratory Loading

This section will treat the behavior of soils under vibratory loadings which develop longitudinal strains of the order of 0.0001 in./in. or shearing strains of 0.0001 rad or less. It is this order of magnitude of strains which are developed in soils supporting vibratory machinery designed for continuous operation.

#### Resonant-Column Tests of Soils

The resonant-column method was employed by Iida (1938, 1940) to study the wave propagation in vertical columns of sand set into longitudinal or torsional oscillations. The frequency at resonance and the height of the specimen provided the information for calculation of the wave velocity. Dry and saturated samples were retained in a cylindrical shape by a cellophane tube, and partially saturated samples were unsupported after being removed from the compaction mold. In all cases the confining pressure was developed by the weight of the samples. During the decade following Iida's tests, little published information was available on the evaluation of soil properties by vibratory methods, but interest picked up in the 1950s and many papers have



been published since that time. A selected list of these references has been given by Hardin and Richart (1963) and by Hardin and Black (1968). The resonant-column device has been used since the mid-1950s for both research and routine soil evaluation (for example, see Shannon, Yamane, and Dietrich, 1959; and Wilson and Dietrich, 1960). Since about 1960 the resonant-column device has been adopted as a research and testing tool in a number of university, government, and consulting laboratories.

In the resonant-column test a vertical cylindrical sample of soil is contained within a rubber membrane and a confining pressure is applied to maintain the shape of the sample during the test. From the preceding discussion of the behavior of ideal spheres under load, we can anticipate that cohesionless materials will respond to applied loadings in a nonlinear, inelastic manner, and that the response will depend on the effective confining pressure  $\bar{\sigma}_o$ . It is important to evaluate the effects of the various factors that influence the shear modulus  $G$  of soils in both the laboratory tests and the prototype situations. An evaluation of the internal damping in the soil and the effective Poisson's ratio are of secondary importance.

#### *Variables Which Affect the Shear Modulus*

Hardin and Black (1968) have indicated the various quantities which exert an influence on the shear modulus of soils in the form of a functional relation for  $G$ , as

$$G = f(\bar{\sigma}_o, e, H, S, \tau_o, C, A, f, t, \vartheta, T) \quad (6-16)$$

in which

$\bar{\sigma}_o$  = effective octahedral normal stress (average effective confining pressure),

$e$  = void ratio,

$H$  = ambient stress history and vibration history,

$S$  = degree of saturation,

$\tau_o$  = octahedral shear stress,

$C$  = grain characteristics, grain shape, grain size, grading, mineralogy,

$A$  = amplitude of strain,

$f$  = frequency of vibration,

$t$  = secondary effects that are functions of time, and magnitude of load increment,

$\vartheta$  = soil structure, and

$T$  = temperature, including freezing.

Of course, several of these quantities may be related as, for example,  $e$ ,  $C$ , and  $\vartheta$ .

In the case of sands, it has been shown that for shearing-strain amplitudes less than about  $10^{-4}$ , and within the range of the variables studied,  $G$  is

essentially independent of each of the variables listed in Eq. (6-16) except for  $\bar{\sigma}_o$  and  $e$ . Hardin and Richart (1963) showed that the grain size and grading of sands retained on the No. 120 sieve had almost no effect on  $G$ , that the grain shape had little effect, and that the degree of saturation had a minor effect which occurred only at low pressures. It was also found that the frequency of vibration had no measurable effect on  $G$  for frequencies less than about 2500 cycles/sec.

#### *Effect of Void Ratio and Confining Pressure*

Figures 6-7 and 6-8 illustrate the influence of void ratio and confining pressure on the shear-wave velocities of clean granular materials over the range of  $(0.37 < e < 1.26)$ . A special note should be made that the *relative density* (see Eq. 6-37) of the material has a negligible influence on the shear-wave velocity. For example, if we examine the wave velocities shown in Fig. 6-7 for the void ratio of 0.61, it can be seen that these are quite similar for the No. 20-30 and No. 80-140 sands, even though the relative densities for the two materials are approximately 47 and 80 per cent, respectively. Furthermore, the maximum variation of shear-wave velocity with change of void ratio may be evaluated for any sand by considering the values of  $v_s$  corresponding to the maximum and minimum void ratios and a given confining pressure. These values will bracket the correct value for  $v_s$  for this sand *in situ* subjected to this same value of confining pressure. Thus, a disturbed sample of sand from a given boring would be satisfactory for determining the maximum and minimum void ratios for this material and, after the confining pressure  $\bar{\sigma}_o$  was established, would provide enough information to establish limits for the probable values of  $v_s$ .

Figure 6-7 illustrates the significant effect the confining pressure has on the shear-wave velocity of clean sands. Straight lines have been fitted through the test points corresponding to the different confining pressures, and these lines are shown in Fig. 6-8 as solid lines. Also shown in Fig. 6-8 are dashed lines which represent the results from tests using clean angular-grained materials in order to extend the range of void ratios considered. For each set of curves the effect of confining pressure on  $v_s$  is shown to be significant.

Figure 6-8 also includes a small diagram which illustrates the variations of the shear modulus  $G$  caused by changes in void ratio or confining pressure. These values may be obtained directly from the shear-wave velocity through the relation

$$G = \rho v_s^2 \quad (6-17)$$

Empirical expressions have been developed for  $v_s$  and  $G$  for round-grained sands and angular-grained crushed quartz. For the *round-grained sands*

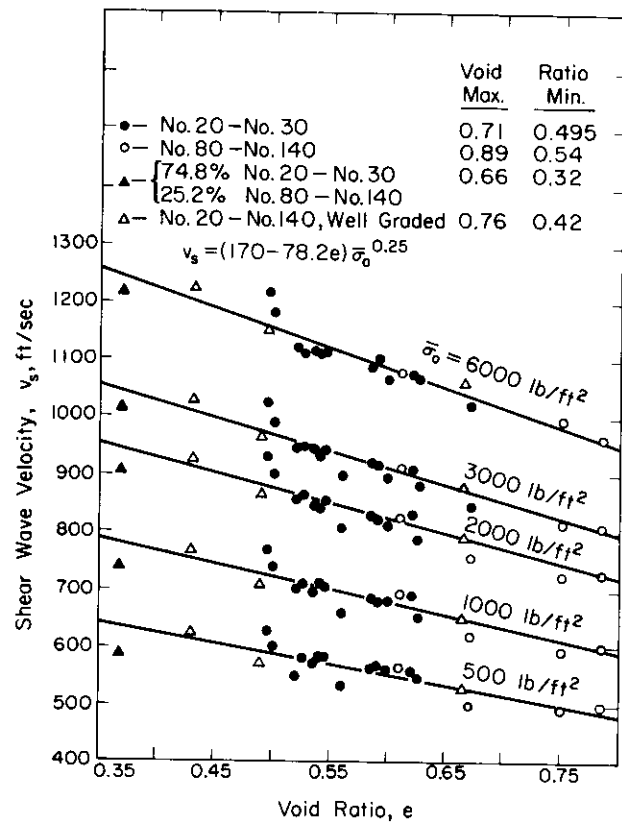


Figure 6-7. Variation of shear-wave velocity with void ratio for various confining pressures, grain sizes, and gradations in dry Ottawa sand (from Hardin and Richart, 1963).

( $e < 0.80$ ) they are

$$v_s = [170 - (78.2)e] (\bar{\sigma}_o)^{0.25} \quad (6-18)$$

(ft/sec)                      (lb/ft<sup>2</sup>)

and

$$G = \frac{2630(2.17 - e)^2}{1 + e} (\bar{\sigma}_o)^{0.5} \quad (6-19)$$

(lb/in.<sup>2</sup>)                      (lb/in.<sup>2</sup>)

and for the angular-grained materials they are

$$v_s = [159 - (53.5)e] (\bar{\sigma}_o)^{0.25} \quad (6-20)$$

(ft/sec)                      (lb/ft<sup>2</sup>)

and

$$G = \frac{1230(2.97 - e)^2}{1 + e} (\bar{\sigma}_o)^{0.5} \quad (6-21)$$

(lb/in.<sup>2</sup>)                      (lb/in.<sup>2</sup>)

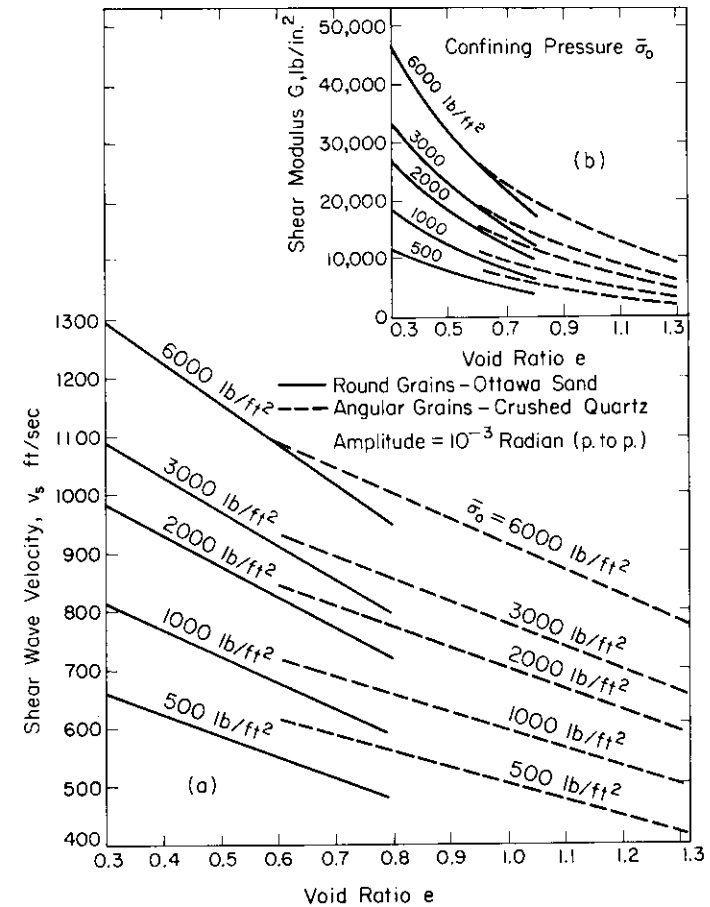


Figure 6-8. Variation of shear-wave velocity and shear modulus with void ratio and confining pressure for dry round and angular-grained sands (from Hardin and Richart, 1963).

Since 1961, numerous independent checks of the wave-propagation velocities of clean, dry, cohesionless materials have been made with at least seven different types of resonant-column devices. The wave-velocity, void-ratio, and confining-pressure data have consistently been found to agree (to within about 10 per cent) with those given by the curves in Fig. 6-8. Additional correlations have been obtained by use of the pulse technique (see Whitman and Lawrence, 1963), although the wave velocities are slightly higher for the pulse than for the steady-state vibration.

Another variable first thought to be significant was the state of shearing stress in the sample identified by the shearing stress on the octahedral plane,

or the *octahedral shearing stress*,

$$\tau_o = \frac{1}{3}\sqrt{(\sigma_1 - \sigma_2)^2 + (\sigma_2 - \sigma_3)^2 + (\sigma_3 - \sigma_1)^2} \quad (6-22)$$

However, Hardin and Black (1966) demonstrated that the shear-wave velocity in sands depended on the confining pressure  $\bar{\sigma}_o$  (normal stress on the octahedral plane, or average of the three principal stresses) and was essentially independent of the state of shearing stress in the sample. This is a significant factor in the design of machine foundations resting on sands because it establishes  $\bar{\sigma}_o$  as the principal quantity to be estimated for a particular bed of sand in order to evaluate  $v_s$  or  $G$  for use in the dynamic analysis.

### Effect of Saturation

In Chap. 5 a theoretical study (Biot, 1956) was described which treated the wave propagation in a fluid-saturated porous medium. It was shown that the presence of the fluid exerted an important influence on the dilatational-wave velocity but produced only a minor effect on the shear-wave velocity. The fluid affects the shear-wave velocity only by adding to the mass of the particles in motion. Figure 6-9 shows the influence of degree of saturation on the shear-wave velocity for a sample made of 20–30 Ottawa sand. Much of the difference between the curves for the dry and saturated conditions can be accounted for by the effect of the weight of the water. Therefore, it is sufficient for an evaluation of  $v_s$  or  $G$  for cohesionless soils to consider the *in-situ* unit weight and the effective  $\bar{\sigma}_o$ .

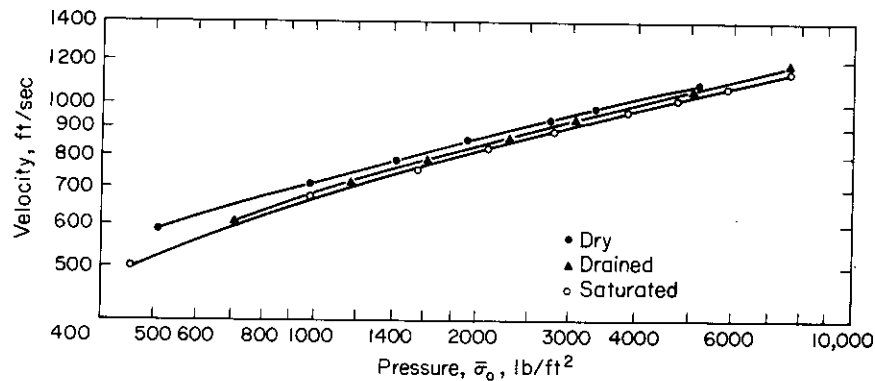


Figure 6-9. Variation of shear-wave velocity with confining pressure for a specimen of Ottawa sand in the dry, saturated, and drained conditions (Test No. 18.  $e = 0.55 - 0.54$ ) (from Hardin and Richart, 1963).

### Behavior of Cohesive Soils

The dynamic response of cohesive soils has been studied by several groups and tentative conclusions have been reached regarding many of the variables indicated by Eq. (6-16). The most important difference between testing cohesionless and cohesive soils is the *time interval* required for consolidation between load increments when establishing curves of the type shown in Fig. 6-9. For samples of 20–30 Ottawa sand it has been found that 6 to 30 minutes were adequate for local adjustments in the sample and reliable and repeatable readings could be obtained using this time interval between pressure changes. Cohesive soils require a much longer time for consolidation between pressure increments, depending on the permeability of the soil, shape of the specimen, and drainage paths. For normally consolidated samples of kaolinite tested in a resonant-column device using specimens of the standard triaxial test size, Hardin and Black (1968) have indicated about two hours as the time required for 100 per cent primary consolidation to be completed. In general, for resonant-column tests on samples of cohesive soils taken from the field, test results involving short time intervals between pressure changes could be expected to be adequate only for pressures corresponding to the “in-situ” confining pressures. However, reliable values of the shear-wave velocity can be obtained at higher confining pressures if enough time is allowed between pressure increments to permit the major part of primary consolidation to be completed.

There is further evidence (Hardin and Richart, 1963; Hardin and Black, 1968; Humphries and Wahls, 1968) that the shear-wave velocity continues to increase during secondary compression. The amount of this increase is not fully accounted for by the change in void ratio, but some part of it is probably associated with the change in soil structure (parameter  $\vartheta$  in Eq. 6-16). There is a need for continued research on the effect of time, or secondary compression, and changes of soil structure on the shear-wave velocity and shear modulus of cohesive soils. Fortunately, there is some relief for the designer in accounting for the effects of secondary compression of soils on the dynamic response of foundations. If serious secondary compression is anticipated, it will have a significant effect on the *static* behavior of the foundation and surrounding structures and will determine the type of foundation which is feasible. Thus, the influence of secondary compression of the underlying soils would first be considered for the static design and then evaluated for dynamic conditions.

In spite of the many variables indicated by Eq. (6-16) and the discussion of the effects of some of these parameters, it appears that in many cases the primary influences on shear-wave velocity are variations of void ratio and confining pressure. Lawrence (1965) used the ultrasonic-pulse technique for tests on kaolinite and Boston blue-clay samples, and Hardin and Black

(1968) and Humphries and Wahls (1968) ran resonant-column tests on kaolinite samples. From an examination of these test results, Hardin and Black (1968) concluded that for *normally consolidated clays of low surface activity, the shear-wave velocity is adequately predicted by Eq. (6-20)* as long as the shearing-strain amplitude is less than about  $10^{-4}$ . This conclusion for certain normally consolidated clays is a significant aid to the designer, even if it represents only a first approximation.

Tests of cohesive soils have shown that there is a stress-history effect which can be important in addition to the secondary compression and time effects. However, additional tests have indicated that some of these effects may be "shaken out" by a few cycles of high-amplitude loading. This will be discussed in the section treating high-amplitude vibrations.

From the foregoing discussions of the effect of vibratory loadings on the dynamic shear modulus of cohesive soils, we may conclude that Eq. (6-21) is adequate for a first estimate, but that extensive studies are still needed to pinpoint the influence on  $G$  of all the variables noted in Eq. (6-16).

#### "High-Amplitude" Resonant-Column Tests

Studies of the effect of amplitude of strains developed in resonant-column samples have been described by Hall (1962), Hall and Richart (1963), Drnevich (1967), and Drnevich, Hall, and Richart (1967). Hall used solid cylindrical samples of 20–30 Ottawa sand, uniform glass beads (avg. dia. = 1.0 mm and 0.06 mm), and Novaculite no. 1250 excited into both longitudinal and torsional modes of resonant vibration. Because the test results were described in terms of the displacement of the top of a sample 11-in. long and fixed at the base, the localized strains are not easily identified. However, the conclusions from tests of the Ottawa sands and glass beads are useful from a qualitative standpoint. These included the observation that both the longitudinal- and shear-wave velocities decreased as the amplitude of vibration was increased. This decrease was as much as 10 to 15 per cent as the double amplitude was increased from  $1 \times 10^{-5}$  to  $2.5 \times 10^{-3}$  rad in the torsion tests or from  $2 \times 10^{-6}$  to  $1 \times 10^{-3}$  in. in the longitudinal tests. Similar tests have also indicated that a decrease of wave velocities of 10 to 15 per cent occurs when the void ratio is changed from the minimum to the maximum value. Thus, the maximum change in the void ratio influences the wave velocities by an amount comparable to that produced by the variations in amplitude used in these tests.

In the resonant-column test of solid cylindrical samples excited into torsional oscillation, it is fairly difficult to evaluate a representative shearing strain. At each cross-section along the sample, the shearing strain varies

from zero at the center to a maximum at the periphery. In addition, the shearing strains vary along the length of the sample in a manner which depends on the ratio of the mass moment of inertia of the sample to the mass moment of inertia of the driving mechanism attached to the upper free end of the sample.

In order to provide a more reliable estimate of the shearing strains developed in the torsional resonant-column test, Drnevich (1967) developed a hollow cylindrical test specimen. Figure 6-10 shows a typical hollow sample mounted on the fixed base. The samples were 30-cm long, 4-cm inside diameter, and either 1-cm or 0.5-cm in wall thickness depending on the grain size of the cohesionless material to be tested. (It was found that the wall thickness should be greater than 10 grain diameters.) With the hollow sample the variation in shearing strain across the sample was minimized and the average shearing strain adequately represented the strain conditions on a particular cross-section. Then by increasing the mass moment of inertia of the driving and pickup device attached to the top end of the sample, the variations in shearing strain along the length of the sample were further reduced.

With the hollow sample in the resonant-column test, Drnevich (1967) was able to evaluate quantitatively the effect of the amplitude of shearing

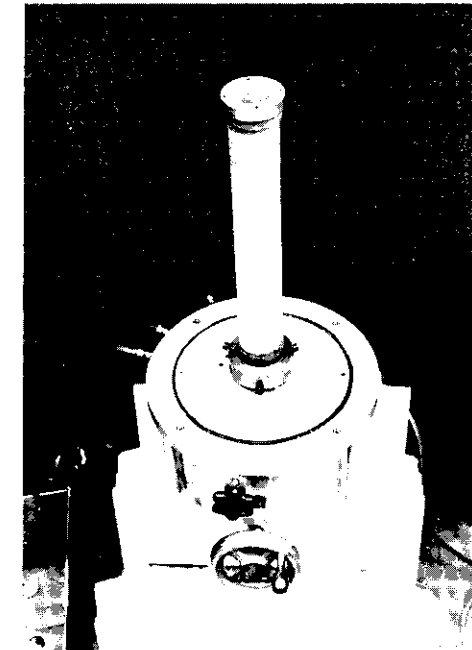


Figure 6-10. Completed hollow sample for resonant-column test.

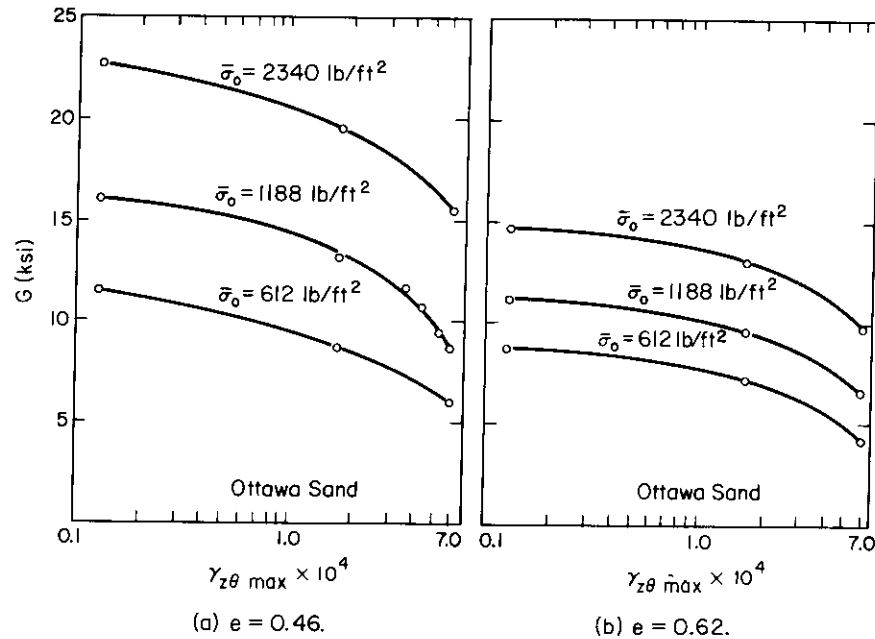


Figure 6-11. Dynamic shear-modulus ( $G = \tau_{\max}/\gamma_{z\theta \max}$ ) variation with maximum shearing-strain amplitude and confining pressure for hollow specimens (from Drnevich, Hall, and Richart, 1967).

strain on the shear modulus of various cohesionless materials. Figure 6-11 shows the decrease in shear modulus of 20-30 Ottawa sand in the dense and loose conditions, with an increase in shearing strain from about  $0.13 \times 10^{-4}$  to  $6.0 \times 10^{-4}$ . These curves are somewhat steeper (greater decrease in  $G$  for increasing amplitude) than was found for the 30-50 Ottawa sand, for example, but Fig. 6-11 does indicate that there is a decrease in  $G$  of the order of 10-15 per cent as the shearing strain increases up to about  $10^{-4}$  and a more significant decrease occurs above this value. Note that the shear modulus identified from the resonant-column test represents the "hysteresis modulus" or the straight line passing through the points 1 and 3 on Fig. 6-4. As the strains increase, the hysteresis loop expands and the hysteresis modulus decreases.

The high-amplitude resonant-column tests were also used by Drnevich to evaluate the influence of strain history on the value of the low-amplitude shear-wave velocity. This has practical applications in providing an estimate of the soil response under machine foundations (small-amplitude vibrations) as a consequence of a variable soil-conditioning process such as compaction by vibrating rollers (large-amplitude vibrations). The principal variables included in the test program were (1) the type of cohesionless materials; (2) void ratio; (3) confining pressure; (4) prestrain amplitude; and (5)

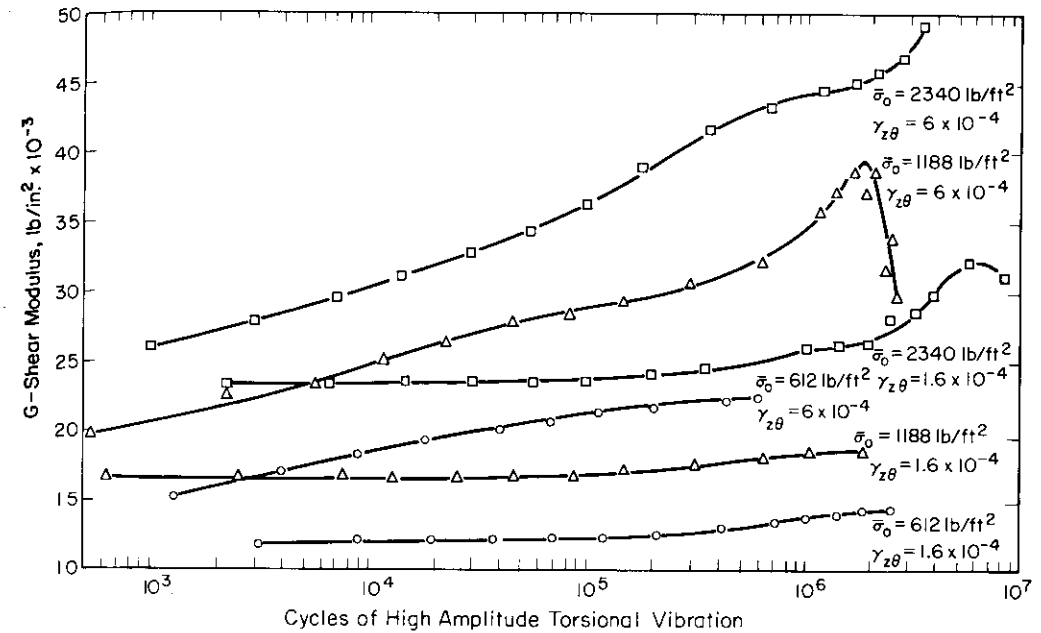


Figure 6-12. Effect of a number of cycles of high-amplitude vibration on the shear modulus at low amplitude (Ottawa sand,  $e = 0.46$ , hollow sample) (from Drnevich, Hall, and Richart, 1967).

number of cycles of prestrain applied. The tests were designed to evaluate the changes in the shear-wave velocity at a low-amplitude shearing strain (less than  $10^{-5}$ ) by application of a varying number of repetitions of high-amplitude shearing strains (greater than  $10^{-4}$ ). Figure 6-12 illustrates typical test results for the 20-30 Ottawa sand. Two values of prestrain amplitudes ( $1.6 \times 10^{-4}$  and  $6.0 \times 10^{-4}$ ) were applied to samples subjected to confining pressures of 612, 1188, and 2340 lb/ft<sup>2</sup>. A virgin sample was used in each test. The testing procedure involved first applying the chosen value of confining pressure and evaluating the shear-wave velocity corresponding to the low-amplitude vibrations. Then the high-amplitude vibration was applied for a particular number of cycles. At the end of this first increment of prestrain, the amplitude was reduced to the low value and the shear-wave velocity determined. From the shear-wave velocity, the value of  $G$  was computed and plotted in Fig. 6-12 at the appropriate number of prestrain cycles. Each point in Fig. 6-12 corresponds to the value of  $G$  evaluated under low-amplitude resonant-column vibrations at the end of the total number of high-amplitude prestrain applications indicated.

The test results in Fig. 6-12 point out several significant phenomena relating to the magnitude and number of cycles of the prestrain. For the

prestrain amplitude of  $1.6 \times 10^{-4}$  and  $\bar{\sigma}_o = 612 \text{ lb/ft}^2$ , no measurable influence was noted for  $10^5$  prestrain cycles, and only a minor influence occurred with  $10^6$  cycles. However, when  $\bar{\sigma}_o$  was increased to  $2340 \text{ lb/ft}^2$ , a peak was reached at about  $6 \times 10^6$  cycles, and a decrease occurred for greater numbers of cycles. For the prestrain amplitude of  $6 \times 10^{-4}$  and  $\bar{\sigma}_o = 1188 \text{ lb/ft}^2$ , the dropoff in low-amplitude  $G$ -value was more striking at prestrain cycles above the peak value. The results shown in Fig. 6-12 indicate that (1) there is probably a lower limiting value of prestrain amplitude which does not induce strain-history effects at the low-amplitude vibration, (2) the maximum strain-history effect occurs at something over  $10^6$  cycles at these levels of prestrain, and (3) a peak value of the prestrain effect may occur after which additional prestrain cycles may reduce or eliminate this gain. From additional tests, Drnevich (1967) determined that a prestrain amplitude of  $10^{-4}$  represented the lower limit of effective prestrain amplitudes. Amplitudes less than this value produced no prestrain effects.

These studies of the strain-history effects on cohesionless soils raise a number of questions and provide few answers. Obviously, there is a need for intensive study of the strain history on the small-amplitude dynamic response of cohesionless, cohesive, and—in particular—partially saturated soils.

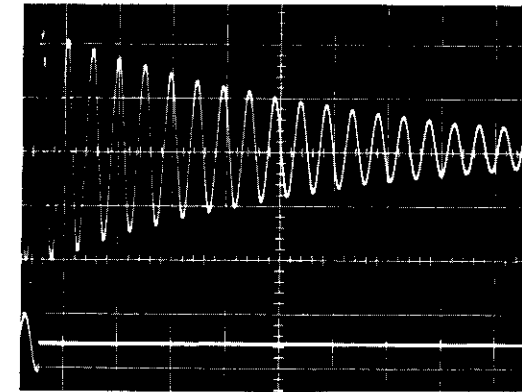
#### Internal Damping in Soils

When a rod of any material is set into a state of free vibration, the vibration will decrease in amplitude and eventually disappear. This reduction in amplitude of vibration is caused by internal damping within the mass of the material, and its decay is similar to that described for free vibration of a viscously damped system. It should be stated at the start of this discussion that the internal damping in soils is *not* considered to be the result of a viscous behavior; nevertheless, the theory for a single-degree-of-freedom system with viscous damping is a useful framework for describing the effect of the damping which actually occurs in soils.

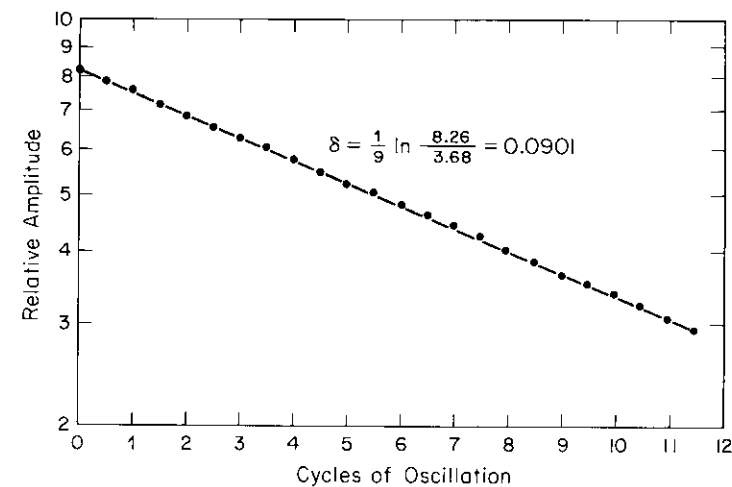
The decay of free vibration of a single-degree-of-freedom system with viscous damping is described by the *logarithmic decrement*, which is defined as the natural logarithm of two successive amplitudes of motion, or

$$\delta = \ln \frac{z_1}{z_2} = \frac{2\pi D}{\sqrt{1 - D^2}} \quad (2-39)$$

The logarithmic decrement is obtained experimentally, for example, from the resonant-column test by setting a soil sample into steady-state forced vibration, then shutting off the driving power and recording the amplitude



(a)



(b)

Figure 6-13. Typical free vibration-decay curves obtained from resonant-column tests of Ottawa sand (from Hall, 1962). (a) Amplitude-time decay curves. (b) Amplitude vs. cycle number plot.

decay with time. Figure 6-13a shows a typical vibration-decay curve obtained from a resonant-column test of Ottawa sand. The evaluation of logarithmic decrement from the decay curve can be accomplished by plotting each amplitude against cycle number on semilog graph paper, as shown in Fig. 6-13b. If the damping in the material produces an effect similar to that predicted by the theory for viscously damped free vibrations, a straight line

will be developed on this semilog plot. Hall found that the damping determined from the decay of steady-state vibrations in resonant-column samples of rounded granular materials behaved like viscous damping. The values of logarithmic decrement varied from 0.02 to approximately 0.20 for the materials and test conditions employed in these tests.

Hardin (1965) described continued and expanded studies of resonant-column tests for evaluating the damping in sands. He also presented an analytical study of the applications of the Kelvin-Voigt model (viscous damping) to represent the material for comparison with the test results. From this study he found that the Kelvin-Voigt model satisfactorily represented the behavior of sands in these small-amplitude vibration tests if the viscosity  $\mu$  in the model was treated as varying with the frequency to maintain the ratio  $\mu\omega/G$  constant. This ratio is related to the logarithmic decrement by

$$\delta = \pi \left( \frac{\mu\omega}{G} \right) \quad (6-23)$$

In his conclusions Hardin recommended values of the ratio of  $\mu\omega/G$  for use in design, which may be represented in terms of the logarithmic decrement as

$$\delta = \pi 9(\gamma_{z\theta})^{0.2}(\bar{\sigma}_o)^{-0.5} \quad (6-24)$$

in which  $\gamma_{z\theta}$  is the shearing-strain amplitude and  $\bar{\sigma}_o$  is the confining pressure (expressed in lb/ft<sup>2</sup>). Note that this empirical equation (Eq. 6-24) is recommended only within the limits of shearing-strain amplitude of  $10^{-6}$  to  $10^{-4}$ , for confining pressures of  $500 \text{ lb/ft}^2 < \bar{\sigma}_o < 3000 \text{ lb/ft}^2$ , and for frequencies less than 600 cycles/sec.

In his study of high-amplitude shearing strains on the dynamic behavior of sands, Drnevich (1967) included studies of damping. He found that no change occurred in damping with cycles of prestrain for prestrain amplitudes less than  $10^{-4}$ , that the logarithmic decrement varied with  $(\bar{\sigma}_o)^{-1/3}$  within the range of 400 to 2000 lb/ft<sup>2</sup> for all shearing-strain amplitudes between  $10^{-5}$  and  $6.0 \times 10^{-4}$ , and that many cycles of high amplitude prestrain increased damping, in some cases, to twice its original value. A part of the reason for the significant increases in damping is related to the testing procedure of controlling the shearing-strain amplitude. As the shear modulus increases because of the prestraining, the procedure of maintaining constant amplitude developed larger strain energy each cycle. It would be expected that the hysteresis loop would then include a larger area which represents increased damping.

The studies of internal damping in soils are by no means complete, and extensive work must be done in evaluating the influence of each of the

variables listed in Eq. (6-16). However, from the studies completed up to the present time, it appears that values of logarithmic decrement for sands may be as large as 0.20 and that they can be estimated from Eq. (6-24). Some additional data corresponding to internal damping for several types of soils are indicated in Table 10-12.

#### *Additional Methods for Evaluating Material Damping*

Some of the quantitative expressions used to define the internal damping of materials are viscosity, damping capacity, constant of internal friction, hysteretic constant, specific damping capacity, logarithmic decrement, elastic phase constant, and coefficient of internal friction. Other terms which may be added to this list are damping modulus, resonance-amplification factor, damping factor, specific damping energy, stress-strain phase angle, specific dissipation function, and attenuation. There are numerous references which treat these terms in detail, including the report by Jensen (1959), the bibliography by Demer (1956), and the book by Lazan (1968).

Of these damping terms, the logarithmic decrement was discussed in the preceding section, and the viscosity term was mentioned. The discussion of amplitude-frequency response curves in Chap. 7 covers the resonance-amplification factor. Of the remaining expressions in the above lists, the specific damping capacity, coefficient of attenuation, and specific dissipation functions occasionally occur in the literature for evaluation of the internal damping in soils.

The term "specific damping capacity" indicates the ratio of the *energy absorbed in one cycle of vibration* to the *potential energy at maximum displacement* in that cycle. The "damping capacity" thus defined has a fairly wide acceptance and may be expressed as a percentage or as a decimal. In terms of the stress-strain diagram, the specific damping capacity represents the ratio of the area enclosed by the hysteresis loop to the total area under the hysteresis loop. For the steady-state condition as shown in Fig. 6-14a (note that the horizontal scale in Fig. 6-14 is greatly exaggerated for simplicity of illustration), the specific damping capacity is given by

$$\Delta_{cs} = \frac{\Delta E_{\sigma}}{E_{\sigma}} \quad (6-25)$$

The term  $E_{\sigma}$  in Eq. (6-25) represents the strain energy described by the area under the hysteresis loop. The condition for a decaying vibration is illustrated in Fig. 6-14b. Point 1 corresponds to the maximum stress of a cycle which starts and ends at points 1 and 2, respectively. It is seen from Fig. 6-14 that the value of  $\Delta_{cs}$  depends on whether the steady-state ( $\Delta_{cs}$ ) or the

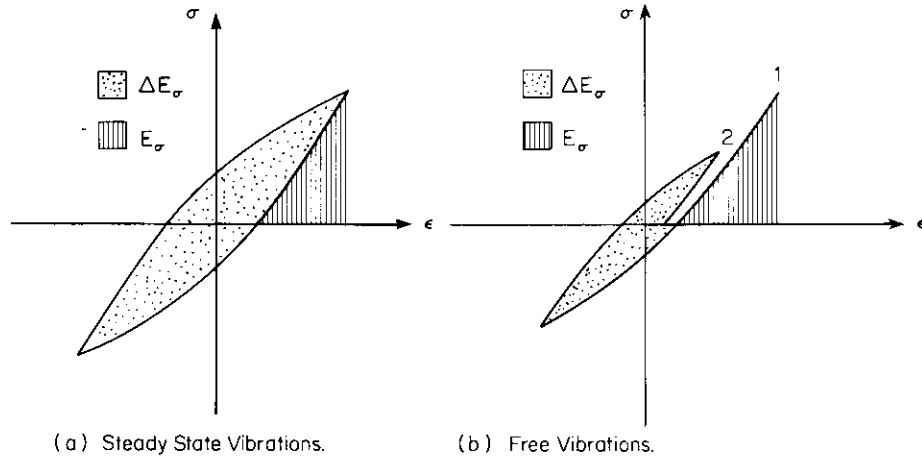


Figure 6-14. Stress-strain curves for a system with hysteresis damping.

decaying-vibration condition ( $\Delta_{cd}$ ) is considered when the damping values are large. For the conditions of decaying vibrations, the relationship between the logarithmic decrement and the specific damping capacity is

$$\Delta_{cd} = 1 - \frac{k_{n+1}}{k_n} \exp(-2\delta) \quad (6-26)$$

in which  $k_n$  represents the proportionality factor between strain energy and the square of the displacement amplitude for the  $n$ th cycle of decaying vibration. It should be emphasized that there is no general relationship between  $\Delta_{cs}$  and  $\delta$ ; but for small values of  $\delta$ ,  $\Delta_{cs} \approx \Delta_{cd}$ , and the ratio of the proportionality constants,  $k_{n+1}/k_n$ , is approximately 1.

It is often desirable to evaluate the decrease in amplitude of vibration with distance from a source which is caused by energy losses in the soil. This is designated as "attenuation," the energy loss as a function of distance, and is measured in terms of the *coefficient of attenuation*  $\alpha$  (1/ft). The coefficient of attenuation is related to the logarithmic decrement by

$$\delta = \frac{2\pi v\alpha}{\omega} = L\alpha \quad (6-27)$$

in which  $v$  is the velocity,  $\omega$  denotes the circular frequency, and  $L$  is the wave length of the propagating wave.

*Attenuation* should be distinguished from *geometrical damping* (see Fig. 3-16 and Sec. 7.7) which occurs in *elastic* systems because of the spreading out of wave energy from a source.

A variation of this attenuation coefficient describes the *specific dissipation function*  $1/Q$  as

$$\frac{1}{Q} = \frac{2\nu\alpha}{\omega} \quad (6-28)$$

Internal damping in materials may also be evaluated by measuring the angle by which the strain lags the stress in a sample undergoing sinusoidal excitation. If the soil is assumed to be a linear viscoelastic solid, the complex shear modulus  $G^*$  is considered to be composed of a real and an imaginary component, each of which is a function of frequency, as

$$G^*(\omega) = G_1(\omega) + iG_2(\omega) \quad (6-29)$$

In Eq. 6-29  $G_1(\omega)$  is the elastic component and  $G_2(\omega)$  is the viscous component. The loss angle  $\delta_L$  is defined by

$$\tan \delta_L = \frac{G_2}{G_1} \quad (6-30)$$

and it is related to the logarithmic decrement  $\delta$  (and the ratio  $\mu\omega/G$ , see Eq. 6-23) by

$$\delta = \pi \tan \delta_L \quad (6-31)$$

Several investigators have adopted theoretical procedures based on the complex modulus and have presented their laboratory-test results in terms of  $\tan \delta_L$ . Equation (6-31) provides the link for interpreting these results in terms of the logarithmic decrement as used in this chapter.

From the preceding paragraphs it is seen that there are several methods for measuring and describing damping in soils. Furthermore, because damping in soils increases with the amplitude of vibration (see Eq. 6-24), it may be convenient to use different methods for different ranges of amplitude. The use of the complex modulus may be warranted for dynamic situations involving large-amplitude vibrations. However, for the order of magnitudes of the vibrations encountered in soils beneath machine foundations, the logarithmic decrement should be less than 0.2. For this value of  $\delta$ , Eqs. (6-29), (6-30), and (6-31) show that the viscous component of the complex modulus is about 6 per cent of the elastic component. This difference of less than 6 per cent between the elastic and complex modulus does not justify adopting the theories of viscoelasticity for the study of response of machine foundations, particularly when we consider the accuracy of present test methods for determining  $G$ . Consequently, the test and design procedures described in this book are based on the assumption of an elastic modulus.



When internal damping in soils is considered, it is represented in terms of the logarithmic decrement.

#### Wave-Propagation Velocity from Field Tests

The general principles involved in the seismic field tests for the compression-wave velocity and the steady-state-vibration method for the Rayleigh-wave velocity were described in Chap. 4. The discussion will be confined here to comparisons between the wave velocities obtained in the field by the steady-state vibrations and in the laboratory by the resonant-column tests.

As noted in Chap. 4, the steady-state-vibration method involves a variable-frequency exciter which produces a vertical oscillating force on the surface of the ground. A pickup is located on the ground surface at varying distances away from the exciter in order to determine the wave length corresponding to a particular frequency of excitation. This wave-length evaluation is recorded for a series of different frequencies and the results shown in a diagram similar to Fig. 4-19. The product of the wave length and frequency is equal to the velocity of the Rayleigh wave, or

$$v_R = fL \quad (6-32)$$

It was demonstrated by Fig. 3-13 that in the ideal elastic body the difference between the Rayleigh-wave velocity and the shear-wave velocity was minor, from an engineering standpoint, for values of Poisson's ratio greater than about 0.25. The ratio of  $v_R/v_S$  is noted below as a function of  $\nu$  (from Knopoff, 1952):

$\nu$	0.25	0.33	0.40	0.50
$v_R/v_S$	0.92	0.933	0.943	0.956

Thus the value of wave-propagation velocity ( $v_R$ ) measured in the field by the steady-state method could be expected to be on the order of 5 to 8 per cent lower than the shear-wave velocity measured in the laboratory with the resonant-column device at the same level of shearing strains.

In the steady-state-vibration method the wave velocities obtained from the field tests are plotted at depths corresponding to a distance equal to one-half the wave length. This type of plot is shown in Fig. 6-15 for *in-situ* tests at the Eglin Field test site (after Fry, 1963). At this site the soil was composed of fine, uniform sand with a void ratio of approximately 0.70. The average effective confining pressure  $\bar{\sigma}_o$  at any depth within the sand mass may be

calculated from

$$\sigma_x = \sigma_y = \frac{\nu}{1 - \nu} \sigma_z \quad (6-33)$$

$$\sigma_z = \gamma z \quad (6-34)$$

$$\bar{\sigma}_o = \frac{\sigma_x + \sigma_y + \sigma_z}{3} \quad (6-35)$$

At the Eglin Field site the unit weight  $\gamma$  was approximately 104 lb/ft<sup>3</sup>. With this value of  $\gamma$  and an assumption of Poisson's ratio of  $\frac{1}{3}$ , the stresses  $\sigma_x$  and  $\bar{\sigma}_o$  were calculated for several depths within the sand mass. Then these values of  $\bar{\sigma}_o$  and ( $e = 0.70$ ) permitted calculations of  $v_S$  at the several depths through the use of Eq. (6-18). Finally, the Rayleigh-wave velocities were obtained from the theoretical relation that  $v_R = 0.933 v_S$  for  $\nu = \frac{1}{3}$ . These calculated values of  $v_R$  are shown on Fig. 6-15 as the dashed line.

At this point, it should be reiterated that the steady-state-vibration method (or half-wave-length method) is an *empirical procedure*, and it is remarkable that it works so well. Equation (6-18) also represents an empirical

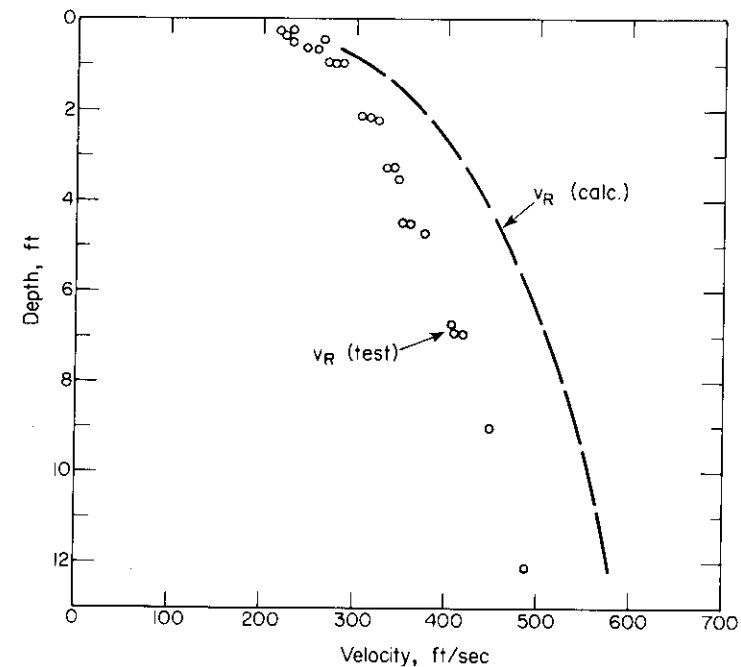


Figure 6-15. Variation of Rayleigh wave velocity with depth—Eglin Field Site (after Fry, 1963).

method for evaluating the shear-wave velocity which is further complicated by difficulties in evaluating  $\bar{\sigma}_v$  for the field conditions. Consequently, a difference of 10 per cent between results obtained by these two methods represents good agreement, and a difference of 20 per cent should be acceptable for most engineering computations.

#### 6.4 Behavior of Soil Under Large-Amplitude Loading

Large-amplitude loadings are designated as those which cause a change in the structure and often a change in the strength of soil. Such loadings may be developed by excessive vibrations of machinery, compaction devices, commercial blasting, nuclear blasts, or earthquakes. Earthquakes, blast loadings, and machinery vibrations generally do not occur until after construction is completed, and the influence of these loadings on the supporting soils must be evaluated during design studies. The construction procedures of compaction and controlled blasting provide a preload for a construction site to minimize further settlements of the operating facility.

It is the purpose of this section to describe some of the changes in soil characteristics which result from these large amplitude loadings. The soil characteristics of primary interest are the shearing strength, change of volume (settlement), dynamic modulus, and internal damping.

##### *Stress-Strain Behavior of Soils Under Dynamic Loads*

Any procedure devised to evaluate the dynamic stress-strain characteristics of a particular soil must attempt to duplicate as closely as possible the boundary conditions which exist in the field. However, it has been customary in the past to evaluate the dynamic stress-strain behavior of soils by means of a dynamic triaxial test. Under these conditions lateral expansion of the soil sample is permitted and the slope of the stress-strain curve decreases as the load increases until it becomes horizontal at the maximum load. An effective confining pressure of undetermined magnitude is introduced by the lateral inertia of the sample. More recently both static and dynamic stress-strain curves have been obtained for different materials using test equipment which did not permit lateral expansion of the sample (for example, Whitman, Roberts, and Mao, 1960; Davisson, 1963; and Zaccor and Wallace, 1963). As noted in Sec. 6.2 and particularly in Fig. 6-5, the overall stress-strain characteristics of soil samples are greatly influenced by lateral deformations which must be considered each time test results are evaluated for use in design.

Numerous investigations utilizing the dynamic triaxial test have been conducted to evaluate the stress-strain characteristics of cohesionless soils loaded to failure by a single application of load. Casagrande and Shannon (1948) presented the results of triaxial tests on dry Manchester sand in which the load was applied by a falling-beam-type apparatus. They found an increase in the ultimate shearing strength of 10 to 15 per cent and an increase in the modulus of deformation of about 30 per cent when the load was applied dynamically rather than statically. The modulus of deformation was defined by a secant modulus obtained by passing a straight line through the origin and a point on the stress-strain curve at one-half the ultimate stress. Seed and Lundgren (1954) investigated the strength and deformation characteristics of saturated specimens of a fine and a coarse sand under dynamic loadings. The rapid loading was applied by a falling-weight-impact testing machine. They found an increase in strength of 15 to 20 per cent and an increase in the modulus of deformation of about 30 per cent under the dynamic loading conditions. They noted that dilatancy effects and lack of drainage contributed to the strength under dynamic loads. Taylor and Whitman (1954) reported results of dynamic triaxial tests of saturated sands in which one of the major objectives was to measure the time change of pore pressures. Since then, the methods for measuring transient pore pressures have been developed to the point where rapid triaxial tests may be conducted with loading times of 0.010 sec with satisfactory measurements of pore pressures. Nash and Dixon (1961) developed a dynamic-pore-pressure measuring device with which they successfully recorded pore pressure changes in triaxial tests of saturated sands under strain rates up to 8000 per cent per minute or loading rates up to about 220 inches per minute. The rapid loadings were developed in the tests by Nash and Dixon by a falling-weight-and-lever system. As a result, this approximated a constant-rate-of-strain-type test. In the course of loading the specimen to its maximum (loading time approximately 0.1 sec), they found several short-time drops in the stress level and simultaneous increases in the pore pressure, as shown in Fig. 6-16. This indicates that the structure collapsed intermittently at a rate which was faster than the loading rate, but the change in the soil structure permitted the sample to carry increasing axial loads

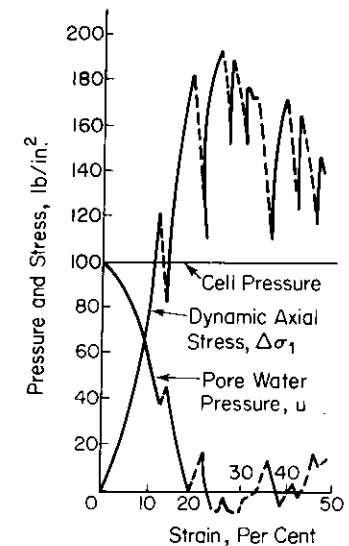


Figure 6-16. Results of dynamic triaxial tests on saturated sand, showing sudden collapses (from Nash and Dixon, 1961).

until the maximum was reached. The time rate of these steps of structural collapse or grain readjustments should be of considerable importance in evaluating the behavior of sands under high rates of loading.

Dynamic triaxial tests have also been conducted on samples of cohesive soils. Casagrande and Shannon (1948) studied intensively the behavior of clays and soft rock under dynamic conditions. Their studies indicated that the water content of the clay has an important influence on the relation between time of loading and compressive strength. The percentage increase of the fast transient strength over the static compressive strength was greatest for specimens of the highest water content and least for specimens of the lowest water content. The fast transient compressive strength, taken at a time of loading of 0.02 sec, ranged between 1.4 and 2.6 times greater than the 10-minute static compressive strength for all tests on clays. For the same dynamic loading conditions the modulus of deformation (secant modulus determined at one-half the ultimate strength) for all types of clays tested was found to be approximately twice that for the 10-minute static loading. Taylor and Whitman (1954) evaluated this strain-rate effect on ten different cohesive materials. Generally, an increase in the strain rate from static to 1000 per cent per second increased the ultimate strength by a factor of 1.5 to 3, which is of the same order of magnitude as that found by Casagrande and Shannon. Tests by Jackson and Hadala (1964) indicated that the strain-rate factor for the compacted clay used in their tests was of the order of 1.5 to 2.0. This strain-rate factor was again the amount of increase in modulus of deformation and ultimate strength in the dynamic test above those measured in the static tests.

This discussion of the rate of loading effects on dynamic triaxial tests of both cohesionless and cohesive soils points out that there is an increase (1.5 to 3 times) in the modulus of deformation and ultimate strength over the static values as loads are applied rapidly. However, these increases are measured in the region of large deformations on the stress-strain curve (i.e., above  $\frac{1}{3}$  of the ultimate strength) and relate to the behavior which develops as the soil sample is in the process of failing.

#### *Liquefaction of Cohesionless Soils*

The term "liquefaction" has been applied to the process by which a saturated mass of soil is caused by external forces to suddenly lose its shearing strength and to behave as a fluid. First consider the expression for the shearing strength of cohesionless soils:

$$\tau = (\sigma - u) \tan \phi' \quad (6-36)$$

in which

$\sigma$  = total normal stress on the failure plane,

$u$  = pore pressure, static plus dynamic, and

$\phi'$  = effective angle of internal friction.

It is evident from the above that an increase in the pore pressure  $u$  will cause a reduction in  $\tau$ . When the pore pressure increases to the point where  $u$  is equal to  $\sigma$ , the shearing strength drops to zero and the "quick" or fluid condition exists. This loss of shearing strength of soils because of high pore pressures, either static or transient, has often produced *flow slides* whereby embankments of submerged sand have run out almost horizontally as a fluid. The liquefied condition may also develop within deposits of loose cohesionless soils having a horizontal surface. In this case the soil loses its bearing capacity and any structure supported thereon will sink or settle. Liquefaction may develop by impacts or repeated loadings (for example, from blasting or earthquakes) applied to loose saturated cohesionless soils. The dynamic forces disturb the soil skeleton and tend to force the particles to compact into a denser arrangement. During the time it takes a sand grain to move into its new position it is, temporarily, partially supported by the pore fluid, and the external loads are transmitted to the fluid thereby increasing the pore pressure  $u$ . Consequently, liquefaction depends upon the ability of a cohesionless material to compact into a denser condition when the soil structure is changed. Numerous studies have established that compaction of saturated sands depends primarily upon the initial void ratio, the confining pressure, and the intensity of the dynamic loading.

Because of the susceptibility of loose saturated sands to compact under dynamic loadings, it was anticipated that controlled blasting by small charges of dynamite or other high explosives should be an effective method of providing compaction. The study by Lyman (1942) showed that blasting was an effective way to compact loose sands, but in order to be successful it was necessary to run field tests at each site to establish the proper charge and spacing. A further description of this method was given by Prugh (1963). The probability of developing an increase in density by blasting depends upon the ability of the material to fall back into a more dense position after it has been disturbed by the charge. Consequently, this method is relatively inefficient close to the surface of submerged slopes where the sand tends to roll back into position down the slope rather than being confined as it falls. Controlled blasting has been used, however, in determining whether submarine slopes might be susceptible to flow slides caused by earthquakes (Kum-meneje and Eide, 1961).

An interesting study of the liquefaction and compaction of granular soils by blasting has been reported by Florin and Ivanov (1961). They found that in impulse tests, loose saturated sands were readily converted into a completely liquefied state over the entire depth of the test stratum. At this time the soil had a bearing resistance which approached zero. Then, with a time rate which depended on the permeability of the material, the sand settled back into place, beginning at the bottom, as the upper layer remained in the liquefied condition for a longer time. The ability of the sand layer to be liquefied depended upon its initial void ratio, the range of confining pressure and, of course, the amount of energy introduced by the blast. The authors concluded, as a result of many field observations, that loose sand is difficult to liquefy at depths ranging between about 10 to 15 meters below ground level. This indicates that surcharge with any material can be used as a method for reducing sand liquefaction.

Florin and Ivanov also produced liquefaction of the sand by steady-state vibrations. By this method liquefaction was not caused simultaneously throughout the depth of the test stratum, but the first vibrations liquefied the upper layer, which carried a comparatively small confining pressure. This then reduced the pressure of the overburden on the lower layers and, as a result, the latter passed into the liquid state with continued vibration; thus, the zone of liquefaction propagated downward. They also indicated that all sufficiently loose cohesionless soils of any grain size may be liquefied, but the time required for compaction depends upon the permeability. Coarse-grained soils compact very rapidly.

Because of this susceptibility of loose saturated sands to compact and possibly to liquefy as a result of impact or repeated loadings, it is probable that difficulties will be encountered with this type of material when it is supporting structures under earthquake loadings. Numerous investigations have ascertained that the structural damage resulting from earthquakes has been a result of liquefaction and compaction of loose saturated sands, for example in the Chilean earthquake of May 1960 (Steinbrugge and Clough, 1960); the Coatzacoalcos, Mexico earthquake of August 26, 1959, (Diaz de Cossio, 1960); the Jaltipan earthquake, Mexico (Marsal, 1961); the Anchorage, Alaska, earthquake of 1964 (Shannon and Wilson, 1964); and the Niigata earthquake, Japan, 1964, (Falconer, 1964, and J.S.S.M.F.E. 1966.) Extensive soil investigations have been conducted following the Anchorage, Alaska, earthquake (Shannon and Wilson, 1964) and the Niigata, Japan, earthquake. For a comprehensive treatment of the development of landslides and liquefaction of soils by earthquakes, the reader is referred to the Fourth Terzaghi Lecture by Professor H. B. Seed (Seed, 1968). This outstanding paper presents a historical review including case histories, the present state of the art, and an extensive bibliography on the subject of landslides during earthquakes due to soil liquefaction.

#### *Failure of Soil Samples in the Repeated-Load Triaxial Test*

The two preceding sections treated the ultimate failure of triaxial samples under a single load which increased continuously to the failure load. However, loads less than the failure load may be applied a number of times before the cumulative deformation reaches a value considered to represent failure. The number of load applications which may be resisted by a particular soil sample depends on the magnitude and type of loading pulse and the characteristics of deformation of the soil.

It has been noted previously that loose saturated sands and silts may liquefy as a result of a single impact or rapidly applied load. These materials may also fail by transient liquefaction *after* a number of load applications have occurred. Figure 6-17 (from Seed and Lee, 1966) illustrates the behavior of a sample of loose saturated sand under repeated triaxial loading conditions. The sample was first subjected to an effective confining pressure  $\bar{\sigma}_o$  of 1 kg/cm<sup>2</sup> (i.e., cell pressure = 2 kg/cm<sup>2</sup>, initial pore pressure = 1 kg/cm<sup>2</sup>) then an alternating axial stress of  $\pm 0.39$  kg/cm<sup>2</sup> was applied. As noted in Fig. 6-17c the pore pressure gradually increased each cycle until transient liquefaction occurred after 8 cycles. In this test the incremental increase in pore pressure each cycle indicated a decrease in void space in the sample caused by minor slips or rearrangements of the soil particles.

The cumulative effects of minor rearrangements of soil particles or slips at the contact points are indicated by gradual increases in axial strain as the number of cycles increases. Figure 6-18 illustrates the behavior of a compacted, silty clay subjected to repeated axial loads in the triaxial test. In one test a total axial strain of 6 per cent was reached after 100,000 cycles of loads applied at a rate of 20 per min. At a slower rate of load applications the cumulative deformation was reduced, which indicated for this material that thixotropic regain in strength occurred between load applications. Thus, the frequency of load application is a factor to be considered when testing materials having thixotropic characteristics.

In the two preceding paragraphs, the results of repeated-loading triaxial tests have been described which, in the first case, caused collapse of the soil structure in 8 cycles of loading and, in the other case, caused about 6 per cent axial strain after 100,000 cycles of loading. Thus, if laboratory tests are to be used to establish numerical values for the response of various soils to repeated dynamic loadings, it is necessary to establish criteria for "failure." For large-amplitude loadings represented by an alternating stress greater than about one-half the allowable static-stress increment, it would be anticipated that failure of the sample under repeated triaxial loads would occur in a few hundred or at the most a few thousand cycles. Failures occurring at this number of stress repetitions are designated as "low-cycle fatigue" in the study

Test No. 114  
 Initial Void Ratio = 0.87  
 Initial Confining Pressure = 2.0 kg/cm<sup>2</sup>

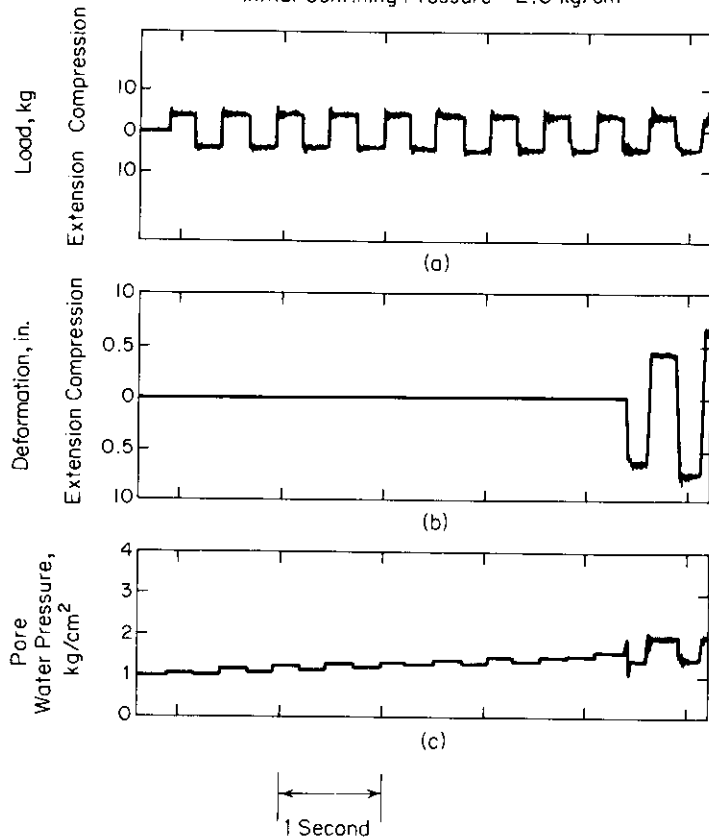


Figure 6-17. Record of a typical pulsating-load test on loose sand (from Seed and Lee, 1966).

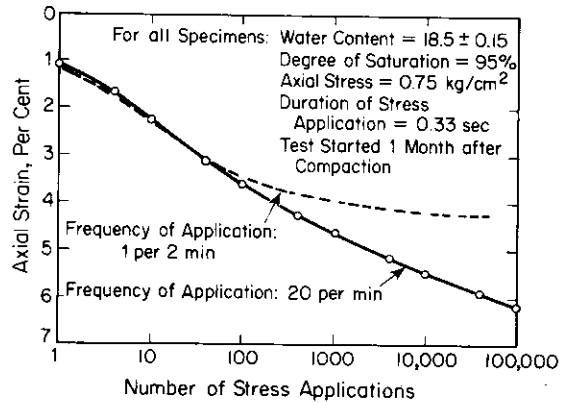


Figure 6-18. Effect of frequency of repeated stress application on deformation of silty clay at high degree of saturation (from Seed, 1957).

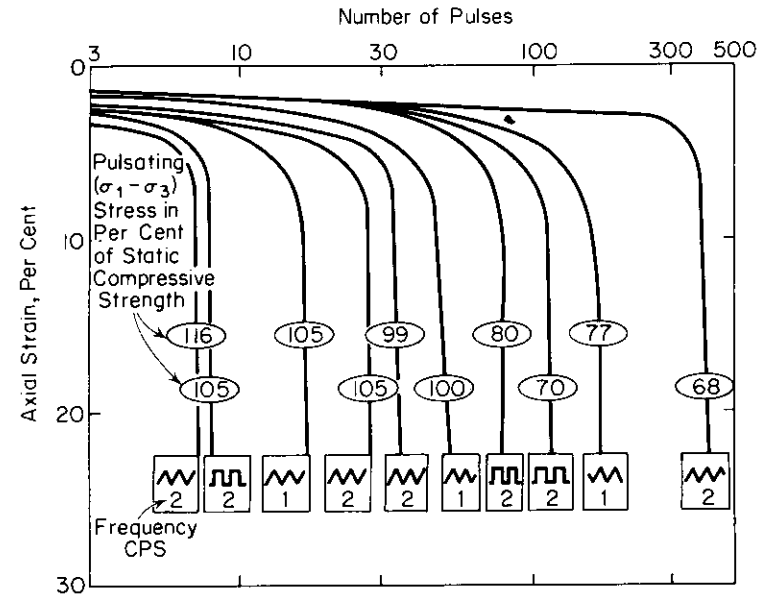


Figure 6-19. Results of pulsating-load tests on samples of silty clay from L Street slide area, Anchorage (from Seed and Chan, 1964).

of fatigue of metals. The low-cycle failure of soils is of particular interest when a soil-structure system must be designed to withstand earthquake loadings.

Following extensive damage which occurred because of slope failures during the Anchorage, Alaska, earthquake in 1964, many repeated-loading triaxial tests were conducted on soil samples from this location. The results are summarized in the report by Shannon and Wilson (1964) and are presented in more detail in papers by Seed and his co-workers. Figure 6-19 (from Seed and Chan, 1964) shows test results for samples of silty clay from the L Street Slide area for different amplitudes of alternating stress and for rectangular and triangular pulse shapes. It is of particular significance that the axial deformations remained relatively small throughout the major part of the test and then increased rapidly as the failure condition was approached. Thus, there was relatively little indication of impending failure. For these tests, an axial deformation of 25 per cent was designated as failure.

From a study of many test results similar to those shown in Fig. 6-19, it is possible to determine the allowable alternating axial stresses which may be superposed on a static axial stress  $\Delta\sigma_1$ , to develop failure at a given number of load applications. Figure 6-20 (from Seed, 1960) illustrates the type of

alternating stress-steady stress diagrams which were established for 1, 10, and 100 transient stress pulses for two soils. This information is in a form similar to the alternating stress-steady stress diagram (see Soderberg, 1933) frequently employed to describe failure conditions for fatigue of metals.

The axial strains developed in the repeated-loading triaxial tests depend upon the levels of stress applied. The results shown in Fig. 6-19 correspond to failures at low numbers of cycles of relatively high stresses. When the level of stress is reduced, it takes many more stress repetitions to develop equivalent axial strains. As illustrated in Fig. 6-18, axial deformations of the sample may increase continuously even after 100,000 cycles of load have been applied. Thus, failure from this type of soil behavior would be established in terms of *limiting total settlement*.

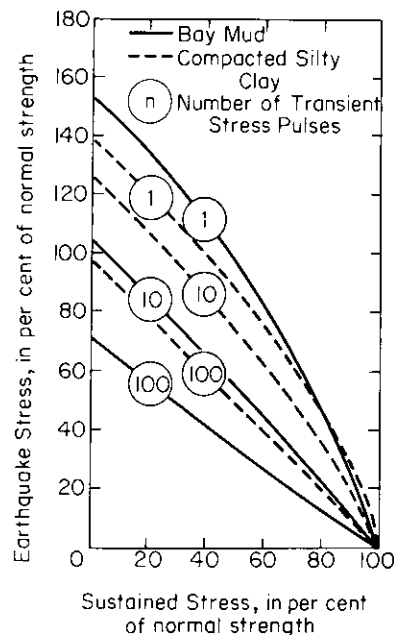


Figure 6-20. Comparison of stress conditions causing failure for compacted and undisturbed samples of silty clay (from Seed, 1960).

### Failure of Sands in the High-Amplitude Resonant-Column Test

In one series of tests conducted in the high-amplitude resonant-column device, Drnevich (1967) attempted to evaluate the progressive settlement of samples of dry 20-30 Ottawa sand. Hollow samples, similar to the one shown in Fig. 6-10, were set into torsional vibration after being subjected to a given confining pressure  $\bar{\sigma}_o$ . The amplitude of reversed shearing strain was maintained constant throughout each test, with the highest strain amplitude amounting to  $6 \times 10^{-4}$ . Repetitions of this amplitude of shearing strain caused a gradual increase in axial strain as shown in Fig. 6-21 for samples prepared in the loose condition. Also shown in Fig. 6-21 is the strain developed in a dense sample with increased cycles of loading. The confining pressure and initial void ratio is noted for each curve, as is the angle of internal friction  $\phi'$ . The maximum shearing stress developed on the horizontal section was established by

$$\tau_{z\theta} = G\gamma_{z\theta}$$

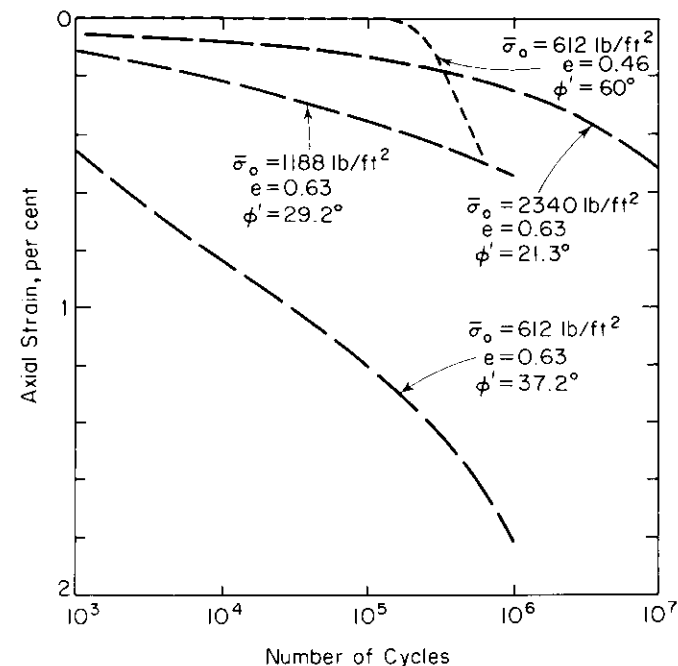


Figure 6-21. Effect of repetitions of high-amplitude torsional prestrain on hollow samples of 20-30 dry Ottawa sand (after Drnevich, 1967).

in which  $\gamma_{z\theta}$  was the amplitude of applied shearing strain and the effective shear modulus at that strain was taken from Fig. 6-11. Then, from the Mohr-circle relation for the applied stress conditions,

$$\tau_{z\theta} = \bar{\sigma}_o \sin \phi'$$

the value of  $\phi'$  can be determined. Table 6-1 includes data for two levels of applied shearing strains applied to samples of 20-30 Ottawa sand in the loose and dense conditions when subjected to three different confining pressures. The cumulative axial strains developed by  $10^6$  cycles were negligible from the applied shearing strains of  $\gamma_{z\theta} = 1.6 \times 10^{-4}$ , but significant strains developed for the shearing-strain amplitude of  $\gamma_{z\theta} = 6.0 \times 10^{-4}$ . This information reinforces previous conclusions that *clean sands behave essentially as elastic materials when subjected to shearing strains of less than  $1 \times 10^{-4}$* . It also points out that axial strains or settlements may continue to develop in loose sands after  $10^6$  or  $10^7$  repetitions of stresses well below the static failure stresses.

Table 6-1. Axial Strains Developed in High-Amplitude Torsional Resonant-Column Tests of Dry 20–30 Ottawa Sand Samples\*

For  $e = 0.46$ 

$\bar{\sigma}_o$ (lb/ft <sup>2</sup> )	$\gamma_{z\theta}$ (10 <sup>-4</sup> rad-in./in.)	$G$ (lb/in. <sup>2</sup> )	$\tau_{z\theta \max}$ (lb/ft <sup>2</sup> )	$\phi'$	$\epsilon_z$ for 10 <sup>6</sup> Cycles (or end of test)
612	1.6	8,700	200	19.1°	0.00017
612	6.0	6,100	530	60.0°	0.00485†
1188	1.6	13,200	305	14.9°	0.00005
1188	5.2	9,500	710	36.7°	neg.
2340	1.6	19,600	450	11.1°	0.00042
2340	6.0	15,600	1350	35.2°	0.00025

For  $e = 0.63$ 

612	1.6	7,200	170	16.1°	0.00034
612	6.0	4,250	370	37.2°	0.01800†
1188	1.6	9,600	220	10.7°	0.00017
1188	6.0	6,700	580	29.2°	0.00540†
2340	1.6	13,200	305	7.5°	0.00080
2340	6.0	9,800	850	21.3°	0.00250†

\* From Drnevich (1967).

† Strain-cycles curves shown in Fig. 6-21.

### Change in Volume of Cohesionless Soils by Vibrations

The two preceding sections included descriptions of axial strains produced in triaxial samples by repeated loads. In the triaxial test, lateral strains of the sample are permitted; consequently, the axial strains may result from a change of shape of the sample as well as from a change of volume.

In order to define the changes in volume of cohesionless soils developed by repeated loadings, tests have been conducted on confined samples. Figure 6-22 shows the testing device used by Whitman and co-workers (see D'Appolonia, 1968; and Luscher, Ortigosa, Rucker, and Whitman, 1967, for example) for repeated air-pressure loadings on the surface of confined samples. The loading rate in this series of tests was slow enough that no dynamic effects were introduced, and the tests established the contributions of repeated static stresses to the compaction of cohesionless soils. Figure 6-23 shows typical results obtained from these tests. Note that the percentage vertical strain also represents change of volume because the confinement permits no lateral deformation of the sample. For this material the relation between percentage vertical strain and logarithm of number of loading cycles was linear up to 10<sup>5</sup> to 10<sup>7</sup> cycles. Similar results have been obtained for samples of other cohesionless soils.

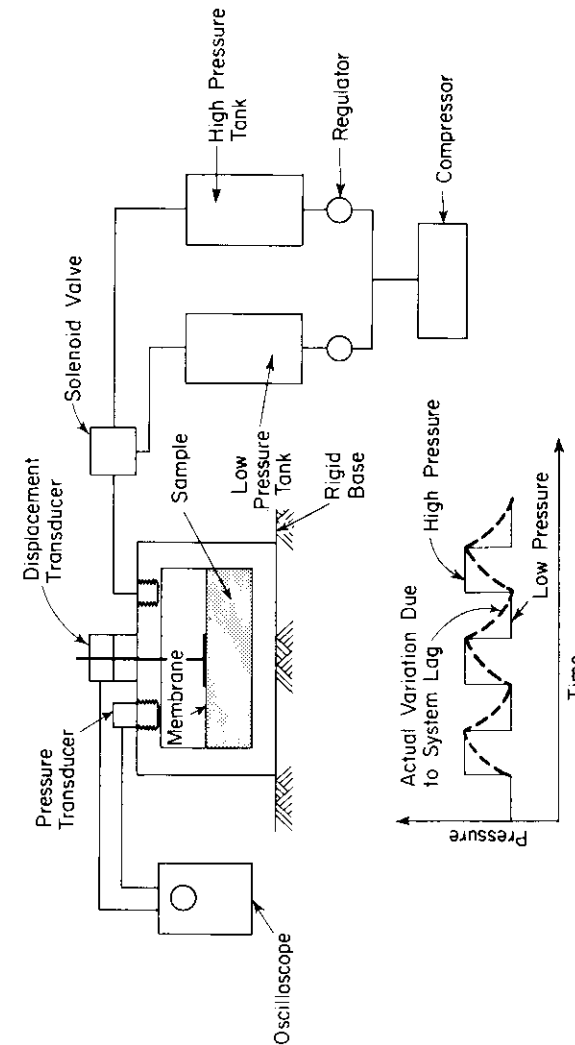


Figure 6-22. Apparatus for conducting cyclic-loading controlled stress tests (from D'Appolonia, 1968).

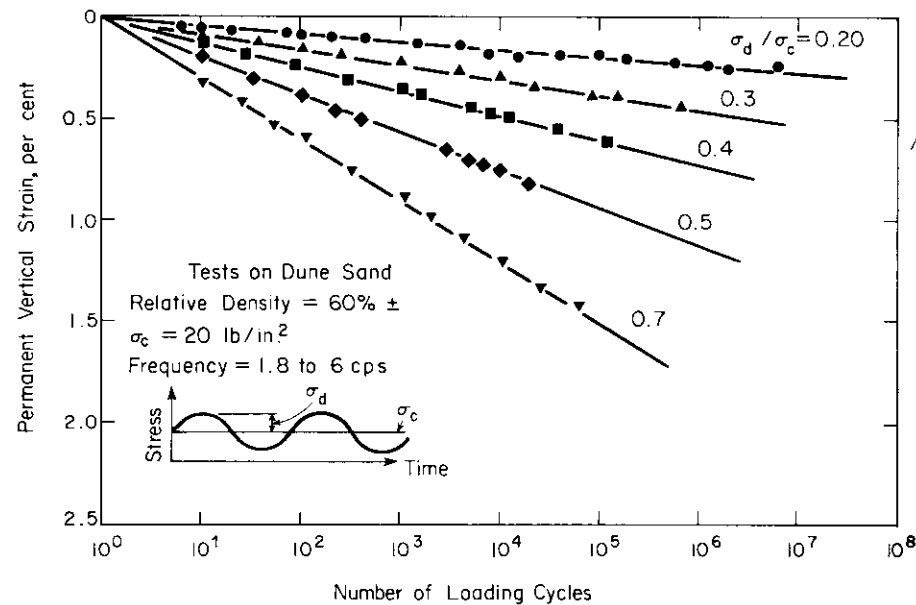


Figure 6-23. Typical results of one-dimensional repeated-loading tests (from D'Appolonia, 1968).

In order to evaluate the influence of vertical *accelerations* on the compaction of cohesionless soils, the loading device shown in Fig. 6-22 was modified slightly. The air pressure applied to the membrane at the top of the sample was held constant throughout the test, and the confining chamber was placed on a vibrating table instead of the rigid base shown in Fig. 6-22. The drive mechanism for the vibrating table was adjustable, so both the frequency of vertical vibration and amplitude of motion could be controlled. Thus, sinusoidal vibrations with a range of peak accelerations could be developed during the program of tests. Variations of this type of vibrating table have been used often for determining the influence of vibrations on the compaction and settlement of cohesionless soils (see, for example, Mogami and Kubo, 1953; Linger, 1963; D'Appolonia and D'Appolonia, 1967; Whitman and Ortigosa, 1968); but recent studies have been concerned specifically with evaluation of the influences of acceleration and confining pressures on settlement.

Figure 6-24 shows results of tests on air-dry samples of dune sand conducted at a specific level of acceleration. These samples had no surcharge pressure and were placed in the container in the loosest condition before each test. Because the value of peak acceleration is the product of amplitude and frequency squared [ $\ddot{z} = A(2\pi f)^2$ ], several values of amplitude were used, as

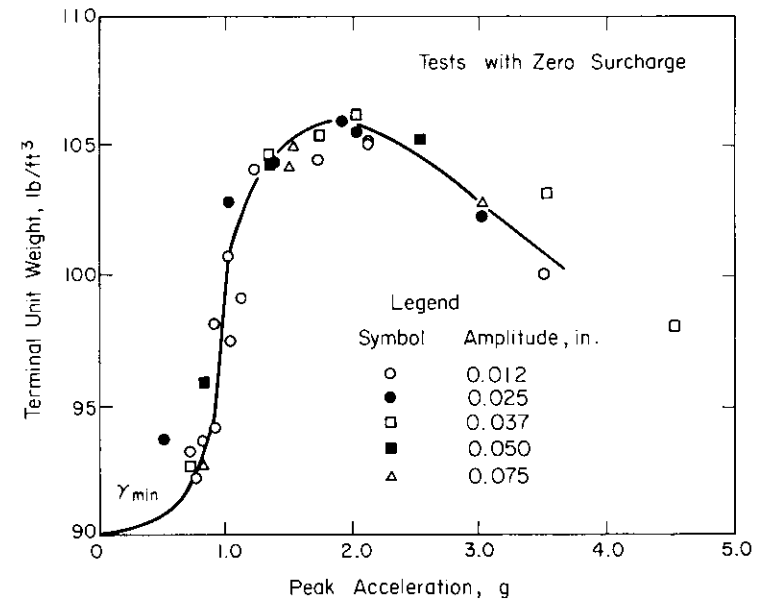


Figure 6-24. Correlation between terminal density and peak acceleration (after D'Appolonia and D'Appolonia, 1967).

noted in Fig. 6-24, in order to develop the same acceleration at different frequencies. It is evident from the test results that there was little effect of frequency over the range used in these tests. The test results show a marked increase in dry unit weight (decrease in volume) as the value of peak acceleration approached 1 g, with the maximum effect produced at about 2 g. For accelerations above 2 g the sample began to loosen or to decrease in volume again. Figure 6-25 illustrates the influence of the air-pressure surcharge on the change in void ratio (decrease in volume) for different values of applied accelerations. It is important to note that an increase in vertical pressure increases the level of acceleration required to initiate the change in void ratio or change in volume of the sample.

The test results shown in Figs. 6-24 and 6-25 reinforce the general conclusions that a change in volume in cohesionless soils, produced by impact or vibratory loads, depends on the confining pressure and intensity of the dynamic load as well as upon the initial void ratio and characteristics of the soil.

#### Field Compaction of Cohesionless Soils by Vibrations

Foundations supported by deposits of cohesionless soils may settle as a result of repeated applications of dynamic forces. The total amount and rate



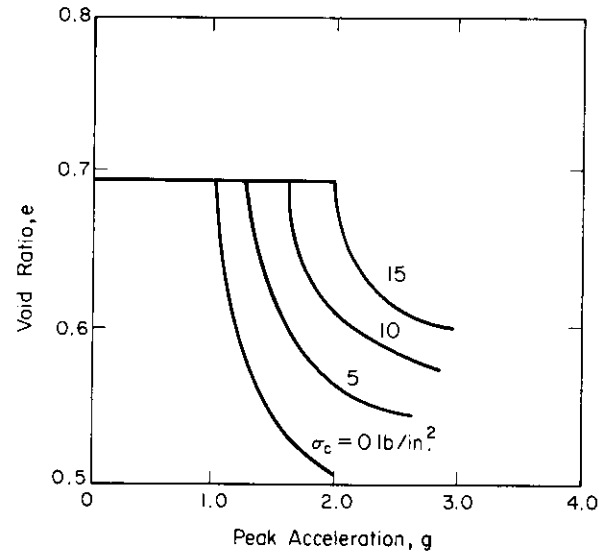


Figure 6-25. Relationship between void ratio and peak acceleration for several values of air pressure surcharge (after Whitman and Ortigosa, 1968).

of settlement depend on the intensity of the dynamic loads applied, the levels of stress developed in the supporting soil, and the changes in volume of the soil mass caused by the particular level and duration of the applied stresses. Changes in soil volume and settlement of the surface of a deposit depend primarily upon the initial condition of the soil. Large settlements are possible if the soil is initially in the *loose* condition, and minor settlements may occur if the soil is initially “*dense*.”

It is convenient to represent the natural condition of a cohesionless soil in terms of its *relative density*  $D_r$ , which is defined in terms of void ratio by

$$D_r = \frac{e_{\max} - e}{e_{\max} - e_{\min}} \quad (6-37)$$

in which

$e$  = measured void ratio of the soil *in situ*,  
 $e_{\max}$  = void ratio for the loosest state, and  
 $e_{\min}$  = void ratio for the densest state.

The relative density may also be defined in terms of the unit weights of the soil by

$$D_r = \frac{\frac{1}{\gamma_{\min}} - \frac{1}{\gamma}}{\frac{1}{\gamma_{\min}} - \frac{1}{\gamma_{\max}}} \quad (6-38)$$

Laboratory procedures for determining maximum and minimum unit weights of cohesionless soils are specified by standard procedures (see *ASTM Standards*, Vol. 11, D-2049).

After the relative density has been evaluated for a particular soil layer of thickness  $H$ , the maximum possible settlement  $\Delta z$  of the surface of this layer may be estimated from

$$\Delta z = \frac{e - e_{\min}}{1 + e} H \quad (6-39)$$

For example, if the layer consists of identical perfect spheres (see Sec. 6.2) initially in the loosest state ( $e_{\max} = e = 0.91$ ) and is subsequently vibrated until it reaches the densest state ( $e_{\min} = 0.35$ ), the surface would settle  $0.293H$ . For this initial condition the relative density was zero. If this layer had an initial void ratio of  $e = 0.63$ , this would correspond to a relative density of 0.50 (or 50 per cent). By vibrating this layer of perfect spheres into the densest condition, the surface would settle by an amount

$$\Delta z = \frac{0.63 - 0.35}{1.63} H = (0.17)H$$

If the layer of perfect spheres was initially at a void ratio of 0.35, the relative density was 1.0 (or 100 per cent) and vibrations would cause no further settlement.

The use of relative density was discussed thoroughly by Burmister (1938, 1948), and a specified value of relative density has often been used as a design criterion or for control of field compaction. However, because relatively small errors in determining  $e_{\min}$  may cause significant errors in  $D_r$  (see D'Appolonia, 1953), the same method should be used for determining  $e_{\min}$  for field control as was used in determining  $e_{\min}$  when establishing the design criterion.

The use of vibratory loadings for compacting cohesionless soils has been studied and evaluated since the early 1930s. These loadings are usually repeated impacts which may be applied at the surface (see, for example, Pippas, 1932; Converse, 1953; Forssblad, 1965; and D'Appolonia, Whitman, and D'Appolonia, 1969) or at a depth within the soil mass (see, for example, Steuerma, 1939; BuRecl, 1948; WES, 1949; Fruhauf, 1949; D'Appolonia, 1953; and Forssblad, 1965). Because the effect of surface compaction extends downward only a few feet, this method is most effective in compacting granular fills which are placed in relatively thin layers. Existing deposits of loose cohesionless materials may be compacted by a vibrator that penetrates into the soil.

The method of compacting cohesionless materials by *vibrations applied at*

the surface has long been employed in the preparation of sub-bases for highways and airport runways and also has been a standard procedure for the construction of earth and rockfill dams. These topics are beyond the scope of this book and will not be treated here. The following discussion is limited to the preparation of sites to support buildings or equipment on soils which will be subjected to vibratory loads during the normal activity of the facility.

Compaction by loads applied at the surface may be accomplished using machines which vary in size from small "one-man" soil compactors to tractor-drawn vibratory rollers producing a dynamic force of 10 tons or more. It should be noted that these vibratory compactors are actually repeated-impact machines in that the vertical accelerations are large enough for the machine to jump free of the ground on the upstroke and act as a hammer on the downstroke. Thus, equipment is available to provide a wide variation in the amount of dynamic force which may be delivered to the soil. In addition to the force amplitude, the number of repetitions delivered to each unit volume of soil is important in causing compaction. The number of stress cycles applied to each spot depends on the number of times the vibrator passes above the given spot, the frequency of vibrations, and the speed of towing. The magnitude of stress developed in any unit volume of soil depends on the intensity of the surface force applied and the distance of this unit volume from the loading point. Thus, there are many combinations of surface force, number of passes, vibration frequency, towing speed, and lift height which may produce satisfactory compaction for a particular cohesionless soil. The most economical combination of these variables must be established by the designer for specific field conditions.

A description of some of the factors to be evaluated when using vibratory compaction for site preparation is included in the study by D'Appolonia, Whitman, and D'Appolonia (1969). This paper describes the field compaction and observations made for a site involving fills of dune sand. The dune sand consisted of poorly graded, angular to subangular, predominantly quartz particles with a mean grain size of 0.18 mm. Following the procedures suggested by Burmister (1964), the former authors found that the minimum unit weight of this material was 88.5 lb/ft<sup>3</sup> and that the maximum unit weight was 110 lb/ft<sup>3</sup>. Initial density measurements from test pits in an 8-ft test embankment gave unit weights of 98 to 100 lb/ft<sup>3</sup> (or 50 to 60 per cent relative density).

Tests to evaluate the increase in compaction with number of vibrating-roller passes were conducted on the 8-foot test embankment. A smooth-drum roller with a dead weight of 12,500 lb and vibrating at a frequency of 27.5 cycles/sec was towed by a D-6 dozer at a speed of 2 ft/sec in all tests. Measurements of the unit weight of the fill were made in test pits after 2, 5, 15, and 45 roller passes. The variation of unit weight with depth is shown in Fig. 6-26a for the original conditions and after 5 roller passes. A composite

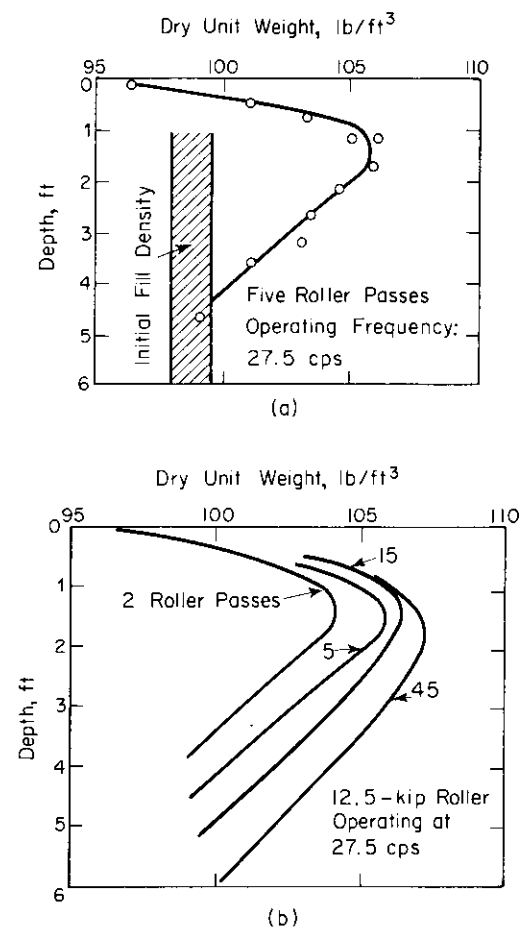


Figure 6-26. Compacted unit weight profile for 8-foot lift height. (a) For five roller passes. (b) For curves showing effect of number of roller passes. (From D'Appolonia, Whitman, and D'Appolonia, 1969.)

diagram shown in Fig. 6-26b illustrates that increasing the number of roller passes increased the unit weights throughout the measured depth, but that the increase was less significant for more than about 5 passes. The maximum compaction occurred at a depth of 1 to 2 ft and decreased with depth until, at a depth of about 6 ft, no measurable effect was noted. Near the surface the compaction was less effective, and for about the upper 6 in., where accelerations were high and confining pressure was low, a loosening occurred.

From the curves shown in Fig. 6-26 it is evident that for this kind of material the most efficient compaction would be obtained for a few roller passes acting on relatively thin lift heights. From subsequent tests using 2-ft lift heights, D'Appolonia et al. (1969) found that superposition of the compactive efforts occurred. Then they proposed a method for specifying compaction procedures by interpreting the density-depth curve of Fig. 6-26a,

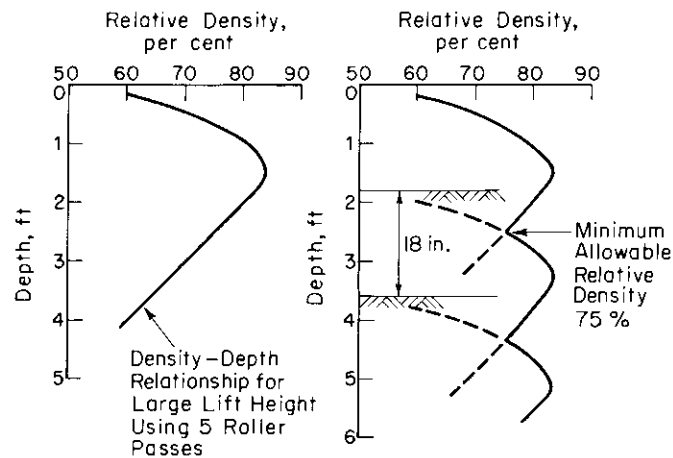


Figure 6-27. Approximate method for determining lift height required to achieve a minimum compacted relative density of 75% with five roller passes using data for a large lift height (from D'Appolonia, Whitman, and D'Appolonia, 1969).

as shown in Fig. 6-27a, in terms of relative density. These curves may be superposed, as shown in Fig. 6-27b, to give the proper lift height to produce a chosen minimum value of relative density. For the case shown in Fig. 6-27b,  $D_r$  was chosen as 75 per cent; and by superposing the 5-pass curves, the minimum lift height was found to be 18 in. For a larger number of passes, the lift height could be increased.

Previous studies (for example, Converse, 1953) have indicated that the most effective compaction is obtained at the resonant frequency of the system. However, in the tests using a 6.3-kip (6300 lb) roller, D'Appolonia et al. (1969) did not find the resonant frequency of the system because the roller was not capable of operating at a high enough frequency. Within the range of operating frequencies, it was found that compaction increased as the frequency increased, as might be anticipated by noting that the exciting force increases with (frequency)<sup>2</sup>. In field situations it may be impossible or uneconomical, from the standpoint of machine maintenance, to operate at the resonant frequency of the system.

Another significant factor associated with vibratory compaction of cohesionless soils was treated in the paper by D'Appolonia et al. (1969). By embedding pressure cells in the fill with the sensing surfaces oriented both horizontally and vertically, they were able to measure the vertical stress and horizontal stresses in the direction of rolling and perpendicular to the direction of rolling. Figure 6-28 shows the resulting *coefficient of horizontal earth pressure*  $K_o$ , which is the ratio of horizontal to vertical static stresses in the

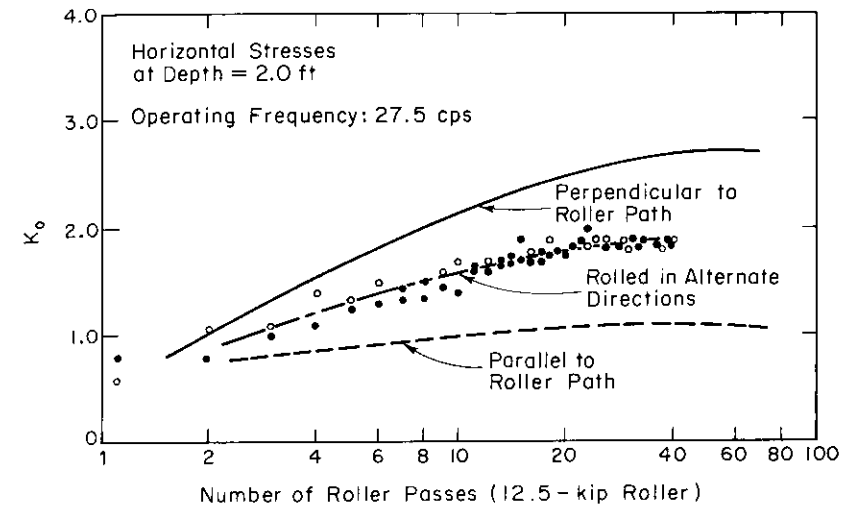


Figure 6-28. Variation of  $K_o$  as a function of number of roller passes (from D'Appolonia, Whitman, and D'Appolonia, 1969).

fill, measured at the end of each series of roller passes. The value

$$K_o = \frac{\sigma_h}{\sigma_v} \quad (6-40)$$

increased with the number of roller passes and was greater in the direction perpendicular to the roller path than it was in the direction parallel to the roller path. Note that these values of  $K_o$  were obtained at a depth of 2 ft below the roller. Undoubtedly as the depths of fill increased above this particular point the value of  $K_o$  would decrease.

When it is necessary to compact existing deposits of loose sand, the vibroflotation process is often used. In this process the vibrating forces are developed by a machine called a "Vibroflot," in which an eccentric mass rotates about a vertical shaft. One model of the Vibroflot has a 16-in. diameter, is 6-ft long, and has a dead weight of 2½ tons. It can develop 10 tons of horizontal force against the soil and has been used effectively to depths of 100 ft. Penetration of the Vibroflot into cohesionless soils is accomplished by a water jet at the tip of the assembly which creates a "quick" condition in the soil. After reaching the desired depth, this tip jet is turned off and a smaller jet at the upper end of the Vibroflot is turned on as the vibrating device is gradually withdrawn to the surface. Additional sand is fed in at the surface as the horizontal impacts compact a column of sand around the vibrator. At the end of the process, a column of compacted sand remains in

the soil mass with the amount of compaction decreasing with radial distance from the line of penetration. The pattern of compacted columns to be developed by this method depends upon the required relative density, the characteristics of the original deposit, and the equipment available. D'Appolonia (1953) has given some criteria which are useful for estimating the required spacings for Vibroflot penetrations.

In these discussions of compaction of cohesionless soils, it was emphasized that a particular value of relative density is desired. For normal machinery vibrations, it is usually satisfactory if the supporting soil is compacted to 70–75 per cent relative density (see D'Appolonia, 1953). However, for foundations subjected to intensive vibrations or earthquake loadings, higher values of  $D_r$  may be required. The final choice of required  $D_r$  at any particular site must be established by the designer.

# 7

## THEORIES FOR VIBRATIONS OF FOUNDATIONS ON ELASTIC MEDIA

### 7.1 Introduction

In this chapter various solutions for the dynamic behavior of foundations supported by an elastic medium are presented and discussed. The principal elastic medium considered is the homogeneous, isotropic, elastic semi-infinite body which is often called simply the “elastic half-space” in following sections. After accepting the assumptions involved in considering a footing resting on the elastic half-space, it is possible to develop mathematical solutions for the dynamic response of footings thus supported. Several solutions which demonstrate the importance of the geometrical variables and types of exciting forces are presented to form a basis for the design procedures which will be treated in Chap. 10.

In Chap. 6 it was demonstrated that soils may be considered to behave approximately as elastic materials for small amplitudes of strain. Furthermore, fairly routine methods for evaluating the “elastic” constants of soils both in the laboratory and in the field have been developed. The elastic soil constants obtained at a given site can be introduced into the appropriate theory to provide an estimate of the dynamic response of a particular foundation. Consequently, theories based on the concepts of elastic media have

engineering value which increases as our knowledge and confidence in estimating the effective values of the elastic soil properties increases.

Following the evaluations of footings resting on the elastic half-space, the change in the dynamic response is considered when the elastic half-space is replaced by an elastic layer resting on a rigid sub-base. Because the theories for this situation are not as well developed, the results are useful primarily to indicate general trends for the dynamic response. Finally, a short section on the influence of piles on the dynamic response of foundations is included to indicate a method of approach which may be useful as a rough guide to design for this condition.

There are also several theories and design procedures which treat the behavior of foundations resting on nonlinear media (Lorenz, 1950, 1953; Novak, 1960; Weissmann, 1966; and Funston and Hall, 1967, for example). These methods will not be considered in this chapter, but they may be considered as supplemental reading. Several of these procedures will become more useful in the future as methods for identifying the nonlinear "elastic" behavior of soils under higher strain amplitudes becomes available.

### 7.2 Lamb (1904) and the Dynamic Boussinesq Problem

The paper by Lamb (1904) has been mentioned previously in Chap. 3 in connection with the theoretical development of ground motions associated with the Rayleigh wave. The Lamb paper is also the cornerstone of theoretical solutions developed from the assumption of an oscillator resting on the surface of a homogeneous, isotropic, elastic, semi-infinite body. In this paper Lamb first studied the response of the elastic half-space as it was excited by oscillating vertical forces acting along a line. Thus, he established the solution for two-dimensional wave propagation. He extended this study to include the condition of oscillating forces acting in a horizontal direction on a line on the surface and for either the vertical or horizontal line source acting at an interior point within the body. The locations of these oscillating line loads are described in Fig. 7-1. He also showed how a series of vertically oscillating forces acting at different frequencies could be combined to produce a single pulse acting on a line on the surface. This pulse was then applied to the surface to produce the surface displacements associated with the compression, shear, and Rayleigh waves.

Lamb followed through the same line of reasoning for the three-dimensional case in which a single oscillating force acted at a point on the surface and within the half-space, and again he developed the solution for both the steady-state oscillation and the transient-pulse loading. It is the oscillating vertical force at the surface, which has often been termed the "dynamic

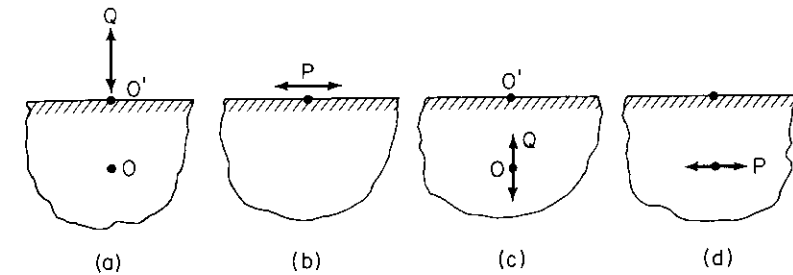


Figure 7-1. Lamb's problems for steady-state oscillating force or pulse loading acting at a point (three-dimensional) or along a line (two-dimensional). (a) For vertical loading at the surface. (b) For horizontal loading at the surface. (c) For vertical loading within the body. (d) For horizontal loading within the body.

Boussinesq loading," which forms the basis for the study of oscillations of footings resting on the surface of the half-space. By integration of the solution for the oscillating vertical force over a finite area of the surface, the contact pressure produced on the half-space by the oscillating footing can be described, and the dynamic response of the footing on the half-space can be evaluated.

Lamb also noted the condition of *dynamic reciprocity*, which is an extension of Maxwell's law of reciprocal deflections to dynamic conditions. Maxwell's law for the usual static case may be stated as follows: The deflection at point 1 in an elastic body due to a unit value of load at point 2 in that body is equal precisely to the deflection at point 2 due to a unit value of load applied at point 1. In using this relation it is necessary to consider the component of each deflection which is in the direction of the applied force at the point under consideration, such that the product of the load and deflection gives work. In the dynamic case, Lamb demonstrated that the horizontal displacement produced at a point on the surface of a semi-infinite elastic body by an oscillating unit vertical force at that point has the same value as the vertical displacement at the same point caused by an oscillating horizontal unit force acting at the point. He noted further that this dynamic reciprocity could be used to evaluate the dynamic motion within an elastic body caused by a point load on the surface by considering the displacement at the surface developed by an oscillating point force acting within the body. This concept is illustrated in Figs. 7-1a and 7-1c, where the vertical displacement at point  $O$  caused by the vertical load  $Q$  acting at  $O'$ , shown in Fig. 7-1a, is equal to the vertical displacement at point  $O'$  caused by the vertical load  $Q$  acting at  $O$  as shown in Fig. 7-1c.

### 7.3 Vertical Oscillation of Footings Resting on the Surface of the Elastic Half-Space

Reissner (1936)

During the early 1930s the Deutschen Forschungsgesellschaft für Bodenmechanik (DEGEBO) investigated the use of mechanical oscillators to evaluate soil properties in the field (see, for example, Hertwig, Früh, and Lorenz, 1933). Because of this activity, E. Reissner attempted to provide a theory for evaluating the dynamic response of a vibrating footing as it was influenced by properties of the soil. He chose the semi-infinite homogeneous, isotropic, elastic body (elastic half-space) to represent the soil mass. The parameters needed to describe the properties of this elastic body were the shear modulus  $G$ , the Poisson's ratio  $\nu$ , and the mass density  $\rho (= \gamma/g)$ . The vibrating footing was represented by an oscillating mass which produced a periodic vertical pressure distributed uniformly over a circular area of radius  $r_o$  on the surface of the half-space.

With the elastic half-space as the mathematical model, Reissner developed an analytical solution for the periodic vertical displacement  $z_o$  at the center of the circular loaded area of the surface. He obtained this solution by integration of Lamb's 1904 solution over a circular area. The mathematical treatment will not be repeated here, but it may be found in the original paper or in the papers by Quinlan (1953) or Sung (1953). The vertical displacement is expressed by

$$z_o = \frac{P_o \exp(i\omega t)}{Gr_o} (f_1 + if_2) \quad (7-1)$$

in which

$P_o$  = amplitude of the total force applied to the circular contact area,

$\omega$  = circular frequency of force application

$G$  = shear modulus of the half-space,

$r_o$  = radius of the circular contact area,

$f_1, f_2$  = Reissner's "displacement functions."

In Eq. (7-1) both the displacement and the force are positive in the downward direction. The expressions for  $f_1$  and  $f_2$  are complicated functions of Poisson's ratio and a dimensionless frequency term  $a_o$ , described by

$$a_o = \omega r_o \sqrt{\frac{\rho}{G}} = \frac{\omega r_o}{v_s} \quad (7-2)$$

In Eq. (7-2)  $v_s$  is the velocity of propagation of the shear wave in the elastic body.

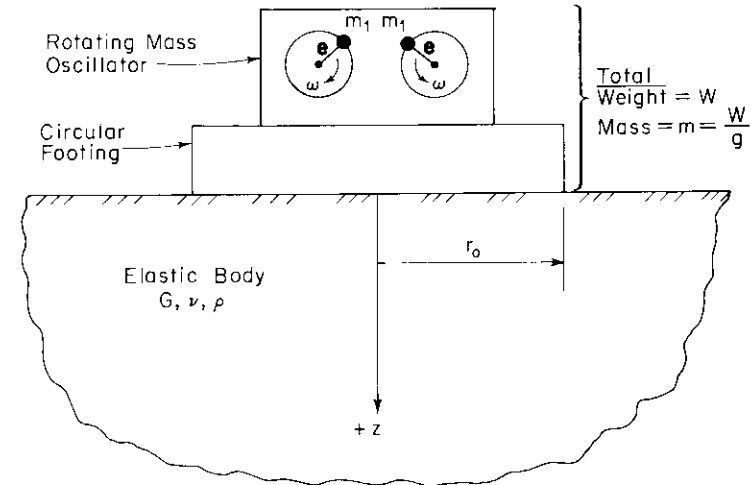


Figure 7-2. Rotating mass oscillator with circular footing resting on semi-infinite elastic body.

Reissner also established a second dimensionless term, designated as the "mass ratio"  $b$ , which is described by

$$b = \frac{m}{\rho r_o^3} \quad (7-3)$$

in which  $m$  is the total mass of the vibrating footing and exciting mechanism which rests on the surface of the elastic half-space (see Fig. 7-2). Equation (7-3) essentially describes a relation between the mass of the rigid body which undergoes vertical motion and a particular mass of the elastic body.

Reissner established expressions for the amplitude of oscillator motion,

$$A_z = \frac{Q_o}{Gr_o} \sqrt{\frac{f_1^2 + f_2^2}{(1 - ba_o^2 f_1)^2 + (ba_o^2 f_2)^2}} \quad (7-4)$$

the phase angle  $\varphi$  between the external force,  $Q = Q_o \exp(i\omega t)$ , and the displacement  $z_o$  was expressed as

$$\tan \varphi = \frac{f_2}{-f_1 + ba_o^2 (f_1^2 + f_2^2)} \quad (7-5)$$

and the input power required was expressed as

$$PR = \frac{Q_o^2}{r_o^2 \sqrt{Gr_o}} \frac{a_o f_1}{(1 - ba_o^2 f_1)^2 + (ba_o^2 f_2)^2} \quad (7-6)$$

The external oscillating force amplitude  $Q_0$  may either be a constant (i.e., independent of the frequency  $\omega$ ) or it may be a function of the frequency of excitation. For the rotating-mass-type exciter with a total mass of  $m_e$  acting at a radius designated as the eccentricity  $e$ , this force is

$$Q_0 = m_e e \omega^2 \quad (7-7)$$

For the two-mass oscillator shown in Fig. 7-2, the total eccentric mass  $m_e$  is equal to  $2m_1$ .

Reissner's theory formed the basis for nearly all further analytical studies of oscillators resting on the half-space, although his theory did not receive immediate adoption by engineers working in the field of soil dynamics because his theoretical results did not completely agree with the results of field tests. There are several reasons for this, including (1) permanent settlements developed during many tests, thereby violating the conditions assumed for an elastic medium; (2) the amplitudes of motion sustained by the model field vibrators were so large (as required for the insensitive recording instruments then available) that the accelerations were often on the order of  $2g$  to  $3g$ , which allowed the vibrator to jump clear of the ground and to act as a hammer; (3) the assumption of a uniformly distributed pressure at the oscillator-soil contact zone was not realistic; and (4) there was an error in the calculation of  $f_2$  which influenced the numerical value of the results. Nevertheless, the study by Reissner is the classic paper in this field.

#### Quinlan (1953) and Sung (1953)

Two papers which appeared at the same time extended Reissner's solution to consider the effects of changes in pressure distribution over the circular area of contact on the surface of the half-space. Quinlan established the equations for oscillating contact pressures which vary across a diameter of the contact area with a parabolic distribution, with a uniform distribution, and with the distribution corresponding to a rigid base. He developed solutions only for the rigid-base case. Sung also established the basic equations for the three pressure distributions and presented solutions for each case. The pressure distributions are identified as

##### (a) Rigid Base (approximation)

$$\begin{aligned} \sigma_z &= \frac{P_0 \exp(i\omega t)}{2\pi r_0 \sqrt{r_0^2 - r^2}} & \text{for } r \leq r_0 \\ \sigma_z &= 0 & \text{for } r > r_0 \end{aligned} \quad (7-8)$$

##### (b) Uniform

$$\sigma_z = \frac{P_0 \exp(i\omega t)}{\pi r_0^2} \quad \text{for } r \leq r_0 \quad (7-9)$$

$$\sigma_z = 0 \quad \text{for } r > r_0$$

##### (c) Parabolic

$$\sigma_z = \frac{2P_0(r_0^2 - r^2) \exp(i\omega t)}{\pi r_0^4} \quad \text{for } r \leq r_0 \quad (7-10)$$

$$\sigma_z = 0 \quad \text{for } r > r_0$$

Sung's solutions described the displacement at the center of the circular area loaded by the three pressure distributions. For the parabolic and uniform-pressure distributions the loaded surface developed larger displacements at the center than at the edges—a displacement pattern which can be developed only by a flexible footing. The rigid-base pressure distribution produced uniform displacement of the loaded surface under static conditions. Thus, the three pressure distributions developed three different shapes of surface displacements.

After determining these center displacements, Sung established the dynamic response of a mass supported on the half-space for each type of contact-pressure distribution by considering that the center of gravity of the mass moved the same distance as the center of the loaded area. This assumption produced exaggerated response curves for the parabolic and uniform-pressure distributions because the center point has greater displacement than the average. However, these response curves are instructive from a qualitative standpoint for visualizing the influence of contact-pressure distribution on the vibration response of the system.

Figure 7-3a shows the amplitude-frequency response curves corresponding to the three pressure distributions in an oscillator-soil system for which  $b = 5$ ,  $\nu = \frac{1}{4}$ , and the exciting force is caused by a rotating-mass exciter (see Eq. 7-7). From Fig. 7-3a it is evident that as the load is progressively concentrated nearer the center of the loaded area, the peak amplitude of motion increases and the dimensionless frequency  $a_0$  at which this peak amplitude occurs is lowered. An improvement on the presentation of the response of footings which develop these pressure distributions was presented by Housner and Castellani (1969). They determined response curves based on a weighted average displacement which was based on the work done by the total dynamic force. The peaks of the corresponding response curves for the weighted average displacements are shown in Fig. 7-3a as the solid circles designated as  $\bar{P}$ ,  $\bar{U}$ , and  $\bar{R}$ . As might be anticipated, the response curves for the weighted average displacements for the parabolic and uniform displacements are closer to the curve for the rigid-base condition than are

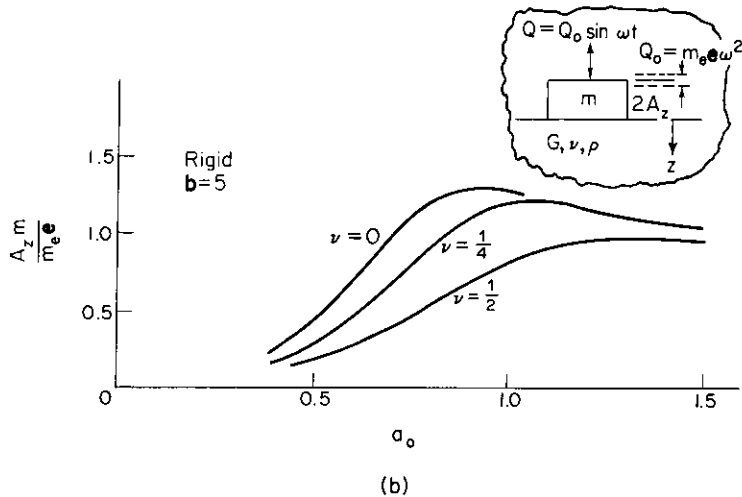
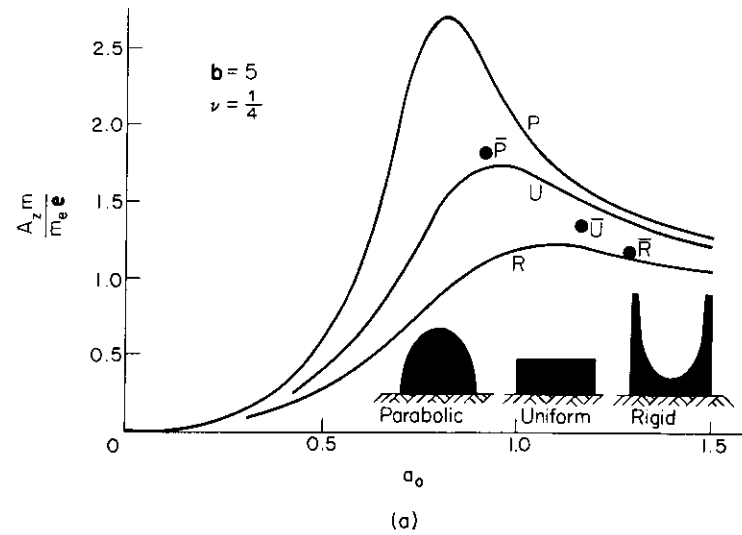


Figure 7-3. Effect of pressure distribution and Poisson's ratio on theoretical response curves for vertical footing motion (after Richart and Whitman, 1967).

Sung's curves; however, the trend is still the same. This diagram should indicate to a designer that he may influence the dynamic response of a foundation by his control of the flexibility of the foundation pad. A practical application of this type of control has been described by Fistedis (1957), who

indicated that adjustment of the resonant frequency of an engine or compressor foundation could be accomplished by post-tensioning a prestressed concrete base pad. By changing the camber of the base pad, the major part of the soil-contact pressure could be moved toward or away from the edges.

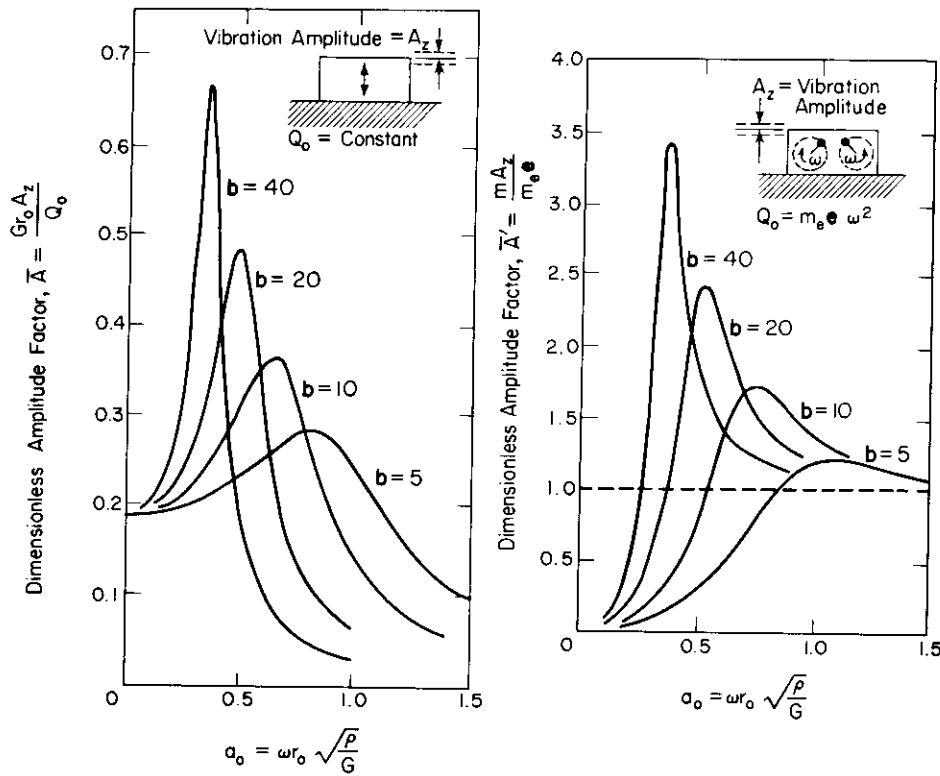
Figure 7-3b illustrates the influence of a change in Poisson's ratio  $\nu$  of the elastic body on the steady-state response for the rigid-base condition and  $b = 5$ . This diagram shows that the amplitude of motion is greater and the frequency at maximum amplitude is lower when  $\nu = 0$ . Because some solutions for other modes of oscillation are available *only* for the case of  $\nu = 0$ , it is useful to have this guide to indicate how the solution for  $\nu = 0$  might vary from a more realistic condition of  $\nu = 0.33$  or  $0.40$ . Generally, the solution for  $\nu = 0$  would represent the "worst case" of a greater motion at a lower frequency.

Sung established values for the displacement functions  $f_1$  and  $f_2$  (used in Eq. 7-1) for values of  $\nu$  of  $0, \frac{1}{4}, \frac{1}{3},$  and  $\frac{1}{2}$  for each of the three base-pressure distributions over the range of  $a_0$  from 0 to 1.5. These displacement functions were then introduced into Eq. (7-4) to evaluate the amplitude-frequency ( $A_z$  vs.  $a_0$ ) response curves for different values of the mass ratio  $b$ . Figure 7-4 illustrates the influence of the mass ratio  $b$  on the shape of the amplitude-frequency response curves for the case of the *rigid-base* pressure distribution and Poisson's ratio of  $\frac{1}{4}$ . By taking the values of the dimensionless amplitudes  $\bar{A}$  or  $\bar{A}'$  and the frequency factor  $a_0$  at the peak of each response curve, a series of curves can be established to relate  $\bar{A}_m$  (or  $\bar{A}'_m$ ),  $a_{0m}$ , and  $b$ , which are useful for establishing the maximum amplitude of motion and the frequency at which it occurs. These curves have been prepared by Richart (1962) for use in analysis or design. The same information is presented in Fig. 7-11 in a more convenient form.

By comparing Fig. 7-4a with Fig. 2-14a, and Fig. 7-4b with Fig. 2-16, we note that the shapes of these response curves are quite similar. The curves for the lower  $b$ -values correspond to the curves with large damping ratios  $D$ . This is a graphical illustration that vertical oscillation of a rigid footing on an elastic semi-infinite body includes a significant loss of energy by radiation of elastic waves from the footing throughout the half-space. This loss of energy through propagation of elastic waves was defined in Sec. 3.3 as *geometrical damping*. Because most footing systems which undergo vertical vibrations lead to  $b$ -values of less than 10, *vertical oscillations are usually highly damped and extreme amplitudes of motion do not occur*.

In Sung's study he assumed that the pressure distribution remained constant throughout the range of frequencies considered. Actually, the rigid-base pressure distribution which correctly predicts a uniform displacement of the loaded surface under static conditions does not produce uniform displacement under dynamic conditions. Bycroft (1956) evaluated the weighted average of the displacements beneath the footing and established





(a) For Constant Amplitude of Exciting Force.

(b) For Exciting Force Amplitude Dependent on Exciting Frequency.

Figure 7-4. Amplitude vs. frequency relations for vertical oscillation of a rigid circular footing on an elastic half-space ( $\nu = \frac{1}{4}$ ). (After Richart, 1962.)

better values for the displacement functions  $f_1$  and  $f_2$ . His values of the displacement functions for the rigid base and for  $\nu = 0, \frac{1}{4}$ , and  $\frac{1}{2}$  are given in Fig. 7-5.

Several important points may be observed in Fig. 7-5. At  $a_o = 0$  (static case),  $f_2 = 0$  and the value of  $f_1$  must produce the correct static displacement when introduced into Eq. (7-1). For the rigid circular footing, the static displacement is

$$z_s = \frac{P_o(1 - \nu)}{4Gr_o} \quad (7-11)$$

It should be noted that the  $f_1$  and  $f_2$  terms are evaluated only over the range

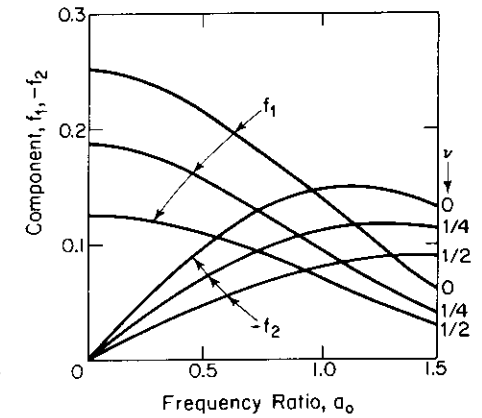


Figure 7-5. Displacement functions for rigid circular footing vibrating vertically on the surface of an elastic half-space (after Bycroft, 1956).

of ( $0 < a_o < 1.5$ ). This is the practical range over which the resonance peaks may occur in the response curves and is satisfactory for most steady-state resonance studies. Finally, the displacement function  $f_2$  essentially describes damping in the system (see Eq. 7-16).

### Hsieh's Equations

By a reorganization of Reissner's basic equations, Hsieh (1962) was able to improve the presentation of the expression for "geometrical damping" which developed from the elastic theory. He considered first a weightless, rigid, circular disk of radius  $r_o$  resting on the surface of the elastic half-space (Fig. 7-6a). The disk was subjected to a vertical periodic loading of

$$P = P_o \exp(i\omega t) \quad (7-12)$$

From Eq. (7-1) it was shown that the vertical displacement is

$$z = \frac{P_o \exp(i\omega t)}{Gr_o} (f_1 + if_2) \quad (7-1)$$

By differentiating with respect to time, he obtained

$$\frac{dz}{dt} = \frac{P_o \omega \exp(i\omega t)}{Gr_o} (if_1 - f_2) \quad (7-13)$$

Thus,

$$f_1 \omega z - f_2 \frac{dz}{dt} = \frac{P_o \omega}{Gr_o} (f_1^2 + f_2^2) \exp(i\omega t) = \frac{P_o \omega}{Gr_o} (f_1^2 + f_2^2)$$

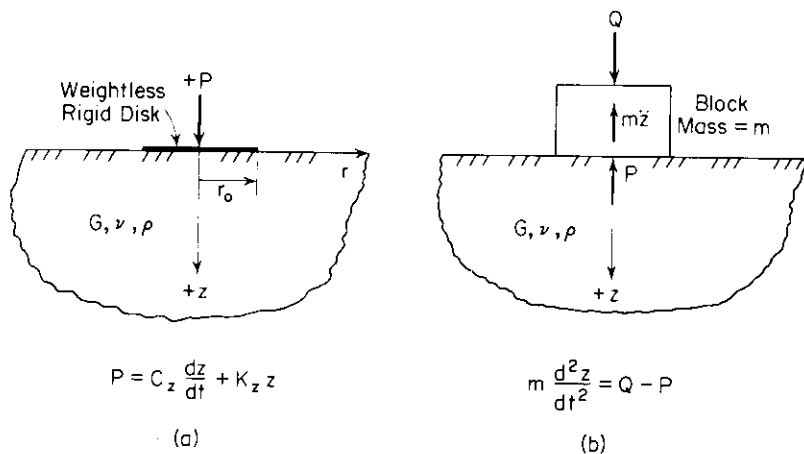


Figure 7-6. Notation for Hsieh's equations.

or

$$P = -\frac{Gr_o}{\omega} \frac{f_2}{(f_1^2 + f_2^2)} \frac{dz}{dt} + Gr_o \frac{f_1}{f_1^2 + f_2^2} z \tag{7-14}$$

Equation (7-14) can be simplified to

$$P = C_z \frac{dz}{dt} + K_z z \tag{7-15}$$

after substituting

$$C_z = \frac{r_o^2}{a_o} \sqrt{G\rho} \left( \frac{-f_2}{f_1^2 + f_2^2} \right) \tag{7-16}$$

and

$$K_z = Gr_o \frac{f_1}{f_1^2 + f_2^2} \tag{7-17}$$

Note that because both  $C_z$  and  $K_z$  include  $f_1$  and  $f_2$ , they also depend on  $a_o$  and  $\nu$ .

Now, if a rigid cylindrical footing of base radius  $r_o$  and total weight  $W$  is placed on the half-space and set into vertical oscillation by an external periodic force  $Q$ , we may write an expression for its dynamical equilibrium as

$$\frac{W}{g} \frac{d^2z}{dt^2} = Q - P \tag{7-18}$$

After substituting Eq. (7-15) and  $m = W/g$ , this reduces to

$$m \frac{d^2z}{dt^2} + C_z \frac{dz}{dt} + K_z z = Q = Q_o \exp(i\omega t) \tag{7-19}$$

Equation (7-19) has the same general form as the equilibrium equation for the damped-single-degree-of freedom system (see Eq. 2-48). The major difference is that the *damping term*  $C_z$  and the *spring-reaction term*  $K_z$  are both functions of the frequency of vibration. However, Eq. (7-16) shows clearly that the geometrical damping in the elastic system is governed by the displacement function  $f_2$ . Equation (7-17) demonstrates that the static displacement and elastic-spring response of the system is governed by the term  $f_1$ .

Hsieh included in this study a description of the frequency-dependent damping and spring functions for horizontal oscillation, rocking, and torsional oscillations and demonstrated their use in establishing equations for coupled oscillations. This will be considered further in Sec. 7.8.

### Lysmer's Analog

To approximate the dynamic response of a rigid circular footing to vertical motion, Lysmer (1965) considered a footing made up of a series of concentric rings. By applying uniform pressures of different magnitudes on each ring, he was able to develop a constant deflection under the footing and to evaluate the dynamic response of the footing to a periodic exciting force. In the process of developing his solution, Lysmer found several notations to be convenient for simplification of the presentation. The displacement function

$$f = f_1 + if_2 \tag{7-20}$$

includes Poisson's ratio, but if it is multiplied by a factor  $4/(1 - \nu)$ , a new displacement function

$$F = \frac{4}{1 - \nu} f = F_1 + iF_2 \tag{7-21}$$

is obtained which is essentially independent of  $\nu$ . Figure 7-7 illustrates the way in which Bycroft's displacement functions collapse onto a nearly common curve when modified by Eq. (7-21). Using this notation, Lysmer calculated values for  $F_1$  and  $F_2$  over the range of frequency ratio ( $0 < a_o < 8.0$ ) and, with an approximation, extended this to  $a_o \rightarrow \infty$ . The curves in Fig. 7-8 show the  $F_1$  and  $F_2$  curves over the range of ( $0 < a_o < 8$ ). It is useful to note that previous analytical solutions only considered the displacement functions up to  $a_o$  of 1.5 and did not clearly identify the peak of the  $F_2$  curve.

With the displacement function  $F$  as noted in Eq. (7-21), and the positive directions of the force  $P$ , and the displacement  $z$  designated as + downward,

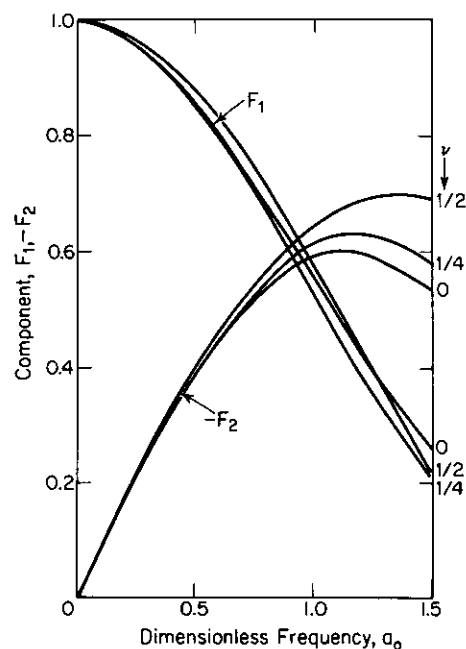


Figure 7-7. Variation of components of  $F$  with Poisson's ratio (after Lysmer and Richart, 1966).

Eq. (7-1) becomes

$$z = \frac{P}{k_z} F \quad (7-22)$$

wherein the directions of the applied force  $P$  and the resulting displacement are the same for static loading. The spring factor  $k_z$  can be developed from Eq. (7-17) after substitution of the terms from Eq. (7-21).

Lysmer further noted that by introducing a modified dimensionless mass ratio

$$\mathbf{B}_z = \frac{1-\nu}{4} \mathbf{b} = \frac{1-\nu}{4} \frac{m}{\rho r^3} \quad (7-23)$$

for the vertical vibration of the rigid circular footing, the influence of Poisson's ratio was essentially eliminated. Then he developed response curves by introducing his modified expressions  $F$  (Eq. 7-21) and  $\mathbf{B}_z$  (Eq. 7-23) into Eq. (7-4). After these substitutions, Eq. (7-4) can be expressed as

$$A_z = \frac{(1-\nu)Q_0}{4Gr_0} M \quad (7-24)$$

in which  $M$  is the magnification factor by which the equivalent static displacement produced by  $Q_0$  is multiplied to give the displacement amplitude

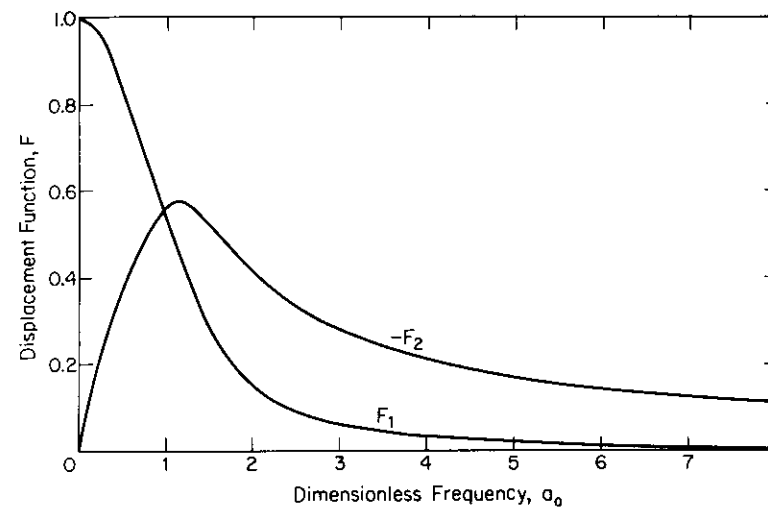


Figure 7-8. Displacement function  $F$  for vertical vibration of a weightless rigid circular disk ( $m = 0$ ) (after Lysmer and Richart, 1966).

$A_z$ . The response curves corresponding to a constant-force excitation  $Q_0$  are shown in Fig. 7-9 for several values of  $\mathbf{B}_z$  as solid curves. Figure 7-10 includes response curves which are produced by the rotating-mass excitation ( $Q_0 = m_e \omega^2$ , Eq. 7-7). After substituting Eq. (7-7) into Eq. (7-24) and simplifying,

$$A_z = \frac{m_e e}{m} M a_0^2 \mathbf{B}_z = \frac{m_e e}{m} M_r \quad (7-25)$$

in which  $M_r$  is the magnification factor by which the quantity  $m_e e/m$  is multiplied to give the displacement amplitude  $A_z$ . From Figs. 7-9 and 7-10, the values of  $M$  and  $M_r$  at the peak of each response curve and the value of  $a_0$  at the peak can be established. These values may then be plotted as  $\mathbf{B}_z$  vs.  $a_{0m}$  (Fig. 7-11a) or  $\mathbf{B}_z$  vs.  $M_m$  or  $M_{rm}$  (Fig. 7-11b). Figures 7-11a and 7-11b provide a simple means for evaluating the maximum amplitude of vertical motion of a rigid circular footing and the frequency at which this occurs for both the constant force and rotating-mass excitation.

After studying the variations of the effective damping and spring factors with frequency ( $a_0$ ) as obtained from the elastic-half-space theory, Lysmer discovered that constant values of these quantities (i.e., independent of  $a_0$ ) could be used. He chose the spring constant equal to the static value

$$k_z = \frac{4Gr_0}{1-\nu} \quad (7-26)$$

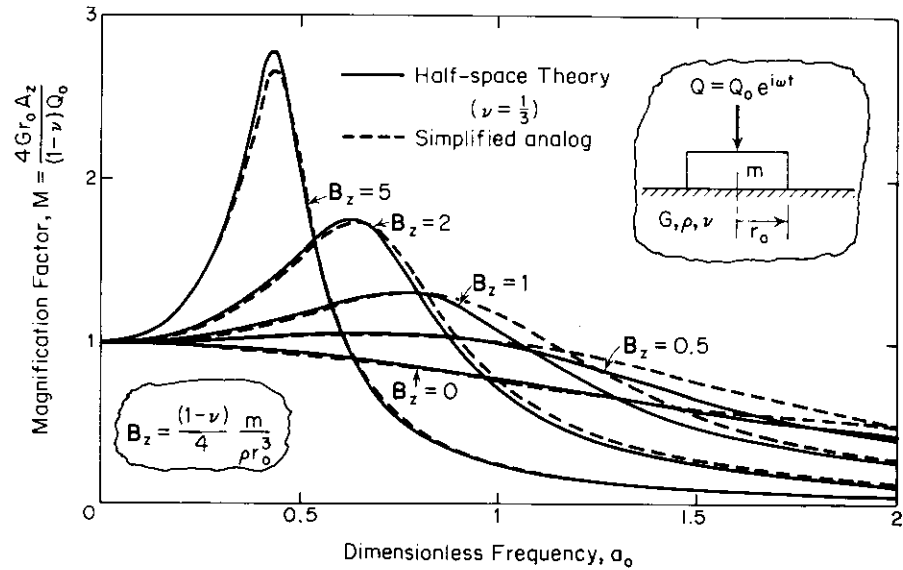


Figure 7-9. Response of rigid circular footing to vertical force developed by constant force excitation (from Lysmer and Richart, 1966).

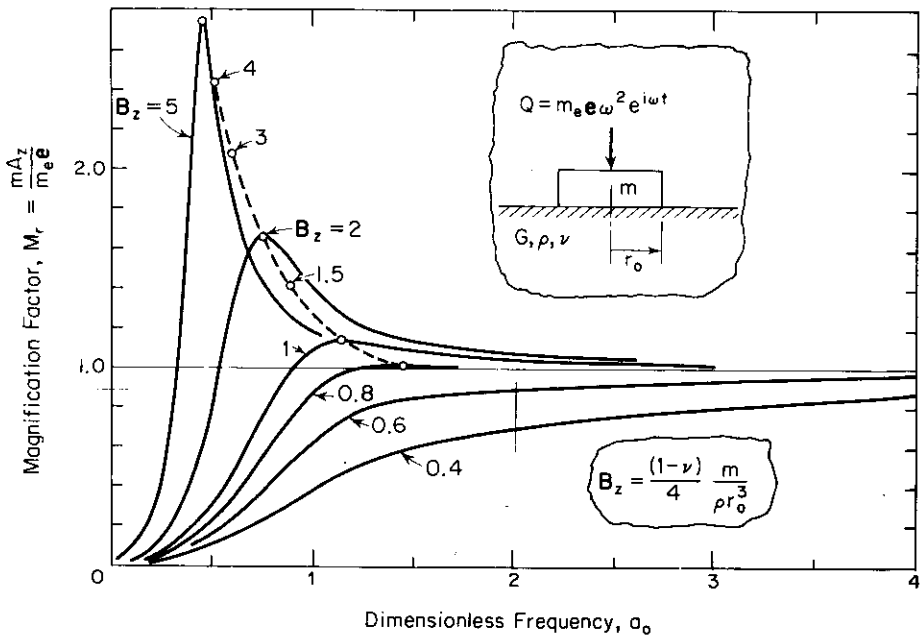


Figure 7-10. Response of rigid circular footing to vertical force developed by rotating mass exciter ( $Q_0 = m_e \omega^2$ ).

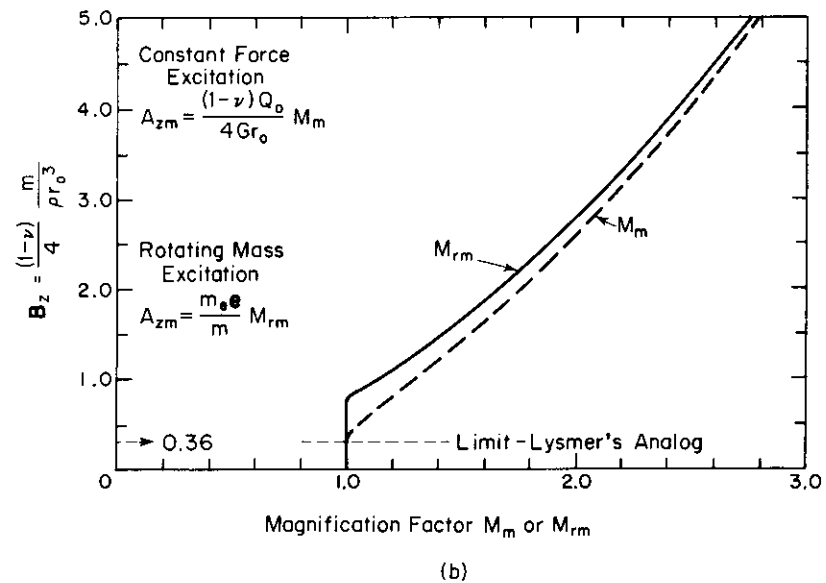
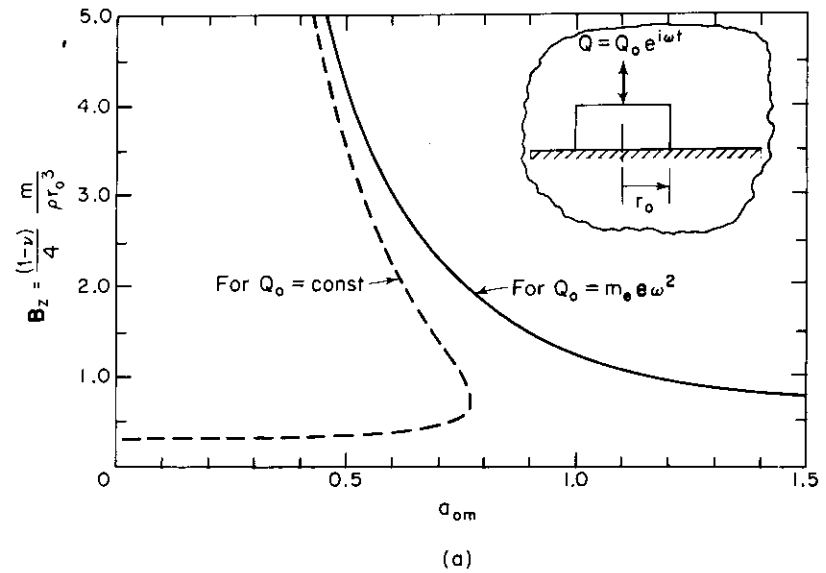


Figure 7-11. Vertical oscillation of rigid circular footing on elastic half-space. (a) Mass ratio vs. dimensionless frequency at resonance. (b) Mass ratio vs. magnification factor at resonance.

and found the best fit for the damping term in the range ( $0 < a_o < 1.0$ ) to be

$$c_z = \frac{3.4r_o^2}{(1-\nu)} \sqrt{\rho G} \quad (7-27)$$

When these values of spring and damping constants were introduced into Eqs. (2-72), (2-73), and (2-74), the steady-state response curves shown as the dashed curves in Fig. 7-9 were obtained. Because the agreement is so remarkable, it is sufficient, for all practical purposes, to use the approximate expressions given in Eqs. (7-26) and (7-27) in the equation of equilibrium (Eq. 7-19) for vertical oscillation of the rigid circular footing on the elastic half-space. The equation of motion for Lysmer's analog is

$$m\ddot{z} + \frac{3.4r_o^2}{(1-\nu)} \sqrt{\rho G} \dot{z} + \frac{4Gr_o}{(1-\nu)} z = Q \quad (7-28)$$

Using the spring constant  $k_z$  (Eq. 7-26) and damping constant  $c_z$  (Eq. 7-27), the functions corresponding to the single-degree-of-freedom system can be established from the procedures described in Chap. 2. The expressions for resonant frequencies depend on the damping ratio  $D$ , which is obtained by dividing the damping constant  $c_z$  (Eq. 7-27) by the critical damping  $c_c$ . For the vertical oscillation of the rigid circular footing, the critical damping is obtained by substituting Eq. (7-26) into Eq. (2-31):

$$c_c = 2\sqrt{k_z m} = 2\sqrt{\frac{4Gr_o m}{(1-\nu)}} \quad (7-29)$$

then

$$D = \frac{c_z}{c_c} = \frac{0.425}{\sqrt{B_z}} \quad (7-30)$$

after substituting  $B_z$  for the expressions noted in Eq. (7-23). For excitation by a force of constant amplitude  $Q_o$ , the resonant frequency is

$$f_m = \frac{1}{2\pi} \sqrt{\frac{k_z}{m}} \sqrt{1 - 2D^2} = \frac{1}{2\pi r_o} \frac{v_S \sqrt{B_z - 0.36}}{B_z} \quad (7-31)$$

When the exciting force is a function of the frequency (Eq. 7-7), Lysmer's expression for the resonant frequency is

$$f_{mr} = \frac{v_S}{2\pi r_o} \sqrt{\frac{0.9}{B_z - 0.45}} \quad (7-32)$$

Note that these approximations give good answers only for  $B_z \geq 1$ .

By substituting the value of  $D$  from Eq. 7-30 into Eqs. 2-56 and 2-61, we can establish expressions for the maximum amplitude of oscillation as

$$A_{zm} = \frac{Q_o(1-\nu)}{4Gr_o} \frac{B_z}{0.85\sqrt{B_z - 0.18}} \quad (7-33a)$$

for constant-force excitation and

$$A_{zm} = \frac{m_e e}{m} \frac{B_z}{0.85\sqrt{B_z - 0.18}} \quad (7-33b)$$

for the rotating-mass excitation. The phase angle  $\varphi$  is determined from

$$\tan \varphi = \frac{0.85a_o}{B_z a_o^2 - 1} \quad (7-34)$$

The most important result of Lysmer's study was establishing the bridge between the elastic-half-space theory and the mass-spring-dashpot system and providing values for the damping and spring constants. Now that the results for the vertically loaded rigid footing can be expressed by Eq. (7-28), we can evaluate the response of this system to either periodic or transient excitation. Further discussions of the development of this study and the use of Eq. (7-28) for conditions of transient loading were given by Lysmer (1965) and by Lysmer and Richart (1966). The response of rigid footings to transient vertical loadings will be discussed in Chap. 10, where Eq. (7-28) will be included in the graphical phase-plane method.

#### Example of Footing Subjected to Steady-State Vertical Oscillation

The report by Fry (1963) contains data from field vibration tests on circular concrete footings which varied from about 5 to 16 ft in diameter. For one series of tests, these model footings rested on the surface of a uniform bed of loess, classified as a silty clay (CL). For this soil the unit weight  $\gamma$  was 117 lb/ft<sup>3</sup> and the properties needed for dynamic analyses were established through seismic and steady-state-vibration tests as described in Chap. 4. These were found to be  $v_S = 460$  ft/sec,  $G = 5340$  lb/in.<sup>2</sup>, and  $\nu = 0.355$ .

The footings were excited into vertical vibration by a four-mass oscillator with eccentric weights arranged as shown in Fig. 10-5c. Each unbalanced weight was 339 lb, giving a total unbalanced weight of  $W_e = 1356$  lb. The dead weight of the oscillator was 5600 lb. The total vibrating weight  $W$

included the dead weight of the oscillator, the weight of the concrete footing, and the weight of the lead ballast which was rigidly attached to the footing.

To illustrate the method for calculation of the amplitude and frequency of resonant vibration, consider a footing with a 62-in. diameter ( $r_o = 31$  in. = 2.583 ft) which has a total weight  $W$  of 30,970 lb. Then, the mass ratio for this test condition is

$$\mathbf{B}_z = \frac{1 - \nu}{4} \frac{W}{\gamma r_o^3} = \frac{1 - 0.355}{4} \frac{30,970}{117(2.583)^3} = 2.48$$

From Fig. 7-11a the dimensionless frequency at maximum amplitude  $a_{om}$  is 0.67. Then the frequency at maximum amplitude may be obtained from Eq. (7-2) after rearranging and substituting quantities:

$$f_{mr} = \frac{\omega}{2\pi} = \frac{a_{om} v_S}{2\pi r_o} = \frac{0.67 \times 460}{2\pi(2.583)} = 19.0 \text{ cycles/sec}$$

The approximate value of resonant frequency obtained from Eq. (7-32) is

$$f_{mr} = \frac{v_S}{2\pi r_o} \sqrt{\frac{0.90}{\mathbf{B}_z - 0.45}} = 18.9 \text{ cycles/sec}$$

The amplitude of vertical oscillation depends on  $\mathbf{B}_z$  and the magnitude of the exciting force. From Fig. 7-11b the magnification factor  $M_{rm}$  is found to be 1.86 for  $\mathbf{B}_z = 2.48$ . Then for the test in which the radius of eccentricity of the unbalanced weights was 0.105 in., the amplitude of motion is calculated as

$$A_{zm} = \frac{m_e e}{m} M_{rm} = \frac{W_e e}{W} M_{rm} = \frac{1356 \times 0.105}{30,970} 1.86 = 0.0086 \text{ in.}$$

The approximate solution obtained from Eq. (7-33b) is

$$A_{zm} = \frac{m_e e \mathbf{B}_z}{m(0.85)\sqrt{\mathbf{B}_z - 0.18}} = 0.0088 \text{ in.}$$

#### Vertical Oscillation of Rigid Rectangular Footing

Analytical solutions for vertical oscillating loads on a rectangular zone of the surface of the elastic half-space have also been developed by integrating

Lamb's solution. Sung (1953a) developed the mathematical expressions for a uniformly distributed oscillating load acting on a rectangular area but did not obtain numerical values. Kobori (1962) and Thomson and Kobori (1963) followed the same procedure and obtained the displacement functions  $f_1$  and  $f_2$  for the case of a uniformly distributed load over the rectangular surface area. They evaluated these functions only in terms of the displacement at the center of the loaded zone, which produced results indicating negative damping at some values of the frequency ratio. (Negative damping cannot occur for this vibrating system.) A recent paper by Elorduy, Nieto, and Szekely (1967) presented solutions for the vertical oscillation of a rigid rectangular base with a length  $2c$  and a width  $2d$  on the surface of the elastic half-space. By superposing the effects of uniform displacement of the surface, they were able to produce uniform displacement of the loaded area. They found, as did Lysmer, that the pressure distribution required to maintain this uniform displacement varied with the frequency of oscillation. They evaluated several of these distributions of pressure and also computed the displacement functions  $f_1$  and  $f_2$  for a square ( $c/d = 1$ ) and rectangular ( $c/d = 2$ ) loading area on an elastic half-space for which the Poisson's ratio was  $\frac{1}{4}$ . These functions are shown as the solid line in Fig. 7-12. Also shown in Fig. 7-12 are the corresponding curves from Sung (1953) and Bycroft (1956) after the radius had been adjusted to give a circular area equal to that for the square or rectangle. Because these curves are approximately the same, for all practical purposes it is satisfactory to use the solution for a circular rigid base of the same area to represent the case of vertical oscillation of a rigid rectangular base (for  $c/d$  up to 2.0).

The limiting condition of a rectangular foundation occurs when the oscillating body is treated as an infinitely long rigid strip. Quinlan (1953) has given a solution for the resonant frequency of such a strip footing of width  $2d$  oscillating vertically in response to excitation of the rotating-mass-type excitation (Eq. 7-7). For this two-dimensional case the mass ratio is

$$\mathbf{b}' = \frac{m'}{\rho d^2} \quad (7-35)$$

in which  $m'$  is the mass per unit length of the footing and  $d$  is one-half its total width. Figure 7-13 shows the mass-ratio-dimensionless-frequency relationships for the two conditions of  $\nu = \frac{1}{2}$  and  $\nu = \frac{1}{4}$ .

For a rectangular footing of finite length-to-width ratio, the resonant frequency should lie between the limits given by the theory for the rigid circular (or square) footing and that for the rigid strip of width  $2d$  and of infinite length.

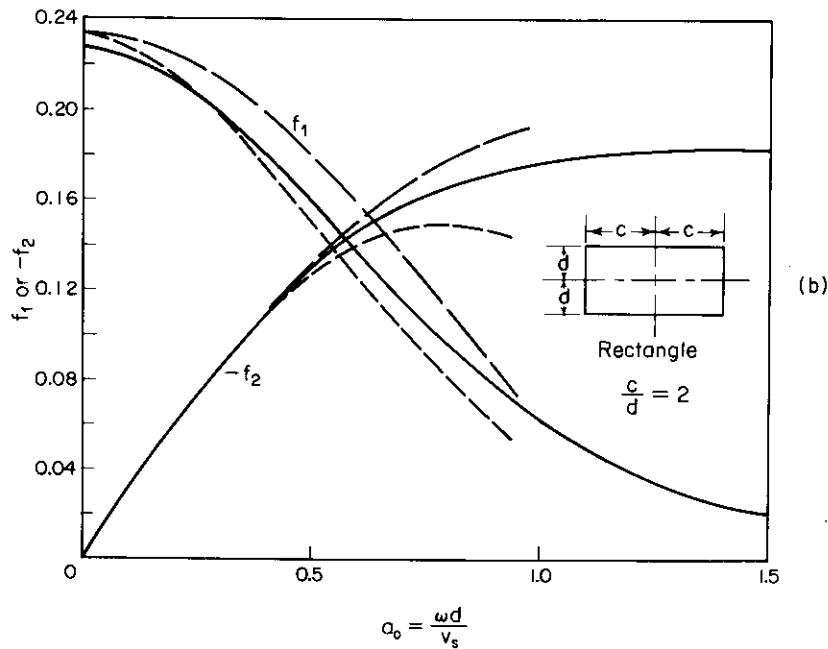
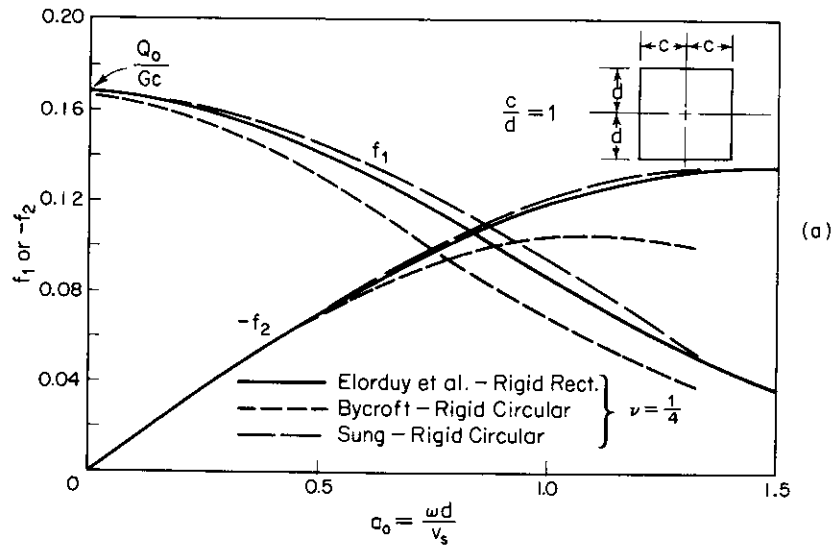


Figure 7-12. Displacement functions for vertical vibration of rigid rectangular and rigid circular footings.

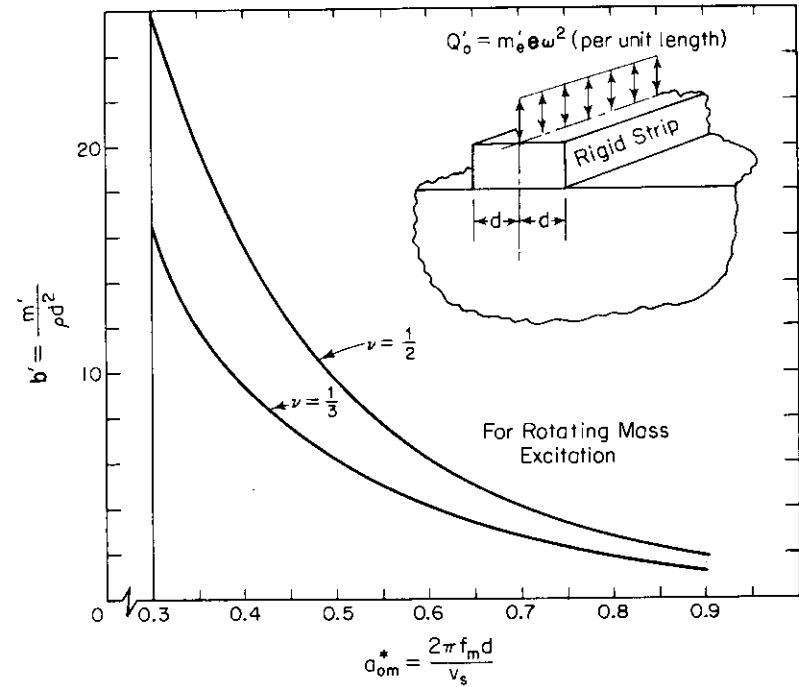


Figure 7-13. Mass ratio vs. dimensionless frequency for vertical oscillation of rigid strip of infinite length (after Quinlan, 1953).

### 7.4 Torsional Oscillation of Circular Footings on the Elastic Half-Space

Reissner (1937) and Reissner and Sagoci (1944) presented analytical solutions for the torsional oscillation of a circular footing resting on the surface of the elastic half-space. In the first paper Reissner considered a linear variation of shearing stress varying from zero at the center of the circle to a maximum at the radius  $r_0$  which bounded the loaded zone. Consequently, this represented a flexible footing. In the second approach, Reissner and Sagoci considered a linear variation in displacement from the center of the circle to the periphery. This represents the movement of a *rigid circular footing* oscillating about a vertical axis through the center of the contact area. Under static conditions the tangential shearing stress  $\tau_{z\theta}$ , which is developed by the applied torque  $T_\theta$ , is given by the expression

$$\tau_{z\theta} = \frac{3}{4\pi} \frac{T_\theta r}{r_0^3 \sqrt{r_0^2 - r^2}} \quad \text{for } 0 < r < r_0 \quad (7-36)$$

Equation (7-36) demonstrates that the shearing stress is zero at the center of the footing and becomes infinite at the periphery. In practical cases the infinite shearing stresses cannot be developed by soils. Thus, it could be anticipated that calculated values of frequency would be higher and amplitudes of motion would be lower than those occurring for real footings. The relation between applied torque  $T_0$  and the resulting rotation  $\theta_s$  under static conditions determines the static spring constant

$$k_{\theta s} = \frac{T_{\theta}}{\Theta_s} = \frac{16}{3} Gr_o^3 \quad (7-37)$$

In the dynamic solutions Reissner, and Reissner and Sagoci again employed the dimensionless frequency  $a_o$  (Eq. 7-2) and the "mass ratio." For torsional oscillation the mass ratio is

$$B_{\theta} = \frac{I_{\theta}}{\rho r_o^5} \quad (7-38)$$

in which  $I_{\theta}$  is the mass moment of inertia of the footing about the axis of rotation. Again, the analytical results can be presented in a simplified form by plotting the peak values of the amplitude-frequency response curves as relations between  $B_{\theta}$ ,  $a_{om}$  (the dimensionless frequency at peak amplitude), and the dynamic magnification factor, which for constant torque excitation is

$$M_{\theta m} = \frac{A_{\theta m}}{\Theta_s} \quad (7-39)$$

For the case of excitation by a rotating-mass system, the exciting torque is

$$T_{\theta} = m_e e x \omega^2 \quad (7-40)$$

in which  $x$  is the horizontal-moment arm of the unbalanced weights from the center of rotation. With this excitation the peak amplitude of motion is given by

$$A_{\theta m} = \frac{m_e e x}{I_{\theta}} M_{\theta rm} \quad (7-41)$$

Values of  $M_{\theta m}$ ,  $M_{\theta rm}$ , and  $a_{om}$  are given in Fig. 7-14 as functions of  $B_{\theta}$ .

The theoretical solution for the torsional oscillation disclosed several significant differences from the case for vertical oscillation: (1) this oscillation is not influenced by Poisson's ratio; (2) it is an uncoupled motion and may

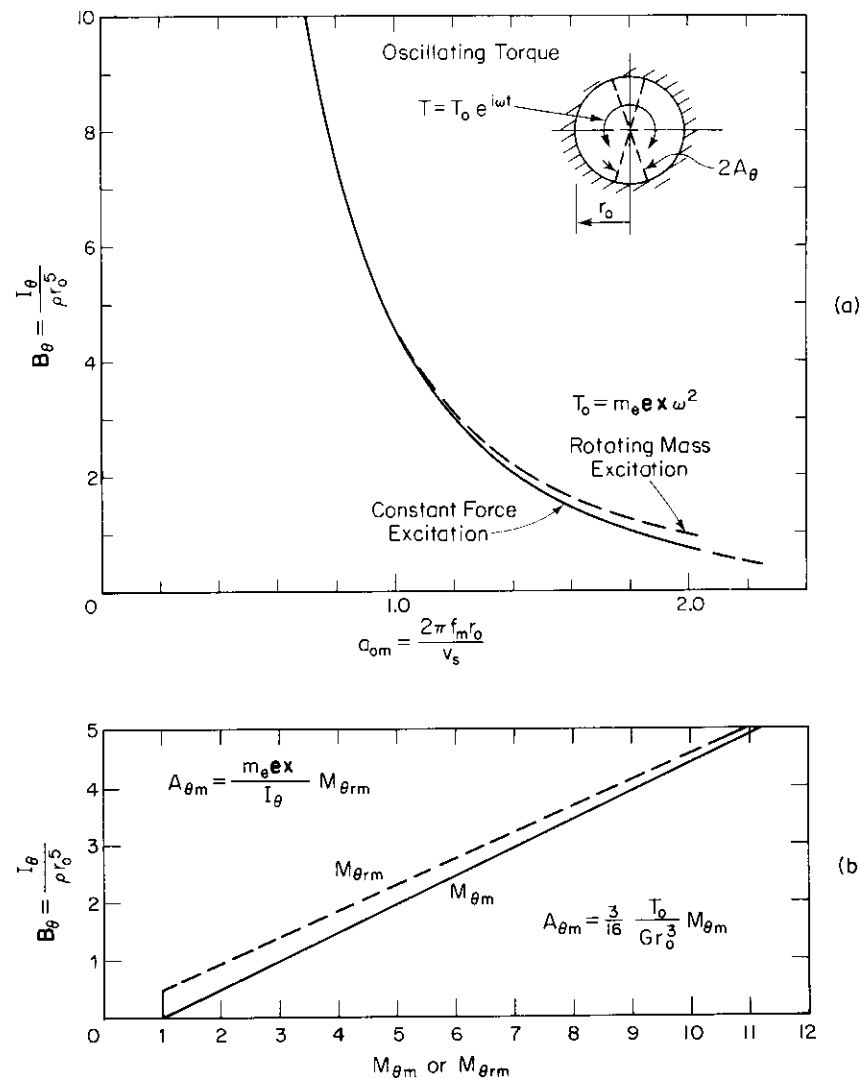


Figure 7-14. Torsional oscillation of rigid circular footing on elastic half-space. (a) Mass ratio vs. dimensionless frequency at resonance. (b) Mass ratio vs. magnification factor at resonance.

be treated independently of the possible vertical motion of the footing; and (3) energy is dissipated by propagation of elastic *shear waves*, only, from the footing; no compression or Rayleigh waves are developed. Furthermore, because this is a rotational-type oscillation, the geometric damping effect contributed by propagation of elastic waves is smaller than occurred for



vertical oscillation. Note in Fig. 7-14b that the magnification factors increase rapidly as  $B_\theta$  increases.

### 7.5 Rocking Oscillation of Footings Resting on the Elastic Half-Space

#### Rigid Circular Footing

Analytical solutions for this problem were presented by Arnold, Bycroft, and Warburton (1955) and by Bycroft (1956). The distribution of vertical pressure on the circular zone of contact was assumed to vary as

$$\sigma_z = \frac{3T_\psi r \cos \theta}{2\pi r_o^3 \sqrt{r_o^2 - r^2}} \exp(i\omega t) \quad \text{for } r \leq r_o \quad (7-42)$$

for rocking about the  $y$ -axis and with  $\theta$  measured from the  $x$ -axis in the  $x$ - $y$  plane. The orientation of rocking is indicated in Fig. 7-16, in which the  $y$ -axis is perpendicular to the plane of the page through point  $O$ . Rocking of the footing occurs about the  $y$ -axis (point  $O$ ) with an angular rotation  $\psi$ . Under static application of the external moment  $T_\psi$ , the static rotation is (from Borowicka, 1943)

$$\psi_s = \frac{3(1 - \nu) T_\psi}{8 Gr_o^3} \quad (7-43)$$

Under dynamic conditions the amplitude of rocking is a function of the mass ratio, which now takes the form

$$B_\psi = \frac{3(1 - \nu) I_\psi}{8 \rho r_o^5} \quad (7-44)$$

and of the dimensionless frequency  $a_o$  (Eq. 7-2). In Eq. (7-44)  $I_\psi$  denotes the mass moment of inertia of the footing in rotation about point  $O$  (see Eq. (7-49) for  $I_\psi$  of a circular footing). With constant amplitude of the exciting moment  $T_\psi$ , the response curves are shown as solid lines in Fig. 7-15 for several values of  $B_\psi$ . The ordinate of the graph in Fig. 7-15 is expressed as the dynamic magnification factor in rocking,

$$M_\psi = \frac{A_\psi}{\psi_s} \quad (7-45)$$

which is recorded on a logarithmic scale because of the large magnitudes

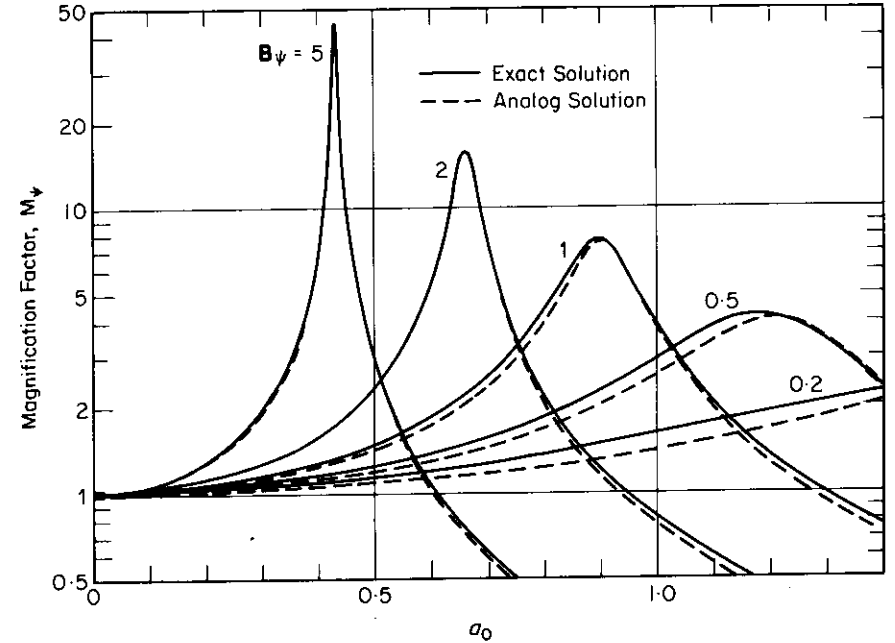


Figure 7-15. Magnification factor vs. dimensionless frequency relations for pure rocking of rigid circular footing on elastic half-space (from Hall, 1967).

involved. Figure 7-15 illustrates the sharp peaks for the response curves, even for small values of  $B_\psi$ . The shape of these curves as well as the high values of peak amplitudes are typical of a simple vibrating system which has *low damping*. From this we may infer that relatively little energy is dissipated into the elastic half-space by elastic waves but that the elastic strain energy in the supporting half-space is transferred back and forth beneath the two halves of the rocking circular footing.

The peak values of dimensionless frequency and magnification factor from Fig. 7-15 provide information for Fig. 7-16. In Fig. 7-16a the frequency at maximum amplitude is shown as a function of  $B_\psi$ . Because of the sharp peaks of the response curves in Fig. 7-15, the two curves in Fig. 7-16a—which denote the cases for constant moment and rotating-mass moment—are essentially identical. The peak values of the magnification factor  $M_{\psi m}$  are shown in Fig. 7-16b as a function of  $B_\psi$ ; the same diagram includes the curve of  $M_{\psi rm}$  vs.  $B_\psi$ .

In order to develop a moment about the  $y$ -axis produced by a rotating mass, it is convenient to express the moment as

$$T_{\psi r} = m_e e z \omega^2 \quad (7-46)$$

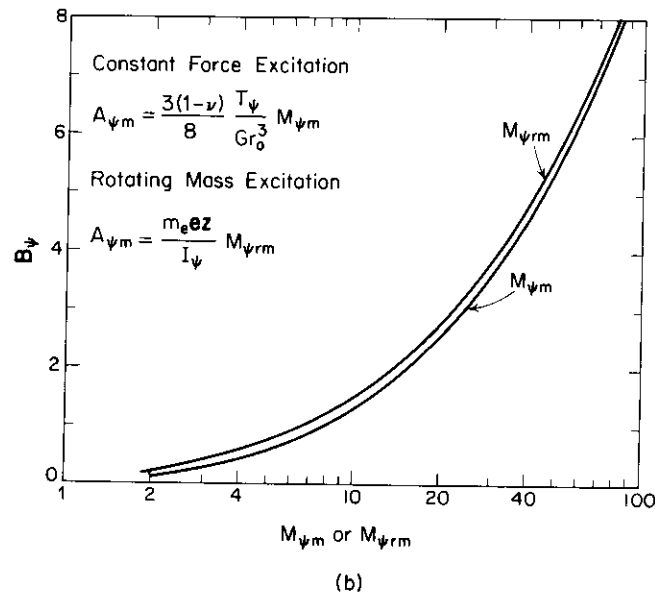
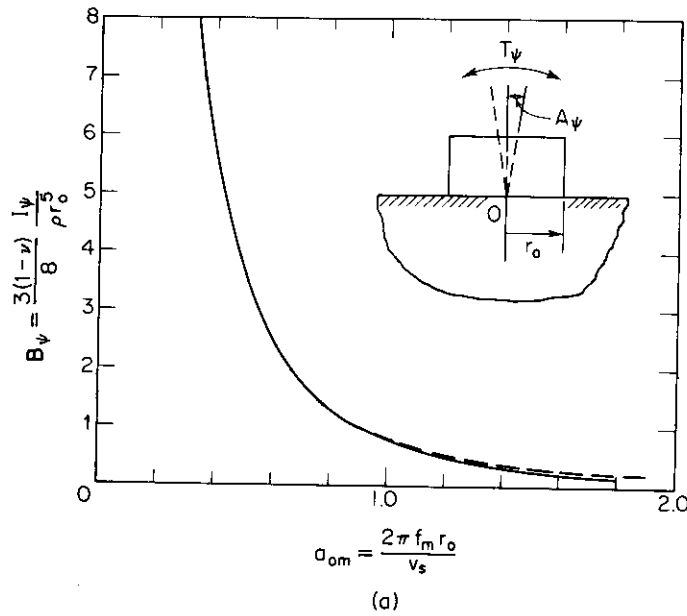


Figure 7-16. Rocking of rigid circular footings on elastic half-space. (a) Mass ratio vs. dimensionless frequency at resonance. (b) Mass ratio vs. magnification factor at resonance.

in which  $z$  represents the vertical distance above point  $O$  of a horizontally oscillating force  $m_e \omega^2$ . By using  $T_{\psi r}$  as the exciting moment, we are replacing a pure moment by a moment developed by an eccentric force. This substitution requires that there be a horizontal force applied to the base of the footing to maintain the center of rocking at point  $O$ . However, when we start by assuming that rocking occurs about point  $O$ , we automatically assume that the required restraints exist. Section 7.8 will treat the problem of coupled rocking and sliding, which happens in real situations when excitation is provided by a moment described by Eq. (7-46). With the exciting moment as indicated by Eq. (7-46), the amplitude of rotation  $A_\psi$  may be evaluated from

$$A_\psi = \frac{m_e e z}{I_\psi} M_{\psi r} \quad (7-47)$$

Rocking of the rigid circular footing on an elastic half-space develops an infinite vertical stress under the edge of the footing (see Eq. 7-42). Real soils cannot sustain this stress; therefore, a soil support is not as stiff as the ideal elastic medium having the same  $G$ . Thus, the actual maximum amplitude of rotation will be somewhat higher and the frequency at this maximum amplitude will be lower than the values calculated from Fig. 7-16.

*Hall's Analog*

Hsieh (1962) showed that all modes of vibration of a rigid circular footing resting on an elastic half-space could be represented in the form of Eq. (7-19), in which the damping and spring factors are functions of the frequency of oscillation. Because Lysmer had been successful in developing a mass-spring-dashpot analog to the vertical vibration of a footing resting on the half-space, Hall (1967) followed this approach to study the rocking problem. This required evaluations of the damping and spring constants for use in the equation of motion:

$$I_\psi \ddot{\psi} + c_\psi \dot{\psi} + k_\psi \psi = T_\psi \exp(i\omega t) \quad (7-48)$$

In Eq. (7-48) the mass moment of inertia of the footing about the center of rotation is designated  $I_\psi$ . For a cylindrical footing of radius  $r_o$  and height  $h$ , with uniformly distributed mass, the expression for  $I_\psi$  is

$$I_\psi = \frac{\pi r_o^2 h \gamma}{g} \left( \frac{r_o^2}{4} + \frac{h^2}{3} \right) \quad (7-49)$$

It was found convenient to introduce the static spring constant as  $k_{\psi s}$  in Eq. (7-48), where  $k_{\psi s}$  is obtained from Eq. (7-43) as

$$k_{\psi s} = \frac{T_{\psi}}{\psi_s} = \frac{8Gr_o^3}{3(1-\nu)} \quad (7-50)$$

Then it was necessary to provide a damping constant, which may be expressed as

$$c_{\psi} = \frac{0.80r_o^4\sqrt{G\rho}}{(1-\nu)(1+B_{\psi})} \quad (7-51)$$

The damping term described by Eq. (7-51) is adequate for establishing the maximum amplitude of rocking motion or the maximum dynamic magnification factor as given in Fig. 7-16b. This can be checked by introducing the expression for critical damping for the mass-spring-dashpot system—

$$c_{\psi c} = 2\sqrt{k_{\psi}I_{\psi}} \quad (7-52)$$

—into the calculation for the damping ratio

$$D_{\psi} = \frac{c_{\psi}}{c_{\psi c}} = \frac{0.15}{(1+B_{\psi})\sqrt{B_{\psi}}} \quad (7-53)$$

and noting that for small damping the maximum magnification factor for rocking is

$$M_{\psi m} \approx \frac{1}{2D_{\psi}} \quad (7-54)$$

In the mass-spring-dashpot system the amplitude of motion at resonance is controlled by the damping; whereas the frequency at maximum amplitude—or “resonant frequency”—is established by the inertia term and spring constant. A discussion of the methods of varying these two quantities to account for the frequency-dependent effect is given in Chap. 10. However, for this particular case Hall found it simplest to consider that an additional mass moment of inertia be added to the real value for the rocking footing in order to force the resonant frequency to agree with the value obtained from the half-space theory. This may be expressed by a magnification factor by which  $B_{\psi}$  (or  $I_{\psi}$ ) must be multiplied to give  $B_{\psi \text{eff}}$  (or  $I_{\psi \text{eff}}$ ), or

$$B_{\psi \text{eff}} = n_{\psi} B_{\psi} \quad (7-55)$$

Values of  $n_{\psi}$  are indicated in the table below:

$B_{\psi}$	5	3	2	1	0.8	0.5	0.2
$n_{\psi}$	1.079	1.110	1.143	1.219	1.251	1.378	1.600

With this modified value of  $B_{\psi \text{eff}}$  (or  $I_{\psi \text{eff}}$ ) and the damping term from Eq. (7-51), Hall found good agreement between the analog solution and the elastic-half-space solution, as indicated by the dashed curves in Fig. 7-15.

## 7.6 Sliding Oscillation of a Circular Disk Resting on the Elastic Half-Space

### Rigid Circular Disk

This problem can exist only in a mathematical sense, for it requires that translation of the disk occur in the horizontal direction without rocking. Physically this requires that the mass of the disk be confined within an infinitely thin layer resting on top of the elastic half-space. Only by concentrating the mass of the disk in this thin layer can the center of gravity of the disk be on the line of action of the restraining force  $P$  developed by the half-space on the bottom face of the disk. The exciting force  $Q$ , the thin disk, and the restraining force  $P$  are shown in the sketch in Fig. 7-17.

In the mathematical treatment it is relatively easy to specify boundary conditions for oscillation of the disk, which demands only horizontal translation without rotation. The analytical solution for translation of the rigid circular disk was presented by Arnold, Bycroft, and Warburton (1955), and by Bycroft (1956), with results expressed in terms of the dimensionless frequency  $a_o$  (Eq. 7-2) and the mass ratio  $b$  (Eq. 7-3). Hall (1967) found that the modified mass ratio

$$B_x = \frac{7-8\nu}{32(1-\nu)} \frac{m}{\rho r_o^3} \quad (7-56)$$

eliminated the effect of Poisson's ratio as a similar modified mass ratio had for the case of vertical oscillation. Consequently, the response parameters will be expressed here in terms of  $B_x$ . Figure 7-17 illustrates the response curves for the horizontal translation of the disk when excited by a horizontal force

$$Q = Q_o \exp(i\omega t) \quad (7-57)$$

for which  $Q_o$  is a constant. The abscissa of Fig. 7-17 is the dimensionless

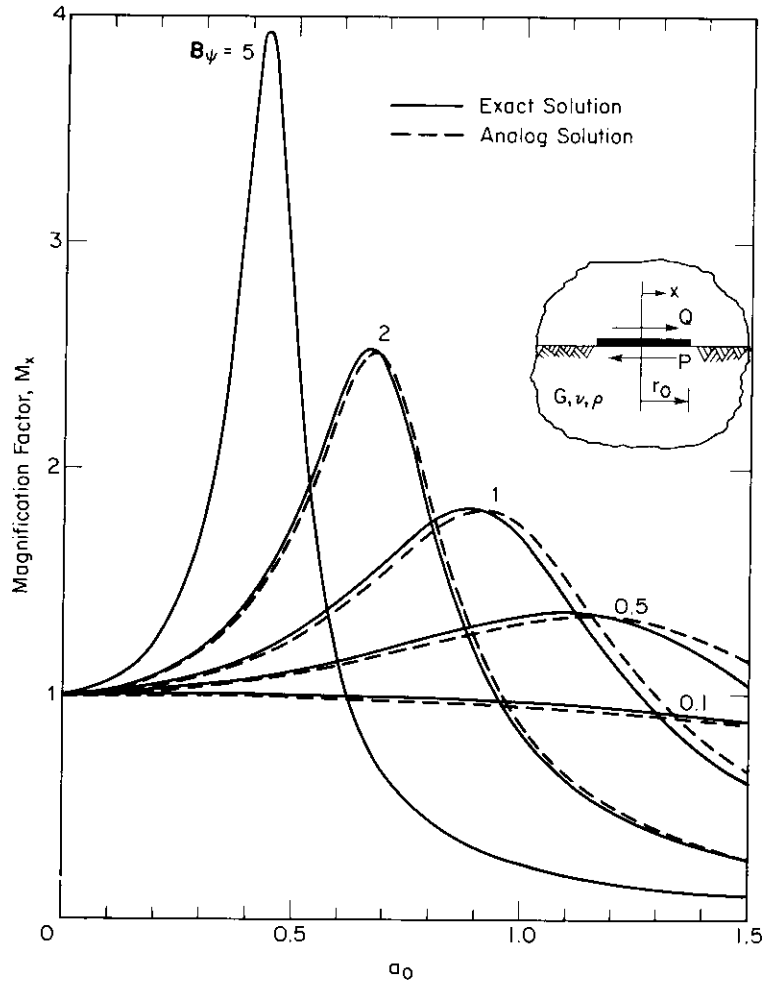


Figure 7-17. Magnification factor vs. dimensionless frequency relations for pure sliding of rigid circular footing on elastic half-space (from Hall, 1967).

frequency  $a_0$ , and the ordinate is the dynamic amplitude magnification factor

$$M_x = \frac{A_x}{x_s} \tag{7-58}$$

in which the static deflection (from Bycroft, 1956) is determined from

$$x_s = \frac{(7 - 8\nu)Q_0}{32(1 - \nu)Gr_0} \tag{7-59}$$

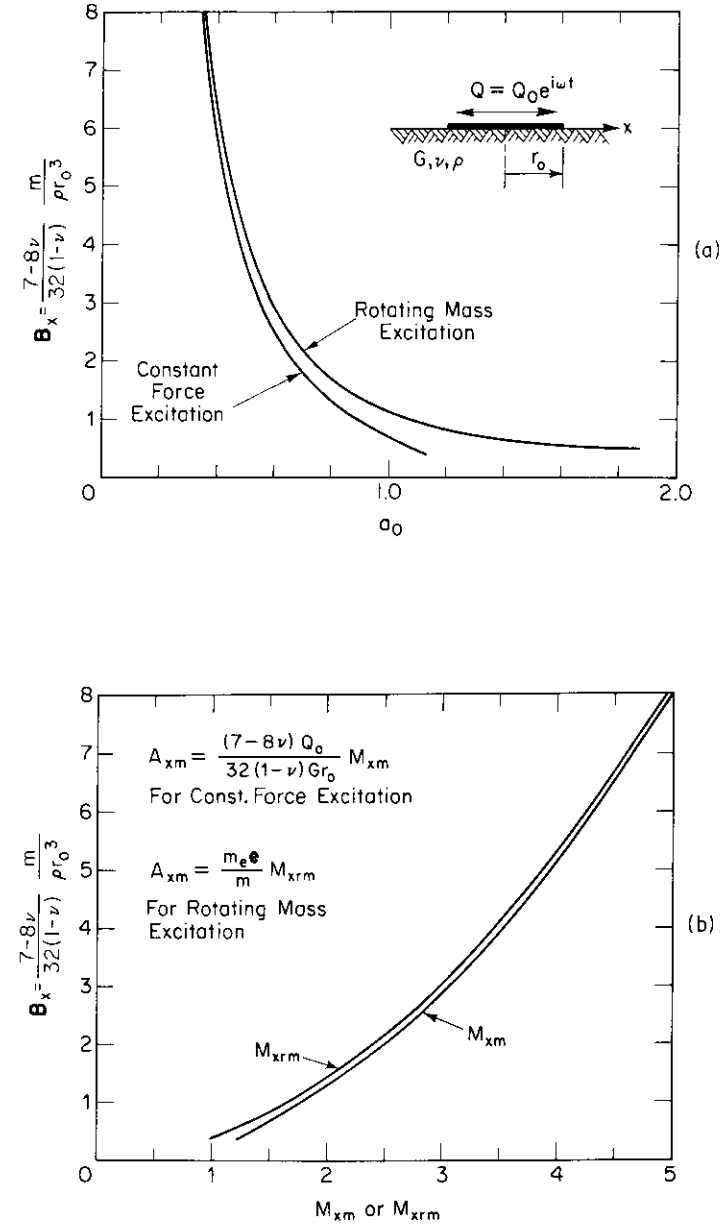


Figure 7-18. Sliding oscillation of rigid circular disk on elastic half-space. (a) Mass ratio vs. dimensionless frequency at resonance. (b) Mass ratio vs. magnification factor at resonance.

Note in Fig. 7-17 that the magnitudes of  $M_x$  are relatively small and that the peaks of the response curves are relatively flat, particularly for the smaller values of  $B_x$ . This indicates that the mode of vibration in horizontal translation is associated with relatively high damping, as was the case for vibration by translation in the vertical direction.

Figure 7-18a again shows the relations between the mass ratio and the value of  $a_0$  at the maximum amplitude of oscillation for both the constant-force and rotating-mass types of excitation. Figure 7-18b shows the magnitudes of the dynamic magnification factors as functions of  $B_x$ . The fact that the frequency at peak amplitude (Fig. 7-18a) develops two distinct curves further demonstrates that a significant damping effect is associated with this mode of vibration.

### Hall's Analog

For the sliding oscillation of a rigid circular disk it was again found possible (Hall, 1967) to describe this motion in terms of the mass-spring-dashpot analog. The mass for the analog was again taken equal to the mass resting on the half-space, and the spring constant was established as equal to the static response of the rigid disk to a horizontal load (see Eq. 7-59),

$$k_{xs} = \frac{32(1-\nu)}{7-8\nu} Gr_o \quad (7-60)$$

Then the damping constant required to provide satisfactory dynamic response for the model was found to be

$$c_x = \frac{18.4(1-\nu)}{7-8\nu} r_o^2 \sqrt{\rho G} \quad (7-61)$$

The dashed curves in Fig. 7-17 illustrate how well the response curves for the analog agree with the response curves for the half-space model.

### 7.7 Geometrical Damping Associated with Vibrations of Rigid Circular Footings on the Elastic Half-Space

It is instructive to stop at this point and review the results so far described for the single-degrees-of-freedom vibration of the rigid circular footing supported by the elastic half-space. We have considered translation along the vertical and horizontal axes, rotation about the vertical axis through

the center, and rotation about a diameter through the base of the footing. All six degrees of freedom are represented by these four solutions because translations and rotations with respect to the  $x$ -axis are identical to similar motions with respect to the  $y$ -axis.

From the magnification-factor-frequency ( $M$  vs.  $a_0$ ) response curves (Figs. 7-9, 7-15, 7-17), it has been demonstrated that the "resonance" condition is associated with a finite amplitude of motion, which indicates that damping is present in the system. However, the assumption of an ideal elastic half-space precludes loss of energy because of inelastic behavior of the material which constitutes the half-space. The indication of damping is evidence that energy is lost in the vibrating system, and in the case of the footing oscillating on the surface of the semi-infinite elastic body, or half-space, the loss of energy occurs through transmission of elastic-wave energy from the footing to infinity. This geometrical distribution of elastic-wave energy has been designated as *geometrical damping*.

From each solution for vibration of the footing on the half-space it is possible to establish a value of the equivalent damping ratio  $D$ , which can then be used in the lumped-parameter analysis. A convenient method for evaluating  $D$  is to equate the peak amplitude of motion from the half-space solution to the amplitude obtained from the mass-spring-dashpot system and then to solve for  $D$ . This procedure has been followed in preparing the curves shown in Fig. 7-19. Approximately the same results can be obtained by calculating  $D$  from the damping constants obtained in the analog solutions and the expression for critical damping,

$$c_o = 2\sqrt{km} \quad (2-31)$$

With this approach the damping ratio is

$$D = \frac{c}{c_o} \quad (2-32)$$

Expressions for the damping ratio are:

For vertical oscillation—

$$D_z = \frac{0.425}{\sqrt{B_z}} \quad (7-62)$$

For horizontal oscillation—

$$D_x = \frac{0.288}{\sqrt{B_x}} \quad (7-63)$$

For rocking oscillations—

$$D_\psi = \frac{0.15}{(1 + B_\psi)\sqrt{B_\psi}} \quad (7-64)$$

For torsional oscillations—

$$D_{\theta} = \frac{0.50}{1 + 2B_{\theta}} \quad (7-65)$$

The variations of the effective-damping ratio  $D$  with  $B$  for the various modes of vibration are shown in Fig. 7-19. The expressions for  $B_z$ ,  $B_x$ ,  $B_{\theta}$ , and  $B_{\psi}$  are given by Eqs. 7-23, 7-56, 7-38, and 7-44, respectively; and it should be noted again that the effect of Poisson's ratio is incorporated into the computation for  $B$ .

From Fig. 7-19 it is evident that appreciable damping is associated with a wide range of  $B$  for the translational modes of vibration. On the other hand, damping is quite low for the rotational modes of vibration, particularly for values of  $B_{\theta} > 2$  in torsional oscillation and for  $B_{\psi} > 1$  in rocking. Because many machine foundations are subjected to some overturning forces, it is probable that some oscillation in the rocking mode will occur. Consequently, the results shown on Fig. 7-19 should indicate to the designer that he should provide the lowest possible value of  $B_{\psi}$  for his machine foundation in order to minimize the rocking motion.

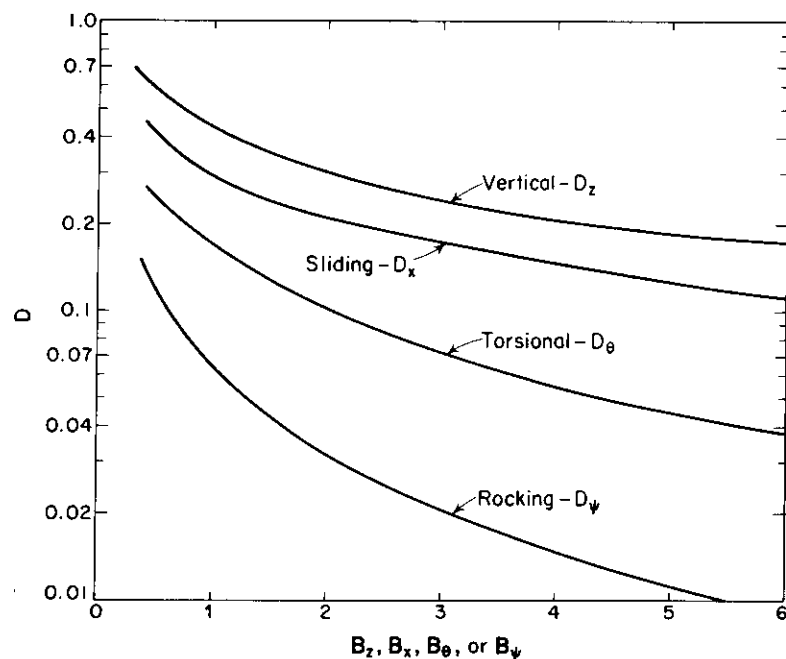


Figure 7-19. Equivalent damping ratio for oscillation of rigid circular footing on the elastic half-space.

### 7.8 Coupled Rocking and Sliding of the Rigid Circular Footing on the Elastic Half-Space

As noted in the preceding article, there are six degrees of freedom possible for the motion of a rigid body: translation in the three coordinate directions— $x$ ,  $y$ , and  $z$ —and rotation about each of these axes. With the information presented in this chapter, it is possible to write the equations of motion for each degree of freedom, thereby establishing six equations of motion. Although this procedure is possible, we usually do not have enough information on the exciting forces or soil parameters to justify the effort involved. Furthermore, it is often found that the vertical mode of oscillation, the torsional mode, or both, occur as uncoupled motions. Coupled motion is most frequently encountered in the design of machine foundations as rocking and sliding. Therefore, the following discussion of coupled vibrations with damping will be restricted to the case of combined rocking and sliding.

Figure 7-20a shows a rigid circular footing which rests on the surface of the elastic half-space. Its center of gravity is assumed to lie on the vertical axis through the center of the circular base and is a distance  $h_0$  above the surface of the half-space. We can express the motion of this rigid body in terms of the horizontal translation  $x_g$  of its center of gravity (CG), and the rotation  $\psi$  of the body about the CG. The sign convention chosen is illustrated in Fig. 7-20b, which indicates that  $+x$  and  $+P$  act to the right and that  $+\psi$  and  $+R_{\psi}$  are clockwise. The force  $P_x$  and the moment  $R_{\psi}$  are developed by the soil reaction on the base of the footing. From Fig. 7-20c it is seen that the resulting motion of the footing can be established by superposing the translation  $x_g$  of the CG and the rotation  $\psi$  about the CG. In this diagram both motions are  $+$  (inphase), which forces the center of rotation to lie *below* the CG; this is designated as the *first mode of vibration*. If the translation is  $+$  while the rotation is  $-$  (motions out of phase), then the center of rotation lies *above* the CG and the motion is designated as the *second mode of vibration*. These designations of first and second modes follow from the fact that resonance in the first mode of vibration occurs at a lower frequency than does resonance in the second mode.

In order to establish the equations of motion from which the amplitudes of motion and the frequencies at maximum amplitude (resonant frequencies) can be calculated, it is useful to designate the translation of the base of the footing as

$$x_b = x_g - h_0\psi \quad (7-66)$$

as noted in Fig. 7-20d. Then the horizontal force on the base of the footing is expressed in terms of this base displacement and velocity as

$$P_x = -c_x\dot{x}_b - k_x x_b \quad (7-67)$$

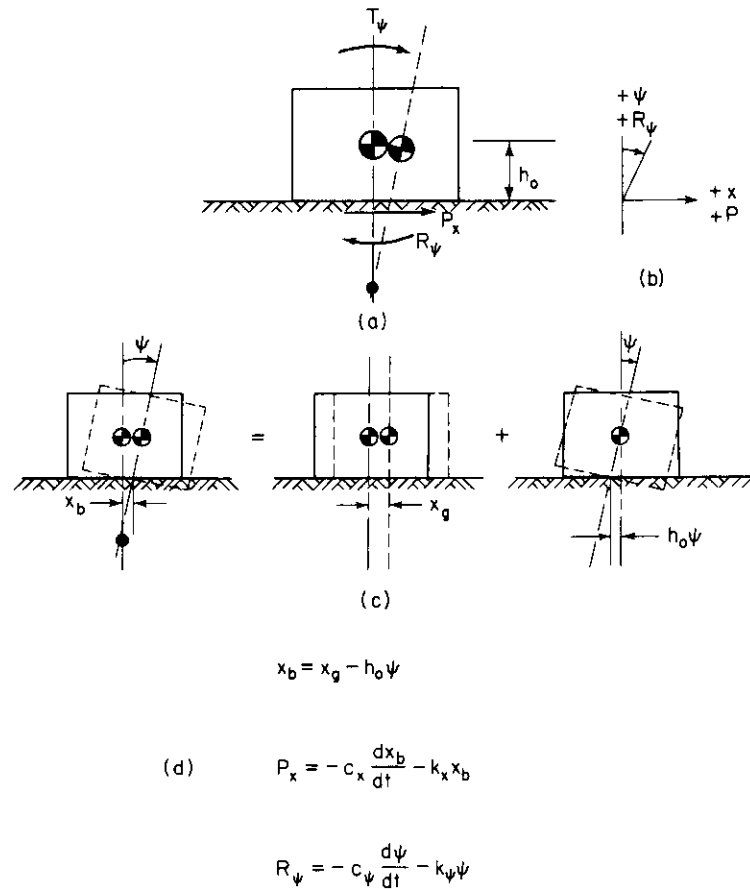


Figure 7-20. Notation for rocking and sliding mode of vibration.

The force described by Eq. (7-67) has the same form as that given in Eq. (7-15) for vertical vibration because they both involve translatory motions. The quantity  $c_x$  represents a damping coefficient and  $k_x$  represents a spring-reaction coefficient. Values of  $c_x$  and  $k_x$  obtained from the half-space theory by Hsieh (1962) are frequency-dependent. We have also seen previously that these quantities can be represented quite satisfactorily by the damping (Eq. 7-61) and spring constants (Eq. 7-60) for the analog. The expression for the resistance of the half-space to rocking of the footing—

$$R_\psi = -c_\psi \dot{\psi} - k_\psi \psi \tag{7-68}$$

—also includes the damping ( $c_\psi$ ) and spring ( $k_\psi$ ) terms which may be frequency-dependent or represented by the analog values (Eqs. 7-51 and 7-50).

The equation of motion for horizontal translation of the center of gravity of the footing is

$$m\ddot{x}_g = P_x = -c_x \dot{x}_b - k_x x_b \tag{7-69}$$

After substituting Eq. (7-66) and rearranging terms, Eq. (7-69) becomes

$$m\ddot{x}_g + c_x \dot{x}_g + k_x x_g - h_o c_x \dot{\psi} - h_o k_x \psi = 0 \tag{7-70}$$

The equation of motion for rotation about the CG is

$$I_g \ddot{\psi} = T_\psi + R_\psi - h_o P_x \tag{7-71}$$

in which  $I_g$  is the moment of inertia of the footing about the CG. Substitutions for  $R_\psi$ ,  $P_x$ , and  $x_b$  change Eq. (7-71) to the form

$$I_g \ddot{\psi} + (c_\psi + h_o^2 c_x) \dot{\psi} + (k_\psi + h_o^2 k_x) \psi - h_o c_x \dot{x}_g - h_o k_x x_g = T_\psi \tag{7-72}$$

With the substitution of

$$x_g = A_{x1} \sin \omega t + A_{x2} \cos \omega t \tag{7-73}$$

$$\psi = A_{\psi 1} \sin \omega t + A_{\psi 2} \cos \omega t \tag{7-74}$$

$$T_\psi = T_{\psi o} \sin \omega t \tag{7-75}$$

into Eqs. (7-70) and (7-72), four equations in four unknowns are established. When the vibrating system is represented by the lumped-parameter analog, the spring and damping coefficients are constants and the solution of the four simultaneous equations at each value of the frequency provide for evaluation of the response. When the footing-soil system is represented by the footing on the elastic half-space, the damping and spring coefficients are frequency-dependent and the values of the coefficients must be calculated at any given frequency before the four simultaneous equations are solved for that value of frequency. In either case the calculations are most conveniently performed with the help of a high-speed digital computer. Hall (1967) has established that for a rigid circular footing the calculated response based on the lumped-parameter analog agrees very well with the "exact" solution.

Equation (7-70) and (7-72) demonstrate that coupling occurs in this problem because the vertical location of the CG of the footing lies *above* the

line of action of the horizontal force  $P_x$  of the half-space on the bottom of the footing. If  $h_o$  is zero, no coupling is present, as demonstrated by the condition that in this case Eq. (7-70) includes only motion related to the coordinate  $x_e$  and Eq. (7-72) includes only motion related to the coordinate  $\psi$ .

### 7.9 Oscillation of the Rigid Circular Footing Supported by an Elastic Layer

For this problem the footing rests on the surface of a layer of thickness  $H$  of isotropic, homogeneous, elastic material which extends to infinity in the horizontal directions only. This layer is supported by a semi-infinite body which is infinitely rigid.

Reissner (1937) outlined the method of solution for the case of torsional oscillation of a circular footing on layered medium and Arnold, Bycroft, and Warburton (1955), and Bycroft (1956) have presented some solutions for this problem. The problem of vertical oscillation of the rigid circular footing on the elastic layer was treated by Arnold et al. (1955), Bycroft (1956), and Warburton (1957). The following discussions indicate only the general trends for the dynamic response of footings on a single layer under restricted conditions. The general problem of the dynamic behavior of footings on layered media or on elastic bodies with stiffness varying with depth needs further investigation, both theoretical and experimental.

#### Torsional Oscillation

In Reissner's (1937) discussion of the torsional oscillation of the circular footing on elastic layers, he established the basic equations for the solution and noted that the application of torsional oscillation at the surface provided one method of estimating the layer thickness. He did not establish the displacement functions  $f_1$  and  $f_2$  needed for evaluation of the dynamic response of the footing. These functions were presented by Arnold et al. (1955) and Bycroft (1956) for a few values of the *layer thickness ratio*  $H/r_o$ , in which  $H$  is the thickness of the elastic layer which is fixed to the rigid support and  $r_o$  is the footing radius (see Fig. 7-21). They computed values of  $f_1$  and  $f_2$  for  $H/r_o$  equal to 10, 1.0, and 0.5, and also indicated the agreement between the theoretical predictions and test results using a model footing resting on a layer of foam rubber. Figure 7-21 was prepared from information given in these two papers.

From both theory and tests they found that a resonant condition exists even when the mass of the footing is zero ( $B_\Theta = 0$ ). The frequency for this

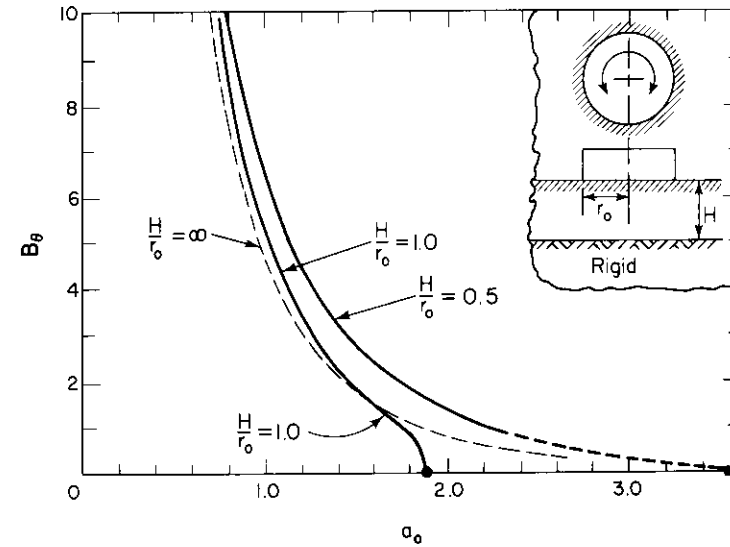


Figure 7-21. Mass ratio vs. dimensionless frequency at resonance for torsional oscillation of rigid circular footing on an elastic layer (after Bycroft, 1956).

condition is shown in Fig. 7-21 as the  $a_0$  value for  $B_\Theta = 0$ . Also note in Fig. 7-21 that for finite values of  $B_\Theta$  the frequency at maximum amplitude is higher than for the case of the semi-infinite elastic medium ( $H/r_o = \infty$ ). This indicates that the presence of the rigid lower boundary introduces a stiffening effect, thereby increasing this frequency. Finally, the presence of the lower rigid boundary acts to reduce the geometrical damping of the system. This is illustrated by an increase in maximum amplitude of motion during vibration. For the footing on the semi-infinite medium the dynamic magnification factor  $M_\Theta$  is 1.0 for  $B_\Theta = 0$ . The dynamic magnification factor was computed to be 1.6 for  $H/r_o = 1.0$  and 2.6 for  $H/r_o = 0.5$ . Thus, as the layer becomes thinner with respect to the radius of the footing, the effective damping is decreased.

Bycroft (1956) made special note of the limiting condition for the frequency of torsional oscillation of a rigid circular footing on an elastic layer. He demonstrated that as  $H/r_o$  became smaller this frequency would approach the natural frequency for a rod of radius  $r_o$ , of length  $H$ , which oscillated as a torsional column fixed at the base and free at the top. The natural frequency of the resonant torsional column is

$$f_n = \frac{v_s}{4H} \quad (7-76)$$



and the dimensionless frequencies ( $a_0$ ) computed from this expression are  $a_0 = 1.57$  for  $H/r_0 = 1$ , and  $a_0 = 3.14$  for  $H/r_0 = 0.5$ . These values may be compared to  $a_0 = 1.87$  for  $H/r_0 = 1$ , and  $a_0 = 3.55$  for  $H/r_0 = 0.5$  as computed from the displacement functions  $f_1$  and  $f_2$ .

### Vertical Oscillation

In the theoretical studies of vertical motion of a circular footing resting on the surface of the elastic layer, the pressure distribution corresponding to the rigid-base condition for the half-space (Eq. 7-8) was assumed. It was recognized that this does not correspond to the correct pressure distribution for a rigid footing on an elastic layer and Bycroft (1956) included a discussion of this point. In his study of the displacement of the footing, represented by the rigid-base pressure distribution, Bycroft computed the average static displacement for several values of the layer-thickness ratio  $H/r_0$ . Figure 7-22 shows the average displacement expressed in terms of the static displacement of the footing on an elastic half-space. This diagram shows clearly that the presence of the underlying rigid boundary provides a significant stiffening effect to the footing motion. The dashed curve in this same diagram illustrates the increase of the static spring constant as the layer thickness ratio  $H/r_0$  decreases. Note that this does not reach a factor of 2 until  $H/r_0$  is

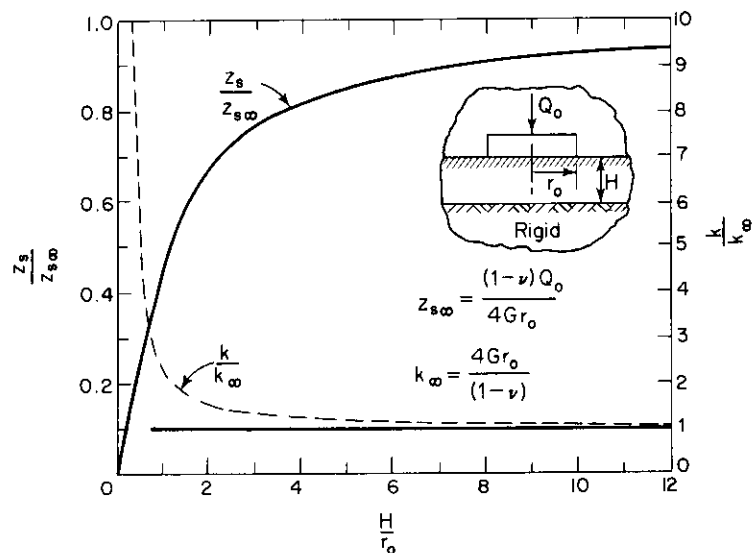


Figure 7-22. Static displacement and spring constant for vertical loading of rigid circular footing on elastic layer (after Bycroft, 1956).

reduced to about 1, but that the spring constant increases rapidly as  $H/r_0$  becomes smaller than 1.

In the studies of the dynamic behavior of the circular footing on the elastic layer, Bycroft (1956) considered only the case for  $\mathbf{b} = 0$ , while Warburton (1957) presented solutions for  $\mathbf{b} > 0$ . Both noted that true resonance, with amplitudes of motion becoming infinite, occurred for  $\mathbf{b} = 0$ . This resonant vibration for  $\mathbf{b} = 0$  occurred when  $f_1 \rightarrow \infty$  at values of  $a_0$  as indicated below:

$$\begin{aligned} \text{for } \nu = 0, \quad f_1 \rightarrow \infty \quad &\text{as} \quad a_0 \frac{H}{r_0} \rightarrow 2.1582 \\ \text{for } \nu = \frac{1}{4}, \quad f_1 \rightarrow \infty \quad &\text{as} \quad a_0 \frac{H}{r_0} \rightarrow 2.5742 \quad (7-77) \\ \text{for } \frac{1}{3} < \nu < \frac{1}{2}, \quad f_1 \rightarrow \infty \quad &\text{as} \quad a_0 \frac{H}{r_0} \rightarrow \frac{\pi}{2} \sqrt{\frac{2(1-\nu)}{1-2\nu}} \end{aligned}$$

Bycroft noted that the case for  $\mathbf{b} = 0$  corresponds to the vibration of a rod of elastic material fixed at the base, free at the top, and constrained at the sides so that no lateral motion occurs. The resonant frequency of vibration of this rod is given by

$$f_0 = \frac{(2n-1)v_P}{4H} = \frac{(2n-1)v_S}{4H} \sqrt{\frac{2(1-\nu)}{1-2\nu}} \quad (7-78)$$

which may be rearranged to

$$a_0 = \frac{(2n-1)\pi r_0}{2H} \sqrt{\frac{2(1-\nu)}{1-2\nu}} \quad (7-79)$$

Note that higher modes of resonant frequency (i.e.,  $n = 1, 2, 3, \dots$ ) are possible for this vertical motion of the weightless rigid plate on the elastic stratum. The vertical displacements of particles at different depths in the stratum are represented by the curves in Fig. 3-8 for the different modes of vibration.

For footings which have weight ( $\mathbf{b} > 0$ ), the amplitudes of motion are finite at the frequency we customarily describe as "resonance" (i.e., frequency for maximum amplitude of vibration). Warburton (1957) has presented curves for this resonant frequency, or frequency at maximum amplitude, as the usual mass ratio  $\mathbf{b}$ -vs.- $a_0$  plots for different values of  $H/r_0$ . He prepared one such diagram for  $\nu = 0$  and a second for  $\nu = \frac{1}{4}$ , which is reproduced here as Fig. 7-23.

Warburton also evaluated the maximum dynamic displacements and expressed them in terms of a magnification of the static displacement.

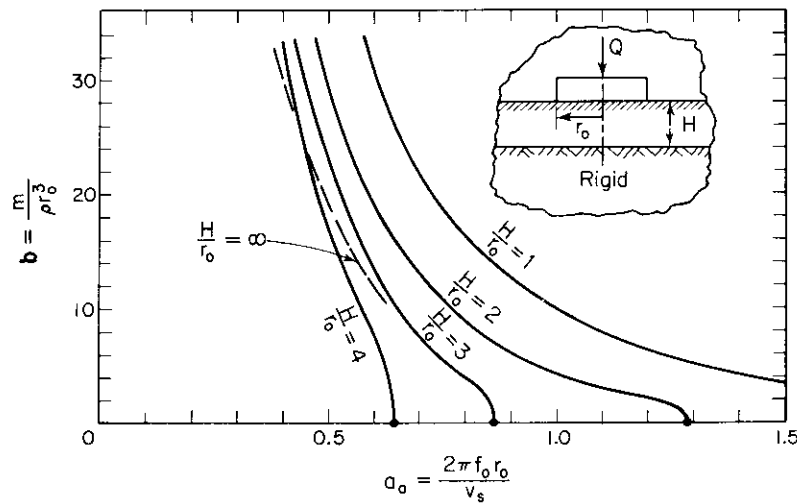


Figure 7-23. Variation of dimensionless frequency at resonance with mass ratio and thickness of the elastic layer for vertical oscillation of rigid circular footing (after Warburton, 1957).

Referring to Fig. 7-22, it is evident that the large magnification factors he presented are not quite as bad as they appear at first glance because they amplify a static displacement which is reduced in magnitude as the layer thickness decreases. The values indicated in Table 7-1 relate Warburton's values for dynamic motion to the static value for displacement of the rigid footing on the semi-infinite body, or

$$M_{Lm} = \frac{A_{2Lm} 4Gr_0}{(1 - \nu)Q_0} \tag{7-80}$$

Table 7-1. Magnification Factors for Vertical Vibration of Rigid Circular Footing Supported by an Elastic Layer ( $\nu = \frac{1}{4}$ )

$\frac{H}{r_0}$	$M_{Lm}$ for				
	$b = 0$	$b = 5$	$b = 10$	$b = 20$	$b = 30$
1	$\infty$	5.8	11.4	20.5	28.9
2	$\infty$	8.0	16.1	30.6	40.8
3	$\infty$	4.7	9.5	23.7	36.0
4	$\infty$	(3.4)	5.9	15.6	27.9
$\infty$	1	1.21	1.60	2.22	2.72

in which  $M_{Lm}$  is the magnification factor for displacement at resonance for the layered system.

Warburton's analysis treated the ideal elastic medium which has no internal damping. For a real footing-soil system, the relatively small amount of material or hysteresis damping will be important in reducing these high magnification factors which have been indicated by the theoretical treatment.

### 7.10 Vibrations of Rigid Foundations Supported by Piles or Caissons

Piles will be effective in resisting vibratory loadings only if they can develop appreciable forces as their tops move through very small distances. As noted in Chap. 10 under *Design Criteria*, the permissible dynamic motions of machine foundations are often of the order of just a few thousandths of an inch. Consequently, the pile must contribute its resisting forces during this kind of movement or it is not effective. Resistances to vertical motion may be provided by end bearing, skin friction, or by a combination of the two. The resistance developed by piles to horizontal forces is provided by horizontal bearing of the pile against the soil. In each of these cases the soil properties involved depend upon the magnitude of the local deformation developed by the pile acting against the soil and must be evaluated from tests involving the same order of magnitude of strain in the soil as occurs in the prototype situation. Fortunately, for these small strains many soils exhibit an approximately elastic response which may be evaluated by laboratory or field tests as described in Chap. 6. Thus, elastic solutions will again be used to estimate the response of pile-supported foundations.

#### Vertical Vibrations of a Foundation Supported by Point-bearing Piles to Rock

Point-bearing piles provide support for a foundation by transferring the vertical loads to a stronger soil stratum at some depth beneath the surface. Under stable dynamic conditions for which no further settlement occurs, the dynamic loads are transferred through the elastic pile to the elastic contact zone at the tip of the pile where the loads are absorbed by the stratum. We can establish the *maximum* influence of piles for stiffening the support for a foundation if we first consider that the *stratum is rigid and no deformation* occurs at the pile tip when dynamic loads are transferred from the pile. This would be approximately true if piles were driven through soft soils to rock.

The theoretical procedure required for this study was discussed in Chap. 3 and is represented by the sketch in Fig. 3-10. It involves an elastic rod fixed

at the base and free at the top, with a mass  $m$  resting on the top. When no weight rests on top we have a solid resonant column with the fixed-free condition, which has a resonant frequency

$$f_n = \frac{v_c}{4\ell} = \frac{1}{4\ell} \sqrt{\frac{E}{\rho}} \tag{7-81}$$

in which

$E$  = Young's modulus of elasticity of the pile,  
 $\rho \left( = \frac{\gamma}{g} \right)$  = mass density of the pile material, and  
 $\ell$  = length of the pile.

For the intermediate case in which the supported mass (i.e., the portion of the total load assigned to each pile) is of the same order of magnitude as the weight of the pile itself, the frequency equation has been given by Eq. (3-33). The solution for Eq. (3-33) is shown graphically by Fig. 7-24, from which  $f_n$  may be calculated. Of course, when the weight of the pile is negligible with respect to the supported weight, the natural frequency is given by Eq. (2-17b).

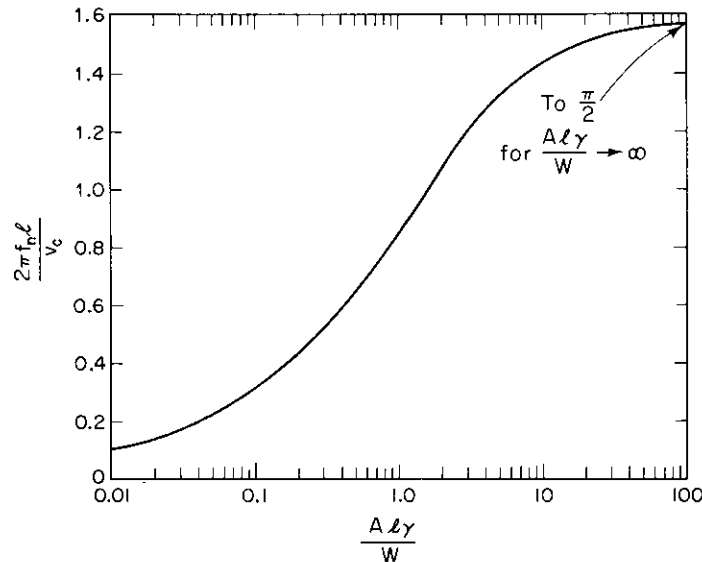


Figure 7-24. Graphical solution for Eq. (3-33).

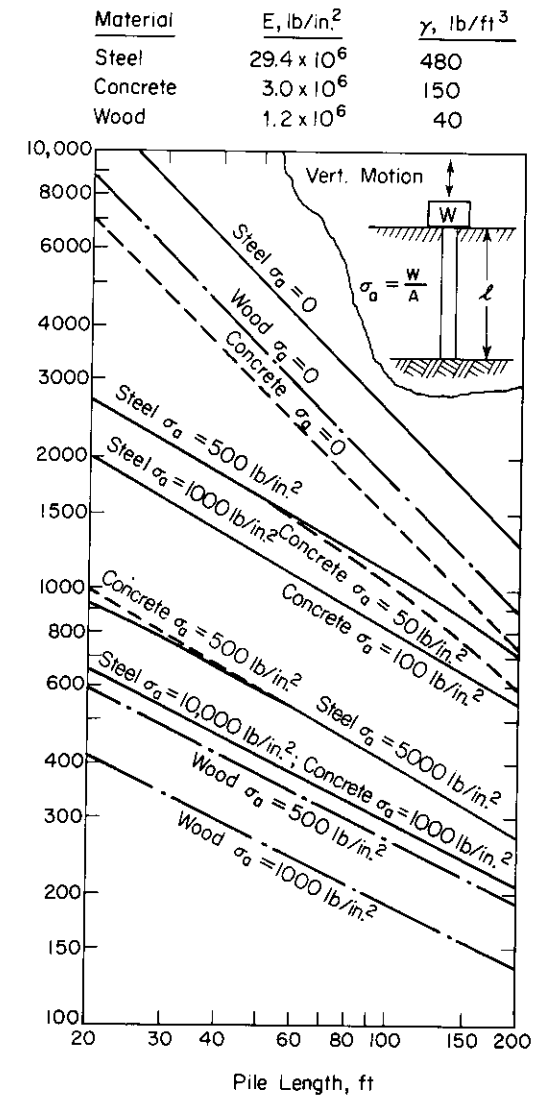


Figure 7-25. Resonant frequency of vertical oscillation for a point-bearing pile carrying a static load  $W$ . (Loaded stratum is rigid.) (From Richart, 1962.)

In order to illustrate the influence of axial loading on the resonant frequency of end-bearing piles to rock, Richart (1962) prepared a diagram which included the parameters of axial load, pile length, and pile material. This diagram is reproduced here as Fig. 7-25. The three curves at the top of the diagram illustrate the resonant frequencies of unloaded steel, concrete, and wooden piles, as computed from Eq. (7-81). As the axial load is increased on a pile of given length, the resonant frequency is reduced.

In this analysis of a pile-supported foundation, only the resonant frequency was considered. From an elastic analysis of a closed system corresponding to this one, no geometrical damping occurs and the amplitudes of motion at resonance are theoretically infinite. Actually, material or hysteresis damping will restrict the motions somewhat, but the resonant motion will still be of large magnitude relative to the static displacement.

*Torsional Vibration of a Circular Foundation Supported by Piles*

The problem of torsional vibration of a circular footing supported by piles is included to illustrate the effectiveness of piles in resisting lateral loads. For the following discussion it will be assumed that the base of the footing is in contact with the soil throughout the dynamic motions and that *no* *slippage* occurs between the base of the foundation and the soil. The piles are considered to be stub piles installed to increase torsional resistance only. The method of analysis involves (1) an estimate of the rotational motion of the soil beneath the footing as the footing twists and imparts shearing forces to the soil surface, (2) an estimate of the relative motion of a pile attached to the footing with respect to the soil motion, and (3) use of the theory of subgrade reaction to estimate the restraining torque provided by the lateral motions of the pile against the soil.

In their studies of torsional oscillations of rigid circular footings resting on the surface of the elastic half-space Reissner and Sagoci (1944) developed solutions for the static rotational displacements (referred to the vertical axis through the center of the footing) within the half-space. Their solution was developed using oblate-spheroidal coordinates. The tangential displacement *s* directly below the periphery of the disk has been evaluated and is illustrated in Fig. 7-26 as  $s/r_0\theta_s$  vs.  $z/r_0$ . The static rotation  $\theta_s$  represents the angular rotation of the disk at the surface, and the displacements vary linearly with the radius.

If a pile is attached to the footing, its point of attachment moves the same distance along a circumferential arc as does a point on the footing base or as does a point on the surface of the soil at the same radius *r*. Therefore, at the footing-soil contact zone the pile does not have any relative motion with respect to the soil and does not develop any lateral force. The only stiffening effect of the pile is through transfer of shear by bending from a deeper location where the pile moves against the soil. The amount of horizontal force developed on the pile at each elevation depends on the relative motion of the pile against the soil. For an infinitely rigid pile attached

to the footing, the motion of the pile against the soil would be

$$s_{rel} = r_0\theta_s \left(1 - \frac{s}{r_0\theta_s}\right) \quad (7-82)$$

where the quantity  $s/r_0\theta_s$  is given in Fig. 7-26 for each depth. However, a real pile will bend because of the forces developed along its length and the relative motion of pile against the soil will be reduced.

The force developed by the pile motion against the soil can be estimated by using the theory of horizontal subgrade reaction. From this approach the horizontal force *P'* per unit length of pile is given by

$$P' = K_h d \cdot s_{rel} \quad (7-83)$$

in which

$K_h$  = coefficient of horizontal subgrade reaction, and  
*d* = pile diameter.

The critical factor in this type of analysis is the proper selection of  $K_h$ , which relates the pressure developed as the surface of the pile moves a unit distance into the soil; that is,

$$K_h = \frac{p}{s} \quad (7-84)$$

The value of  $K_h$  must be related to the order of magnitude of the motions involved, and for vibration problems these motions are very small. Because methods are available for evaluating the "elastic" constants for soils for these small strains, it is useful to employ the theory of elasticity to establish  $K_h$ . If we consider first the behavior of a circular pile, we can approximate this by considering the pressure required to expand a cylindrical hole in an elastic medium. Westergaard (1952) gives the radial expansion of a hole of diameter *d* as

$$\frac{\Delta d}{2} = \frac{pd}{4G} \quad (7-85)$$

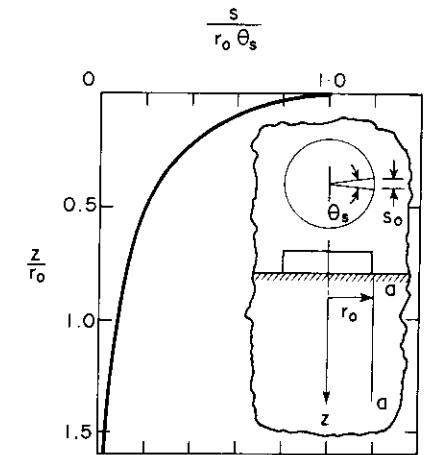


Figure 7-26. Tangential displacements along line *a-a* beneath the edge of a circular footing which has been rotated through an angle  $\theta_s$ .

from which the coefficient of subgrade reaction is approximately

$$K_h = \frac{2p}{\Delta d} = \frac{4G}{d} \tag{7-86}$$

This approach has been followed because the inaccuracies introduced by the geometry of the problem were considered to be less important than the potential errors in  $G$ .

Now if we return to a consideration of the infinitely rigid cylindrical pile which extends downward from the base of a circular footing, this pile will move laterally a distance  $s_o$  as the footing rotates through an angle  $\theta_s$ , as shown in the sketch in Fig. 7-27a. At the same time, the soil moves laterally because of the shearing forces introduced by the footing on the surface (Fig. 7-27b). The net motion is illustrated in Fig. 7-27c. Then, according to Eq. (7-83), the lateral force developed at each elevation is

$$P' = \frac{4G}{d} r \theta_s d \left(1 - \frac{s}{r \theta_s}\right) \tag{7-87}$$

in which the displacement  $s$  is a function of the depth involved—or the length of the pile. By integrating Eq. (7-87) from  $z = 0$  to  $z = \ell$  we can evaluate the efficiency of rigid piles in developing resistance to lateral motion as they penetrate to greater depths. The efficiency factor is designated by

$$(EF)_M = \frac{\int_0^\ell P' dz}{K_h s_o \ell d} \tag{7-88}$$

and represents the total horizontal force developed as a fraction of the total force which *could* be developed if the soil did *not* move. Figure 7-28 illustrates the variation of this efficiency factor with length of rigid pile for the condition of  $K_h$  constant with depth.

For real piles the flexibility of the pile itself is of importance because pile bending will reduce the relative motion of pile against the soil. Thus, the flexibility introduces an efficiency factor which decreases as the pile length increases.

**EXAMPLE.** To illustrate the combined effects of soil motion and pile flexibility, consider 6-in.-diameter stub piles located along a 50-in.-diameter circle on the base of a 62-in.-diameter circular concrete footing. The footing is to be subjected to torsional oscillations and the stub piles are for the purpose of increasing the torsional rigidity of the foundation.

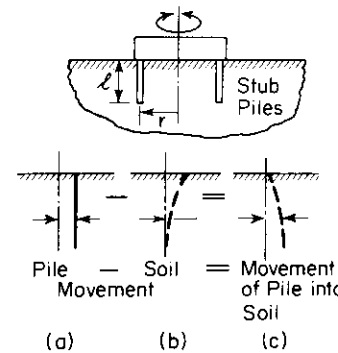


Figure 7-27. Action of stub piles.

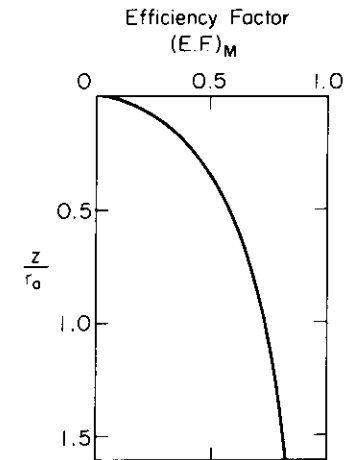


Figure 7-28. Efficiency factor for rigid stub piles attached to a circular footing twisted against the soil.

For this example the shear modulus  $G$  of the soil is taken as 4500 lb/in.<sup>2</sup> and the footing is not permitted to slip. Then the static torsional stiffness of the rigid footing on the soil is given by

$$\left(\frac{T_\theta}{\theta_s}\right)_F = \frac{16}{3} G r_o^3 = \frac{16}{3} (4500)(31)^3 = 7.15 \times 10^8 \text{ in.-lb/rad}$$

When the stub piles are introduced on a 50-in. diameter, the contribution to the torsional stiffness of the system by *each* pile is

$$\left(\frac{T_\theta}{\theta_s}\right)_p = \frac{P_o r^2}{s_o} \tag{7-89}$$

in which  $P_o$  and  $s_o$  are the horizontal force and displacement, respectively, at the top of the pile. Because we have already considered the effect of soil motion in reducing the pile efficiency below that for the infinitely rigid pile moving against still soil, we may express Eq. (7-89) as

$$\left(\frac{T_\theta}{\theta_s}\right)_p = \frac{K_h d s_o r^2}{s_o} (EF)_M (EF)_F \tag{7-90}$$

in which  $(EF)_M$  is the efficiency factor for a rigid pile including the effect of soil

motion, and  $(EF)_F$  is the efficiency factor which takes into account the pile flexibility.

In order to evaluate the effect of pile flexibility, we must first evaluate  $K_h$  from Eq. (7-86):

$$K_h = \frac{4G}{d} = \frac{4(4500)}{6} = 3000 \text{ lb/in.}^3 \quad (7-91)$$

Then the stiffness for the infinitely rigid pile moving against still soil is

$$\left(\frac{T_\Theta}{\Theta_s}\right)_R = K_h t r^2 d = 11.25 \times 10^6 \text{ in.-lb/rad} \quad (7-92)$$

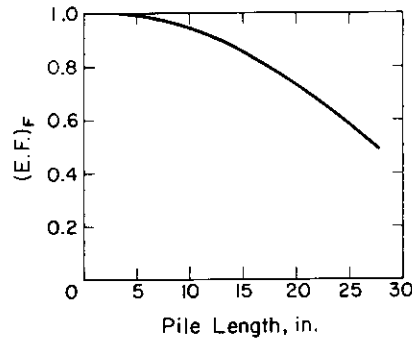
Now, if the 6-in.-diameter stub pile is assumed to be made of reinforced concrete with  $E = 5 \times 10^6$  psi, the effect of pile flexibility may be evaluated from the theory for beams on an elastic foundation (Hetenyi, 1946). For  $K_h$  constant with depth and a constant  $EI$  pile, we first calculate the value of  $\lambda$  as

$$\lambda = \sqrt[4]{\frac{K_h d}{4EI}} = 0.0613 \left(\frac{1}{\text{in.}}\right) \quad (7-93)$$

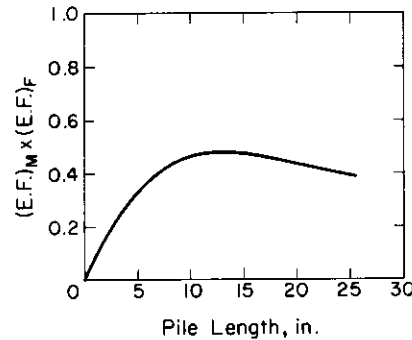
For a pile of finite length, Hetenyi gives separate solutions for deflection and slope for end shear only, and deflection and slope for end moment only. Then, for a stub pile assumed fixed into the circular footing, it is only necessary to calculate the force required to produce unit translation of the point of fixity. The ratio of the stiffness of the flexible pile to the stiffness of a rigid pile, both moving against soil at rest, gives the efficiency factor for flexibility  $(EF)_F$ . The decrease of this quantity with length of the 6-in.-diameter stub pile is shown in Fig. 7-29a.

The combined effect of soil motion and pile flexibility is shown by the curve in Fig. 7-29b. Thus, the lateral resistance to rotation provided by a 6-in.-diameter stub pile 20-in. long is given by

$$\left(\frac{T_\Theta}{\Theta_s}\right)_p = \left(\frac{T_\Theta}{\Theta_s}\right)_R (EF)_M (EF)_F = 11.25 \times 10^6 \times 20 \times 0.44 = 99 \times 10^6 \text{ in.-lb/rad}$$



(a)



(b)

Figure 7-29. Efficiency factor for six-inch diameter concrete stub piles. (a) Effect of pile flexibility. (b) Combined effects of flexibility and soil motion.

From this analysis it is seen that each 20-in.-long stub pile contributes a torsional stiffness equal to about 13.8 per cent of that due to the contact between the circular footing and the soil. Thus, the torsional stiffness of the foundation system could be doubled, theoretically, by adding seven of these stub piles.

The foregoing discussion was restricted to a consideration of stub piles which do not absorb any appreciable vertical load. However, it is possible for real piles to absorb the entire vertical load of the footing if the soil settles away from the footing. If this happens, the torsional resistance of the footing against the soil is lost and the *entire* torsional resistance must be provided by the piles. It should be evident from this example that the torsional restraint provided by the footing twisting against the soil is important and should be maintained if torsional oscillations of the footing are anticipated.

# 8

## ISOLATION OF FOUNDATIONS

Foundation isolation, as the term is used in this chapter, implies the isolation of entire machine–foundation systems or of entire structures. There is, of course, another field of engineering specialization associated with mechanical isolation of machines, machine components, or structural components. Mechanical isolation in this context means the isolation of machines or structures from their foundations or from larger structural elements using localized isolators. Some isolators which are commonly used in mechanical isolation are rubber or composite pads, springs or spring-damper systems, and pneumatic springs. It is important in any specific situation involving vibrations to distinguish between vibration problems that can be resolved using mechanical isolation and those which cannot. For this reason a foundation engineer must have a basic understanding of mechanical isolation. The basis for understanding mechanical isolation is available in Chap. 2, but for a more detailed treatment of mechanical isolation techniques, see Crede (1951) or Harris and Crede (1961). For those vibration problems in which mechanical isolation is inadequate, foundation isolation may provide the required protection. The selection and design of foundation-isolation systems is the topic of this chapter.

### 8.1 Isolation by Location

#### Attenuation with Distance

It was shown in Chap. 3 that in an elastic half-space both body waves and Rayleigh waves decrease in amplitude with increased distance from a

source of vibration simply due to the geometry of the half-space. Rayleigh waves decrease in amplitude more slowly than body waves and propagate in a restricted zone close to the surface of the half-space; therefore, they are of primary importance in any attempt to isolate foundations. The decrease in amplitude of the vertical component of the  $R$ -wave with distance due to geometry alone—*geometrical damping*—can be expressed as

$$w = w_1 \sqrt{\frac{r_1}{r}} \tag{8-1}$$

where

$r_1$  = distance from source to point of known amplitude,

$r$  = distance from source to point in question,

$w_1$  = amplitude of the vertical component of the  $R$ -wave at distance  $r_1$  from source, and

$w$  = amplitude of the vertical component of the  $R$ -wave at distance  $r$  from source.

Considering geometrical damping alone, it can be seen that a large degree of isolation can be achieved by locating a structure as far as possible from a known vibration source.

Because soil is not perfectly elastic, there is another consideration which influences the attenuation of  $R$ -waves. In real earth materials, energy is lost by *material damping*. The existence of material damping in soils is demonstrated by the fact that amplitude attenuation measured in the field is greater than would be predicted by geometric damping alone. Figure 8-1 shows amplitude–decay curves obtained in the field at the four sites described in Table 8-1. The dashed curves through the data points (solid circles) represent the measured attenuation of vertical-displacement amplitude of the ground surface, and the solid straight line (slope =  $-\frac{1}{2}$  on log–log plot) represents

Table 8-1. Site Conditions and Source of Excitation for Field Data Presented in Fig. 8-1

Curve Identification	Soil Conditions	Source of Excitation	Frequency (cycles/sec)
WES (1965)	uniform, fine sand	rotating-mass vibrator (vertical)	20
Forssblad (1965)	morainic (silty, gravelly sand)	7260-lb vibrating roller	26.7
Richart (1962)	4–6-in. concrete slab over compact granular fill	single-cylinder internal-combustion engine	40
Woods (1967)	silty, fine sand	electromagnetic vibrator (vertical)	200

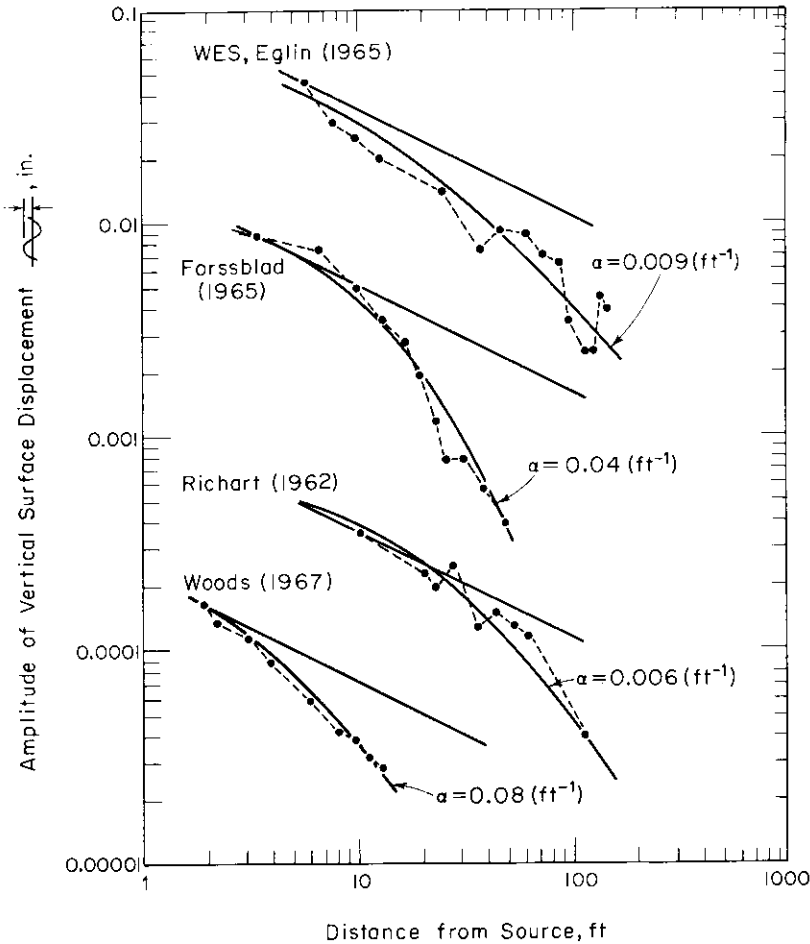


Figure 8-1. Attenuation of surface wave with distance from source of steady-state excitation.

the theoretical attenuation predicted by Eq. (8-1). All four sets of field data indicate amplitude attenuation greater than predicted by geometrical damping alone.

Both geometrical and material damping can be included in an expression for  $R$ -wave attenuation (Bornitz, 1931) as follows:

$$w = w_1 \sqrt{\frac{r_1}{r}} \exp[-\alpha(r - r_1)] \quad (8-2)$$

where  $\alpha$  is the coefficient of attenuation, having dimensions of 1/distance (see Eq. 6-27). Equation (8-2) implies that the total energy on two concentric circles at radii  $r_1$  and  $r$  from a point energy source is constant except for the

energy lost through material damping. Barkan (1962) suggested values of  $\alpha$  ranging from 0.01 to 0.04 (1/feet) for various types of soils. The solid curves in Fig. 8-1 represent Eq. (8-2) with  $\alpha$  selected to fit each set of data. The range of  $\alpha$  in Fig. 8-1 is from 0.006 to 0.08 (1/feet). Although material damping occurs in real soils, as shown in Fig. 8-1, it is geometrical damping which contributes most to the attenuation of  $R$ -waves.

The attenuation considered so far has been associated only with horizontal (radial) distance from the source. An additional degree of isolation from  $R$ -wave energy can be obtained by locating foundations below the surface. It was shown in Chap. 3 that  $R$ -waves attenuate with depth; therefore, it may be useful for isolation purposes to seat a foundation as deep as practical while keeping the sides of the foundation separated from the surrounding soil.

### Geologic Formations

If it is possible to select the site for sensitive structures or instruments, advantage may be taken of basic geologic formations. Foundations on sound, deep-seated bedrock, for example, will experience smaller vibration amplitudes than foundations on weathered materials or soils subject to the same excitation. Seismologists have found that abandoned rock quarries provide excellent sites for "quiet" seismograph stations. The depth of the quarry screens local microseismic noise and the freshly exposed rock at the quarry floor is an excellent foundation for instruments. Mines and underground caverns have similar advantageous properties.

It has been suggested by geophysicists that isolation can be achieved by locating a foundation in a protective natural geologic structure like a syncline. Also a deep valley or a mountain range may act as a barrier to long-period surface waves if it is situated between the source of excitation and a site to be isolated.

## 8.2 Isolation by Barriers

### Examples from Practice

Isolation of structures and machine foundations from ground-transmitted vibrations by the installation of wave barriers has been attempted many times, and has met with various degrees of success. Barkan (1962) reported on an application of an open-trench and sheet-wall barrier to isolate a building from traffic induced vibrations, as shown in Fig. 8-2. This installation was unsuccessful and vibrations from the street continued to



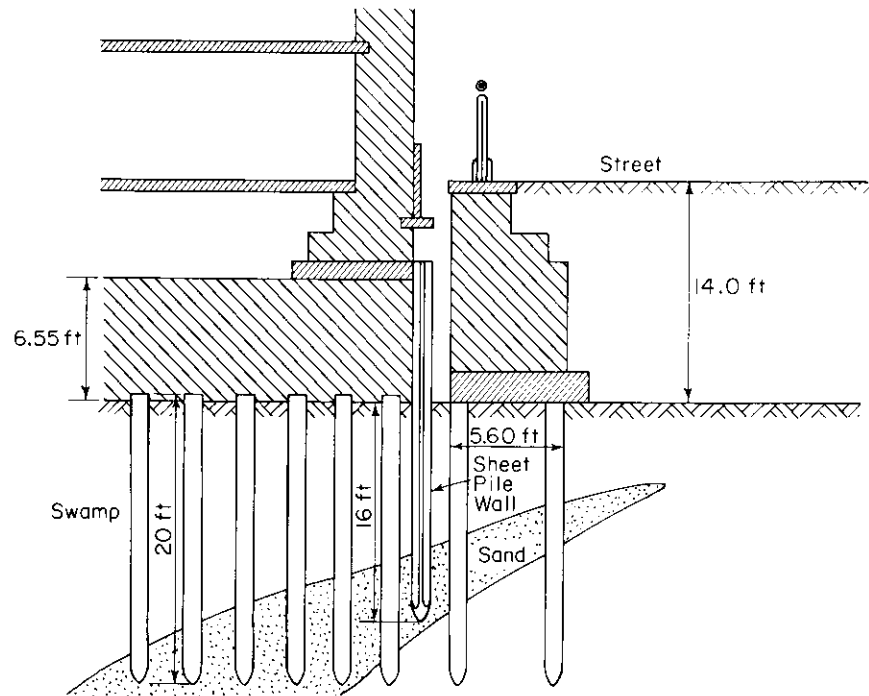


Figure 8-2. Isolation of building from traffic induced vibrations (after Barkan, 1962).

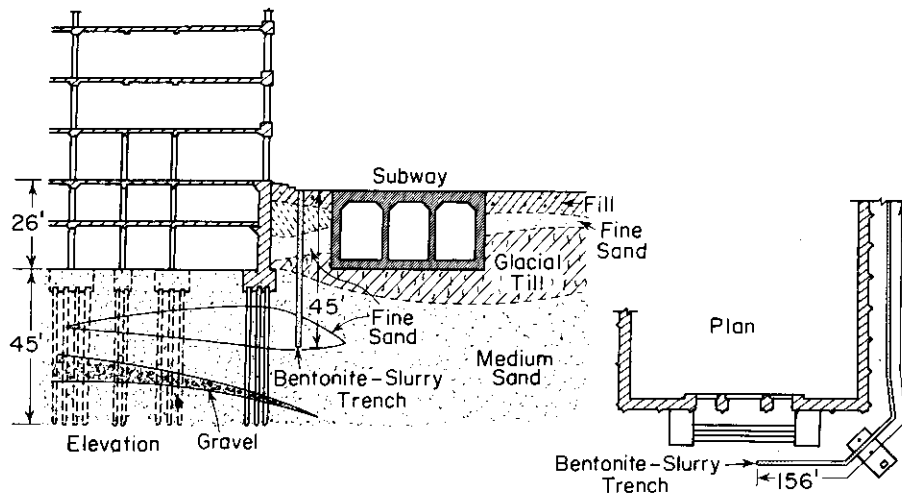


Figure 8-3. Building isolation using bentonite-slurry filled trench (after Neumeuer, 1963).

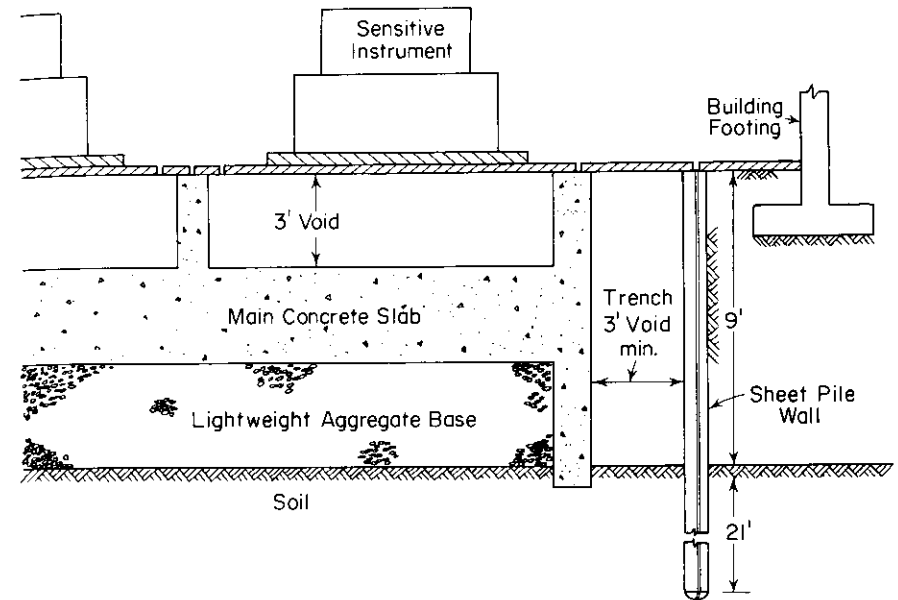


Figure 8-4. Isolation of standards laboratory (after McNeill et al., 1965).

affect the building adversely. Dolling (1965) and Neumeuer (1963) reported on the use of a bentonite-slurry-filled trench to isolate a printing plant in Berlin from vibrations generated by subway trains. This application, as shown in Fig. 8-3, was reported as successful because the amplitude of vibration in the printing plant after trench installation was about one-half the amplitude before trench installation. It should be noted that a reduction of one-half in vibration amplitude would usually not be considered adequate. McNeill, Margason, and Babcock (1965) reported the successful application of a trench and sheet-wall barrier to isolate a sensitive dimensional-standards laboratory, as shown in Fig. 8-4. This isolation system effectively limited acceleration of the slab to the owners' specification (maximum acceleration of 100 micro-g).

#### Experimental Study of Trench and Sheet-Wall Barriers

In most applications of isolation barriers, the shape and size of the barriers have been selected without benefit of a rational design procedure. Barkan (1962) and Dolling (1965) reported on field investigations studying the effectiveness of barriers, and some guidelines for barrier size and shape were indicated. The tests by these investigators were limited in scope,

however, and did not provide sufficient background on which adequate barrier dimensions could be established. Recently, broader investigations have been conducted to determine the effectiveness of trench and sheet-wall barriers as vibration isolators and to develop guidelines for the design of these barriers, (see Woods and Richart, 1967; and Woods, 1968). The following paragraphs describe these investigations.

The concept of isolation by wave barriers is based on reflection, scattering, and diffraction of wave energy. Wave barriers may consist, in general, of solid, fluid, or void zones in the ground. The partition of elastic-wave energy at a solid-to-solid interface was described in Chap. 4. Partitions of wave energy at a solid-to-fluid interface or a solid-to-void interface are special cases of the solid-to-solid problem, and detailed analyses can be found in Kolsky (1963) and Ewing, Jardetzky, and Press (1957). At a solid-to-solid interface, both *P*-waves and *S*-waves are transmitted; at a solid-to-fluid boundary only *P*-waves are transmitted; and at a solid-to-void interface, no waves are transmitted. The most effective barrier is that which transmits the minimum wave energy; that barrier would be, of course, the void. Thau and Pao (1966) have shown theoretically that a thin crack is sufficient to screen vertically polarized *SH*-waves in an elastic medium. Figure 8-5 (after Thau and Pao) shows the relative amplitude of a plane *SH*-wave which encountered a semi-infinite crack parallel to its wave front. Particle motion in Fig. 8-5 is normal to the plane of the figure and is, therefore, analogous to the vertical component of the *R*-wave at the surface of a half-space. On the basis of the preceding considerations, open trenches were used as the barriers in these isolation studies.

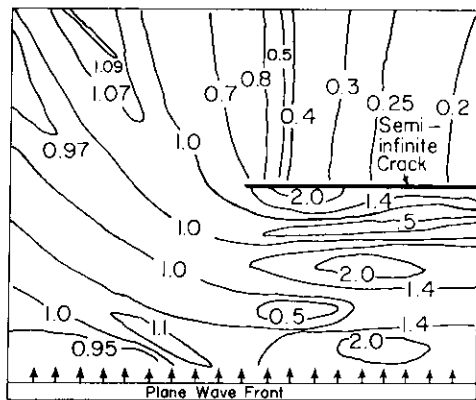


Figure 8-5. Amplitude-ratio contour diagram for *SH*-wave at a crack in an elastic medium (after Thau and Pao, 1966).

(Note: A comparison of Fig. 8-5 for shear waves in an elastic solid with Fig. 5-3 for gravity waves in water shows the analogous scattering and diffraction characteristics of a void barrier in a solid and a solid barrier in water.)

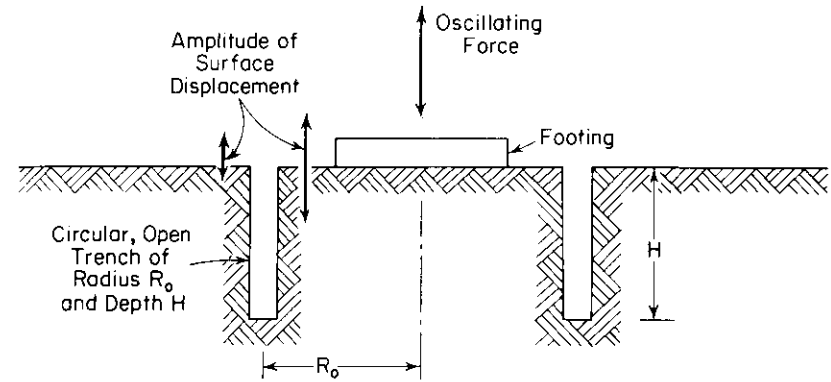


Figure 8-6. Schematic of vibration isolation using a circular trench surrounding the source of vibrations—active isolation (from Woods, 1968).

It is convenient to subdivide the problem of screening of elastic waves by trenches into two categories: (1) active isolation (isolation at the source), and (2) passive isolation (screening at a distance). Active isolation, as shown schematically in Fig. 8-6, is the employment of barriers close to or surrounding the source of vibrations to reduce the amount of wave energy radiated away from the source. Passive isolation, as shown schematically in Fig. 8-7 is the employment of barriers at points remote from the source of vibrations but near a site where the amplitude of vibration must be reduced. Both types of foundation isolation problems were investigated.

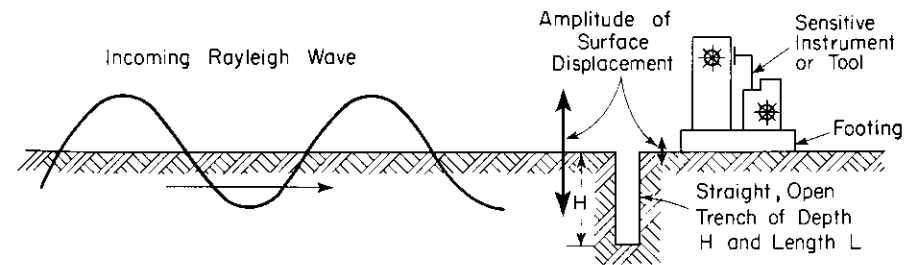


Figure 8-7. Schematic of vibration isolation using a straight trench to create a quiescent zone—passive isolation (from Woods, 1968).

The isolation tests were performed at the field-test site shown in Fig. 8-8. This site was situated on a sand-and-silt deposit in an area remote from sources of manmade seismic noise. A profile showing the pertinent properties of the soil at the field site is shown in Fig. 8-9. The angle of internal friction  $\phi'$  was  $38^\circ$  and the cohesion intercept *c* was 700 lb/ft<sup>2</sup>. In a moist condition (water content *w* = 5 to 15 per cent), this soil maintained vertical-walled

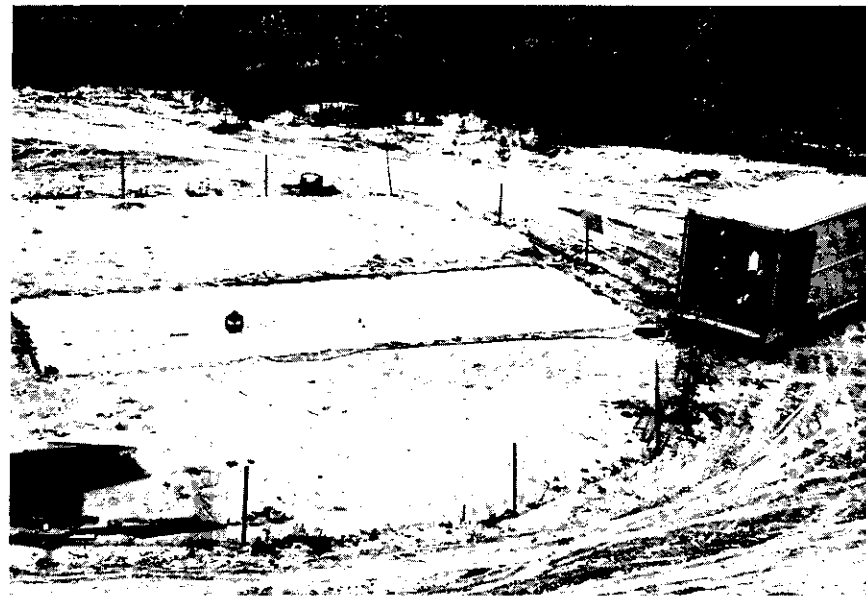


Figure 8-8. Field site.

open trenches up to 4-ft deep. Each field-test layout consisted of a vibration exciter as the source of input motion, a trench to screen displacement waves, and pickup points at which were measured the amplitude of vertical ground motion.

Wave-length scaling was determined appropriate for these model tests (Woods, 1967); therefore, the wave length of the Rayleigh wave,  $L_R$ , had to be determined at the field site for several frequencies of vibrations. Rayleigh-wave velocities  $v_R$  and wave lengths  $L_R$ , as determined in the field by the method described in Chap. 4, are given in Table 8-2. Critical

Table 8-2. Wave Length and Wave Velocity for the Rayleigh Wave at the Field Site

Frequency (cycles/sec)	$L_R$ (ft)	$v_R$ (ft/sec)
200	2.25	450
250	1.68	420
300	1.38	415
350	1.10	385

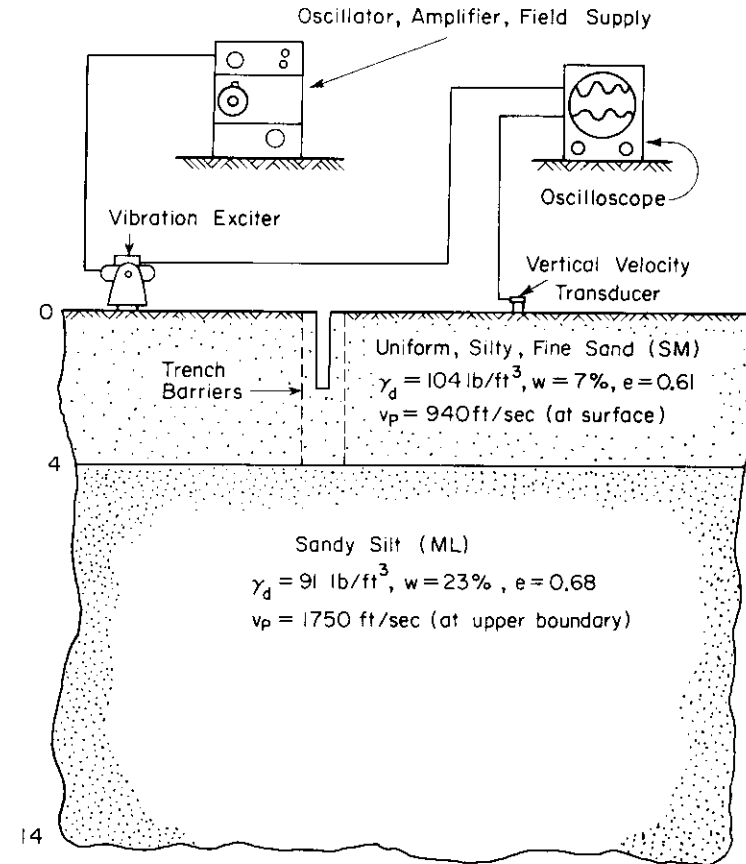


Figure 8-9. Field-site soil properties and schematic of instrumentation (from Woods, 1968).

dimensions of the trenches used in all tests were normalized on  $L_R$  for the appropriate frequency when used to compare results of two or more tests at different frequencies.

**Active-isolation tests.** The primary variables in the active isolation tests were  $H$  and  $\theta$ , where  $H$  was the trench depth and  $\theta$  was the angular length of the trench. Barrier trenches 0.5-ft to 2.0-ft deep composed of segments of annuli ranging from  $90^\circ$  to  $360^\circ$  were employed. Figure 8-10 shows a schematic diagram of the experimental setup for these tests with the critical dimensions labeled. The radii  $R_o$  of the annular trenches were 0.50 ft and 1.00 ft. By employing trenches at these two radii and by using four exciter

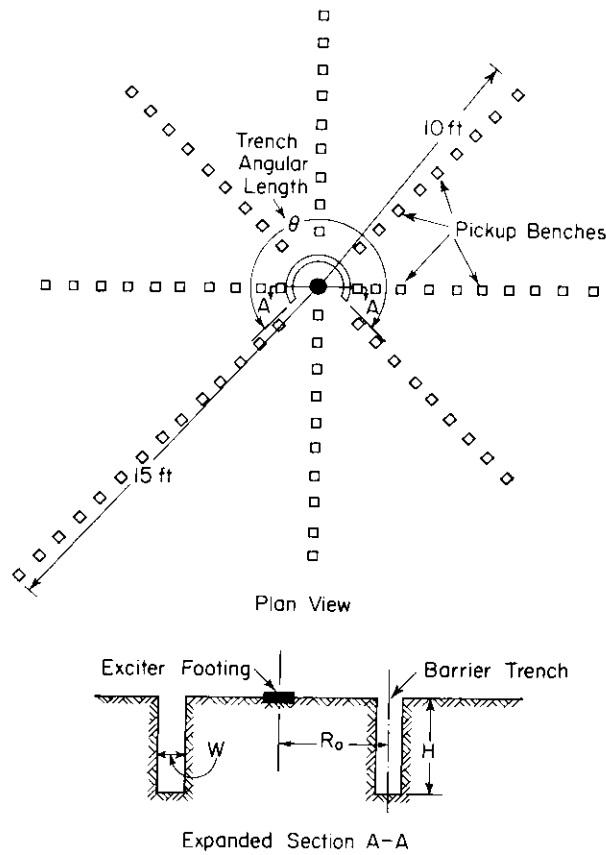


Figure 8-10. Schematic of test layout for active isolation in the field (from Woods, 1968).

frequencies (200, 250, 300 and 350 cycles/sec) it was possible to obtain ratios of trench radius to wave length ( $R_o/L_R$ ) ranging from 0.222 to 0.910.

In these tests, one criterion of effectiveness was a reduction in the amplitude of vertical ground motion of 0.25. By recording the vertical surface displacement at many points with and without a trench barrier, a *ratio of amplitude* after trench installation to amplitude before trench installation could be computed. By plotting these *amplitude ratios* on a plan diagram of the field-test site, contour diagrams of amplitude ratio were obtained. These contour diagrams provided the means of evaluating the effectiveness of each trench barrier. An example of an *amplitude-ratio contour diagram* is shown in Fig. 8-11.

From these test results it was concluded that for trenches fully surrounding the source of vibration at a distance of one wave length or less, the scaled

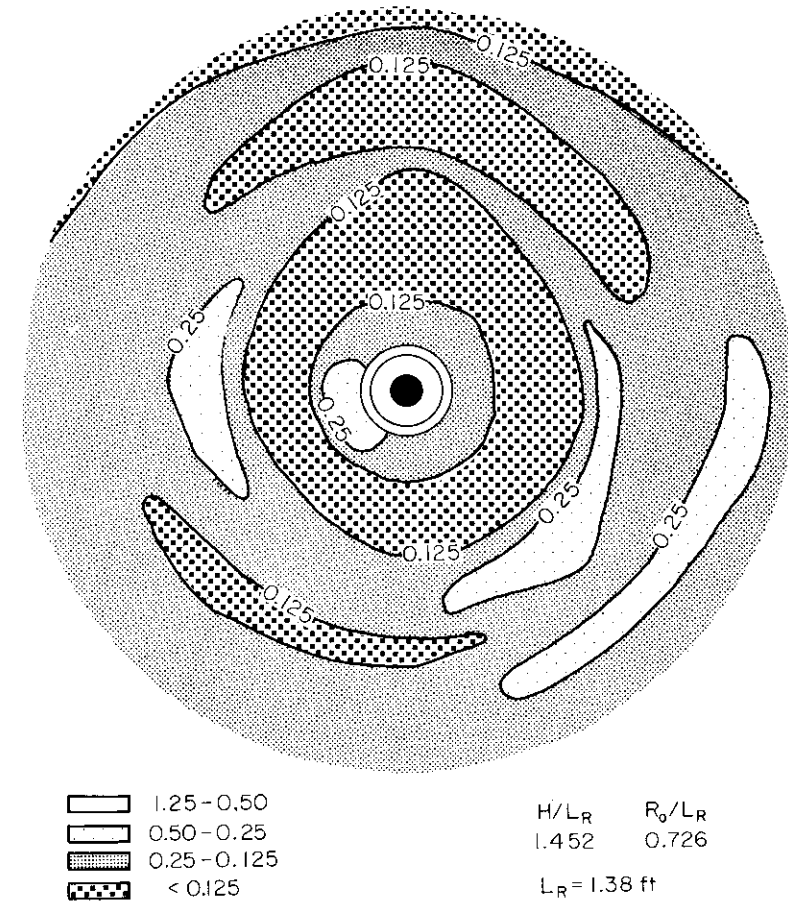


Figure 8-11. Amplitude ratio contour diagram (from Woods, 1968).

depth of the trench must be about 0.6 for the trench to be effective. For full-circle trenches the screened zone included an area of the half-space outside of the trench extending to a radius of at least 10 wave lengths. Data was not obtained beyond 10 wave lengths due to the site size and the power limitations of the vibration exciter.

For trenches of angular length less than  $360^\circ$ , the screened zone was an area symmetrical about a radius from the source of excitation through the center of the trench and was bounded laterally by two radial lines extending from the center of the source of excitation through points  $45^\circ$  from each end of the trench (Fig. 8-12). This definition of the screened zone excludes trenches of arc length less than  $90^\circ$ , and *all data confirmed that  $90^\circ$  trenches were not effective*. Also, in these tests the screened zone extended at least

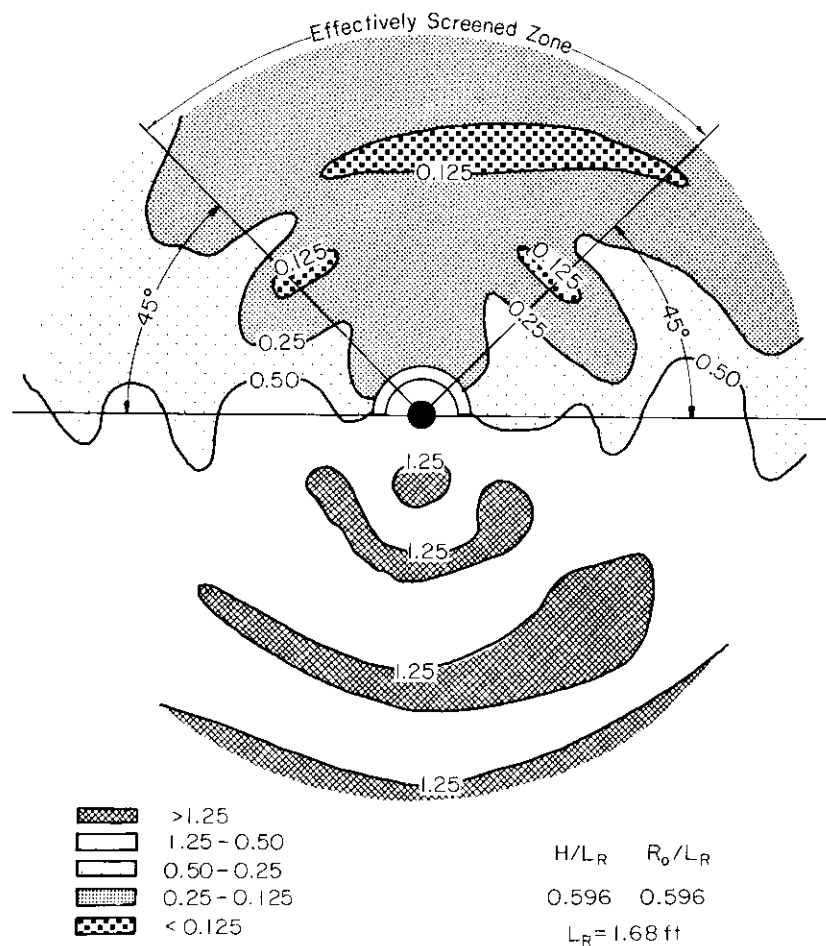


Figure 8-12. Amplitude ratio contour diagram (from Woods, 1968).

10 wavelengths from the source. The same criterion for screening effectiveness (amplitude reduction of 0.25 or less) when applied to trenches of angular length less than  $360^\circ$  showed that the same scaled trench depth  $H/L_R = 0.6$  is required to produce an effectively screened zone.

Further examination of all tests for active isolation indicated that amplitude reductions greater than one order of magnitude are not likely to be achieved using trench barriers up to 2 wave lengths ( $H/L_R = 2.0$ ) deep. The tests by Barkan (1962) and Dolling (1965) indicated similar results.

**Passive-isolation tests.** The test setup for passive isolation is shown schematically in Fig. 8-13. The layout consisted of two vibration-exciter

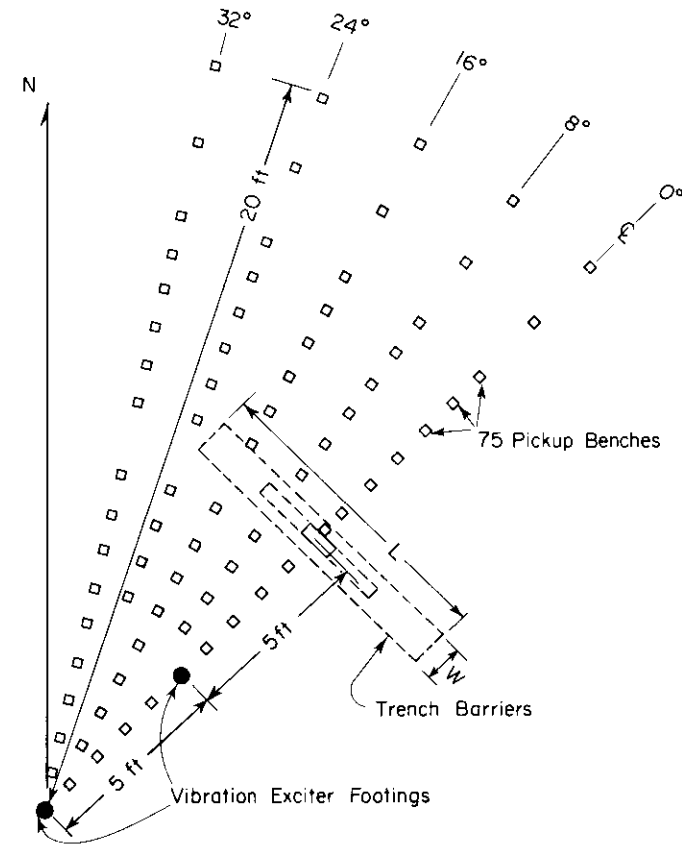


Figure 8-13. Plan view of field-site layout for passive isolation (from Woods, 1968).

footings, a trench barrier, and 75 pickup benches. For this series of tests it was assumed that the zone screened by the trench would be symmetrical about the  $0^\circ$  line; therefore, surface-motion measurements were made for only one-half of the screened zone. Symmetry of screening effects had been already sufficiently established in the active-isolation tests. The variables in these tests were trench depth  $H$ , trench length  $L$ , trench width  $W$ , and the distance from the source of excitation to the trench,  $R$ .

To study passive isolation, trenches ranging in size from 1.0-ft deep by 1.0-ft long by 0.33-ft wide, to 4.0-ft deep by 8.0-ft long by 1.0-ft wide were employed. By locating the vibration exciter at two distances from these trenches and using four frequencies of excitation (200, 250, 300, and 350 cycles/sec) a range of eight  $R/L_R$  ratios ( $R/L_R = 2.22$  to 9.10) was obtained. This range in  $R/L_R$  was necessary to evaluate the effects of the exciter-trench distance  $R$  on trench performance.

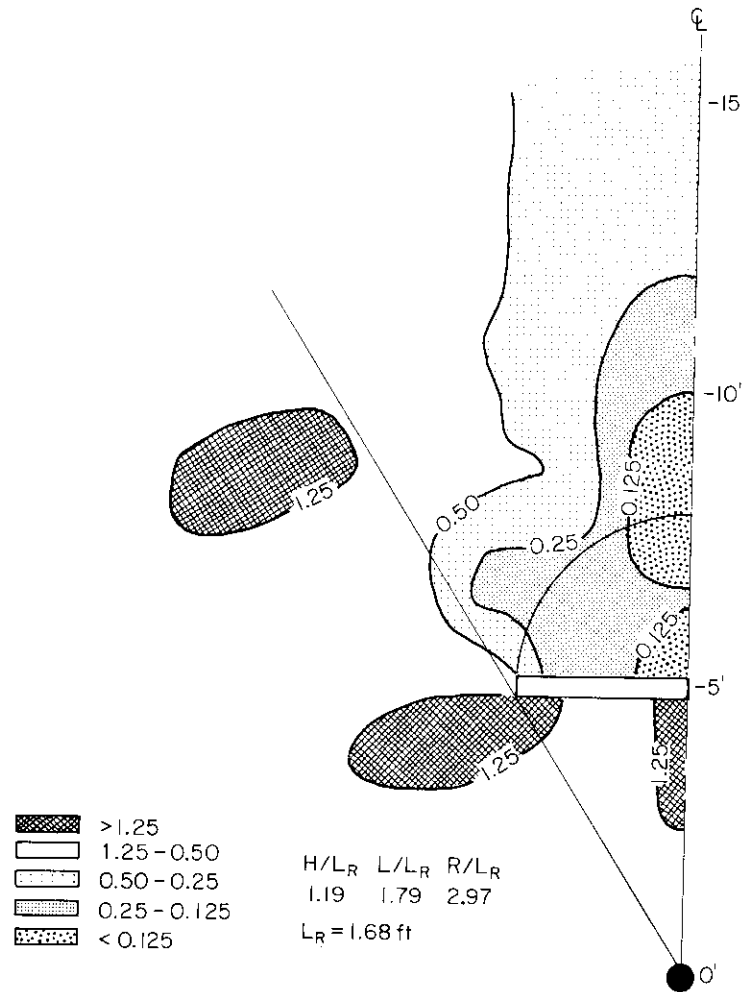


Figure 8-14. Amplitude-ratio contour diagram (from Woods, 1968).

From practical considerations, the critical dimension for trench barriers was the scaled depth  $H/L_R$ ; therefore, for each distance from the source the shallowest trench which satisfied the criteria was determined. The minimum scaled depth for the passive trenches was generally between  $H/L_R = 1.2$  and  $H/L_R = 1.5$ . To evaluate the effect of total trench area on the screened zone, a quantity  $HL/L_R^2$  (scaled trench length times scaled trench depth) was computed for each trench. There was a general trend toward increasing  $HL/L_R^2$  with increasing  $R/L_R$ . Figure 8-14 shows the amplitude-ratio contour diagram for a trench which satisfies the criteria.

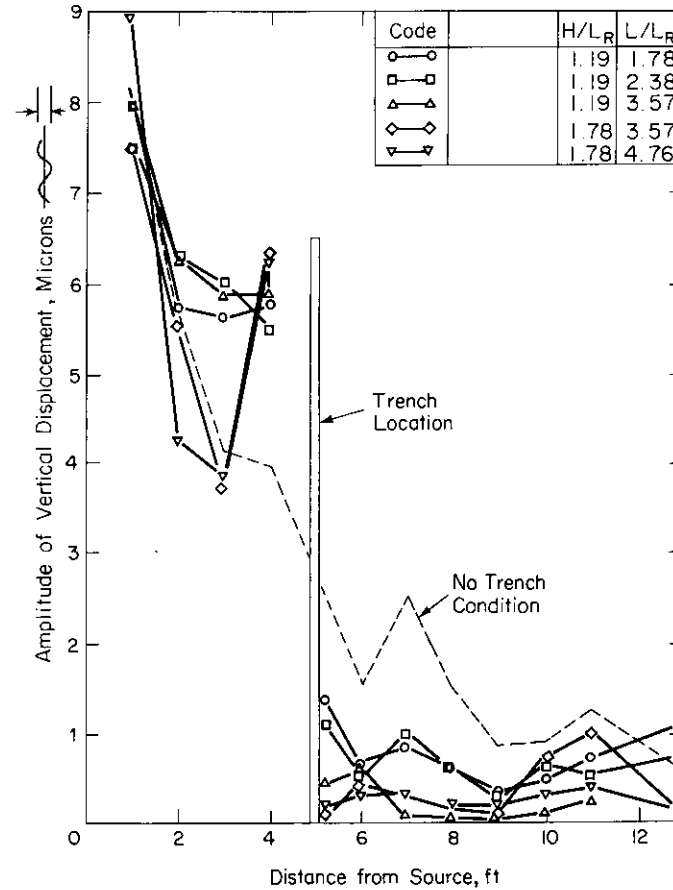


Figure 8-15. Amplitude of vertical displacement vs. distance from source for five tests (from Woods, 1968).

Amplitude magnification (indicated by amplitude-reduction-factor contours greater than 1.0) can be seen in Fig. 8-14 in front of and near the end of the trench. This phenomenon may explain some of the first unsatisfactory applications of trench barriers referred to earlier in this chapter. This magnification phenomenon was also noted in the work by Thau and Pao (1966) and can be seen in Fig. 8-5.

Curves of amplitude of vertical displacement vs. distance along a line of symmetry from the vibrator through the trench for five tests are shown in Fig. 8-15. The increasing effectiveness of the larger trenches can be seen in the region beyond the trench by the relative position of the curves for each test. Also apparent in this figure are the magnification in front of the trench and maximum reduction at some distance behind the trench.

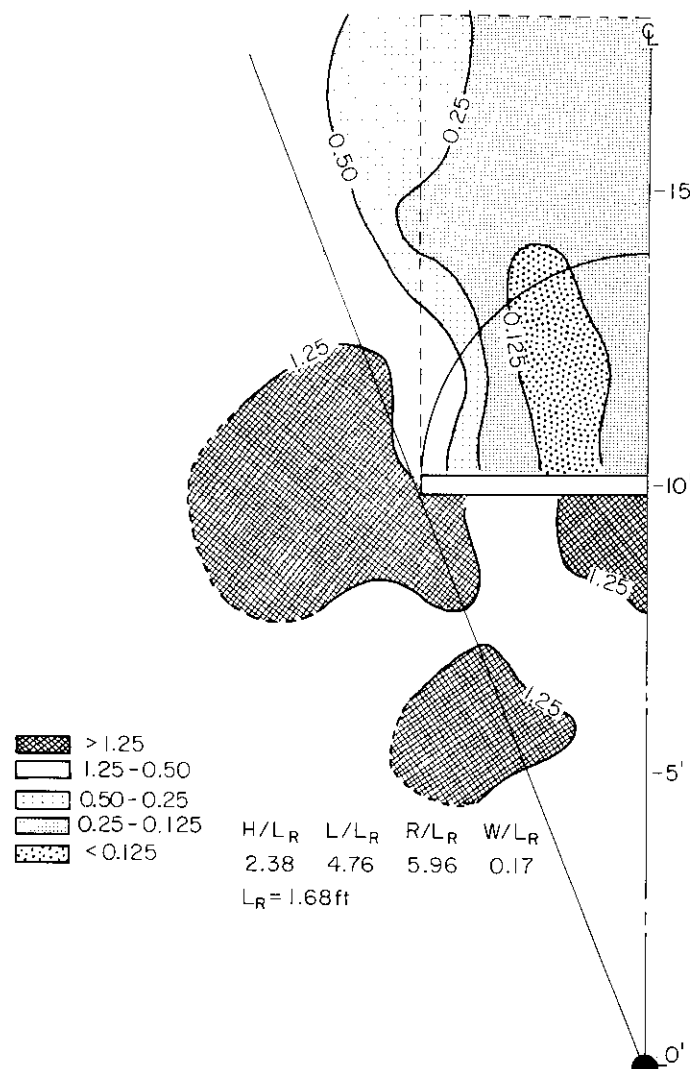


Figure 8-16. Amplitude-ratio contour diagram (from Woods, 1968).

In planning the tests it was assumed that the width of an open trench would not be an important variable and that, in fact, a small crack or slit would be sufficient to screen elastic waves. A few tests were performed to evaluate this assumption and it was found that an increase in width did not cause a significant change in either the magnitude of reduction or the shape of the screened zone. These results tend to confirm the assumption that *trench width is not an important variable*.

Another assumption made in planning the trench study was that open trenches would be more effective than sheet walls as surface-wave barriers; therefore, a few sheet-wall-barrier tests were performed. An aluminum sheet  $\frac{3}{16}$ -in. thick, 4-ft deep, and 8-ft long was used as the barrier. For comparison, the length and depth of the sheet-wall barrier were the same as the length and depth of the trench barrier shown in Fig. 8-16. In general, the sheet-wall barriers were *not as effective* in reducing amplitude of vertical ground motion as the trench barriers.

It is interesting to compare the general positions and shapes of the amplitude-ratio contours in Figs. 8-5 and 8-16. For example, the contours of 0.50 and 0.25 on both figures show a definite similarity in position and shape. There is also an overall correspondence in the regions of amplitude magnification in front of and at the side of the barriers. The correspondence of these features is remarkable because the contours in Fig. 8-5 are for a plane shear wave encountering a semi-infinite barrier (crack) in a homogeneous, isotropic, elastic solid, while the contours in Fig. 8-16 are for a cylindrical surface wave encountering a finite barrier (trench) in a real soil.

#### Conclusions Pertinent to Design of Isolation Barriers

The following recommendations for trench size and shape are influenced by the criteria used in judging the isolation effectiveness of the trenches tested. For this reason the effectiveness criteria are included in the design recommendations. Two general criteria are required—one specifying the amplitude reduction and the other specifying the area of influence.

For *active isolation* with trenches that fully surround the source of vibration, a trench is considered effective if the amplitude of vertical ground motion is reduced to 25 per cent of the no-trench motion within an annular zone extending from the outer edge of the trench to a circle with a radius of at least  $10L_R$ . To accomplish this degree of isolation, the ratio of trench depth to wave length of the *R*-wave ( $H/L_R$ ) should be about 0.6. For active isolation with partially surrounding trenches, the same  $H/L_R$  is recommended for an amplitude reduction of 0.25, but the area of influence must be specified in more detail. In this case the zone of influence is an area symmetrical about a radius from the source of excitation through the center of the trench and is bounded by two radial lines extending from the center of the source through points  $45^\circ$  from each end of the trench and by a circular arc of radius equal to  $10L_R$  (see Fig. 8-12). Note, this criterion excludes trenches of angular length less than  $90^\circ$ .

For *passive isolation* a trench is considered effective if the amplitude of vertical surface motion is reduced to 25 per cent of the no-trench motion within a semicircular area with radius of one-half the trench length ( $L/2$ )

and center at the center of the trench (see Fig. 8-14). For trenches located between  $2L_R$  and  $7L_R$  from the source ( $2L_R \leq R \leq 7L_R$ ),  $H/L_R$  must be about 1.33. Furthermore, to maintain the same degree of isolation, the scaled area of the vertical projection of the trench ( $H/L_R \times L/L_R = HL/L_R^2$ ) should be increased as the distance from the source ( $R$ ) increases. The scaled area should be at least 2.5 at  $R = 2L_R$  and at least 6 at  $R = 7L_R$ . Experimental data is not available for source-to-trench distances greater than about  $7L_R$ .

For both active and passive isolation, the trench width  $W$  is determined solely on the basis of the trench-construction requirements. The recommended trench dimensions for both types of isolation are a function of  $L_R$  which, in turn, is a function of the frequency of the disturbance and the wave-propagation velocity of the foundation material. For installations that are already in operation, the frequency of ground motion should be measured at the site of the proposed trench; while for a new installation the frequency of the proposed equipment may be used. The wave-propagation velocity should be measured *in situ* by the method described in Sec. 4.3 or estimated on the basis of soil properties and confining pressure. The wave length  $L_R$  can then be computed from Eq. (4-45):

$$L_R = \frac{v_R}{f}$$

Caution must be exercised with respect to focusing or amplitude magnification in the selection of trench shape and trench location for active isolation with partially surrounding trenches, and for passive isolation. Also, it should be recognized that soil layering, a high water table, or other foundation or building details may alter wave-propagation phenomena and require additional considerations in the selection of a trench barrier.

There are problems, of course, associated with keeping trenches open for depths of practical concern—say, 20 to 50 ft. One method of overcoming this difficulty is to use bentonite-slurry-filled trenches as described by Dolling (1965). However, more data is needed comparing slurry-filled trenches with open trenches before this technique can be used generally. Another promising possibility is to replace the trench by single or multiple rows of thin-shell-lined cylindrical holes.

## 9

### INSTRUMENTATION FOR LABORATORY AND FIELD MEASUREMENTS

In order to compare the actual performance of a dynamic system with the calculated performance, it is necessary to use relatively complex instrumentation. The same type instrumentation is also used for laboratory studies of dynamic soil properties. For all cases the problem involves a transducer which converts the physical quantity to be measured into an electrical signal which is related to the physical quantity through a calibration factor for the transducer. The electrical signal is measured and read directly or recorded so that the information can be analyzed in more detail at a later time. Engineering judgment is needed in many cases to insure that the most significant quantities are measured. This judgment is most often called for during measurement, since prior planning cannot anticipate all details which might significantly affect the measurements. Thus, the person making the measurements must not only be trained in dynamics but he must also have the knowledge required to understand the operation of the instruments he is using. Without a good understanding of the basic operation of electronic instruments, the operator will not know when his equipment is performing properly or be able to cope with difficult circumstances in taking the measurements.



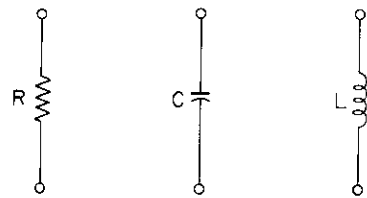


Figure 9-1. Basic elements of electrical circuits.

The objectives of this chapter are to provide a review of the basic electronic principles which are applicable to vibration measurements and to provide information on the types of instruments most commonly used for dynamic measurements. There is also a section on the types of equipment used for the resonant-column method of determining dynamic soil properties.

### 9.1 Basic Electrical Elements

Figure 9-1 shows the three basic elements used in electrical circuits, along with the symbols used to describe them. Vacuum tubes, transistors, diodes, and other components will not be considered as they are beyond the scope of this text. In order to understand the behavior of basic elements in an electrical circuit we shall make use of an analogy between electrical and mechanical components. The force-current analog is most suited for this purpose. In this analog, the current  $I$  in the electrical circuit is analogous to force in a mechanical system. Each electrical element has a corresponding mechanical element which responds in a manner which is mathematically the same.

#### Resistance

First consider the relationships for a resistor having a resistance  $R$ , expressed in ohms. If a direct current (dc) flows through the resistor, a voltage difference  $E$  will exist across the resistor having a value given by

$$E = IR \quad (9-1)$$

which is an expression of Ohm's law. We are all familiar with the fact that when current flows through a wire it gets warm due to the resistance in the wire. This heat represents a loss of energy. In a mechanical system a dashpot is an energy-absorbing element having the relationship

$$\text{Force} = (\text{Viscous-damping coeff.}) \times (\text{Velocity}) \quad (9-2)$$

By rewriting Eq. (9-1) as

$$I = \frac{1}{R} E \quad (9-3)$$

we see that  $1/R$  is analogous to the viscous-damping coefficient and voltage is analogous to velocity. Equation (9-3) applies at any instant of time and therefore can be used for alternating-current (ac) relationships just as the analogous dashpot relationship applies to sinusoidal forces.

The power  $P$  absorbed by a pure resistance and converted into heat is given by

$$P = I^2 R = \frac{E^2}{R} \quad (9-4)$$

#### Capacitance

A capacitive element is one which has the ability to store an electrical charge. Current passes through the conductors leading to the capacitor only when the charge on the capacitor changes. Thus, in a dc circuit no current passes to the capacitor after it has become charged. The amount of charge in a capacitor is given by the expression

$$q = CE \quad (9-5)$$

where

$$\begin{aligned} q &= \text{charge in coulombs and} \\ C &= \text{capacitance in farads.} \end{aligned}$$

The amount of charge is related to current by

$$q = \int_0^t I dt \quad (9-6)$$

This equation is analogous to the impulse equation in mechanics. Introducing Eq. (9-6) into (9-5) and taking the derivative with respect to time gives

$$I = C \frac{dE}{dt} \quad (9-7)$$

For our analogous physical element we have

$$\text{Force} = \text{Mass} \times \text{Acceleration} \quad (9-8)$$

Thus, we see that capacitance is analogous to mass.

If a sinusoidal voltage is applied to a capacitor, we can calculate the charging current that will occur using Eq. (9-7). If

$$E = E_0 \sin \omega t \quad (9-9)$$

then

$$I = C \frac{dE}{dt} = C\omega E_o \sin\left(\omega t + \frac{\pi}{2}\right) \quad (9-10)$$

This is most easily visualized by taking a sinusoidal force (current) acting on a free mass (capacitor) and considering the resulting velocity (voltage). When a force is first applied to a mass, there is a time lag before the mass can achieve a velocity due to its inertia. Thus, velocity lags force just as voltage lags current in a capacitor.

### Inductance

An inductive element consists of a coil having zero resistance surrounded by a magnetic field due to the current passing through it. Any change in current will change the magnetic field and induce a voltage in the coil, which tends to oppose the change in current. The relationship for an inductive element may be written

$$E = L \frac{dI}{dt} \quad (9-11)$$

where  $L$  is the coil inductance in henrys. Integration of Eq. (9-11) with respect to time gives

$$I = \frac{1}{L} \int E dt \quad (9-12)$$

Since the integration of voltage (velocity in a mechanical system) with respect to time is equivalent to displacement, an inductor is analogous to the mechanical spring where

$$\text{Force} = (\text{Spring constant}) \times (\text{Displacement}) \quad (9-12)$$

In this case the spring constant is analogous to the reciprocal of the inductance. If an alternating voltage is applied to an inductor, the resulting current can be calculated from Eq. (9-12) as

$$I = \frac{E_o}{\omega L} \sin\left(\omega t - \frac{\pi}{2}\right) \quad (9-13)$$

In this case the current lags the voltage. It can be visualized by remembering that for a spring no force (current) occurs until a displacement is produced (voltage  $\times$  time).

Table 9-1. Analogous Relationships between Mechanical and Electrical Systems

Mechanical	Electrical
Force = $Q$	Current = $I$
Velocity = $\dot{z}$	Voltage = $E$
Displacement = $z$	$\int E dt$
Acceleration = $\ddot{z}$	$\frac{dE}{dt}$
Damping = $c$	$\frac{1}{\text{Resistance}} = \frac{1}{R}$
Spring = $k$	$\frac{1}{\text{Inductance}} = \frac{1}{L}$
Mass = $m$	Capacitance = $C$

For convenience, the analogous relationships have been listed in Table 9-1. Use will be made of these relationships in describing various electronic circuits.

### Impedance

The term *impedance* is used to describe the characteristics of an electrical circuit. It is analogous to mechanical impedance, which is a measure of the opposition of a system to an applied force (current), usually taken as a sinusoidal force. Thus, the ratio of velocity amplitude (voltage amplitude) to force amplitude (current amplitude) as a function of frequency is the quantity used to describe impedance. In view of the phase difference between current and voltage for capacitors and inductors, it is convenient to introduce complex notation and express the impedance in vector form. Thus, for pure elements, the impedances  $Z$  are expressed by

$$Z_R = R \quad (\text{ohms}) \quad (9-14)$$

$$Z_C = -i \frac{1}{\omega C} \quad (\text{ohms}) \quad (9-15)$$

$$Z_L = i\omega L \quad (\text{ohms}) \quad (9-16)$$

where  $i = \sqrt{-1}$ . Impedances of the input and output terminals of electronic instruments are usually expressed in terms of the element values and how they are connected. For instance, the input terminals of an oscilloscope might have an impedance composed of a resistance of 1 megohm ( $10^6$  ohms) in parallel with a capacitance of 47 picofarads ( $47 \times 10^{-12}$  farad).

Table 9-2. Prefixes Commonly Used in Electrical Measurements

giga	= $10^9$
mega	= $10^6$
kilo	= $10^3$
milli	= $10^{-3}$
micro	= $10^{-6}$
nano	= $10^{-9}$
pico	= $10^{-12}$

Due to the fact that both very large and very small quantities are found in electrical components, prefixes are often used. Table 9-2 is a list of these prefixes and the multipliers that they represent.

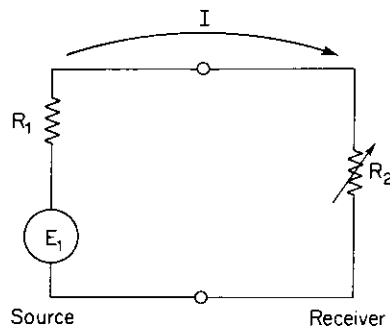


Figure 9-2. Simplified diagram of a source and receiver having resistive impedances.

**Matched impedance.** If two instruments are connected together such that the main function is to transfer power or energy from one to the other, there exists an optimum relationship between the output impedance of the source and the input impedance of the receiver. For simplicity we shall consider the source to be represented by an electromotive force (emf) having a voltage output  $E_1$  in series with an output impedance having pure resistance  $R_1$ , as shown in Fig. 9-2. The receiver has an adjustable input impedance  $R_2$ ,

which is to be adjusted so that the maximum power is absorbed. The current flowing in the circuit is given by

$$I = \frac{E_1}{R_1 + R_2} \quad (9-17)$$

The power absorbed by  $R_2$  is

$$P_2 = I^2 R_2 = \frac{E_1^2 R_2}{(R_1 + R_2)^2} \quad (9-18)$$

Taking the derivative of  $P_2$  with respect to  $R_2$ , we get

$$\frac{dP_2}{dR_2} = E_1^2 \left[ \frac{-2R_2}{(R_1 + R_2)^3} + \frac{1}{(R_1 + R_2)^2} \right] \quad (9-19)$$

Setting this equal to zero, we get

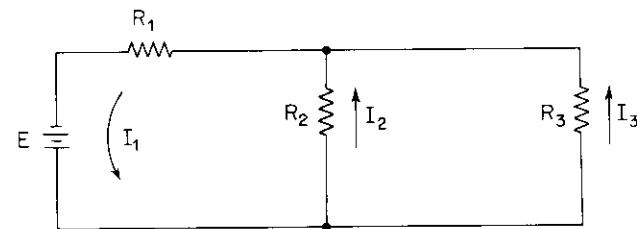
$$R_2 = R_1 \quad (9-20)$$

Thus, the condition of maximum transfer of energy occurs when the input impedance of the receiver matches the output impedance of the source—hence, the condition of *matched impedance*. For the measurement of the voltage output of vibration transducers, matching impedance is of no importance. In fact,  $R_2$  is usually made large with respect to  $R_1$  in order to obtain the maximum voltage across  $R_2$ . However, if the source is an oscillator which is being used to drive a vibration generator, then it is important to match the output impedance of the oscillator to the input impedance of the vibration generator to obtain the maximum power output. A similar example is found on the output connections of an ordinary hi-fi amplifier. Output impedances of 4, 8, and 16 ohms are usually provided to match the impedances of different types of speakers that may be used. When the impedances are matched, there is an additional advantage in that the distortion of the signal is reduced to a minimum.

## 9.2 Instruments for Electrical Measurements

### Direct-Current Meters

The dc meter is a fundamental component of many instruments available for making electrical measurements. Most dc meters are incorporated into an instrument that will measure voltage, current, or resistance by setting a switch to the desired function. Basically the dc meter only measures current, but measurements of voltage or resistance can be accomplished by inserting additional elements between the meter and the circuit. The meter has a very low resistance coil surrounded by a magnetic field. The coil moves when a current passes through it. The electrical resistance of this coil is made as small as possible so that it will not influence the circuit being measured. In some cases, however, the readings of a meter are meaningless, especially when the circuit resistances are of the same magnitude as the meter resistance. For example, consider the circuit shown in Fig. 9-3a. If we wish to measure the current  $I_2$  flowing through the resistance  $R_2$ , we break the connection to  $R_2$  and insert the meter as shown in Fig. 9-3b. The meter resistance  $R_m$  is shunted with a resistance  $R_s$ , which is used to provide various ranges of current measurement by allowing only a certain percentage of the current actually to pass through the meter. The net meter resistance is  $R_m R_s / (R_m + R_s)$ . If the net meter resistance is only a small percentage of the value of  $R_2$ , then the current indicated by the meter will be very close to the original current  $I_2$ . However, it can easily be seen that if the net meter resistance is nearly as large as  $R_2$ , or if the circuit is very sensitive to changes in  $R_2$ , then the meter reading may be completely different than the original value of  $I_2$ .



(a) Original Circuit.

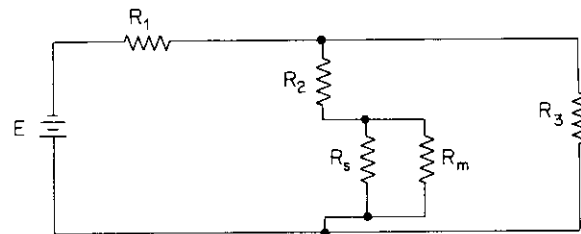
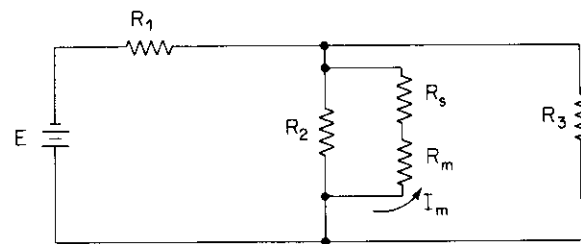
(b) Measurement of  $I_2$ .(c) Measurement of Voltage Across  $R_2$ .

Figure 9-3. Effects of meter impedance on circuit measurements.

In order to measure voltages, a resistance is placed in series with the meter to produce a high net resistance equal to  $(R_m + R_s)$ . If the meter is connected to two points in a circuit, as in Fig. 9-3c, a small current  $I_m$  will flow through the meter and will be proportional to the voltage difference between the two points. In order not to affect the characteristics of the original circuit, it can be seen that the current  $I_m$  must be as small as possible. This condition is met by having the net meter resistance large compared to the resistances that make up the circuit in which the voltage measurements are made.

Measurements of resistance may be made by applying a known voltage across the unknown resistance and measuring the current that flows through it. Application of the relationship  $R = E/I$  provides the value of the unknown resistance.

### Electronic Meters

The application of the dc meter as discussed in the preceding paragraphs has certain disadvantages. The main disadvantage lies in the fact that the presence of the meter changes the voltages and currents that are being measured. In order to overcome this problem an electronic circuit containing rectifiers, amplifiers, and other active components is used to generate the signal which is applied to the meter. Input impedances for an electronic meter used as a voltmeter range from  $10^6$  to as high as  $10^{14}$  ohms. A meter system of this type is commonly referred to as a *vacuum-tube voltmeter*.

### Alternating-Current Meters

When ac currents are applied to a dc meter, the variations in voltage or current are so rapid that the meter cannot respond fast enough and no measurement can be obtained. This problem is overcome in several ways. One method is to rectify the signal so that only components having the *same sign* are measured. Another method uses a thermocouple to generate a direct current from the heat generated by the alternating current passing through the thermocouple. Other methods are also used to measure alternating currents, but the important consideration is the response of the meter to different wave forms. Since a meter reading can only convey one piece of information about a voltage or current, meters are designed to measure one of three characteristics: the *average value*, *peak value*, or *root-mean-square (rms) value* of current or voltage. *In almost all cases, however, the dial face is calibrated so that the readings correspond to the rms value of a pure sinusoidal signal.* Thus, the readings will be in error if the wave form is not sinusoidal except for the true rms-responding meter. For sinusoidal quantities,

$$E_{\text{rms}} = 0.707E_{\text{peak}} \quad (9-21a)$$

and

$$E_{\text{rms}} = 1.111E_{\text{avg}} \quad (9-21b)$$

From this it can be seen that a 200-volt peak-to-peak square wave would read 70.7 V (volts) on a peak-responding meter, 100 V on an rms-responding meter, and 111.1 V on an average-responding meter. This points out the fact that care should be used when interpreting meter readings if the wave form is not sinusoidal.

### Galvanometers

A galvanometer is nothing more than a sensitive dc meter that is mechanically designed to respond to rapidly varying signals. Its response

may be described accurately by the equation for the dynamic magnification factor of a damped single-degree-of-freedom system (Eq. 2-53). Typical values of undamped natural frequency range from less than 1 cycle/sec to greater than 1000 cycles/sec. In general, the sensitivity of the galvanometer decreases as its undamped natural frequency is increased. Since the main purpose of the galvanometer is to measure dynamic signals, a means must be provided to record its response. There are two methods by which this is accomplished. One method is to attach a pen to the end of the galvanometer and record the signal on a roll of paper passing under the pen at a known velocity to provide a time scale. (The pen is actually part of the galvanometer since its mass affects the response characteristics of the galvanometer.) The other method records the galvanometer movement using a beam of light reflected onto a light-sensitive photographic paper from a mirror attached to the galvanometer coil. Since the mirror can be made very small, this system is used where high values of undamped natural frequencies are required in the galvanometer system. The maximum frequency response of a pen-type system is about 100 cycles/sec, whereas frequencies as high as several thousand cycles per second may be measured with the mirror-type system.

The methods used to record the signal onto paper are of importance only in terms of convenience. For the pen-type system, there is a choice between ink- and thermal-writing. The ink-writing pen requires a less expensive paper for recording but requires a lot of maintenance if the system is not in near-continuous use. The thermal-writing pen has a hot tip which melts a coating on a special type of recording paper. The paper is more expensive but the savings in maintenance time often offset the difference in price. The light-beam systems are made to record on either ordinary photographic paper or ultraviolet-sensitive paper. The only difference in the two types of paper is that the ordinary photographic paper must be handled and processed in complete darkness, whereas the ultraviolet paper develops automatically when exposed to daylight or to a fluorescent lamp. The ultraviolet-type system provides the convenience of making the recording almost immediately visible after it is made without imposing a wait while the paper is processed in a photographic laboratory. The choice of which system to use of course depends upon each particular application or need since all of the systems will give the same degree of accuracy.

### *Oscilloscopes*

A cathode-ray oscilloscope is one of the most versatile measuring instruments available. It provides a visual display of the wave form being measured, from which it is possible to obtain accurate measures of voltage and time. The heart of the instrument is a cathode-ray tube in which a beam of electrons

illuminates a spot on its phosphor-coated face. This spot can be accurately positioned both horizontally and vertically by application of voltages across pairs of deflection plates between which the beam passes. One set is used to control the vertical position and the other the horizontal position of the beam. For most applications a calibrated sawtooth voltage is applied to the horizontal-deflection plates so that the beam moves from left to right at a known velocity and then rapidly returns to the left side of the tube to repeat its sweep from left to right. This provides a *time scale* on the face of the cathode-ray tube. The signal to be measured is amplified and applied to the vertical-deflection plates. With this arrangement, complete information is displayed showing the variation of voltage with time, which can be recorded photographically if a permanent record is desired. The applications of this type instrument are almost unlimited in view of the availability of transducers which can convert such quantities as force, displacement, velocity, acceleration, pressure, strain, and temperature into voltages proportional to the quantity being measured.

### *Magnetic-Tape Recorders*

Magnetic-tape recorders provide a means of recording dynamic signals for subsequent reproduction. The system has a great advantage over paper-recording systems in which the signal is recorded permanently and cannot be regenerated as an electrical signal. Since the magnetic-tape recorder can reproduce the original signal, it is possible to make a much more detailed analysis by using filters, wave-form analyzers, integrators, analog computers, or other types of instruments depending on the information desired. In many instances, the ability to regenerate the original signal permits the system to provide more information than can be obtained using paper-recording systems.

Two methods are used to record and play back signals on a magnetic tape; the *direct-record/reproduce* method and the *FM-record/reproduce* method. The direct-record/reproduce method amplifies a signal and applies it directly to the recording head, which magnetizes the tape by an amount proportional to the signal level. When the tape is played back, a voltage is generated by the reproducing head which is proportional to the *rate of change* of the magnetic field on the tape. Thus, it is the derivative of the recorded signal and not the signal itself which is sensed by the reproducing head. In order to obtain the original signal, the signal from the reproducing head is integrated. It is obvious that this system will have a lower limit on the frequency that it can record since no voltage will be reproduced by the reproducing head if the magnetic field is constant. There are other inherent problems involved with the direct-recording method that are associated with the

magnetic hysteresis of the tape, but a discussion of these will not be included here.

The FM-record/reproduce method eliminates the problems of magnetic hysteresis and inability to record dc signals by converting signal levels into frequency deviations from a center frequency. A positive signal causes an increase in frequency while a negative signal causes a decrease in frequency. When the signal is reproduced, changes from center frequency are converted to signal levels by means of relatively complex electronics. Although this method appears to have great advantages over direct recording, other problems arise that are not associated with the direct-recording method. In the FM method the system is extremely sensitive to slight variations in tape speed, since such variations have the same effect as a change in frequency. Thus, the system requires a much more sophisticated tape-drive system than can be used for the direct-record method. However, an FM system will give better performance than the direct-record system except in the area of maximum frequency response. An FM system can record signals from dc to 1250 cycles/sec at a tape speed of  $7\frac{1}{2}$  in./sec, while a direct record system can record from 100 to 12,000 cycles/sec at the same tape speed. The upper limits on frequency response are directly proportional to tape speed. Thus, since most soil-dynamics problems involve frequencies of less than 100 cycles/sec, the FM-record/reproduce system is usually the only one that can be used.

### Amplifiers

An amplifier is an instrument whose main function is to increase the voltage or current amplitude of a weak signal. In measurement applications it is the voltage amplitude which is amplified. Current is amplified to provide sufficient power to drive a galvanometer, vibration generator, or other physical system. (The comments below are limited to *voltage amplifiers*.)

Whenever a low-level voltage is amplified, one of the greatest problems that arises is *noise*—that part of the signal which does not represent the quantity that is being measured. This unwanted part is generated by several sources: differences in ground potential at various parts in a measuring system (ground loops), voltages induced into the cables that connect the signal source to the instrument, and the internal circuitry of the amplifier. This last source is usually given in the instrument specifications in terms of a voltage level over a given frequency range. Noise picked up by cable leads or produced by ground loops can be reduced to a minimum with shielded cables connected in the proper way. However, at some point the noise level reaching the amplifier will be reduced to a minimum. At the input to the amplifier, one side of the signal source is connected to ground and, since the amplifier

cannot distinguish between signal and noise, both will appear in the amplified signal. This condition is described as a "single-ended input," since one side of the signal source is grounded. However, if the signal source is not grounded, the noise will occur as a voltage common to each terminal and the generated signal will occur as a difference in voltage between each terminal. It can be seen that for this case the noise could be eliminated by measuring the algebraic difference of the voltage at each terminal. This is accomplished using a *differential* or *push-pull* amplifier. Such an amplifier actually consists of two nearly identical amplifiers, one producing an output having the same sign as the input and the other producing an output which is the negative of the input. The outputs of both amplifiers are added together to give the final amplified signal. Since the noise has the same level and sign at the input to each amplifier, it will be rejected and will not appear in the amplified signal. Since two amplifiers are never exactly identical, some of the noise will appear at the output of the amplifier. The ratio of the noise signal at the input to that at the output is referred to as the *common-mode rejection ratio*; typical values range from 100:1 to as high as 100,000:1. Since neither connection to the signal source is grounded in a differential amplifier, the input is sometimes referred to as a *floating input*. Although noise reduction is a main feature of the differential amplifier, it can also be used where a common dc voltage exists, as might be the case in a bridge circuit where the power source is not grounded.

### 9.3 Vibration Transducers and Their Calibration

The vibration-displacement amplitudes most often measured in soils and foundations range from millionths to thousandths of an inch and occur at frequencies ranging from less than 10 cycles/sec to more than 100 cycles/sec. The instruments required to measure motions of this magnitude are designed on the basis of a single-degree-of-freedom system. Instruments based on this design have two distinct advantages. First, in the single-degree-of-freedom system a suspended mass is used as a reference from which to measure vibrations, because in cases such as ground-motion measurements no reference is available: the single-degree-of-freedom system circumvents this problem. The second advantage is that certain electrical phenomena are readily adapted to measuring the response of the system by producing an electrical signal which can be observed with an oscilloscope or recorded for subsequent analysis.

An instrument which converts mechanical motion into an electrical signal is called a *transducer*. For vibration measurements there are three general types of transducers: displacement transducers, velocity transducers, and acceleration transducers. The theory of operation and methods of calibration for each type of transducer will be discussed in the following sections.

### Displacement Transducers

**Single-degree-of-freedom type.** The response of a single-degree-of-freedom system due to motion of its support was analyzed in Sec. 2.3. However, for the displacement transducer, the relative motion  $z_r$  between the mass and its support is the quantity desired. This relative displacement can be found easily by setting up the differential equation for the system shown in Fig. 9-4a. The acceleration of the mass will be

$$\ddot{z} = \ddot{z}_1 + \ddot{z}_r \quad (9-22)$$

The spring force and damping force are both directly proportional to  $z_r$ ; thus, the equation of motion is

$$m(\ddot{z}_1 + \ddot{z}_r) + c\dot{z}_r + kz_r = 0 \quad (9-23)$$

which may be written as

$$m\ddot{z}_r + c\dot{z}_r + kz_r = -m\ddot{z}_1 \quad (9-24)$$

The quantity on the right-hand side of Eq. (9-24) represents the forcing function which produces  $z_r$ . Substitution of  $A_1 \sin \omega t$  for  $z_1$  gives

$$-m\ddot{z}_1 = m\omega^2 A_1 \sin \omega t \quad (9-25)$$

which is similar in form to Eq. (2-57). Calculation of the equivalent  $Q_o/k$

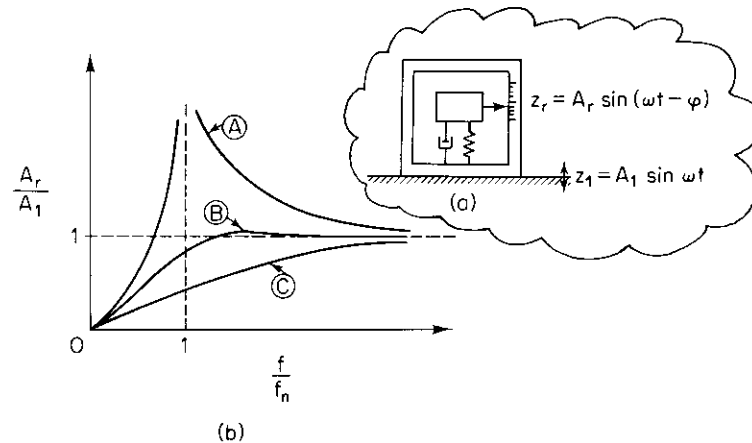


Figure 9-4. Ratio of relative to absolute displacement amplitude as a function of frequency.

provides the solution to the problem:

$$\frac{Q_o}{k} = \frac{m\omega^2 A_1}{k} = \left(\frac{\omega}{\omega_n}\right)^2 A_1 \quad (9-26)$$

Hence  $A_r/A_1 = (\omega/\omega_n)^2 M$  follows from comparison with Eq. (2-53) and  $\varphi$  is given by Eq. (2-54). For convenience, the solutions are repeated here:

$$\frac{A_r}{A_1} = \frac{\left(\frac{\omega}{\omega_n}\right)^2}{\sqrt{\left[1 - \left(\frac{\omega}{\omega_n}\right)^2\right]^2 + \left(2D \frac{\omega}{\omega_n}\right)^2}} \quad (2-53)$$

$$\tan \varphi = \frac{2D \frac{\omega}{\omega_n}}{1 - \left(\frac{\omega}{\omega_n}\right)^2} \quad (2-54)$$

Equation (2-53) has been plotted in Fig. 9-4b for three values of damping ratio  $D$ . All three curves have the property that they approach a value of 1.0 for frequencies greater than the undamped natural frequency. This means that the relative motion between the mass and its support is essentially the same as the motion of the support for frequencies above a particular value. The lowest frequency for which  $A_r/A_1$  remains within a specified variation from 1.0 depends on the value of  $D$ . For small  $D$ , a curve such as  $\textcircled{A}$  in Fig. 9-4b will be obtained. This condition is undesirable not only because of its slow convergence to  $A_r/A_1 = 1.0$  but also because vibrations at frequencies near the natural frequency of the transducer are exaggerated. For large  $D$ , a curve similar to  $\textcircled{C}$  will be obtained which eliminates the amplification of components near the resonant frequency by actually eliminating the resonant frequency. Furthermore, the curve does not rapidly approach  $A_r/A_1 = 1.0$ . The optimum value of  $D$  is 0.6 because  $A_r/A_1$  rapidly approaches 1.0 at this damping ratio and the amplification at resonance is only 4 per cent. Most displacement transducers designed on the basis of a single-degree-of-freedom system have damping ratios as close as possible to 0.6. Using this system, measurements of  $z_r$  provide a direct measure of  $z_1$  as long as the frequency components of the vibrations are within the range where the relationship is one-to-one.

Unfortunately, it is difficult actually to measure  $z_r$ . However, one available method uses a system of mirrors to magnify the motion of a light-beam reflected from the moving mass. The lightbeam is recorded on photographic paper which is later developed to obtain a record of the vibration.

Calibration of a displacement transducer is usually not necessary because the mirror system provides a fixed amount of magnification of the motion of the mass. A simple check can be made by comparing the output with a known displacement of the mass.

**Relative-displacement type.** An instrument commonly used to measure the relative displacement between two objects is a *linearly variable differential transformer* (LVDT). In some cases it is used as the sensing device for the displacement transducer described above. A diagram of an LVDT, which consists of a center primary coil and two outer secondary coils, is shown in Fig. 9-5a. An iron core placed along the axis of the coils causes equal ac voltages,  $180^\circ$  out of phase, to be induced into each secondary coil. The secondary coils are connected so that there is no net ac output voltage when the iron core is in the center position. However, as the core is moved away from the center position, the ac voltage in one secondary coil is increased while the other is decreased. The relationship between ac-voltage output and core displacement is linear within a small range each side of the null

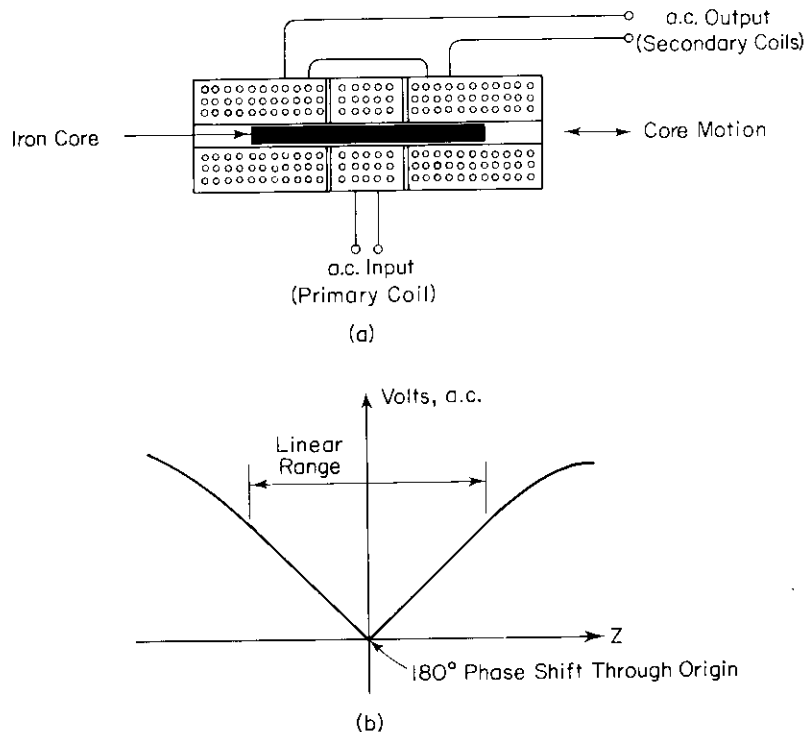


Figure 9-5. Linearly variable differential transformer.

position. Since there is a  $180^\circ$  phase shift as the core passes through the null position, it is possible to determine the position of the core by using a phase-sensitive instrument to convert the ac output into a dc-voltage level. The sign of the dc voltage depends on the position of the core with respect to the null position.

It is obvious that the frequency response of an LVDT depends on the frequency of the excitation voltage. The frequency-response limit is normally equal to 10 per cent of the excitation frequency, which typically ranges from 60 to 2400 cycles/sec.

Calibration of an LVDT may be accomplished by attaching a dial indicator or micrometer to an extension of the core.

**Optical type.** Many instances require the measurement of vibrations of small objects to which it is not practical to attach a transducer. Even if a transducer could be attached, the added mass would alter the dynamic response to such an extent that any measurements would be meaningless. Optical-displacement transducers overcome these difficulties by using an optical connection. Two types of systems are commonly used. In one system a beam of light from a cathode tube is focused on a half-reflecting, half-absorbing foil target attached to the object. The lightbeam is adjusted so that it is centered on the interface between the reflecting portion and the non-reflecting portion of the target, as shown in Fig. 9-6. The position of the object or the instrument is adjusted so that the beam reflects back into the

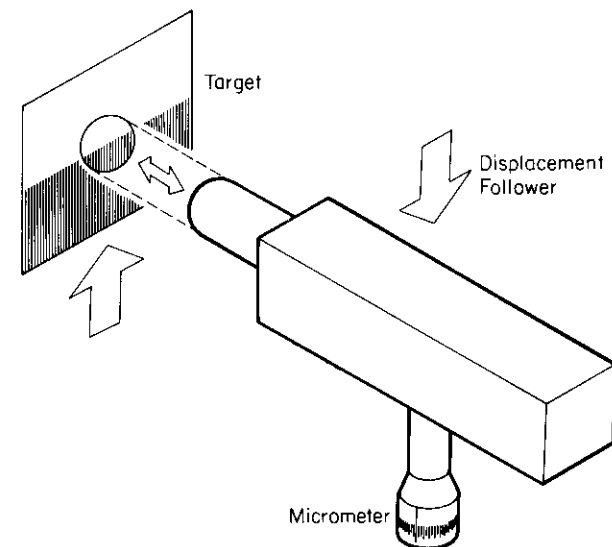


Figure 9-6. Schematic diagram of an optical displacement transducer.



lens of the instrument. When properly positioned, the instrument will continually adjust the spot of light so that only half of it falls on the reflective portion of the target. If the target moves, the instrument automatically repositions the spot. The spot position is directly proportional to the voltage applied to the deflection plates of the cathode-ray tube; this voltage is used as the output voltage. Since the instrument responds to the *relative* position of the object with respect to the instrument, calibration of the system can be accomplished by moving the instrument a known distance and measuring the change in output voltage. The static calibration factor obtained in this manner is applicable to frequencies as high as 5000 cycles/sec or higher.

Another type optical-displacement system uses a scanning technique to determine the position of an object. The only requirement for the object is that it have sufficient visual contrast such as dark against light, painted lines or even a machined edge. As the instrument scans the image, it detects the point of discontinuity and generates an output voltage proportional to the position of the discontinuity. With this arrangement it is possible to measure simultaneously the position of several points. Calibration of the output voltage in terms of displacement can be accomplished in the same manner as described for the other system.

The limit of resolution for the two types of optical-displacement transducers depends on the focal length of the lens used. The lower limit is about 10 to  $100 \times 10^{-6}$  in. The upper limit on displacement for the beam-type instrument is about 2 in., but for the scanning type there is no limit since the distance from the instrument to the object is not restricted by the requirement of being able to detect a small beam of light reflected from the object.

Optical-displacement transducers fulfill a need where vibration measurements must be made without touching the object to be measured. However, they are relatively expensive—prices for typical systems range from \$5,000 to \$10,000, depending on the accessories included with the instrument.

### Velocity Transducers

**Single-degree-of-freedom type.** The system shown in Fig. 9-4a may also be used as a velocity transducer. The relationship between the relative-velocity amplitude and the base-velocity amplitude is identical to Eq. (2-53), since multiplication of  $A_r$  and  $A_1$  by  $\omega$  leaves the equation unchanged. The comments on the optimum amount of damping for a displacement transducer apply equally well to the velocity transducer.

The output from a velocity transducer is generated by a coil moving through a magnetic field. Since the voltage induced in the coil is directly proportional to the relative velocity between the coil and the magnetic field, either the coil or the magnet is made part of the mass and the other component

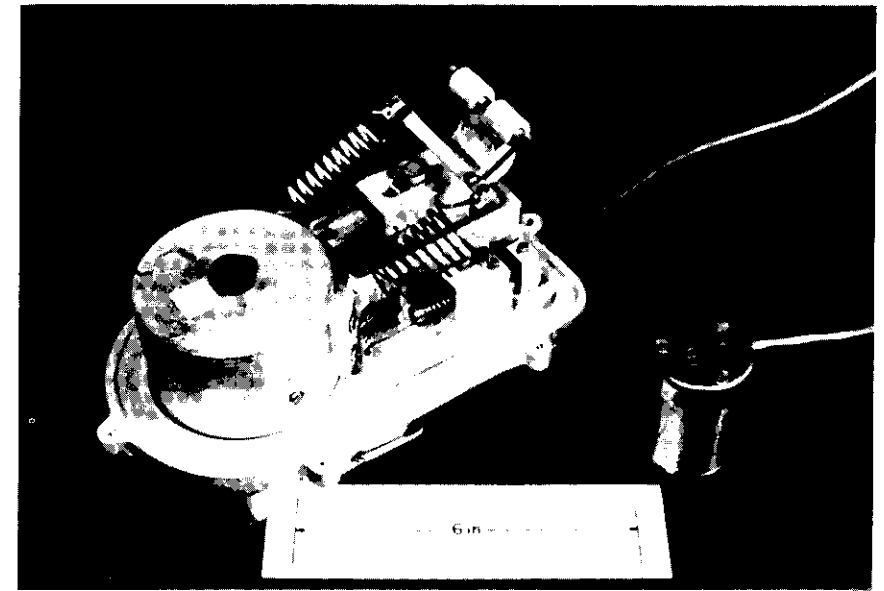


Figure 9-7. Velocity transducers.

is attached to the frame. The output voltage is then directly proportional to  $\dot{z}_r$ . Two types of velocity transducers and their components are shown in Fig. 9-7. For the larger transducer the circular mass is the permanent magnet and the coil is attached to the frame directly beneath it. The transducer is required to be relatively large in order to provide a low undamped natural frequency of 1 cycle/sec. The smaller transducer has an undamped natural frequency of about 7 cycles/sec. Its component parts, shown in Fig. 9-8, consist of a coil suspended by springs and a permanent magnet which is held by the case of the instrument.

The equivalent electrical circuit for a velocity transducer is shown in Fig. 9-9. The transducer is represented by a voltage generator  $E_o$  and a coil resistance  $R_{coil}$ . The oscilloscope impedance is shown as a pure resistance  $R_{scope}$ . The shunt resistance  $R_{shunt}$  is used to control the amount of damping in the transducer. Some of the damping arises from eddy currents caused by the relative motion between the magnetic field and metallic components of the transducer. A significant part of the damping is caused by the loss of energy associated with an electrical current passing around the loops of the circuit through each resistor. Since the damping is proportional to current, which is in turn proportional to voltage, the damping is exactly like viscous damping. By decreasing  $R_{shunt}$  the amount of damping is increased, but at the same time the output voltage to the oscilloscope is decreased. The normal

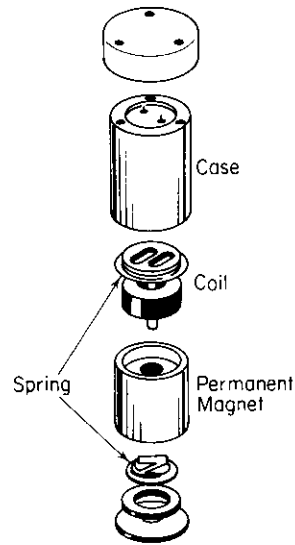


Figure 9-8. Schematic diagram of the components of a velocity transducer.

procedure is to choose  $R_{shunt}$  so that the damping is 60 per cent of critical. This is determined from the shape of the output-sensitivity curve for various values of  $R_{shunt}$ . Once the desired value is determined, a resistor having this value is permanently attached to the terminals of the velocity transducer.

Calibration of the transducer is achieved by exciting it with a known vibration. An electromagnetic vibration generator may be used to calibrate velocity transducers within the range of 5–2000 cycles/sec. Most vibration generators are specified in terms of output-force-amplitude capabilities. A small unit of 20-lb-force capacity will normally work well for calibration of transducers. Larger units having force-output capabilities in the tens of thousands of pounds are also available; however, the larger units are not readily portable because the weight of the vibration generator will be from

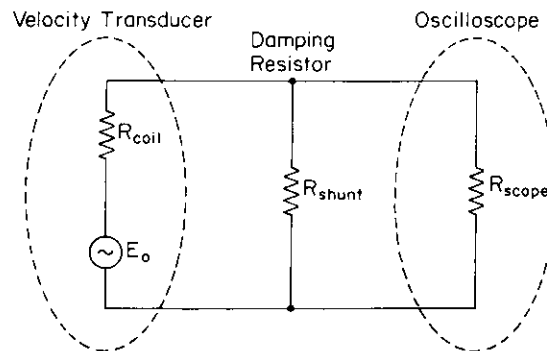


Figure 9-9. Schematic representation of a velocity transducer with a shunt resistance and connected to an oscilloscope.

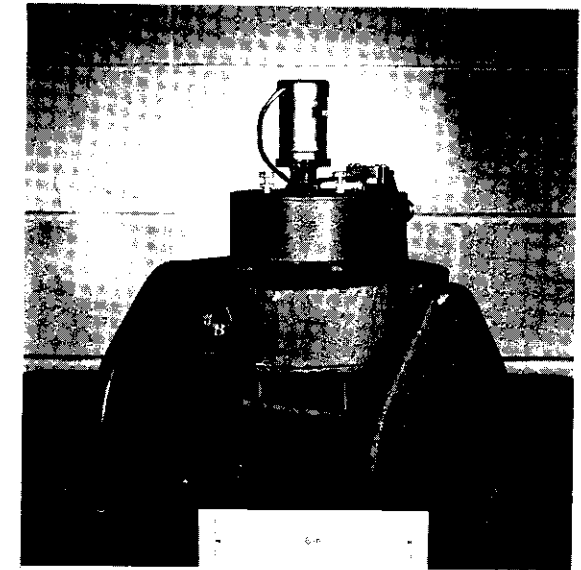


Figure 9-10. Electromagnetic vibration generator.

1 to 3 times its force-output capacity. Figure 9-10 shows an electromagnetic vibration generator having a 25-lb-force capacity. A velocity transducer is shown attached to the end of the armature of the vibration generator. The large circular component is an electromagnet which produces the magnetic field surrounding the driving coil attached to the armature. An oscillator is used to supply ac current to the driving coil at a controlled amplitude and frequency to provide the desired vibration.

The determination of the calibration curve by subjecting the transducer to a known vibration amplitude requires a means of determining accurately the amplitude of vibration. The simplest method is to have a transducer of known calibration mounted along with the transducer to be calibrated on a common rigid block. The output voltage of the transducer to be calibrated is compared to the standard to obtain the calibration factor, which is expressed as volts/(in./sec) for a velocity transducer. The disadvantage of this method is that no indication is available to tell whether or not the calibration factor of the standard is correct. Fortunately, it is possible to make an independent check by making use of the visual persistence of the human eye. It is found that for vibrations above about 30 cycles/sec, geometric patterns such as those in Fig. 9-11 can be used to determine the peak-to-peak-displacement amplitude. A spot will look like a line having a length equal to  $2A$ , as shown in Fig. 9-11a. The length of this line may be measured accurately with a microscope. Other patterns are also used, such as the two parallel lines in Fig. 9-11b and the wedge in Fig. 9-11c. The appearance at rest

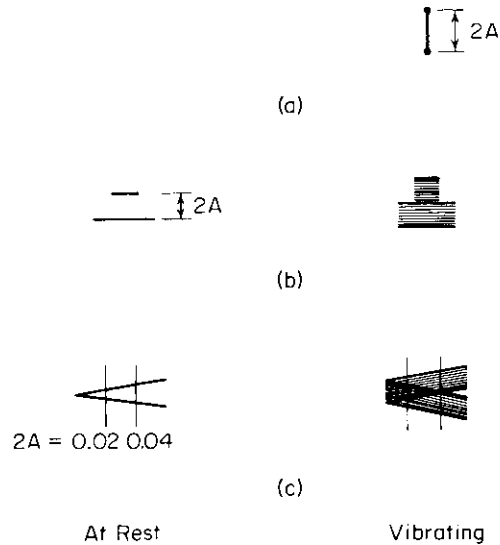


Figure 9-11. Geometric patterns used in the visual persistence method of measuring displacement amplitude.

and during vibration is shown for both of these patterns. Once the peak-to-peak-displacement amplitude is measured, it is possible, using the relationships for sinusoidal motion, to convert this measurement to velocity or acceleration.

When an optical-displacement transducer is used as the calibration standard, the calibration factor can be statically determined; and since the static calibration is applicable to frequencies of 5000 cycles/sec or more, this calibration will be adequate for the ranges of frequency used with most velocity transducers.

**Relative-velocity type.** There are many applications for which a relative-velocity transducer is the ideal instrument for making vibration measurements. The resonant-column apparatus for measuring dynamic properties of soils uses this type of transducer for measuring vibrations of a soil specimen: a typical coil-and-magnet system is shown in Fig. 9-12. The same unit can also be used to produce vibrations by connecting a source of alternating current to the coil. The permanent magnet is normally connected to a rigid frame and the coil is attached to the object to be vibrated or from which vibration measurements are to be made.

**Influence of cable length.** There are some circumstances in which the length of the cable between the velocity transducer and the measuring instrument must be relatively long. An equivalent-circuit diagram of a velocity transducer connected to an oscilloscope is shown in Fig. 9-13a. The circuit can be greatly simplified by first considering the relative



Figure 9-12. Driving coil and permanent magnet for a resonant-column device.

magnitudes of the various components. The velocity transducer and its shunt can be replaced by a single equivalent resistance  $R_o$ . This value will fall within the range of 500-5000 ohms for most velocity transducers. The cable resistance and capacitance depend on cable length. Typical values are near 0.01 ohm/ft and 30 picofarads/ft, respectively. If the oscilloscope impedance is 1 megohm, it can be seen that the effect of cable resistance is not important since 1,000,000 ft of cable would be required to produce a cable resistance of only one per cent of the oscilloscope resistance. The effect of cable capacitance on the circuit can be easily calculated by assuming  $R_{scope}$  to be infinite and analyzing the equivalent circuit in Fig. 9-13b. From

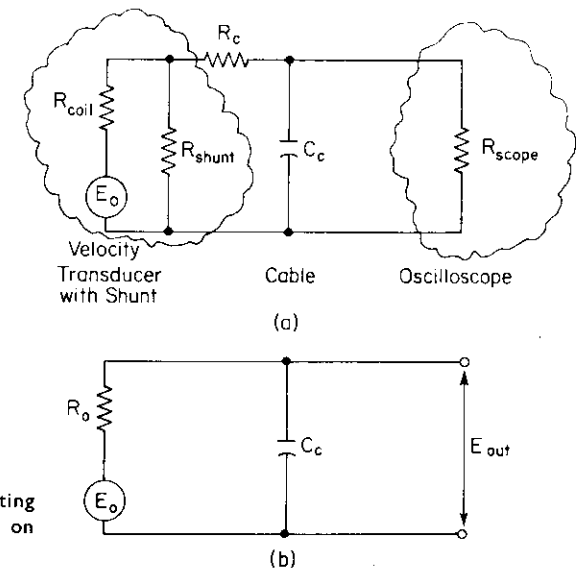


Figure 9-13. Circuits representing the effect of cable length on velocity transducers.

this we get

$$\begin{aligned} \frac{E_{out}}{E_o} &= \frac{Z_{cable}}{Z_o + Z_{cable}} = \frac{\frac{1}{\omega C_c}}{\sqrt{R_o^2 + \left(\frac{1}{\omega C_c}\right)^2}} \\ &= \frac{1}{\sqrt{1 + \omega^2 R_o^2 C_c^2}} \end{aligned} \quad (9-27)$$

For  $R_o = 1000$  ohms, and a cable 1000 ft long, the value of  $E_{out}/E_o$  is 0.995 at  $f = 1000$  cycles/sec. Thus, cable length for the average case may be ignored. If the cable length is such as to make a significant change in the output or if the effects cannot be calculated, the best approach is to calibrate the transducer with the cable in the circuit at the time of calibration.

*Acceleration Transducers*

The construction of an acceleration transducer, or accelerometer, is slightly different from the displacement or velocity transducer. Whereas a low natural frequency was required for the previous cases, a high natural frequency is required for an accelerometer. Figure 9-14 shows the basic principles applicable to the design of an accelerometer. The quantity of

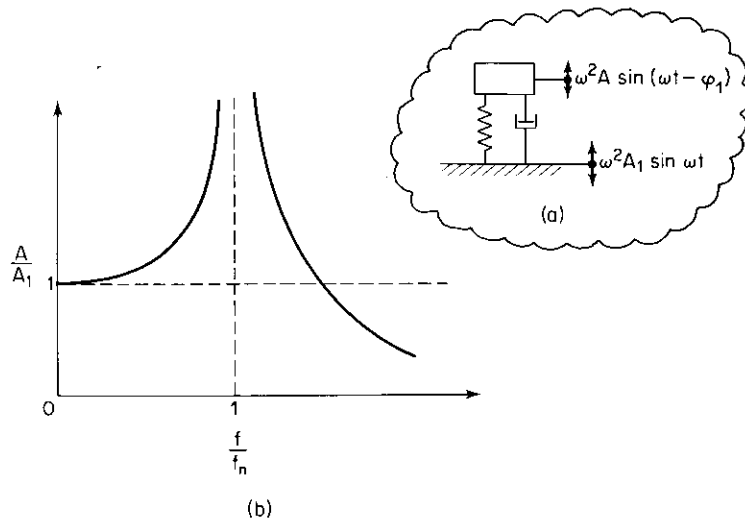


Figure 9-14. Ratio of the acceleration amplitudes of the mass and the support as a function of frequency.

interest for this case is the absolute acceleration of the suspended mass. Its relationship to the acceleration of the base is given by Eq. (2-66), which is repeated here for convenience:

$$\frac{A}{A_1} = \frac{\sqrt{1 + \left(2D \frac{\omega}{\omega_n}\right)^2}}{\sqrt{\left[1 - \left(\frac{\omega}{\omega_n}\right)^2\right]^2 + \left[2D \frac{\omega}{\omega_n}\right]^2}} \quad (2-66)$$

The phase angle between the acceleration of the base and the mass is given by

$$\tan \phi_1 = \frac{2D \left(\frac{\omega}{\omega_n}\right)^3}{1 - \left(\frac{\omega}{\omega_n}\right)^2 (1 - 4D^2)} \quad (2-68)$$

These have been plotted in Fig. 2-20.

At frequencies well below the natural frequency of the accelerometer, the accelerations of the mass and base are nearly the same. If the damping is small, measurements of the force in the spring attached to the mass provide a quantity that is directly proportional to the acceleration of the mass. Within the frequency range described above, this gives a measure of the acceleration of the base. The most common method of constructing an accelerometer is to use a quartz crystal or other piezoelectric material for the spring. A material having *piezoelectric* properties will develop an electrical charge directly proportional to the pressure applied to it. Hence, in a quartz-type accelerometer, the charge is directly proportional to the acceleration of the base at frequencies within the range where the acceleration of the mass and the frame are equal. A high-impedance instrument called a *cathode follower* is used to measure the charge developed by the piezoelectric crystal. A cathode follower is actually an impedance transformer that allows an oscilloscope or other measuring instrument to be used for measuring a charge voltage.

Accelerometer calibration is the same as for the velocity transducer. However, cable length is a critical part of the measuring circuit, in contrast to the relative insignificance of cable length for velocity-transducer calibration.

**Influence of cable length.** The circuit for a quartz accelerometer attached to a cathode follower is shown in Fig. 9-15. The value of the input resistance  $R_i$  of the cathode follower is greater than  $10^{12}$  ohms and can be considered infinite for periods of vibration that are less than the product  $R_i(C_i + C_c + C_a)$

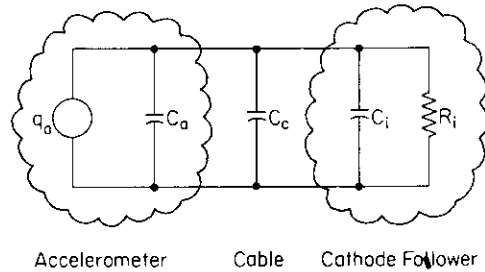


Figure 9-15. Circuit representing a piezoelectric transducer.

sec, which represents the  $RC$  time constant of the circuit. The  $RC$  time constant is found by multiplying the resistance in ohms by the capacitance in farads. The time in seconds obtained from this product represents the time for a charge in the circuit to decay to 36.8 per cent of its initial value. The per cent of the open-circuit output (output when  $R_i = \infty$ ) as a function of  $RCf$  is shown in Fig. 9-16. For high-frequency characteristics, the output voltage is governed by the total capacitance in the circuit. From Fig. 9-15 the voltage  $E_i$  measured by the cathode follower will be

$$E_i = \frac{q_a}{C_a + C_c + C_i} \quad (9-28)$$

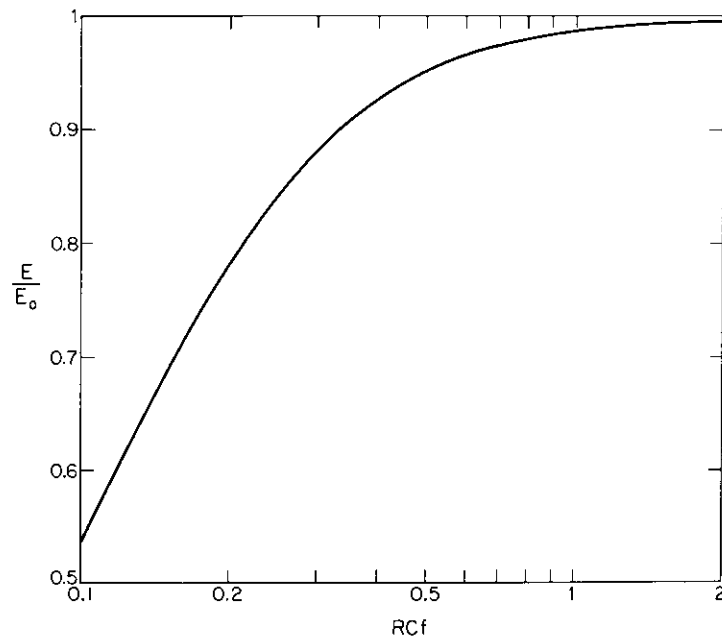


Figure 9-16. Effect of  $RC$  time constant on voltage sensitivity of a piezoelectric transducer.

where

- $C_a$  = accelerometer capacitance,
- $C_i$  = input capacitance of the cathode follower, and
- $q_a$  = charge developed by the accelerometer.

For the average accelerometer, the value of the cable capacitance  $C_c$  is of the same order as the other terms in Eq. (9-28), thus making cable capacitance an important factor. For this reason *very short cables must be used in order to prevent large reductions in the sensitivity of the accelerometer*. For example, a typical accelerometer may have a sensitivity of 60 mV/g with a 10-ft cable but a sensitivity of only 15 mV/g with a 100-ft cable.

The maximum range of frequency response of a piezoelectric accelerometer is limited to about 50 per cent of its natural frequency. However, this poses no serious problems, since for most cases the limit is hardly ever less than 1000 cycles/sec and is usually considerably higher.

A final word should be included regarding frequency measurements. For most cases the frequency indicated by the dial of the oscillator used to drive the vibration generator is sufficiently accurate. However, if a conversion is made from displacement to acceleration amplitude, the error will be approximately twice the error of the frequency measurement since the quantity  $\omega^2$  is involved. An oscillator-frequency error of 10 per cent will mean a 20 per cent error on acceleration. For critical work a more accurate frequency generator or an accurate frequency-measuring instrument is required.

#### 9.4 Cables and Connectors

There is an almost unlimited variety of cable and connector types available for electronic instrumentation. The purpose of this section is to acquaint the reader with the more common components and their application to vibration instrumentation.

##### Cable Characteristics

An ideal cable would act as a pure conductor of electricity and would have no effect on the signal that is transmitted through it. For many cases this condition can be assumed to exist, but in others the cable characteristics may be an important factor. A good example is the effect of cable capacitance on the calibration factor of a piezoelectric accelerometer. Most cable specifications include the amount of capacitance and resistance per foot of cable—although the latter quantity is sometimes omitted since it can be found in any

handbook or text on electrical engineering if the size of the conductor is known.

The term *characteristic cable impedance*, frequently encountered in the literature, refers to the impedance at the terminals of a semi-infinite cable. An analysis of such a cable indicates that it behaves like a pure resistance the value of which is specified as its characteristic impedance. An interesting aspect of this characteristic is that if a finite length of cable is terminated with a resistor having a value equal to its characteristic impedance, its electrical characteristics are the same as the semi-infinite cable. For example, when a regular TV-antenna cable, which is designated 300-ohm cable, is connected to the antenna terminals of a TV set that has an input impedance of 300 ohms it is the same as having the antenna connected to a semi-infinite cable. The reason for having this characteristic is so that high-frequency signals propagating along the cable will be completely absorbed at the end of the cable. If not properly terminated, some of the signal will be reflected back to the source and distort the transmitted signal. Fortunately, this problem does not have to be considered in the range of frequencies encountered in vibration measurements. As a rough guide, characteristic-impedance considerations do not become important until the wave length of the electrical signals is of the same magnitude as cable length.

### Cable Types

Figure 9-17 shows four types of conductors commonly used for instrumentation and which are discussed below.

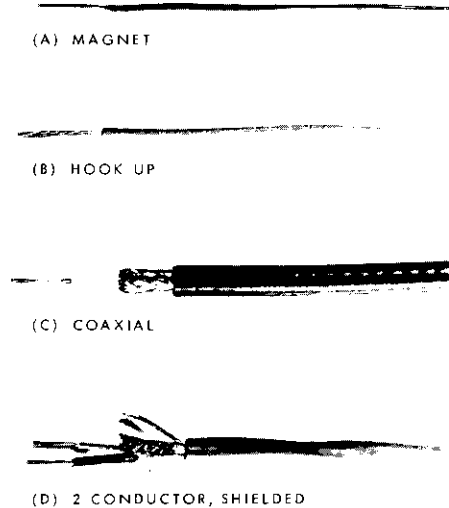


Figure 9-17. Wire and cable used for instrumentation.

**Magnet wire.** This type wire is used for winding coils for velocity pickups and other applications where many turns of wire are required. It has a special enamel insulation which increases the wire diameter by only a small percentage of its original diameter.

**Hookup wire.** This type wire is used for connections within electronic circuits and has a rubber or plastic insulation. The conductor is either solid or stranded depending on the flexibility requirements.

**Coaxial cable.** This cable contains a single insulated conductor surrounded by a conducting shield. This cable is used for signal measurements when the source is grounded on one side. The shield acts as the ground wire and the center conductor carries the signal.

**Two-conductor shielded cable.** This type cable contains two insulated conductors surrounded by a shield. The cable shown in Fig. 9-17d has a bare wire which makes contact with the foil shield and is used for the shield connection. The primary use of two-conductor shielded cable is for signal measurements with a differential amplifier. In this case, the signal is balanced between the two conductors and the shield is grounded to reduce electrostatic-noise pickup.

The foil shield has several advantages over braided shielding. It is much easier to work with when making connections and provides a 100 per cent shield cover, whereas the braided type provides only 70–95 per cent shield cover. In addition, in many cases the foil shield costs less than the braided shield.

### Connectors

Figure 9-18 shows most of the connectors commonly used with the cables in Fig. 9-17. The UHF and the BNC connectors are used with coaxial cables and are the most common types of connectors used on oscilloscopes. The UHF connector is a screw-type connection, while the BNC connector is attached to the instrument with a locking half-twist.

The Microdot connector is also used with a coaxial cable but is more specialized in its application, the most common being the connection between a piezoelectric transducer and a cathode follower. This connection requires a special coaxial cable which does not change capacitance when it is mechanically distorted. A change in capacitance would result in a change in signal level and a change in signal level is no different than unwanted noise; hence, it is necessary to use special low-noise coaxial cable.

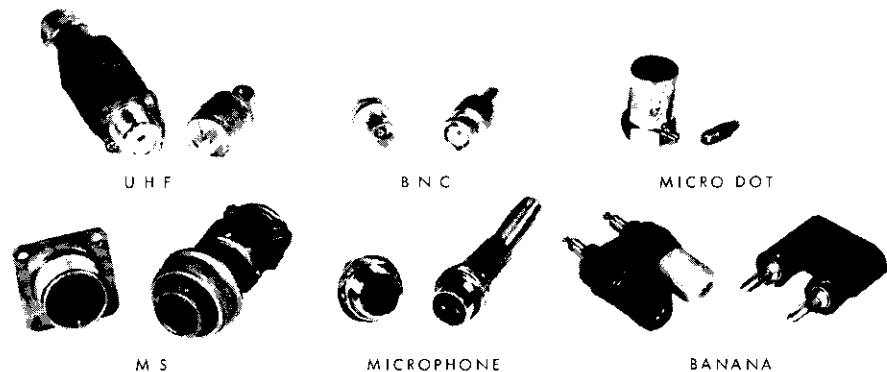


Figure 9-18. Connectors used for instrumentation.

The MS- and microphone-type connectors are used with two-conductor cables with the shield connected to the body of the connector. Both connectors come in various numbers of cable contacts, but the MS type has the greatest selection. The microphone-type connector has the distinct advantage of being easier to connect and disconnect. When the MS-type connector is used to connect two cables, it is almost impossible for the inexperienced person to decide what part to unscrew to disconnect the cables. This often causes the wires to be broken off inside the connector. With the microphone connector, this problem does not exist.

The banana-plug connector can be used where shielding is not important. Its low cost and ease of assembly make it a popular connector where large-level signals are involved.

### 9.5 Vibration Measurements for Field Tests

In general, there are two testing methods for measuring dynamic soil properties in the field. One method uses a source of steady-state vibration and the other method uses a single impact as a source of vibration. Theories given in Chap. 4 provide the basis for interpreting the measurements from these two tests. The steady-state-vibration test is used for determining the velocity of Rayleigh waves, from which the shear modulus of the soil can be calculated. The impact test provides information on the velocity of the *P*-wave. Both methods provide information on the variation of soil properties with depth and can be used to determine the location of boundaries between layers. Field methods and instrumentation used in performing these tests will be considered in this section.

After an installation is completed, it is desirable to make measurements to compare the performance of the design facility with that predicted by

design. Measurements are also required for analyzing vibrations of foundation and structural systems before and after corrective work. The results of these measurements may be used to develop refinements for the methods of design and analysis. Measurements may also assist in evaluating dynamic loads developed by machines.

#### *Vibration-Measuring Systems*

For most field work, velocity or acceleration transducers are used due to their small size, portability and ruggedness. Displacement measurements can be made using the same transducers with the addition of electronic integrators.

Vibration-measurement systems to be used in the field should meet several basic requirements. The first and most important requirement is the ability to measure vibrations over as wide a range as possible for both frequency and amplitude. This allows the person making the measurements to cope with unexpected vibration characteristics which often occur in real problems. A second requirement is that the system provides for recording the vibration for later analysis. The recording should permit inspection at the measurement site so that another recording can be made if the first one is incomplete. A third requirement is that the system obtain two simultaneous vibration measurements recorded on a common time base in order to verify phase relationships needed to determine modes of motion or any other quantity requiring two simultaneous measurements. As a final requirement, the system must be capable of being easily transported by one or two persons.

Two general systems meeting the above requirements are used at the University of Michigan Soil Dynamics Laboratory. These are shown in Figs. 9-19 and 9-20. The system shown in Fig. 9-19 consists of a dual-beam oscilloscope and a Polaroid camera. The two velocity transducers shown can be used to measure vibrations simultaneously at any two locations. Two-conductor shielded cables are used with the differential amplifiers of the oscilloscope in order to eliminate electrostatic noise from the traces. The distinct advantages of this system are the wide ranges of velocity amplitude and frequency that can be measured and the ability to observe vibrations without recording them. Typical specifications for the components of this system are given in Table 9-3. The average cost of this system is about \$1500-2000.

The system shown in Fig. 9-20 consists of a dual-channel recorder with two velocity transducers. Two-conductor shielded cables are also used with this system to eliminate electrostatic noise from the two traces. The pens for this recorder use a heated stylus that writes on a special wax-coated paper by melting the wax. Writing by this method rather than by ink writing

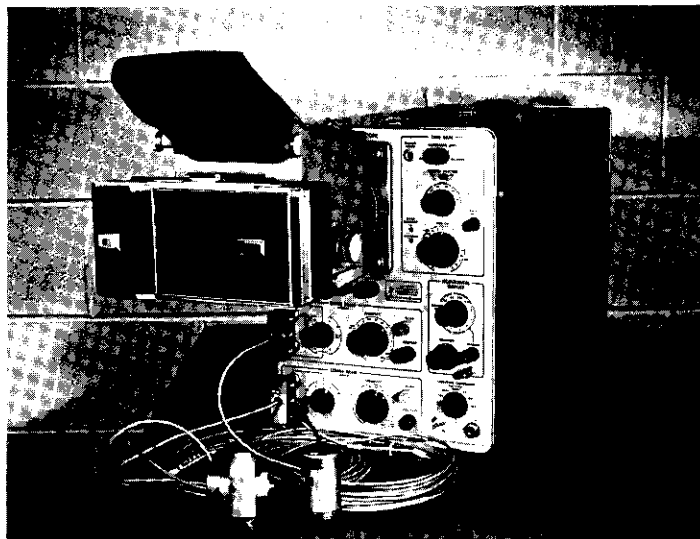


Figure 9-19. Dual beam oscilloscope and accessories used for vibration measurements.

is recommended for portable systems as it requires much less maintenance. There are two advantages of this system over that shown in Fig. 9-19. First, the operation of the instrument is so simple that a person can learn to operate it within a very short time. The operation of an oscilloscope, however, requires a certain degree of practice to become proficient. Second, it is possible, with the system in Fig. 9-20, to obtain continuous recordings over a longer time interval than obtainable with an oscilloscope. The disadvantages of the recorder when compared with the oscilloscope are that it is less sensitive and the frequency response is limited to about 100 cycles/sec. However, except in a few cases, these are not important drawbacks. The cost of a system like that shown in Fig. 9-20 is about \$2500-3000. Typical specifications are listed in Table 9-4.

Table 9-3. Typical Specifications for the Vibration Measuring System in Fig. 9-19

Oscilloscope	
Sensitivity:	0.2 mV/cm-20 V/cm
Horizontal Sweep:	5 sec/cm-1 microsec/cm
Velocity Transducers	
Natural Frequency:	7 cycles/sec
Nominal Sensitivity:	1.0 volt/(in./sec)

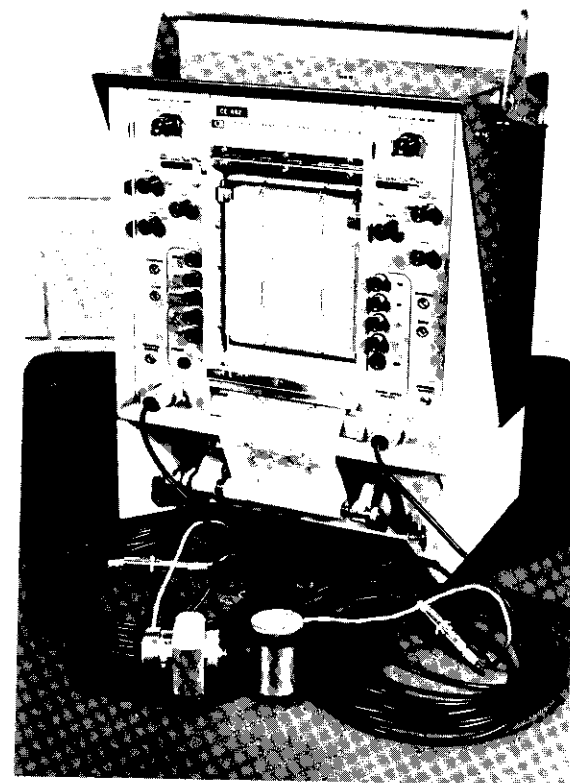


Figure 9-20. Two-channel recorder used for vibration measurements.

Table 9-4. Typical Specifications for the Vibration-Measuring System in Fig. 9-20

Recorder	
Sensitivity:	5 mV/cm-50 V/cm
Chart Speed:	0.1-10 cm/sec
Velocity Transducers	
Same as in Table 9-3	

#### *Vibration Measurements of Rigid Foundations*

Vibration measurements of a rigid foundation can reveal not only the amplitudes of vibration but also the mode of vibration. An understanding of what to measure and where to measure it will save time in the field and



provide more complete information from which to make an analysis or check a design.

The first requirement in making a satisfactory vibration measurement is good coupling between the transducer and the vibrating object. For measuring low-amplitude vibrations of hard surfaces, the weight of the transducer is sufficient to hold it in place. For vibration levels greater than several tenths the acceleration of gravity, hand pressure can be used to hold the transducer firmly against the vibrating object. It is also possible to use a quick-drying glue or even wax squeezed between two flat surfaces for a quick, temporary connection.

Using two vibration transducers makes it possible to determine the mode of vibration of a rigid foundation. There are essentially two types of motion to be measured; translation and rotation. These may occur along or about any axis of the foundation. In Fig. 9-21, four independent motions are shown for a rectangular foundation. It is recognized that in general the motion of a foundation will be a superposition of any number of these, but they are separated here for ease of illustration.

**Vertical motion.** For a foundation vibrating in the vertical mode, the amplitude of motion will be equal at all points and in-phase as shown in Fig. 9-21a. If the output of one transducer is used as a reference signal, the output from the other transducer placed on at least three noncollinear points

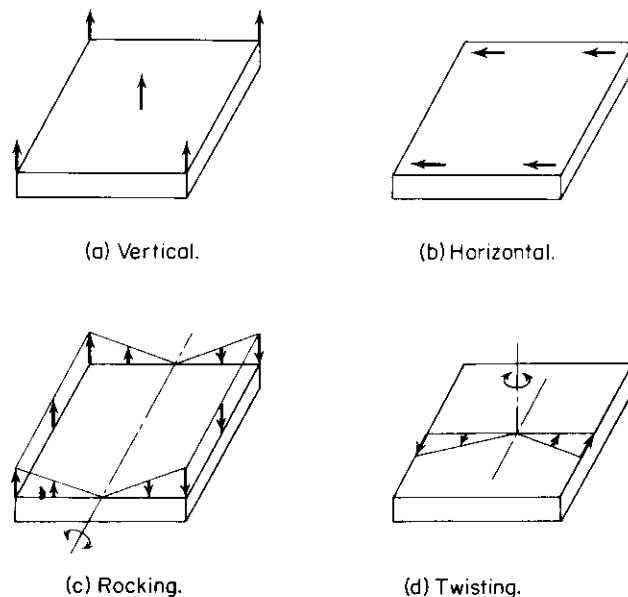


Figure 9-21. Components of motion for a rigid footing.

may be compared for both amplitude and phase relationships. This will indicate immediately whether or not the motion is predominantly in the vertical direction.

**Horizontal motion.** Horizontal motion as shown in Fig. 9-21b is indicated by in-phase equal horizontal vibration of at least three noncollinear locations on the foundation. This is the same type measurement as used to detect vertical motion.

**Rocking motion.** In Fig. 9-21c, the relative vertical amplitudes increase linearly with respect to the distance from a horizontal line across the foundation. However, there is a  $180^\circ$  phase difference between vibrations on opposite sides of the line of zero displacement. Vibrations measured at the ends and at the center will clearly show this if rocking motion is present.

**Twisting motion.** For the rectangular foundation shown in Fig. 9-21d, twisting motion will result in horizontal vibrations in a direction perpendicular to a radius from the axis of rotation. The amplitude increases in direct proportion to the distance from the axis of rotation. There is also the  $180^\circ$  phase shift on opposite sides of the axis of rotation.

#### *Rayleigh-Wave-Velocity Measurements*

The procedure for determining dynamic soil properties from the measurements of Rayleigh-wave velocities requires a source of harmonic vibration at the surface of the soil. The wave length of the resulting surface waves is determined by measuring the distance between points that are vibrating in phase with the vibration source. Moduli may then be computed from the measured wave length and frequency of vibration.

The source of steady-state vibration can be either an electromagnetic oscillator modified to produce vibrations when it is placed on the surface of the soil or a rotating-mass mechanical oscillator. The U.S. Army Waterways Experiment Station has developed equipment for producing steady-state vibrations and has used it extensively to obtain soil data for dynamics problems. A small electromagnetic oscillator of about 25-lb-force capacity, shown in Fig. 9-22, is used for high-frequency vibrations (30–1000 cycles/sec). Wave lengths produced in this frequency range are generally less than 20 ft and hence only provide information to depths of 10 ft or less. Longer wave lengths may be obtained using lower frequencies. These may be generated using a rotating-mass oscillator like the one shown in Fig. 9-23. The greatest problem at low frequencies is producing enough vibration to make the resulting ground motions greater than the ambient level. This requires larger

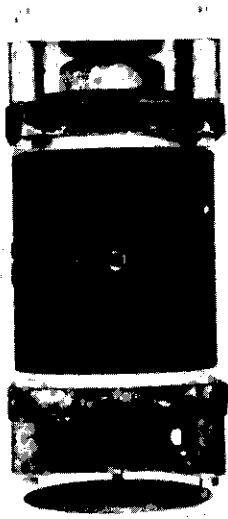


Figure 9-22. Electromagnetic oscillator modified to produce ground vibrations (U.S. Army photograph).

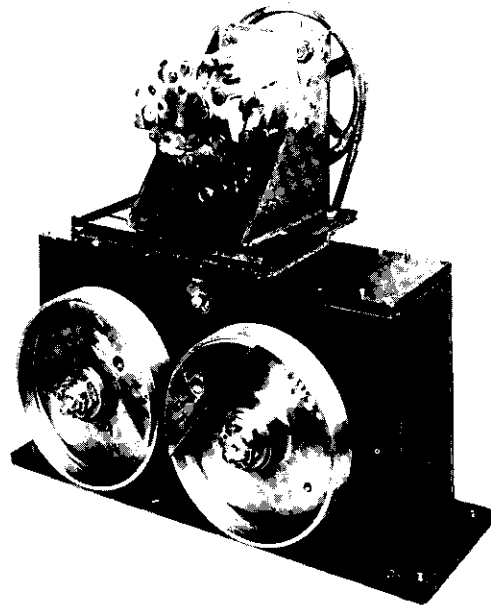


Figure 9-23. Rotating mass type oscillator used to produce low-frequency ground vibrations (U.S. Army photograph).

input forces than are possible with electromagnetic oscillators; the rotating-mass oscillator is the easiest method of obtaining them at low frequencies.

Once a source of vibrations is established, the wave lengths are measured by comparing the phase relationship of vibrations at various radii from the source with the vibrations of the source. Normally, points that are in phase as well as points that are  $180^\circ$  out of phase are measured, the latter representing half-wave-length intervals. A typical set of data is shown in Fig. 4-19 with the wave number plotted as a function of distance from the source for various values of frequency. This information is used directly in the calculation of Rayleigh-wave velocity for each wave length.

#### *P-wave-Velocity Measurements*

The measurement of *P*-wave velocity through a soil is done using the refraction survey, for which a source of impulsive energy is required along with

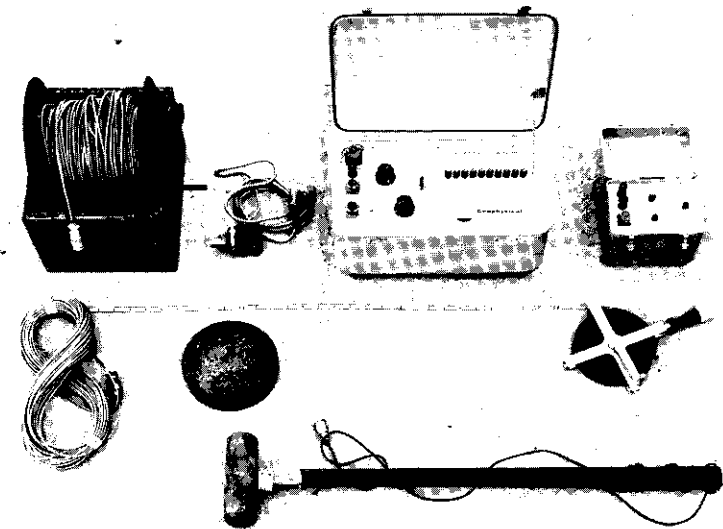


Figure 9-24. Electronic timer and accessories used for refraction surveys (U.S. Army photograph).

a method of measuring the time interval between the instant of impact and the first arrival of a *P*-wave at a known distance from the source. The source of impulsive energy may be an explosive charge or a hammer struck against the ground. If an explosive charge is used, a vibration transducer and a recording channel are necessary for every point on the ground at which measurements are to be taken. The hammer-blow method allows the impulse to be repeated; thus, only one vibration transducer is required. Except for oil-exploration surveys, the hammer-blow method is used most extensively because of its simplicity.

The measurement of the time interval from impact to first arrival can be made either with an electronic timer or with an oscilloscope. A portable system with an electronic timer is shown in Fig. 9-24. The timer is started by a switch that is activated by the impact of the hammer, and the signal from the transducer at the time of arrival of the first wave stops the timer. The gain of the amplifier can be adjusted so that background noise does not stop the timer. However a disadvantage is that the instrument does not provide a picture of the wave form. An oscilloscope overcomes this disadvantage, and is also very useful when the level of background vibration is high. The essential parts of the system are shown in Fig. 9-25. Measurement of travel time with an oscilloscope is done by triggering the horizontal sweep with a signal generated by the impact of the hammer. When this is done, a trace

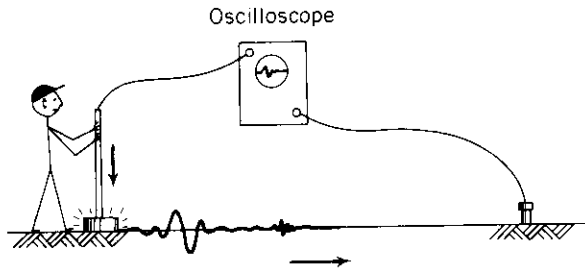


Figure 9-25. Basic system for a refraction survey.

may be observed, as shown in Fig. 9-26. The travel time is calculated by multiplying the sweep rate of the oscilloscope by the distance from the beginning of the trace to the point of first arrival. By using repeated blows with the hammer, it is possible to pick out the first arrival even in the presence of ambient vibrations. A high-persistence or storage oscilloscope has a distinct advantage for this type of work. By changing slightly the vertical position of the sweep between consecutive impacts of the hammer, several traces can be stored and viewed simultaneously to pick off the trace distance used in the travel-time computation. Using a normal oscilloscope requires picking off the trace distance as the sweep occurs, and many blows may be required to obtain an accurate reading. The storage oscilloscope eliminates this problem since the trace can be studied for as long as necessary.

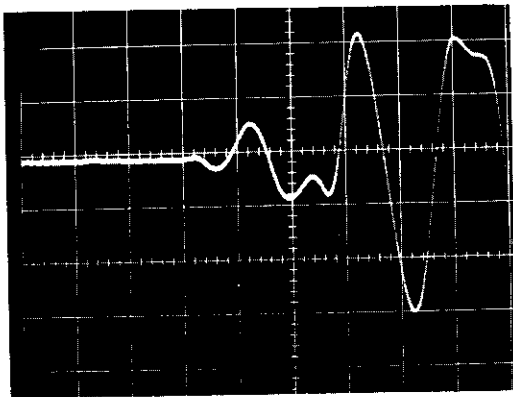


Figure 9-26. Oscilloscope trace obtained for measuring the time of arrival of a *P*-wave using the system shown in Fig. 9-25.

### 9.6 The Resonant-Column Test

For laboratory measurements of dynamic soil properties, the resonant-column test is the most convenient. This test is based on theoretical solutions given in Chap. 3 which relate the dynamic modulus of the column to its resonant frequency. Other solutions that take internal damping of the soil

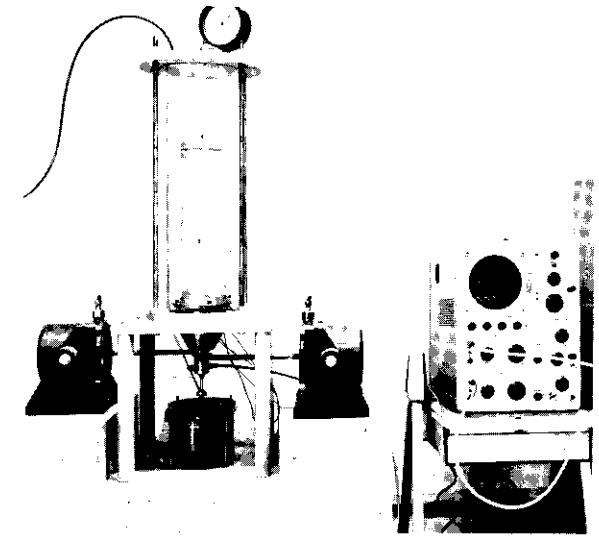


Figure 9-27. Resonant-column apparatus used at the U.S. Army Waterways Experiment Station, Vicksburg, Mississippi (U.S. Army photograph).

into account (for example, Hardin, 1965) have shown that the elastic solutions are satisfactory within the range of damping developed for small-strain amplitudes in the resonant-column test.

The various types of apparatus that have been used in the resonant-column test all give similar results. However, the designs differ primarily because of the boundary conditions imposed on the soil column. Wilson and Dietrich (1960) described an apparatus in which the soil column is attached to a vibrating base having a resonant frequency several times that of the specimen. The boundary conditions for this system closely represent a fixed-free condition. The base is constructed so that both longitudinal and torsional vibrations may be applied to the specimen. An apparatus based on the same principle and used by the U.S. Army Waterways Experiment Station is shown in Fig. 9-27. Note that three electromagnetic vibration generators are used to apply the vibrations to the base of the specimen. The middle vibrator is used for longitudinal vibrations, while the other two are arranged for application of torsional vibrations. Accelerometers are attached to the top of the soil specimen, which is enclosed in a pressure cell. The frequency of the vibration generators may be adjusted to the maximum response of the specimen in order to determine its resonant frequency.

Hardin and Richart (1963) described two types of apparatus for running the resonant-column test, and components of these are shown in Fig. 9-28. Figure 9-28a shows the torsional-vibration exciter for a free-free end condition. An identical unit attached to the opposite end of the specimen acted as a transducer to measure torsional vibrations. Each unit consisted of four electromagnets wired to produce an oscillating torque on a bar magnet

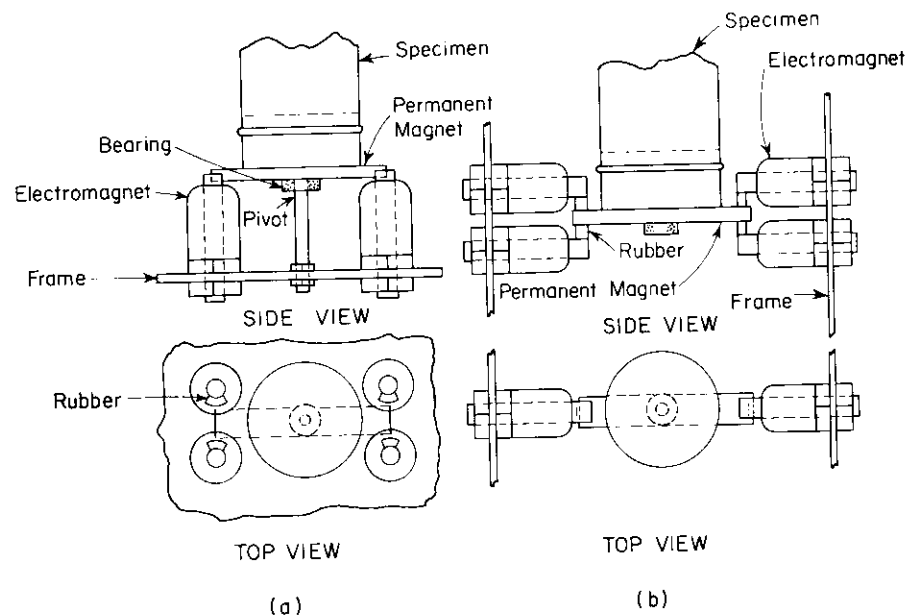


Figure 9-28. Driving components for a free-free resonant-column apparatus (from Hardin and Richart, 1963).

attached to the end cap of the specimen. Small rubber pads prevented the magnet from attaching itself to the end of one of the electromagnets, while at the same time offering very little torsional restraint to small-amplitude vibrations. This system produced resonance with maximum amplitudes occurring at each end of the specimen and a node point in the center. A similar arrangement was used to apply longitudinal oscillations (Fig. 9-28b); the same permanent magnet is used but the electromagnets are placed and wired to produce vibrations in the longitudinal direction.

Hall and Richart (1963) described two fixed-free resonant-column devices, the main components of which are shown in Fig. 9-29. The base of the specimen was rigidly attached to a frame and the top was left free. For torsional vibrations the mechanism shown in Fig. 9-29a was used both to apply a torque and to measure torsional oscillations. Both the driver and pickup consisted of a coil surrounding a small permanent magnet. The only physical connection between the top of the specimen and the frame of the apparatus was the small wires attached to the coils. The well-defined boundary conditions offered by this apparatus allowed the measurement of soil damping to be made by turning off the driving coil and recording the decay of vibrations. For longitudinal vibrations the mechanism shown in Fig. 9-29b was attached to the top of the specimen. Two coils surrounded by magnetic fields provided the oscillating axial force and the means of measuring

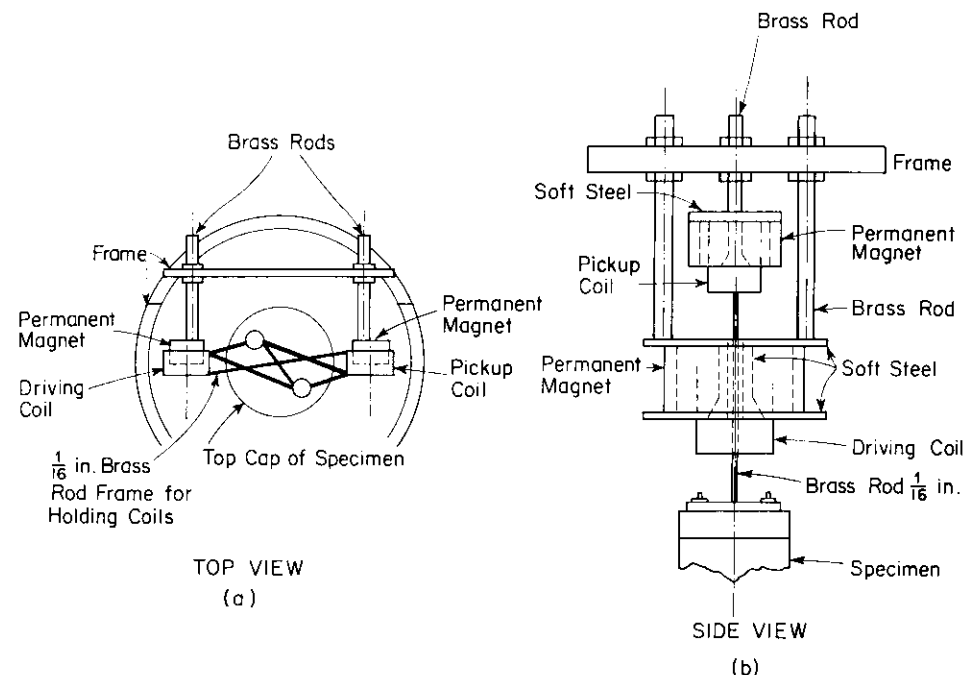


Figure 9-29. Driving and measuring components for a fixed-free resonant-column apparatus (from Hall and Richart, 1963).

the resulting vibrations. This system also made it possible to measure damping by recording the decay of free vibrations.

For the fixed-free systems described, only small changes in specimen length could be tolerated before interference between coils and magnets occurred. When this happened, the apparatus no longer worked unless adjustments were made. To overcome this problem, a torsional resonant-column apparatus was developed at the University of Michigan; it has rectangular coils and magnets in the shape of C-clamps as shown in Fig. 9-30. With this arrangement the specimen could change length by 0.5 in. without affecting the operation of the apparatus. In this apparatus as well as in the torsional apparatus described by Hall and Richart (1963), only one coil was used to apply the torque to the free end of the specimen. This introduced a transverse force to the specimen and caused bending. However, the resonant frequencies for bending and torsion are different and the damping is small enough so that at the torsional resonant frequency of the specimen the amount of bending was insignificant.

For the system shown in Fig. 9-30, the driving coil and pickup coil were oriented  $90^\circ$  to each other. There are two reasons for this. First, when two

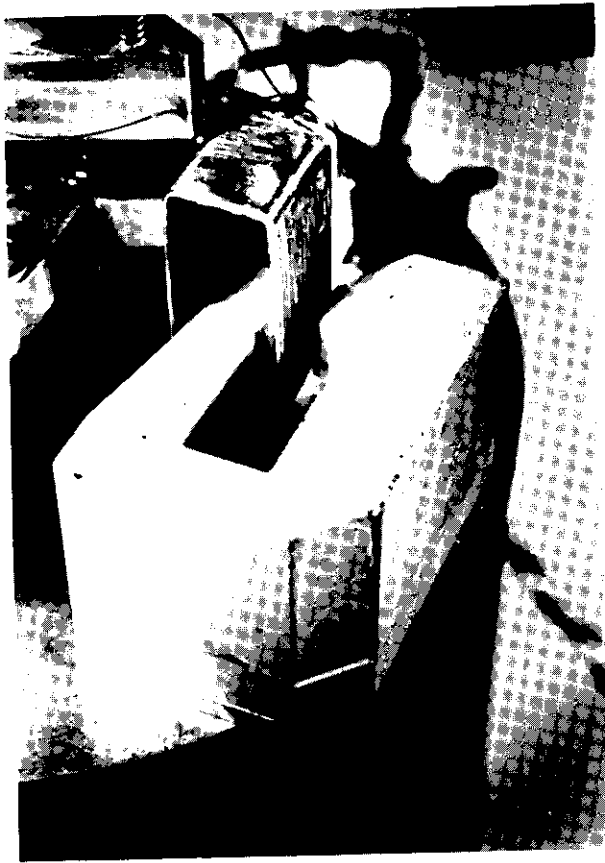


Figure 9-30. Rectangular driving coil and permanent magnet used to allow movement in the vertical direction.

coils are placed next to each other, an alternating current flowing in one coil will induce in the adjacent coil a voltage whose magnitude is dependent on the orientation of the coils. By orienting the coils at  $90^\circ$  the induced voltage is reduced to a minimum. Any remaining induced voltage may be reduced further using a differential amplifier. The second advantage of using the  $90^\circ$  orientation is that only torsional vibrations produced by the driving force are measured, since any bending would move the coil parallel to the magnetic field and produce no signal. The torsional vibrations cause the coil to move perpendicular to the magnetic field and generate a signal proportional to the rotational velocity.

Hardin and Music (1965) developed a resonant-column device which allowed axial loads to be applied to the specimen during the measurement of the resonant frequency. The previous equipment could be used only to test soils under the application of pressure in an enclosed cell. The key part to Hardin's apparatus is the top-cap system shown in Fig. 9-31.

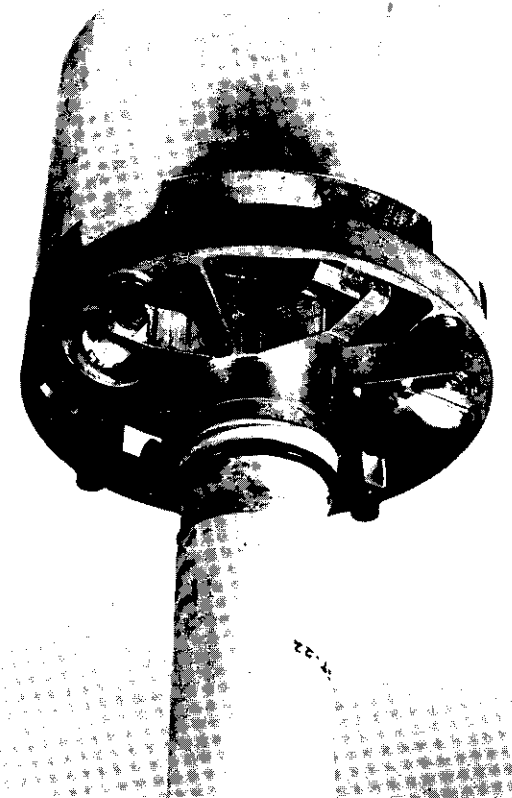


Figure 9-31. Top cap system of the Hardin oscillator.

The bottom of the specimen is attached to an ordinary base plate of a triaxial cell; the top-cap system is then lowered and connected to the top of the specimen. The top cap is initially counterbalanced so that no load is applied to the soil specimen. Once the system is set up, stresses can be applied to the specimen as they are applied in an ordinary triaxial test. Figure 9-31 shows the thin flexible members that connect the top cap to the outer edge of the frame. These provide flexibility in the torsional direction but are stiff axially for application of axial loads. The influence of the apparatus is calibrated and taken into account when calculating the modulus of the soil from test data.

In addition to the resonant-column apparatus there are other components used to perform the test. The first item is an oscillator to provide a source of ac voltage at frequencies over the range anticipated for the apparatus. Any commercially available low-frequency oscillator is adequate. The output of the oscillator is fed into a power amplifier to supply current to the driving coils of the resonant-column device. In some cases, however, the output from the oscillator is sufficient and the power amplifier is not necessary. To

determine the resonant frequency of the soil column from the output of the vibration transducer, an oscilloscope is used. Although a meter will work as well as an oscilloscope for determining the resonant frequency, it does not indicate the wave form of the output, which is a check on whether the system is operating properly. When a malfunction occurs, it usually appears in the output signal as a distortion of the sine wave.

Although the above instruments are all that are needed for the routine test, research purposes often require more accurate frequency measurements. Resonant-frequency readings with a precision of a few parts in 100,000 have been measured using a digital counter. Obtaining the point of resonance with such precision cannot be accomplished by observing the frequency at peak response because the method is insensitive to slight errors in frequency. The

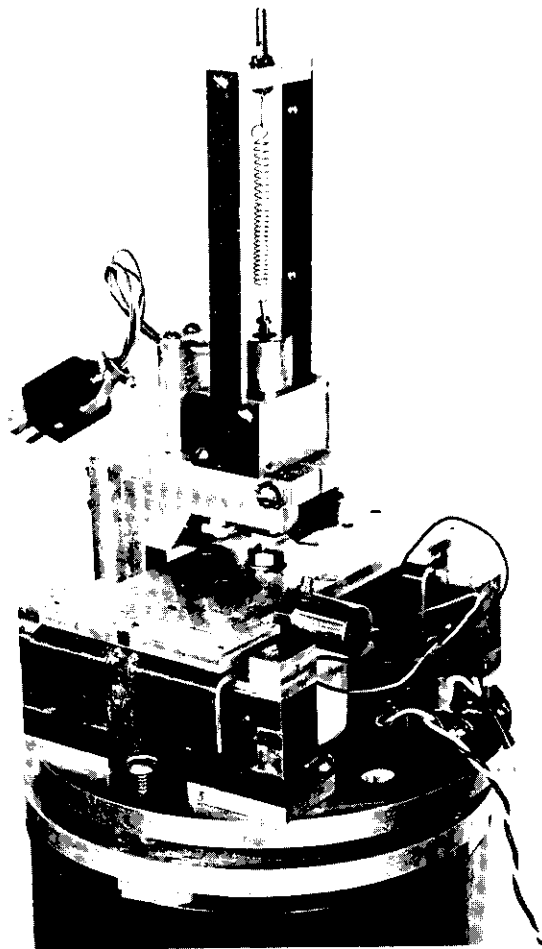


Figure 9-32. Driving system for a fixed-free resonant-column apparatus designed for large strain amplitudes.

required precision is obtained by measuring the point at which force—or torque—and velocity are in phase. This corresponds to a  $90^\circ$  phase angle between force and displacement and, since the damping is small, the phase angle changes rapidly near resonance. If force and velocity signals are viewed as an  $x$ - $y$  plot on an oscilloscope, the point of resonance will produce a display which is a straight line. If the frequency is slightly off resonance, an ellipse will appear. This method of measuring resonance has been found much faster than any other method and is actually used as a routine method.

All of the resonant-column systems described above were designed to operate at small-strain amplitudes (less than  $10^{-5}$ ). Studies of dynamic soil behavior at relatively high strain levels (greater than  $10^{-4}$ ) were conducted by Drnevich (1967) using a torsional resonant-column apparatus developed at the University of Michigan. The driving system used is shown in Fig. 9-32. It consisted of four driving coils, three of which can be seen in the figure. Permanent magnets in the shape of C-clamps were used to provide the magnetic field for each coil. Also shown in the figure is an LVDT with the core attached to a spring supported by a frame. This was used to measure changes in the length of the soil specimen during tests.

Since a solid cylindrical specimen is not subjected to uniform-strain conditions when twisted, a hollow specimen was used. One of these is shown in Fig. 6-10. Results of some of the tests using this apparatus are presented in Chap. 6.

The resonant-column test may be considered by some to be a tool only for soil dynamics, but this is not true. Insofar as many static soil-mechanics problems deal with small-elastic-strain conditions, the resonant-column test can provide information at these strain levels. The test can also be used as a research tool to study changes in soil properties at small strains. This can be accomplished without disturbing the specimen and hence provides a non-destructive testing technique. Because of recent improvements in testing apparatus and theories for analysis, the resonant-column test is becoming a common laboratory procedure.

# 10

## DESIGN PROCEDURES FOR DYNAMICALLY LOADED FOUNDATIONS

### 10.1 Introduction

A design procedure must deal with three major questions: (1) What is the condition for failure of the design function and how is it defined? (2) What are the loads or external conditions which produce the failure? (3) What is the analytical procedure to be followed for relating the applied loadings to the failure condition? Another factor, introduced after evaluating the uncertainties related to each of foregoing, is the factor of safety.

In the design of machine foundations or other dynamically loaded foundations, successive corrections are used to arrive at the final physical system. A set of physical parameters are assumed and then analyzed to determine if the design conditions are satisfied. If they are not satisfied, then some of the physical parameters are varied and the process is repeated. With this approach the *criteria for failure of the design function and the applied loadings* must be carefully determined, because these establish a control of the procedure. The analysis should describe clearly the influence of each of the major physical variables involved, in order that an intelligent choice can be made during successive corrections in design.

The design procedures to be discussed in this chapter relate primarily to the dynamic response of foundations subjected to steady-state vibrations or

transient loadings. Generally, the supporting soil is considered to be in a stable condition such that it does not compact or change geometry unless the design conditions are exceeded. The emphasis of the chapter lies in the procedure for carrying out the dynamic analyses after the design conditions have been established.

### 10.2 Design Criteria

The end product of the design procedure is the determination of a foundation-soil system which satisfactorily supports equipment or machinery. The supported unit may be the source of dynamic loads applied to the system or it may require isolation from external excitation. In each case the criteria for satisfactory operation of the unit dictate the design requirements.

In Table 10-1 are listed some criteria which may be considered during the design of the foundation system. This checklist is included only as a guide; all topics may not be applicable to a particular problem, and additional topics may be included to cover special installations.

The design criteria most often encountered relate to the dynamic response of the foundation. These are expressed in terms of the limiting amplitude of vibration at a particular frequency or a limiting value of peak velocity or peak acceleration. Figure 10-1 indicates the order of magnitudes which may be involved in the criteria for dynamic response. Five curves limit the zones for different sensitivities of response by persons, ranging from "not noticeable" to "severe." These categories are for persons standing and being subjected to vertical vibrations. The boundary between "not noticeable" and "barely noticeable" is defined by a line at a slope of  $-1$  on the log-log plot which represents a peak *velocity* of about 0.01 in./sec. The line dividing the zones of "easily noticeable" and "troublesome" represents a peak *velocity* of 0.10 in./sec.

The envelope described by the shaded line in Fig. 10-1 as "limit for machines and machine foundations" indicates a limit for *safety* and *not a limit for satisfactory operation of machines*. Operating limits for machines are discussed in the next section. The shaded limit for machines in Fig. 10-1 is composed of two straight lines. Below about 2000 cycles/min this limit represents a peak velocity of 1.0 in./sec, and above 2000 cycles/min it corresponds to a peak acceleration of  $(0.5)g$ .

Two curves are also included in Fig. 10-1 to indicate limiting dynamic conditions associated with *blasting*. These magnitudes of motion correspond to effects applied once, or at most repeated a few times. They definitely do not apply for steady-state vibrations. The line at the lower limit of the zone "caution to structures" corresponds to a peak velocity of 3 in./sec.

Table 10-1. Checklist for Design Criteria

- I. Functional Considerations of Installation
  - A. Modes of failure and the design objectives
  - B. Causes of failure
  - C. Total operational environment
  - D. Initial cost and its relation to item A
  - E. Cost of maintenance
  - F. Cost of replacement
- II. Design Considerations for Installations in Which the Equipment Produces Exciting Forces
  - A. Static bearing capacity
  - B. Static settlement
  - C. Bearing capacity: Static -- Dynamic loads
  - D. Settlement: Static + Repeated dynamic loads
  - E. Limiting dynamic conditions
    - 1. Vibration amplitude at operating frequency
    - 2. Velocity
    - 3. Acceleration
  - F. Possible modes of vibration—coupling effects
  - G. Fatigue failures
    - 1. Machine components
    - 2. Connections
    - 3. Supporting structure
  - H. Environmental demands
    - 1. Physiological effects on persons
    - 2. Psychological effects on persons
    - 3. Sensitive equipment nearby
    - 4. Resonance of structural components
- III. Design Considerations for Installation of Sensitive Equipment
  - A. Limiting displacement, velocity, or acceleration amplitudes
  - B. Ambient vibrations
  - C. Possible changes in ambient vibrations
    - 1. by construction
    - 2. by new equipment
  - D. Isolation of foundations
  - E. Local isolation of individual machines

It is important to note from Fig. 10-1 that the magnitudes of vibration involved in these criteria are much smaller than the displacements usually considered in the designs of foundations for static loads. For example, at a frequency of 1000 cycles/min, an amplitude of 0.0001 in. may be noticed by persons, whereas it takes a motion of 0.01 in. at the same frequency to cause damage to machinery or machine foundations. Therefore, the order of magnitude of vibration amplitudes to be considered in this chapter will nearly always be less than 0.01 in. and will usually be of the order of 0.005 to 0.0001 in.

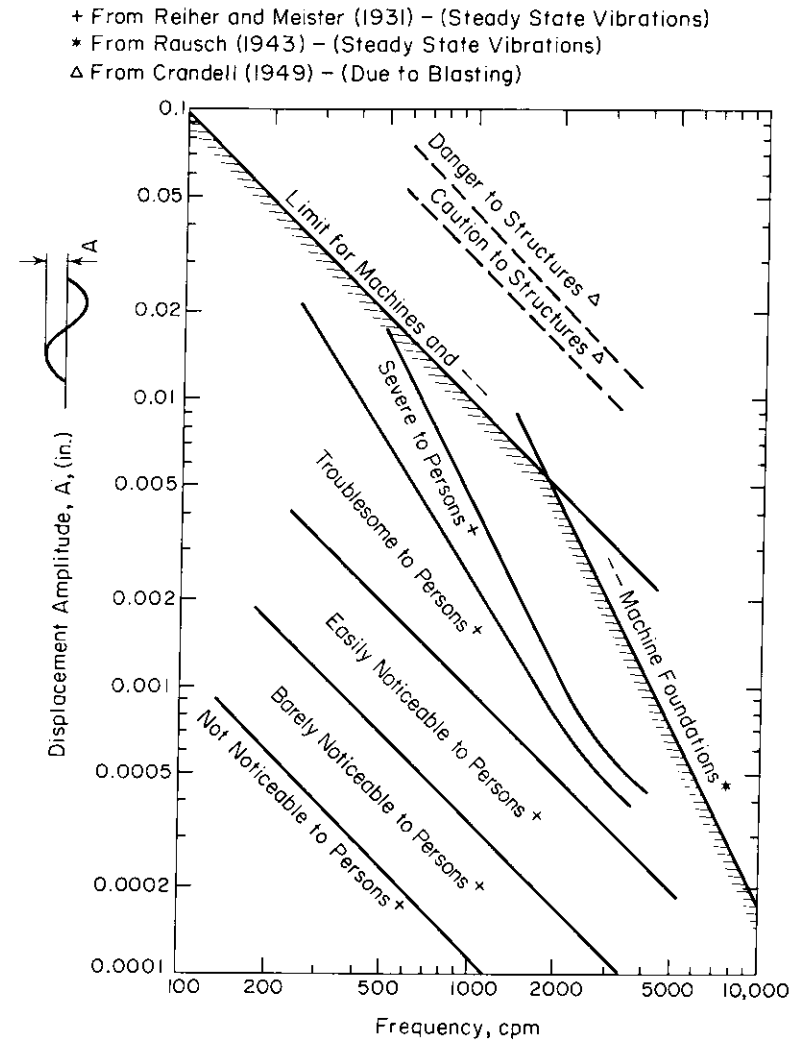


Figure 10-1. General limits of displacement amplitude for a particular frequency of vibration (from Richart, 1962).

*Steady-State Vibrations of Machinery*

The design criteria related to operation of machinery depend on the prime function of the entire installation and the importance of each machine unit to this function. Thus, the design criteria involve considerations of the initial cost, cost of maintenance (which includes the economic significance of



“down time”), and the cost of replacement of the unit. The foundation system must be designed to accommodate the level of operation desired by the owner.

For rotating machinery the information presented by Blake (1964) may be used to establish the permissible amplitudes of motion at the operating speed. Figure 10-2 illustrates the categories of performance *A* through *E* on the amplitude-vs.-frequency diagram. Note that the amplitude of vibration refers to horizontal motions measured on the bearing (not the shaft) of the machine. Blake (1964) has also introduced the concept of *service factor* (see Table 10-2), which indicates the importance of the particular machine to the prime function of the plant. The higher numerical values for the service factor indicate the more critical machines.

With the introduction of the service factor, Fig. 10-2 may be used to evaluate the performance of a wide variety of machines. Several examples (from Blake, 1964) are included below to illustrate the use of the service factor.

- A. Measurements on an electric motor show 2 mils (0.002-in. single amplitude) at 3600 rpm. From Table 10-2 the service factor is 1, and the effective vibration is  $2 \times 1 = 2$  mils. Enter Fig. 10-2 at 3600 rpm and go up to 2 mils. This point falls in class *D*. See “Explanation of Cases” at the bottom of Fig. 10-2 for recommended action.
- B. A stiff-shafted centrifuge shows 7 mils (0.007 in.) at 1000 rpm. The service factor is 2. Thus, the effective vibration is  $7 \times 2 = 14$  mils. From Fig. 10-2 at 1000 rpm and 14 mils (0.014 in.), the point falls in Class *E*. See notes to Fig. 7-2 for recommended action.

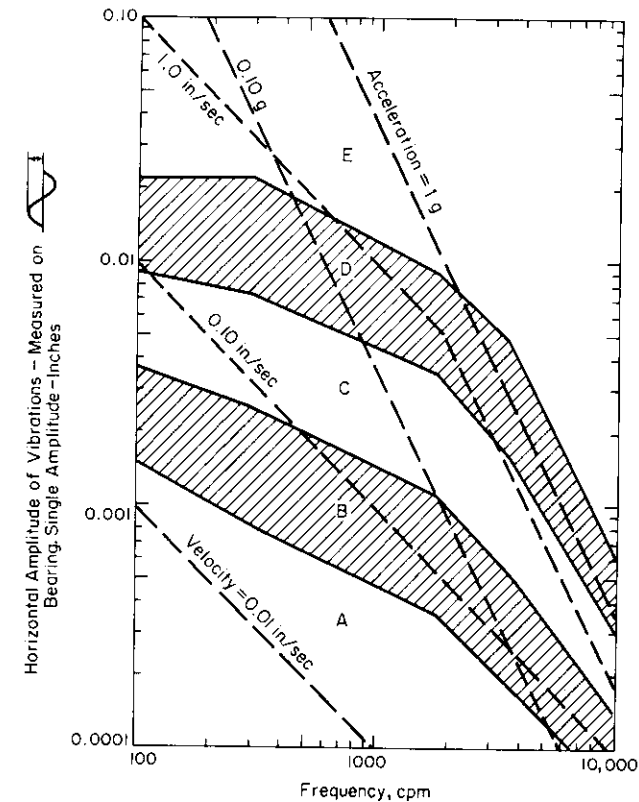
Table 10-2. Service Factors\*

Single-stage centrifugal pump, electric motor, fan	1
Typical chemical processing equipment, noncritical	1
Turbine, turbogenerator, centrifugal compressor	1.6
Centrifuge, stiff-shaft†; multistage centrifugal pump	2
Miscellaneous equipment, characteristics unknown	2
Centrifuge, shaft-suspended, on shaft near basket	0.5
Centrifuge, link-suspended, slung	0.3

Effective vibration = measured *single amplitude* vibration, inches multiplied by the *service factor*.  
 Machine tools are excluded. Values are for bolted-down equipment; when not bolted, multiply the service factor by 0.4 and use the product as a service factor.  
*Caution:* Vibration is measured on the bearing housing, except as stated.

\* From Blake (1964).

† Horizontal displacement on basket housing.



Explanation of cases:

- E Dangerous. Shut it down now to avoid danger.
- D Failure is near. Correct within two days to avoid breakdown.
- C Faulty. Correct within 10 days to save maintenance dollars.
- B Minor faults. Correction wastes dollars.
- A No faults. Typical new equipment.

Figure 10-2. Criteria for vibrations of rotating machinery (after Blake, 1964).

- C. A link-suspended centrifuge operating at 950 rpm shows 2.5 mils, with the basket empty. The service factor is 0.3 and the effective vibration is 0.75 mils (0.00075 in.). The point at 950 rpm and 0.00075 in. in Fig. 7-2 falls in Class *B*.

For special types of machines, the organizations concerned with their manufacture, installation, and operation often develop ratings for different operating conditions. For example, Parvis and Appendino (1966) give values for vibrations at the bearings of turboalternator sets operating at 3000 rpm which have the ratings indicated in Table 10-3.

Table 10-3. Range of Values of Vibrations for Turboalternators Operating at 3000 rpm\*

Rating of Turboalternator Operation	Vibration (Single-Amplitude)		
	On Bearing Caps (in.)	On Shaft (in.)	On Turbine Table (in.)
Excellent	0.0002	0.0010	0.00002
Good	0.0004	0.0020	0.00004
Fair	0.0008	0.0040	0.00008
Bad	0.0016	0.0080	0.00016
Dangerous	0.0032	0.0160	0.00032

\* After Parvis and Appendino (1966).

Additional information relating to the operation of rotating machinery in general is noted in Table 10-4 (from Baxter and Bernhard, 1967). These limits are based on peak-velocity criteria alone and would be represented by straight lines on plots similar to those of Figs. 10-1 and 10-2. Note the similarity in values of peak velocity for the lower limit of the range for machines as "smooth" (0.010 in./sec in Table 10-4) and the lower limit of the range "barely noticeable to persons" (0.01 in./sec in Fig. 10-1). Similarly, note the lower limits for "slightly rough" for machines (0.160 in./sec in Table 10-4) and "troublesome to persons" (0.10 in./sec in Fig. 10-1), and the danger limits of "very rough" (>0.63 in./sec in Table 10-4) and the Rausch limit for machines (1.0 in./sec in Fig. 10-1). The "dangerous" rating for turboalternators of 0.0032 in. at 3000 rpm (Table 10-3) also corresponds to 1.0 in./sec.

Baxter and Bernhard (1967) have also given a tentative guide to vibration tolerances for machine tools—this information is shown in Table 10-5. The

Table 10-4. General Machinery-Vibration-Severity Data\*

Horizontal Peak Velocity (in./sec)	Machine Operation
< 0.005	Extremely smooth
0.005-0.010	Very smooth
0.010-0.020	Smooth
0.020-0.040	Very good
0.040-0.080	Good
0.080-0.160	Fair
0.160-0.315	Slightly rough
0.315-0.630	Rough
> 0.630	Very rough

\* After Baxter and Bernhard (1967).

Table 10-5. Tentative Guide to Vibration Tolerances for Machine Tools\*

Type Machine	Displacement of Vibrations as Read with Pickup on Spindle-Bearing Housing in the Direction of Cut
Grinders	Tolerance Range (mils†)
Thread grinder	0.01-0.06
Profile or contour grinder	0.03-0.08
Cylindrical grinder	0.03-1.0
Surface grinder (vertical reading)	0.03-0.2
Gardner or Besly type	0.05-0.2
Centerless	0.04-0.1
Boring machines	0.06-0.1
Lathe	0.2-1.0

\* These values came from the experience of personnel who have been troubleshooting machine tools for over ten years. They merely indicate the range in which satisfactory parts have been produced and will vary depending on size and finish tolerance. After Baxter and Bernhard (1967).  
 † 1 mil = 0.001 in.

motions indicated in this table represent only general magnitudes; actual operating tolerances must depend on the size and finish tolerances of the parts to be machined.

*Vibrations of Structures*

Although the topics of vibrations of structures and the allowable limits for such vibrations are beyond the scope of this book, it is useful to include a few comments on this subject. This is particularly important in relation to the problem of preventing damage to structures because of machine operations or construction operations in the immediate vicinity.

In Fig. 10-1 and in the text describing this figure, it was noted that limits have been established (Crandell, 1949) for motions of structures caused by blasting. Although the lower limit for the zone (in Fig. 10-1) denoted "caution to structures" represents a peak velocity of 3 in./sec, it is general practice to limit the peak velocity to 2 in./sec (see Wiss, 1968). The U.S. Bureau of Mines criteria for structural safety against damage from blasting involve both a limiting peak velocity and a limiting peak acceleration. Below 3 cycles/sec the limit is 2 in./sec peak velocity, and above 3 cycles/sec the limit is (0.10)g peak acceleration.

For failure conditions governed by limiting values of peak velocity or acceleration, it is sometimes more convenient to plot this information on a

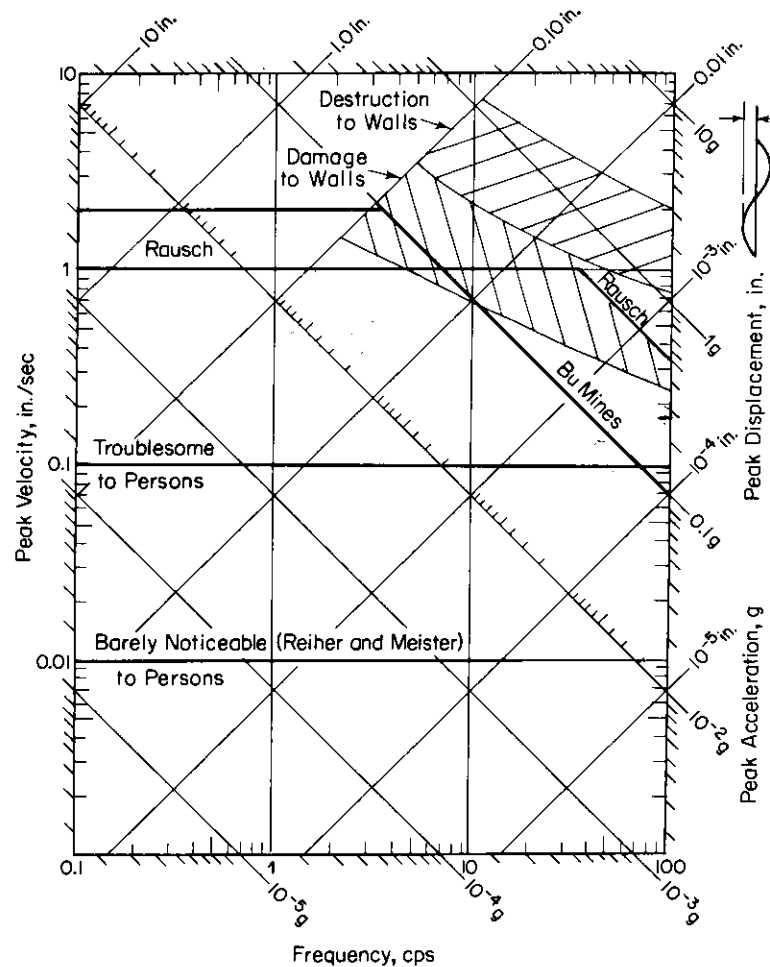


Figure 10-3. Response spectra for vibration limits.

diagram similar to Fig. 10-3, which shows simultaneous values of displacement, velocity, and acceleration. The limiting condition for each of these three quantities forms an envelope on this diagram. Points falling above this envelope violate the "failure" conditions, while those points falling below the envelope represent satisfactory conditions. In Fig. 10-3 are shown the limiting conditions for (1) the "people" limits of "barely noticeable" and "troublesome to persons," (2) the Rausch limits for machines and machine foundations, and (3) the U.S. Bureau of Mines criteria. Also shown in Fig. 10-3 are two shaded zones which describe the possibility of structural damage, particularly to walls, which may be caused by steady-state vibrations (see "Building Research Station," 1955). Diagrams similar to Fig. 10-3 are quit

useful for evaluating the dynamic response of a vibrating system and are often designated as *shock or response-spectra diagrams*.

### Effects of Vibrations on Persons

When the design of a foundation-soil system involves the consideration of people in the immediate vicinity, the problem may become complex. The first point to be established is the tolerable level of vibration for the area where persons are to be located. The next step is to ascertain if this level is possible within the ranges of vibration input, distances, and soil conditions anticipated.

In Fig. 10-1 several ranges of human tolerances to vibrations were noted which had been established experimentally by subjecting people to vertical vibrations as they stood on a shaking table (see Reiher and Meister, 1931). Generally, people are most susceptible to vibrations applied in the direction of the long axis of the body. The human tolerance limits of Reiher and Meister have been confirmed by subsequent investigations and are generally accepted as useful physiological vibration limits for people. For a comprehensive discussion of the effect of shock and vibrations on man; see Chap. 44, by Goldman and von Gierke, in the book edited by Harris and Crede (1961).

The physiological vibration limits represent only the first step in evaluating the effects of vibrations on persons. The next and often more important consideration is the psychological effect on persons. If the vibration is being generated "in his interest," then a person may accept the physiological vibration limit. However, if the vibration is generated "for someone else's benefit," a vibration which is "barely noticeable" may be effectively transformed into the "troublesome" category. Another example of the psychological effect occurs when a new foundation-soil system is designed for a dynamic unit. It is not satisfactory to provide the same level of vibration to persons in the neighborhood of the new unit as had existed from the old installation. Even though they had accepted the previous vibration levels and possibly even found them tolerable, people "expect" the new installation to perform better. Consequently, the reactions of people in the immediate vicinity of vibration-generating equipment may introduce a significant factor when establishing design criteria. It should be possible to make up a table similar to Table 10-2 (service factors for machinery) to indicate the variations in sensitivity of persons to vibrations, according to their psychological response.

### Criteria for Transient Loadings

The report by Steffens (1952) includes a summary of the various methods proposed for assessment of vibration intensity and their application

Table 10-6. Some Typical Vibration Data\*

Vibration from	Authority	Details	Observed		Reiher & Meister Classification	Derived	
			Amplitude (in.)	Frequency (cycles/sec)		Max. Velocity (microinches/sec)	Acceleration (g)
Traffic	Hyde and Lintern (1929)	Single-deck motor bus, 18 mph, 30 ft away	0.00012	26	Just perceptible	19,700	0.0082
Traffic	Hyde and Lintern (1929)	Light truck, 13.6 mph, 20 ft away; rough road	0.00012	20	Just perceptible	15,100	0.0049
Traffic	BRS (1934)	General traffic at Brentford	0.00012	19	Just perceptible	14,300	0.0044
Traffic	Tillman (1933)	Measurements in house 30-50 ft from traffic	0.00025	24	Clearly perceptible	37,700	0.0145
Traffic	BRS (1950)	Vibrations from London; traffic as measured inside a building	0.00014	25	Just perceptible	22,000	0.009
Traffic	BRS (1950)	Traffic measurements in Queens Street, London	0.00031	14	Just perceptible	27,000	0.0062
Traffic	BRS (1950)	Traffic measurements in Farrington Street, London	0.00036	10	Just perceptible	22,600	0.003
Railways	US	Measurements of vibration in Times Building (N.Y.), subway; floor vibrations	0.00078	15-20	Clearly perceptible	85,000	0.024

Railways	Mallock (1902)	Hyde Park area; building vibrations due to subway	0.001	10-15	Clearly perceptible	78,000	0.01
Railways	C. C. Williams	Freight train at 65 ft; passenger train at 25-30 ft	0.0009 0.0037				
Pile Driving	BRS	Close to occupied building	0.00053	30	Clearly perceptible—annoying	100,000	0.049
Blasting	BRS and RAE (1950)	Measurements in bomb-damaged tunnel; no damage caused by blasting vibration	0.0015 0.00007	6 80	Clearly perceptible Clearly perceptible	57,500 36,000	0.006 0.045
Blasting	G. Morris (1950)	Vibrations in villa 1100 ft away; firing 2000-lb explosive	0.0017	9.4	Clearly perceptible—annoying	100,000	0.015
Machinery	Tillman (1933)	Vibration from chocolate factory; measurements in nearby house	0.00056	42	Annoying	147,500	0.09
Machinery	Tillman (1933)	Vibration in houses (3rd storey), 400 ft from 120-hp diesel	0.0008	3.5	Just perceptible	17,500	0.01
Machinery	BRS	Vibrating table; measurements on table	0.005	25	Painful	780,000	0.32
Machinery	Tillman (1933)	Vibration in 70-year-old house adjacent to six lithographic presses	0.00031	64	Annoying	125,000	0.133

Notes:

(1) From the foregoing results it would appear that the maximum velocities involved at the various stages of perceptibility are (approximately) in microinches per second.

Just perceptible 10,000 to 30,000  
Clearly perceptible 30,000 to 100,000  
Annoying Over 100,000

(2) Digby gives a nuisance-vibration velocity of 86,000 to 250,000 microinches per second and a faintly-perceptible-vibration of 25,000 to 63,000.

\* From Steffens (1952).

to the study of building vibrations. With relation to the effect of vibrations on people, he concluded that the criteria presented by Reiher and Meister (1931) for any particular frequency cover reasonably well the values given by other investigators. The Reiher and Meister limits, established by tests, are shown in Fig. 10-1. Steffens also included tables which describe the ranges of intensity for the "Modified Mercalli Scale" of 1931 (abridged), Seiberg's "Mercalli-Cancani Scale" (abridged), the "Rossi-Forel Scale," and the "Omori Scale" (abridged) for earthquakes and attempted to apply these to industrial vibrations. Generally, he found that the information provided by the earthquake scales was of little use for the industrial-vibration problem. He found the Reiher and Meister data useful and suggested that the Zeller scale, based on a unit called the "Pal," might have potential. The Pal is determined by  $10 \log 2X$  (see for example Zeller, 1933) in which  $X$  is equal to  $16\pi^4 z^2 f^3$  or  $16\pi^4$  (amplitude)<sup>2</sup>  $\times$  (frequency)<sup>3</sup> of the exciting motion. The vibrations considered by Zeller ranged from 0 to 80 Pal; a vibration equivalent to 55 Pal causes seasickness and a vibration of 70 Pal causes a painful sensation to people. Finally, Steffens included a table containing typical vibration data from traffic, blasting, and machinery. These data are reproduced herein as Table 10-6.

The problem of vibrations produced by impact loads on soils or soil-supported structures is of considerable importance. In Table 10-6 only one case for pile driving and two cases for blasting are noted; but these are routine construction procedures, and many consulting firms, contractors, and insurance companies have extensive files relating to vibrations generated by pile driving and blasting. One criteria for evaluating the influence of impact or vibratory energy on soils and structures is the "energy ratio" (Crandell, 1949) given by

$$E.R. = \frac{(\text{Acceleration})^2}{(\text{Frequency})^2} \left( \frac{\text{ft}}{\text{sec}^2} \right)^2 \left( \frac{\text{sec}}{\text{cycles}} \right)^2 \quad (10-1)$$

The energy ratio decreases with distance from the source with the rate of decay depending on the type of soil and local conditions; but Crandell indicates a general trend of decrease of energy ratio according to (distance)<sup>-2</sup>. From his study Crandell concluded that damage to structures did not occur when the energy ratio produced by blasting was less than 3. The concept of the energy ratio has also been selected as a criterion for evaluating the excitation required to compact cohesionless soils (D'Appolonia, 1966). However a lower limit of energy ratio which does *not* affect soil structure does not seem to be well-defined at the present time (1969). Tschebotarioff (1965) has pointed out at least one instance for which energy ratios of 0.01 to 0.001 developed by repeated impacts from pile driving have caused serious settlement of soils in the vicinity of the construction. Consequently, the total influence of vibratory loading on soil structure cannot be evaluated by a simple

limit indicated by the energy ratio because the *number of repetitions* is also important.

Several bits of information on the vibrations resulting from traffic are noted in Table 10-6. It is important to evaluate the influence of traffic and other background vibrations when considering the design criteria for a particular installation. The evaluation should include a range of the potential variables involved, such as the type and frequency of vehicles passing; the roughness of the road surface, including the effects of ice in cold climates; the influence of changing soil conditions, including frost and seasonal moisture variations; and the possible effects of the changes in soil geometry, during construction, on the wave-energy transmission from the traffic source to the selected site. Several of these factors were investigated by Sutherland (1950), who found the effect of irregularities in the road to be the most significant. The ambient or background vibration level at a particular location is of particular significance when foundations for sensitive equipment are to be designed.

#### *Foundations for Sensitive Equipment*

Occasionally it is necessary to design a foundation which is "vibration-free." This is impossible, of course, but it indicates an extremely low value of permissible motion. This requirement is often specified for sensitive equipment such as electron microscopes, calibration test stands, precision-machining operations, and radar towers. For installations in which the equipment itself is not a significant source of vibration, it is necessary to evaluate the ambient vibrations at the site and then to provide isolation of the foundation and of the individual pieces of equipment by the methods indicated in Chap. 8. Generally, the design criteria should be established by the owner or equipment manufacturer because they must be satisfied with the eventual operation of the equipment. In the case of the electron microscope, a limiting criteria of  $10^{-4}g$  at the machine has been established by tests (Sell, 1963). In this particular instance, local isolation pads may provide about one order of magnitude of reduction in  $g$  values. Criteria for calibration test stands and similar facilities are often of the order of  $10^{-4}g$  with some variations according to the frequency of input vibrations. The interesting part of the requirement of many of these "vibration-free" facilities is that they are often located relatively close to a major source of vibrations, which complicates the isolation problem.

Radar tracking towers are one type facility which require stable foundations and are at the same time often located near rocket-launching facilities. For satisfactory operation of the equipment, Pschunder (1966) has indicated

that the total allowable tilt of the tower is of the order of  $\frac{1}{3}$  of the total pointing error. This includes the tilt induced by the flexibility of the tower structure in addition to the tilt introduced by rocking of the foundation mat. Maxwell (1965) has noted that typical values for the angular rotation in tilting of radar towers is often of the order of 0.02 mils (1020 mils = 1 radian, or 1 mil = 0.05617°); similar limits apply to the torsional motions. In addition, criteria for radar-tower foundations usually include a range of resonant frequencies to be avoided because of resonance in the structural or electrical systems. Each particular type radar tower has its own set of design criteria which must be satisfied by the foundation designer.

### 10.3 Dynamic Loads

Before a satisfactory design can be made for a machine foundation, it is necessary to obtain as much information as possible about the magnitude and characteristics of the dynamic loads involved. Often this is a relatively difficult task because manufacturers may not wish to admit that any unbalanced forces occur from operation of their equipment. However, there are certain basic types of equipment for which the unbalanced forces can be calculated, and a brief discussion of some of these are included in the following paragraphs. There is a definite need for reliable measurements of machine-induced forces which are transmitted to foundations, and the reader is encouraged to obtain this kind of information at every opportunity.

#### Rotating Machinery

Rotating machinery designed to operate at a constant speed for long periods of time includes turbines, axial compressors, centrifugal pumps, turbogenerator sets, and fans. In the case of each it is possible, theoretically, to balance the moving parts to produce no unbalanced forces during rotation. However, in practice, some unbalance always exists, and its magnitude includes factors introduced by design, manufacture, installation, and maintenance. These factors may include an axis of rotation which does not pass through the center of gravity of a rotating component; an axis of rotation which does not pass through the principal axis of inertia of a unit, thereby introducing longitudinal couples; gravitational deflection of the shaft; misalignment during installation; damage, corrosion, or wear of moving parts; improper tightening of components; or unbalances introduced by movement of materials being processed. The cumulative result of the unbalanced forces must not be great enough to cause vibrations of the machine-foundation system which exceed the design criteria. When excessive vibrations do occur, the obvious remedy is to reduce the unbalanced forces.

In certain types of machines, unbalanced forces are developed on purpose. Compaction machinery often contains unbalanced masses which rotate at a fixed eccentric radius about either a horizontal or vertical axis. The vibratory rollers for surface compaction have a horizontal axis of rotation, whereas the Vibroflot has a vertical axis. In either case the exciting-force amplitude can be evaluated from

$$Q_o = m_e e \omega^2 \quad (10-2)$$

in which  $m_e$  is the total unbalanced mass and  $e$  is the eccentric radius to the center of gravity of the total unbalanced mass. The force transmitted to the soil by this type compacting machinery depends on the resulting motion of the contact faces of the machine against the soil. It is the purpose of this type device to produce inelastic deformations in the soil, and much of the input energy is absorbed in changing the soil structure.

Another type rotary mechanism which often develops unbalanced forces is the solid-waste shredder, rotary rock crusher, or hammermill. In this kind of machine a row of heavy steel weights or "hammers" are attached to disks or arms which rotate at relatively high speeds (See Fig. 10-4). When solid wastes, rocks, or automobile bodies are fed into this machine, the material is smashed against a slotted anvil by the rotating hammers, thereby fracturing or shredding the material because of the high shearing stresses involved. During this shredding operation the hammers are worn down. This changes the total rotating weight and possibly the eccentricity if the hammers wear unevenly or are not matched during replacement. Because of the need for frequent replacement of the hammers in this kind of machine, the operating unbalanced forces depend on the owner's maintenance procedure.

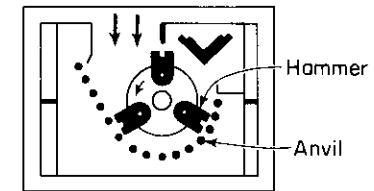


Figure 10-4. Elements of a hammermill.

#### Multimass Vibrators

The centripetal force developed by a single rotating mass Eq. (10-2) is a vector force  $Q_o$  which acts outward from the center of rotation (Fig. 10-5a). By combining two rotating masses on parallel shafts within the same mechanism, it is possible to produce an oscillating force with a controlled direction. As shown in Fig. 10-5b, counterrotating masses can be so arranged that the horizontal-force components cancel but the vertical components are

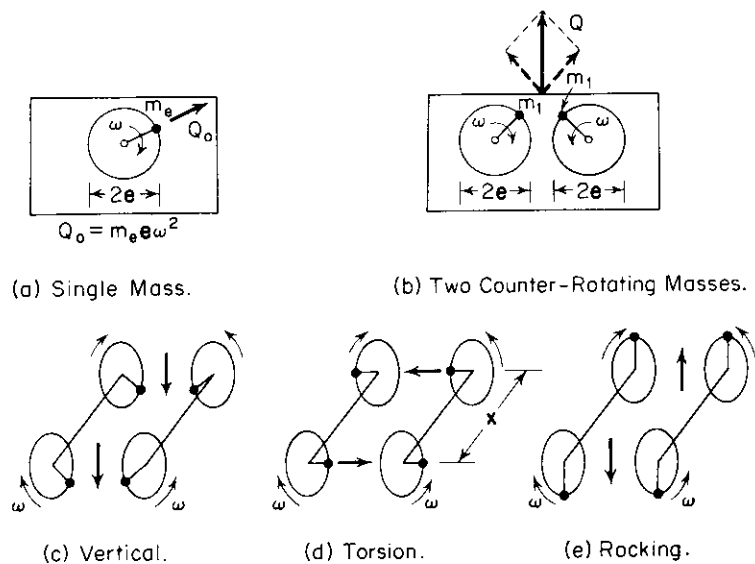


Figure 10-5. Forces from rotating mass exciters.

added. If each mass  $m_1$  has an eccentricity  $e$ , the vertical force produced is

$$Q = Q_o \sin \omega t = 2m_1 e \omega^2 \sin \omega t \tag{10-3}$$

In order to improve the flexibility of this type of vibrator, four masses may be arranged with one at each end of the two parallel shafts. A vertical oscillating force is developed by the arrangement of weights shown in Fig. 10-5c, a torsional couple about a vertical axis results from the arrangement of Fig. 10-5d, and a rocking couple is produced when the masses are located as in Fig. 10-5e. Vibrators of this design often include mechanisms which permit different settings of the eccentricities of the weights (see, for example, Bernhard and Spaeth, 1928; Hertwig, Früh, and Lorenz, 1933; or Fry, 1963). Note that for the rocking or torsional forces developed from the four-mass exciter, the torque or moment is given by

$$T = 4m_1 e \frac{x}{2} \omega^2 \sin \omega t \tag{10-4}$$

in which  $x$  represents the distance between the weights at the ends of each shaft.

Usually these multimass vibrators are designed such that adjustments of the size of the weights or of the throw of the eccentric are fixed before each

test and then maintained constant during the test. For this situation the exciting force increases as the square of the rotating speed.

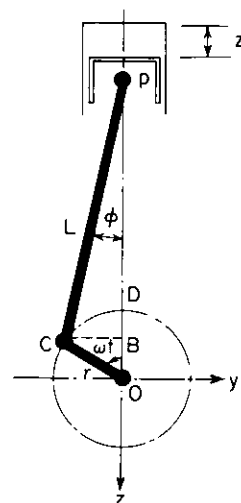
### Single-Cylinder Engines

Internal-combustion engines, piston-type compressors and pumps, steam engines, and other machinery involving a crank mechanism produce reciprocating forces. The crank mechanism transfers a reciprocating motion to a rotary motion, or vice versa. After the weight and center of gravity of each of the moving parts are determined, the forces resulting from operation of the machine can be evaluated.

The basic crank mechanism is shown in Fig. 10-6. It consists of a piston which moves vertically within a guiding cylinder, a crank of length  $r$  which rotates about point  $O$ , and a connecting rod of length  $L$  attached to the piston at point  $p$  and to the crank at point  $C$ . Thus, the crank pin  $C$  follows a circular path, while the wrist pin  $p$  oscillates along a linear path. Points on the connecting rod between  $C$  and  $p$  follow elliptical paths.

If the crank is assumed to rotate at a constant angular velocity  $\omega$ , we may evaluate the acceleration of the piston along its axis of translation. In Fig. 10-6 the vertical displacement of the piston is  $z_p$ , measured from the top dead-center position at which  $\omega t$  is taken as zero. The total motion of the piston is

$$z_p = \overline{DB} + L(1 - \cos \phi) \tag{10-5}$$



$$z_p = \left(r + \frac{r^2}{4L}\right) - r(\cos \omega t + \frac{r}{4L} \cos 2\omega t)$$

$$\dot{z}_p = r\omega \left(\sin \omega t + \frac{r}{2L} \sin 2\omega t\right)$$

$$\ddot{z}_p = r\omega^2 \left(\cos \omega t + \frac{r}{L} \cos 2\omega t\right)$$

Figure 10-6. Crank mechanism.

From the geometry of the diagram (Fig. 10-6),

$$\overline{DB} = r(1 - \cos \omega t) \tag{10-6}$$

and

$$\sin \phi = \frac{r}{L} \sin \omega t \tag{10-7}$$

With the introduction of expressions obtained from Eqs. (10-6) and (10-7) into Eq. (10-5), the displacement becomes

$$z_p = r(1 - \cos \omega t) + L \left( 1 - \sqrt{1 - \frac{r^2}{L^2} \sin^2 \omega t} \right) \tag{10-8}$$

Because the ratio  $r/L$  is seldom greater than  $\frac{1}{4}$ , the expression beneath the radical in Eq. (10-8) can be replaced by the first two terms of the expansion into a power series by the binomial theorem, or

$$\sqrt{1 - \frac{r^2}{L^2} \sin^2 \omega t} \approx 1 - \frac{r^2}{2L^2} \sin^2 \omega t \tag{10-9}$$

and after substituting, Eq. (10-8) becomes

$$z_p = r(1 - \cos \omega t) + \frac{r^2}{2L} \sin^2 \omega t \tag{10-10}$$

The  $\sin^2$  term in Eq. (10-10) can be represented by its equivalent expression for the double angle in order to simplify the differentiation of the displacement expression; thus,

$$z_p = \left( r + \frac{r^2}{4L} \right) - r \left( \cos \omega t + \frac{r}{4L} \cos 2\omega t \right) \tag{10-11a}$$

Then the velocity and acceleration are

$$\dot{z}_p = r\omega \left( \sin \omega t + \frac{r}{2L} \sin 2\omega t \right) \tag{10-11b}$$

and

$$\ddot{z}_p = r\omega^2 \left( \cos \omega t + \frac{r}{L} \cos 2\omega t \right) \tag{10-11c}$$

The expressions for velocity and acceleration provide the momentum and inertia forces for the piston after multiplying by its mass. Note that one term

varies with the *same frequency* as the rotation; this is called the *primary term*. The term which varies at *twice* the frequency of rotation is called the *secondary term*. The importance of the secondary term is established by the ratio  $r/L$ . If the connecting rod is infinitely long the secondary term disappears and the piston executes harmonic motion. For a connecting rod of finite length the motion of the piston is periodic but not harmonic. Figure 10-7 illustrates the influence of the secondary term on the piston acceleration for a crank mechanism having  $r/L = \frac{1}{4}$ .

With Eqs. (10-11) to describe the dynamic characteristics of the piston, we may now consider the rotating parts of the crank. If there is any unbalance in the crankshaft, this may be replaced by a mass concentrated at the crank pin  $C$ , which produces the same inertia forces as the original system. The vertical motion of point  $C$  is

$$z_C = r(1 - \cos \omega t) \tag{10-12a}$$

from which the velocity and acceleration are

$$\dot{z}_C = r\omega \sin \omega t \tag{10-12b}$$

and

$$\ddot{z}_C = r\omega^2 \cos \omega t \tag{10-12c}$$

The horizontal components are

$$y_C = -r \sin \omega t \tag{10-13a}$$

$$\dot{y}_C = -r\omega \cos \omega t \tag{10-13b}$$

$$\ddot{y}_C = r\omega^2 \sin \omega t \tag{10-13c}$$

The motions of the piston and the crank have now been established, leaving the characteristics of the connecting rod to be determined. Because the wrist pin  $p$  follows a linear path, the crank pin  $C$  a circular path, and all

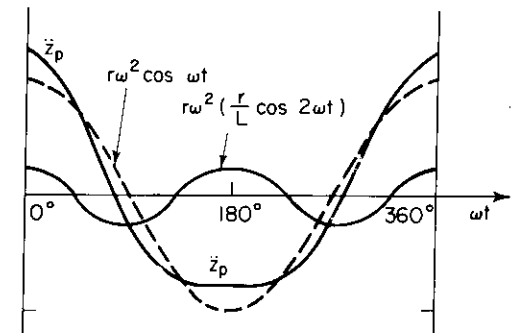


Figure 10-7. Piston acceleration as function of crank angle for  $r/L = \frac{1}{4}$ .



points in between an elliptical path, the exact evaluation of the motions and resulting forces developed by the connecting rod is fairly complicated. However, it is satisfactory to replace the connecting rod by an equivalent structure consisting of a mass at the wrist pin and a mass at the crank pin which produce the same total mass and the same center of gravity. This procedure is correct for evaluating the inertia forces but is an approximation when establishing the inertia couple.

After adopting this procedure of dividing the connecting rod into two masses, one moving with the piston (reciprocating) and one moving with the crank pin (rotating), the total reciprocating and rotating masses may be designated by  $m_{rec}$  and  $m_{rot}$ , respectively. Then the total vertical-inertia force  $F_z$  and total horizontal-inertia force  $F_y$  are given by

$$F_z = (m_{rec} + m_{rot})r\omega^2 \cos \omega t + m_{rec} \frac{r^2}{L} \omega^2 \cos 2\omega t \quad (10-14)$$

and

$$F_y = m_{rot}r\omega^2 \sin \omega t \quad (10-15)$$

It should be noted that the vertical force has both a *primary* component acting at the frequency of rotation and a *secondary* component acting at twice that frequency. The horizontal force has only the *primary* component.

The torque of the inertia forces can also be evaluated from the arrangement of the masses and the geometry described in the preceding paragraphs. The torque is about the longitudinal axis  $O$  (perpendicular to plane of figure) in Fig. 10-6 and represents the torque acting on the shaft in the direction of rotation or the torque on the frame in the opposite direction. Its magnitude is given by

$$M = -m_{rec}\omega^2 r^2 \sin \omega t \left( \frac{r}{2L} + \cos \omega t + \frac{3r}{2L} \cos 2\omega t \right) \quad (10-16)$$

By "counterbalancing," the inertia forces due to the rotating masses can be reduced or eliminated completely. Usually this is done in the design of internal-combustion engines or piston-type pumps or compressors. However, the reciprocating mass still produces unbalance in a simple system corresponding to that shown in Fig. 10-6. Thus, a *single-cylinder engine is inherently unbalanced.*

The following example illustrates the calculation for the primary and secondary unbalanced forces for a single-cylinder engine. Typical data for two single-cylinder engines are given in Table 10-7.

It will be assumed that the rotating mass is balanced. Then Eq. (10-14) is reduced to

$$F_z = m_{rec}r\omega^2 \cos \omega t + m_{rec} \frac{r^2}{L} \omega^2 \cos 2\omega t$$

Table 10-7. Data for Single-Cylinder Engines

Bore (in.)	Stroke (in.)	Crank $r$ (in.)	Rod $L$ (in.)	$\frac{r}{L}$	Piston Weight (lb)	Pin Weight (lb)	Rod Weight (lb)	Total Recip. Weight (lb)	Total Engine Weight (lb)
$5\frac{3}{4}$	8	4	15	0.267	10.6	2.9	18.0	19.0	2270
$5\frac{1}{4}$	$6\frac{1}{2}$	$3\frac{1}{4}$	$10\frac{3}{4}$	0.302	7.19	1.88	11.18	11.87	2270

For the  $5\frac{3}{4}$ -by-8-in. single-cylinder engine, the amplitude of the primary force is

$$F' = \frac{19}{386} 4 \frac{4\pi^2}{(60)^2} (\text{rpm})^2 = 0.00216 (\text{rpm})^2$$

and the amplitude of the secondary force is

$$F'' = \frac{r}{L} F' = (0.267)F' = 0.000576 (\text{rpm})^2$$

Then at an operating speed of 1000 rpm, these force amplitudes amount to

$$F' = 2160 \text{ lb}$$

and

$$F'' = 576 \text{ lb}$$

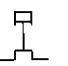


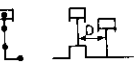

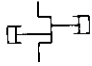


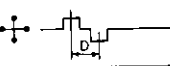
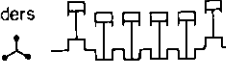
which are significant when compared with the machine weight of 2270 lb. Note that for this machine 30.6 per cent of the connecting-rod weight was considered to act as part of the reciprocating weight.

### Multicylinder Machines

In multicylinder engines and compressors it is possible to arrange the cylinders in a manner which minimizes the unbalanced forces. Table 10-8 illustrates the forces developed by multicylinder machines for different crank arrangements and numbers of cylinders. For a particular machine the unbalanced primary and secondary forces as well as the torques should be available from the manufacturer because these quantities were required for the original design of the machine.

It should be noted that Table 10-8 illustrates the unbalanced forces developed for multicylinder engines having the same bore and stroke for each cylinder. For this condition the six-cylinder engine can be completely balanced. Consequently, a V-12 engine made up of two in-line 6's would also be balanced. However, if the bore and stroke of the cylinders are *not* all the

Table 10-8. Unbalanced Forces and Couples for Different Crank Arrangements (after Newcomb, 1951)

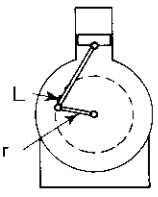

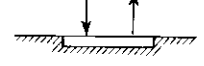
Crank Arrangements	Forces		Couples	
	Primary	Secondary	Primary	Secondary
Single crank 	$F'$ without counterwts. $(0.5)F'$ with counterwts.	$F''$	None	None
Two cranks at 180° In-line cylinders 	0	$2F''$	$F'D$ without counterwts. $\frac{F'}{2}D$ with counterwts.	None
Opposed cylinders 	0	0	Nil	Nil
Two cranks at 90° 	$(1.41)F'$ without counterwts. $(0.707)F'$ with counterwts.	0	$(1.41)F'D$ without counterwts. $(0.707)F'D$ without counterwts.	$F''D$
Two cylinders on one crank Crank at 90° 	$F'$ without counterwts 0 with counterwts	$(1.41)F''$	Nil	Nil
Two cylinders on one crank Opposed cylinders 	$2F'$ without counterwts. $F'$ with counterwts.	0	None	Nil
Three cranks at 120° 	0	0	$(3.46)F'D$ without counterwts. $(1.73)F'D$ with counterwts.	$(3.46)F''D$
Four cylinders Cranks at 180° 	0	0	0	0
Four cylinders Cranks at 90° 	0	0	$(1.41)F'D$ without counterwts. $(0.707)F'D$ with counterwts.	$4.0F''D$
Six cylinders 	0	0	0	0

$r$  = crank radius (in.)  
 $L$  = connecting-rod length (in.)  
 $D$  = cylinder-center distance (in.)  
 $W$  = recip. wt. of one cylinder (lb)  
 $F' = (0.0000284) r W (\text{rpm})^2 = \text{Primary}$   
 $F'' = \frac{L}{r} F' = \text{Secondary}$

same, then Table 10-8 should not be used, but the unbalanced forces should be computed for each cylinder and the results superposed.

Table 10-9 illustrates the order of magnitude of forces which may be developed by one- and two-cylinder engines or compressors. For the single-cylinder engines oriented vertically, both the primary and secondary vertical forces are significant. An engine usually drives some additional machinery, and a compressor needs something to drive it. Consequently, these forces

Table 10-9. Order of Magnitude of Forces Developed by One- and Two-Cylinder Engines

Single-Cylinder Engine - Vertical		
Bore = 5.125 in.	Stroke = 6.5 in.	
$r = 3.25$ in.	$L = 10.75$ in.	Total Wt. = 2270 lb Reciprocating Weight = 11.87 lb Operating Speed = 1800 rpm Unbalanced Forces Primary = 3450 lb at 1800 rpm Secondary = 1075 lb at 1800 rpm
Single-Cylinder Compressor - Vertical		
Bore = 14.5 in.	Stroke = 9 in.	Vert. { Primary = 9180 lb Secondary = 2210 lb Horiz. { Primary = 310 lb Secondary = 0
Total Wt. = 10,900 lb	Forces at Operating Speed of 450 rpm	
Horizontal Compressor - 2 Unequal Cylinders		
Low Pressure Cyl.: Bore = 23", Stroke = 14", Unbal. Wt. = 1130 lb		
High Pressure Cyl.: Bore = 14", Stroke = 14", Unbal. Wt. = 890 lb, Wt. Compressor = 22,400 lb		
Unbalanced Forces at 277 rpm		
Horiz. { Primary = 6190 lb Secondary = 730 lb	Vert. { Primary = 5300 lb Secondary = 0	 
Unbalanced Moment at 277 rpm		
Horiz. { Primary = 22,400 ft lb Secondary = 11,300 ft lb	Vert. { Primary = 19,300 ft lb Secondary = 0	

shown on Table 10-9 constitute only a part of the loads acting on a particular foundation. The response of the foundation will depend on the resultant forces developed from the entire package of machinery and the location of these forces.

The two-cylinder horizontal compressor described on Table 10-9 illustrates the additional problems associated with the motion of two horizontal in-line cylinders of different bore. Because of the large moving masses involved, the vertical components of the primary force and moment are nearly as large as the horizontal components. Furthermore, forces are developed which will cause horizontal and vertical translation as well as rocking and

twisting of the foundation for this machine. It is also probable that pitching and lateral motions would occur because of coupling. Consequently, the forces developed by this two-cylinder compressor would excite vibrations of its foundation in all six degrees of freedom.

In general, multicylinder engines have smaller unbalanced forces than do the one- and two-cylinder engines and compressors. However, in each case it is necessary to evaluate the influence of the unbalanced forces and couples on the response of the machine foundation in *all six* modes of vibration.

#### Forces from Vibratory Conveyors

Vibratory conveyors are often used to transport masses of solid particles. Figure 10-8 illustrates the elements of this type machine, which consists essentially of the conveyor trough, supporting springs, a reaction block, and a motor-crank-drive mechanism. The springs may be either leaf springs, as shown, or coil springs. Horizontal movements of particles in the conveyor trough are developed by oscillation of the trough along a path which produces a forward and upward acceleration of particles, then a backward and downward acceleration. This causes the particles to move forward in a small "hop" each oscillation. The sketch in Fig. 10-8 shows leaf springs inclined at  $60^\circ$  from the horizontal, which forces the conveyor trough to move along a path inclined at  $30^\circ$  from the horizontal. A crank mechanism provides the input oscillation at a given amplitude of motion. Usually there is a speed-reduction system between the motor and crank-drive mechanism to provide a wide range of operating frequency of oscillation. If the operating frequency is "tuned" to the resonant frequency of the mass-spring system, then minimum input force is required to maintain the oscillation. The moving mass is primarily the weight of the conveyor trough but may include a portion of the transported material.

The foundation block is required to absorb an inclined oscillating force, indicated as  $Q_o$  in Fig. 10-8. There may also be a pitching moment developed if the line of action of the resultant force  $Q_o$  does not coincide with the center of the resistance developed by the foundation block. In any case, a horizontal

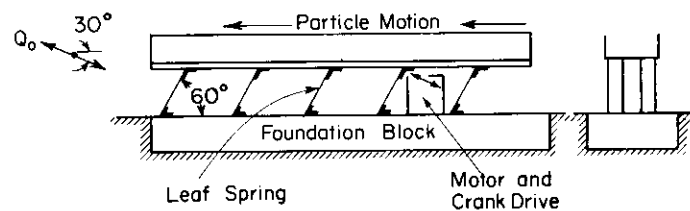


Figure 10-8. Elements of vibratory conveyor.

and a vertical force will be transmitted to the supporting soil, and wave energy will be propagated from the foundation block outward. Because the horizontal component of the force applied to the soil is predominant, the elastic waves propagating outward from the foundation will have a greater intensity along the axis of conveyor vibration. This directional effect should be considered in the layout of vibrating conveyor systems if there is any vibration-isolation problem in the vicinity.

As indicated in Fig. 10-8, the oscillating force is inclined at an angle to the horizontal and has a magnitude

$$Q_o = me4\pi^2f_o^2 \quad (10-17)$$

in which  $m$  is the total oscillating mass,  $e$  is the crank throw or eccentricity, and  $f_o$  is the operating frequency of vibration. This force is then broken down into its horizontal and vertical components in order to estimate the dynamic motions of the foundation block.

#### Loads Developed by Intermittent Machine Operation—Pulse Loads

Many types of machines produce intermittent loads which must be transmitted through the foundation block to the supporting soil. The operation of punch presses, forging hammers, drop tests, and stamping machines, for example, produce impulsive loads which may be considered as single pulses because the effect of one load dies out before the next load occurs.

In order to evaluate the response of a foundation block to a pulse-type load, it is necessary to have reliable information about the force-time relation of the pulse. This information is often not readily available, and the reader is encouraged to obtain this information experimentally whenever possible. Two pulse loads will be described to illustrate the needed information and to provide loads which will be employed later (in Sec. 10.6) in the evaluation of the dynamic response of footings. The pulse shown in Fig. 10-9b was obtained experimentally from a load-sensitive column which supported a loading platen on a model footing (see Drnevich and Hall, 1966). Figure 10-9a illustrates the general test setup in which the load was applied by dropping a 5-lb sandbag a distance of 1 ft onto the loading platen. The shape of the pulse and in particular the rise time were controlled by placing different thicknesses of foam-rubber sheets on the surface of the loading platen. The solid curve in Fig. 10-9b represents the experimental load-time pulse for test Q-2 and the dashed rectangles constitute a step-type approximation to

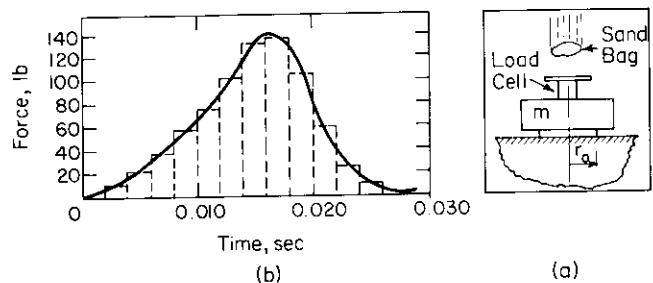
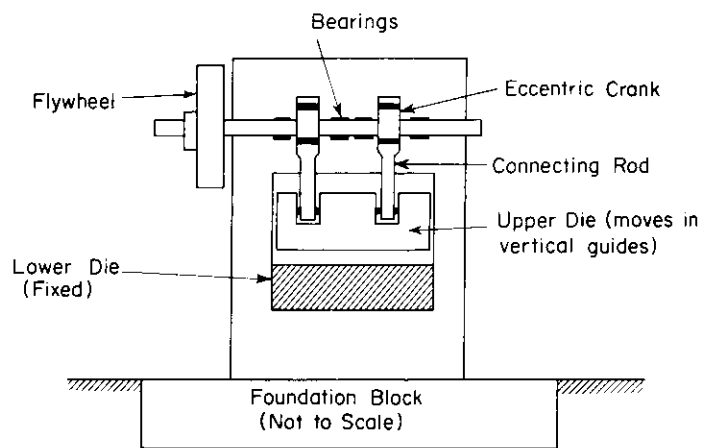


Figure 10-9. Impact load on model footing. (a) Test setup showing sandbag dropping onto loading platen to force mass  $m$  to load soil through circular footing having  $r_0 = 6$  in. (b) Load-time pulse measured in load-sensitive column for test Q-2 (after Drnevich and Hall, 1966).

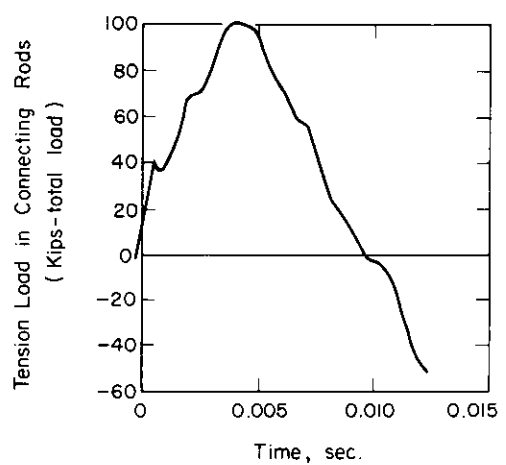
the loading pulse which will be used in the phase-plane solution for the footing response.

Figure 10-10a shows the elements of a punch press—a machine which punches shapes from sheet metal by forcing a moving upper die against a fixed lower die. The upper die moves vertically in guides and is actuated by an eccentric crank and connecting rods. As the upper die is forced downward against the metal to be processed, compression loads are built up in the connecting rods. These forces are resisted by developing tension in the structural frame; thus, the loads are contained within the machine. However, when the upper die punches through the sheet metal, there is a sudden release of this compressive energy in the connecting rods along with a loss of support for the weight of the upper die. These two forces accelerate the mass of the upper die in a downward direction. This results in a tension shock imparted to the connecting rods as they stop the motion of the die. Because this tension shock in the connecting rods is developed by inertia loads, it is an external load on the machine. The result is a downward force on the crankshaft which then causes motion of the entire machine and foundation block.

Figure 10-10b shows the tensile forces developed in the connecting rods of a punch press which has a capacity of 250 tons of compressive force between the dies. In this case, it is seen that the maximum transient tensile load in the connecting rods (or downward force on the machine and foundation) was of the order of 40 per cent of the rated capacity of the machine. This transient-load pulse reached a maximum of about 100,000 lb, but the pulse duration was only about 0.010 sec. This loading pulse, the weight of the machine and its moving parts, and soil data obtained by one of the methods described in Chap. 6 provide the information needed to design a foundation which will restrict the motion of the machine to acceptable limits.



(a) Elements of Punch Press Mechanism.



(b) Force-Time Pulse for Tension Load Developed in Connecting Rods after Upper Die Punches Through Metal Stock.

Figure 10-10. Impulse developed by punch press operation.

Random Vibrations

Earthquakes, wind, and certain manmade forces have a random pattern which provides excitation to structures and foundations. In order to establish force or displacement patterns to be applied as design loads, it is necessary to obtain reliable field data from previous excitations considered similar to the proposed design conditions. For example, ground-motion records from previous earthquakes are often used to represent probable earthquake excitations when analyzing the dynamic response of a proposed structure.

10.4 Brief Review of Methods for Analyzing Dynamic Response of Machine Foundations

DEGEBO

An intensive study of the effect of vibrations on foundation response and upon soil properties was carried out by the Deutschen Forschungsgesellschaft für Bodenmechanik (DEGEBO) in Berlin primarily during the period 1928–1936. This group developed a rotating-mass mechanical oscillator with four eccentric masses to excite model footings into the vertical and torsional modes of vibration. The drive mechanism for the eccentric masses was arranged as shown in Fig. 10-11, with four shafts driven by bevel gears—instead of four masses on two parallel shafts as shown in Fig. 10-5c and d; but the principle is the same.

In the first major report on their investigations (DEGEBO No. 1) Hertwig, Früh, and Lorenz (1933) described the test equipment and included an extensive evaluation of the dynamic response of the oscillator and footing plate in vertical vibration. They attempted to fit the test results into the framework of the single-degree-of-freedom mass-spring-dashpot system and found it possible to do so for any particular test. However, the damping constant, in particular, was appreciably different for different tests. They noted that the dynamic response was nonlinear and that progressive settlements developed during vibration tests when the oscillator was supported on sand. The dynamic response was found to depend on the total weight of the oscillator and base plate, on the area of the base plate, and on the dynamic

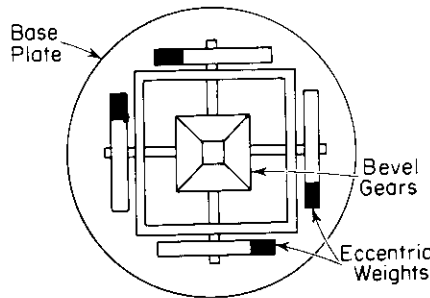


Figure 10-11. DEGEBO Oscillator (top view).

force applied as well as on the characteristics of the soil. At the end of the report is a table which indicates the “characteristic frequency” for a variety of soils. This table has been reproduced many times in the literature, to the point that many people believe that soil has a “natural frequency” and attempt to use this value in design. The table represents information obtained from a particular set of test conditions and should be considered only as interesting qualitative information.

In subsequent publications (for example, Lorenz, 1934) the effect of oscillator weight, base-plate area, and exciting force were studied for their influence on the resonant frequency. It was found that for the same base-plate area and exciting force, increasing the total weight lowered the resonant frequency. For a constant total weight and exciting force, an increase in base-plate area raised the resonant frequency; and for a constant weight and constant base-plate area, an increase in exciting force lowered the resonant frequency. Hertwig and Lorenz (1935) obtained similar results for both vertical and torsional tests of footings on sand and on clay.

The change in frequency with a change in exciting force indicated that the soil response was nonlinear. This is true and it is particularly important at the magnitude of motions involved in the DEGEBO tests, which often involved vertical accelerations of the oscillator of more than ±1g. Thus, for many tests the oscillator was acting as a hammer. A discussion of the influence of range of strain on the effective modulus of elasticity of soils was presented in Chap. 6; this influence on the design of machine foundations will be discussed in Sec. 10.7.

Methods Based on the “In-Phase Mass”

From the DEGEBO tests and subsequent analyses there developed the concept that a mass of soil moved with the footing. This is illustrated by the zone labeled  $m_s$  beneath the footing in Fig. 10-12. By working backward from the equation for the resonant frequency—

$$f_n = \frac{1}{2\pi} \sqrt{\frac{k}{m + m_s}} \quad (10-18)$$

—one is able to evaluate  $m_s$  for each test. However, it was found that  $m_s$  varied with the dead load, exciting force, base-plate area, mode of vibration, and type of soil on which the oscillator rested.

In spite of the difficulties in obtaining specific values of  $m_s$ , the mass of soil that

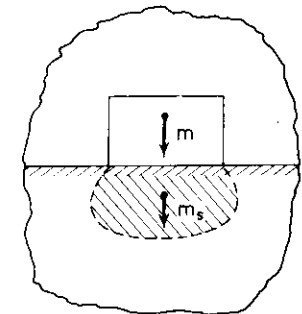


Figure 10-12. “In-phase mass” of soil.

supposedly moves with the footing or is "in phase" with the footing, the concept has appeared periodically in the literature. Crockett and Hammond (1949) and Rao (1961), for example, have attempted to estimate a weight of soil within a "bulb of pressure" in order to force Eq. (10-18) to fit test results. These procedures are principally intuitive; reliable numbers are difficult to obtain for design purposes. Even if the "in-phase mass" could be determined satisfactorily, this information would not lead directly to an evaluation of the amplitude of vibration needed for design purposes. Consequently, at this stage of development of design procedures for dynamically loaded foundations, the "in-phase mass" is not a significant factor.

*Tschebotarioff's "Reduced Natural Frequency"*

In an attempt to improve the methods for evaluating the resonant frequency of machine foundations supported by different soils, Tschebotarioff and Ward (1948) and Tschebotarioff (1953) developed an expression for a "reduced natural frequency" of the system. Beginning with the DEGEBO expression (Eq. 10-18) for the resonant frequency of a foundation (including the effect of an "in-phase mass"), the spring constant  $k$  was replaced by  $k'A$ , where  $k'$  is the dynamic modulus of subgrade reaction (i.e., lb/ft<sup>3</sup>) and  $A$  is the contact area (ft<sup>2</sup>) of the foundation against the soil. With this substitution Eq. (10-18) takes the form

$$f_n = \frac{1}{2\pi} \sqrt{\frac{k'A}{m + m_s}} \tag{10-19}$$

This equation was further rearranged to

$$f_n = \sqrt{\frac{A}{W}} \frac{1}{2\pi} \sqrt{\frac{k'g}{1 + \frac{m_s}{m}}} = \frac{1}{\sqrt{q_0}} f_{nr} \tag{10-20}$$

in which  $q_0$  is the average vertical contact pressure between the base of the foundation and the soil, and the remaining terms are lumped together and called the "reduced natural frequency  $f_{nr}$ ." Then from an evaluation of a limited number of case histories available at the time (1953), Tschebotarioff prepared curves which related  $f_{nr}$  to the base area of the foundation for several soils. These relations appear as straight lines on the log-log plot of Fig. 10-13a. In order to calculate the resonant frequency for a given size footing on a particular soil, Fig. 10-13a gives a value of  $f_{nr}$  which then leads to  $f_n$  by the use of Eq. (10-20) and of the design value of  $q_0$ . It should be noted that

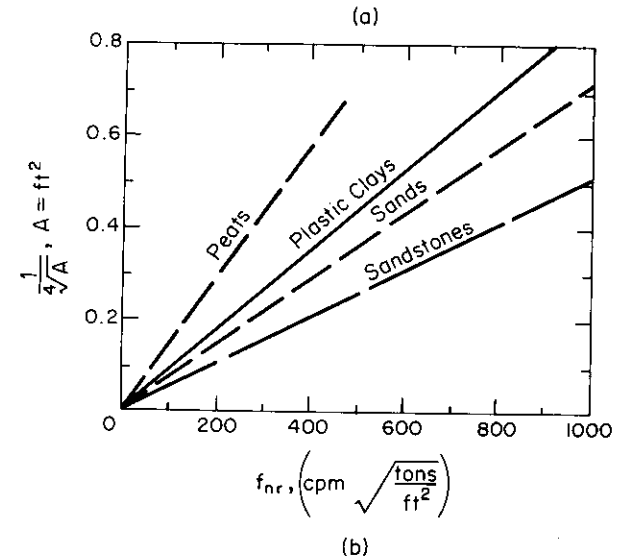
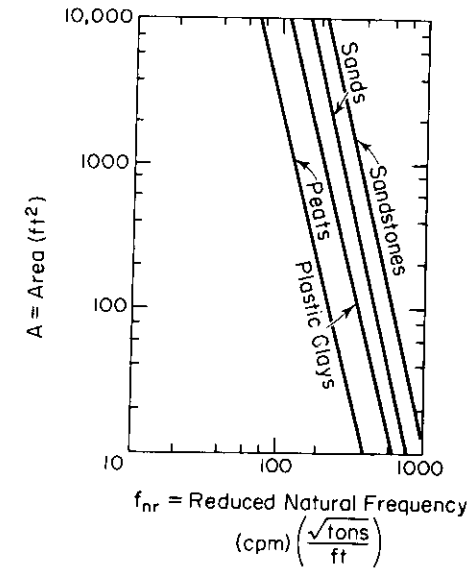


Figure 10-13. Tschebotarioff's "Reduced Natural Frequency."

this method gives *only* an estimate of the resonant *frequency* and tells us nothing about the amplitude of vibration.

Figure 10-13a may be replotted as  $f_{nr}$  vs.  $A^{-1/4}$  to give the diagram shown in Fig. 10-13b. It is of interest to note that relations similar to those in Fig. 10-13b can be predicted from the elastic-half-space theory described in

Chap. 7. For vertical vibrations the mass ratio  $\mathbf{b}$  (Eq. 7-3) can be expressed as

$$\mathbf{b} = \frac{m}{\rho r_o^3} = \frac{W}{\gamma r_o^3} = \frac{W}{\frac{\gamma r_o}{\pi} \pi r_o^2} = \frac{q_o}{\frac{\gamma r_o}{\pi}} \quad (10-21)$$

and the dimensionless frequency  $a_{on}$  (Eq. 7-2) as

$$a_{on} = \omega r_o \sqrt{\frac{\rho}{G}} = 2\pi f_n r_o \sqrt{\frac{\rho}{G}} \quad (10-22a)$$

and

$$a_{on}^2 = 4\pi^2 f_n^2 r_o^2 \frac{\rho}{G} \quad (10-22b)$$

Then,

$$\mathbf{b} a_{on}^2 = \frac{4\pi^3 r_o}{gG} q_o f_n^2 = \frac{4\pi^{5/2} \sqrt{A}}{gG} q_o f_n^2 \quad (10-23)$$

if we substitute  $A = \pi r_o^2$  Equation (10-23) represents the reduced natural frequency:

$$f_n \sqrt{q_o} = \sqrt{\frac{gG \mathbf{b} a_{on}^2}{4\pi^{5/2}}} \frac{1}{\sqrt[4]{A}} = K \frac{\sqrt{G}}{\sqrt[4]{A}} \quad (10-24)$$

For any particular  $\mathbf{b}$ ,  $a_{on}$  is fixed. Thus, Eq. (10-24) illustrates that for a constant value of  $G$  we get a linear relation between  $f_{nr}$  ( $= f_n \sqrt{q_o}$ ) and  $A^{-1/4}$ . Therefore, the lines in Fig. 10-13b designated as peat, plastic clays, sands, and sandstones actually represent typical values of shear modulus  $G$  for these materials.

#### Method Based on the Dynamic Subgrade Reaction

One method for estimating the deflection of a loaded structure resting on soil involves replacing the soil by a set of independent elastic springs which produce an equivalent reactive force to the displacement developed. This concept has been designated as the theory of elastic subgrade reaction. It is discussed in the books by Hayashi (1921), Terzaghi (1943), and Hetenyi (1946), for example, and a comprehensive discussion of methods for evaluating the *coefficients* of elastic subgrade reaction was given by Terzaghi (1955).

Figure 10-14 illustrates the approximations involved in replacing the soil beneath a rigid foundation by a series of springs. Once the representative

values are chosen for the reaction springs, these values are fixed and there is no further modification of their behavior as a consequence of changing the total weight of the oscillating block (i.e., change in confining pressure in the soil) or of the amplitude of vibration (effect of strain). Furthermore, this elastic subgrade rests on a rigid base, and for the dynamic condition it represents a *closed* system. When the system shown in Fig. 10-14 is set into vertical vibration, it responds as an *elastic undamped* system with *amplitudes* of motion at resonance which *approach infinity*. Such a closed system does not include the damping of energy by radiation as does the elastic-half-space theory and gives *no* useful information on the amplitude of motion at frequencies near resonance. *This theory gives useful results only for the undamped natural frequency of vibration.*

As indicated in the previous section, the coefficient of subgrade reaction is related to a spring constant for a given system by

$$k = k'A \quad (10-25)$$

in which the spring constant (lb/ft) is represented as the product of  $k'$  (lb/ft<sup>3</sup> or pressure per unit displacement) multiplied by the foundation-contact area ( $A = \text{ft}^2$ ). Therefore, if we can obtain test information relating the applied load to the displacement we have evaluated  $k$ , and from Eq. (10-25) we can obtain  $k'$ .

Information from plate-bearing tests and field tests on foundations has been used to establish  $k$  for machine foundations. Barkan (1962) has cited numerous field tests which demonstrate that the spring constant applicable to dynamic motion is essentially equal to the ratio of increment of load to increment of deflection (or moment to rotation) during static repeated-loading tests. The resonant frequency observed during dynamic tests on a foundation block was compared with the undamped natural frequency computed using just the mass of the foundation block plus machinery and using the value of  $k$  measured during a static repeated-loading test on the same foundation block. From 15 data points from tests on foundations ranging from 5-ft<sup>2</sup> to 161-ft<sup>2</sup> base area resting on sand, clay, or loess, he found that the observed frequency averaged 97 per cent of the computed frequency and that the extremes ranged from 85 to 121 per cent. Therefore, it was considered that the procedure was satisfactory for estimating resonant frequencies.

The key to the procedure described by Barkan is the use of *repeated* loadings in the static tests. Furthermore, it is important that the magnitudes of the "dead load" and of the "live load" be similar to those anticipated

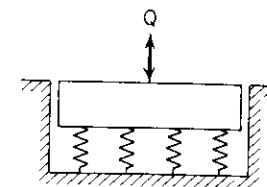


Figure 10-14. Springs replacing soil support to provide "dynamic subgrade reaction."

under the actual foundation. Because of the small movements anticipated (note displacements allowed for prototype foundations given in Fig. 10-1), the process of obtaining reliable load-deformation data from model or prototype footings is not easy. Special instrumentation is usually required for these measurements and particular care is needed in carrying out the tests.

After field data are obtained from tests on model footings, the next problem involves extrapolating this information to prototype dimensions. The discussion by Terzaghi (1955) and others concerning the choice of a modulus of subgrade reaction for static loadings applies as well to the machine-foundation problem. Suggested methods for extrapolating test information are given by Terzaghi (1955) and are indicated below for vertical motions.

For cohesive soils: 
$$k'_z = k'_{z1} \frac{1}{2d} \quad (10-26a)$$

For cohesionless soils: 
$$k'_z = k'_{z1} \left( \frac{2d+1}{4d} \right)^2 \quad (10-26b)$$

in which

$2d$  = width of a beam, or least dimension of foundation base,

$k'_z$  = coefficient of vertical subgrade reaction for base of least dimension of  $2d$  (lb/ft<sup>3</sup>), and

$k'_{z1}$  = coefficient of vertical subgrade reaction for base of least dimension of 1 ft (lb/ft<sup>3</sup>).

Thus, the test data provide information for establishing the values of  $k'_{z1}$  for the unit dimensions, then Eqs. (10-26a) and (10-26b) are used to adjust the subgrade coefficient to correspond to the prototype dimensions. This procedure is reasonable only when both the model footing and the prototype footing produce equivalent stresses in similar soils.

Barkan (1936, 1962) has utilized the concept of elastic-subgrade reaction extensively and has indicated spring constants for the various modes of vibration of rigid foundations in the following form:

For vertical motion:

$$k_z = k'_z A$$

For horizontal motion:

$$k_x = k'_x A$$

For rocking motion:

$$k_\psi = k'_\psi I' \quad (10-27)$$

For torsional motion:

$$k_\theta = k'_\theta I''$$

in which

$A$  = contact area between foundation and soil,

$I'$  = second moment of contact area about a horizontal axis normal to the plane of rocking through the centroid, and

$I''$  = second moment of the contact area about a vertical axis through the centroid.

The coefficients  $k'_z$ ,  $k'_x$ ,  $k'_\psi$ , and  $k'_\theta$  are coefficients of subgrade reaction and are functions of soil type and of size and shape of the foundation. However, these are often assumed to be functions only of soil type. Barkan (1962) provided the data in Table 10-10 for  $k'_z$  and has suggested that the remaining coefficients can be evaluated as

$$\begin{aligned} k'_x &\approx 0.5k'_z \\ k'_\psi &\approx 2k'_z \\ k'_\theta &\approx 1.5k'_z \end{aligned} \quad (10-28)$$

The spring constants computed on the basis of Eq. (10-28) and Table 10-10 could be used for preliminary design when reliable soil information is not available. However, it is recommended that the procedures outlined in Secs. 10-6 and 10-7 be used for design purposes.

Table 10-10. Recommended Design Values for Subgrade Coefficient  $k'_z$ \*

Soil Group	Allowable Static Bearing Stress (ton/ft <sup>2</sup> )	Coefficient $k'_z$ (ton/ft <sup>3</sup> )
Weak soils (clay and silty clays with sand, in a plastic state; clayey and silty sands)	1.5	95
Soils of medium strength (clays and silty clays with sand, close to the plastic limit; sand)	1.5-3.5	95-155
Strong soils (clay and silty clays with sand, of hard consistency; gravels and gravelly sands, loess and loessial soils)	3.5-5	155-310
Rocks	5	310

\* After Barkan (1962).

### Elastic-Half-Space Theory

The representation of a foundation on soil by a footing resting on a semi-infinite elastic body was discussed extensively in Chap. 7. This elastic-half-space theory includes the dissipation of energy throughout the half-space



by "geometrical damping." This theory permits calculation of finite amplitudes of vibration at the "resonant" frequency. The entire amplitude-frequency response curve may be obtained as well as the phase angle between the exciting force and footing motion and the input power required. Because the elastic-half-space theory is an analytical procedure, certain mathematical simplifications have been introduced which are not quite realistic. The footing is assumed to rest on the surface of the half-space and to have simple geometrical areas of contact, usually circular but occasionally rectangular or a long strip. The half-space itself is assumed to consist of an ideal elastic, homogeneous, isotropic material. However, the analytical solutions serve as a useful guide for evaluation of the dynamic response of simple footings undergoing single modes of vibration. They also provide a rational means of evaluating the spring and damping constants which may then be incorporated into the lumped-parameter, mass-spring-dashpot vibrating system.

### 10.5 Lumped-Parameter Vibrating Systems

In a study by Richart and Whitman (1967) it was shown that the dynamic behavior of actual foundations could be predicted by the elastic-half-space theory. Furthermore, Lysmer (1965) had shown that vertical vibrations of a rigid circular footing on the elastic half-space could be represented quite satisfactorily by a mass-spring-dashpot system if the damping constant and spring constant were chosen correctly. Therefore, it followed that the lumped-parameter system represented by a mass, spring, and dashpot could be used to represent the motion of rigid foundations. The lumped-parameter system treats all the masses, springs, and damping components of the system as if they were lumped into a single mass, single spring, and single damping constant for each mode of vibration. A description of the lumped-parameter system equivalent to the half-space model for each mode of vibration was given in Chap. 7; Fig. 10-15 illustrates typical equivalent lumped systems for foundations subjected to vertical, horizontal, and torsional exciting forces. Note that in Fig. 10-15 the vertical and torsional excitations produce motion with a single degree of freedom but that the horizontal excitation produces a coupled motion involving both rocking and sliding.

For a single-degree-of-freedom system the lumped parameters lead to an equation of motion of the type

$$m\ddot{z} + c\dot{z} + kz = Q(t) \tag{2-48}$$

in which

- $m$  = equivalent mass,
- $c$  = effective damping constant,
- $k$  = effective spring constant,

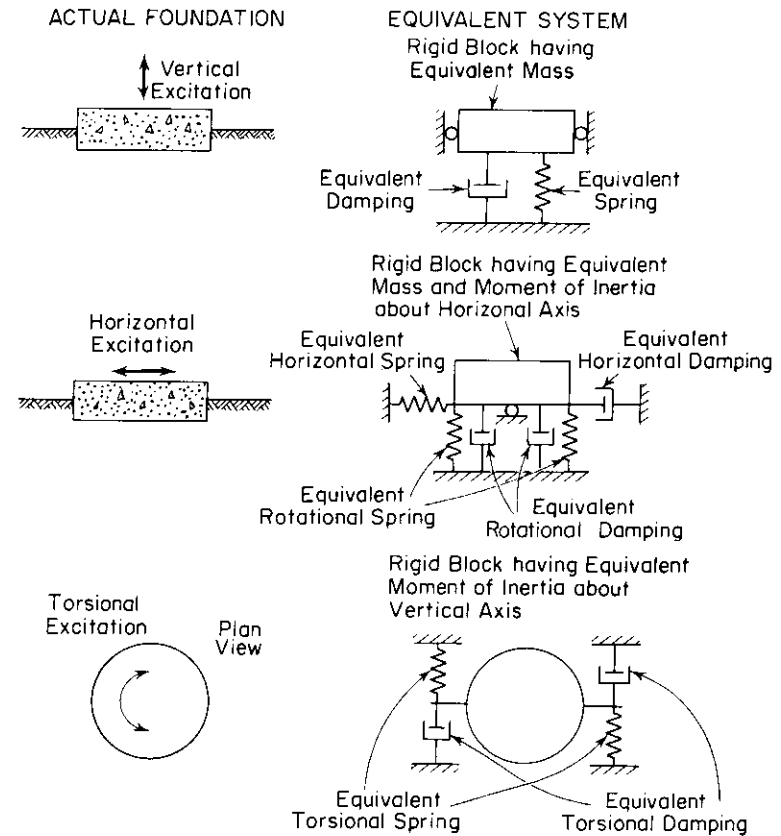


Figure 10-15. Typical equivalent lumped systems.

$Q(t)$  = time-dependent exciting force, and

$z, \dot{z}, \ddot{z}$  = displacement, velocity, and acceleration, respectively, of the mass in the direction of the chosen coordinate (in this example the vertical direction was chosen).

Analytical and graphical methods for treating the lumped-parameter systems were described in Chap. 2, and many books are available which include comprehensive discussions of this topic. Consequently, any procedure which permits a dynamically loaded foundation to be represented by lumped parameters simplifies our analysis of the foundation response.

In Chap. 2 it was noted that the exciting force  $Q(t)$  in Eq. (2-48) can be expressed as  $(Q_0 \sin \omega t)$ , in which the force amplitude  $Q_0$  is either a constant or a function of the circular frequency  $\omega$ . When the force amplitude is a function of the frequency it is evaluated from Eq. (10-2). The expressions which describe the response of a mass  $m$  to either type of exciting force are

Table 10-11. Summary of Parameters Required for Dynamic Analysis

Analysis	Factors Required	
Approximate estimate for resonant frequency	$k$ and $m$	
Approximate estimate for motion at frequencies well away from resonance	$\ll f_0$	$k$
	$\gg f_0$	$m$
Upper limit for motion at frequencies near resonant frequency	$D$ and $k$ or $m$	

summarized in Table A-1 in the Appendix for the single-degree-of-freedom system. Note that the relations in Table A-1 apply to each of the six modes of vibration, but that the vertical coordinate  $z$  was chosen for the example. From Table A-1 it can be seen that the lumped parameters influence different expressions relating to the response of the mass  $m$ ; these effects are summarized in Table 10-11.

*Choice of Mass for Equivalent Lumped Systems*

The method recommended in this text for establishing the lumped parameters for the equivalent mass-spring-dashpot system is based on the elastic-half-space theory. *The lumped mass is chosen as the mass of the foundation and supported machinery.* Then the damping and spring constants are developed through the theory and have values as indicated in Table A-2 for the case of rigid circular footings.

The method based upon the concept of an "in-phase mass" of soil leads only to an estimate of the natural frequency of the system and gives no information relating to the amplitude of vibration at resonance. Consequently, this method is not satisfactory for determining the lumped parameters for a vibrating system which includes damping.

*Choice of Damping for Equivalent Lumped Systems*

The dashpots of the lumped system represent the damping of the soil in the foundation-soil system. There are two types of damping in the real system: one introduced by the loss of energy through propagation of elastic

waves away from the immediate vicinity of the footing, the other associated with internal energy losses within the soil due to hysteretic and viscous effects. The equivalent damping corresponding to the elastic-wave propagation has been designated as "geometrical damping" (Chap. 7) or is occasionally called "radiation damping." Expressions for the damping ratio  $D$  obtained through the half-space theory and corresponding analogs for *rigid circular footings* are summarized in Table A-2. This information is also shown in graphical form in Fig. 7-19.

The equations and diagrams for geometrical damping developed by vibrations of a rigid circular footing on the elastic half-space may also be used to provide estimates for the geometrical damping developed by footings with rectangular-plan form. This is accomplished by converting the rectangular base of dimensions  $2c$ -by- $2d$  into an equivalent circular base having a radius  $r_0$ , determined by the following:

For translation: 
$$r_0 = \sqrt{\frac{4cd}{\pi}} \tag{10-29a}$$

For rocking: 
$$r_0 = \sqrt{\frac{16cd^3}{3\pi}} \tag{10-29b}$$

For torsion: 
$$r_0 = \sqrt[4]{\frac{16cd(c^2 + d^2)}{6\pi}} \tag{10-29c}$$

in which

$2c$  = width of the foundation (along axis of rotation for the case of rocking), and

$2d$  = length of the foundation (in the plane of rotation for rocking).

The internal damping in soils has been discussed in Chap. 6. Table 10-12 summarizes some of the available information relating to internal damping of soils at the level of stress changes occurring under machine foundations. (Where the test results are given as damping capacity or log decrement, they are expressed in terms of an equivalent damping ratio  $D$ .) From Table 10-12 it is evident that a typical value of  $D$  is on the order of 0.05 for internal damping in soils.

The lumped damping parameter for any particular foundation-soil system will include both the effects of geometrical and internal damping. If we take the value of 0.05 to represent a typical internal-damping ratio, then by comparing this value with the geometrical damping from Fig. 7-19, we can estimate the contribution of each. It is evident from this examination that for vibrations in translatory modes, the geometrical damping overshadows the internal damping to the point where the latter may be disregarded in

Table 10-12. Some Typical Values of Internal Damping in Soils

Type Soil	Equivalent $D$	Reference
Dry sand and gravel	0.03–0.07	Weissmann and Hart (1961)
Dry and saturated sand	0.01–0.03	Hall and Richart (1963)
Dry sand	0.03	Whitman (1963)
Dry and saturated sands and gravels	0.05–0.06	Barkan (1962)
Clay	0.02–0.05	Barkan (1962)
Silty sand	0.03–0.10	Stevens (1966)
Dry sand	0.01–0.03	Hardin (1965)

preliminary analyses. On the other hand, for the rotary modes of vibration—torsion and rocking—the geometrical damping is small and, for rocking in particular, these two damping terms may be of the same order of magnitude. In this case, the internal damping is important and should be included.

This comparison of the effectiveness of geometrical damping and internal damping illustrates the value of the elastic-half-space theory in establishing values for geometrical damping for motions of simple footings in each of the modes of vibration. The values of geometrical damping thus obtained should be considered as a first approximation, however, because the theory treats footings resting *on the surface* of the elastic half-space; whereas actual foundations are often partially embedded. Barkan (1962), Pauw (1952), and Fry (1963) have reported on tests of footings partially embedded as well as on footings resting on the surface of the soil. In general, partial embedment reduced the amplitude of motion at the resonant peaks and increased the value of the resonant frequency. This indicates an increase in the effective spring constant as well as a probable increase in the effective damping ratio. However, the effects on amplitude and frequency in the tests depended upon the mode of vibration and magnitude of the motion. For motions within the range of design criteria for machinery, it appears that this reduction in amplitude resulting from partial embedment is on the order of 10 to 25 per cent. Therefore, the design calculations will err on the conservative side if the footing is considered to rest on the surface. Further field tests are needed to establish the influence of partial embedment, particularly for the rocking mode.

A second major discrepancy between the assumptions made in the theoretical treatment and real conditions is the assumption that the soil is a homogeneous, isotropic, elastic body. Often a soil stratum is layered and may have a hard stratum of soil or rock at a shallow depth below the footing. This problem was discussed briefly in Sec. 7.9, in which it was noted that

the amplitudes of vibration at resonance were increased by the presence of the underlying rigid layer. This indicates that radiation of energy from the footing was impeded by the presence of the rigid layer and that part of this elastic-wave energy was reflected back to the footing. Further studies should be directed toward evaluations of the geometrical damping related to vibrations of footings supported by layered media as well as of footings supported by soils which vary in stiffness with depth or confining pressure.

#### *Choice of Spring Constant for Equivalent Lumped Systems*

The spring constant  $k$  is the most critical factor in the lumped-parameter analysis. It governs the static displacement of the foundation which would be developed by application of a static force equal to the dynamic force  $Q_0$ ; and this static displacement is multiplied by a magnification factor  $M$  to establish the maximum amplitude of dynamic motion. The magnification factor (Eq. 2-53) is influenced by  $k$  through its contribution to the critical-damping coefficient  $c_c$  (Eq. 2-31), and thus to the damping ratio  $D$  (Eq. 2-32). Finally,  $k$  is the significant unknown in establishing the resonant frequency (Eqs. 2-17, 2-55, or 2-60). Methods for establishing  $k$  include static field tests of prototype foundations, static or dynamic field tests of model foundations, or theoretical methods.

**Tests on prototype foundations.** Tests on the prototype foundations are, of course, preferable if the tests are carefully conducted to include ranges of load and deformations corresponding to acceptable operating conditions. Pile-loading tests and tests of foundations supported by pile groups have often been conducted, but usually these have been for the purpose of evaluating the load-carrying capacity rather than the spring constant. The same type of test can provide useful information about the  $k$  required for dynamic analysis if repeated static loadings or vibratory loadings are applied and realistic ratios of steady load to alternating load are maintained. Tests of prototypes are recommended if several foundations of similar characteristics are to be built at one construction site. However, if only one structure is planned, the test on the prototype may indicate either a satisfactory or unsatisfactory performance. An unsatisfactory performance may require costly repairs that could have been minimized by a more careful design in the first place.

**Tests on model footings.** Static or dynamic tests of model footings are useful for establishing relations between the applied loads and response of these footings for particular subsoil conditions. A comprehensive program of carefully controlled model tests, exemplified by the vibration tests reported by Fry (1963), provides not only information about the response of the

individual footings but also permits evaluation of the best methods for extrapolating this information for use in the design of prototype foundations. It is the extrapolation procedure which governs the value of model-footing tests for design purposes.

**Formulas for spring constants.** The spring constant represents a linear relation between applied load and displacement of the foundation which implies a linear stress-strain relation for the soil. Therefore, it follows that theory of elasticity can provide useful formulas for the spring constants for footings of simple shapes. Tables 10-13 and 10-14 include spring constants obtained through the theory of elasticity for circular and rectangular footings resting on the surface of the elastic half-space. These expressions have been obtained for rigid footings except for the case of horizontal motion, for which the spring constant was obtained by assuming a uniform distribution of shearing stress on the contact area and computing the average horizontal displacement of this area. These formulas apply for situations corresponding to rigid block or mat foundations with shallow embedment.

Table 10-13. Spring Constants for Rigid Circular Footing Resting on Elastic Half-Space

Motion	Spring Constant	Reference
Vertical	$k_z = \frac{4Gr_o}{1-\nu}$	Timoshenko and Goodier (1951)
Horizontal	$k_x = \frac{32(1-\nu)Gr_o}{7-8\nu}$	Bycroft (1956)
Rocking	$k_\psi = \frac{8Gr_o^3}{3(1-\nu)}$	Borowicka (1943)
Torsion	$k_\Theta = \frac{16}{3}Gr_o^3$	Reissner and Sagoci (1944)

(Note:  $G = \frac{E}{2(1+\nu)}$ )

Table 10-14. Spring Constants for Rigid Rectangular Footing Resting on Elastic Half-Space

Motion	Spring Constant	Reference
Vertical	$k_z = \frac{G}{1-\nu} \beta_z \sqrt{4cd}$	Barkan (1962)
Horizontal	$k_x = 4(1+\nu)G\beta_x \sqrt{cd}$	Barkan (1962)
Rocking	$k_\psi = \frac{G}{1-\nu} \beta_\psi 8cd^2$	Gorbunov-Possadov (1961)

(Note: values for  $\beta_z, \beta_x,$  and  $\beta_\psi$  are given in Fig. 10-16 for various values of  $d/c$ )

The effect of embedment is to increase the soil resistance to motion of the foundation; thus, the effective spring constant is increased. Figure 10-17 illustrates the change in vertical spring constants for circular footings as the depth of embedment increases. Curve *a* represents a rigid footing which adheres to the soil along the vertical surface, thereby developing skin-friction resistance to vertical motion of the block as well as developing resistance by pressure on the base. Curve *b* corresponds approximately to the situation of an embedded foundation which is isolated from the soil along the vertical surfaces. It is included to point out the increase in spring constant developed only by base pressure applied at different depths. The spring constants corresponding to curve *b* were obtained from the average settlement produced by a uniformly distributed load applied at the different depths of embedment. By comparing the spring constants for curve *a* (with side adhesion) and curve *b* (without side adhesion), it is possible to separate the effects of end bearing and skin friction. The information shown in Fig. 10-17 was prepared by Kaldjian (1969) from a solution of the elasticity problem by the finite-element method.

The depth of embedment should produce even more significant effects on the spring constants for rocking and sliding motions of the foundation. However, by the end of the 1960s, satisfactory solutions for these problems were not known to the writers.

Another effect which provides a stiffening to the spring constant of the foundation is the presence of a rigid boundary beneath an elastic layer. That is, a thin elastic layer supported by a rigid base permits a smaller displacement of a footing for a given load than does the elastic half-space. This was

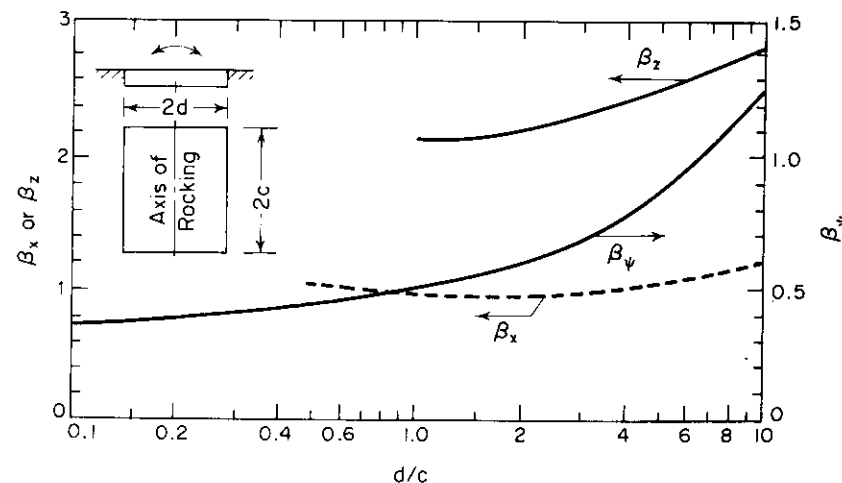


Figure 10-16. Coefficients  $\beta_z, \beta_x,$  and  $\beta_\psi$  for rectangular footings (after Whitman and Richart, 1967).

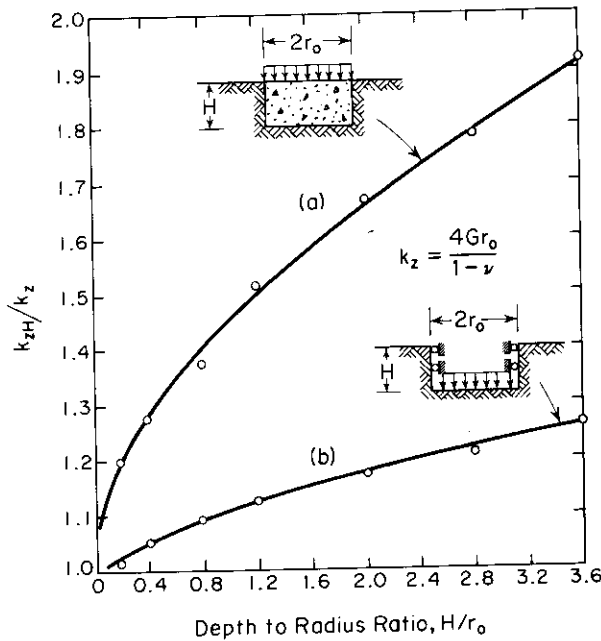


Figure 10-17. Effect of depth of embedment on the spring constant for vertically loaded circular footings (from Kaldjian, 1969).

illustrated by Fig. 7-22, in which the increase in  $k$  (for vertical loading) was shown to be significant as the value of  $H/r_0$  (where  $H$  is the thickness of the elastic layer) decreased below about 2.

**Elastic constants for soils.** In the preceding section, which discussed formulas for spring constants, it was indicated that these were derived from solutions by the theory of elasticity. It should be emphasized that the elastic medium was assumed to be isotropic and homogeneous; therefore, only two elastic constants are required in the solution. Throughout this book the elastic constants chosen have been the modulus of elasticity in shear,  $G$ , and Poisson's ratio  $\nu$ . Consequently, in order to evaluate spring constants for foundations from the formulas, we need reliable values for  $G$  and  $\nu$  for the soil beneath the proposed foundation.

It is possible to compute Poisson's ratio for soils from measured values of the compression-wave and shear-wave velocities through the soil (see Chap. 3). However, these computations involve small differences of rather large numbers, and significant errors are possible. Generally, it has been found that Poisson's ratio varies from about 0.25 to 0.35 for cohesionless soils and from about 0.35 to 0.45 for cohesive soils which are capable of supporting block-type foundations. Consequently, for design purposes little error is introduced if Poisson's ratio is assumed as  $\frac{1}{3}$  for cohesionless soils and as 0.40 for cohesive soils.

Values of the shear modulus  $G$  may be evaluated in the field or from samples taken to the laboratory. Static plate-bearing tests in the field can establish an experimental value of the spring constant  $k$ , from which the shear modulus can be calculated (Table 10-13). *In-situ* steady-state-vibration tests may also be used to establish values of  $G$  at the construction site (see Sec. 4.3). In the laboratory the resonant-column test (see Sec. 9.6) is now a standard method for determining the effective  $G$  of soil samples for design purposes as well as being a research tool. Consequently, several methods are available for obtaining useful values of  $G$  by testing the actual soil which will support the proposed foundation. In the event the design study represents only a preliminary estimate or a feasibility study, reasonable values of  $G$  for soils can be estimated if we have some information on the void ratio of the soil and of the probable confining pressure  $\bar{\sigma}_o$ . Figure 6-8 illustrates the dependence of the shear-wave velocity of quartz sand on the void ratio and confining pressure. The shear modulus can be obtained from the shear-wave velocity given in Fig. 6-8 and the relation

$$G = \rho v_s^2 \tag{6-17}$$

For round-grained sands ( $e < 0.80$ ) the shear modulus can be estimated from the empirical equation

$$G = \frac{2630(2.17 - e)^2}{1 + e} (\bar{\sigma}_o)^{0.5} \tag{6-19}$$

and, for angular-grained materials ( $e > 0.6$ ), from

$$G = \frac{1230(2.97 - e)^2}{1 + e} (\bar{\sigma}_o)^{0.5} \tag{6-21}$$

in which both  $G$  and  $\bar{\sigma}_o$  are expressed in lb/in.<sup>2</sup>. Hardin and Black (1968) have indicated that Eq. (6-21) is also a reasonable approximation for the shear modulus of normally consolidated clays with low surface activity.

### 10.6 Analysis and Design for Vertical Vibrations of Foundations

In many cases machines which produce vertical forces can be located centrally on foundation blocks or mats with the result that only vertical vibrations of the machine-foundation system are important. This section includes examples of analyses of such systems based on both the elastic-half-space theory (Chap. 7) and on the lumped-parameter analog.

Steady-State Vibrations of Model Footings

It is useful to begin this section with a comparison of the vibration response estimated by theory and that measured in carefully controlled field tests on model footings. Fry (1963) has reported on tests conducted on model footings from about 5-ft to 16-ft diameter constructed at the U.S. Army Waterways Experiment Station in Vicksburg, Mississippi, and at Eglin Field, Florida. The basic dimensions and weights of the footings are given in Table 10-15. All of these circular footings were constructed on the surface of the soil, except for base 5 at the Eglin Field site, which was embedded 25 in. The soil at the WES site was a silty clay (CL), for which typical parameters needed for dynamic analysis are

$$\begin{aligned} \gamma &= 117 \text{ lb/ft}^3 \\ v_s &= 460 \text{ ft/sec} \\ G &= 5340 \text{ lb/in.}^2 \\ \nu &= 0.35 \end{aligned}$$

The water table was approximately 16 ft from the surface. At the Eglin Field site the soil was a nonplastic uniform fine sand (SP) with uniform conditions indicated from borings to 25 ft below the surface as well as reasonably uniform conditions indicated throughout the test area. The water table was deep and was not encountered in any of the boreholes. For this material a typical void ratio was  $e = 0.70$ .

The footings were excited by a rotating-mass vibrator of the type illustrated in Fig. 10-5c. The four eccentric masses each had a weight of 339 lb; so the total eccentric weight was 1356 lb. The total static weight of the vibrator was 5600 lb. Four eccentric settings were used in the testing program: 0.105 in., 0.209 in., 0.314 in., and 0.418 in. Values of force output from

Table 10-15. Data on WES Test Bases

Base No.	$r_o$ (in.)	Thickness (in.)	Wt. of Base + Vibrator (lb)
1—1st pour	31	14.3	12,820
1—2nd pour	31	29.7	25,640
1—3rd pour	31	36.0	30,970
2	43.81	20.5	18,465
3	54.0	24.0	24,315
4	62.0	24.5	30,970
5	43.81	25.0	18,465
16	96.0	24.0	64,961

Table 10-16. Vertical Forces from Four-Mass WES Oscillator

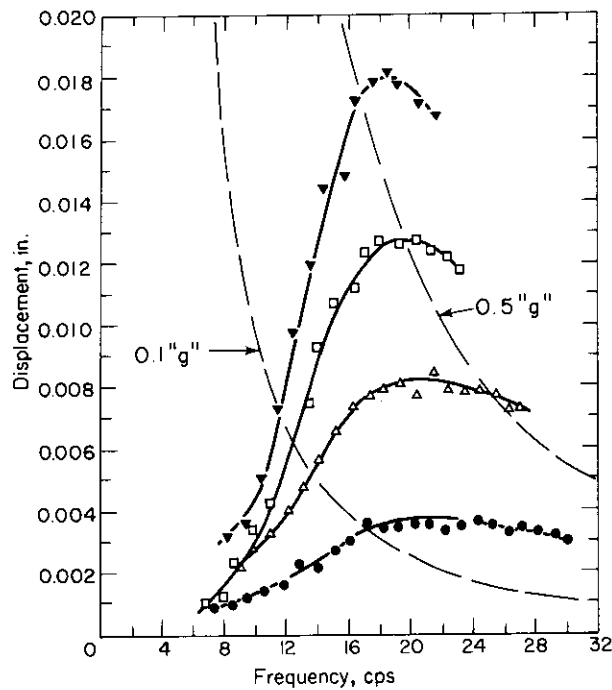
Rotating Frequency (cycles/sec)	15	20	25	30
$Q_o$ (lb) for $e = 0.105$ in.	3,285	5,840	9,125	13,140
$Q_o$ (lb) for $e = 0.209$ in.	6,540	11,620	18,160	26,160
$Q_o$ (lb) for $e = 0.314$ in.	9,825	17,460	27,290	39,300
$Q_o$ (lb) for $e = 0.418$ in.	13,020	23,140	36,160	52,070

this vibrator can be calculated from Eq. (10-2), and several values are indicated in Table 10-16 to establish the order of magnitude of forces involved.

By comparing the static weights of the footings in Table 10-15 with the dynamic forces available from the vibrator at the higher speeds from Table 10-16, it is evident that the vibrator was capable of lifting some of the lighter footings free of the ground during vibration. Consequently, for some of the tests, additional weights were rigidly attached to the footing.

For the purpose of comparing theoretical and test results, three tests at the WES site and three tests at the Eglin Field site were chosen. In each of these tests the vibrator had an eccentricity setting of 0.105 in., which produced the smallest set of exciting forces and the lowest accelerations in each pattern of tests. Figure 10-18 (after Fry, 1963) illustrates the effect on the amplitude-frequency response curve developed by changing the eccentric settings of the rotating weights for particular test conditions. Note that for WES test 3-6 in Fig. 10-18 a motion of about 0.0037 in. was developed at 20 cycles/sec. Dashed curves are shown in Fig. 10-18 which correspond to peak accelerations of (0.1)g and (0.5)g. The response curves shown in Fig. 10-18 could also have been plotted in Fig. 10-3, which would permit an easier evaluation of the peak velocities and accelerations. From Fig. 10-18 it can be noted that the peak accelerations for tests 3-7, 3-8, and 3-9 were greater than (0.5)g. The largest value of peak acceleration for test 3-9 was (0.7)g.

The test results for the model footings can be evaluated better when they are presented on dimensionless plots. For example, we may consider three tests at the WES site, tests 2-18, 3-6, and 4-5, for which the mass ratios were  $b = 3.12$ ,  $b = 2.83$ , and  $b = 3.1$ , respectively. Points representing test data are shown in Fig. 10-19a for comparison with the theoretical curves for  $b = 3$  and  $\nu = \frac{1}{3}$  (or  $B_z = 0.5$ ). Theoretical curves for the rigid-base pressure ( $R$ ) and the uniform-pressure ( $U$ ) distribution (from Sung, 1953) are shown. From Fig. 10-19a it is evident that the agreement between the test results and the  $R$ -curve is reasonably good with respect to amplitude of vibration, but that the theoretical curve indicates a higher frequency at maximum amplitude



Legend.

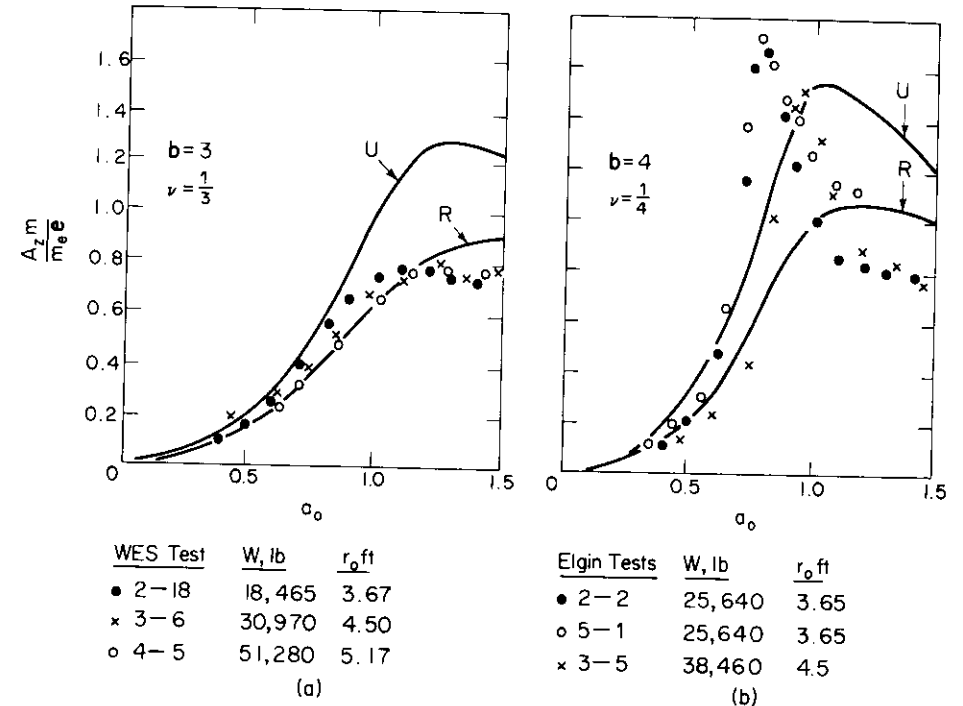
Symbol.	Run No.	ECC Setting—in.
●	6	0.105
▲	7	0.209
□	8	0.314
▼	9	0.418

Note: 6655 lb ballast, 30,970 lb total weight including vibrator

Fig. 10-18. Typical amplitude-frequency response curves for tests on model footings (after Fry, 1963).

than that shown by test. For these tests, in which the footings were supported by a cohesive soil, it appears that the rigid-base condition is approximated.

Tests 2-2, 5-1, and 3-5 run at the Eglin Field site provided the dimensionless test data shown in Fig. 10-19b. For these tests the *b*-values were 4.5, 4.5, and 3.61, respectively; so they were compared with the theoretical values for *b* = 4.



WES Test	W, lb	r <sub>0</sub> ft
● 2-18	18,465	3.67
× 3-6	30,970	4.50
○ 4-5	51,280	5.17

(a)

Eglin Tests	W, lb	r <sub>0</sub> ft
● 2-2	25,640	3.65
○ 5-1	25,640	3.65
× 3-5	38,460	4.5

(b)

Figure 10-19. Comparison of test results with theory for vertical oscillation (a) Data from WES test site. (b) Data from Eglin Field test site.

In order to interpret the test frequency in terms of the dimensionless frequency

$$a_0 = \frac{2\pi f r_0}{v_s} \tag{7-2}$$

it is necessary to obtain a representative value of *v<sub>s</sub>*. At the Eglin Field site the footings were poured on the sand surface (except for base 5, which was embedded). Thus, the sand beneath the footing was loaded by the weight of the footing and ballast as well as by its own weight. For an approximation to the pressure developed below the periphery of the footing, the theoretical solution obtained by Prange (1965) for a rigid circular footing on the isotropic, homogeneous, elastic half-space was used. These relations are given below for  $\nu = \frac{1}{4}$ . It is obvious that a bed of sand develops a different

$\frac{z}{r_0}$	0.1	0.2	0.4	0.6	0.8	1.0	1.5	2.0	3.0
$\frac{\bar{Q}_0}{\pi r^2 \bar{\sigma}_0}$	0.642	0.440	0.293	0.222	0.178	0.147	0.096	0.067	0.037

distribution of pressure under loading than does the ideal half-space, and further information is needed on the effects of repeated loadings on the distribution of contact pressure at the footing base, as well as information on the vertical and horizontal pressures within the soil mass.

Figure 10-20a shows a rigid circular footing resting on the surface of a soil mass. The radius and weight of the footing correspond to that for base 3 used in the Eglin Field tests. The average contact pressure was  $q = 604.6$  lb/ft<sup>2</sup>; Fig. 10-20b shows how the average confining pressure  $\bar{\sigma}_{oq}$  caused by this surface pressure decreases with depth below the periphery of the footing according to Prange's solution.

The unit weight of the sand at the Eglin Field site was approximately 97 lb/ft<sup>3</sup> and it was assumed that Poisson's ratio was  $\frac{1}{4}$  for this material. Then the vertical and horizontal stresses at a depth in the soil mass were

$$\sigma_z = \gamma z \tag{10-34a}$$

and

$$\sigma_x = \sigma_y = \frac{\nu}{1 - \nu} \sigma_z = \frac{\gamma z}{3} \tag{10-34b}$$

These stresses established  $\bar{\sigma}_{os}$  as  $(1.67/3)\gamma z$ .

The total average confining pressure at any depth below the perimeter of the footing is the sum of  $\bar{\sigma}_{oq}$  and  $\bar{\sigma}_{os}$ , as shown by Fig. 10-20d. A minimum value of  $\bar{\sigma}_{o\ tot}$  usually occurs at a depth of  $z/r_o \leq 1$ . This minimum value of  $\bar{\sigma}_{o\ tot}$  and the void ratio of the sand ( $e = 0.7$  at the Eglin Field site) were introduced into the equation for velocity of the shear wave

$$v_s = [170 - (78.2)e](\bar{\sigma}_o)^{0.25} \tag{6-18}$$

By this procedure, values of  $v_s$  of 460, 470, and 500 ft/sec were determined for the soil directly beneath Eglin Field bases 2, 3, and 5, respectively.

Note that errors in the calculation of  $v_s$  (or  $G$ ) have an important influence on the value of  $a_o$  for maximum amplitude of vibration. Conversely, if the theoretical curves are to be used for predicting the frequency for design or analysis, this also depends on the value of  $v_s$ . In Fig. 10-19b the peak amplitudes are at a lower value of  $a_o$  than indicated by theory, and the shapes of the response curves indicate less damping than might be indicated from theory. Part of this difference could be assigned to a probable change in pressure distribution beneath the footing from the assumed rigid-base ( $R$ ) condition to one more nearly uniform. The theoretical curve for the uniform ( $U$ ) pressure distribution for  $b = 4$  and  $\nu = \frac{1}{3}$  is shown in Fig. 10-19b for comparison. The amplitudes of oscillation for the test footings agree fairly well with those predicted from the uniform pressure distribution condition.

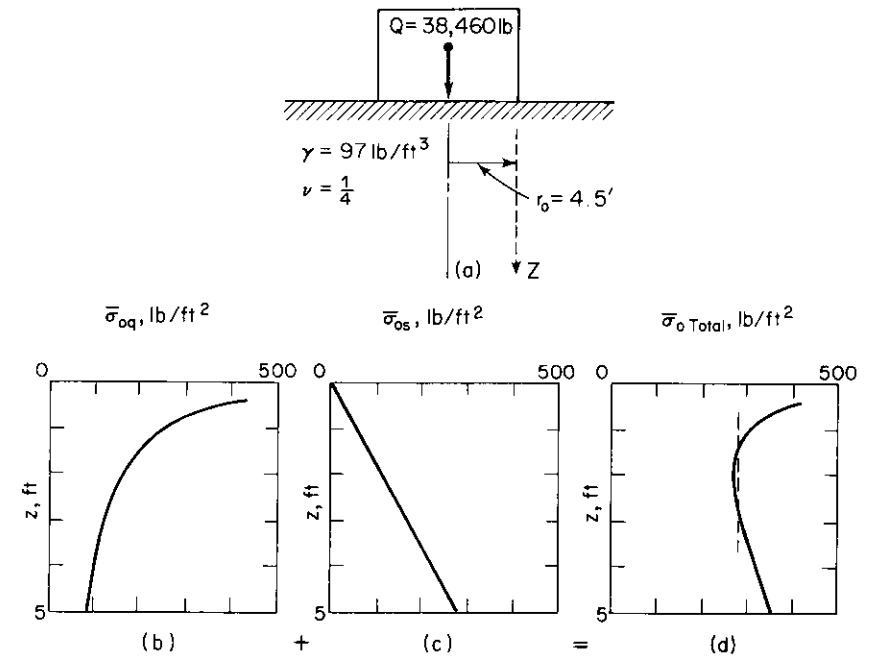


Figure 10-20. Distribution of average confining pressure,  $\bar{\sigma}_o$ , beneath periphery of rigid footing. (a) Vertical load on footing. (b)  $\bar{\sigma}_{oq}$  from footing load. (c)  $\bar{\sigma}_{os}$  from unit weight of soil. (d) Total  $\bar{\sigma}_o = \bar{\sigma}_{oq} + \bar{\sigma}_{os}$ .

The entire test program of vertical vibrations of the model footings included 94 tests. Figure 10-21 illustrates the relations between the maximum amplitudes of motion as computed from the half-space theory and those measured in the WES tests. The abscissa of Fig. 10-21 represents the maximum vertical acceleration of the footing as compared with the acceleration

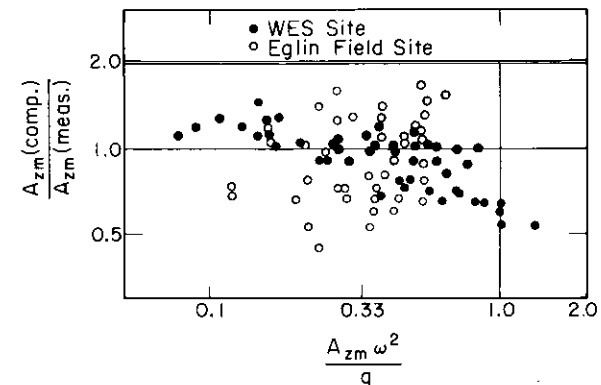


Figure 10-21. Vertical vibration of model footings, summary of 94 tests.



of gravity  $g$ . From Fig. 10-21 it is seen that the theoretical and test values for tests at the WES site agree closely for  $A_{zm}\omega^2/g$  less than about  $\frac{1}{3}$ . As the acceleration ratio increases, these test and theoretical values differ more. The test results from the Eglin Field site show considerably more scatter throughout the entire range of acceleration ratios. However, the overall agreement between test and theory is within a factor of about 2, which is considered good for dynamic problems.

One item which should be noted with regard to the tests at the Eglin Field site is the matter of *total settlement* of the footings over the course of the vibration tests. For each pattern of tests, the response curves were obtained by increasing the eccentricity of the rotating mass successively through the four settings; then the dead load was changed and the next loading pattern was applied. By this procedure the soil beneath the footing had been subjected to a complex load-history by the time the second loading pattern was applied. Converse (1953) has shown that vibrating footings on sand tend to develop a "hard zone" beneath the center of the footings after sustained high-amplitude vibrations; so it would be anticipated that the pressure distribution beneath the footing would change as the loading history of the sand changed. Finally, settlement records were kept and the average total settlements at the end of the test program were about  $4\frac{3}{8}$  in. for base 2,  $1\frac{1}{2}$  in. for base 3,  $\frac{5}{8}$  in. for base 4, and 3 in. for base 5. Consequently, these footings produced local failures and compaction of the supporting soil during some parts of the test program. For an actual machine foundation, a proper design would prevent this progressive settlement, and it could be anticipated that the soil would behave more nearly like the elastic half-space.

*Vertical Single-Cylinder Compressor*

This type of machine develops vertical periodic forces which can produce a vertical motion of the machine and its foundation block. This motion must be restricted to acceptable values, as noted in Sec. 10.2, to provide for satisfactory operation of the machine. The following discussion treats a method for establishing the foundation-block size for a vertical single-cylinder compressor having the following characteristics:

- Bore = 14.5 in.
  - Stroke = 9 in.
  - Operating frequency = 450 rpm
- Unbalanced forces
- Vertical: primary = 9,180 lb

- secondary = 2,220 lb
- Horizontal: primary = 310 lb
- secondary = 0 lb
- Weight of compressor
- + motor = 10,900 lb

The vertical primary and secondary forces produce a periodic vertical force as indicated in Fig. 10-22 by the heavy solid curve. However, for purposes of analysis, the reduced lower portion of the real-force-time curve will be ignored and the excitation will be considered to be developed by a sinusoidal force having an amplitude of  $Q_o = 11,400$  lb at 450 rpm.

This compressor is to be supported by a foundation block resting directly upon the soil. From resonant-column tests of samples of the silty clay at the proposed site, the shear-wave velocity  $v_s$  was found to be 806 ft/sec. This value of  $v_s$  and the unit weight  $\gamma$  of 100 lb/ft<sup>3</sup> establish the shear modulus  $G$  as 14,000 lb/in.<sup>2</sup>. Poisson's ratio  $\nu$  was chosen as  $\frac{1}{3}$  for the following calculations.

The first step in the design procedure is to establish the acceptable limits of motion (criterion of "failure"). For this example it is assumed that vertical motions equal to the horizontal motions noted as "case B" in Fig. 10-2 are acceptable. At 450 rpm the upper limit of case B corresponds to a

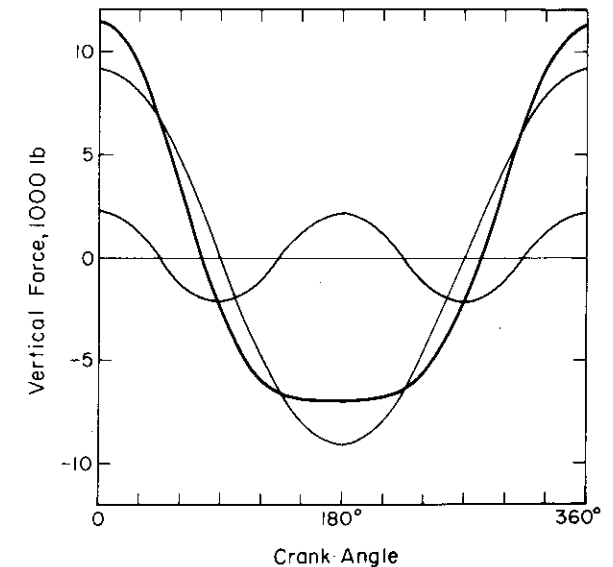


Figure 10-22. Unbalanced vertical force from vertical single-cylinder compressor.

single amplitude of 0.0021 in. Thus, the design criterion for the foundation-soil system requires the maximum amplitude of vertical motion to be less than 0.0021 in.

The first approximation for the foundation-plan dimensions may be obtained from the base area required to limit the static displacement, caused by  $Q_o = 11,400$  lb, to a value of 0.002 in. The equivalent rigid circular footing will be used in both the static and dynamic analysis, although a rectangular foundation plan is needed. The static deflection

$$z_s = \frac{(1 - \nu)Q_o}{4Gr_o} = 0.002 \text{ in.} = \frac{\frac{3}{4} \times 11,400}{4 \times 14,000 \times r_o}$$

leads to a required radius  $r_o = 67.9$  in. = 5.66 ft. For convenience in further calculations, assume  $r_o = 6$  ft, which determines a base area of 113 ft<sup>2</sup>. With this assumed value of  $r_o$ , the corrected static displacement is now  $z_s = 0.0019$  in.

The rigid circular footing of  $r_o = 6$  ft will be used in further calculations to represent a rectangular foundation block 16-ft long and 7-ft wide. For a block 3-ft thick the total weight is

$$W_b = 16 \times 7 \times 3 \times 150 = 50,400 \text{ lb}$$

The total oscillating weight  $W$ , which includes the block and machinery supported upon it, is

$$W = 50,400 + 10,900 = 61,300 \text{ lb}$$

Then for the equivalent circular footing,

$$B_z = \frac{(1 - \nu)W}{4\gamma r_o^3} = \frac{\frac{3}{4} \times 61,300}{4 \times 100(6)^3} = 0.473$$

From Fig. 7-19 the damping ratio  $D$  is 0.60 for this value of  $B_z$ . The natural frequency  $f_n$  of the system depends upon the oscillating mass and the spring constant

$$k_z = \frac{4Gr_o}{1 - \nu} = \frac{3}{2} \times 4 \times 14,000 \times 72 = 6.048 \times 10^6 \text{ lb/in.}$$

Then

$$f_n = \frac{1}{2\pi} \sqrt{\frac{k_z}{m}} = \frac{1}{2\pi} \sqrt{\frac{6.048 \times 10^6 \times 386}{61,300}} = 31.1 \text{ cycles/sec}$$

or

$$f_n = 1864 \text{ cycles/min}$$

Thus, the operating frequency of 450 rpm corresponds to  $(0.24)f_n$ . From Fig. A-1,

$$M = \frac{A_z}{z_s} = 1.02 \quad \text{at} \quad \frac{f}{f_n} = 0.24 \quad \text{for} \quad D = 0.6$$

which permits calculation of the maximum amplitude of vertical motion

$$A_z = 1.02 \times z_s = 0.00194 \text{ in.}$$

This value of motion satisfies the design criterion.

For this example the 16-by-7-by-3-ft concrete block and the soil with  $G = 14,000$  lb/in.<sup>2</sup> form a satisfactory foundation for vertical vibration. However, it has been assumed in the analysis that the input force, center of gravity of the oscillating mass, and the center of pressure of the soil on the base of the foundation block all lie along the same vertical line. In assembling the machinery on the foundation block, care should be taken to align these exciting and resisting forces as closely as possible to reduce coupling between the vertical and rocking or pitching modes of vibration.

The solution for the maximum amplitude of vertical vibration was obtained from the response curve (Fig. A-1) for constant amplitude of force excitation ( $Q_o = \text{const.} = 10,900$  lb). It could have been obtained also from Fig. A-2, which corresponds to the frequency-dependent excitation ( $Q_o = m_e e \omega^2$ ). In Chap. 2 it was noted that the ordinate of each curve on Fig. A-2 may be obtained at each frequency ratio from the ordinate of a similar curve on Fig. A-1 by

$$M\left(\frac{f}{f_n}\right)^2 = \frac{A_z k_s (2\pi)^2 \omega^2}{Q_o (2\pi)^2 \frac{k_z}{m}} = \frac{A_z m \omega^2}{m_e e \omega^2} = \frac{A_z m}{m_e e}$$

The force of  $Q_o = 11,400$  lb at 450 rpm is developed by

$$m_e e = \frac{Q_o}{\omega^2} = \frac{11,400}{4\pi^2 \left(\frac{450}{60}\right)^2} = 5.13 \text{ lb-sec}^2$$

Then

$$1.02(0.24)^2 = 0.0587 = \frac{A_z \times 61,300}{386 \times 5.13}$$

or

$$A_z = 0.0019 \text{ in.}$$

as was obtained in the previous calculation. Note that the value of  $A_z m/m_e e$

is usually obtained directly from Fig. A-2 at  $f/f_n = 0.24$  on the curve for  $D = 0.6$ . However, in this low frequency range ( $f/f_n < 0.3$ ) the curves are very steep on the semilog plot and more accurate values are obtained by calculation, as indicated above.

### Response of Foundations to Transient Vertical Loads

In order to evaluate the motions of foundations responding to transient loadings, it is necessary to have reliable information on the load-time-pulse to be applied. This pulse is then applied to the lumped-parameter analog of the foundation-soil system and a solution can be obtained from the phase-plane method.

**Drop test on model footing.** The first example to be considered here was illustrated in Fig. 10-9a. A footing of 1-ft diameter rested on the surface of a bed of compacted Ottawa sand. This footing supported a dead weight and a loading platen onto which a 5-lb sandbag was dropped. For test Q-2 the force-time-pulse shown by the solid curve in Fig. 10-9b was developed, and the rectangular force-time-pulse approximations, also shown on this figure, were used in the phase-plane analysis of the footing response. The following quantities related to the footing-soil system entered into the computations:

$r_o$ = Radius of the circular footing	= 6 in.
$W$ = Weight of the footing	= 150 lb
$\gamma$ = Unit weight of the sand	= 109 lb/ft <sup>3</sup>
$\mathbf{b} = \frac{W}{\gamma r_o^3}$ = Mass ratio	= 11.0
$\mathbf{B}_z = \frac{1 - \nu}{4} \mathbf{b}$ = Modified mass ratio	= 2.07
$D = \frac{0.425}{\sqrt{\mathbf{B}_z}}$ = Damping ratio	= 0.296
$G$ = Shear modulus of soil	= 3400 lb/in. <sup>2*</sup>
$\nu$ = Poisson's ratio of soil	= $\frac{1}{4}$
$k_z = \frac{4Gr_o}{1 - \nu}$ = Static spring constant	= 108,800 lb/in.

\* The effective  $G$  for the sand beneath the footing was established by the procedure described by Fig. 10-20.

$$m = \frac{W}{g} = \text{Mass of footing} = 0.389 \text{ lb-sec}^2/\text{in.}$$

$$\omega_n = \sqrt{\frac{k_z}{m}} = \text{Undamped natural frequency} = 529 \text{ rad/sec}$$

$$\omega_d = \sqrt{\frac{k_z}{m}} \sqrt{1 - D^2} = \text{Damped frequency} = 505 \text{ rad/sec}$$

$$T_d = \frac{2\pi}{\omega_d} = \text{Natural period of footing} = 0.0124 \text{ sec}$$

$$\varphi_1 = \arcsin D = \text{Angle of inclination of ordinate} = 17.2^\circ$$

The rectangular force-time-pulse approximations to the pulse-loading curve indicate a constant-force amplitude over an interval of 0.002 sec (2 msec). This time interval corresponds to an angular movement  $\omega_d \Delta t$  on the phase-plane of

$$\omega_d \Delta t = \frac{\Delta t}{T_d} 360 = \frac{0.002}{0.0124} 360 = 58^\circ$$

The values of input force for each time interval establish the static displacements  $z_{s4}, z_{s6}, \dots$  shown in the phase-plane solution (Fig. 10-23a).

The phase-plane solution shown in Fig. 10-23a is constructed by the procedure described in Chap. 2. The circled numbers, ④, ⑥, ... designate the points on the phase plane from which the displacement and velocity can be evaluated, corresponding to the time of 4, 6, ... msec. For example, to find the displacement at point ⑩ (end of 10 msec. of loading), a line is drawn from ⑩ parallel to the  $\dot{z}/\omega_n$  axis until it intersects the  $z$ -axis at point ⑩'. This value of  $z$  is 0.0005 in. The circles in Fig. 10-23b represent the displacements at the end of the time intervals as obtained from the phase-plane solution shown in Fig. 10-23a. The length of the line ⑩-⑩' represents the value of  $\dot{z}/\omega_n$  at the end of 10 msec of loading from which a velocity of 0.09 in./sec is calculated.

The acceleration at the end of each time interval could also be evaluated from Fig. 10-23a by the method described in Chap. 2, but because rather large instantaneous-force jumps are represented by the rectangles used to approximate the force pulse (Fig. 10-9b), the values of acceleration would be fairly crude. In order to improve the calculations of accelerations, it is preferable to use smaller time intervals for the force-pulse blocks. The problem described by the graphical phase-plane method can also be solved readily with a digital computer, which makes it easy to cut down the time duration on the force-time-pulse blocks. Figure 10-23c shows the acceleration-time diagrams obtained from the computer solution and the curve obtained from the test.

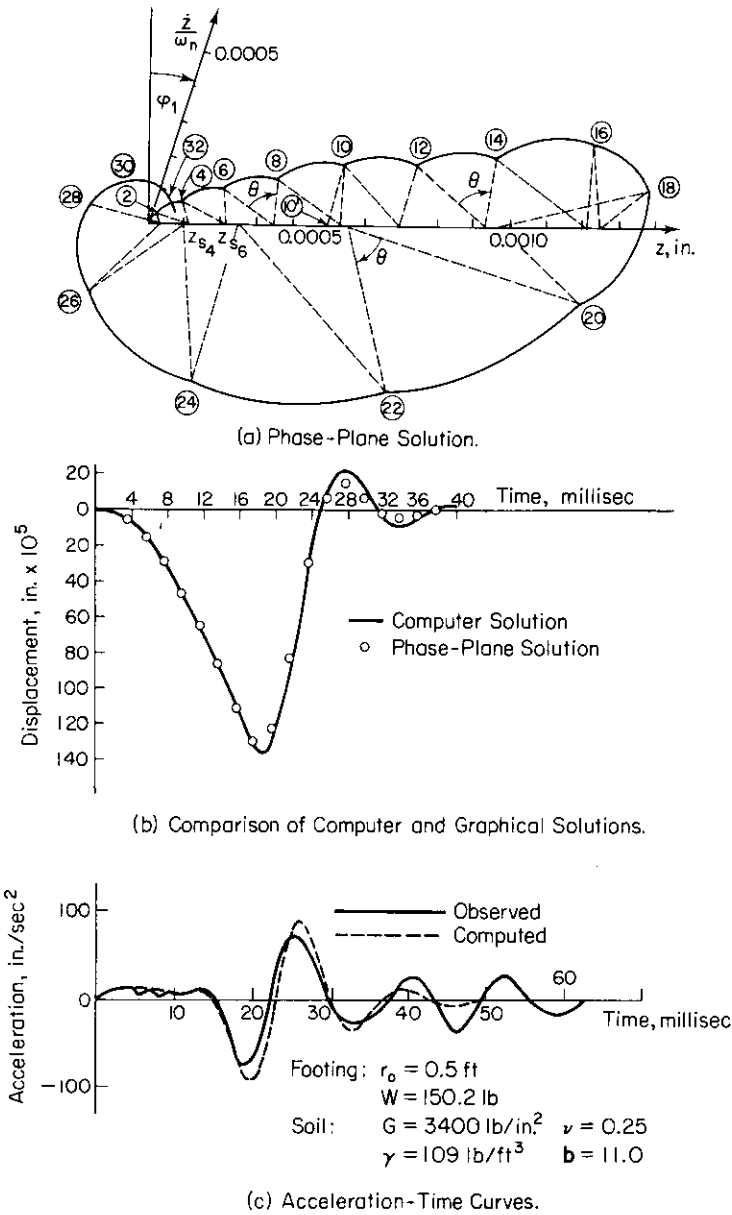


Figure 10-23. Dynamic response of model footings—transient loading test Q-2.

This good agreement between test and computed values is typical of the results reported by Drnevich and Hall (1966). The computed value of the displacement-time curve is shown as the solid curve on Fig. 10-23b, and it should be noted that the phase-plane solution produces a displacement-time curve which agrees closely with the computed solution.

From transient-loading tests on model footings similar to the one described for Test Q-2, it was demonstrated that theoretical methods may predict the displacement-time and acceleration-time behavior of the footing quite satisfactorily. The phase-plane solution provides approximate answers in a relatively short time, and the accuracy may be improved by taking smaller time intervals in the force-time-pulse approximations.

**Impact on punch-press foundation.** The loading pulse described in Fig. 10-10b resulted from a sudden release of elastic energy as the upper die of a punch press sheared through a metal blank. This loading pulse is reproduced in Fig. 10-24a along with the rectangular force-pulse approximations to this curve. This pulse is associated with a machine having a dead weight of 30,000 lb which rests on a concrete-block foundation. The block is supported directly on a soil for which  $G = 10,000$  psi and  $\nu = \frac{1}{4}$ .

Table 10-17 includes the significant quantities needed for a phase-plane solution for the response of a machine-foundation-soil system set into motion by this loading pulse. Three choices for the foundation block are noted in Table 10-17 having dimensions of 18 by 18 by 3 ft, 18 by 18 by 4 ft, and 15 by 15 by 3 ft. The phase-plane solution shown in Fig. 10-24b and the

Table 10-17. Data for Analysis of Response of Block Foundation to Transient Vertical Loading

Block Dimensions	18 × 18 × 3 ft	18 × 18 × 4 ft	15 × 15 × 3 ft
$W^*$	175,800 (lb)	224,400 (lb)	131,250 (lb)
effective $r_o$	10.16 (ft)	10.16 (ft)	8.46 (ft)
$b$	1.40	1.78	1.81
$B_s$	0.26	0.334	0.339
$D$	0.83	0.735	0.730
$k$	$6.5 \times 10^6$ (lb/in.)	$6.5 \times 10^6$ (lb/in.)	$5.41 \times 10^6$ (lb/in.)
$\phi_1$	56.2°	47.3°	46.9°
$\omega_n$	119.5 (rad/sec)	105.8 (rad/sec)	126.2 (rad/sec)
$\omega_d$	66.6 (rad/sec)	71.8 (rad/sec)	86.3 (rad/sec)
$T_d$	0.0943 (sec)	0.0876 (sec)	0.0729 (sec)
$\theta$	3.82°	4.11°	4.94°
$z_{max}$	0.0042 (in.)	0.0041 (in.)	0.0048 (in.)
time for $z_{max}$	0.0125 (sec)	0.0130 (sec)	0.0126 (sec)

\*  $W$  = wt. of foundation block + machine.

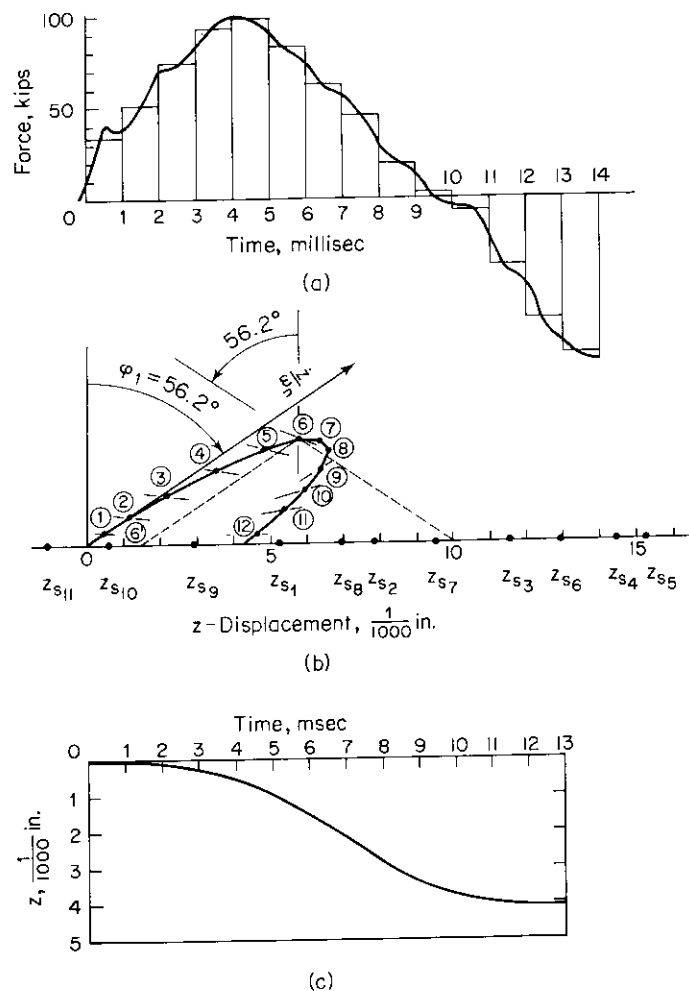


Figure 10-24. Transient loading of 18-ft-by-18-ft-by-3-ft foundation block. (a) Force-time diagram. (b) Phase-plane solution. (c) Displacement-time diagram.

displacement-time curve in Fig. 10-24c are shown for the 18-by-18-by-3-ft foundation block to illustrate the method of analysis. Note from Table 10-17 that for vertical loading the weights and dimensions of each of these foundations lead to extremely high computed values for the geometrical damping. High damping ratios limit the maximum amplitude of motion developed during response to the impact.

The phase-plane solution shown in Fig. 10-24b was constructed by the same procedure followed for the phase-plane solution shown in Fig. 10-23a.

However, the construction lines have been eliminated from Fig. 10-24b to simplify the drawing. This phase-plane solution was discontinued after the displacement had reached the maximum amplitude, again for convenience in illustration. As before, the displacement  $z$  is evaluated from Fig. 10-24b by following from a point on the curve—for example, point ⑥—down along a line parallel to the  $z/\omega_n$  axis to the abscissa. Thus, the displacement corresponding to point ⑥ (at end of 6 msec) is 0.0015 in. The velocity at this time is represented by the length of the line ⑥-⑥' (i.e.,  $z/\omega_n$ ) multiplied by  $\omega_n$ , which gives a value of  $\dot{z} = 0.62$  in./sec at the end of 6 msec. The acceleration at this time is obtained by projecting a line at  $-56.2^\circ$  from the vertical through point ⑥ to the abscissa. This intersection at  $z = 0.010$  in. is a distance of  $-0.0029$  in. to the left of  $z_{s6}$ , from which the acceleration at the end of 6 msec is calculated to be

$$\ddot{z} = (0.0029)\omega_n^2 = 41.4 \text{ in./sec}^2$$

Data from phase-plane solutions of the three block foundations loaded by the same pulse are given in Table 10-17 for comparison. Note that the maximum displacement only increases from 0.0042 in. to 0.0048 in. by decreasing the side of the square block from 18 to 15 ft. The final choice of block size depends on the design criteria, which includes cost for a particular installation.

### 10.7 Analysis and Design for Rocking Vibrations of Foundations

In contrast to the high values of geometrical damping generally associated with vertical oscillations, rocking oscillations develop relatively low values of geometrical damping. This was illustrated in Fig. 7-19, where it was shown that for rigid circular footings a value of  $B_\psi$  of 0.75 or less was required in order to raise  $D$  above 0.10. The consequence of low damping is exhibited by large values for the magnification factor  $M_\psi$ , shown in Fig. 7-16. Consequently, the dynamic response at the resonant frequency for rocking will result in large amplitudes of motion.

Design procedures for footings subjected to rocking motions must either provide such a low value for  $B_\psi$  (i.e.,  $B_\psi \leq 0.5$ ) that the magnification factors become small or assure that the resonant frequency for rocking is well above (by at least a factor of 2) the proposed operating frequency.

#### Rocking Tests of Model Footings

The series of tests on model footings described by Fry (1963) included excitation of the footings in the rocking mode of vibration by adjusting the

vibrator to operate as indicated in Fig. 10-5e. Even though a pure couple was generated by the vibrator, the response of the footing involved both rocking and a horizontal translation because the center of gravity of the footing was above the center of sliding resistance (see Fig. 7-20). Therefore, a coupled motion resulted, and two modes of resonant vibration were possible, as indicated in Fig. 10-25. The lower-frequency mode is designated as mode I. Another resonant frequency, mode II, occurs at a higher frequency and corresponds to an out-of-phase relation between rotation and translation. In mode II the footing rotates clockwise about the center of gravity as the center of gravity moves to the left. Thus, the footing moves about some center of rotation which is above the center of gravity (Fig. 10-25b).

The design restrictions placed on the model footings by the limited range of frequencies available from the mechanical oscillator, as well as the desire to limit all resonant vibrations to relatively small amplitudes, affected the response of the footings in the rocking mode of vibration. Only base 1 (see Fig. 10-26b) had geometrical configurations which permitted mode-II rocking vibrations to develop within the range of available frequencies. The other footings developed only mode-I rocking vibrations.

For base 1—test 36 at the Vicksburg site, the test results for the rocking

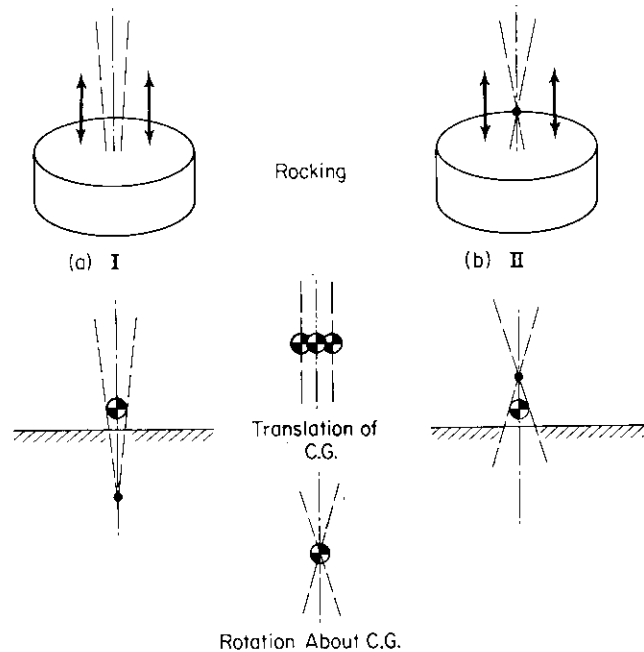


Figure 10-25. First (I) and second (II) coupled modes of rocking vibrations of model footings.

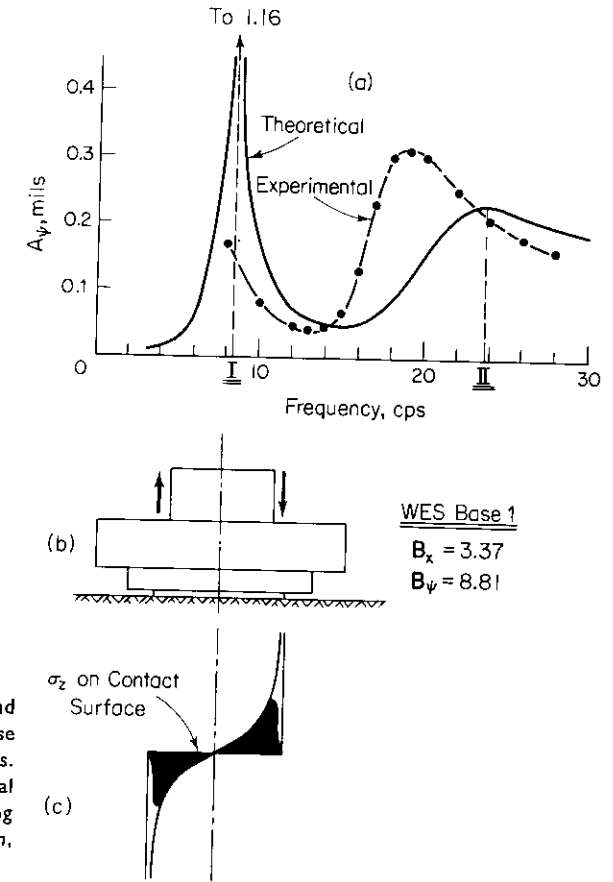


Figure 10-26. Coupled rocking and sliding vibrations of WES Base 1, Test 36. (a) Response curves. (b) Footing geometry. (c) Vertical pressure distribution on footing base. (After Richart and Whitman, 1967.)

mode of vibration are shown by the dashed curve in Fig. 10-26a. These values were obtained from the vertical displacement measured 2 in. from the periphery of the upper surface of the concrete base on a diameter perpendicular to the axis of rocking. These vertical displacements were divided by the radius to the center of the circular top surface of the base to describe the amplitude of rotation  $A_{\psi}$ . A theoretical curve for the corresponding amplitude of rotation is also shown in Fig. 10-26a, as obtained by the analysis for coupled rocking and sliding described in Sec. 7.8. Because the theoretical solution for rocking of the rigid disk was available only for the case of  $\nu = 0$ , the theoretical coupled solution applies only for  $\nu = 0$ .

Figure 10-26b shows the general configuration of WES base 1 which had a circular base of 62-in. diameter in contact with the soil and additional cylindrical concrete masses of 88-in. and 112-in. diameter added above. The 5600-lb mechanical vibrator was attached to the top of the footing, which then

constituted a relatively "top-heavy" mass as indicated by the mass ratio of  $B_w = 8.81$  for rocking.

From the results of the theoretical solution shown in Fig. 10-26a, it is seen that a resonant peak of 1.16 mils (1020 mils = 1 radian) was reached in mode I of the coupled motion at about 8.4 cycles/sec. The theoretical peak for mode-II vibration is 0.23 mil of rotation at 23.8 cycles/sec. The significant point brought out by the theoretical curve is that in order to obtain the resonant conditions for mode-II vibration, it is necessary to *pass through mode I*, which develops high-amplitude motions. Note that in the discussion of allowable rotations for radar towers in Sec. 10.2 we were considering acceptable motions in the range of 0.05 mil. Thus, it is evident that the test footing passed through mode-I vibrations at a relatively high amplitude of motion before reaching the peak motion in mode II, which occurred at a much smaller amplitude. The test data were not available for frequencies less than 8 cycles/sec because of rough operating characteristics of the mechanical vibrator below this speed, but there is little doubt that mode-I vibrations did occur in the tests.

By comparing the amplitude-frequency curves obtained from theory and test, it is seen that the mode-II peak for the test conditions represents a higher amplitude of motion at a lower frequency than those predicted by theory. Part of this discrepancy lies in the fact that real soils *cannot* develop the pressure distributions on the footing base that correspond to the rigid-base condition for rocking. The curve in Fig. 10-26c representing the vertical pressure  $\sigma_z$  along a diameter in the plane of rocking of the footing goes to infinity at the periphery of the footing. Real soils have a limiting pressure, and the shaded distribution shown in Fig. 10-26c illustrates a more probable distribution of pressure provided by a real soil against the footing base. This pressure distribution has lost the moment resistance provided by pressures near the edge of the diagram; thus, the effective-moment arm of the resisting couple is reduced. Consequently, we would expect that a shift of the center of pressure toward the center of the footing would reduce the effective geometrical damping. A reduction in effective geometrical damping would affect the dynamic characteristics of the system by increasing the maximum amplitude of vibration and by causing it to occur at a lower frequency. Thus, this type of change in base-pressure distribution would cause the theoretical-response curve better to approximate the test curve.

Additional comparisons have been made between the WES test data and theoretical predictions for rocking tests. These comparisons are shown on Table 10-18 for tests in which the lowest exciting-force input (i.e., eccentricity = 0.105 in.) was applied. From this table it is seen that the computed amplitude of motion varied from 0.72 to 3.94 times the measured value and the computed value of frequency at maximum amplitude varied from 0.7 to 1.27 times the test values. Only for mode-II vibration was the computed

value lower than the measured value, and a possible explanation for this discrepancy was discussed in the previous paragraph. For mode-I vibrations which are most likely to occur in prototype footings, the theoretical amplitudes were larger than those measured and the frequency for maximum amplitude was generally lower. Except for WES test 3-26, the computed amplitudes of motion were within a factor of 2 of the measured value. For some reason, test 3-26 (on a base of 9-ft diameter weighing 24,315 lb) developed a lower amplitude of motion than did WES test 4-18A (on a base of 10.33-ft diameter weighing 30,970 lb). Both bases were subjected to the same rocking couple by the mechanical oscillator.

In addition to the comparisons of peak values indicated in Table 10-18, a more complete study of the shapes of the amplitude-frequency response curves from both test and theory has indicated that in all but a few cases the agreement throughout the frequency range was within a factor of 2. For the exceptions the theoretical values were higher—as for WES test 3-26.

Table 10-18. Comparison of Test and Theoretical Results for Rocking and Sliding Vibrations of Rigid Circular Footings\*

Test No.	Vibration Mode	$A_{\psi \text{ Vert Meas.}}$ (mil)	$\frac{A_{\psi \text{ Comp}}}{A_{\psi \text{ Meas}}}$	$\frac{f_{\text{Comp}}}{f_{\text{Meas}}}$	$A_{\psi \text{ Horiz Meas.}}$ (mil)	$\frac{A_{\psi \text{ Comp}}}{A_{\psi \text{ Meas}}}$	$\frac{f_{\text{Comp}}}{f_{\text{Meas}}}$
WES 1-36	I	—	—	—	—	—	—
1-36	II	0.315	0.73	1.27	0.095	1.24	1.17
2-23	I	0.28	1.04	0.70	0.24	1.96	0.99
3-26	I	—†	—	—	0.047	3.94	0.83
4-18A	I	—†	—	—	0.055	1.96	1.09
Eglin Field 2-13	I	0.185	1.62	0.85	0.335	1.49	0.78
3-13	I	0.142	1.06	0.94	0.193	1.02	0.91
4-13	I	0.110	—†	—	0.156	0.72	0.94

\* Test data from Fry (1963).

† No peak of amplitude-frequency response curve reached within frequency range available.

#### Analysis of Rocking of Machine Foundation

Figures 10-27a and b show the plan and elevation of a foundation proposed to support rotating machinery. The upper slab is at the first-floor level, and the lower slab rests directly on the soil at an elevation of 1.5 ft below the

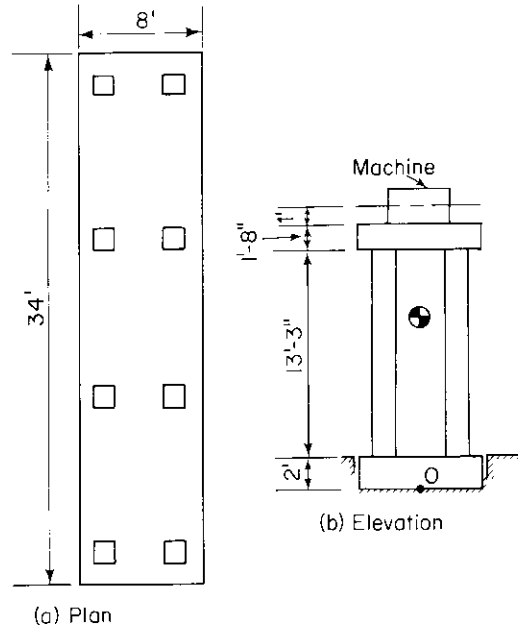


Figure 10-27. Machine foundation.

Total Weight = 272,100 lb  
 Mass Moment of Inertia in Rocking about Point O  
 $I_{\psi} = \frac{4.81 \times 10^7}{32.2}$  ft lb sec<sup>2</sup>  
 Elevation of C.G. above Point O = 11.2 ft

top of the basement slab. For this installation the soil properties needed in the dynamic analysis of the foundation-soil system are:  $G = 12,300$  psi,  $v_S = 720$  ft/sec,  $\nu = 0.25$ , and  $\gamma = 110$  lb/ft<sup>3</sup>.

The problem is to evaluate the dynamic response of this foundation to the horizontal and vertical forces generated by rotating machinery. This will be carried out by analyses based on the elastic-half-space theory (Chap. 7) for separate single-degree-of-freedom responses of the foundation to the vertical and to the horizontal (or rocking) forces. For the vertical response the first step is to calculate the radius of the equivalent circular area (Eq. 10-29a)—

$$r_o = \sqrt{\frac{4cd}{\pi}} = \sqrt{\frac{34 \times 8}{\pi}} = 9.30 \text{ ft}$$

—to be used in the calculation for the modified mass ratio,

$$B_z = \frac{(1 - \nu) W}{4 \gamma r_o^3} = \frac{0.75 \times 272,100}{4 \times 110(9.3)^3} = 0.58$$

From Fig. 7-11 the dynamic magnification factor is about 1.1, and from Fig. 7-19 or Eq. (7-30) the damping ratio  $D$  is 0.56. This demonstrates that the vertical motion is highly damped and that the maximum amplitude of dynamic motion will be only slightly greater than the static displacement produced by the input force. Therefore, for the preliminary calculation, it appears that this foundation is satisfactory from the standpoint of vertical vibrations.

For rocking vibrations excited by the horizontal component of the machine forces, again we calculate the radius of an equivalent circular base, this time from Eq. (10-29b), as

$$r_o = \sqrt[4]{\frac{2c(2d)^3}{3\pi}} = \sqrt[4]{\frac{34 \times 8^3}{3\pi}} = 6.55 \text{ ft}$$

Then

$$B_{\psi} = \frac{3(1 - \nu) I_{\psi}}{8 \rho r_o^5} = \frac{2.25 \times 4.81 \times 10^7}{8 \times 110(6.55)^5} = 10.2$$

Figure 7-16 indicates that the dynamic amplitude magnification factor for this value of  $B_{\psi}$  is greater than 100. From Eq. (7-64),

$$D_{\psi} = \frac{0.15}{(1 + B_{\psi})\sqrt{B_{\psi}}} = 0.0042$$

from which the magnification factor can be calculated as

$$M_{\psi m} \approx \frac{1}{2D} = 119$$

With this low value of damping ratio, or high magnification factor, the peak of the amplitude-frequency response curve will occur at a frequency almost identical with the natural frequency. The dimensionless frequency  $a_{om}$  can be estimated from Fig. 7-16a as 0.30, from which the resonant frequency is

$$f_m = \frac{a_{om} v_S}{2\pi r_o} = \frac{0.30 \times 720}{2\pi \times 6.55} = 5.25 \text{ cycles/sec} = 315 \text{ cycles/min}$$

As a check, the resonant frequency for the lumped-mass system can be evaluated through Eq. (2-17). For this calculation the expression for the spring constant of the rectangular footing may be taken from Table 10-14, and with  $\beta_{\psi}$  from Fig. 10-16,

$$k_{\psi} = \frac{G}{1 - \nu} \beta_{\psi} 8cd^2 = \frac{12,300 \times 144}{0.75} \times 0.40 \times 34 \times 8^2 = 2.055 \times 10^9 \text{ ft-lb/rad}$$



Then from Eq. (2-17),

$$f_n = \frac{1}{2\pi} \sqrt{\frac{k_v}{I_w}} = \frac{1}{2\pi} \sqrt{\frac{2.055 \times 10^9 \times 32.2}{4.81 \times 10^7}}$$

$$= 5.90 \text{ cycles/sec} = 354 \text{ cycles/min}$$

The difference between the resonant frequencies calculated by these two methods is due primarily to the differences in the  $k_v$  values computed from Table 10-13 and Table 10-14. However, these are reasonably close, and either is satisfactory to indicate the order of magnitude of the resonant frequency.

From this preliminary analysis, it is evident that the foundation will experience a severe rocking oscillation at a frequency in the range of 320–350 rpm. This particular foundation was scheduled to support several different combinations of rotating machinery at different times, and all of the machines operated around this range of frequencies or higher. When operating at the higher frequencies, there was always the necessity for passing through the resonant condition during starting up or stopping. Consequently, this configuration was considered unsuitable for the purpose of resisting rocking motions. In this particular case, several proposed foundations of this general type were located parallel and relatively close together. Therefore, it was expedient to tie these together with a shear wall at each end to develop a box-type foundation which was stable against rocking.

It should be fairly obvious that foundations needed to resist rocking forces induced by machines should be low and wide. This is demonstrated by the dependence of the dynamic response of foundations to the mass ratio  $B_v$  (Eq. 7-44) for rocking. Whenever possible, the best procedure for reducing the value of  $B_v$  is to increase the size of the footing, because  $r_o$  enters the computation as  $r_o^5$ .

#### Rocking of a Radar Tower

The supporting structure for a radar antenna must have dynamic responses which do not interfere with the operation of the electronic equipment. The radar disk itself must be rigid enough so that it does not distort unduly as the mechanism moves in azimuth and elevation; the rotating mechanisms must have close tolerances; the vertical tower must be stiff and must not develop resonant responses; and finally, the foundation which bears against the soil must not permit large motions of the entire tower.

As noted in the discussion of design criteria (Sec. 10.2), permissible rotations of radar-tower foundations are often of the order of 0.05 mil (or about 0.00005 rad). Figure 10-28 illustrates the rotation of the radar antenna

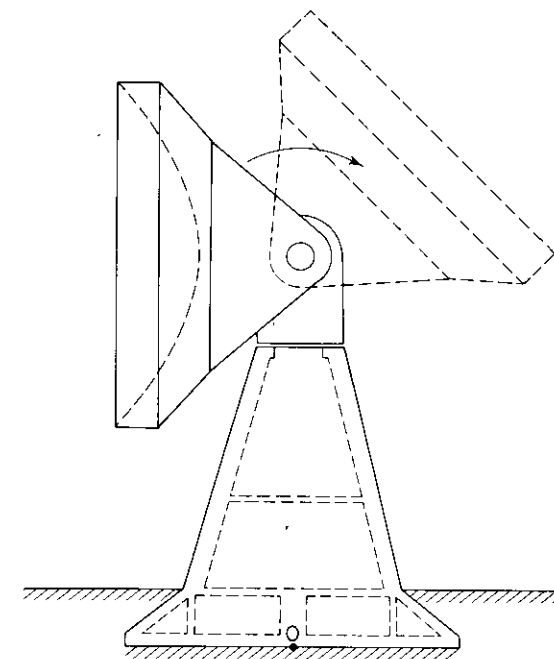


Figure 10-28. Rocking of radar tower.

in elevation about a horizontal axis. This motion introduces a transient rocking pulse into the tower which then may cause the tower to rock at its natural frequency because of the flexible connection between the foundation and the soil or because of the various flexibilities in the structural system. Obviously, the entire radar tower has many degrees of freedom in vibration, but a standard design can be prepared for the structural system to avoid the critical resonant frequencies. It is the foundation–soil flexibility which will vary from site to site and which must be evaluated for each tower installation. This section will consider only the rocking of the radar tower, considering the tower itself as a rigid mass and all the flexibility to be concentrated in the supporting soil.

The radar tower shown in Figure 10-28 is supported by a rigid circular concrete base 60 ft in diameter which rests directly on the soil. Field measurements were made of the dynamic soil properties (see WES Misc. Paper No. 4-584, July 1963), and values of the shear modulus between 12,000 and 20,000 psi and a Poisson's ratio of 0.43 were determined by the steady-state-vibration method (see Sec. 4.3). Because slightly higher confining pressures were to be developed in this soil under the completed structure, the limiting values of  $G = 14,000$  psi and  $G = 20,000$  psi were used in the original design computations.

The analysis for rocking of the tower as a rigid body is analyzed here by the lumped-parameter analog to the elastic theory for rocking of the rigid

circular foundation. For this tower the circular foundation was 60 ft in diameter, or  $r_o = 30$  ft. The mass moment of inertia in rocking about a diameter through the base (point  $O$ , Fig. 10-28) was calculated to be

$$I_\psi = 80.545 \times 10^6 \text{ lb-ft-sec}^2$$

With the unit weight of the soil of approximately 100 lb/ft<sup>3</sup>, this leads to the calculation of the mass ratio in rocking as

$$B_\psi = \frac{3(1 - \nu)}{8} \frac{80.545 \times 10^6}{\frac{100}{32.2} (30)^5} = (1 - \nu)0.400$$

Calculations for the maximum amplitude of rotation and the frequency at which this occurs for an overturning moment of 212,000 ft lb, considered as a constant-moment excitation, are shown in Table 10-19.

Field tests were conducted on this tower after construction to evaluate the prototype performance (see Ballard and Fowler, 1967). A summary of the test results from excitation of the tower in the rocking mode are given in Table 10-20 along with the original design estimates, which were prepared with the aid of the elastic-half-space theory (with the assumption of  $\nu = 0$ ). Note that there is reasonably good agreement between the calculated and measured amplitudes and frequencies.

Table 10-19. Calculations for Rocking of Radar Tower

Constant-Force Excitation, $T = T_o \sin \omega t$ ; $T_o = 212,000$ ft-lb			
	For $\nu = 0$	For $\nu = 0.4$	Eq. No.
$B_\psi$	0.40	0.24	7-44
$D_\psi$	0.169	0.247	7-53
$\sqrt{1 - D_\psi^2}$	0.986	0.969	
$\sqrt{1 - 2D_\psi^2}$	0.971	0.937	
$M_{\psi m}$	2.96	2.02	2-56
For $G = 14,000$ psi			
$\psi_s$ (rad)	$1.46 \times 10^{-6}$	$0.876 \times 10^{-6}$	7-43
$A_\psi$ (rad)	$4.26 \times 10^{-6}$	$1.72 \times 10^{-6}$	7-45
$f_m$ (cycles/sec)	6.56	8.2	2-55
For $G = 20,000$ psi			
$\psi_s$ (rad)	$1.022 \times 10^{-6}$	$0.613 \times 10^{-6}$	7-43
$A_\psi$ (rad)	$2.98 \times 10^{-6}$	$1.20 \times 10^{-6}$	7-45
$f_m$ (cycles/sec)	7.8	9.8	2-55

Table 10-20. Comparison of Measured and Calculated Values for Rocking of Radar Tower\*

	Frequency Range (cycles/sec)	Rotation ( $10^{-6}$ rad)
Design	6.0-9.0	3.6-5.1
Measured	4.9-7.7	1.60

\* From Ballard and Fowler (1967).

The design of the foundation for a radar tower should also include consideration of the torsional resistance of the foundation as well as rocking, and should include an evaluation of the coupling between the structural and foundation flexibilities. Additional design criteria may be found—in Fu and Jepson (1959), Horn (1964), and Pschunder (1966), for example—and useful data on foundation and tower stiffnesses are given by Weissmann and White (1961), Weissmann (1966) and Pschunder (1965, 1966).

### 10.8 Conclusions

This chapter has treated methods of analysis and design of dynamically loaded foundations. These methods depend on the design criteria, applied forces, soil response, and analytical procedures for relating these quantities.

The design criteria were based on a failure criterion of a limiting amplitude of motion, or a limiting velocity or acceleration of the foundation. In nearly all cases the motions involved were on the order of a few thousandths of an inch up to perhaps a few hundredths, and general guidelines have been established.

A critical part of the study of the dynamic response of a given system is to evaluate the type and magnitude of the input forces to be resisted. These may be calculated readily for certain types of machinery and can usually be evaluated experimentally for machines producing transient loads. It becomes more difficult to estimate the loads introduced by natural forces of wind, water waves, or earthquakes. Thus, it may be concluded that much more information is needed on the forces to be applied to foundations by machines or external sources.

Chapter 6 included a discussion of the response of soils to dynamic loads which produce small deformations. Because the design criteria for foundation behavior restrict motions to small values, it follows that the supporting soils will normally be subjected to small strains only. Consequently, the dynamic soil parameters described in Chap. 6 and the methods described in Chaps. 4 and 9 for determining these characteristics constitute a reasonably satisfactory part of the design procedure at the present (1969). However, it is

anticipated that a considerable amount of effort will continue to be directed toward laboratory and field evaluation of soil behavior under dynamic loading.

The analytical procedures for establishing the dynamic behavior of a foundation relate the applied forces, soil properties, and foundation weights and geometry to the response. By successive corrections of the design parameters, the analytical procedures provide a method for developing a dynamic response of the foundation which falls within the design limits. Several simplified methods of analysis have been discussed in Chaps. 7 and 10; these have been found satisfactory when the prototype conditions correspond to the assumptions made in establishing the theory. Much more work is required in developing analytical procedures to cover the variables of shape of foundation, depth of embedment, variations of soil properties with depth, geometrical vs. hysteresis damping, coupling effects, and effects of adjacent footings. Very little information is available on the dynamic behavior of foundations supported by piles or caissons, or on flexible mats.

A final conclusion relates to the continuing need for field data from tests on prototype foundations: The only justification for using any design procedure is that it provides a reliable estimate for the behavior of the prototype. Thus, it is necessary to compare predicted and measured values at all opportunities in order to provide a realistic basis for subsequent efforts to improve the methods of design.

## APPENDIX

Information that is needed frequently in design or analysis is included in the following two tables and four figures.

Table A-1. Summary of Relations for Single-Degree-of-Freedom Vibration (z-coordinate chosen for illustration)

Critical Damping	$c_c = 2\sqrt{km}$	(2-31)
Damping Ratio	$D = \frac{c}{c_c}$	(2-32)
Undamped "Natural Frequency"	$f_n = \frac{1}{2\pi} \sqrt{\frac{k}{m}}$	(2-17b)
Static Displacement	$z_s = \frac{Q_o}{k}$	(2-13)
Amplitude-Magnification Factor During Vibration	$M = \left[ \left( 1 - \frac{f^2}{f_n^2} \right)^2 + \left( 2D \frac{f}{f_n} \right)^2 \right]^{-1/2}$	(2-53)
For Constant-Force Excitation ( $Q_o = \text{constant}$ )	For Rotating-Mass Excitation ( $Q_o = m_e e \omega^2$ )	
Amplitude at Frequency $f$		
$A_z = \frac{Q_o}{k} M$	$A_z = \frac{m_e e}{m} \left( \frac{f}{f_n} \right)^2 M$	
Maximum Amplitude of Vibration		
$A_{zm} = \frac{Q_o}{k} \frac{1}{2D\sqrt{1-D^2}}$	$A_{zm} = \frac{m_e e}{m} \frac{1}{2D\sqrt{1-D^2}}$	
Frequency for Maximum Amplitude		
$f_m = f_n \sqrt{1-2D^2}$	(2-55)	$f_{mr} = f_n \frac{1}{\sqrt{1-2D^2}}$
		(2-60)

Table A-2. Equivalent Damping Ratio for Rigid Circular Footings

Mode of Vibration	Mass (or Inertia) Ratio	Damping Ratio $D$
Vertical	$B_z = \frac{(1-\nu)m}{4\rho r_o^3}$	$D_z = \frac{0.425}{\sqrt{B_z}}$
Sliding	$B_x = \frac{(7-8\nu)m}{32(1-\nu)\rho r_o^3}$	$D_x = \frac{0.288}{\sqrt{B_x}}$
Rocking	$B_\psi = \frac{3(1-\nu)I_\psi}{8\rho r_o^5}$	$D_\psi = \frac{0.15}{(1+B_\psi)\sqrt{B_\psi}}$
Torsional	$B_\Theta = \frac{I_\Theta}{\rho r_o^5}$	$D_\Theta = \frac{0.50}{1+2B_\Theta}$

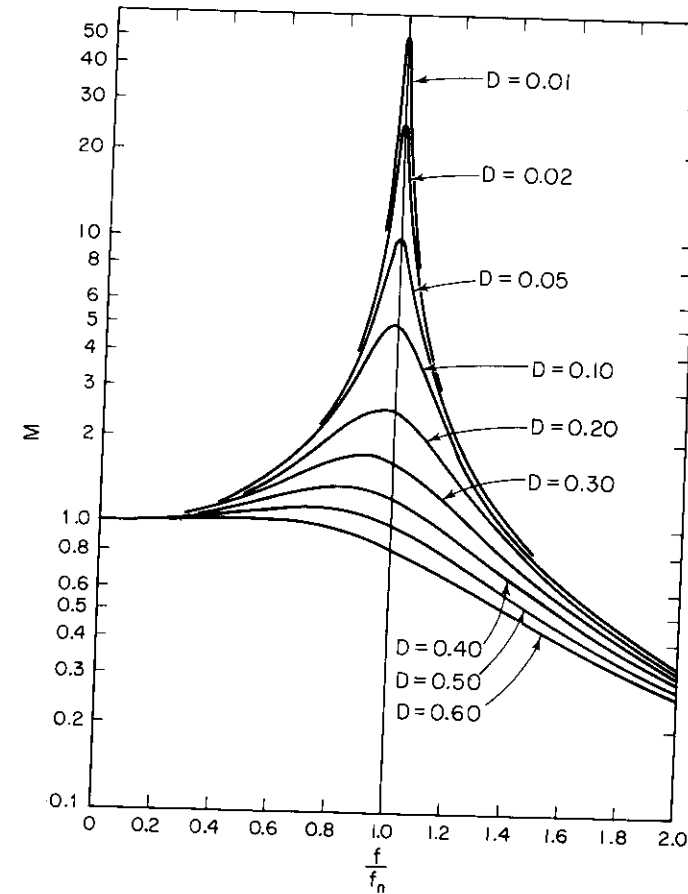


Figure A-1. Response curves for a viscously damped single-degree-of-freedom system (constant force amplitude excitation —  $Q_o = \text{const}$ ).

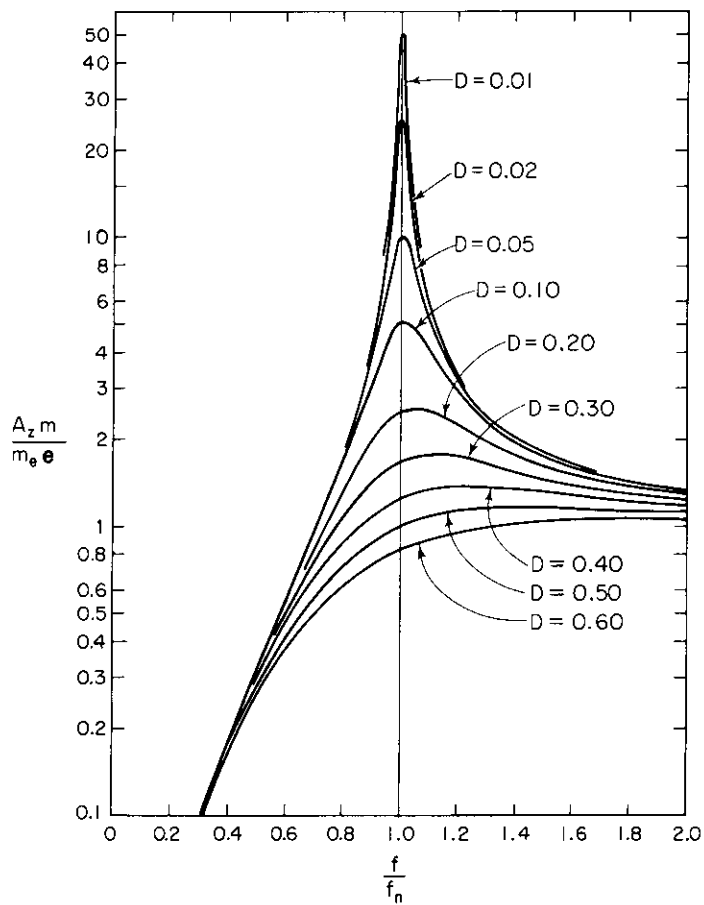


Figure A-2. Response curves for rotating-mass-type excitation of viscously damped single-degree-of-freedom system.

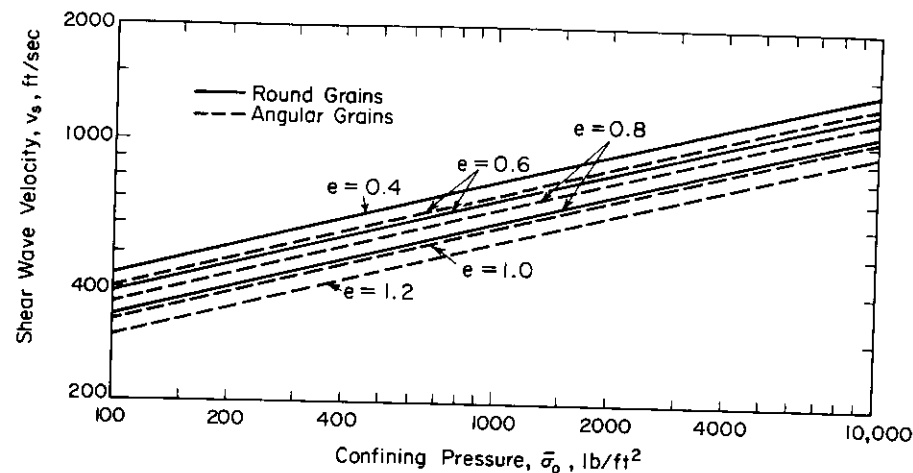


Figure A-3. Variation of shear-wave velocity in dry sands with void ratio and confining pressure.

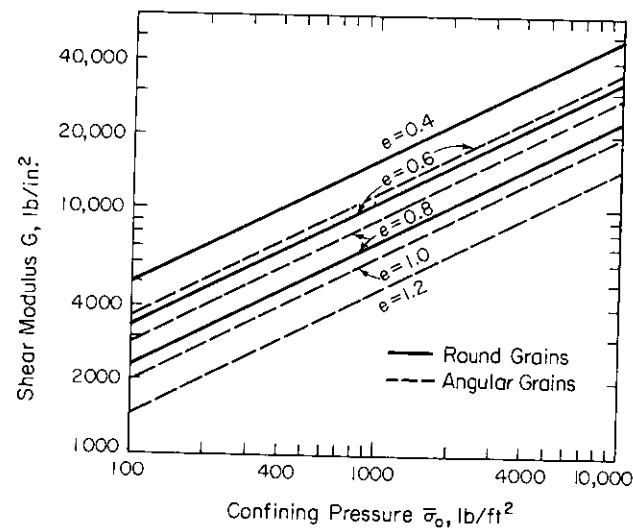


Figure A-4. Variation of shear modulus of dry sands with void ratio and confining pressure.

## REFERENCES

Throughout the reference list several publications and organizations occur repeatedly. Standard abbreviations have been established for these to achieve a more compact reference form. The abbreviations are as follows:

ASCE	American Society of Civil Engineers
ASME	American Society of Mechanical Engineers
ASTM	American Society for Testing and Materials
<i>ASTM-STP</i>	<i>American Society for Testing and Materials, Special Technical Publication</i>
<i>Bull. ERI</i>	<i>Bulletin of the Earthquake Research Institute Tokyo Imperial Univ., Japan</i>
DEGEBO	Deutschen Forschungsgesellschaft für Bodenmechanik
<i>ENR</i>	<i>Engineering News-Record</i>
<i>J. Soil Mech. and Found. Div., Proc. ASCE</i>	<i>Journal of the Soil Mechanics and Foundations Division, Proceedings of the American Society of Civil Engineers</i>
<i>J. Appl. Mech., Trans. ASME</i>	<i>Journal of Applied Mechanics, Transactions of the American Society of Mechanical Engineers, Series E</i>
<i>Proc. [number] ICSMFE</i>	<i>Proceedings of the [number] International Conference on Soil Mechanics and Foundation Engineering</i>
<i>Trans. ASCE</i>	<i>Transactions of the American Society of Civil Engineers</i>
<i>VDI</i>	<i>Verein Deutscher Ingenieure (Berlin)</i>
WES	U.S. Army Engineer Waterways Experiment Station, Corps of Engineers, Vicksburg, Miss.

- Albers, V. M. (1960), *Underwater Acoustics Handbook*, The Pennsylvania State Univ. Press, 290 pp.
- Arnold, R. N., Bycroft, G. N., and Warburton, G. B. (1955), "Forced Vibrations of a Body on an Infinite Elastic Solid," *J. Appl. Mech., Trans. ASME*, Vol. 77, pp. 391-401.
- Ballard, R. F., Jr. (1964), "Determination of Soil Shear Moduli at Depth by In-Situ Vibratory Techniques," WES, Misc. Paper No. 4-691, Dec.
- Ballard, R. F., Jr., and Casagrande, D. R. (1966), "Dynamic Foundation Investigation Roi-Namur, Kwajalein Atoll, Marshall Islands," WES, Misc. Paper No. 4-858, Nov.
- Ballard, R. F., Jr., and Casagrande, D. R. (1967), "Dynamic Foundation Investigations, TAA-2A Radar Site, Cape Kennedy, Florida," WES, Misc. Paper No. 4-878, Feb.
- Ballard, R. F., Jr., and Fowler, J. (1967), "Effect of Antenna Operation on Structure and Foundation Behavior, AMRAD and RAMPART Towers, White Sands Missile Range, New Mexico," WES, Misc. Paper No. 4-955, Dec.
- Barkan, D. D. (1936), "Field Investigations of the Theory of Vibration of Massive Foundations under Machines," *Proc. 1st ICSMFE* (Harvard Univ., Cambridge, Mass.), Vol. II, pp. 285-288.
- Barkan, D. D. (1962), *Dynamics of Bases and Foundations* (translated from the Russian by L. Drashevskaya, and translation edited by G. P. Tschebotarioff), McGraw-Hill Book Co. (New York), 434 pp.
- Baxter, R. L., and Bernhard, D. L. (1967), "Vibration Tolerances for Industry," ASME Paper 67-PEM-14, presented at Plant Eng. and Maintenance Conf., Detroit, Mich., April 10-12.
- Bernhard, R., u. Spaeth, W. (1929), "Rein dynamische Verfahren zur Untersuchung der Beanspruchungen von Bauwerken," *Stahlbau*, Vol. 2, S. 61/8.
- Biot, M. A. (1956), "Theory of Propagation of Elastic Waves in A Fluid-Saturated Porous Solid," *J. Acoustical Society of America*, Vol. 28, Mar. pp. 168-191.
- Blake, M. P. (1964), "New Vibration Standards for Maintenance," *Hydrocarbon Processing and Petroleum Refiner*, Vol. 43, No. 1 (Jan.), pp. 111-114, (copyrighted in 1962 by Gulf Publishing Company, Houston, Texas).
- Bornitz, G. (1931), *Über die Ausbreitung der von Groszkolbenmaschinen erzeugten Bodenschwingungen in die Tiefe*, J. Springer (Berlin).
- Borowicka, H. (1943), "Über ausmittig belastete starre Platten auf elastischisotropem Untergrund," *Ingenieur-Archiv*, 1:1-8.
- Brandt, H. (1955), "A Study of the Speed of Sound in Porous Granular Media," *J. Appl. Mech., Trans. ASME*, Vol. 22, No. 4 (Dec.), pp. 479-486.
- BRS (1955), "Vibrations in Buildings," *Building Research Station Digest*, No. 78, published by Her Majesty's Stationery Office, York House, Kingsway, London, W.C.2.
- BuRecl (1948), "Vibroflotation Experiments at Enders Dam, Frenchman Cambridge Unit, Missouri Basin Project," U.S. Bur. of Reclamation, Research and Geology Div., Denver, Colo.
- Burmister, D. M. (1938), "The Grading-Density Relations of Granular Materials," *Proc. ASTM*, Vol. 38, Part II, pp. 587-596.
- Burmister, D. M. (1948), "The Importance and Practical Use of Relative Density in Soil Mechanics," *Proc. ASTM*, Vol. 48, pp. 1249-1268.
- Burmister, D. M. (1964), "Suggested Methods of Test for Maximum and Minimum Densities of Granular Soils," *Proc. for Testing Soils, ASTM*.
- Bycroft, G. N. (1956), "Forced Vibrations of a Rigid Circular Plate on a Semi-infinite Elastic Space and on an Elastic Stratum," *Philosophical Trans., Royal Society, London*, Ser. A, Vol. 248, pp. 327-368.
- Casagrande, A., and Shannon, W. L. (1948), "Stress Deformation and Strength Characteristics of Soils under Dynamic Loads," *Proc. 2nd ICSMFE*, Vol. V, pp. 29-34.
- Cattaneo, C. (1938), "Sul contatto di due corpi elastici," *Accademia dei Lincei Rendiconti*, Ser. 6, Vol. 27, pp. 342-348, 434-436, 474-478.
- Converse, F. J. (1953), "Compaction of Sand at Resonant Frequency," *Symposium on Dynamic Testing of Soils, ASTM-STP No. 156*, pp. 124-137.
- Crandell, F. J. (1949), "Ground Vibration due to Blasting and Its Effect on Structures," *J. Boston Society of Civil Engineers*, April.
- Crede, C. E. (1951), *Vibration and Shock Isolation*, John Wiley & Sons, Inc. (New York), 328pp.
- Crockett, J. N. A., and Hammond, R. E. R. (1949), "The Dynamic Principles of Machine Foundations and Ground," *Proc. Institution of Mechanical Engineers, London*, Vol. 160, No. 4, pp. 512-523.
- D'Appolonia, D. J., and D'Appolonia, E. (1967), "Determination of the Maximum Density of Cohesionless Soils," *Proc. 3rd Asian Regional Conference on Soil Mechanics and Foundation Eng.*, Haifa, Israel, Sept.
- D'Appolonia, D. J., Whitman, R. V., and D'Appolonia, E. (1969), "Sand Compaction with Vibratory Rollers," *J. Soil Mech. and Found. Div. Proc. ASCE*, Vol. 95, No. SM 1, Jan.
- D'Appolonia, E. (1953), "Loose Sands—Their Compaction by Vibroflotation," *Symposium on Dynamic Testing of Soils, ASTM-STP No. 156*, pp. 138-154.

- D'Appolonia, E. (1966), "The Performance of Spread Footings on Vibratory Compacted and Preloaded Fine Sands," paper presented at ASCE Meeting, Miami, Fla., Jan.
- D'Appolonia, E. (1968), "Dynamic Loadings," presented at ASCE Specialty Conference on Placement and Improvement of Soil to Support Structures, Massachusetts Inst. of Technology, Aug.
- Davisson, M. T. (1963), "Static and Dynamic Behavior of a Playa Silt in One-Dimensional Compression," Air Force Weapons Laboratory, Kirtland Air Force Base, New Mexico, Tech. Documentary Rep. No. RTD TDR-63-3078, Sept.
- deBremaecker, J. Cl. (1958), "Transmission and Reflection of Rayleigh Waves at Corners," *Geophysics*, Vol. 23, pp. 253-266.
- Demer, L. J. (1956), *Bibliography of the Material Damping Field*, Wright Air Development Center, Tech. Rep. 56-180, 92 pp.
- Den Hartog, J. P. (1956), *Mechanical Vibrations*, 4th Edition, McGraw-Hill Book Co. (New York), 448 pp.
- Deresiewicz, H. (1958), "Stress-Strain Relations for a Simple Model of a Granular Medium," *J. Appl. Mech., Trans. ASME*, Sept., pp. 402-406.
- Diaz de Cossio, R. (1960), "Foundation Failures During the Coatzacoalcos (Mexico) Earthquake of 26 Aug. 1959," *Proc. 2nd World Conference on Earthquake Engineering*, 1, pp. 473-486.
- Dolling, H. J. (1965), "Schwingungsisolierung von Bauwerken durch tiefe, auf geeignete Weise stabilisierte Schilte," Sonderdruck aus *VDI-Berichte* 88, S. 3741.
- Drnevich, V. P. (1967), "Effect of Strain History on the Dynamic Properties of Sand," Ph.D. dissertation, Univ. of Michigan, 151 pp.
- Drnevich, V. P., and Hall, J. R., Jr. (1966), "Transient Loading Tests on a Circular Footing," *J. Soil Mech. and Found. Div. Proc. ASCE*, Vol. 92, No. SM 6, Nov., pp. 153-167.
- Drnevich, V. P., Hall, J. R., Jr., and Richart, F. E., Jr. (1967), "Effects of Amplitude of Vibration on the Shear Modulus of Sand," *Proc. International Symposium on Wave Propagation and Dynamic Properties of Earth Materials*, Albuquerque, N.M., Aug.
- Duffy, J., and Mindlin, R. D. (1957), "Stress-Strain Relations of a Granular Medium," *J. Appl. Mech., Trans. ASME*, Dec., pp. 585-593.
- Elorduy, J., Nieto, J. A., and Szekely, E. M. (1967), "Dynamic Response of Bases of Arbitrary Shape Subjected to Periodic Vertical Loading," *Proc. International Symposium on Wave Propagation and Dynamic Properties of Earth Materials*, Albuquerque, N.M., Aug.
- Evans, J. T. (1956), "Pneumatic and Similar Breakwaters," *Proc. Institution of Civil Engineers*, Vol. 5, No. 1, Part II, Feb., pp. 91-93.
- Ewing, W. M., Jardetzky, W. S., and Press, F. (1957), *Elastic Waves in Layered Media*, McGraw-Hill Book Co. (New York), 380 pp.
- Falconer, B. H. (1964), "Niigata Earthquake, Japan, 1:02 p.m., 16 June, 1964," *International Inst. of Seismology and Earthquake Eng.*, Tokyo, Japan, 41 pp.
- Fistedis, S. H. (1957), "Vibration-Resistant Prestressed Concrete Foundations for Engines and Compressors," *Proc. World Conference on Prestressed Concrete*, San Francisco, pp. 10-1-10-6.
- Florin, V. A., and Ivanov, P. L. (1961), "Liquefaction of Sandy Soils," *Proc. 5th ICSMFE*, Vol. I, pp. 107-111.
- Forssblad, L. (1965), "Investigations of Soil Compaction by Vibration," *ACTA Polytechnica Scandinavia*, Civil Eng. and Building Construction Series No. 34, Ci 34, UDC 624.138.22, Royal Swedish Acad. of Eng. Sciences, Stockholm.
- Fruhauf, B. (1949), "Wet Vibration Puts Strength into Sand," *ENR*, July 23.
- Fry, Z. B. (1963), "Development and Evaluation of Soil Bearing Capacity, Foundations of Structures," WES, *Tech. Rep. No. 3-632*, Report No. 1. Jul.
- Fry, Z. B. (1965), "Dynamic Soils Investigations Project Buggy, Buckboard Mesa Nevada Test Site, Mercury, Nevada," WES, Misc. Paper No. 4-666, Jan.
- Fu, C., and Jepson, J. W. (1959), *Criteria for Design of Foundations for Precision Tracking Radars Considering Dynamic Response*, ASME Paper 59-A-328.
- Funston, N. E., and Hall, W. J. (1967), "Footing Vibration with Nonlinear Subgrade Support," *J. Soil Mech. and Found. Div., Proc. ASCE*, Vol. 93, No. SM 5, Sept., pp. 191-211.
- Godden, W. G. (1965), *Numerical Analysis of Beam and Column Structures*, Prentice-Hall, Inc. (Englewood Cliffs, N.J.), 309 pp.
- Gorbulov-Possadov, M. I., and Serebrajanyi, R. V. (1961), "Design of Structures upon Elastic Foundations," *Proc. 5th ICSMFE*, Vol. I, pp. 643-648.
- Grant, F. S., and West, G. F. (1965), *Interpretation Theory in Applied Geophysics*, McGraw-Hill Book Co. (New York), 584 pp.
- Graves, M. (1968), "Air Bubble Curtain in Sub-Aqueous Blasting at Muddy Run," *Civil Engineering*, June, pp. 58-61.
- Griffiths, D. H., and King, R. F. (1965), *Applied Geophysics for Engineers and Geologists*, Pergamon Press (New York), 223 pp.
- Hall, J. R., Jr. (1962), "Effect of Amplitude on Damping and Wave Propagation in Granular Materials," Ph.D. dissertation, Univ. of Florida, Aug., 172 pp.



- Hall, J. R., Jr. (1967), "Coupled Rocking and Sliding Oscillations of Rigid Circular Footings," *Proc. International Symposium on Wave Propagation and Dynamic Properties of Earth Materials*, Albuquerque, N.M., Aug.
- Hall, J. R., Jr., and Richart, F. E., Jr. (1963), "Dissipation of Elastic Wave Energy in Granular Soils," *J. Soil Mech. and Found. Div., Proc. ASCE*, Vol. 89, No. SM 6, Nov., pp. 27-56.
- Hamilton, E. L. (1963), "Sediment Sound Velocity Measurements Made In Situ from Bathyscaph Trieste," *J. Geophysical Research*, Vol. 68, No. 21, Nov. 1, pp. 5991-5998.
- Hardin, B. O. (1961), "Study of Elastic Wave Propagation and Damping in Granular Materials," Ph.D. dissertation, Univ. of Florida, Aug., 207 pp.
- Hardin, B. O. (1965), "The Nature of Damping in Sands," *J. Soil Mech. and Found. Div., Proc. ASCE*, Vol. 91, No. SM 1, Jan., pp. 63-97.
- Hardin, B. O., and Black, W. L. (1966), "Sand Stiffness Under Various Triaxial Stresses," *J. Soil Mech. and Found. Div., Proc. ASCE*, Vol. 92, No. SM 2, March, pp. 27-42.
- Hardin, B. O., and Black, W. L. (1968), "Vibration Modulus of Normally Consolidated Clay," *J. Soil Mech. and Found. Div., Proc. ASCE*, Vol. 94, No. SM 2, March, pp. 353-369.
- Hardin, B. O., and Music, J. (1965), "Apparatus for Vibration During the Triaxial Test," *Symposium on Instrumentation and Apparatus for Soils and Rocks, ASTM STP*, No. 392.
- Hardin, B. O., and Richart, F. E., Jr. (1963), "Elastic Wave Velocities in Granular Soils," *J. Soil Mech. and Found. Div., Proc. ASCE*, Vol. 89, No. SM 1, Feb., pp. 33-65.
- Harris, C. M., and Crede, C. E. (1961), *Shock and Vibration Handbook*, (3 vols.), McGraw-Hill Book Co. (New York).
- Hayashi, K. (1921), *Theorie des Trägers auf elastischer Unterlage*, Julius Springer (Berlin), 301 pp.
- Hendron, A. J., Jr., Fulton, R. E., and Mohraz, B. (1963), "The Energy Absorption Capacity of Granular Materials in One-Dimensional Compression," Tech. Doc. Rep. No. AFSWC-TDR-62-91, Dept. of Civil Eng., Univ. of Illinois, report to AFSWC, Kirtland AFB, N. M.
- Hertwig, A., Früh, G., and Lorenz, H. (1933), "Die Ermittlung der für das Bauwesen wichtigsten Eigenschaften des Bodens durch erzwungene Schwingungen," DEGEBO No. 1, J. Springer (Berlin), 45 pp.
- Hertwig, A., and Lorenz, H. (1935), "Das Dynamische Bodenuntersuchungsverfahren," *Der Bauingenieur*, Vol. 16, June 21, pp. 279-285.
- Hertz, H. (1881), "Über die Berührung fester elastischer Körper," *J. reine u. angew Math.*, Vol. 92, pp. 156-171.

- Hetényi, M. (1946), *Beams on Elastic Foundation*, The University of Michigan Press (Ann Arbor) 255 pp.
- Heukelom, W., and Foster, C. R. (1960), "Dynamic Testing of Pavements," *J. Soil Mech. and Found. Div., Proc. ASCE*, Vol. 86 No SM1, part 1 Feb., pp. 1-28.
- Hirona, T. (1948), "Mathematical Theory on Shallow Earthquake," *The Geophysical Magazine*, Vol. 18, No. 1-4, Oct.
- Horn, H. M. (1964), "The Analysis and Design of Antenna Tower Foundations," *J. Boston Society of Civil Engineers*, Vol. 51, pp. 215-245.
- Housner, G. W., and Castellani, A. (1969), Discussion of "Comparison of Footing Vibration Tests with Theory" by F. E. Richart, Jr., and R. V. Whitman, *J. Soil Mech. and Found. Div. Proc. ASCE*, Vol. 95, No. SM 1, Jan., pp. 360-364.
- Hsieh, T. K. (1962), "Foundation Vibrations," *Proc. Institution of Civil Engineers*, Vol. 22, pp. 211-226.
- Humphries, W. K., and Wahls, H. E. (1968), "Stress History Effects on Dynamic Modulus of Clay," *J. Soil Mech. and Found. Div., Proc. ASCE*, Vol. 94, No. SM 2, Mar., pp. 371-389.
- Iida, K. (1938), "The Velocity of Elastic Waves in Sand," *Bull. ERI*, Vol. 16, pp. 131-144.
- Iida, K. (1940), "On the Elastic Properties of Soil particularly in relation to its Water Content," *Bull. ERI*, Vol. 18, pp. 675-690.
- Jackson, J. G., Jr., and Hadala, P. F. (1964), "Dynamic Bearing Capacity of Soils, Report 3: The Application of Similitude to Small-Scale Footing Tests," WES, Tech. Rep. No. 5-399, Dec.
- Jacobsen, L., and Ayre, R. S. (1958), *Engineering Vibrations*, McGraw-Hill Book Co. (New York), 564 pp.
- Jensen, J. W. (1959), "Damping Capacity—Its Measurement and Significance," *Bur. of Mines Report 5441*, U.S. Dept. of the Interior, Wash., D.C.
- Johnson, J. W. (1953), "Engineering Aspects of Diffraction and Refraction," *Trans. ASCE*, Vol. 118, pp. 617-648.
- Jones, R. (1958), "In-Situ Measurement of the Dynamic Properties of Soil by Vibration Methods," *Geotechnique*, Vol. 8, No. 1, Mar., pp. 1-21.
- J.S.S.M.F.E. (1966), Japanese Society of Soil Mechanics and Foundation Engineering, Vol. 6, No. 1, Jan.
- Kaldjian, M. J. (1969), Discussion of "Design Procedures for Dynamically Loaded Foundations" by R. V. Whitman and F. E. Richart, Jr., Paper No. 5569, *J. Soil Mech. and Found. Div. Proc. ASCE*, Vol. 95, No. SM 1, Jan., pp. 364-366.
- Kane, J., and Spence, J. (1963), "Rayleigh Transmission on Elastic Wedges," *Geophysics*, Vol. 28, No. 5, Oct., pp. 715-723.

- Knopoff, L. (1952), "On Rayleigh Wave Velocities," *Bulletin of the Seismological Society of America*, Vol. 42, pp. 307-308.
- Knopoff, L., and Gangi, A. F. (1960), "Transmission and Reflection of Rayleigh Waves by Wedges," *Geophysics*, Vol. 25, pp. 1203-1214.
- Kobori, T. (1962), "Dynamical Response of Rectangular Foundations on an Elastic Half-Space," *Proc. Japanese National Symposium on Earthquake Eng.*, pp. 81-86.
- Kolsky, H. (1963), *Stress Waves in Solids*, Dover Publications, Inc. (New York) and Clarendon Press (Oxford), 1953, 213 pp.
- Kummeneje, O., and Eide, O. (1961), "Investigation of Loose Sand Deposits by Blasting," *Proc. 5th ICSMFE*, Vol. I, pp. 491-497.
- Kurihara, M. (1958), "Pneumatic Breakwaters I," translation by K. Horikawa from *1st Conference on Coastal Engineering*, Japan, Nov. 1954, Dept. of Eng., U. of Cal. Inst. of Eng. Research, Wave Research Lab, Tech. Rep. Series 104, Issue 4, Berkeley, Cal., 14 pp.
- Lamb, H. (1879, 1945), *Hydrodynamics*, Cambridge Univ. Press; 1945 ed.: Dover Publications (New York), 738 pp.
- Lamb, H. (1904), "On the Propagation of Tremors over the Surface of an Elastic Solid," *Philosophical Transactions of the Royal Society, London*, Ser. A, Vol. 203, pp. 1-42.
- Lawrence, F. V., Jr. (1965), "Ultrasonic Shear Wave Velocities in Sand and Clay," *Rep. R65-05*, Dept. of Civil Eng., Massachusetts Inst. of Technology Cambridge, Mass., to WES.
- Lazan, B. J. (1968), *Damping of Materials and Members in Structural Mechanics*, Pergamon Press, Inc. (New York), 317 pp.
- Linger, D. A. (1963), "Effect of Vibration on Soil Properties," *Proc. 42nd Annual Meeting Highway Research Board*.
- Lorenz, H. (1934), "Neue Ergebnisse der dynamische Baugrunduntersuchung," *Z VDI*, Vol. 78, No. 12, March 24, pp. 379-385.
- Lorenz, H. (1950), "Der Baugrund als Federung und Dämpfung Schwingender Körper," *Der Bauingenieur*, Heft 10, pp. 365-372.
- Lorenz, H. (1953), "Elasticity and Damping Effects of Oscillating Bodies on Soil," *Symposium on Dynamic Testing of Soils, ASTM STP No. 156*, pp. 113-122.
- Lorenz, H. (1960), *Grundbau-Dynamik*, J. Springer (Berlin), 308 pp.
- Luscher, U., Ortigosa, P., Rocker, K., and Whitman, R. V. (1967), "Repeated Load and Vibration Tests upon Sand," Progress Report No. 1, Dept. of Civil Eng., Massachusetts Inst. of Technology, Research Report R67-29, *Soils Publication No. 203*, Aug.

- Lyman, A. K. B. (1942), "Compaction of Cohesionless Foundation Soils by Explosives," *Trans. ASCE*, Vol. 107, pp. 1330-1348.
- Lysmer, J. (1965), *Vertical Motion of Rigid Footings*, Dept. of Civil Eng., Univ. of Michigan Report to WES Contract Report No. 3-115 under Contract No. DA-22-079-eng-340; also a Ph.D. dissertation, Univ. of Michigan, Aug.
- Lysmer, J., and Richart, F. E., Jr. (1966), "Dynamic Response of Footings to Vertical Loading," *J. Soil Mech. and Found. Div., Proc. ASCE*, Vol. 92, No. SM 1, Jan., pp. 65-91.
- Lysmer, J. (1966), private communication with F. E. Richart, Jr., dated Feb. 2.
- Major, A. (1962), *Vibration Analysis and Design of Foundations for Machines and Turbines*, Collet's Holdings Ltd. (London) and Akadémiai Kiadó (Budapest).
- Marsal, R. J. (1961), "Behavior of a Sandy Uniform Soil During the Jaltipan Earthquake, Mexico," *Proc. 5th ICSMFE*, Vol. I, pp. 229-232.
- Maxwell, A. A. (1965), Panel Discussion on Session IV, "Dynamically Loaded Foundations," *Proc. of Symposium, Bearing Capacity and Settlement of Foundations*, Duke Univ., pp. 136-139.
- McCamy, K., Meyer, R. P., and Smith, T. J. (1962), "Generally Applicable Solutions of Zoeppritz' Amplitude Equations," *Bulletin of the Seismological Society of America*, Vol. 52, No. 4, Oct., pp. 923-955.
- McNeill, R. L., Margason, B. E., and Babcock, F. M. (1965), "The Role of Soil Dynamics in the Design of Stable Test Pads," *Guidance and Control Conference*, Minneapolis, Minn., Aug. 16-18.
- Miller, G. F., and Pursey, H. (1954), "The Field and Radiation Impedance of Mechanical Radiators on the Free Surface of a Semi-Infinite Isotropic Solid," *Proc. Royal Society, London, A*, Vol. 223, pp. 521-541.
- Miller, G. F., and Pursey, H. (1955), "On the Partition of Energy Between Elastic Waves in a Semi-Infinite Solid," *Proc. Royal Society, London, A*, v. 233, pp. 55-69.
- Mindlin, R. D. (1949), "Compliance of Elastic Bodies in Contact," *JAM*, Sept. pp. 259-268.
- Mindlin, R. D. (1954), "Mechanics of Granular Media," *Proc. 2nd U.S. National Congress of Appl. Mech., ASME*, pp. 13-20.
- Mindlin, R. D., and Deresiewicz, H. (1953), "Elastic Spheres in Contact under Varying Oblique Forces," *J. Appl. Mech., Trans. ASME*, Sept., pp. 327-344.
- Mindlin, R. D., Mason, W. P., Osmer, T. F., and Deresiewicz, H. (1951), "Effects of an Oscillating Tangential Force on the Contact Surfaces of Elastic Spheres," *Proc. 1st U.S. National Congress of Appl. Mech., ASME*, pp. 203-208.
- Mogami, T., and Kubo, K. (1953), "The Behavior of Soil During Vibration," *Proc. 3rd ICSMFE*, Vol. I, p. 152.

- Morse, P. M. (1948), *Vibration and Sound*, McGraw-Hill Book Co. (New York), 468 pp.
- Morse, P. M. (1952), "Acoustic Propagation in Granular Media," *J. Acoustical Society of America*, Vol. 24, No. 6, Nov., pp. 696-700.
- Nash, K. L., and Dixon, R. K. (1960), "The Measurement of Pore Pressure in Sand Under Rapid Triaxial Test," *Proc. Conference on Pore Pressure and Suction in Soils*, Butterworths (London).
- Neumeuer, H. (1963), "Untersuchungen über die Abschirmung eines bestehenden Gebäudes gegen Erschütterungen beim Bau und Betrieb einer U-Bahnstrecke," *Baumaschine und Bautechnik-10*, Jahrgang, Heft 1, Jan.
- Newcomb, W. K. (1951), "Principles of Foundation Design for Engines and Compressors," *Trans. ASME*, Vol. 73, pp. 307-312; disc.—pp. 313-318.
- Newmark, N. M. (1943), "Numerical Procedure for Computing Deflections, Moments, and Buckling Loads," *Trans. ASCE*, Vol. 108, pp. 1161-1188.
- Novak, M. (1960), "The Vibrations of Massive Foundations on Soil," *International Association of Bridge and Structural Engineering*, Vol. 20, pp. 263-281.
- Parvis, E., and Appendino, M. (1966), *Large Size Turbogenerator Foundations—Dynamic Problems and Considerations on Designing*, Ente Nazionale per l'Energia Elettrica, Department of Milan, Steam Power Plant Design, Eng. and Constr. Div., Milan, Italy.
- Paterson, N. R. (1955), "Elastic Wave Propagation in Granular Media," Ph.D. thesis, Dept. of Physics, Univ. of Toronto.
- Pauw, A. (1952), "A Rational Design Procedure for Machine Foundations," Ph.D. thesis, California Inst. of Technology, 178 pp.
- Pilant, W. L., Knopoff, L., and Schwab, F. (1964), "Transmission and Reflection of Surface Waves at a Corner, 3, Rayleigh Waves (Experimental)," *J. Geophysical Research*, Vol. 69, No. 2.
- Pippas, D. A. (1932), "Über die Setzungen und Dichtigkeitsänderungen bei Sandschüttungen infolge von Erschütterungen," DEGEBO Pub. No. 4, J. Springer (Berlin).
- Prange, B. (1965), "Ein Beitrag zum Problem der Spannungsmessung im Halbraum," dissertation, Technischen Hochschule Karlsruhe, Germany, O. Berenz (Karlsruhe), 159 pp.
- Prugh, B. J. (1963), "Densification of Soils by Explosive Vibration," *J. Constr. Div. Proc. ASCE*, Vol. 89, No. CO 1, pp. 79-100.
- Pschunder, R. J. (1965), "Tilt and Deflection of Tapered Polygonal Towers," *J. Struct. Div., Proc. ASCE*, Vol. 91, No. ST 3, Proc. 4373, June, pp. 151-169.
- Pschunder, R. J. (1966), "Radar Tower and Foundation Analysis," *ASME Deep Space and Missile Tracking Antennas*, pp. 78-100.
- Quinlan, P. M. (1953), "The Elastic Theory of Soil Dynamics," *Symposium on Dynamic Testing of Soils, ASTM STP No. 156*, pp. 3-34.
- Rao, H. A. Balakrishna (1961), "The Design of Machine Foundations Related to the Bulb of Pressure," *Proc. 5th ICSMFE*, Vol. 1, pp. 563-568.
- Rausch, E. (1943), *Maschinenfundamente und andere dynamische Bauaufgaben*, Vertrieb VDI Verlag G.M.B.H. (Berlin).
- Rayleigh, Lord (1877, 1945), *The Theory of Sound*, 1945 Ed.: Dover Publications (New York).
- Rayleigh, Lord (1885), "On Waves Propagated Along the Plane Surface of an Elastic Solid," *London Mathematical Society Proc.*, 17, pp. 4-11.
- Reiher, H., and Meister, F. J. (1931), "Die Empfindlichkeit der Menschen gegen Erschütterungen," *Forsch. Gebiete Ingenieurwesen*, Vol. 2, No. 11, pp. 381-386.
- Reissner, E. (1936), "Stationäre, axialsymmetrische durch eine Schüttelnde Masse erregte Schwingungen eines homogenen elastischen Halbraumes," *Ingenieur-Archiv*, Vol. 7, Part 6, Dec., pp. 381-396.
- Reissner, E. (1937), "Freie und erzwungene Torsionschwingungen des elastischen Halbraumes," *Ingenieur-Archiv*, Vol. 8, No. 4, pp. 229-245.
- Reissner, E., and Sagoci, H. F. (1944), "Forced Torsional Oscillations of an Elastic Half-Space," *J. of Appl. Phys.*, Vol. 15, pp. 652-662.
- Richart, F. E., Jr. (1962), "Foundation Vibrations," *Trans. ASCE*, Vol. 127, Part 1, pp. 863-898.
- Richart, F. E., Jr. (1962a), Private communication with Moran, Proctor, Mueser, and Rutledge.
- Richart, F. E., Jr., and Whitman, R. V. (1967), "Comparison of Footing Vibration Tests with Theory," *J. Soil Mech. and Found. Div., Proc. ASCE*, Vol. 93, No. SM 6, Nov., pp. 143-168.
- Sato, Y. (1952), "Velocity of Elastic Waves Propagation in Media with Small Holes," *Bull. ERI*, Vol. 30, pp. 179-190.
- Seed, H. B., and Lundgren, R. (1954), "Investigation of the Effect of Transient Loading on the Strength and Deformation Characteristics of Saturated Sands," *Proc. ASTM*, Vol. 54, pp. 1288-1306.
- Seed, H. B. (1957), Discussion on "Soil Properties and their Measurement," *Proc. 4th ICSMFE*, Vol. 3, pp. 86-87.
- Seed, H. B. (1960), "Soil Strength During Earthquake," *Proc. 2nd World Conference on Earthquake Eng.*, Vol. 1, p. 183-194.
- Seed, H. B., and Chan, C. K. (1964), "Pulsating Load Tests on Clays," Appendix D of Shannon and Wilson (1964) report, *Anchorage Area Soil Studies, Alaska*.

- Seed, H. B., and Lee, K. L. (1966), "Liquefaction of Saturated Sands during Cyclic Loading," *J. Soil Mech. and Found. Div., Proc. ASCE*, Vol. 92, No. SM 6, Nov., pp. 105-134.
- Seed, H. B. (1968), "The Fourth Terzaghi Lecture: Landslides during Earthquakes due to Liquefaction," *J. Soil Mech. and Found. Div., Proc. ASCE*, Vol. 94, No. SM 5, Sept., pp. 1053-1122.
- Sell, J. C. (1963), "Further Study on the Vibration Limits for the Successful Operation of Electron Microscopes in Health Research Facilities," U.S. Dept. of Health, Education, and Welfare, Public Health Service, National Institutes of Health, Division of Research Services.
- Shannon and Wilson, Inc. (1964), *Anchorage Area Soil Studies, Alaska*, Report to U.S. Army Engineer District, Anchorage, Alaska.
- Shannon, W. L., Yamane, G., and Dietrich, R. J. (1959), "Dynamic Triaxial Tests on Sand," *Proceedings, First Panamerican Conference on Soil Mechanics and Foundation Engineering*, Mexico City, Vol. 1, pp. 473-486.
- Shumway, G. (1960), "Sound Speed and Absorption Studies of Marine Sediments by a Resonance Method—Parts I and II," *Geophysics*, Vol. 25, No. 2, April, pp. 451-467; No. 3, June, pp. 659-682.
- Soderberg (1933), "Working Stresses," *Trans. ASME, Appl. Mech. Div.*, Vol. 1, No. 3, pp. 131-140.
- Steffens, R. J. (1952), "The Assessment of Vibration Intensity and Its Application to the Study of Building Vibrations," *National Building Studies Special Report No. 19*, Dept. of Scientific and Ind. Research, Building Research Station, London.
- Steinbrugge, K. V., and Clough, R. W. (1960), "Chilean Earthquake of May, 1960, A Brief Report," *Proc. 2nd World Conference on Earthquake Eng.*, Vol. 1, pp. 629-637.
- Steurman, S. (1939), "A New Soil Compaction Device," *ENR*, July 20.
- Stevens, H. W. (1966), "Measurement of the Complex Moduli and Damping of Soils under Dynamic Loads," U.S. Army Cold Regions Research and Eng. Laboratory, Hanover, N.H., Tech. Rep. No. 173.
- Streeter, V. L. (editor) (1961), *Handbook of Fluid Dynamics*, McGraw-Hill Book Co. (New York).
- Streeter, V. L., and Wylie, E. B. (1967), *Hydraulic Transients*, McGraw-Hill Book Co. (New York), 329 pp.
- Sung, T. Y. (1953), "Vibrations in Semi-Infinite Solids due to Periodic Surface Loadings," *Symposium on Dynamic Testing of Soils, ASTM-STP No. 156*, pp. 35-64.
- Sung, T. Y. (1953a), "Vibration in Semi-Infinite Solids due to Periodic Surface Loading," S.D. thesis, Harvard University, May.
- Sutherland, H. B. (1950), "A Study of the Vibrations Produced in Structures by Heavy Vehicles," *Proc. 30th Annual Meeting of the Highway Research Board*, Dec., pp. 406-419.
- Taylor, D. W., and Whitman, R. V. (1954), *The Behavior of Soils under Dynamic Loadings—3, Final Report on Laboratory Studies*, Aug., Massachusetts Inst. of Technology Dept. of Civil and Sanitary Engineering Soil Mechanics Lab.
- Terzaghi, K. (1943), *Theoretical Soil Mechanics*, John Wiley and Sons, Inc. (New York).
- Terzaghi, K. (1955), "Evaluation of Coefficients of Subgrade Reaction," *Geotechnique*, Vol. 5, pp. 297-326.
- Thau, S. A., and Pao, Y. (1966), "Diffractions of Horizontal Shear Waves by a Parabolic Cylinder and Dynamic Stress Concentrations," *J. Appl. Mech., Trans. ASME*, Dec., pp. 785-792.
- Thomson, W. T., and Kobori, T. (1963), "Dynamical Compliance of Rectangular Foundations on an Elastic Half-Space," *J. Appl. Mech., Trans. ASME*, Dec., pp. 579-584.
- Timoshenko, S. P., and Goodier, J. N. (1951), *Theory of Elasticity*, McGraw-Hill Book Co. (New York), 506 pp.
- Tschebotarioff, G. P., and Ward, E. R. (1948), "The Resonance of Machine Foundations and the Soil Coefficients Which Affect It," *Proc. 2nd ICSMFE*, Vol. 1, pp. 309-313.
- Tschebotarioff, G. P. (1953), "Performance Records of Engine Foundations," *Symposium on Dynamic Testing of Soils, ASTM STP No. 156*, pp. 163-173.
- Tschebotarioff, G. P. (1965), Panel Discussion on Session IV, "Dynamically Loaded Foundations," in *Proc. Symposium on Bearing Capacity and Settlement of Foundations*, Duke University, pp. 135-136.
- Viktorov, I. A. (1958), "The Effects of Surface Defects on the Propagation of Rayleigh Waves," *Soviet Physics, Doklady*, 3, pp. 304-306.
- "A Wall of Bubbles Controls the Waves," *ENR*, Jan. 22, 1959, pp. 57-58.
- Warburton, G. B. (1957), "Forced Vibration of a Body Upon an Elastic Stratum," *J. Appl. Mech., Trans. ASME*, Vol. 24, pp. 55-58.
- Weissmann, G. F. (1966), "A Mathematical Model of a Vibrating Soil-Foundation System," *The Bell System Technical Journal*, Vol. 45, No. 1, Jan., pp. 177-228.
- Weissmann, G. F., and Hart, R. R. (1961), "Damping Capacity of Some Granular Soils," *ASTM STP No. 305*, pp. 45-54.
- Weissmann, G. F., and White, S. R. (1961), "Small Angular Deflexions of Rigid Foundations," *Geotechnique*, Vol. 11, No. 3, pp. 186-202.
- WES (1949), *Compaction Studies on Sand Subgrade*, Soil Compaction Investigation Report No. 3, Tech. Memo No. 3-271.

- WES (1963), "Nondestructive Dynamic Testing of Proposed Radar Sites, White Sands Missile Range, New Mexico," Misc. Paper No. 4-584, July.
- WES (1965), Private communication between F. E. Richart and Z. B. Fry of WES.
- Westergaard, H. M. (1952), *Theory of Elasticity and Plasticity*, Harvard Univ. Press (Cambridge) and John Wiley and Sons, Inc. (New York), 176 pp.
- Whitman, R. V., Roberts, J. E., and Mao, S. W. (1960), "The Response of Soils to Dynamic Loadings, Rep. 4, One-Dimensional Compression and Wave Velocity Tests," Massachusetts Inst. of Technology, Soils Eng. Div. Rep. to WES, Contract DA-22-079-eng-224, Aug.
- Whitman, R. V., and Lawrence, F. V., Jr. (1963), Discussion of "Wave Velocities in Granular Soils," by B. O. Hardin and F. E. Richart, Jr., *J. Soil Mech. and Found. Div., Proc. ASCE*, Vol. 89, No. SM 5, Sept., pp. 112-118.
- Whitman, R. V. (1963), "Stress-Strain-Time Behavior of Soil in One Dimensional Compression," *Rep. R 63-25*, Dept. Civil Eng. Massachusetts Inst. of Technology, to WES.
- Whitman, R. V., and Ortigosa dePablo, P. (1968), "Densification of Sand by Vertical Vibrations, Rep. No. 4—Repeated Load and Vibration Tests upon Sand," Dept. of Civil Eng., Massachusetts Inst. of Technology, Tech. Paper No. T68-5, Soils Pub. No. 222, Aug.
- Whitman, R. V., and Richart, F. E., Jr. (1967), "Design Procedures for Dynamically Loaded Foundations," *J. Soil Mech. and Found. Div., Proc. ASCE*, Vol. 93, No. SM 6, Nov., pp. 169-193.
- Wiegel, R. L. (1964), *Oceanographical Engineering*, Prentice-Hall, Inc. (Englewood Cliffs, N.J.), 532 pp.
- Wilson, S. D., and Dietrich, R. J. (1960), "Effect of Consolidation Pressure on Elastic and Strength Properties of Clay," *Proc. ASCE Research Conference on Shear Strength of Cohesive Soils*, Boulder, Colo., June.
- Wiss, J. F. (1968), "Effects of Blasting Vibrations on Buildings and People," *Civil Engineering*, July, pp. 46-48.
- Wood, A. B. (1930), *A Textbook of Sound*, G. Bell and Sons (London).
- Woods, R. D., and Richart, F. E., Jr. (1967), "Screening of Elastic Surface Waves by Trenches," *Proc. International Symposium on Wave Propagation and Dynamic Properties of Earth Materials*, Albuquerque, N.M., Aug.
- Woods, R. D. (1967), "Screening of Elastic Surface Waves by Trenches," Ph.D. dissertation, Univ. of Michigan, 160 pp.
- Woods, R. D. (1968), "Screening of Surface Waves in Soils," *J. Soil Mech. and Found. Div., Proc. ASCE*, Vol. 94, No. SM 4, July, pp. 951-979.
- Zaccor, J. V., and Wallace, M. R. (1963), "Techniques and Equipment for Determining Dynamic Properties of Soils," The United Research Services, Burlingame, California, Rep. for Defense Atomic Support Agency, on Contract No. DA-49-146-XZ-019, DASA 1421.
- Zeller, W. (1933), "Vorschlag für ein Mass der Schwingungsstärke" *Z. VDI*, v. 77, No. 12, p. 323.
- Zoeppritz, K. (1919), "Nach d. Konigl. Gesell. d. Wissen, z. Gottingen," *Math-Phys.*, Berlin, pp. 66-94.
- Zwikker, C., and Kosten, C. W. (1949), *Sound Absorbing Materials*, Elsevier (New York).

## AUTHOR INDEX

### A

Albers, V. M. 124  
Appendino, M. 313, 314  
Arnold, R. N. 216, 221, 230  
Ayre, R. S. 32, 43, 45, 58

### B

Babcock, F. M. 249  
Ballard, R. F., Jr. 113, 115, 116, 138, 378, 379  
Barkan, D. D. 1, 247, 248, 249, 256, 341, 342, 343, 348, 351  
Baxter, R. L. 314, 315  
Bernhard, D. L. 314, 315  
Bernhard, R. 324  
Biot, M. A. 132, 156  
Black, W. L. 152, 156, 157, 158, 353  
Blake, M. P. 312, 313  
Bornitz, G. 246  
Borowicka, H. 216, 351  
Brandt, H. 132  
BRS 316  
BuRecl 185  
Burmister, D. M. 185, 186  
Bycroft, G. N. 199, 201, 211, 216, 221, 222, 230, 231, 232, 233, 351

### C

Casagrande, A. 171, 172  
Casagrande, D. R. 115, 116, 138  
Castellani, A. 197  
Cattaneo, C. 146  
Chan, C. K. 177  
Clough, R. W. 174  
Converse, F. J. 185, 188, 360  
Crandell, F. J. 315, 320  
Crede, C. E. 1, 244, 317  
Crockett, J. N. A. 338

### D

D'Appolonia, D. J. 182, 183, 185, 186, 187, 188, 189  
D'Appolonia, E. 180, 181, 182, 183, 185, 186, 187, 188, 189, 190, 320  
Davisson, M. T. 170  
deBremaecker, J. Cl. 98, 99  
Demer, L. J. 165  
Den Hartog, J. P. 50  
Deresiewicz, H. 146, 147  
Diaz de Cossio, R. 174  
Dietrich, R. J. 152, 301  
Dixon, R. K. 171  
Dolling, H. J. 249, 256, 262

Drnevich, V. P. 158, 159, 160, 161, 162,  
164, 178, 179, 180, 307, 333, 334, 367  
Duffy, J. 148, 150, 151

## E

Eide, O. 173  
Elorduy, J. 211  
Evans, J. T. 131  
Ewing, W. M. 75, 92, 100, 103, 250

## F

Falconer, B. H. 174  
Fistedis, S. H. 198  
Florin, V. A. 174  
Forssblad, L. 185, 245  
Foster, C. R. 113, 116, 117  
Fowler, J. 378, 379  
Früh, G. 194, 324, 336  
Fruhauf, B. 185  
Fry, Z. B. 113, 116, 118, 168, 169, 209, 324,  
348, 349, 354, 355, 356, 369, 373  
Fu, C. 379  
Fulton, R. E. 148  
Funston, N. E. 192

## G

Gangi, A. F. 98  
Godden, W. G. 58  
Goodier, J. N. 66, 75, 143, 351  
Gorbunov-Possadov, M. I. 351  
Grant, F. S. 76  
Graves, M. 132  
Griffiths, D. H. 103

## H

Hadala, P. F. 172  
Hall, J. R., Jr. 158, 160, 161, 163, 217, 219,  
221, 222, 224, 229, 302, 303, 333,  
334, 348, 367  
Hall, W. J. 192  
Hamilton, E. L. 129  
Hammond, R. E. R. 338

Hardin, B. O. 135, 136, 152, 153, 154, 155,  
156, 157, 158, 164, 301, 302, 304,  
348, 353

Harris, C. M. 1, 244, 317  
Hart, R. R. 348  
Hayashi, K. 340  
Hendron, A. J., Jr. 148  
Hertwig, A. 194, 324, 336, 337  
Hertz, H. 143  
Hetenyi, M. 242, 340  
Heukelom, W. 113, 116, 117  
Hirona, T. 92  
Horn, H. M. 379  
Housner, G. W. 197  
Hsieh, T. K. 201, 219, 228  
Humphries, W. K. 157

## I

Iida, K. 151  
Ivanov, P. L. 174

## J

Jackson, J. G., Jr. 172  
Jacobsen, L. 32, 43, 45, 58  
Jardetzky, W. S. 75, 92, 100, 103, 250  
Jensen, J. W. 165  
Jepson, J. W. 379  
Johnson, J. W. 127  
Jones, R. 118, 120  
J.S.S.M.F.E. 174

## K

Kaldjian, M. J. 351, 352  
Kane, J. 98  
King, R. F. 103  
Knopoff, L. 98, 99, 168  
Kobori, T. 211  
Kolsky, H. 66, 75, 250  
Kosten, C. W. 132  
Kubo, K. 182  
Kummeneje, O. 173  
Kurihara, M. 131

## L

Lamb, H. 80, 88, 90, 122, 192

Lawrence, F. V., Jr. 155, 157  
Lazan, B. J. 165  
Lee, K. L. 175, 176  
Linger, D. A. 182  
Lorenz, H. 1, 192, 194, 324, 336, 337  
Lundgren, R. 171  
Luscher, U. 180  
Lyman, A. K. B. 173  
Lysmer, J. 31, 91, 203, 204, 205, 206, 209,  
345

## M

Mao, S. W. 170  
Major, A. 1  
Margason, B. E. 249  
Marsal, R. J. 174  
Mason, W. P. 147  
Maxwell, A. A. 322  
McCamy, K. 96, 97  
McNeill, R. L. 249  
Meister, F. J. 311, 317, 320  
Meyer, R. P. 96, 97  
Miller, G. F. 92  
Mindlin, R. D. 146, 147, 148, 150, 151  
Mogami, T. 182  
Mohraz, B. 148  
Morse, P. M. 122, 124, 132  
Music, J. 304

## N

Nash, K. L. 171  
Neumeuer, H. 248, 249  
Newcomb, W. K. 330  
Newmark, N. M. 57  
Nieto, J. A. 211  
Novak, M. 192

## O

Osmer, T. F. 147  
Ortigosa, P. 180, 182, 184

## P

Pao, Y. 250, 259

Parvis, E. 313, 314  
Paterson, N. R. 132  
Pauw, A. 348  
Pilant, W. L. 98, 99  
Pippas, D. A. 185  
Prange, B. 357  
Press, F. 75, 92, 100, 103, 250  
Prugh, B. J. 173  
Pschunder, R. J. 321, 379  
Pursey, H. 92

## Q

Quinlan, P. M. 194, 196, 211, 213

## R

Rao, H. A. 338  
Rausch, E. 1  
Rayleigh, Lord 80, 122  
Reiher, H. 311, 317, 320  
Reissner, E. 194, 213, 230, 238, 351  
Richard, F. E., Jr. 86, 152, 153, 154, 155,  
156, 157, 158, 160, 161, 198, 199,  
200, 204, 205, 206, 209, 237, 245,  
250, 301, 302, 303, 311, 345, 348,  
350, 371  
Roberts, J. E. 170  
Rocker, K. 180

## S

Sagoci, H. F. 213, 238, 351  
Sato, Y. 132  
Schwab, F. 98, 99  
Seed, H. B. 171, 174, 175, 176, 177, 178  
Sell, J. C. 321  
Serebrajanyi, R. V. 351  
Shannon, W. L. 152, 171, 172, 174, 177  
Shumway, G. 129  
Soderberg 178  
Smith, T. J. 96, 97  
Spaeth, W. 324  
Spence, J. 98  
Steffens, R. J. 317  
Steinbrugge, K. V. 174  
Steuerman, S. 185  
Stevens, H. W. 348

Streeter, V. L. 122, 131  
 Sung, T. Y. 194, 196, 211, 355  
 Sutherland, H. B. 321  
 Szekely, E. M. 211

## T

Taylor, D. W. 171, 172  
 Terzaghi, K. 340, 342  
 Thau, S. A. 250, 259  
 Thomson, W. T. 211  
 Timoshenko, S. P. 66, 75, 143, 351  
 Tschebotarioff, G. P. 320, 338

## V

Viktorov, I. A. 98, 99

## W

Wahls, H. E. 157  
 Wallace, M. R. 170  
 Warburton, G. B. 216, 221, 230, 233, 234  
 Ward, E. R. 338

Weissmann, G. F. 192, 348, 379  
 WES 185, 245, 377  
 West, G. F. 76  
 Westergaard, H. M. 239  
 White, S. R. 379  
 Whitman, R. V. 155, 170, 171, 172, 180,  
 182, 184, 185, 186, 187, 188, 189,  
 198, 345, 348, 350, 371

Wiegel, R. L. 123, 127, 128  
 Wilson, S. D. 152, 174, 177, 301  
 Wiss, J. F. 315  
 Wood, A. B. 129  
 Woods, R. D. 91, 245, 250, 251, 252, 253,  
 254, 255, 256, 257, 258, 259, 260  
 Wylie, E. B. 131

## Y

Yamane, G. 152

## Z

Zaccor, J. V. 170  
 Zeller, W. 320  
 Zoppertz, K. 93  
 Zwicker, C. 132

## SUBJECT INDEX

## A

Acceleration:  
 gravity 9  
 from phase plane 41, 46  
 pickups 286  
 Accelerometer 286  
 influence of cable length 287  
 Acoustic waves 123  
 Active isolation:  
 definition 251  
 field tests 253  
 Amplifiers 274  
 differential, common-mode rejection  
 ratio 275  
 floating input 275  
 Amplitude of motion, half-space theory 195  
 Analog:  
 electrical to mechanical 264, 267  
 Hall's 219, 224  
 Lysmer's 203  
 Approximate methods:  
 beam frequencies 58  
 Rayleigh method 58  
 Southwell-Dunkerley method 58  
 Attenuation 166 (*see also* Damping)  
 coefficient of 246  
 of Rayleigh wave with distance 244

## B

Beams 58  
 Bentonite-slurry trench 249  
 Blasting, vibrations from 315, 319  
 Body waves (*see P-wave and S-wave*)  
 Boundary conditions (end conditions),  
 semi-infinite rods 66  
 Breakwater 128  
 pneumatic 131  
 refraction by 128  
 Bulk modulus 129 (*see also* Modulus, of  
 volume compressibility)

## C

Cable 289  
 capacitance 285  
 characteristic impedance 290  
 characteristics 289  
 electrical termination 290  
 influence on calibration factor 284, 287  
 resistance 285  
 types 290  
 Caissons, vertical vibrations 235  
 Calibration of transducers 278, 279, 282,  
 283, 287



- Capacitance, electrical 265  
 Cathode follower 287  
 Circular footing on half-space, vertical oscillation:  
   distribution of energy from 92  
   waves generated by 90  
 Coaxial cable 291  
 Coefficient of attenuation 166, 246  
 Compaction:  
   of in-situ soils 183  
   of samples by vibrations 180  
   by vibrating rollers 185  
 Compression waves, ideal fluids 123  
 Connectors 291  
   banana-plug 292  
   BNC 291  
   microdot 291  
   microphone 292  
   UHF 291  
 Contact pressure, base of foundations:  
   parabolic, vertical motion 197  
   rigid, circular, rocking 216  
   rigid base approximation, vertical motion 196  
   uniform, vertical motion 197  
 Coulomb damping (*see* Damping, friction)  
 Coupled motion:  
   damped system 55  
   forced vibration 54  
   rocking and sliding 227  
     field test data 371  
     translation 49  
     and rotation 51  
 Critical angle of refraction 98  
 Critical damping 16  
 Cross-over distance 106  
 Current measurement 269
- D**
- Damping 15  
   coefficient of attenuation 166, 246  
   constant, geometrical, rigid circular footing:  
     rocking 220  
     sliding 224  
     vertical 208  
   critical 16  
   friction 37  
   geometrical 199, 245  
   vertical vibration 199
- Damping (cont.):*  
   internal hysteretic, soils 162, 165, 245  
   logarithmic decrement 18, 26, 162  
     soils, experimental 163  
   loss angle 167  
   material 165, 245  
   specific damping capacity 165  
   specific dissipation function 167  
   viscous 15, 39  
 Damping ratio, geometrical, rigid circular footing: 17  
   horizontal 225  
   rocking 220, 225, 226  
   torsion 226  
   vertical 208, 225, 226  
 Damping resistor 282  
 Dashpot 15  
 Decibel 124  
 Design criteria isolation, foundations for sensitive equipment 309, 321  
   machinery, steady-state 311  
   radar towers 322, 379  
   transient loading 315, 317  
 Diffraction 127  
   of gravity waves in water 128  
 Dilation (cubical dilation, dilatation) 77  
   definition for plane wave 80  
 Dilatational wave:  
   propagation velocity 78  
   synonyms 79  
 Dip angle:  
   apparent 108  
   true 108, 111  
 Displacement:  
   complex notation 56  
   dynamic rigid circular footing, rocking 218  
   Lysmer, vertical oscillation 203  
   Reissner, vertical oscillation 194  
   static, elastic layer, rigid circular footing, vertical 232  
   static rigid circular footing:  
     rocking 216  
     sliding 222  
 Displacement functions:  
   Lysmer's 203  
   Reissner's 194  
 Displacement measurements:  
   geometric patterns, visual observation 283  
   transducers 276

- Distortional wave:  
   propagation velocity 79  
   synonyms 79  
 Dynamic loads 322  
   from multicylinder engines 330  
   from rotating machinery 322  
   from single-cylinder engines 325  
   transient:  
     pulse 333  
     from punch press 334  
     from vibratory conveyors 332  
 Dynamic magnification factor 20  
 Dynamic modulus, measurement 300  
 Dynamic reciprocity 193
- E**
- Eccentric mass 23, 196  
 Eccentricity 23, 196  
 Elastic half-space, kinds of waves possible 80  
 Elastic layer, rigid circular footing:  
   torsional oscillation 230  
   vertical oscillation 232  
 Elastic moduli, experimental determination:  
   resonant-column method 72, 300  
   travel-time method 72  
 Elastic solids, porous, saturated, wave propagation 132  
 Elastic waves, wave equation 60, 78, 123  
 Electrical circuit:  
   current measurement 269  
   piezoelectric accelerometer 287  
   velocity transducer 280  
   voltage measurement 269  
 Electronic terms, prefixes 268  
 Embedment, effect on spring constant circular footings 352  
 Energy ratio 320  
 Equation of motion for infinite, homogeneous, isotropic elastic medium 75, 77, 78  
 Equivoluminal wave 78  
 Exciting force, by rotating mass 196

**F**

- Failure of soil samples:  
   in resonant-column tests 178  
   triaxial test, repeated loads 175

- Field measurements:  
   *P*-wave velocity 298  
   Rayleigh wave velocity 297  
   refraction survey 104, 298  
   travel time 299  
 Finite rods, end conditions:  
   fixed-fixed 71  
   fixed-free 70  
   free-free 69  
 Force transmission 30  
 Forced vibrations 19, 20  
 Foundation isolation, definition of 244  
 Foundation vibrations, measurement 295  
 Free vibration:  
   damped 15  
   undamped 11  
 Frequency:  
   circular 6  
   dimensionless 194  
   dimensionless factor 31  
   natural:  
     beams 57  
     of continuous system 57  
     damped 17  
     Newmark's method 57  
     Rayleigh approximation 58  
     relationship to static deflection 13, 58  
     Southwell-Dunkerley approximation 58  
   resonant rigid circular footing, vertical 208  
   undamped natural 13  
 Frequency equation:  
   fixed-fixed rod 71  
   fixed-free rod 70  
   free-free rod 70  
 Frequency measurement errors 289  
 Friction damping 37
- G**
- Galvanometers 271  
 Geologic formations, as vibration isolators 247  
 Geometrical damping:  
   definition 92, 225  
   vertical vibration 199, 225, 226  
 Geophone 275 (*see also* Transducer)

**H**

- Hardin oscillator 304

Harmonic motion 6  
 vector representation 10  
 Head wave 104  
 Hertz 6  
 Hollow cylindrical specimen 159  
 Horizontal vibration:  
 measurement 297  
 sliding 221  
 Huygens' principle 125

I

Impedance 267  
 Inductance 266  
 Inelastic behavior 44, 192  
 In-phase mass 337  
 Irrotational wave 78 (*see also* Dilatational wave)  
 Isolation:  
 by barriers 247  
 criteria for field tests 261  
 by geologic formations 247  
 by trenches 247  
 Isolation trenches, design dimensions 261

J

Jerk 9

L

Laplacian operator 78  
 Lateral earth pressure developed by vibrating compactors 188  
 Layered media (*see* Elastic layer)  
 Layering, horizontal 100  
 Liquefaction 172, 175  
 Logarithmic decrement 18 (*see also* Damping, logarithmic decrement)  
 Logarithmic spiral, construction of 45, 46  
 Longitudinal waves, rods 61  
 Love waves 100, 118  
 LVDT 278

## M

Machine foundations:  
 methods for analyzing:  
 DEGEBO 336

*Machine foundations (cont.):*  
 dynamic subgrade reaction 340  
 lumped-parameter system 345  
 rocking, example 373  
 Machinery, vibrations from 245, 319  
 Magnification factor 20  
 elastic layer, rigid circular footing, vertical 234  
 half-space theory, rigid circular footing:  
 rocking 216, 220  
 sliding 222  
 torsional vibration 214  
 vertical vibration 204, 205  
 Mass, dimensionless factor 31  
 Mass moment of inertia, rigid cylindrical footing, rocking 219  
 Mass ratio:  
 modified, vertical oscillation 204  
 rigid circular footing:  
 horizontal, sliding 221  
 rocking 216  
 torsion 214  
 vertical oscillation 195  
 Modes of vibration 53  
 coupled translation and rotation 53  
 experimental determination 296  
 Modulus:  
 shear:  
 complex 167  
 granular soils 154  
 tangent, cubic packing of spheres 145  
 of volume compressibility:  
 cubic packing of spheres 145  
 mixture of air and water 131  
 mixture of solids and liquid 129  
 of water 125  
 Mohr's circle 50  
 Moment of inertia, mass (*see* Mass moment of inertia)  
 Meters 269  
 ac 271  
 dc 269

## N

Newmark's method 57  
 Noise, electronic 274  
 Nomograph, vibration 10

## O

Octahedral shearing stress 156  
 Ohm's Law 264  
 Oscillator:  
 electromagnetic 283, 298  
 rotating mass 24, 298, 324  
 Oscilloscope 272, 293

## P

*P*-wave synonyms 79  
*P*-wave velocity, measurement 298  
 Pal 320  
 Particle velocity:  
 definition of 64  
 equation 64  
 Passive isolation:  
 definition 251  
 field tests 256  
 Persons, effects of vibrations on 311, 317  
 Phase angle 6  
 half-space theory 195  
 Phase-plane 32  
 acceleration 41, 46  
 free vibrations 32  
 friction damping 37  
 inelastic behavior 44  
 motion of the support 40  
 multilinear springs 42  
 oblique coordinates 45  
 solution:  
 drop test on model footing 366  
 punch press 368  
 step function 33  
 viscous damping 39  
 Pickup (*see also* Transducer) 275  
 Piezoelectric material 287  
 Piles:  
 natural frequency:  
 loaded 236  
 unloaded 236  
 torsional vibrations 238  
 vertical vibrations 235  
 Poisson's ratio:  
 effect on vertical vibrations 199  
 effect on wave velocity 86  
 Porosity 121  
 Potential functions 80  
 Power, electrical 265  
 Power required, half-space theory 195

Prefixes of electronic terms 268  
 Pressure, contact (*see* Contact pressure)  
 Primary unbalanced force 327

## R

Radar tower analysis, example, rocking vibrations 378  
 Railways, vibrations from 318  
 Rayleigh approximation to natural frequency 58  
 Rayleigh wave (*R*-wave):  
 attenuation of 245  
 definition 80  
 at interface 98  
 length 113  
 particle motion at surface 90  
 partition of at a corner 99  
 refraction of 127  
 relative displacement 88  
 velocity 80, 85, 86  
 measurement 297  
 wave length, field method 111  
*RC* time constant 288  
 Recorders 272  
 magnetic tape 273  
 paper 272, 295  
 Rectangular foundation:  
 equivalent radius 347  
 vertical oscillation 210  
 Reduced natural frequency 338  
 Reflection 93, 125  
 Reflection survey 101  
 Refracted waves, definition of for refraction survey 104  
 Refraction 93, 127  
 of gravity waves in water 127  
 Snell's law 94, 127  
 Refraction survey 104, 298  
 horizontal layering 104  
 inclined layering 106  
 reversed profile 109  
 Relative density 184  
 Resistance, electrical 264  
 Resonance curves, shape of 25  
 Resonant-column method:  
 with added mass:  
 longitudinal vibration 73  
 torsional vibration 73  
 description of 72

- Resonant-column test 300
  - hollow sample 159
  - of perfect spheres 150
  - of soils 151
- Resonant frequency 22, 25
- Reversed profile 109
- Rocking vibration:
  - measurement 297
  - radar tower 376
  - rectangular foundation analysis, example 373
  - rigid circular footings, field test data 369
- Rods, vibrations in:
  - flexural 61
  - longitudinal 61
  - torsional 61, 65
- Rotating mass excitation 24
- Rotating mass oscillator 298
- Rotation, definition for plane wave 80

## S

- S-wave synonyms 79
- Saturation, degree of 122
- Scaling law, wave length scaling for isolation tests 252
- Secondary unbalanced force 327
- Seismic methods 100
  - reflection survey 101
  - refraction survey 104
  - steady-state vibration 111
- Settlement 185
- Shear modulus:
  - cohesionless soils:
    - effect of amplitude 160
    - effect of prestrain 161
    - equations for 154, 353
  - complex 167
  - evaluation beneath footing 358
- Shear waves, horizontally polarized (Love waves) 100, 118
- Shear window, definition 92
- Shielded cable 291
- Shunt resistance 269, 281
- Single-degree-of-freedom system 11
  - force transmission 30
  - forced vibrations 19, 20
    - constant force 22
    - motion of the support 27, 40
    - rotating mass 23
  - vector representation 21

- Single-degree-of-freedom system (cont.):
  - free vibrations 11
  - frequency factor 31
  - friction damping 37
  - Lysmer's representation 31
  - mass factor 31
  - phase-plane solution 32
  - resonant frequency 22
  - steady-state solution 20
- Sinusoidal motion 6
- Sliding (*see* Horizontal oscillation)
- Slurry-trench, bentonite 249
- Snell's law 94, 127
- Soil properties, in-situ determination 100
- Sound, velocity of, in:
  - air 123, 124
  - water 124
- Southwell-Dunkerley approximation 58
- Spheres in contact:
  - contact pressure, normal loads 144
  - normal compliance 145
  - radius of contact, normal loads 144
- Spring constants:
  - rectangular footing, static, formulas for 350
  - rigid circular footing, static:
    - formulas for 350
    - rocking 220
    - sliding 224
    - torsion 214
    - vertical 205
  - static, elastic layer, rigid circular footing, vertical 232
- Springs 14
  - multilinear 42
  - parallel 14
  - rotational 51
  - series 14
- Static deflection methods 58
- Static displacement, rigid circular footing, vertical motion 200
- Steady-state vibrations 20
- Step function 33
- Strain-displacement relationship, ideal elastic medium 77
- Stress-strain behavior:
  - soils under dynamic loads 170
  - theoretical, spheres 149
- Stress-strain relationships, ideal elastic medium 77
- Subgrade reaction:
  - coefficient of 342

- Subgrade reaction (cont.):
  - horizontal, on piles 239
  - dynamic 338, 340

## T

- Tape recorders 273
- Termination resistance 290
- Torsional oscillation, rigid circular footing 213
- Torsional vibration, measurement 297
- Torsional waves, rods 65
- Traffic, vibrations from 318, 321
- Transducer 275
  - acceleration 286
  - calibration 278, 279, 282, 283, 287
  - displacement 276
  - LVDT 278
  - optical 279
  - relative displacement 278
  - relative velocity 284
  - velocity 280
- Transmissibility 30
- Transmission of force 30
- Travel time 299
- Travel-time method, elastic moduli 72
- Trenches:
  - dimensions for isolation 261
  - as isolation barriers 247
  - slurry-trench as isolation 249
- Two degrees of freedom 48
  - coupled translation 48
  - coupled translation and rotation 51
  - damped system 55
  - forced vibration 54
  - Mohr's circle 50

## U

- Unit weight:
  - submerged 122
  - total 122
  - unit dry weight 122

## V

- Vectors 11
- Velocity:
  - P-wave 78

- Velocity (cont.):
  - R-wave 86
  - S-wave 79
  - shear wave 66
- Velocity transducer 280
  - equivalent electrical circuit 285
- Vertical vibration:
  - measurement 296
  - rigid circular footing, field test data 356
  - single-cylinder compressor, analysis, example 360
  - transient loading:
    - analysis, example for model footing 364
    - analysis, punch press 367
- Vibrating roller 185
- Vibration:
  - amplitude 6
  - free 11
  - frequency 6
  - generator 282, 298
  - harmonic 6
  - measuring systems 293
  - period 6
  - periodic 7
  - random 7
  - sinusoidal 6
  - transient 7
  - vector 10
- Viscous damping 15, 39
- Void ratio 121
  - cubic packing of spheres 141
  - tetrahedral packing of spheres 143
- Voltage measurement 269

## W

- Water table, effect on wave velocities 136
- Waves:
  - direct 103
  - distribution of energy 95
  - head 104
  - reflected 93
  - refracted 94
  - refraction survey 104
  - shear, components 93
  - Snell's law 94, 127
  - transmitted 93
- Wave equation 60, 123
  - ideal elastic medium 78, 79

*Wave equation (cont.):*

- for longitudinal waves in a rod 62
- solution for finite rods 69
- torsional waves in a rod 66

Wave front:

- cylindrical (*R*-wave) 91
- hemispherical (*P*, *S*-waves) 91

Wave length, measurement 297

Wave number (*N*), definition 82

Wave propagation velocity, distinguished  
from particle velocity 63

Wave reflection, rods 67

Wave system at surface of half-space 88

- major tremor 89
- minor tremor 89

Wave velocity:

- acoustic waves in air 123, 124

*Wave velocity (cont.):*

apparent 106

compression waves:

- in mixture of air and water 131
- in mixture of solids and liquids 129
- in porous saturated solids 135, 136

effect of saturation 156

in elastic solids, effect of Poisson's ratio  
86, 168

pressure waves in water 124

Rayleigh waves, steady-state method,  
field 168

shear waves:

- cohesive soils 157
- granular soils 154
- porous saturated solids 134
- spheres 151